MARINE BIVALVE RECORDS OF ANTARCTIC SEASONALITY AND BIOLOGICAL RESPONSES TO ENVIRONMENTAL CHANGE OVER THE CRETACEOUS-PALEOGENE MASS EXTINCTION INTERVAL

Joanna Louise Ong Hall

Submitted in accordance with the requirements for the degree of
Doctor of Philosophy

The University of Leeds

School of Earth and Environment

December 2017

The candidate confirms that the work submitted is her own, except where work which has formed part of jointly authored publications has been included.

The contribution of the candidate and the other authors to this work has been explicitly indicated below. The candidate confirms that appropriate credit has been given within the thesis where reference has been made to the work of others.

The work in Chapter 6 of the thesis has been accepted for publication pending revision as follows:
Hall, J.L.O.; Newton, R.J.; Witts, J.D.; Francis, J.E.; Hunter, S.J.; Jamieson, R.A.; Harper, E.M.; Crame, J.A.; Haywood, A.M.
Sulfate and seasonality: Extreme methane signals in Late Cretaceous Antarctic bivalves
In revision for Earth and Planetary Science Letters
The candidate is the lead author and is responsible for all data analysis, interpretation and for writing the manuscript. Fieldwork and fossil sampling in Antarctica was conducted by Francis and Crame. Witts and Jamieson provided additional isotope data from sediments and bulk bivalves for comparison. Hunter assisted with hydrate modelling. All co-authors provided intellectual input and editorial changes to the draft manuscript.

ABSTRACT

The Cretaceous-Paleogene mass extinction event occurred 66 million years ago and had a profound effect on the course of evolutionary history, with the extinction of up to 75% of life and larger effects on the broader Earth system. A number of studies posit that the severity of this extinction event may have been amplified by climate variability and destabilisation in the latest Cretaceous – immediately prior to the extinction event. The strong seasonal forcing in the polar high latitudes is likely to have enhanced any such effects during this time period; additionally, the historical mismatch between late Cretaceous proxy data and climate simulations is particularly pronounced at high latitudes and both the effects of a stronger seasonal cycle on proxy temperature conversions, and misrepresentation of seasonality in climate models have been suggested as factors in the mismatch. This makes the Antarctic an extremely valuable location to study with regards to seasonality from a proxy- and model- based perspective. Seymour Island is a rare and valuable Antarctic K-Pg boundary site with a good framework of fossil, stratigraphic and sedimentological study, which makes fossil material ideal for investigation of the effects and impacts of seasonality and environmental change across the mass extinction interval.

This thesis presents a detailed study focusing on using fossil bivalve shell material from the Seymour Island section to reconstruct records of Antarctic climate and seasonality across the K-Pg mass extinction event. New data were obtained about the seasonal growth patterns of these bivalves to understand their growth and ontogenetic response to potential climate variability and the effects of the mass extinction. For the first time, sub-annual resolution stable carbon and oxygen isotopic data were produced from Seymour Island's bivalve shells to show seasonal changes in temperatures and detect changes in biogeochemical cycling and methane influence through the section. These data were integrated with a series of oxygen isotope enabled climate simulations to address potential issues converting from isotopic to temperature data in a highly seasonal environment and provide further information regarding the influence of sea ice. Combining new proxy- and model- based knowledge in a series of sensitivity experiments, it was shown that both sets of data display good agreement under realistic sets of parameters, suggesting that seasonality was important for the development of polar ecosystems. Warm summer temperatures may have been key in permitting the ecological strategy in these bivalves of slow growth to large sizes, which in turn may have contributed to survivorship across the K-Pg boundary.

ACKNOWLEDGMENTS

Firstly, I would like to thank my many supervisors, Alan Haywood, Rob Newton, Jane Francis, Liz Harper, Alistair Crame and Steve Hunter for all of their guidance, enthusiasm and encouragement over the course of this project. Thank you for lending me some of your scientific knowledge and for your patience whenever I was unable to see the way forward. I am also grateful to the Natural Environment Research Council for financial support to allow this research, and the British Antarctic Survey for their CASE funding.

I would also like to thank Rowan Whittle and the PalaeoPOLAR Research Group for helping to put everything Seymour Island into context and Cris Little, Christian Marz, Ben Mills and members of the Palaeo@Leeds Group for useful scientific discussions over Friday fish and chips throughout my time at Leeds. To everybody I've shared an office with; James, Laura, Tom, Rhian, Autumn, Carl, Adam and the various office pets. Thank you for many years of your advice, support and distractions.

Thanks go to my friends outside of Leeds as well as everybody I have gamed, travelled and sparkled with along the way. Thank you for providing so many wonderful spaces to escape to and reminding me that I am lucky to have been able to work on this project for the past four years. Special mentions go to Rhiannon for giving me so many remedial grammar lessons without complaint, and to Luke for fixing both my maths and my brain every time I broke them.

Finally, I would like to thank my parents, Mike and Chew-Lan for always trying to understand and not letting me give up and my brother, Jonny for somehow being able to say, "do it" exactly once to push me through any mental block: I'm glad you use your powers for good and not evil. None of this would have been possible without all of you.

CONTENTS

LIST OF TABLES

LIST OF FIGURES

CHAPTER 1

INTRODUCTION

1.1 Introduction

The Cretaceous-Paleogene (K-Pg) mass extinction event of 66 million years ago (Ma) is the most studied of the major mass extinction events of Earth history and is famed not only for its high-profile victims, including non-avian dinosaurs, marine reptiles and ammonites (MacLeod et al. 1997; Brusatte et al. 2014) but for the fundamental restructuring of global ecosystems it caused. These environmental and ecological changes may have ultimately contributed to the rise of modern fauna and flora (Alroy 1998; Krug et al. 2009).

There is still considerable debate over the cause of the K-Pg mass extinction with two principal hypotheses for the triggering event. The leading hypothesis is the impact of a major bolide (Alvarez et al. 1980) linked to the Chicxulub crater in Yucatan peninsula (Hildebrand et al. 1991; Arenillas et al. 2006). This would have led to rapid and severe global environmental changes (Schulte et al. 2010) and food chain collapse due to a reduction in available sunlight (Esmeray-Senlet et al. 2015). The most prominent alternative hypothesis is volcanism from the Deccan Traps large igneous province (LIP) in continental India (Schoene et al. 2015; Font et al. 2016). Although two of the three main phases occur before and after the K-Pg mass extinction, the largest phase is co-incident with the mass extinction (Chenet et al. 2009). Major volcanism would have released large volumes of CO_2 and other volatiles leading to alteration of atmospheric chemistry, short-term warming and longer-term cooling. Cause-and-effect relationships have also been proposed whereby the second phase of Deccan Traps volcanism may have been triggered by the seismic impact of a major bolide collision (Renne et al. 2015; Richards et al. 2015).

The proximate environmental killing mechanisms are also widely debated. Survivor taxa in the immediate post-extinction recovery period can be used to gauge the ecological effects. The effects of the mass extinction were geographically widespread, with even the middle to high-palaeolatitude oceanic

shelf sites far from either the Chicxulub impact site or Deccan Traps affected by a reduction in primary productivity (Aberhan et al. 2007). Multiple sites show a prevalence of starvation-resistant low-nutrient-adapted benthic species in the recovery faunas and the preferential extinction of groups dependent on photosynthetic organisms (Rhodes & Thayer 1991; Sheehan et al. 1996; Aberhan et al. 2007). There was also a change in ecospace occupation, particularly within molluscs with an overall decrease in suspension feeding and increase in deposit feeding across the K-Pg boundary (Aberhan & Kiessling 2015).

The impact of an asteroid at Chixulub was likely to have been the cause of the observed crisis in primary productivity and the collapse of photosynthesis-dependent food webs (e.g. Rhodes & Thayer 1991; Sheehan et al. 1996; Aberhan et al. 2007; Esmeray-Senlet et al. 2015). There is also evidence for additional environmental effects including metal poisoning (Jiang et al. 2010), surface water acidification (Alegret et al. 2012) and short-lived global cooling (Vellekoop et al. 2014). Deccan Trap volcanism may have provided additional stressors due to changes in the global carbon cycle and the resultant global warming followed by cooling, increased continental weathering, and run-off leading to changes in ocean chemistry (Kump & Arthur 1999; Renne et al. 2013).

It has been hypothesised that long-term environmental stresses, such as climate destabilisation and variability in the lead up to the K-Pg mass extinction may have primed environments and increased the severity of the extinction event itself (e.g. Arens & West 2008). The geological period across the K-Pg boundary from the latest Cretaceous Maastrichtian Stage (72.1 to 66 Ma) to the earliest Paleogene Danian Stage (66 to 61.6 Ma) has long been highlighted as a time of extreme temperature seasonality and variability on a scale unseen in modern temperate climates in contrast to more equable Cretaceous conditions (Barrera et al. 1987; Wolfe & Upchurch 1987; Pirrie & Marshall 1990; Barrera 1994; Ditchfield et al. 1994; Huber et al. 1995; Li & Keller 1998; Dingle & Lavelle 2000; Francis & Poole 2002; Gallagher et al. 2008).

The high latitudes in particular have the potential for heightened seasonal variability compared to lower latitudes due to strong forcing from the annual insolation regime which can involve long periods of continuous darkness or sunlight. Existing studies highlight the potential for strong seasonality around the Antarctic continent during the latest Cretaceous, including indicators of sea ice (Bowman et al. 2013; Petersen et al. 2016) in apparent contrast to the lush cool-temperate rainforests, large reptiles and abundant diverse marine life found

in the fossil record which are indicative of much warmer temperatures (Francis & Poole 2002; Martin & Crame 2006). There is no modern ecological analogue for a warm vegetated high latitude setting with an extremely seasonal light regime and energy budget, however it is expected that seasonality is likely to have played an important role in the evolution of high latitude environments and biotas, even during warmer periods of climate. This makes it extremely valuable to look in the Antarctic fossil record for evidence of the effects of high latitude seasonality and climate variability with regards to the K-Pg mass extinction and because of the key role that the continent played, and continues to play, in modulating global climate.

Annual seasonal temperature change driven by insolation provides one of the largest sources of climate variability on one of the shortest timescales. This is particularly important in the high latitudes, where the change in insolation is extremely large over the course of a year. Temperature seasonality and intra-annual climate change may be more important to understand from a palaeoecological angle than longer timescale mean-state climate conditions (e.g. Guthrie 1984) as seasonal temperature changes drive physical systems such as ocean currents and nutrient cycling (Marshall & Speer 2012). The amount of seasonality experienced by organisms may even affect global patterns of evolution and extinction (Bartlein & Prentice 1989; Sheldon 1996; Li & Keller 1998; Davis et al. 2005) with some studies suggesting that seasonal temperatures may have a stronger effect than mean annual temperatures on evolution and diversification (Parmesan et al. 2000; Archibald et al. 2010). Yet very little work has been done to examine the records and effects of seasonality in the geological record as it is extremely difficult to quantify seasonality in deep time due to a reliance on the ability to discern sub-annual temperature variations

The potential for heightened seasonal variability – in both the Maastrichtian to Danian and at high latitudes in general – is largely overlooked in interpretations of geochemical proxy records which often use modern calibrations to middle- and low-latitude mean annual temperatures and may result in misleading palaeoenvironment reconstructions (Wolfe 1993; Markwick 1996; Price et al. 1997; Pearson et al. 2001; Huber et al. 2002). In spite of a rich fossil and proxy data record, Late Cretaceous climate models often fail to match the conditions expected, with mean annual temperatures often predicted by models to be several degrees cooler than the proxy data suggest (Donnadieu et al. 2006). The effect of seasonality in the proxy interpretation of data may be an important source of data-model discrepancy and accurately quantifying past Antarctic climate

behaviour on a sub-annual scale is therefore important for assessing the veracity of palaeoclimate models.

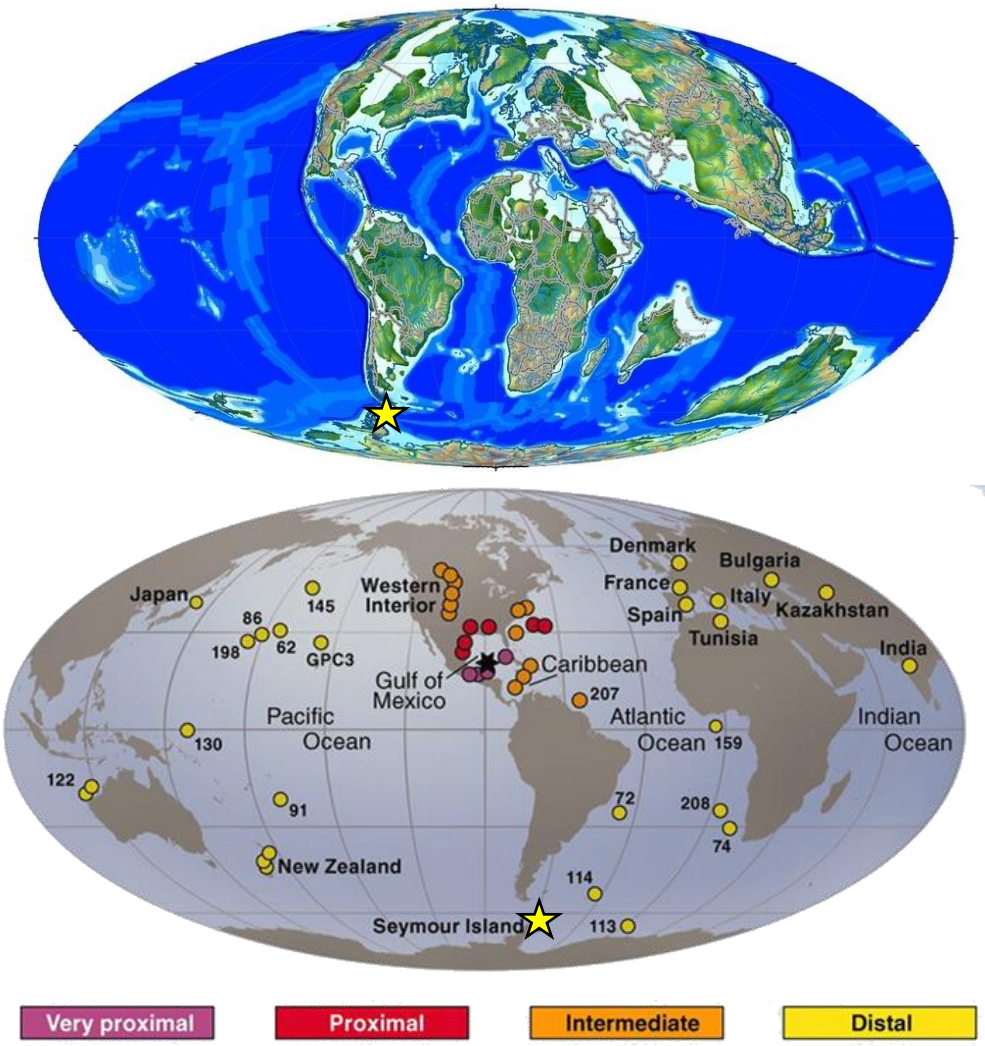

Figure 1.1: Maastrichtian palaeogeographic reconstruction showing the approximate palaeolocation of Seymour Island (yellow star). And map of modern locations of key K-Pg boundary data locations. Reconstruction based on Markwick & Valdes (2004), locations from Schulte et al. (2010). Note that maps are not centred on the same line of longitude; the present-day location of Seymour Island shows little movement from its Cretaceous location.

The effects of the mass extinction event have long been thought to have been muted at high latitudes (e.g. Barrera & Keller 1994), however, the latest studies suggest that the extinction event was probably just as rapid and severe in Antarctica as it was in lower latitudes (Witts et al. 2016). Studies from Cretaceous to Paleogene sections around the Antarctic Peninsula have proved particularly important in adding to the discussion of the climate and effects of the mass extinction event. This region of the Antarctic is an area which has been identified as being both sensitive to environmental change, and an important location for both deep-water formation, and upwelling during the Late Cretaceous and Paleogene.

Within the region of the Antarctic Peninsula, Seymour Island contains a rare and extremely scientifically important high latitude K/Pg boundary locality. The island possesses a near-continuous section of shallow marine sedimentary deposits ranging from the latest Cretaceous to Eocene with abundant well-preserved fossil material. Palaeogeographic reconstructions (Figure 1.1) and magnetostratigraphic data place the depositional basin at around 65°S during the events of the K-Pg mass extinction (e.g. Lawver et al. 1992; Hay et al. 1999). These outcrops therefore represent a true high latitude record of events during this critical period of time as well as the only outcropping marine rocks of these ages in Antarctica (Marvin & Post 1982; Schulte et al. 2010) and the highest-latitude continuous K/Pg boundary section (Figure 1.1). Fossil material from this section is therefore ideal for examining records of high latitude seasonality during the boundary interval.

There are a large number of intact macrofossil specimens collected from traverses across the Seymour Island K-Pg boundary section available to study, and the basic framework of species identification, broad palaeoenvironment and sedimentology is available evidence (Macellari 1988; Zinsmeister & Macellari 1988; Crame et al. 2004; Thorn et al. 2009; Olivero 2012), so more detailed analysis can be undertaken without the need to start entirely blind. Infaunal bivalves have been particularly important in previous studies; several genera of large-shelled infaunal bivalves are abundant in pre- and post- extinction faunas and have the potential to both record and respond to changes in environmental conditions (e.g. Zolotarev 1980; Jones et al. 1989; Buick & Ivany 2004; Butler et al. 2010, 2013). Bivalve specimens from the Eocene of this area have been found to be preserved sufficiently well for sub-annual stable isotopic analysis (Buick & Ivany 2004), and attempts have been made to produce clumped isotopic data from shell material across the boundary section including broad estimates of

minimum seasonality from differences between juvenile and mature mean recorded temperatures (Petersen et al. 2016). However, specimens from the K-Pg boundary have not been well studied on sub-annual timescales, and the data produced by such analysis is likely to provide a useful understanding of processes that affected the high latitudes during a climatologically important time period.

1.2 Aims and Objectives

The aim of this thesis is to understand the nature of seasonality in Cretaceous and early Cenozoic Antarctic climates and the impact of seasonality and environmental variability on the growth and survival of polar marine bivalves across the K-Pg boundary interval. Specifically, this thesis will aim to answer the following research questions:

- What were the climate conditions of the marine environment in the James Ross Basin during the late Maastrichtian and early Paleogene; how seasonal and climatologically variable was it and what were the likely drivers of variability. What is the potential for seasonal bias in temperature proxies at high latitudes
- Can high resolution stable carbon and oxygen isotopic data be used to detect changes in biogeochemical cycling throughout this time period?
- How do global patterns of seasonality from climate models and data throughout the Maastrichtian compare to the data from Seymour Island?
- How did infaunal bivalves respond to climate variability, seasonality and environmental changes in the lead up to and aftermath of the K-Pg mass extinction?

In order to answer these questions, this thesis is divided into 7 chapters as follows, each drawing on the work done in the previous chapters. The remainder of Chapter 1 provides an overview of the thesis rationale and structure.

Chapter 2 presents a summary of the geological setting of the marine sedimentary sequence on Seymour Island, which presents a rare Antarctic Cretaceous and early Paleogene boundary succession and fossil material with which to look for evidence for seasonal effects on marine fauna.

Chapter 3 identifies the suitable bivalves in the Seymour Island section to use to look for signals of seasonality and presents the results of morphometric analysis of several species of bivalves through the stratigraphic section. Also included are the results of preservation tests to determine suitability of these specimens for geochemical analysis, along with tests for growth ring periodicity and analysis of ontogenetic trends in species where annual growth rings can be confirmed.

Chapter 4 focuses on geochemical analysis, using well preserved fossil specimens to reconstruct sub-annual temperature records using stable isotopic and clumped isotopes. These results have been compared to oxygen isotope enabled model data under a number of different CO2 and river output conditions.

In Chapter 5, seasonality and climate variability are examined in shell-derived data through stratigraphy and compared to modelled seasonal temperature outputs under different boundary conditions.

The biogeochemical conditions of the Late Cretaceous and early Paleogene and their potential impact on local and global climate are considered in Chapter 6, where seasonal stable carbon isotopic data is used to examine the marine sedimentary carbon cycle under low sulfate conditions. This chapter has been formatted for publication.

Chapter 7 brings together these results and additional data from other terrestrial and marine proxies for seasonal climate conditions into an overall discussion of the effects of seasonality within the Seymour Island section and in the context of global Maastrichtian conditions, and summarises the findings related to each of the research questions detailed above.

1.3 References

Aberhan, M. and Kiessling, W. (2015) 'Persistent ecological shifts in marine molluscan assemblages across the end-Cretaceous mass extinction', *Proceedings of the National Academy of Sciences*, 112(23), 7207– 7212.

Aberhan, M., Weidemeyer, S., Kiessling, W., Scasso, R. A. and Medina, F. A. (2007) 'Faunal evidence for reduced productivity and uncoordinated recovery in Southern Hemisphere Cretaceous-Paleogene boundary

sections', *Geology*, 35(3), 227–230.

Alegret, L., Thomas, E. and Lohmann, K. C. (2012) 'End-Cretaceous marine mass extinction not caused by productivity collapse', *Proceedings of the National Academy of Sciences*, 109(3), 728–732.

Alroy, J. (1998) 'Cope's rule and the dynamics of body mass evolution in North American fossil mammals.', *Science*, 280(5364), 731–4.

Alvarez, L. W., Alvarez, W., Asaro, F. and Michel, H. V. (1980) 'Extraterrestrial Cause for the Cretaceous-Tertiary Extinction', *Science*, 208(4448), 1095–1108.

Archibald, J. D., Clemens, W. A., Padian, K., Rowe, T., Macleod, N., Barrett, P. M., Gale, A., Holroyd, P., *et al.* (2010) 'Multiple Causes Cretaceous Extinctions : Cretaceous Extinctions ':, *Science*, 328, 973–976.

Arenillas, I., Arz, J. A., Grajales-Nishimura, J. M., Murillo-Muñ etó n, G., Alvarez, W., Camargo-Zanoguera, A., Molina, E. and Rosales-Domí nguez, C. (2006) 'Chicxulub impact event is Cretaceous/Paleogene boundary in age: New micropaleontological evidence', *Earth and Planetary Science Letters*, 249(3–4), 241–257.

Arens, N. C. and West, I. D. (2008) 'Press-pulse: a general theory of mass extinction?', *Paleobiology*, 34(4), 456–471.

Barrera, E. (1994) 'Global environmental changes preceding the Cretaceous-Tertiary boundary: Early-late Maastrichtian transition', *Geology*, 22(10), 877–880.

Barrera, E., Huber, B. T., Savin, S. M. and Webb, P. N. (1987) 'Antarctic marine temperatures: Late Campanian through early Holocene', *Paleoceanography*, 2, 21–47.

Barrera, E. and Keller, G. (1994) 'Productivity across the Cretaceous/Tertiary boundary in high latitudes', *Geological Society of America ..*, (10).

Bartlein, P. J. and Prentice, I. C. (1989) 'Orbital variations, climate and paleoecology', *Trends in Ecology & Evolution*, 4(7), 195–199.

Bowman, V. C., Francis, J. E. and Riding, J. B. (2013) 'Late Cretaceous winter sea ice in Antarctica?', *Geology*, 41(12), 1227–1230.

Brusatte, S. L., Lloyd, G. T., Wang, S. C. and Norell, M. A. (2014) 'Gradual assembly of avian body plan culminated in rapid rates of evolution across the dinosaur-bird transition.', *Current biology : CB*, 24(20), 2386–92.

Buick, D. P. and Ivany, L. C. (2004) '100 years in the dark: Extreme longevity

of Eocene bivalves from Antarctica', *Geology*, 32(10), 921.

Butler, P. G., Richardson, C. A., ., Scourse, J. D., Wanamaker, A. D., Shammon, T. M. and Bennell, J. D. (2010) 'Marine climate in the Irish Sea: analysis of a 489-year marine master chronology derived from growth increments in the shell of the clam *Arctica islandica*', *Quaternary Science Reviews*, 29(13–14), 1614–1632.

Butler, P. G., Wanamaker, A. D., Scourse, J. D., Richardson, C. A. and Reynolds, D. J. (2013) 'Variability of marine climate on the North Icelandic Shelf in a 1357-year proxy archive based on growth increments in the bivalve *Arctica islandica*', *Palaeogeography, Palaeoclimatology, Palaeoecology*, 373, 141–151.

Chenet, A.-L., Courtillot, V., Fluteau, F., Gérard, M., Quidelleur, X., Khadri, S. F. R., Subbarao, K. V. and Thordarson, T. (2009) 'Determination of rapid Deccan eruptions across the Cretaceous-Tertiary boundary using paleomagnetic secular variation: 2. Constraints from analysis of eight new sections and synthesis for a 3500-m-thick composite section', *Journal of Geophysical Research*, 114(B6), B06103.

Crame, J. A., Francis, J. E., Cantrill, D. J. and Pirrie, D. (2004) 'Maastrichtian stratigraphy of Antarctica', *Cretaceous Research*, 25(3), 411–423.

Davis, M. B., Shaw, R. G. and Etterson, J. R. (2005) 'Evolutionary Responses To Changing Climate', *Ecology*, 86(7), 1704–1714.

Dingle, R. V. and Lavelle, M. (2000) 'Antarctic Peninsula Late Cretaceous-Early Cenozoic palaeoenvironments and Gondwana palaeogeographies', *Journal of African Earth Sciences*, 31(1), 91–105.

Ditchfield, P. W., Marshall, J. D. and Pirrie, D. (1994) 'High latitude palaeotemperature variation: New data from the Thithonian to Eocene of James Ross Island, Antarctica', *Palaeogeography, Palaeoclimatology, Palaeoecology*, 107(1–2), 79–101.

Donnadieu, Y., Pierrehumbert, R., Jacob, R. and Fluteau, F. (2006) 'Modelling the primary control of paleogeography on Cretaceous climate', *Earth and Planetary Science Letters*, 248, 426–437.

Esmeray-Senlet, S., Wright, J. D., Olsson, R. K., Miller, K. G., Browning, J. V. and Quan, T. M. (2015) 'Evidence for reduced export productivity following the Cretaceous/Paleogene mass extinction', *Paleoceanography*, 30(6), 718–738.

Font, E., Adatte, T., Sial, A. N., Drude de Lacerda, L., Keller, G. and Punekar, J. (2016) 'Mercury anomaly, Deccan volcanism, and the end-Cretaceous mass extinction', *Geology*, 44(2), 171–174.

Francis, J. E. and Poole, I. (2002) 'Cretaceous and early Tertiary climates of Antarctica: evidence from fossil wood', *Palaeogeography, Palaeoclimatology, Palaeoecology*, 182(1), 47–64.

Gallagher, S. J., Wagstaff, B. E., Baird, J. G., Wallace, M. W. and Li, C. L. (2008) 'Southern high latitude climate variability in the Late Cretaceous greenhouse world', *Global and Planetary Change*, 60(3), 351–364.

Guthrie, R. D. (1984) 'Mosaics, allelochemics and nutrients: an ecological theory of late Pleistocene megafaunal extinctions.', in *Quaternary Extinctions: A Prehistoric Revolution*, 259–98.

Hay, W. W., DeConto, R. M., Wold, C. N., Wilson, K. M., S., V., M., S., Wold, A. R., Balukhovsky, A. N., *et al.* (1999) 'Alternative global Cretaceous paleogeography', *Geological Society of America Special Papers*, 332, 1–47.

Hildebrand, A. R., Penfield, G. T., Kring, D. A., Pilkington, M., Camargo Z., A., Jacobsen, S. B. and Boynton, W. V (1991) 'Chicxulub Crater: A possible Cretaceous/Tertiary boundary impact crater on the Yucatan Peninsula, Mexico', *Geology*, 19(9), 867–871.

Huber, B. T., Hodell, D. A. and Hamilton, C. P. (1995) 'Middle-Late Cretaceous climate of the Southern High Latitiudes: Stable isotope evidence for minimal equator-to-pole thermal gradients', *Geological Society of America Bulletin*, 107(10), 1164–1191.

Huber, B. T., Norris, R. D. and MacLeod, K. G. (2002) 'Deep-sea paleotemperature record of extreme warmth during the Cretaceous', *Geology*, 30(2), 123–126.

Jiang, S., Bralower, T. J., Patzkowsky, M. E., Kump, L. R. and Schueth, J. D. (2010) 'Geographic controls on nannoplankton extinction across the Cretaceous/Palaeogene boundary', *Nature Geoscience*, 3(4), 280–285.

Jones, D. S., Arthur, M. A. and Allard, D. J. (1989) 'Sclerochronological records of temperature and growth from shells of *Mercenaria mercenaria* from Narragansett Bay, Rhode Island', *Marine Biology*, 102(2), 225–234.

Krug, A. Z., Jablonski, D. and Valentine, J. W. (2009) 'Signature of the end-Cretaceous mass extinction in the modern biota.', *Science*, 323(5915), 767–71.

Kump, L. R. and Arthur, M. A. (1999) 'Interpreting carbon-isotope excursions: carbonates and organic matter', *Chemical Geology*, 161(1–3), 181–198.

Lawver, L. A., Gahagan, L. M. and Coffin, M. F. (1992) 'The development of paleoseaways around Antarctica', in Kennett, J. P. and Warnke, D. A. (eds) *The Antarctic Paleoenvironment: A Perspective on Global Change Antarctic Research Series*, 7–30.

Li, L. and Keller, G. (1998) 'Abrupt deep-sea warming at the end of the Cretaceous', *Geology*, 26(11), 995–998.

Macellari, C. E. (1988) 'Stratigraphy, sedimentology, and paleoecology of Upper Cretaceous / Paleocene shelf-deltaic sediments of Seymour Island', *Geological Society of America Memoirs*, 169, 25–54.

MacLeod, N., Rawson, P. F., Forey, P. L., Banner, F. T., Boudagher-Fadel, M. K., Bown, P. R., Burnett, J. A., Chambers, P., *et al.* (1997) 'The Cretaceous-Tertiary biotic transition', *Journal of the Geological Society*, 154(2), 265–292.

Markwick, P. J. (1996) *Late Cretaceous to Pleistocene Climates: Nature of the Transition from 'Hot-House' to an 'Ice-House' World*.

Marshall, J. and Speer, K. (2012) 'Closure of the meridional overturning circulation through Southern Ocean upwelling', *Nature Geoscience*, 5(3), 171–180.

Martin, J. E. and Crame, J. A. (2006) 'Palaeobiological significance of high-latitude Late Cretaceous vertebrate fossils from the James Ross Basin, Antarctica', *Geological Society, London, Special Publications*, 258(1), 109–124.

Marvin, U. B. and Post, J. (1982) 'Searching for evidence of an impact event at the Cretaceous/Tertiary boundary on Seymour Island', *Antarctic Journal*, 17(5).

Olivero, E. B. (2012) 'Sedimentary cycles, ammonite diversity and palaeoenvironmental changes in the Upper Cretaceous Marambio Group, Antarctica', *Cretaceous Research*, 34, 348–366.

Parmesan, C., Root, T. L., Willig, M. R., Parmesan, C., Root, T. L. and Willig, M. R. (2000) 'Impacts of Extreme Weather and Climate on Terrestrial Biota *', *Bulletin of the American Meteorological Society*, 81(3), 443–450.

Pearson, P. N., Ditchfield, P. W., Singano, J., Harcourt-Brown, K. G., Nicholas, C. J., Olsson, R. K., Shackleton, N. J. and Hall, M. A. (2001) 'Warm

tropical sea surface temperatures in the Late Cretaceous and Eocene epochs', *Nature*, 413(6855), 481–487.

Petersen, S. V., Dutton, A. and Lohmann, K. C. (2016) 'End-Cretaceous extinction in Antarctica linked to both Deccan volcanism and meteorite impact via climate change', *Nature Communications*, 7(May), 12079.

Pirrie, D. and Marshall, J. D. (1990) 'High-paleolatitude Late Cretaceous paleotemperatures: New data from James Ross Island, Antarctica', *Geology*, 18(1), 31–34.

Price, D. A., Valdes, P. J. and Sellwood, B. W. (1997) 'Quantitative palaeoclimate GCM validation: Late Jurassic and mid-Cretaceous case studies', *Journal of the Geological Society*, 154, 769–772.

Renne, P. R., Deino, A. L., Hilgen, F. J., Kuiper, K. F., Mark, D. F., Mitchell, W. S., Morgan, L. E., Mundil, R., *et al.* (2013) 'Time Scales of Critical Events Around the Cretaceous-Paleogene Boundary', *Science*, 339(6120), 684–687.

Renne, P. R., Sprain, C. J., Richards, M. A., Self, S., Vanderkluysen, L. and Pande, K. (2015) 'State shift in Deccan volcanism at the Cretaceous-Paleogene boundary, possibly induced by impact', *Science*, 350(6256), 76–78.

Rhodes, M. C. and Thayer, C. W. (1991) 'Mass extinctions: Ecological selectivity and primary production', *Geology*, 19(9), 877.

Richards, M. A., Alvarez, W., Self, S., Karlstrom, L., Renne, P. R., Manga, M., Sprain, C. J., Smit, J., *et al.* (2015) 'Triggering of the largest Deccan eruptions by the Chicxulub impact', *Geological Society of America Bulletin*, 127(11–12), 1507–1520.

Schoene, B., Samperton, K. M., Eddy, M. P., Keller, G., Adatte, T., Bowring, S. A., Khadri, S. F. R. and Gertsch, B. (2015) 'U-Pb geochronology of the Deccan Traps and relation to the end-Cretaceous mass extinction', *Science*, 347(6218), 182–184.

Schulte, P., Alegret, L., Arenillas, I., Arz, J. A., Barton, P. J., Bown, P. R., Bralower, T. J., Christeson, G. L., *et al.* (2010) 'The Chicxulub asteroid impact and mass extinction at the Cretaceous-Paleogene boundary.', *Science (New York, N.Y.)*, 327(5970), 1214–8.

Sheehan, P. M., Coorough, P. J., Fastovsky, D. E. and Ryder, G. (1996) 'Biotic selectivity during the K/T and Late Ordovician extinction events',

Geological Society of America Special Paper, 307, 477–489.

Sheldon, P. R. (1996) 'Plus ça change — a model for stasis and evolution in different environments', *Palaeogeography, Palaeoclimatology, Palaeoecology*, 127(1–4), 209–227.

Thorn, V. C., Francis, J. E. and Riding, J. B. (2009) 'The Late Cretaceous dinoflagellate cyst *Manumiella* — Biostratigraphy, systematics, and palaeoecological signals in Antarctica', *Review of Palaeobotany and Palynology*, 156(3–4), 436–448.

Vellekoop, J., Sluijs, A., Smit, J., Schouten, S., Weijers, J. W. H., Sinninghe Damste, J. S. and Brinkhuis, H. (2014) 'Rapid short-term cooling following the Chicxulub impact at the Cretaceous-Paleogene boundary', *Proceedings of the National Academy of Sciences*, 111(21), 7537–7541.

Witts, J. D., Whittle, R. J., Wignall, P. B., Crame, J. A., Francis, J. E., Newton, R. J. and Bowman, V. C. (2016) 'Macrofossil evidence for a rapid and severe Cretaceous–Paleogene mass extinction in Antarctica', *Nature Communications*, 7, 11738.

Wolfe, J. A. (1993) 'A method of obtaining climatic parameters from leaf assemblages', *U.S. Geological Survey Bulletin*, 2040.

Wolfe, J. A. and Upchurch, G. R. (1987) 'North American nonmarine climates and vegetation during the Late Cretaceous', *Palaeogeography, Palaeoclimatology, Palaeoecology*, 61, 33–77.

Zinsmeister, W. J. and Macellari, C. E. (1988) 'Bivalvia (Mollusca) from Seymour Island , Antarctic Peninsula', *Geological Society of America Memoirs*, (169).

Zolotarev, V. (1980) 'The life span of bivalves from the Sea of Japan and Sea of Okhotsk', *Biologiya morya-Marine Biology*, 6, 3–12.

CHAPTER 2

GEOLOGICAL SETTING AND MATERIALS

2.1 Introduction

This chapter presents the stratigraphic, sedimentological and palaeoenvironmental context for the fossil bivalve specimens studied in the following chapters. It begins with a discussion of the evolution and tectonic history of the Antarctic Peninsula and the eastern back-arc basin where Seymour Island's sediments were deposited followed by an overview of the Cretaceous to Paleogene sedimentary succession from which the fossil bivalve material was collected. An overview of existing records of marine and terrestrial palaeoenvironmental conditions around the Antarctic Peninsula over this interval of sedimentation is also presented. Fossil collection methods, locality specifics, and nomenclature used within this study are described, and the chapter concludes with the results of initial preservation tests to determine the suitability of these specimens for the geochemical analysis which forms the basis of the following chapters.

2.2 Regional Tectonics and Palaeogeography

The rocks outcropping on modern-day Seymour Island were deposited in the James Ross basin; the northernmost sub-basin of the much larger Larsen Basin which developed in the back-arc of the Antarctic Peninsula (del Valle et al. 1992; Hathway 2000). From the Jurassic to the Eocene, the Antarctic Peninsula was an active and evolving volcanic arc, fed by the subduction of the proto-Pacific to the west under the Antarctic plate (Figure 2.3, Elliot 1988). Crustal extension is likely to have formed a number of basins along the margins of the tectonic remnants of the break-up of Gondwana during this period (Zinsmeister 1982)

and subduction led to the formation of basins in the fore-arc to the west of the Antarctic Peninsula, and back-arc basins such as the Larsen Basin to the East.

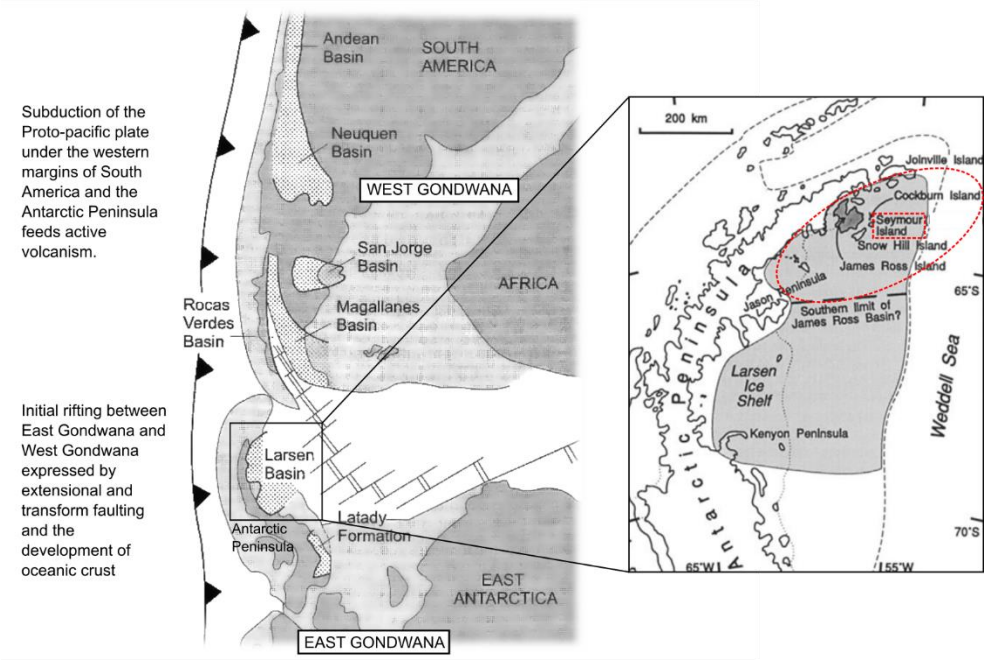

Figure 2.1: Tectonic and subduction regime of the early rifting between East and West Gondwana (Late Jurassic to Cretaceous), modified from Hathway (2000). Inset; the approximate position and extent of Seymour Island and the James Ross Basin (red dashed line) within the larger Larsen Basin, modified from del Valle et al. (1992).

During the Late Cretaceous to Paleocene which is the focus of this study, the Larsen basin was open to the east and bounded to the west by the coastal plains and flanks of the volcanically active and emergent Antarctic Peninsula, with a shoreline trending roughly NNE – SSW. A southern limit to the Larsen Basin has tentatively been placed along the 69°S parallel (Macdonald et al. 1988), with the James Ross basin within it bounded at roughly the 65°S parallel (Figure 2.1, del Valle et al. 1992). Rivers flowing ESE from the Antarctic Peninsula provided the main clastic source to the basin and delivered siliciclastic sediments to the deltaic or estuarine systems offshore (Pirrie 1989; Scasso et al. 1991; Olivero et al. 1992). Analysis of the distribution of fossil invertebrates and trace fossils suggest that Seymour Island was located in a relatively central part of the basin some 150 km to the southeast of the principal magmatic arc, and approximately 300 km from the trench (Figure 2.6) (Elliot 1997; Olivero et al. 2008).

During the deposition of the Maastrichtian to Danian succession, palaeogeographic reconstruction suggests that the northern tip of the Antarctic Peninsula was connected via a shallow water archipelago to the southern tip of the Fugeian Andes of South America (Figure 2.2, Markwick & Valdes 2004; Markwick 2007). This allowed ocean contact into the Weddell sea, but there is no evidence for a deep circumpolar flow until the earliest Oligocene (Katz et al. 2011).

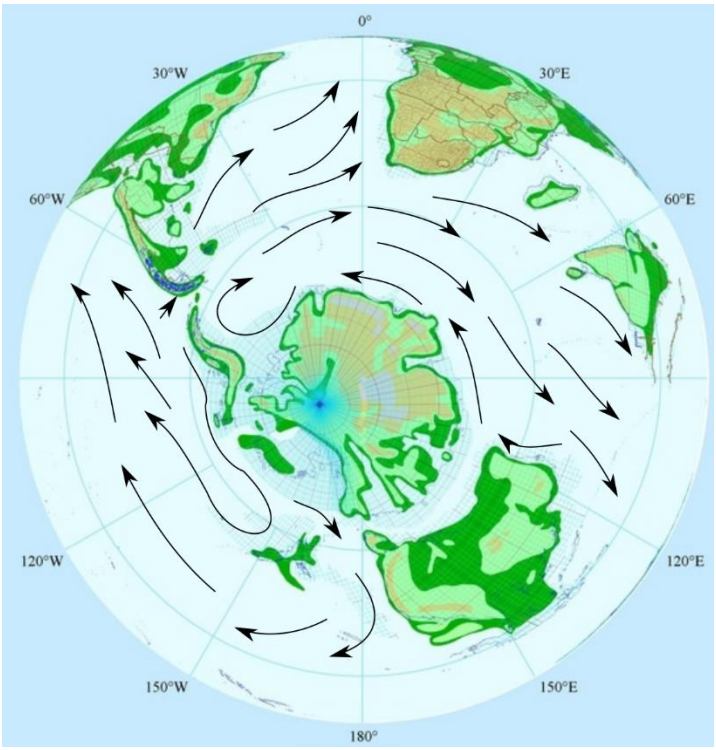

Figure 2.2: Palaeogeographical map of the south polar region and oceanic connectivity during the Maastrichtian (Base map from Markwick 2007, ocean circulation based on the top 450m of currents modelled using HadCM3L (Hunter 2009).

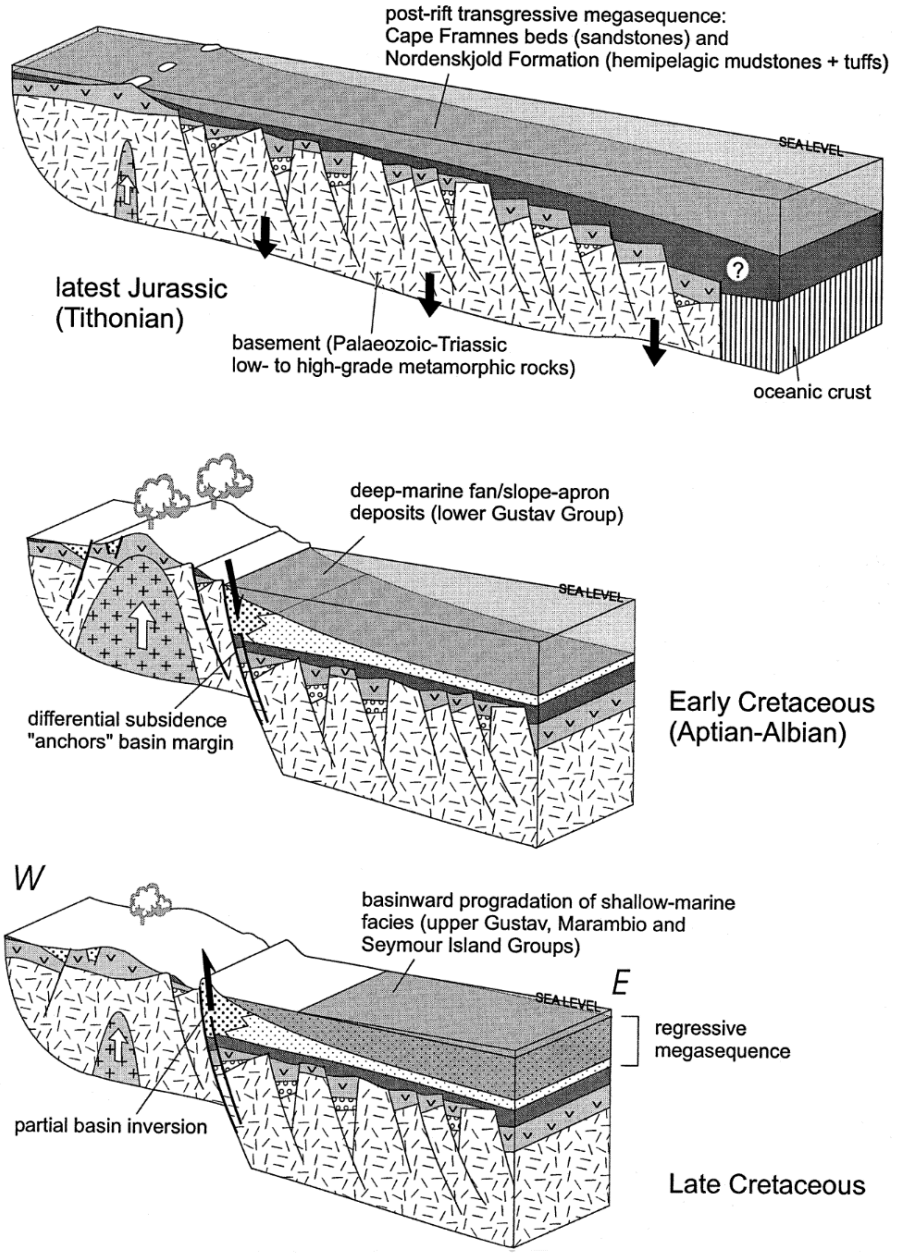

Figure 2.3: Geological evolution of the Antarctic Peninsula (western volcanics) and Larsen Basin (eastern marine sequences), from the Late Jurassic onset of rifting to the Late Cretaceous deposition of basin fill sediments, altered from Hathway (2000).

2.3 General Stratigraphy of the James Ross Basin

The islands of the modern James Ross basin preserve a thick and relatively complete volcaniclastic succession throughout the evolution of the basin from the Late Cretaceous (approximately Aptian Stage 125 Ma) to the Late Eocene (33.9 Ma). The sedimentary basin-fill of the James Ross Basin has been classified as a regressive megasequence (Macdonald et al. 1988) and can be divided into three main sequences; the Aptian to Coniacian Gustav group (Riding & Crame 2002; Crame et al. 2006; Kennedy et al. 2007), the latest Coniacian to Paleocene Marambio Group (Rinaldi et al. 1978; Crame et al. 1991; McArthur et al. 2000; Olivero 2012) and the Paleocene to Eocene Seymour Island Group (Elliot & Trautman 1982; Marenssi et al. 1998). These groups are divided by major regional unconformities representing a change in palaeoenvironment and basin configuration; likely driven by a mixture of tectonic changes, global sea-level regressions or potentially glacioeustatic sea level change (Pirrie et al. 1991; Crame et al. 2004; Olivero et al. 2008; Olivero 2012).

The similar and homogeneous nature of much of the fine-grained sedimentary succession has led to difficulties correlating smaller units across the basin. This is of particular issue for members of the Marambio Group, which has key outcrops spread over a wide area on disparate small islands of the James Ross Basin. Macrofossils (e.g. ammonites, Olivero & Medina 2000) and microfossils (e.g. dinoflagellates, Pirrie et al. 1997; Riding & Crame 2002; Bowman et al. 2012) have been used to define the stratigraphy and correlate well with sedimentological features such as major unconformities (Crame et al. 1991). Recent additions of absolute age controls in the form of strontium iotope chemostratigraphy (McArthur et al. 2000) and magnetostratigraphy (Tobin et al. 2012; Milanese et al. 2013, 2017) to the existing biostratigraphic and sedimentological framework has provided much more precise age constraints to the basin succession. Each megasequence broadly represents a different set of environmental and depositional conditions within the evolution of the James Ross Basin, and the associated environments and compositions are briefly detailed below.

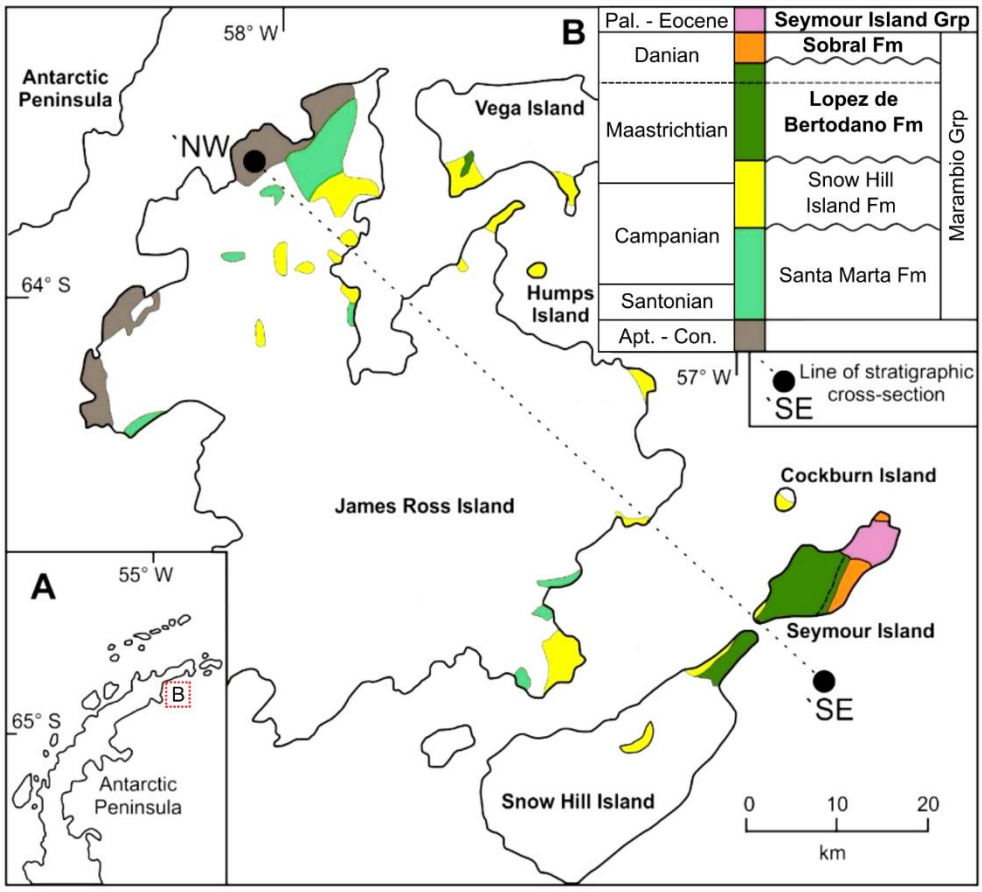

Figure 2.4: Geographical setting (A) and geological map (B) of the James Ross Island cluster within the James Ross basin showing the distribution of the main sedimentary groups. K-Pg boundary position is indicated on Seymour Island in the upper layers of the López de Bertodano Formation. Line of section refers to Figure 2.5. Modified from Witts (2016).

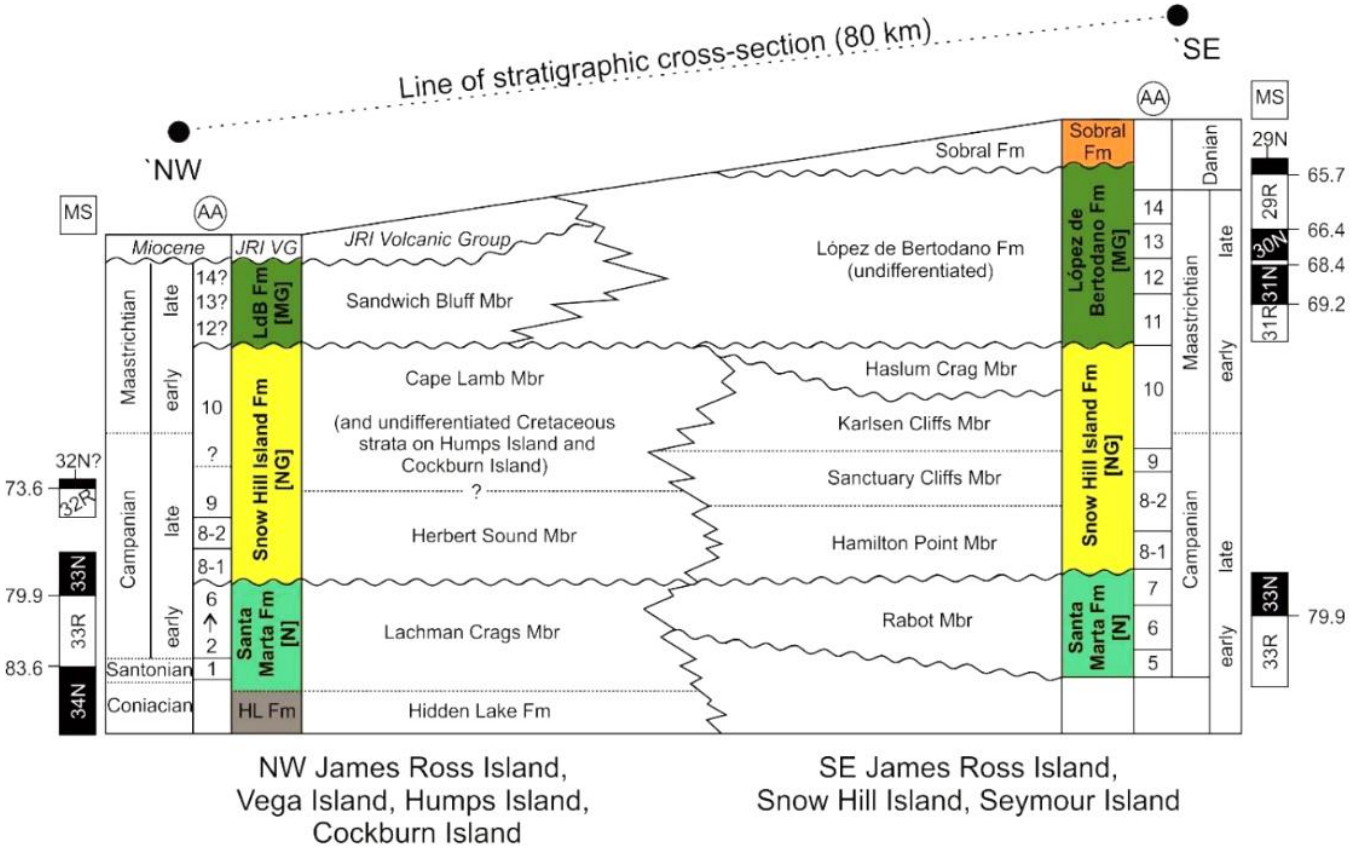

Figure 2.5 Correlation cross section based on line in Figure 2.4. Includes correlations made using magnetostratigraphy (MS), ammonite assemblage biostratigraphy (AA) and lithostratigraphy from multiple sources. Taken from Witts (2016).

2.3.1 Gustav Group

The Gustav Group was deposited in the Aptian to Coniacian (Riding & Crame 2002; Crame et al. 2006; Kennedy et al. 2007) and includes the Lagrelius Point Formation, Kotick Point Formation, Whiskey Bay Formation and Hidden Lake Formation. These can all be found as outcrops along the northwest coast of the James Ross Island and are thought to represent the deepest marine sedimentation in the basin. During the period of deposition, rapid basin extension and uplift of the Antarctic Peninsula volcanic arc produced high sedimentation rates, resulting in a basin-infill sequence roughly 3000m thick (Whitham et al. 2006). The sedimentary deposits are largely fine grained sandstones and mudstones, with volcaniclastics including pyroclastic flows and fragments of pumice and volcanic bombs present in the Coniacian strata (Hathway 2000; Whitham et al. 2006).

2.3.2 Marambio Group

The Marambio Group was deposited from the latest Coniacian to the Paleocene and its members are exposed across a much larger geographical area than the Gustav Group. It consists of the Santa Marta Formation, present in several locations across James Ross Island, the Snow Hill Island Formation, found across James Ross Island, Snow Hill Island, Vega Island and Humps Island, the López de Bertodano Formation on Vega Island, Snow Hill Island and Seymour Island, and the Sobral Formation, which only outcrops on Seymour Island (Rinaldi et al. 1978; Crame et al. 1991; McArthur et al. 2000; Olivero 2012). The increased number of outcrops and locations display some environmental difference across the roughly 80 km of the modern-day James Ross island chain, which has made correlating the units and members within the Marambio Group quite challenging. The overall sedimentological environment is interpreted as a shallower marine environment than the Gustav Group, with the Marambio Group representing an overall regressive megasequence prograding East from the Antarctic Peninsula towards the Weddell Sea. Consequently, the northwest parts of the James Ross island chain (e.g. Vega Island and northern James Ross Island) represent proximal deposition, whereas the southeast parts of the section (e.g. south James Ross Island, Snow Hill Island and Seymour Island) represent more distal deposition near the centre of the basin. In addition, the change from crustal extension to a compressional tectonic regimen produced reverse faulting along

the western edge of the Larsen Basin, causing uplift in the James Ross Basin (Hathway 2000). As a result, the stratigraphically older Santa Marta Formation deposited in the outer margins of a deep water delta shows shallowing upwards to finer grained inner shelf deposits (Olivero 2012). The Snow Hill Island Formation, López de Bertodano Formation and Sobral Formation all represent more upper slope to inner shelf environments (Macellari 1988; Pirrie et al. 1997; Crame et al. 2004, 2014). The exact palaeoenvironments of the López de Bertodano and Sobral Formations on Seymour Island are discussed further in Sections 2.4.2 and 2.4.3.

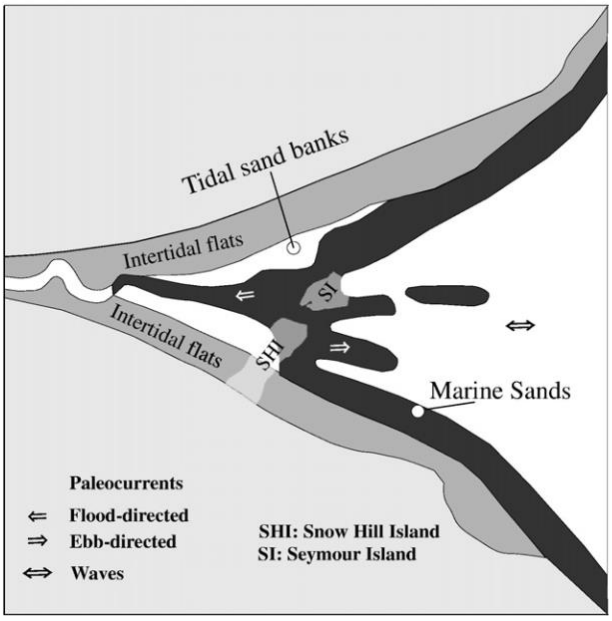

Figure 2.6: Simplified geomorphology and facies distribution scheme of a typical tide-dominated estuary similar to the proposed palaeogeographical setting of Seymour Island during deposition of the Marambio Group based on sedimentology and palaeocurrent data. Taken from Olivero et al (2008).

2.3.3 Seymour Island Group

The Seymour Island Group was deposited in the Paleocene and Eocene and is comprised of the Cross Valley Formation and the La Meseta Formation which crop out on Seymour Island and Cockburn Island, which are in the southeast of the James Ross island cluster (Figure 2.4). These represent further shallowing of the inverting basin with sedimentation mainly influenced by eustatic sea level

changes (Marenssi 2006). The sedimentology consists of fluvial and shallow marine shelf successions and includes conglomerates and channel flows with some volcaniclastic units. Further details of these units as they appear on Seymour Island are also discussed in Section 2.4.

2.4 Stratigraphy and Palaeoenvironments of Seymour Island

Seymour Island has been studied extensively since the early 20th century (Andersson 1906; Zinsmeister 1988) with many expeditions undertaken to document and sample the sedimentary and macro- and micro-fossil material. The island is ice-free during Austral summers, but is unvegetated and has close to 100% rock exposure. As a result, the succession has been dated and correlated via a number of methods including magnetostratigraphy (Tobin et al. 2012), palynology (Elliot et al. 1994; Bowman et al. 2012) and strontium isotopes (McArthur et al. 1998; Crame et al. 2004) and a detailed geological map exists (Montes et al. 2010). The palaeontology has also been studied extensively, with reasonably well defined marine vertebrate and invertebrate faunal taxonomy (Blake & Zinsmeister 1988; Feldmann & Woodburne 1988; Zinsmeister & Macellari 1988) and stratigraphic ranges (Witts et al. 2016). Several studies have been made using floral, faunal and sedimentological evidence to produce interpretations of the palaeoenvironmental conditions throughout the succession (Feldmann & Woodburne 1988, summarised in Bowman et al 2012).

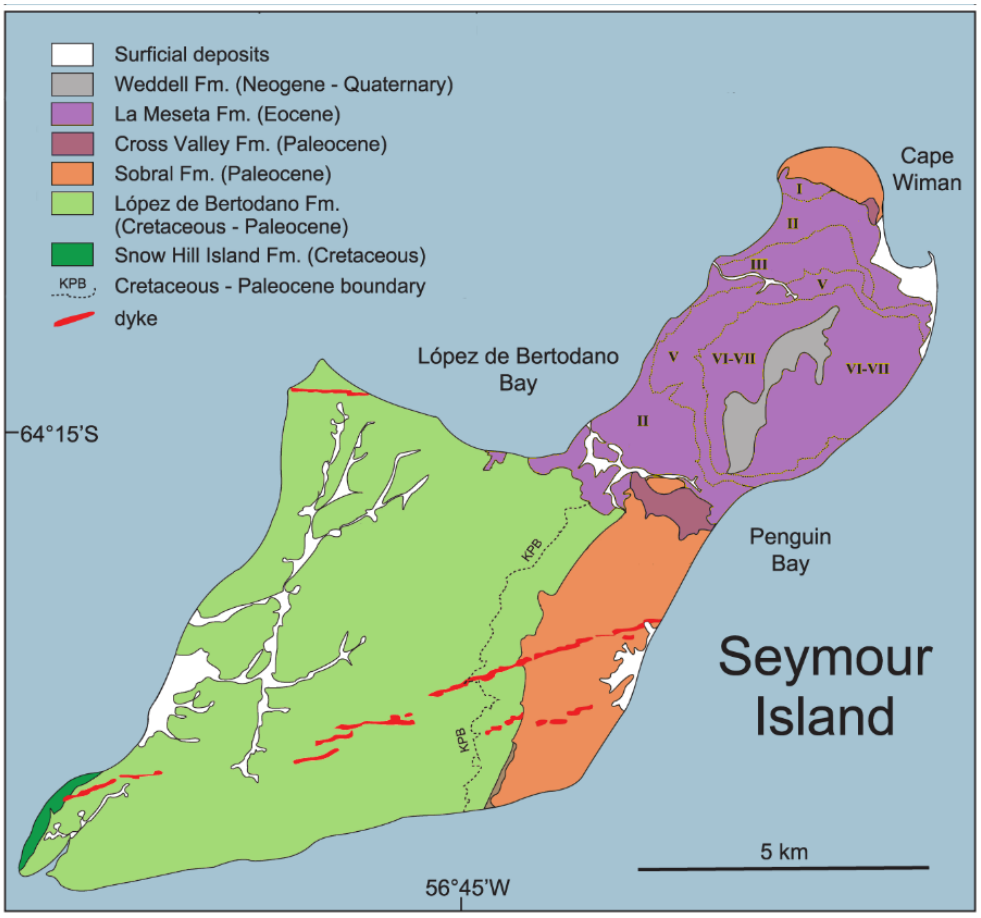

Figure 2.7: Geological map of Seymour Island. Modified from Crame et al 2014; based on work by Montes et al (2010).

The sedimentary succession on Seymour Island consists of five main formations, the oldest three of which form part of the larger Coniacian to Danian Marambio Group, while the younger of two comprise the Seymour Island Group. The overall stratigraphy has a dip of roughly 10° towards the southeast with older units exposed on the western side of the island and younger units in the north and east and represents an overall prograding palaeo-shoreline oriented roughly NE – SW (Figure 2.1).

This thesis focuses predominantly on the fossils of the López de Bertodano Formation, which contains the Cretaceous-Paleogene boundary sequence; covering both the pre-and post-extinction faunas. Specimens from the Paleocene Sobral and Eocene La Meseta formations are also included. The Haslum Crag

Member, and Cross Valley Formation have been excluded due to the potential for fossil reworking (Marenssi et al. 2012).

2.4.1 Haslum Crag Member

The Haslum Crag Member is a 200m thick layer of glauconitic sandstone with prominent lenticular bedding, described predominantly from Snow Hill Island (Pirrie et al. 1997). On Snow Hill Island, it has been interpreted as a set of deep sub-tidal channels in an estuarine environment (Olivero et al. 2008), and contains abundant eastward directed sedimentary structures including coarse grained sandstone-filled channels which grade into finer sandstones and mudstones. A small area of the member, roughly 68m thick is visible on the stratigraphically oldest western shore of Seymour Island (Crame et al. 2004; Olivero et al. 2008), where it has been interpreted as a shallow marine to tidal deposit with potential for reworked deposits. As a result, fossils from this formation are not suitable for this study.

2.4.2 López de Bertodano Formation

The López de Bertodano Formation (Rinaldi et al. 1978) is comprised of approximately 1100m of near-uniform sedimentary deposits unconformably overlying the Haslum Crag Member. It extends over most of the southern half of Seymour Island as a continuous sedimentary succession of a similar mix of clayey silts to silty clays with additional fine to medium sands which have been extensively bioturbated (Macellari 1988). This Maastrichtian to Danian Formation represents a unit deposited during a major transgression onto a pre-existing fluvially or tidally scoured topographic depression (Olivero et al. 2008). The sedimentary deposits have been interpreted as predominantly shallow-marine deltaic to estuarine, with sedimentology and faunal assemblage suggesting a fully marine continental shelf setting, with water depths of between 50−200m (Macellari 1988; Crame et al. 2004). The formation is thought to record a period of deposition during a marine transgression with little volcanic activity (Olivero et al. 2008). The uppermost levels of the formation, including the Danian sediments, have been interpreted as recording a weak regression based on slight grain-size changes, macrofossil and palynological evidence (Macellari 1988;

Crame et al. 2004; Thorn et al. 2009; Olivero 2012) but shallow-water facies and structures are absent, indicating sub-wave-base depths.

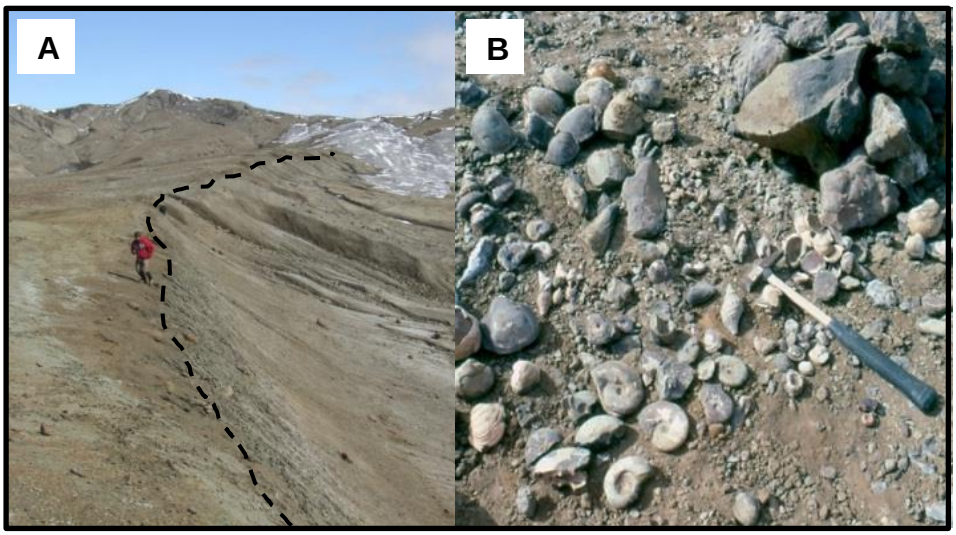

Figure 2.8: A) K-Pg Boundary on Seymour Island (dotted line) as it appears in the field. Note visible green colour of glauconite-rich interval immediately below marked line. B) carbonate concretions containing a variety of macrofossil material. Photography from the British Antarctic Survey.

This formation contains the exceptionally complete and expanded Cretaceous-Paleogene boundary sequence (Zinsmeister et al. 1989), which is the focus of this body of work. The K-Pg boundary is found near the top of the formation and is marked by a laterally continuous 40cm thick glauconite-rich interval which is clearly visible in the field (Figure 2.8). A minor iridium anomaly has been detected, marking the base of the Paleogene, however the boundary layer lacks the ash and clay material commonly found in lower latitude boundary sites (Elliot et al. 1994). The boundary is defined by the disappearance of many groups of fossil marine fauna, including the loss of all vertebrates, ammonites and many species of bivalves and gastropods.

The López de Bertodano Formation has many well-described locally fossiliferous layers, containing invertebrate and vertebrate macrofaunal and macroflora in the form of calcified wood (e.g. Zinsmeister et al. 1989; Zinsmeister 1998; Tobin et al. 2012; Witts et al. 2016). The uppermost 500m of this formation (termed KLB7 to KLB9, see discussion below) in particular contain large amounts of abundant and diverse well-preserved marine macrofossil material, including complete and articulated infaunal bivalves. Fossil material is often found within metre-scale

early-diagenetic carbonate concretions which occur at roughly 10m intervals (Tobin et al. 2012) and are heavily bioturbated with *Taenidium* and *Thalassinoides* burrows. The macrofossil record has been well defined and the stratigraphic representation is remarkably complete, with many species persisting up to the K-Pg boundary (Figure 2.9, Witts et al. 2016). The microfossil record has also been well described, including foraminifera (Huber 1988), silicoflagellates and marine and terrestrial palynomorphs (e.g. Askin 1988; Thorn et al. 2009; Bowman et al. 2012). The marine faunal assemblage contains many species endemic to the Antarctic Peninsula, which has historically made dating and subdivision of the formation difficult.

A number of attempts have been made to subdivide the sedimentary deposits of the López de Bertodano Formation based on sedimentology and fossil content. Early studies (Sadler 1988b) divided the formation into 10 informal units, but the oldest (KLB1) has since been assigned to the Haslum Crag Member (Crame et al. 2004). The lower units (KLB2 to KLB6) were called the Rotularia Units based on the abundance of *Rotularia*; a genus of polychaete worm. The upper Maastrichtian units (KLB7 to KLB9) have been termed the Molluscan Units and are subdivided based on the appearance and abundance of various bivalve species, and the Danian sedimentary deposits (KPLB10) described as the recovery unit was bounded by the K-Pg boundary (Macellari 1988). This subdivision based on fossil data has recently been challenged (Pirrie et al. 1997; Crame et al. 2004; Bowman et al. 2012). Subsequent studies across the Island have highlighted the lateral variation of sedimentology within the formation, and it may be more meaningful to subdivide the formation based on ammonite zones (e.g. Crame et al. 2004) or palynology (Bowman et al. 2012). However, this study will continue to use the informal definitions of Units 7-9 (KLB 789) to denote the immediate pre-extinction and Unit 10 (KPLB 10) to denote the recovery interval. Further details of the correlation and nomenclature used are described in detail in Figure 2.10 and Section 2.6.1

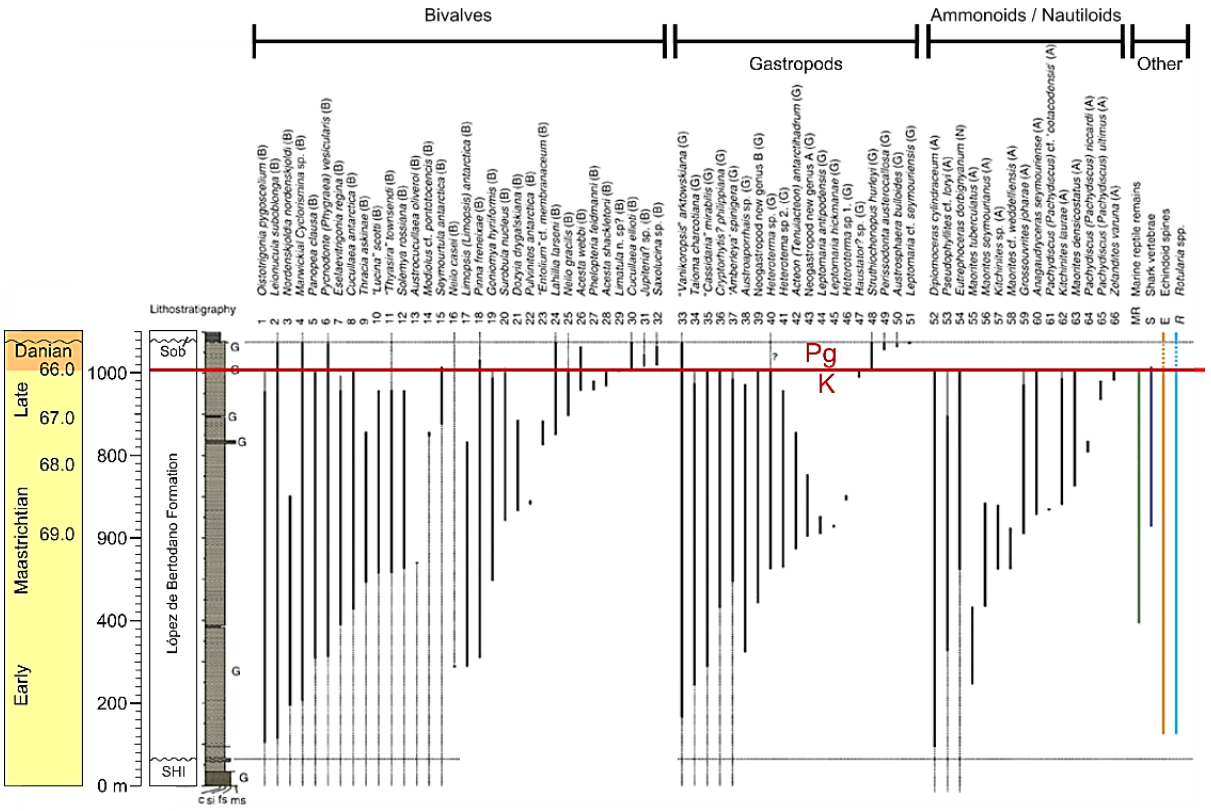

Figure 2.9: Stratigraphic ranges of macrofossil fauna across the K-Pg boundary section on Seymour Island showing a remarkably complete stratigraphic representation of many species up to and across the boundary. Modified from Witts et al (2016).

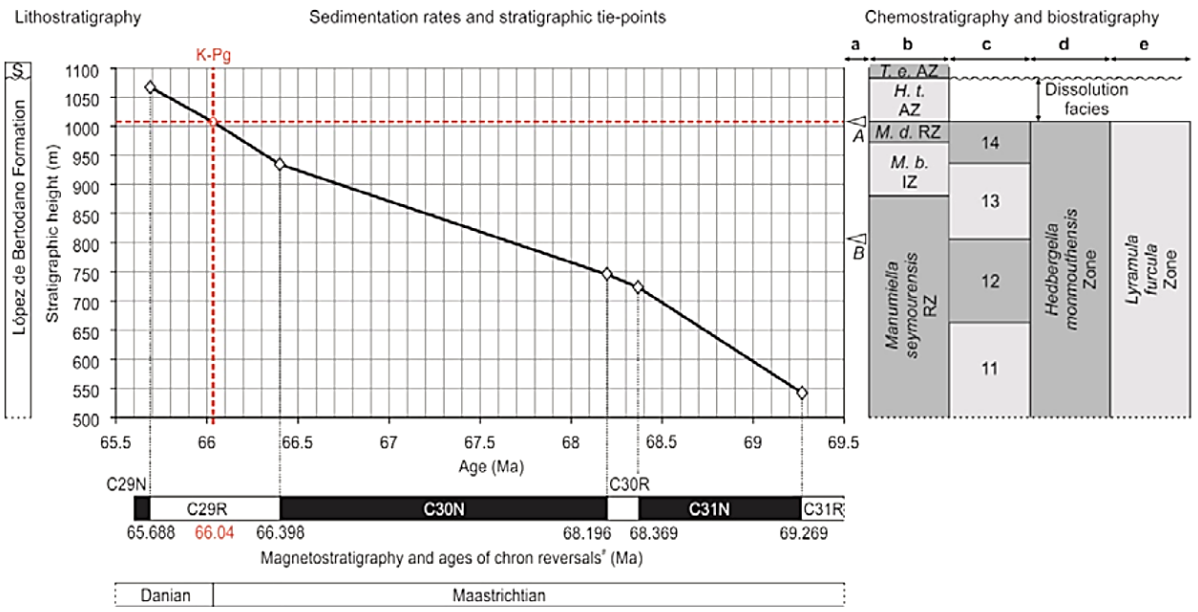

Figure 2.10: Age model and sedimentation rates for the López de Bertodano Formation. Taken from Witts et al (2016).

Palaeomagnetic dating of the succession suggests a relatively rapid 0.01 to 0.02 cm/year sedimentation rate (Figure 2.10, Tobin et al. 2012), likely driven by volcanic activity and uplift in the Antarctic Penninsula, directly to the west of the basin (Pirrie et al. 1991). The great thickness of the formation indicates formation during high-frequency sea-level changes and an increased subsidence rate driven by tectonic activity (Olivero et al. 2008). Numerous glauconite-rich beds prominent in the uppermost 100m of the Maastrichtian units may indicate temporary reductions in the rate of deposition leading to sediment starvation (Zinsmeister 1998), but no major hiatus.

A homoclinal tilt of 5-7° to the strata with little additional deformation suggests minimal tectonic activity has occurred during the intervening time (Hathway 2000). As a result, the rocks and fossils of the López de Bertodano Formation provide an ideal unit to examine in order to determine the biotic effects of climate variability.

2.4.3 Sobral Formation

The Sobral Formation is present above the López de Bertodano Formation on the southern east coast of Seymour Island. It is roughly 250 to 400m thick and separated from the underlying López de Bertodano formation by an erosional unconformity surface marked by phosphatic nodules (Macellari 1988; Sadler 1988a; Marenssi et al. 2012; Olivero 2012). The presence of channelised relief of up to 50m along the erosional surface indicates scouring along a storm-weather wave base and a more significant fall in sea level during the beginning of the Danian (Stilwell et al. 2004). There are few changes in the benthic faunal composition from the uppermost López de Bertodano Formation into the Sobral Formation, which suggests that the time period of the discontinuity was a brief one (Stilwell et al. 2004).

The Sobral Formation consists of clay-rich silts, sands and subordinate sandstones (Macellari 1988). Sedimentary deposits show an overall coarsening-upward regressive trend, reflecting eastward progradation of a marine delta fed from the Antarctic Peninsula to the west (Macellari 1988; Marenssi et al. 2012). Tuff beds produced by the active Antarctic Peninsula volcanism are common in the lower part of the section, with glauconite beds becoming more common above

the basal 60m, indicating periods of slow deposition. The depositional setting is interpreted to have been wave dominated; produced in a shallower marine environment than the López de Bertodano Formation, and influenced by tidal processes (Macellari 1988). It is thought to represent a regressional sequence from a mid-shelf setting to a more proximal delta-front depositional environment. As a result, analysis of fossils from this formation may be influenced by terrestrial or riverine processes to a greater extent than in the marine-dominated López de Bertodano Formation, although trace fossil evidence does indicate an environment that is still marine.

Marine fauna are notably less abundant in the Sobral Formation than the López de Bertodano Formation, and the entire succession is heavily bioturbated with a number of identifiable trace fossils including *Teichichnus*, *Helminthopsis*, *Diplocraterion*, *Chondrites*, *Taenidium* and *Thalassinoides* in the lower 200m which also support the interpretation of a shoreline to shelf facies environment. A switch to higher energy shore-face to foreshore characteristic trace fossils including *Ophiomorpha nodosa*, *Skolithos*, *Arenicolites*, *Rhizocorallium* and *Thalassinoides* supports the interpretation of upper units as being much shallower and proximal to the delta-front. Fossil wood and pollen are abundant throughout the sequence, and foraminifera and dinoflagellates have been used to date the formation to the early Paleocene (Danian to Thanetian age; 66 to 56 Ma) (Bowman et al. 2016)(Askin 1988a). The Sobral Formation has been divided into 7 depositional environments (Ineson *et al.* in prep).

2.4.4 Cross Valley Formation

Two formations of younger strata crop out on the north end of Seymour Island from Cross valley to Cape Winman, unconformably overlying the Marambio Group sediments (Figure 2.7). The Cross Valley Formation (formalised by Elliot & Trautman 1982) outcrops in a small area at the head of the Cross Valley and has been interpreted as a prograding non-marine delta (Elliot & Trautman 1982) or channel-fill (Sadler 1988b) which incises into both the Sobral Formation and López de Bertodano Formation.

The Cross Valley Formation consists of between 100 to 200m of poorly sorted silty sandstones and pebbly sandstones with a high proportion of volcanic tuffaceous material, including both volcanic glass and pumice (Elliot et al. 1975,

Marenssi et al. 2012, Ineson et al in prep). The lowest strata are composed of immature sandstones, which coarsen upwards into gravelly to pebbly sandstones which suggest terrestrial deposition, potentially deposited rapidly by a high-energy surge or lahar (Doktor et al. 1988). The upper strata contain finer grained sandy material with mudstone units indicating a return to marine environments which is also reflected by the presence of marine oyster fossils and *Skolithos* burrows (Ineson *et al.* in prep). Charcoalified wood and lignite logs are common in the lower strata, while the finer grained upper layers preserve abundant leaf and plant debris.

Palynological data indicate that the formation is late Paleocene in age (Wrenn & Hart 1988), however, it has a distinctive sedimentology, including diagenetic dolomite infill (Larkin 2014)and fossil content, including fossils potentially reworked from stratigraphically older units (Macellari 1988; Sadler 1988b). Sedimentology and fossil content also indicates that the environment of deposition was not fully marine, as a result, specimens from this formation will not be examined by this body of work.

7.1.1 La Meseta Formation

The Eocene La Meseta Formation (Elliot & Trautman 1982) rests unconformably on top of both the Marambio Group, and the Cross Valley Formation and is present in the northeastern prominence of Seymour Island. The sedimentology consists of approximately 700m of loosely consolidated sandstones and silty sandstones with interbedded pebbly conglomerates. The formation is floored by an erosional surface which intersects all of the older units of the island in a complex system of incised valleys (Marenssi et al. 2015). This topography is interpreted as erosion into the emerged shelf of Marambio Group and Cross-Valley sedimentary deposits (Sadler 1988b; Marenssi et al. 1998) infilled mostly within a northwest to southeast trending valley with clastic material sourced from the Antarctic Peninsula (Marenssi et al. 2002).

Fossil content includes abundant plant wood and leaf material (e.g. Case 1988); indicative of the more proximal shoreline. Marine macrofaunal fossils occur in a number of fossiliferous horizons and include shark and fish teeth and bones, and diverse and abundant molluscs, crabs, echinoderms and brachiopods (e.g. Zinsmeister 1977; Feldmann & Zinsmeister 1984; Doktor et al. 1996). Terrestrial mammal and bird bones are also found and have been used in addition to marine

faunas to define the age and as indicators of relative sea level throughout the formation (Marenssi et al. 2015).

The formation has been variously divided into a number of informal groups, known as Telms (Tertiary Eocene La Meseta, Sadler 1988b) based on unconformities. The number of attempts to formalise the stratigraphy (Sadler 1988b; Marenssi et al. 2002, 2015) is a testament to the complexity of the sedimentology, which consists of a mix of sandstones, mudstones, and both reworked (Zinsmeister 1984) and in-situ (Elliot & Trautman 1982) shell banks, thought to represent a shallow marine succession or deltaic environment (Elliot 1988; Macellari 1988). There is still debate regarding the exact Eocene age of the La Meseta Formation (Ivany et al. 2008; Pross et al. 2012), and the depositional setting (Sadler 1988b; Porebski 1995, 2000, Marenssi et al. 1998, 2002). As a result, specimens from this formation will not be separated by stratigraphy, but will predominantly be used to present a generic Eocene "warmer world scenario" (Figure 2.11) in comparison with specimens from the cooler main Cretaceous/Paleogene boundary section.

2.5 Palaeoclimate Records

Global marine proxy evidence suggests that Maastrichtian climates were considerably less warm and equable than the preceding mid and Late Cretaceous (Wolfe & Upchurch 1987; Barrera et al. 1987; Pirrie & Marshall 1990; Barrera 1994; Ditchfield et al. 1994; Huber et al. 1995, 2002; Barrera & Savin 1999; Dingle & Lavelle 2000; Francis & Poole 2002; Gallagher et al. 2008; Friedrich et al. 2012). Following a thermal maximum during the Cenomanian to Turonian interval, proxy records indicate a distinct global cooling trend recorded in marine and terrestrial sections worldwide (Friedrich et al. 2012; Ando et al. 2013; Linnert et al. 2014). This cooling trend reached a peak during the Campanian to Maastrichtian interval, but was interrupted several times by episodes of geologically rapid global cooling and warming (e.g. Li & Keller 1998b; Barrera & Savin 1999; Bowman et al. 2013; Thibault et al. 2016). These intervals of climate instability highlight the potential for variability in the latest Cretaceous and early Paleogene.

The Antarctic Peninsula is an area of specific interest to modern and past climatic studies, as it appears particularly sensitive to change (e.g. Bowman et

al. 2013). It is also a key location for changes in circulation, with studies proposing that climate shifts through the Maastrichtian may have driven changes in ocean circulation and bottom-water formation around Antarctica (Robinson et al. 2010; Jung et al. 2013) or that the changes in global climate may have even been driven by circulation changes (Barrera & Savin 1999; Frank & Arthur 1999; Friedrich et al. 2009; Jung et al. 2013). However, there appears to be a disparity between Late Cretaceous Antarctic climate records from marine and terrestrial proxies which will be reviewed in the following section.

2.5.1 Antarctic Marine Records

Most of the evidence for increased climate variability and seasonality in the Antarctic Peninsula region during the Late Cretaceous is from the marine realm. However, with the exception of the Seymour Island section, high-resolution marine temperature data from around Antarctica are limited, with few well-studied sections.

Planktic and benthic foraminiferal $\delta^{18}O$ data show an overall cooling trend of approximately 4.3℃ at high southern latitudes during the Maastrichtian (Barrera 1994; Barrera et al. 1997) accompanied by falling sea levels (Miller et al. 2005; Kominz et al. 2008). A distinct pulse of warming is observed in the latest Maastrichtian, close to chron C30N, less than 0.5 Ma prior to the K-Pg event (Wilf et al. 2003; Bowman et al. 2013). Benthic foraminiferal compilations from a number of high latitude Antarctic marine sites show similar short-interval warming in high southern latitudes at the K-Pg boundary against a relatively cool Maastrichtian–Paleocene background state followed by a warmer early Eocene (Cramer et al. 2009; Hollis et al. 2012).

Analysis of $\delta^{18}O$ of fossil shell material from the James Ross Basin has been used to estimate sea surface and seafloor temperatures (Tobin et al. 2012, Peter Frost unpublished). But uncertainties have recently arisen in the choice of the correct $\delta^{18}O$ seawater value in the calibration of molluscan temperature data (e.g. Ivany et al. 2008; Petersen et al. 2016). This will be examined further in the rest of this thesis.

2.5.2 Antarctic Terrestrial Records

Current knowledge of continental Antarctic Late Cretaceous and Paleogene climate conditions is poorer than marine conditions due to the generally lower temporal resolution of terrestrial records. Continental terrestrial records have been generated from material washed into the James Ross Basin using both the MBT′/CBT thermometer in fossil soils (Kemp et al. 2014), and palaeofloral analysis (Greenwood & Wing 1995; Francis & Poole 2002; Poole et al. 2005) and terrestrial palynology (Bowman et al. 2013, 2014). These proxies tend to indicate a relatively stable, persistently cool temperate climate on the Antarctic Peninsula across the Cretaceous-Paleogene boundary with temperatures averaging 7 to 14°C (Figure 2.11). Chemical weathering and compositional maturity of sediments also suggest probable cool to subantarctic temperatures for the Antarctic interior during the Maastrichtian (Dingle & Lavelle 1998).

The absence of climate variability in Antarctic terrestrial soil records could be affected by an inherent bias towards summer month temperatures at high latitudes using the MBT′/CBT thermometer (e.g. Pross et al. 2012) or could be a result of aliasing due to the sparse stratigraphic resolution of terrestrial data compared to a marine record. Given the apparent disparity between the marine and terrestrial records, it is likely that studying the effects of seasonality and continentality may give a better reflection of the dynamical causes of climate change, rather than the simple observation that the Earth warmed or cooled on average through a geological interval.

There is also mixed evidence for ephemeral high latitude ice sheets in the Antarctic during the latest Maastrichtian, both from eustatic studies (Miller et al. 2005), latitudinal temperature gradients (Amiot et al. 2004) and palynological studies (Bowman et al. 2013, 2014). Some of the lower CO_2 estimates also allow the formation of Maastrichtian Antarctic ice (Hong & Lee 2012). However, there are no records of glacial sedimentary deposits of this age, and climate models have been unable to reproduce seasonal ice under the suggested boundary conditions (Otto-Bliesner & Upchurch 1997; Hunter et al. 2008, 2013). Evidence for sea ice influence around the James Ross Basin will also be examined in this thesis.

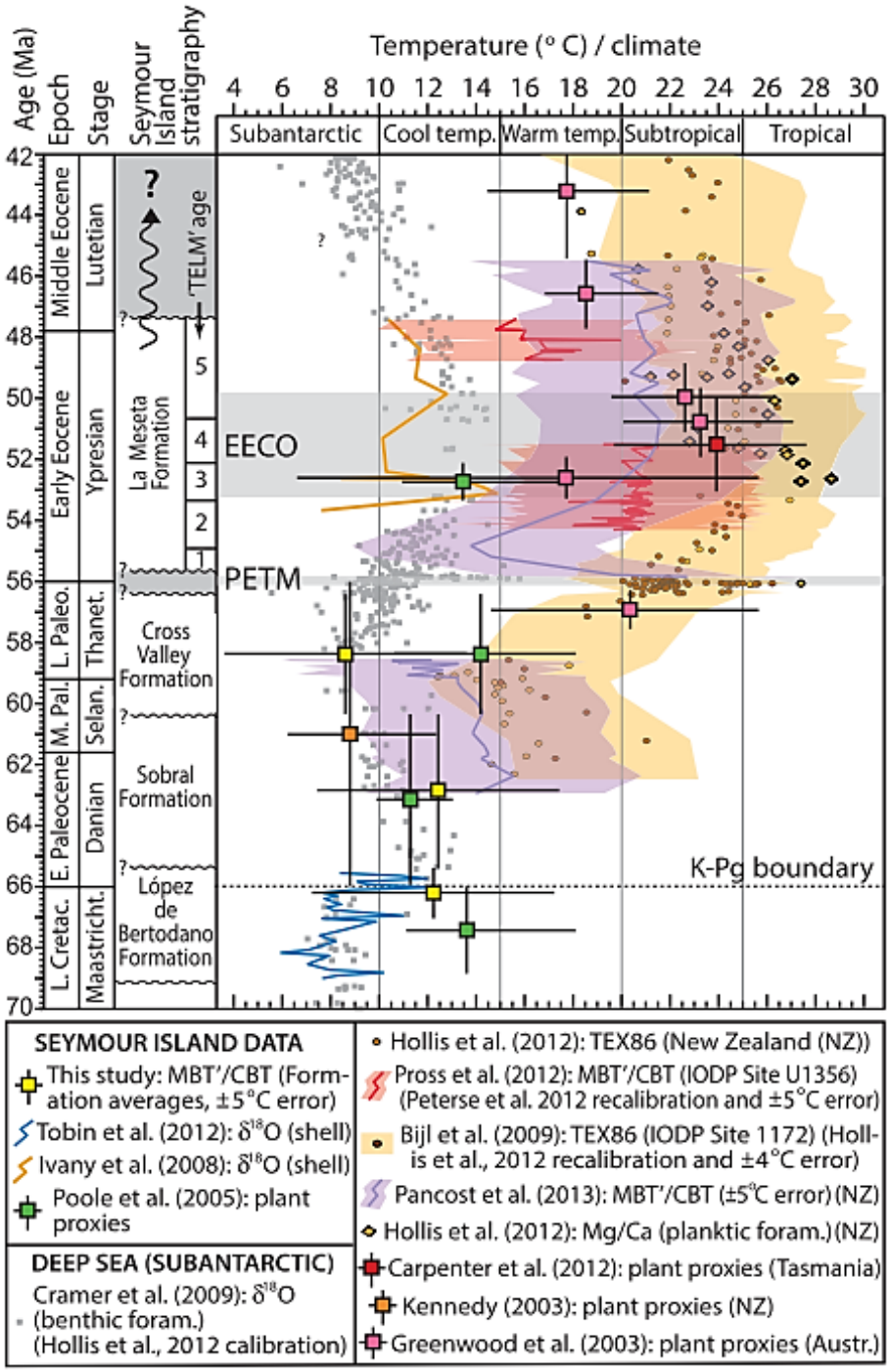

Figure 2.11: Summary figure of existing palaeoclimate temperature proxies from the James Ross Basin area. Showing the difference between relatively low temperatures in the Lopez de Bertodano Formation and the much warmer Paleocene and Eocene temperatures. Taken from Kemp et al. (2014).

2.6 Specimen Collection

This study focuses on several taxa of infaunal bivalves; examples of the genera *Lahillia*, *Cucullaea* and *Leionucula*. The rationale for the selection of each taxon is detailed in Section 3.3. This body of work makes use of a large number of pre-collected fossil bivalves of these taxa taken from stratigraphic sections measured perpendicular to strike using a Jacob's staff and tape measure during three field seasons across southern Seymour Island (Figure 2.12). The sections have been correlated by using several stratigraphic tie-points, including the well-defined K-Pg boundary layer and a prominent glauconitic horizon ~170 m below as a datum (Figure 2.10). For correlations planar bedding along strike is assumed, as is the absence of significant hiatuses in the Maastrichtian, based on field observation and previous studies (Bowman et al. 2013; Witts et al. 2015). A robust age model exists for the López de Bertodano Formation based on strontium isotope chemostratigraphy (McArthur et al. 1998; Crame et al. 2004), marine palynology (Elliot et al. 1994; Bowman et al. 2012) and magnetostratigraphy (Tobin et al. 2012) (see Bowman et al. 2013, Witts et al. 2016 and references therein for details).

Macrofossil collections were made at varying scales during each field excursion with topography in the field area preventing standardization of bin size or collecting time. Sample bins ranged from 1 m to 15 m thickness and stratigraphic height of each specimen is taken as the mid-point of each bin. Sample numbers of all specimens examined are catalogued in Dataset S1. Additional specimens from the Zinsmeister Collection have also been used. Details of all collections and field seasons are presented in Table 2.1 and Appendix A.

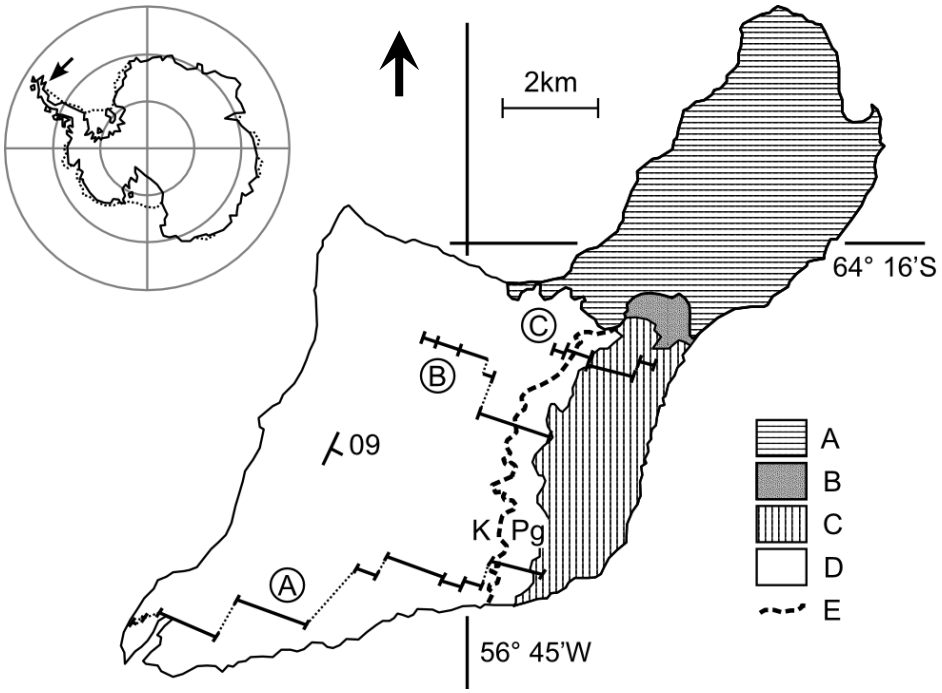

Figure 2.12: Modern geographic index map and geologic map of Seymour Island showing major stratigraphic units: (A) Eocene, La Meseta Formation; (B), Paleocene, Cross Valley Formation; (C) Paleocene, Sobral Formation; (D) Maastrichtian to lower Paleocene, López de Bertodano Formation; (E)– K-Pg Boundary. Section lines; A– AFI 2004 composite D5.251 (Bowman et al. 2014); B– BAS 1999 composite DJ.959-957-953-952 (Crame et al. 2004); C– D9 BAS 2010 composite D9.205-206-207-209-210-211 (Crame et al. 2014).

Table 2.1: Specimens have been referred to by number throughout this work. These numbers correspond to the different field seasons and section locations and collection types. Lists of specimens used for specific geochemical, preservation or morphometric tests are available in Appendix A.

Year of Field Season	Sites / Sub-sections used	Naming convention	Focus	Collection bin sizes
1999	DJ.959, DJ.957, DJ.952, DJ.953	e.g. DJ.953.533 DJ = location (Seymour Island) 953 = Site 335 = Fossil number from that site	Maastrichtian López de Bertodano Fm	0.75 – 34.5 m
2006	D5.212, D5.215, D5.218, D5.219, D5.220, D5.222, D5.229	e.g. D5.220.1223.2 D5 = year (2005/6) 220 = Site 1226 = Overall fossil number 2 = Macrofossil	Maastrichtan López de Bertodano Fm to Paleocene Sobral Fm	1 m
2010	D9.205, D9.206 D9.207	e.g. D9.207.1 D9 = year (2009/10) 207 = Site 1 = Fossil number from that site	Boundary interval López de Bertodano Fm, Soral Fm and La Meseta Fm	0.5 – 27 m
Zinsmeister Collection PRI Ithaca	3 decades of spot collections (see Appendix A for details)		Maastrichtian López de Bertodano Fm, Sobral Fm and La Meseta Fm	N/A spot collections only

2.6.1 Stratigraphic Nomenclature

In order to directly compare trends between collections made by different field groups from different section lines using different methods of sampling and unequal bin widths, the stratigraphic section was divided into stratigraphic intervals at approximately 50m spacing. These 50m bins represent between 250 and 500 kyr of sedimentation (Tobin et al. 2012).

For the Maastrichtian López de Bertodano formation, stratigraphic intervals were calculated down-stratigraphy using the K-Pg boundary as a baseline. The

Danian López de Bertodano formation was divided up-stratigraphy using the K-Pg boundary as a baseline to account for the uneven stratigraphic boundary with the overlying Sobral formation. Intervals in the Sobral Formation were calculated from the base of the succession where it was observed in each individual section line. Specimens from the La Meseta were considered as a single group. A visual representation of this division strategy is visible below (Figure 2.13).

In addition, this work uses the informal division of the López de Bertodano formation into pre-and post-extinction units for ease of referral when discussing the effects of the Mass Extinction and recovery interval. The pre-extinction unit is referred to as KLB789, and the post-extinction as KPLB10. Similarly, the Sobral Formation and La Meseta Formation are often referred to as SOB and TELM in figures.

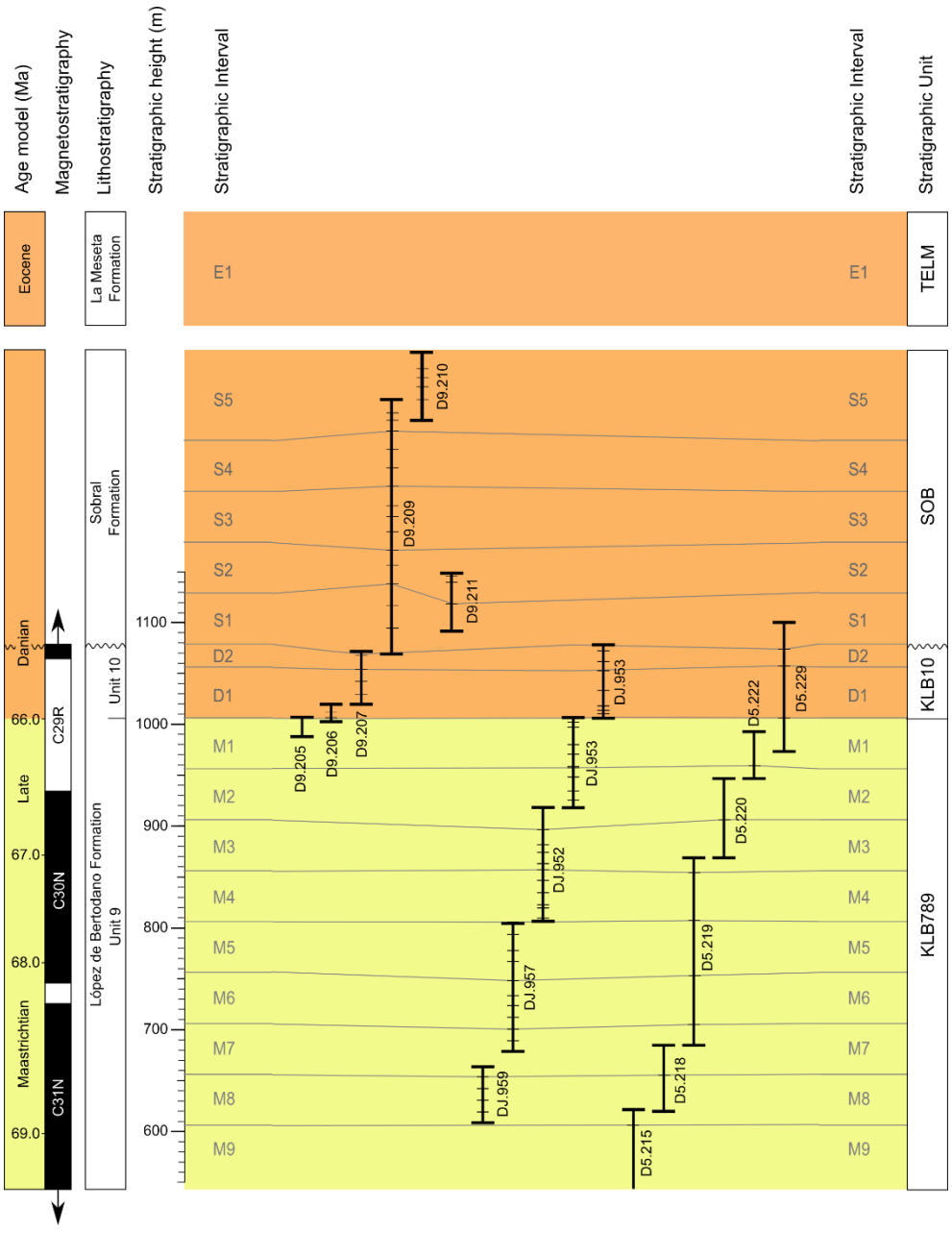

Figure 2.13: Details of informal subdivisions used in this work (Stratigraphic Units KLB789, KPLB10, SOB and TELM, and Stratigraphic intervals M1-9, D1-2, S1-5 and E1) and distribution of specimen collection intervals within the subdivisions. Each measured section is represented with a bold vertical line. In the 1999 (DJ) and 2010 (D9) sections, each collection interval is marked with a horizontal stroke on the vertical section line. In the 2006 (D5) section, collections were more densely spaced, so only the collections closest to each stratigraphic interval boundary are marked.

2.6.2 Collection Bias

Seymour Island's rocks are sufficiently fossiliferous that not all of the samples within a horizon were able to be collected (J.E. Francis Pers. Comm. 2013). It is possible that some bimodality can be introduced from sampling bias if (for example) very small and very large specimens are favoured for collection. Data pooled for this research were therefore tested by examining morphometric and size trends in representative *Lahillia* in order to get a rough estimate as to whether certain collections may have been subject to poor practices.

The morphometric trends within each collection's *Lahillia* (Figure 2.14) are very similar, and can be accounted for by the difference in the number of specimens collected from each stratigraphic unit. These results suggest that the patterns visible in the data are unlikely to be a result of sampling bias, and the samples examined are likely to represent real trends in the fossil record.

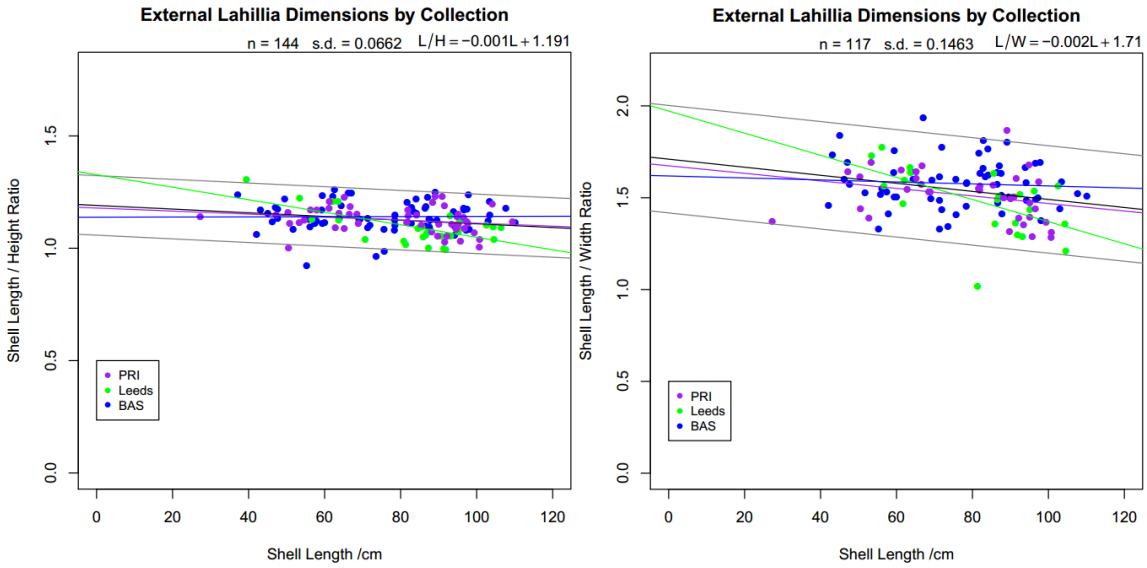

Figure 2.14: External *Lahillia* shell dimension Length/Height and Length/Width against Length plots separated by specimen collection. Regression lines from each section show no significant difference, and suggest that all collections have a similar distribution of specimens.

2.7 Specimen Preservation

Only specimens of *Lahillia* and *Cucullaea* were tested to determine their preservation, as modern members of these clades are known to mineralise aragonitic shells, which have a well-defined relationship between $\delta^{18}O$ and temperature (Grossman & Ku 1986). *Leionucula* however mineralise shells with a nacre structure, which although composed primarily of aragonite, contains a much higher proportion of shell organics and may be more prone to diagenesis.

Preservation tests were designed to test the suitability of shells for stable isotopic analysis. Diagenetically altered or recrystallized shell material will tend to form in equilibrium with pore water, obliterating any previously preserved geochemical signals within the shells.

Several bivalves of both genera were examined using a scanning electron microscope (SEM), cathodoluminescence microscope (CL) and x-ray diffraction (XRD) of shell material to confirm preservation of the original microstructure and aragonitic mineralogy. Full details of each technique are found in Appendix A. A summary of the results of all the preservation tests carried out is presented below.

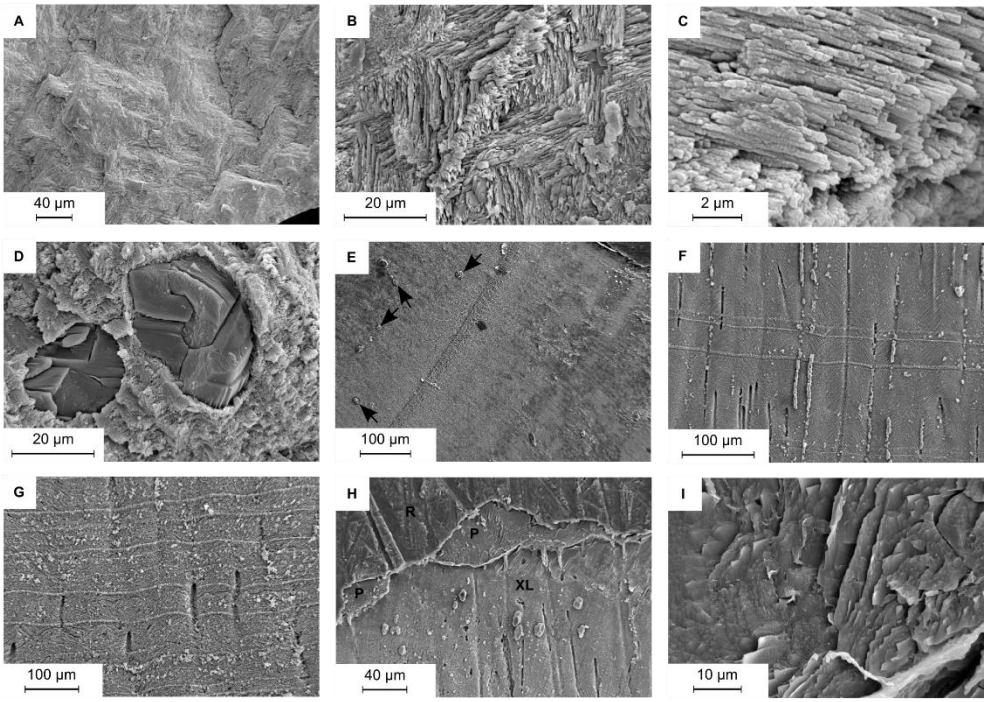

Figure 2.15: Scanning electron microscope images on the microstructures and diagenetic textures of *Lahillia* (A-E) and *Cucullaea* (F-I). (A) Overview image of pristine aragonite crossed lamellae. (B) Prismatic growth line between first order crossed-lamellar chevron domains. (C) Etched surface and interior myostracal prismatic layers. (D) Recrystallised calcite in algal borings. (E) Algal borings (arrows) estimated at 1.3% of typical surface area; in line with XRD data. (F) Crossed-lamellar aragonite with both calcite filled and hollow tubules. (G) Inner complex crossed-lamellar aragonite in inner shell with periodic prismatic growth lines. (H) Intermittent Mg rich outer shell layer; possible periostracal remnants (P), Resin (R) and crossed lamellar layer (XL). (I) Magnification of intermittent outer layer showing possible calcite crystals.

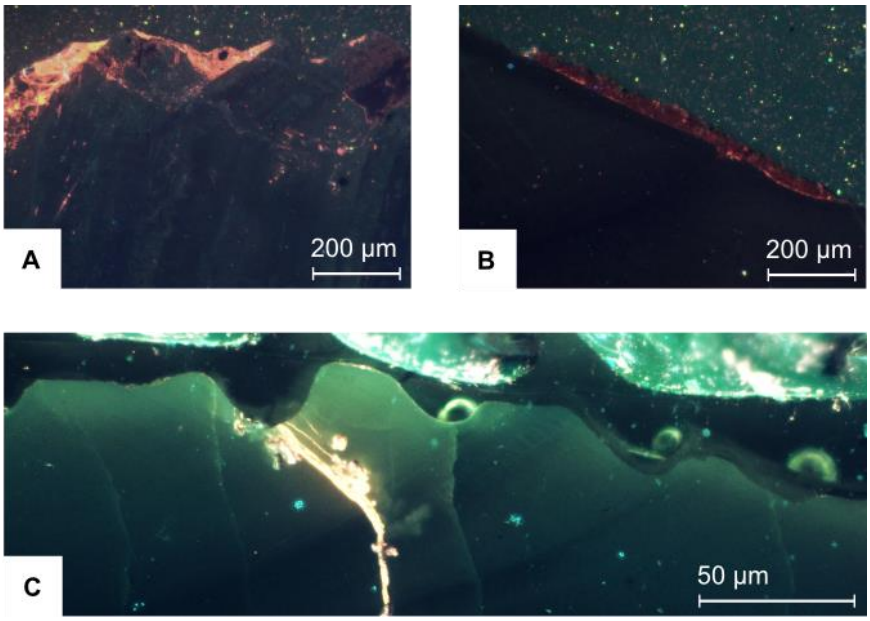

Figure 2.16: Cathodoluminescence microscope images of *Cucullaea* (A) and *Lahillia* (B-C). (A) Bright luminescence of intermittent surface layer. (B) Bright luminescence of thin surface layer. (C) Surface sampling pits and bright luminescence of Mg-rich diagenetic infilling within a crack in shell.

Table 2.2: XRD Results from sampled shell layers. The periostracal layers and samples from the whole shell including surface contained the highest percentage calcite. All other samples from the top 1 mm of shells contained less than 3% calcite and the remainder aragonite.

Specimen	Sample Details	wt% Calcite
D5.219.1185.2	upper 0.2 mm of outer layer of valve	1.37
D5.219.1185.2	upper 0.2 mm of lower layer of valve	1.95
D5.219.1185.2	whole shell sample (from surface to 2.5 mm depth)	7.22
D9.207.1	Upper 1 mm	2.93
Fragment	Internal crossed lamellar layer	2.37
DJ.952.516	surface layer	1.22
DJ.952.529	surface layer	2.31
D5.219.1185.2	Periostracal remnants	14.03

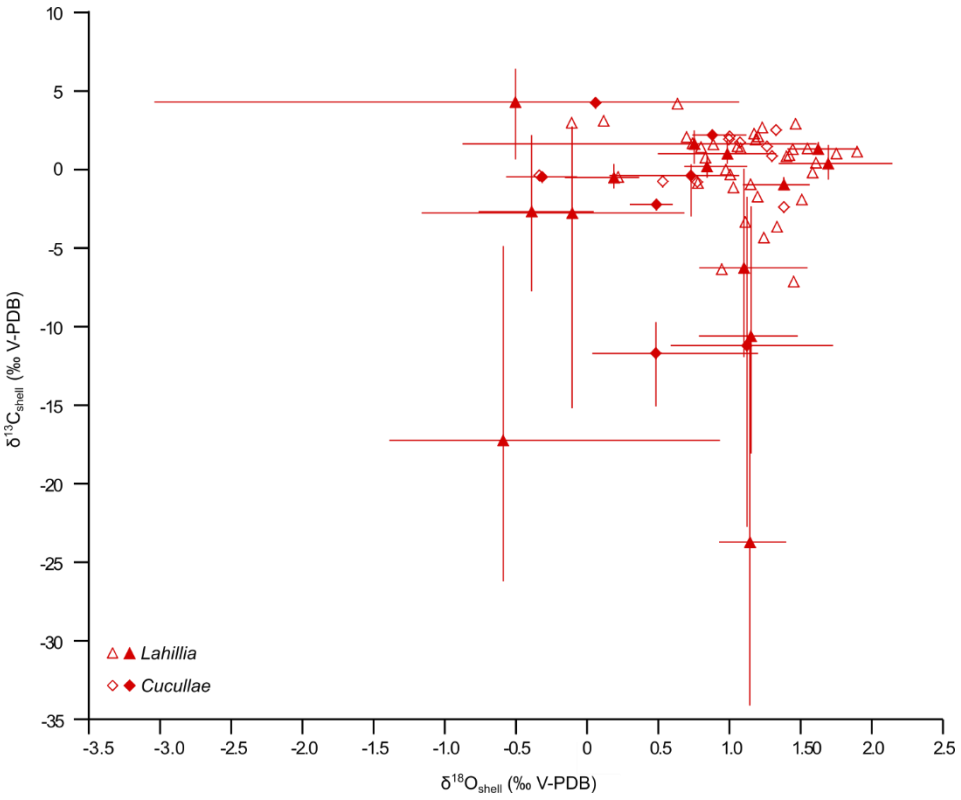

Figure 2.17: Bulk and average shell carbon-oxygen stable isotope cross-plot of *Lahillia* (triangles) and *Cucullaea* (diamonds). Range bars with filled markers represent the mean and range of microsampled data points produced within one shell. Hollow markers represent bulk data from a single shell. Analytical reproducibilities of ±0.06‰ for $\delta^{13}C$ and ±0.08‰ for $\delta^{18}O$ do not plot at this resolution.

SEM observations of *Lahillia* cross sections (Figure 2.15) show a well preserved inner crossed-lamellar layer typical of heterodont bivalves with a thin layer of prismatic crystals visible at growth lines and the outer shell layer (Bieler et al. 2014). The crossed-lamellar layer in some specimens was observed to contain up to 1 to 2% algal boreholes filled with recrystallized calcite, calculated by area coverage of representative sections. *Cucullaea* sections show an outer layer of crossed-lamellar aragonite with clearly visible tubules, similar to the typical structure of modern arcoids (Bieler et al. 2014). The inner shell has a complex crossed-lamellar structure with periodic fine layers of prisms; an intermittent layer which may be periostracal remnants is present on the surface of some specimens and appears to have been replaced with calcite. Preservation of the internal microstructures alone suggests that the shell microstructure is diagenetically un-altered; the micron-scale crystals have no spaces for authigenic

calcite precipitation and would be an early casualty to overprinting by calcite diagenesis (Figure 2.15.D).

Cold cathode CL images confirmed SEM observations, with the only evidence for alteration confined to a thin strongly luminescent Mg-rich coating near the external surface of a small number of valves and in some large cracks (Figure 2.16) which were avoided by subsequent sampling.

X-Ray diffraction analysis of the non-luminescing crossed-lamellar layers of *Lahillia* indicate predominantly aragonite mineralogy in all specimens. A maximum of 3% calcite was observed in the internal layers. Material from the outer layer in *Lahillia* which fluoresced visibly under CL was also sampled and found by XRD to be only 85% aragonite. This was considered too diagenetically altered to produce reliable stable isotope data and was removed by grinding prior to geochemical sampling in all specimens.

Cross-plot comparisons of stable isotope values (Figure 2.17) show no significant statistical trends (Appendix Figure B.2) for either species and are consistent with a fully marine environment. Therefore, any stable isotope signals produced are likely to be original signals.

The preservation is suitable to allow these shells to be used for further geochemical analysis. Combined observations strongly indicate that the original aragonitic mineralogy is intact in both *Lahillia* and *Cucullaea*. Small areas of surface alteration detected during the preservation testing process were able to be identified and avoided or removed by grinding or sectioning prior to geochemical work. The reliability of the stable isotopic signals is supported by the presence of annual cycles visible in both the oxygen and carbon data, which suggest that no isotopic resetting has occurred. Cross-plots of the stable isotope values (Figure 2.17) are consistent with a fully marine environment without substantial riverine input.

2.8 Summary

Fossil infaunal bivalve shells are present in sedimentary deposits from the James Ross Basin with several species surviving across the K-Pg boundary. Bivalve shells are abundant in the López de Bertodano Formation and Sobral Formation

on Seymour Island where they are likely to have lived under normal marine continental shelf conditions making them ideal for study of environmental conditions across the K-Pg boundary. Similar fossils are also present in the La Meseta Formation, but this portion of stratigraphy lacks the well-defined chronology of the former units.

Seymour Island's sedimentary deposits have been well correlated and defined within regional stratigraphy, although stratigraphic subdivision of units has not always been formalised, making it necessary to use an informal naming system throughout this thesis for the López de Bertodano Formation, Sobral Formation and La Meseta Formation.

During the Late Cretaceous and Early Paleogene, Antarctic palaeoclimate shows evidence for increased climate variability and temperature seasonality with potential ephemeral ice sheets, and short-lived warming and cooling periods in the late Maastrichtian particularly in the marine realm.

Specimens of *Lahillia* and *Cucullaea* from a number of traverses across Seymour Island have been compared and suggest little evidence for potential collection bias meaning measurements and observations from shells across the island and through stratigraphy can be consolidated.

Combined observations of shell preservation in *Lahillia* and *Cucullaea* suggest that much of the original aragonite microstructure is preserved, and stable carbon and oxygen isotope ratios are likely to be original. Initial stable isotopic results also support the interpretation of a normal marine sedimentary environment without significant freshwater input.

2.9 References

Amiot, R., Lecuyer, C., Buffetaut, E., Fluteau, F., Legendre, S. and Martineau, F. (2004) 'Latitudinal temperature gradient during the Cretaceous Upper Campanian-Middle Maastrichtian: −"oxy" record of continental vertebrates', *Earth and Planetary Science Letters*, 226(1–2), 255–272.

Andersson, J. G. (1906) 'On the geology of Graham Land', *Bulletin of the Geological Institute, University of Upsala*, (7), 19–71.

Ando, A., Huber, B. T. and Premoli Silva, I. (2013) 'Paraticinella rohri as the valid name for the latest Aptian zonal marker species of planktonic foraminifera traditionally called bejaouaensis or eubejaouaensis', *Cretaceous Research*, 45, 275–287.

Askin, R. A. (1988a) 'Campanian to Paleocene palynological succession of Seymour and adjacent islands , northeastern Antarctic Peninsula', *Geological Society of America Memoir*, 169.

Askin, R. A. (1988b) 'The palynological record across the Cretaceous/Tertiary transition on Seymour Island, Antarctica Rosemary', *Geological Society of America Memoir*, 169.

Barrera, E. (1994) 'Global environmental changes preceding the Cretaceous-Tertiary boundary: Early-late Maastrichtian transition', *Geology*, 22(10), 877–880.

Barrera, E., Huber, B. T., Savin, S. M. and Webb, P. N. (1987) 'Antarctic marine temperatures: Late Campanian through early Holocene', *Paleoceanography*, 2, 21–47.

Barrera, E. and Savin, S. M. (1999) 'Evolution of late Campanian-Maastrichtian marine climates and oceans', *Geological Society of America*, Special pa, 245–278.

Barrera, E., Savin, S. M., Thomas, E. and Jones, C. E. (1997) 'Evidence for thermohaline-circulation reversals controlled by sea-level change in the latest Cretaceous', *Geology*, 25(8), 715–718.

Bieler, R., Mikkelsen, P. M., Collins, T. M., Glover, E. A., González, V. L., Graf, D. L., Harper, E. M., Healy, J., *et al.* (2014) 'Investigating the Bivalve Tree of Life – an exemplar-based approach combining molecular and novel morphological characters', *Invertebrate Systematics*, 28(1), 32.

Blake, D. B. and Zinsmeister, W. J. (1988) *Geology and Paleontology of Seymour Island Antarctic Peninsula*, *Geological Society of America Memoirs*.

Bowman, V. C., Francis, J. E., Askin, R. A., Riding, J. B. and Swindles, G. T. (2014) 'Latest Cretaceous–earliest Paleogene vegetation and climate change at the high southern latitudes: palynological evidence from Seymour Island, Antarctic Peninsula', *Palaeogeography, Palaeoclimatology, Palaeoecology*, 408, 26–47.

Bowman, V. C., Francis, J. E. and Riding, J. B. (2013) 'Late Cretaceous winter sea ice in Antarctica?', *Geology*, 41(12), 1227–1230.

Bowman, V. C., Francis, J. E., Riding, J. B., Hunter, S. J. and Haywood, A. M. (2012) 'A latest Cretaceous to earliest Paleogene dinoflagellate cyst zonation from Antarctica, and implications for phytoprovincialism in the high southern latitudes', *Review of Palaeobotany and Palynology*, 171, 40–56.

Bowman, V., Ineson, J., Riding, J., Crame, J., Francis, J., Condon, D., Whittle, R. and Ferraccioli, F. (2016) 'The Paleocene of Antarctica: Dinoflagellate cyst biostratigraphy, chronostratigraphy and implications for the palaeo-Pacific margin of Gondwana', *Gondwana Research*, 38, 132–148.

Case, J. A. (1988) 'Paleogene floras from Seymour Island , Antarctic Peninsula', *Geological Society of America Memoir*, 169.

Crame, J. A., Beu, A. G., Ineson, J. R., Francis, J. E., Whittle, R. J. and Bowman, V. C. (2014) 'The Early Origin of the Antarctic Marine Fauna and Its Evolutionary Implications.', *PloS one*, 9(12), e114743.

Crame, J. A., Francis, J. E., Cantrill, D. J. and Pirrie, D. (2004) 'Maastrichtian stratigraphy of Antarctica', *Cretaceous Research*, 25(3), 411–423.

Crame, J. A., Pirrie, D. and Riding, J. B. (2006) 'Mid-Cretaceous stratigraphy of the James Ross Basin, Antarctica', *Geological Society, London, Special Publications*, 258(1), 7–19.

Crame, J. A., Pirrie, D., Riding, J. B. and Thomson, M. R. A. (1991) 'Campanian-Maastrichtian (Cretaceous) stratigraphy of the James Ross Island area, Antarctica', *Journal of the Geological Society*, 148(6), 1125–1140.

Cramer, B. S., Toggweiler, J. R., Wright, J. D., Katz, M. E. and Miller, K. G. (2009) 'Ocean overturning since the Late Cretaceous: Inferences from a new benthic foraminiferal isotope compilation', *Paleoceanography*, 24(4), 4216.

Dingle, R. V. and Lavelle, M. (1998) 'Late Cretaceous-Cenozoic climatic variations of the northern Antarctic Peninsula: new geochemical evidence and review', *Palaeogeography, Palaeoclimatology, Palaeoecology*, 141(3–4), 215–232.

Dingle, R. V. and Lavelle, M. (2000) 'Antarctic Peninsula Late Cretaceous-Early Cenozoic palaeoenvironments and Gondwana palaeogeographies', *Journal of African Earth Sciences*, 31(1), 91–105.

Ditchfield, P. W., Marshall, J. D. and Pirrie, D. (1994) 'High latitude

palaeotemperature variation: New data from the Thithonian to Eocene of James Ross Island, Antarctica', *Palaeogeography, Palaeoclimatology, Palaeoecology*, 107(1–2), 79–101.

Doktor, M., Gazdzicki, A., Jerzmanska, A., Porebski, S. J. and Zastawniak, E. (1996) 'A Plant-And-Fish Assemblage From The Eocene La Meseta Formation Of Seymour Island (Antarctic Peninsula) And Its Environmental Implications', 128–138.

Doktor, M., Gaździcki, A., Marenssi, S. A., Porębski, S. J., Santillana, S. N. and Vrba, A. V. (1988) 'Argentine-Polish geological investigations on Seymour (Marambio) Island, Antarctica', *Polish Polar Research*, 9(4), 521–541.

Elliot, D. H. (1988) *Geology and Paleontology of Seymour Island Antarctic Peninsula*, *Geological Society of America Memoirs*.

Elliot, D. H. (1997) 'The Planar Crest of Graham Land, Northern Antarctic Peninsula: Possible Origins and Timing of Uplift', in, 51–73.

Elliot, D. H., Askin, R. A., Kyte, F. T. and Zinsmeister, W. J. (1994) 'Iridium and dinocysts at the Cretaceous-Tertiary boundary on Seymour Island, Antarctica: Implications for the K-T event', *Geology*, 22(8), 675.

Elliot, D. H. and Trautman, T. A. (1982) 'Lower tertiary strata on Seymour island', in *Antarctic Peninsula*, 287–297.

Feldmann, R. M. and Woodburne, M. O. (1988) *Geology and Paleontology of Seymour Island Antarctic Peninsula*.

Feldmann, R. M. and Zinsmeister, W. J. (1984) 'New Fossil Crabs (Decapoda: Brachyura) from the La Meseta Formation (Eocene) of Antarctica: Paleogeographic and Biogeographic Implications', *Journal of Paleontology*, 1046–1061.

Francis, J. E. and Poole, I. (2002) 'Cretaceous and early Tertiary climates of Antarctica: evidence from fossil wood', *Palaeogeography, Palaeoclimatology, Palaeoecology*, 182(1), 47–64.

Frank, T. D. and Arthur, M. A. (1999) 'Tectonic forcings of Maastrichtian ocean-climate evolution', *Paleoceanography*, 14(2), 103–117.

Friedrich, O., Herrle, J. O., Wilson, P. A., Cooper, M. J., Erbacher, J. and Hemleben, C. (2009) 'Early Maastrichtian carbon cycle perturbation and cooling event: Implications from the South Atlantic Ocean', *Paleoceanography*, 24.

Friedrich, O., Norris, R. D. and Erbacher, J. (2012) 'Evolution of middle to Late

Cretaceous oceans—A 55 m.y. record of Earth's temperature and carbon cycle', *Geology*, 40(2), 107–110.

Gallagher, S. J., Wagstaff, B. E., Baird, J. G., Wallace, M. W. and Li, C. L. (2008) 'Southern high latitude climate variability in the Late Cretaceous greenhouse world', *Global and Planetary Change*, 60(3), 351–364.

Greenwood, D. R. and Wing, S. L. (1995) 'Eocene continental climates and latitudinal temperature gradients', *Geology*, 23(11), 1044–1048.

Grossman, E. L. and Ku, T.-L. (1986) 'Oxygen and carbon isotope fractionation in biogenic aragonite: Temperature effects', *Chemical Geology: Isotope Geoscience section*, 59, 59–74.

Hathway, B. (2000) 'Continental rift to back-arc basin: Jurassic-Cretaceous stratigraphical and structural evolution of the Larsen Basin, Antarctic Peninsula', *Journal of the Geological Society*, 157(2), 417–432.

Hollis, C. J., Taylor, K. W. R., Handley, L., Pancost, R. D., Huber, M., Creech, J. B., Hines, B. R., Crouch, E. M., *et al.* (2012) 'Early Paleogene temperature history of the Southwest Pacific Ocean: Reconciling proxies and models', *Earth and Planetary Science Letters*, 349–350, 53–66.

Hong, S. K. and Lee, Y. Il (2012) 'Evaluation of atmospheric carbon dioxide concentrations during the Cretaceous', *Earth and Planetary Science Letters*, 327–328, 23–28.

Huber, B. T. (1988) 'Upper Campanian-Paleocene foraminifera from the James Ross Island region, Antarctica Peninsula', in Feldman, R. M. and Woodburne, M. O. (eds) *Geology and Paleotology of Seymour Island, Antarctica Peninsula*, 163–252.

Huber, B. T., Hodell, D. A. and Hamilton, C. P. (1995) 'Middle-Late Cretaceous climate of the Southern High Latitiudes: Stable isotope evidence for minimal equator-to-pole thermal gradients', *Geological Society of America Bulletin*, 107(10), 1164–1191.

Huber, B. T., Norris, R. D. and MacLeod, K. G. (2002) 'Deep-sea paleotemperature record of extreme warmth during the Cretaceous', *Geology*, 30(2), 123–126.

Hunter, S. J. (2009) *Modelling Antarctic Ice Sheets*.

Hunter, S. J., Haywood, A. M., Valdes, P. J., Francis, J. E. and Pound, M. J. (2013) 'Modelling equable climates of the Late Cretaceous: Can new boundary conditions resolve data-model discrepancies?', *Palaeogeography,*

Palaeoclimatology, Palaeoecology, 392, 41–51.

Hunter, S. J., Valdes, P. J., Haywood, A. M. and Markwick, P. J. (2008) 'Modelling Maastrichtian climate: investigating the role of geography, atmospheric CO2 and vegetation', *Climate of the Past Discussions*, 4(4), 981–1019.

Ivany, L. C., Lohmann, K. C., Hasiuk, F., Blake, D. B., Glass, A., Aronson, R. B. and Moody, R. M. (2008) 'Eocene climate record of a high southern latitude continental shelf: Seymour Island, Antarctica', *Geological Society of America Bulletin*, 120(5–6), 659–678.

Jung, C., Voigt, S., Friedrich, O., Koch, M. C. and Frank, M. (2013) 'Campanian-Maastrichtian ocean circulation in the tropical Pacific', *Paleoceanography*, 28(3), 562–573.

Katz, M. E., Cramer, B. S., Toggweiler, J. R., Esmay, G., Liu, C., Miller, K. G., Rosenthal, Y., Wade, B. S., *et al.* (2011) 'Impact of Antarctic Circumpolar Current Development on Late Paleogene Ocean Structure', *Science*, 332(6033), 1076–1079.

Kemp, D. B., Robinson, S. A., Crame, J. A., Francis, J. E., Ineson, J., Whittle, R. J., Bowman, V. and O'Brien, C. (2014) 'A cool temperate climate on the Antarctic Peninsula through the latest Cretaceous to early Paleogene', *Geology*, 42(7), 583–586.

Kennedy, W. J., Crame, J. A., Bengtson, P. and Thomson, M. R. (2007) 'Coniacian ammonites from James Ross Island, Antarctica', *Cretaceous Research*, 28(3), 509–531.

Kominz, M. A., Browning, J. V., Miller, K. G., Sugarman, P. J., Mizintseva, S., Scotese, C. R., Miller, D. J., Sugarman, P. J., *et al.* (2008) 'Late Cretaceous to Miocene sea-level estimates from New Jersey and Delaware coastal plain coreholes: an error analysis', *Basin research*, 20(2), 211–226.

Larkin, C. (2014) *Clumped Isotope analysis of Antarctic Molluscs from the Late Cretaceous to Early Paleogene*, *University of Cambridge*.

Li, L. and Keller, G. (1998) 'Maastrichtian climate, productivity and faunal turnovers in planktic foraminifera in South Atlantic DSDP sites 525A and 21', *Marine Micropaleontology*, 33(1–2), 55–86.

Linnert, C., Robinson, S. A., Lees, J. A., Bown, P. R., Perez-Rodriguez, I., Petrizzo, M. R., Falzoni, F., Littler, K., *et al.* (2014) 'Evidence for global cooling in the Late Cretaceous', *Nat Commun*, 5(May), 4194.

Macdonald, D. I. M., Barker, P. F., Garrett, S. W., Ineson, J. R., Pirrie, D., Storey, B. C., Whitham, A. G., Kinghorn, R. R. F., *et al.* (1988) 'A preliminary assessment of the hydrocarbon potential of the Larsen Basin, Antarctica', *Marine and Petroleum Geology*, 5(1), 34–53.

Macellari, C. E. (1988) 'Stratigraphy, sedimentology, and paleoecology of Upper Cretaceous / Paleocene shelf-deltaic sediments of Seymour Island', *Geological Society of America Memoirs*, 169, 25–54.

Marenssi, S. A. (2006) 'Eustatically controlled sedimentation recorded by Eocene strata of the James Ross Basin, Antarctica', *Geological Society, London, Special Publications*, 258(1), 125–133.

Marenssi, S. A., Net, L. I. and Santillana, S. N. (2002) 'Provenance, environmental and paleogeographic controls on sandstone composition in an incised-valley system: the Eocene La Meseta Formation, Seymour Island, Antarctica', *Sedimentary Geology*, 150(3–4), 301–321.

Marenssi, S. A., Santillana, S. N. and Rinaldi, C. A. (2015) 'STRATIGRAPHY OF THE LA MESETA FORMATION (EOCENE), MARAMBIO (SEYMOUR) ISLAND, ANTARCTICA', *Publicación Electrónica de la Asociación Paleontológica Argentina*, 5(1).

Marenssi, S. A., Santillana, S. N., Rinaldi, C. A. and Rinaldi., C. A. (1998) 'Paleoambientes sedimentarios de la Aloformación La Meseta (Eoceno), Isla Marambio (Seymour)', *Dirección Nacional del Antártico, Instituto Antártico Argentino*, 464.

Marenssi, S., Santillana, S. and Bauer, M. (2012) 'Stratigraphy, sedimentary petrology and provenance of the Sobral and Cross Valley formations (Paleocene), Marambio (Seymour) Island, Antarctica', *Andean geology*, 39(1), 67–91.

Markwick, P. J. (2007) 'The palaeogeographic and palaeoclimatic significance of climate proxies for data-model comparisons', in Williams, M., Haywood, A. M., Gregory, D., and Schmidt, D. N. (eds) *Deep-Time Perspectives on Climate Change: Marrying the Signal from Computer Models and Biological Proxies*.

Markwick, P. J. and Valdes, P. J. (2004) 'Palaeo-digital elevation models for use as boundary conditions in coupled ocean–atmosphere GCM experiments: a Maastrichtian (late Cretaceous) example', *Palaeogeography, Palaeoclimatology, Palaeoecology*, 213(1), 37–63.

McArthur, J. M., Crame, J. A. and Thirlwall, M. F. (2000) 'Definition of Late Cretaceous Stage Boundaries in Antarctica Using Strontium Isotope Stratigraphy', *The Journal of Geology*, 108(6), 623–640.

McArthur, J. M., Thirlwall, M. F., Engkilde, M., Zinsmeister, W. J. and Howarth, R. J. (1998) 'Strontium isotope profiles across K/T boundary sequences in Denmark and Antarctica', *Earth and Planetary Science Letters*, 160(1–2), 179–192.

Milanese, F., Kirschvink, J., Olivero, E. and Rapalini, A. (2013) 'Magnetostratigraphy of an Upper Cretaceous Section of James Ross Basin, Antarctica', *Latinmag Letters*, (3), 1–9.

Milanese, F. N., Olivero, E. B., Kirschvink, J. L. and Rapalini, A. E. (2017) 'Magnetostratigraphy of the Rabot Formation, Upper Cretaceous, James Ross Basin, Antarctic Peninsula', *Cretaceous Research*, 72, 172–187.

Miller, K. G., Wright, J. D. and Browning, J. V. (2005) 'Visions of ice sheets in a greenhouse world', *Marine Geology*, 217(3–4), 215–231.

Montes, N., Nozal, F., Santillana, S., Marenssi, S. A. and Olivero, E. B. (2010) *Mapa geológioco de la Isla Marambio (Seymour) Escala 1:20,000*, *Inst. Ant. Arg. Inst. Geol. Min. España*.

Olivero, E. B. (2012) 'Sedimentary cycles, ammonite diversity and palaeoenvironmental changes in the Upper Cretaceous Marambio Group, Antarctica', *Cretaceous Research*, 34, 348–366.

Olivero, E. B., Martinioni, D. R. and Mussel, F. J. (1992) 'Upper Cretaceous sedimentology and biostratigraphy of western Cape Lamb (Vega Island, Antarctica). Implications on sedimentary cycles and evolution of the basin', *Geología de la Isla James Ross*, 147–166.

Olivero, E. B. and Medina, F. A. (2000) 'Patterns of Late Cretaceous ammonite biogeography in southern high latitudes: the family Kossmaticeratidae in Antarctica', *Cretaceous Research*, 21(2–3), 269–279.

Olivero, E. B., Ponce, J. J. and Martinioni, D. R. (2008) 'Sedimentology and architecture of sharp-based tidal sandstones in the upper Marambio Group, Maastrichtian of Antarctica', *Sedimentary Geology*, 210(1–2), 11–26.

Otto-Bliesner, B. L. and Upchurch, G. R. (1997) 'Vegetation-induced warming of high latitude regions during the Late Cretaceous period', *Nature*, 385, 804–807.

Petersen, S. V., Dutton, A. and Lohmann, K. C. (2016) 'End-Cretaceous

extinction in Antarctica linked to both Deccan volcanism and meteorite impact via climate change', *Nature Communications*, 7(May), 12079.

Pirrie, D. (1989) 'Shallow marine sedimentation within an active margin basin, James Ross Island, Antarctica', *Sedimentary Geology*, 63(1–2), 61–82.

Pirrie, D., Crame, J. A., Lomas, S. A. and Riding, J. B. (1997) 'Late Cretaceous stratigraphy of the Admirality Sound region, James Ross Basin, Antarctica', *Cretaceous Research*, 18, 109–137.

Pirrie, D., Crame, J. A. and Riding, J. B. (1991) 'Late Cretaceous stratigraphy and sedimentology of Cape Lamb, Vega Island, Antarctica', *Cretaceous Research*, 12(3), 227–258.

Pirrie, D. and Marshall, J. D. (1990) 'High-paleolatitude Late Cretaceous paleotemperatures: New data from James Ross Island, Antarctica', *Geology*, 18(1), 31–34.

Poole, I., Cantrill, D. J. and Utescher, T. (2005) 'A multi-proxy approach to determine Antarctic terrestrial palaeoclimate during the Late Cretaceous and Early Tertiary', *Palaeogeography, Palaeoclimatology, Palaeoecology*, 222, 95– 121.

Porebski, S. J. (1995) 'Facies architecture in a tectonically-controlled incised-valley estuary: La Meseta Formation (Eocene) of Seymour Island, Antarctic Peninsula.', *Studia Geologica Polonica*, (107), 7–97.

Porebski, S. J. (2000) 'Shelf-valley compound fill produced by fault subsidence and eustatic sea-level changes, Eocene La Meseta Formation, Seymour Island, Antarctica', *Geology*, 28(2), 147–150.

Pross, J., Contreras, L., Bijl, P. K., Greenwood, D. R., Bohaty, S. M., Schouten, S., Bendle, J. A., Röhl, U., *et al.* (2012) 'Persistent near-tropical warmth on the Antarctic continent during the early Eocene epoch', *Nature*, 488(7409), 73–77.

Riding, J. B. and Crame, J. A. (2002) 'Aptian to Coniacian (Early–Late Cretaceous) palynostratigraphy of the Gustav Group, James Ross Basin, Antarctica', *Cretaceous Research*, 23(6), 739–760.

Rinaldi, C. A., Massabie, A., Morelli, J., Rosenman, H. L. and Del Valle, R. (1978) 'Geologia de la isla Vicecomodoro Marambio', *Contribución del Instituto Antártico Argentino*, (217), 1–37.

Robinson, S. A., Murphy, D. P., Vance, D. and Thomas, D. J. (2010) 'Formation

of "Southern Component Water" in the Late Cretaceous: Evidence from Nd-isotopes', *Geology*, 38(10), 871–874.

Sadler, P. M. (1988a) *Geology and Paleontology of Seymour Island Antarctic Peninsula*, *Geological Society of America Memoirs*.

Sadler, P. M. (1988b) *Geometry and stratification of uppermost Cretaceous and Paleogene units on Seymour Island, northern Antarctic Peninsula*, *Geological Society of America Memoirs*.

Scasso, R. A., Olivero, E. B. and Buatois, L. A. (1991) 'Lithofacies, biofacies, and ichnoassemblage evolution of a shallow submarine volcaniclastic fan-shelf depositional system (Upper Cretaceous, James Ross Island, Antarctica)', *Journal of South American Earth Sciences*, 4(3), 239–260.

Stilwell, J. D., Zinsmeister, W. J. and Oleinik, A. E. (2004) 'Early Paleocene Mollusks of Antarctica: systematics, paleoecology and paleobiogeographic significance', 369(365).

Thibault, N., Harlou, R., Schovsbo, N. H., Stemmerik, L. and Surlyk, F. (2016) 'Late Cretaceous (late Campanian-Maastrichtian) sea-surface temperature record of the Boreal Chalk Sea', *Climate of the Past*, 12(2), 429–438.

Thorn, V. C., Francis, J. E. and Riding, J. B. (2009) 'The Late Cretaceous dinoflagellate cyst Manumiella — Biostratigraphy, systematics, and palaeoecological signals in Antarctica', *Review of Palaeobotany and Palynology*, 156(3–4), 436–448.

Tobin, T. S., Ward, P. D., Steig, E. J., Olivero, E. B., Hilburn, I. A., Mitchell, R. N., Diamond, M. R., Raub, T. D., *et al.* (2012) 'Extinction patterns, δ18 O trends, and magnetostratigraphy from a southern high-latitude Cretaceous–Paleogene section: Links with Deccan volcanism', *Palaeogeography, Palaeoclimatology, Palaeoecology*, 350, 180–188.

del Valle, R. A., Elliot, D. H. and Macdonald, D. I. M. (1992) 'Short note Sedimentary basins on the east flank of the Antarctic Peninsula : proposed nomenclature', *Antarctic Science*, 4(4), 477–478.

Whitham, A. G., Ineson, J. R. and Pirrie, D. (2006) 'Marine volcaniclastics of the Hidden Lake Formation (Coniacian) of James Ross Island, Antarctica: an enigmatic element in the history of a back-arc basin', *Geological Society, London, Special Publications*, 258(1), 21–47.

Wilf, P., Johnson, K. R. and Huber, B. T. (2003) 'Correlated Terrestrial and Marine Evidence for Global Climate Changes before Mass Extinction at

the Cretaceous-Paleogene Boundary', *Proceedings of the National Academy of Sciences of the United States of America*, 100(2), 599–604.

Witts, J. D. (2016) *Marine biodiversity during the latest Cretaceous in Antarctica and the nature of the Cretaceous – Paleogene mass extinction*.

Witts, J. D., Bowman, V. C., Wignall, P. B., Alistair Crame, J., Francis, J. E. and Newton, R. J. (2015) 'Evolution and extinction of Maastrichtian (Late Cretaceous) cephalopods from the López de Bertodano Formation, Seymour Island, Antarctica', *Palaeogeography, Palaeoclimatology, Palaeoecology*, 418, 193–212.

Witts, J. D., Whittle, R. J., Wignall, P. B., Crame, J. A., Francis, J. E., Newton, R. J. and Bowman, V. C. (2016) 'Macrofossil evidence for a rapid and severe Cretaceous–Paleogene mass extinction in Antarctica', *Nature Communications*, 7, 11738.

Wolfe, J. A. and Upchurch, G. R. (1987) 'North American nonmarine climates and vegetation during the Late Cretaceous', *Palaeogeography, Palaeoclimatology, Palaeoecology*, 61, 33–77.

Wrenn, J. H. and Hart, G. F. (1988) 'Paleogene dinoflagellate cyst biostratigraph of Seymour Island, Antarctica', *Geological Society of America Memoirs*, 169(1).

Zinsmeister, W. J. (1977) 'Note on a New Occurrence of the Southern Hemisphere Aporrhaid Gastropod Struthioptera Finlay & Marwick on Seymour Island, Antarctica', *Journal of Paleontology*, 399–404.

Zinsmeister, W. J. (1982) 'Late Cretaceous-Early Tertiary Molluscan Biogeography of the Southern Circum-Pacific', *Journal of Paleontology*, 84–102.

Zinsmeister, W. J. (1984) 'Late Eocene bivalves (Mollusca) from the La Meseta Formation, collected during the 1974-1975 joint Argentine-American expedition to Seymour Island, Antarctic Peninsula', *Journal of Paleontology*, 58(6), 1497–1527.

Zinsmeister, W. J. (1988) 'Early geological exploration of Seymour Island, Antarctica', *Geological Society of America Memoirs*, 169.

Zinsmeister, W. J. (1998) 'Discovery of fish mortality horizon at the K-T Boundary on Seymour Island: Re-evaluation of events at the end of the Cretaceous', *Journal of Paleontology*, 72(3), 556–571.

Zinsmeister, W. J., Feldmann, R. M., Woodburne, M. O. and Elliot, D. H. (1989)

'Latest Cretaceous/earliest Tertiary transition on Seymour Island, Antarctica', *Journal of Paleontology*, 63(6), 731–738.

Zinsmeister, W. J. and Macellari, C. E. (1988) 'Bivalvia (Mollusca) from Seymour Island , Antarctic Peninsula', *Geological Society of America Memoirs*, (169).

CHAPTER 3

GROWTH PATTERNS AND LONGEVITY

The aim of this chapter is to determine whether environmental or biological change exerts a major control on growth of bivalve specimens from Seymour Island and investigate changes in growth rate and morphology of high latitude marine bivalves in response to the Cretaceous-Paleogene mass extinction event.

3.1 Introduction

The previous two chapters have outlined the importance of understanding seasonality, climate variability and their potential effects on organisms over the Cretaceous to Paleogene interval of the Seymour Island section. In addition to the effects of the mass extinction itself, it is likely that marine organisms would have reacted the environmental stress of the purportedly variable climate of the late Maastrichtian.

Changes in temperature, primary productivity and water salinity can all affect the growth patterns of marine organisms (e.g. Brown & Hartwick 1988; Schone et al. 2002). The K-Pg boundary has long been associated with temperature fluctuations and the potential for anoxia and regional primary productivity collapse (Arthur et al. 1987; Smith et al. 1998; Aberhan et al. 2007; Alegret et al. 2012). It is likely that the effects of this will have caused a size difference in survivor taxa.

Studies of morphometric changes across major mass extinctions have reported significant dwarfing in an effect known as the Lilliput effect (Urbanek 1993). The Lilliput effect is a general description for a temporary decrease in body size among post-extinction organisms. The effect has been widely reported in many animal groups, both in holdover taxa and long-term survivors in the aftermaths of all five past mass extinction events including the K-Pg mass extinction

(Hansen et al. 1993; Smith & Jeffery 1998; Jeffery 2001; Lockwood 2005; Aberhan et al. 2007).

Some studies of the K-Pg and other mass extinction events dispute the ubiquity of the Lilliput effect; particularly in within-lineage size studies (e.g. Brayard et al. 2010; Sogot et al. 2014). Increases in body size of some clades due to reduced competition and predation by other organisms has also been reported (e.g. Case 1978; McClain et al. 2006; Harries & Knorr 2009). It is becoming more and more accepted that size change at mass extinction horizons is likely to be complex and it cannot be expected that all clades will respond in the same manner, or that all mass extinctions will have the same effects (Harries & Knorr 2009; Friedman & Sallan 2012).

It is therefore useful to examine the environmental and biological context for size change in order to understand the variability of behaviour between clades and extinction events. The K-Pg succession on Seymour Island is ideal for such investigations into morphological change as it contains an abundance of largely intact skeletal fossils and several species which survive and can be compared across the mass extinction event. Patterns of change can be examined across several taxa in order to determine whether environmental or biological change is likely to exert a major control on shell size and growth.

It is also likely that mean-state climates around the Antarctic Peninsula during this period were warmer than present high latitude areas, with annual temperature estimates between 6 and 14°C (Figure 2.11; Poole et al. 2005; Tobin et al. 2012; Kemp et al. 2014). Body size is important for generation times, energy demands and population sizes (Pianka 1970; Heim et al. 2015) and the effect of such a climate regime on biological groups has received relatively little attention, with high latitude fossil taxa, even from warmer global climate states, often directly compared to modern taxa (e.g. Moss et al. 2016).

This chapter addresses both the change in size across the K-Pg boundary and the changes in growth rates which may result from differences in climate. Size and growth rate of 3 taxa of fossil bivalves from the lead up to and the aftermath of the Cretaceous-Paleogene mass extinction interval on Seymour Island were studied in order to determine whether significant changes that may have been associated with environmental fluctuations across this interval are observable.

Morphology and size were compared in specimens at intervals through the stratigraphic section and from each side of the boundary, to look for signs of dwarfing which could relate to environmental instability across the mass extinction period. The periodicity of visible growth lines in shells was also tested using stable oxygen isotope analysis to determine the seasonality of growth ring formation. This allowed the longevity and growth rate of specimens from the Maastrichtian and Danian to be compared.

As each method of analysis of these bivalves directly allows for the subsequent method to be used, the methodology, results and a brief discussion of the implications of the growth seasonality, shell morphometrics and then shell growth rates will be presented before being discussed within the context of the K-Pg mass extinction even.

3.2 Objectives

- Assess the evidence for annual seasonal signals in bivalve shell material and the periodicity of internal and external shell growth rings.

- Study morphometrics and growth patterns in order to determine whether there are significant size changes or dwarfing in groups that survived the mass extinction and to determine whether size changes are due to changes in juvenile growth duration or growth rate.

- Comparison with modern data in order to determine whether Seymour Island's bivalves are consistent with the established trends of increased longevity at high latitudes, during a time when the high latitudes were significantly warmer than modern.

3.3 Rationale of Taxon Choice

The Seymour Island section is fossil rich with abundant and well-described skeletal material as discussed in Chapter 2. This study focuses on several taxa

of infaunal bivalves; examples of the genera *Lahillia*, *Cucullaea* and *Leionucula* (Figure 3.1). Infaunal bivalves were chosen because they had a greater survivorship across the Cretaceous-Paleogene boundary than epifaunal taxa. They also mineralise aragonitic shells which are more susceptible to diagenetic effects than calcite shells, and easier to discern areas of the shell which have been affected by diagenesis (refer to Section 2.7 for details).

Examples of these genera were chosen because they produced large sized robust shells and are abundant as fossils throughout the stratigraphic sections, with many specimens collected in an intact or near-intact condition. A number of species from these genera are present in Seymour Island's succession; the taxonomic classifications and faunal ranges of the species examined are summarised in Figure 3.1, with full details available in Appendix B. *Lahillia larseni*, and *Leionucula suboblongata* are both examples of species which survive and thrive across the mass extinction, whereas *Cucullaea* is represented by *Cucullaea antarctica* in the pre-extinction Maastrichtian fauna, and *Cucullaea elliotti* in the post-extinction Danian. *Lahillia* are likely to have been shallow-burrowing mobile infaunal suspension feeders; *Cucullaea* were likely endobyssally infaunal suspension feeders (Zinsmeister & Macellari 1988); and *Leionucula* are likely to have been deposit feeders. This choice of genera therefore provides a range of feeding strategies and responses to the effects of the mass extinction event.

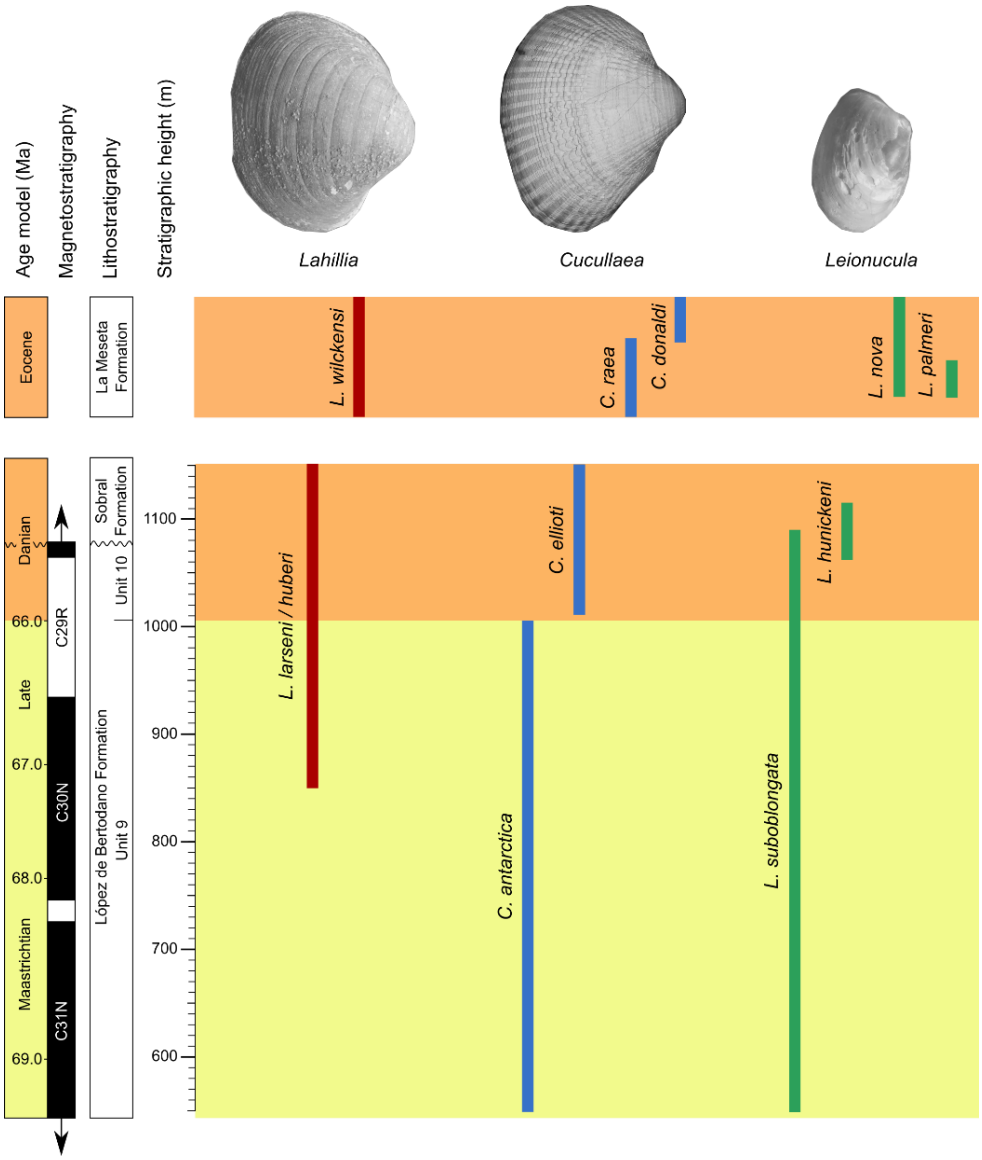

Figure 3.1: Biostratigraphic ranges of bivalve species used for morphometric analysis. Range data based on Crame et al 2014 and Witts et al 2016.

Lahillia are also notable for their clearly visible external growth lines which are extremely advantageous for measuring rates of growth and ontogenetic trajectories. Many species of bivalve produce visible external or internal growth lines, with a distinct periodicity (e.g. annual, monthly or daily) which can be used to determine the relative age of shell material and compare rates of shell accretion (Schöne et al. 2004; Immenhauser et al. 2016).

Bivalves are among the most long-lived animals on the planet, with several species exhibiting lifespans of over 100 years (Buick & Ivany 2004; Butler et al. 2013a). As a result, the shells produce long continuous records of the environmental factors affecting shell production (e.g. Zolotarev 1980; Jones et al. 1989; Buick & Ivany 2004; Butler et al. 2010, 2013). Shell growth rates are recorders of secondary productivity (Jones et al. 1989), and have been found in several species of modern bivalves to be strongly regulated by temperature (e.g. Schöne et al. 2004 and many more). A pattern of increasing longevity and slower growth rates towards the high latitudes has also been noted across studies of many modern taxa (Moss et al. 2016).

Bivalve molluscs are also excellent archives for seasonal climate data because they grow carbonate shells by periodic accretion, which can incorporate a number of ambient water signals during growth, such as stable isotopes and trace elements which can be used as palaeoenvironmental proxies. These can be used to determine the period and season of active growing and growth pauses.

3.4 Seasonality of Growth

Most bivalves do not grow continuously year-around. Most species have been observed to pause growth for spawning or when water temperatures exceed a tolerated threshold range. This causes production of a visible – often macroscopic – growth-check line in the entire valve and tooth. This line may possess a different microstructure or incorporate a higher proportion of organic material, making it easily discernible from small scale accretionary banding (Shirai et al. 2014). These internal or external growth rings are produced by many species of bivalve during periods of slower growth or metabolism, however some species are prone to producing "false" growth lines (e.g. Lutz & Rhoads 1980; Thompson et al. 1980; Ropes 1984), or ridges as surface ornamentation.

The season and periodicity of growth can be identified in fossil material using geochemical temperature proxies, which will show cuspate data where records have been truncated across growth checks (Figure 3.2). Here, $\delta^{18}O$ measurements have been used to establish whether the ornamentations of *Lahillia* and *Cucullaea* (Figure 3.4) are produced with regular periodicity and if

growth lines can be used as a source of age data to compare the growth of different specimens.

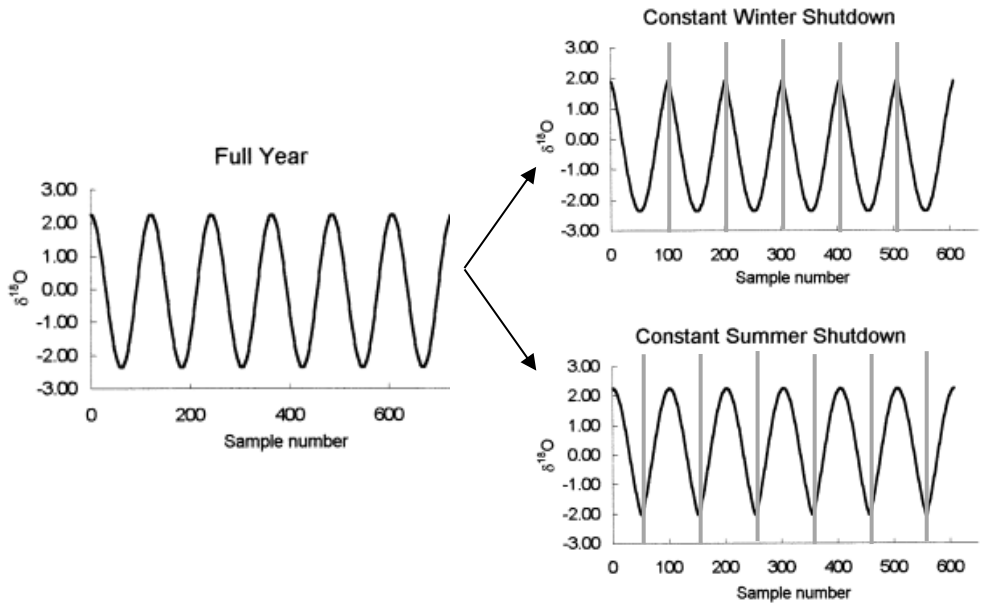

Figure 3.2: Examples of δ^{18}O shell data for uninterrupted shell growth (left) and winter and summer shutdowns (right), modified from Goodwin et al. 2003.

3.4.1 Methods

Once preservation was confirmed to be suitable for geochemical analysis, high resolution δ^{18}O measurements were carried out to determine the periodicity of internal and external growth lines in *Lahillia* and *Cucullaea* specimens.

This chapter uses δ^{18}O variation as a rough indicator of relative water temperature, and therefore a method to determine the approximate periodicity of shell growth between visible structural growth features. Seminal papers from around the mid-century (Urey 1947; Urey et al. 1951; Epstein et al. 1953) showed that oxygen isotopes in biogenic carbonates are a function of temperature and isotopic composition of the water. The amount of biological fractionation has been experimentally determined in aragonitic (Grossman & Ku 1986) and calcitic (Anderson & Arthur 1983) molluscs. Further details of this process and factors affecting the relationship between shell δ^{18}O composition and temperature are discussed in Chapter 4.

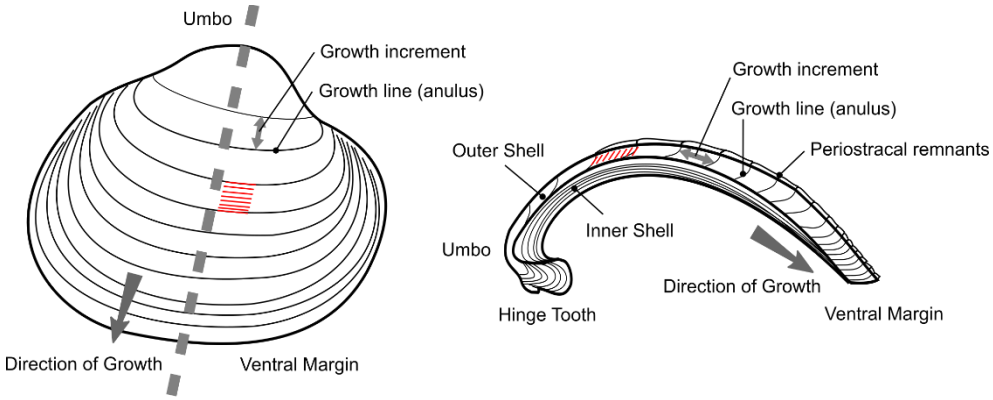

Figure 3.3: Representative diagram of bivalve shell (left) and shell cross section (right) taken along dashed line. Diagrams show the main anatomical features including growth lines, growth increments and shell layers with aproximate microsampling pathways (red lines).

High resolution stable carbon and oxygen isotope microanalysis was performed for 29 specimens. The specimens chosen for stable isotope analysis have extremely well preserved original aragonite shell mineralogy which was microsampled following standard procedures (Dettman & Lohmann 1995 and Appendix B). Microsampling was undertaken using a Merchantek MicroMill at a resolution of between 5 and 10 samples per visible growth increment. *Lahillia* were polished by Dremel to remove any of the previously identified altered surface layers and sampled on the outer surface. *Cucullaea* were sectioned along the line of maximum growth and sampled from the cut face to avoid the intermittent periostracal layer identified by SEM (Figure 2.15) and shell ornamentations which tended to obscure the external position of true growth lines (Figure 3.4). Additional bulk shell powders produced by grinding shell fragments were also tested for stable isotope composition. Full methodology for this stable isotopic analysis is presented in Section 4.4.1.

Leionucula mineralise shells in aragonitic nacre, which has finer crystals than those found in the crossed-lamellar layers of *Lahillia* and *Cucullaea* and has a much greater organic component. As a result, their shells may be more susceptible to the effects of diagenesis than the other two genera, and have not been sampled for stable isotope measurements.

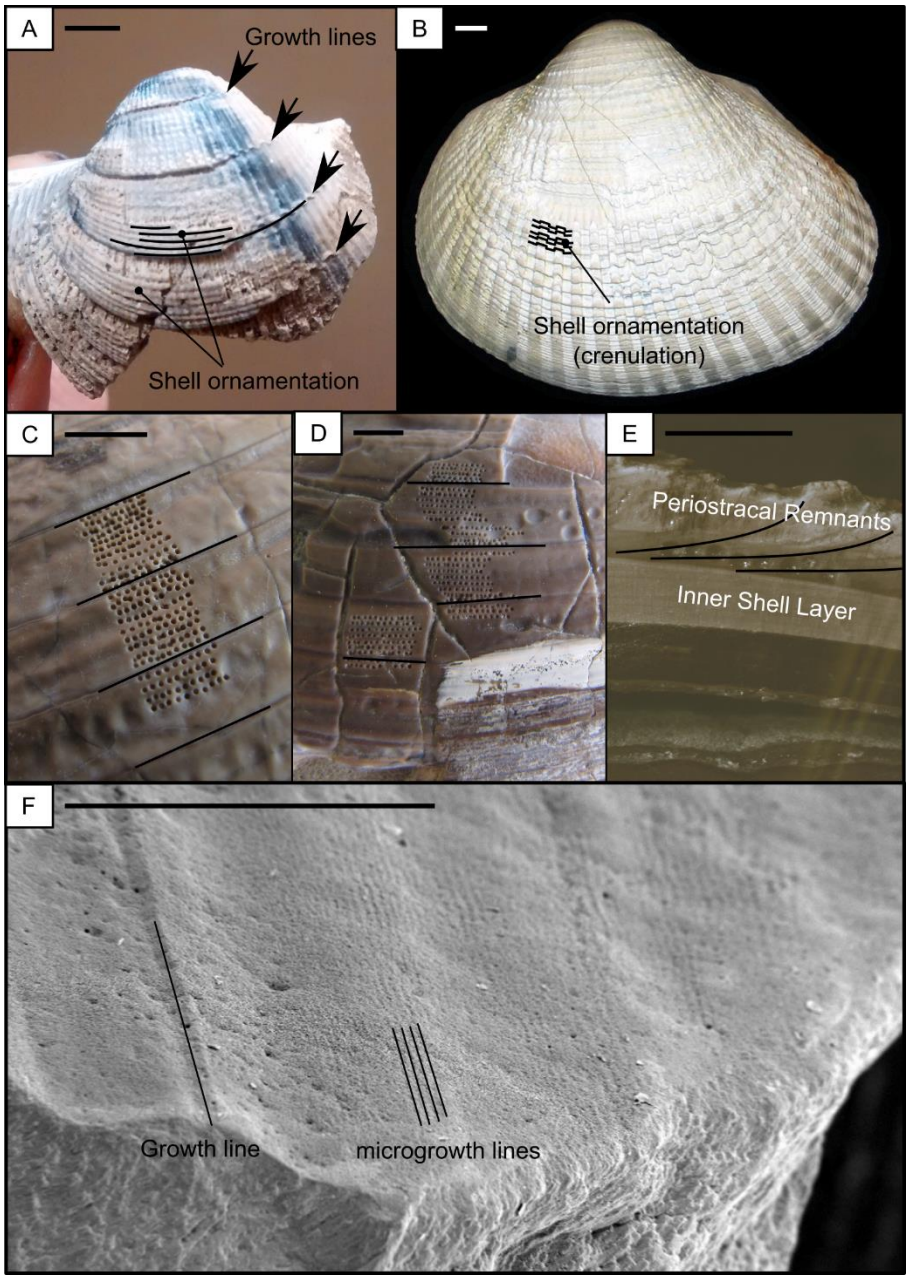

Figure 3.4: Photographs showing details of shell ornamentation and sampling paths; scale bar = 5mm. (A) *Cucullaea* fragment showing true growth lines (arrows) and shell ornamentations (lines) which are shallower and can be weathered off. (B) less weathered *Cucullaea* shell showing the crenulated pattern of this ornamentation and the obscuration of the growth lines by the shell crenulations. (C, D) *Lahillia* shell showing growth lines (black lines) and rows of microdrilled sample pits drilled to avoid cracks and potential alteration. (E) *Cucullaea* section showing shell layers, growth lines (black lines) and location of microdrilled sample pits. (F) SEM image of *Lahillia* shell surface showing growth line and sub-annual microgrowth lines (periodicity unknown)

3.4.2 Results

Nineteen specimens were successfully microsampled to produce high resolution seasonal data. Ten did not have sufficient preservation of continuous wide growth line sections without cracks to produce seasonal time-series, results from these specimens were averaged to produce additional bulk data points (Appendix B). In order to remove obvious outliers which may be a result of sampling small patches of diagenetically altered material in microborings or cracks, mean and 3σ values were calculated for the oxygen isotope data from each specimen and any outliers were disregarded during further analysis. This removed a total of 5 data points out of the 564 stable isotope samples.

Measurements of isotopic data are presented in Appendix B. The data have been plotted here as graphs in Figure 3.5 to Figure 3.7. Many of these graphs show cuspate trajectories truncated against visible external or internal shell lines (grey vertical bars).

In *Lahillia* from the López de Bertodano Formation (Figure 3.5), the growth increments incorporate more negative $\delta^{18}O$ signals, whereas the growth check lines incorporate more positive $\delta^{18}O$ signals. A characteristic concave-up shape of the trend in $\delta^{18}O$ data throughout the growth increment between growth lines indicates shell production in warmer temperatures with the growth line forming in cooler temperatures.

Cucullaea have a highly ornamented external valve surface (Figure 3.4:) with evidence for alteration of the outer layers (Figure 2.16), so were sampled only in cross-section. Due to the lower sampling resolution in *Cucullaea*, the concave-up pattern of temperature data between growth lines is not as clear as in *Lahillia*, but the oxygen isotopic trend in *Cucullaea* from the López de Bertodano Formation (Figure 3.6) is very similar. *Cucullaea* show generally more positive $\delta^{18}O$ signals near the growth lines indicating lower temperatures during growth cessations, and more negative $\delta^{18}O$ signals within the growth increment indicating warmer temperatures during the active growing season.

In addition to the $\delta^{18}O$ cyclicity, the high resolution $\delta^{13}C$ data in *Lahillia* and *Cucullaea* shows interesting seasonal trends which will be discussed in further detail in Chapter 6.

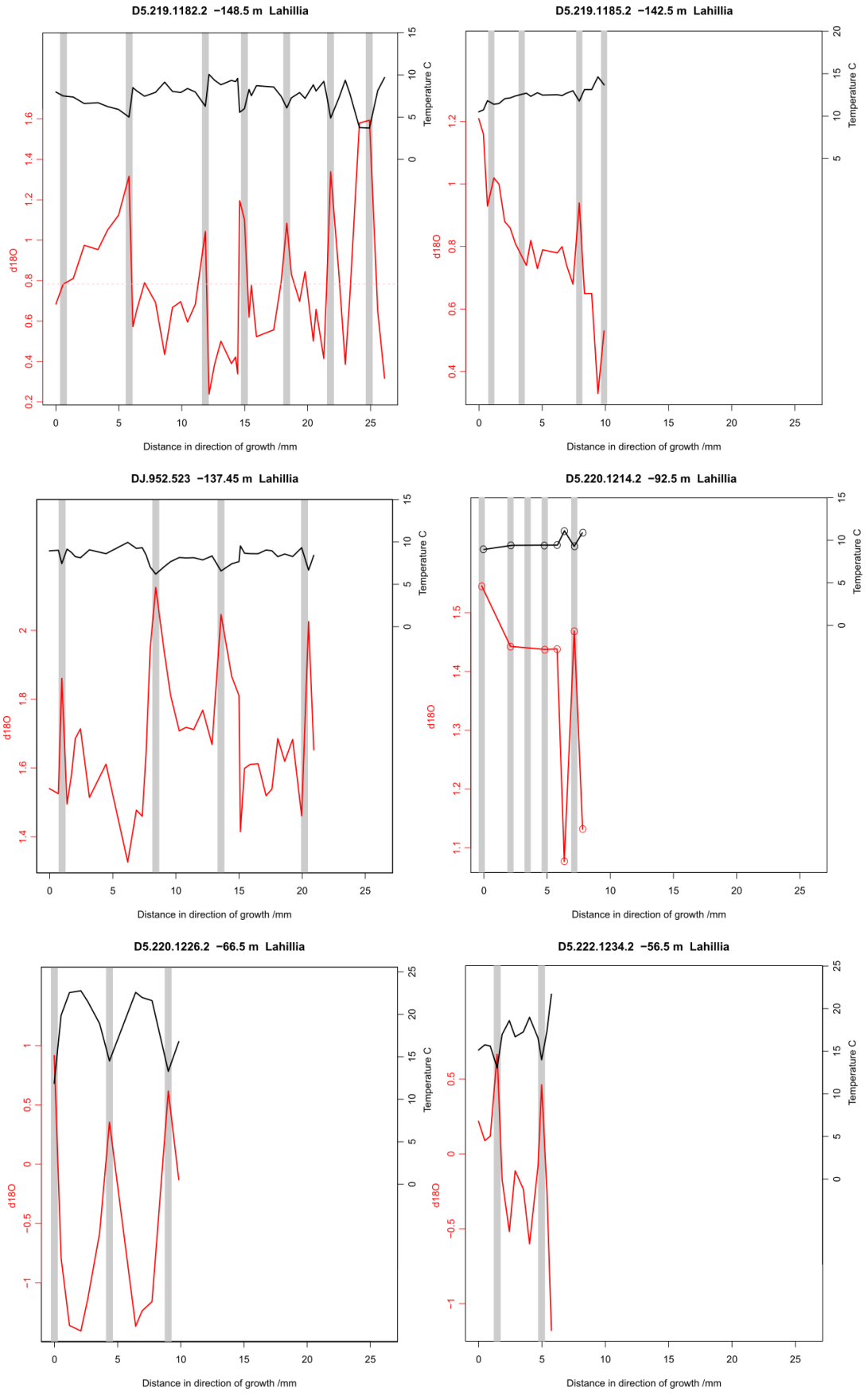

Figure 3.5A: δ^{18}**O (red) and approximate converted temperature (black) in López de Bertodano Formation *Lahillia* labelled with relative height to the K-Pg boundary. Distance axis begins at an arbitrary point within shells. Vertical grey bars locate positions of growth lines.**

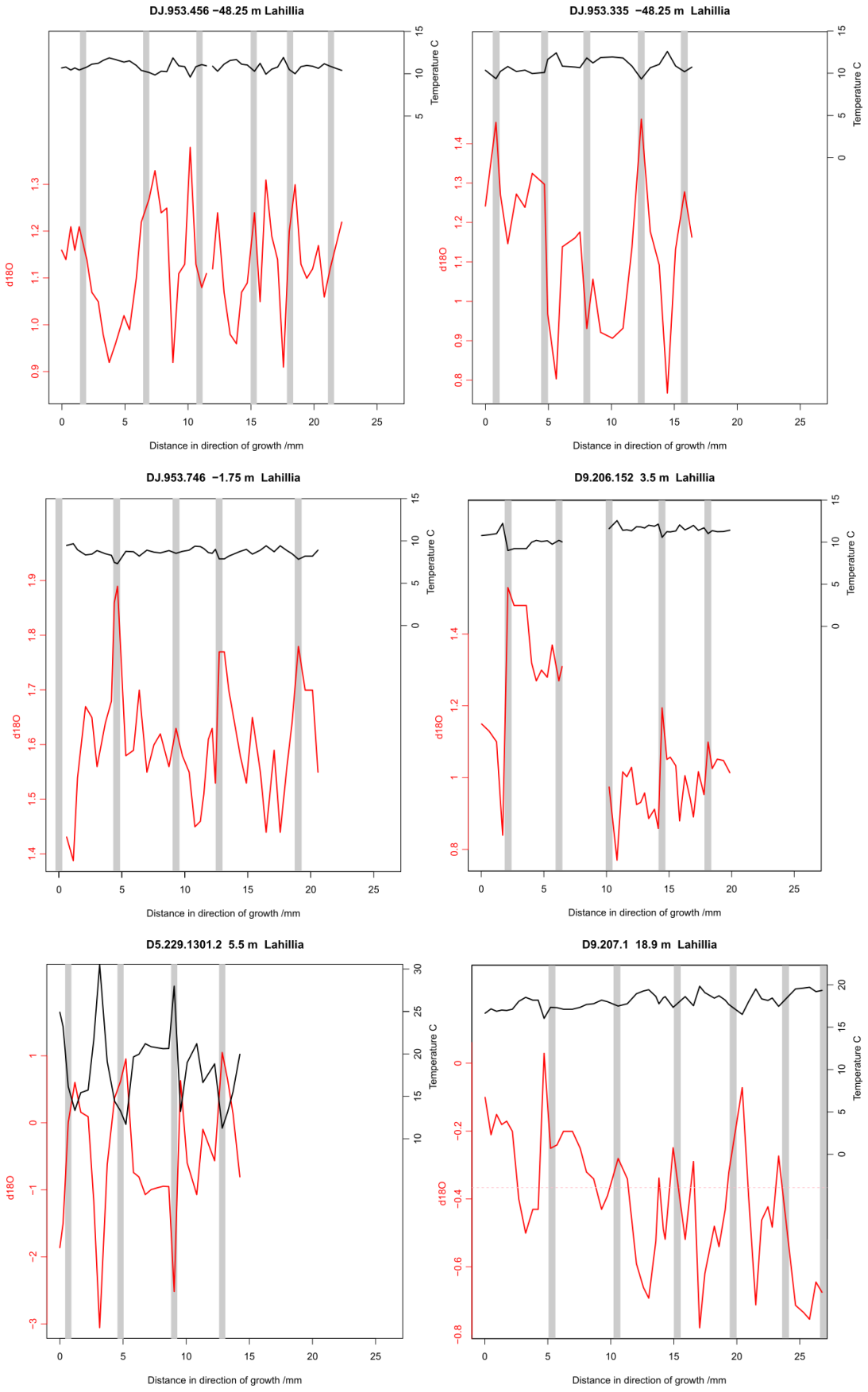

Figure 3.5B: δ^{18}**O (red) and approximate converted temperature (black) in López de Bertodano Formation *Lahillia* labelled with relative height to the K-Pg boundary. Distance axis begins at an arbitrary point within shells. Vertical grey bars locate positions of growth lines.**

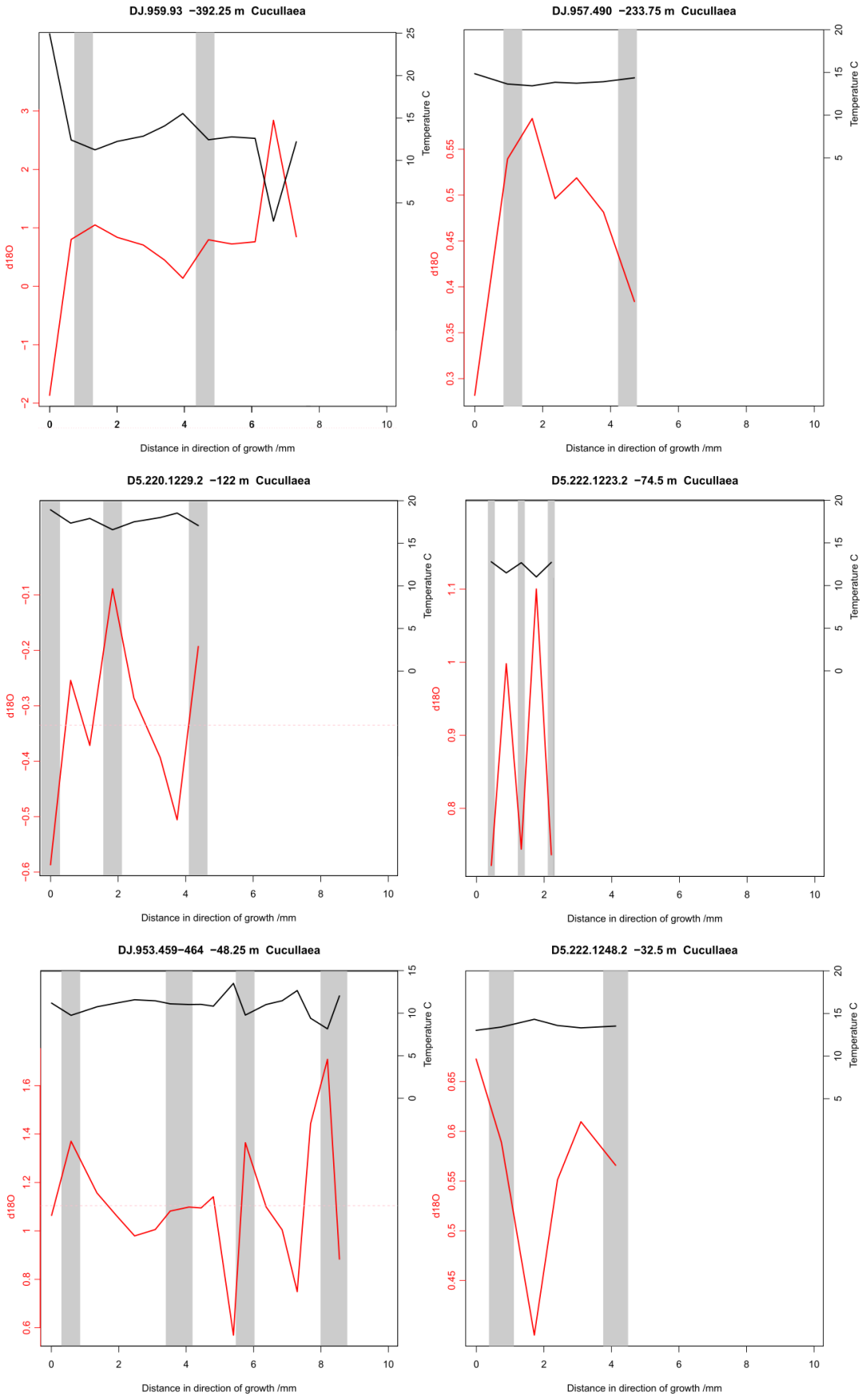

Figure 3.6: δ^{18}**O (red) and approximate converted temperature (black) in López de Bertodano Formation *Cucullaea* labelled with relative height to the K-Pg boundary. Distance axis begins at an arbitrary point within shells. Vertical grey bars locate positions of growth lines.**

All of the specimens in Figures 3.5 and 3.6 were collected from the López de Bertodano formation, however some of the specimens from stratigraphically higher rock units displayed a reversed trend of $\delta^{18}O$ and temperatures. These specimens show the highest relative temperatures during the growth pause, and grow during periods of low temperatures (Figure 3.7).

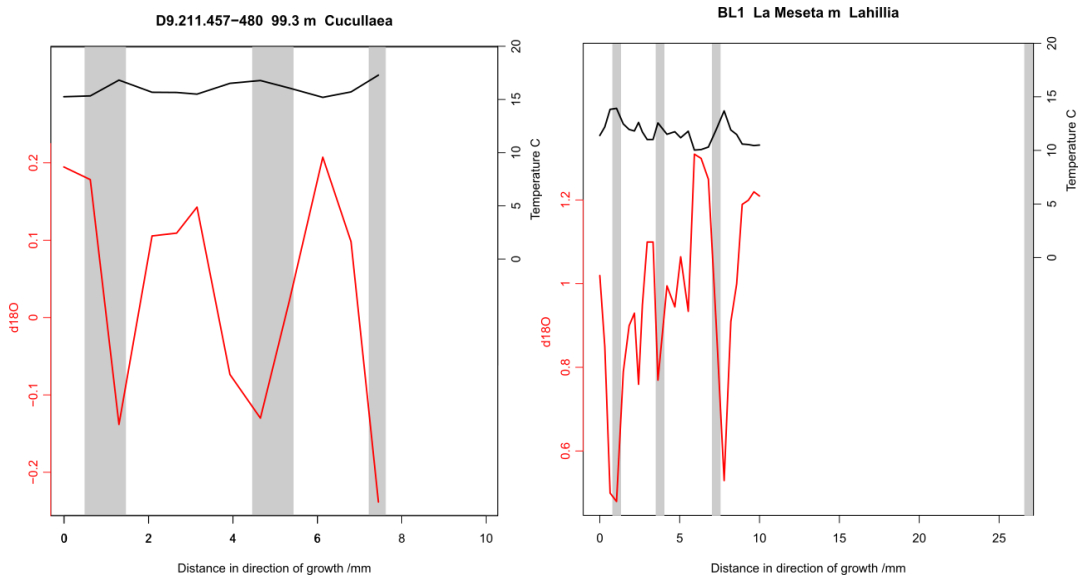

Figure 3.7: $\delta^{18}O$ (red) and approximate converted temperature (black) in specimens of *Cucullaea* from the Sobral Formation (A) and *Lahillia* from the La Meseta Formation (B). Distance axis begins at an arbitrary point within the shell. Vertical grey bars locate positions of growth lines.

3.4.3 Discussion

In species of *Lahillia*, SEM imagery (Figure 2.15) shows visible growth rings of short prisms on the inside and surface of the valve. Stable isotope results (Figure 3.5Figure 3.6) show cuspate trajectories truncated against these shell lines (grey vertical bars). The concave-up shape to the $\delta^{18}O$ data between growth lines in *Lahillia* indicates active shell production throughout the warmer seasons, whereas a more positive $\delta^{18}O$ signal on the growth lines suggests that growth lines incorporate cooler water signals from colder seasons.

The presence of microgrowth rings visible in SEM imagery (Figure 3.4F) suggests that higher resolution (e.g. tidal, daily or lunar cycle related) growth

patterns are also present, which also supports the conclusion that the larger macrogrowth rings are produced with annual cyclicity rather than a shorter period of temperature cyclicity.

Combining results from microstructure and geochemistry strongly suggests that the periodicity of the growth rings is annual, with each growth line representing the pause in shell production in the winter following one cycle of shell growth during the spring and summer. As a result, external growth rings can be used as an indication of shell age in *Lahillia* for the analysis reconstructing growth rates and trajectories in Section 3.5.3.

It appears that internal growth lines in *Cucullaea* are also produced annually, as in *Lahillia*, but because the valve surface is heavily ornamented, it is difficult to discern the annual growth rings from ornaments without destructively sectioning individuals. As a result, only *Lahillia* have been used for growth rate analysis from external growth rings in Section 3.5.3.

Some of the specimens from stratigraphically higher Danian and Eocene rock units displayed a reversed trend of $\delta^{18}O$ and temperatures. These specimens show the highest relative temperatures during the growth pause, and grew during low-temperature portions of the year. This is an interesting trend, as it suggests that the season of growth of bivalves was temperature related. It has also been reported that Seymour Island's Eocene *Cucullaea raea* have a cold-temperature growing season and warm temperature growth pause (Buick & Ivany 2004). It is possible that this may be related to elevated mean-annual temperatures during these times compared to the cooler Maastrichtian and Danian (Figure 2.11).

The season during which bivalves produce this annual growth check shows potential as a temperature indicator; modern day bivalves tend to grow during the summer at the poles and during the winter near the equator, even within the same species at different latitudes along the same coast (Jones & Quitmyer 1996). It is possible this effect is being shown by the species living during the generally warmer Eocene epoch at the same latitude (Buick & Ivany 2004).

3.5 Morphometrics

3.5.1 Methods

Specimens from Seymour Island collections were examined and measured using Vernier callipers to the nearest 0.01mm. All 3 major axes were measured where possible on all specimens (Figure 3.8). The shells of around 30% of these specimens were broken to reveal an internal mould either by taphonomic processes, or through previous destructive geochemical analyses (e.g. Witts et al. 2018). Major axis dimensions of internal moulds were also measured and catalogued separately from the intact specimens. Measurements from internal moulds are not included in data presented in the chapter, but have been presented separately in Appendix B.

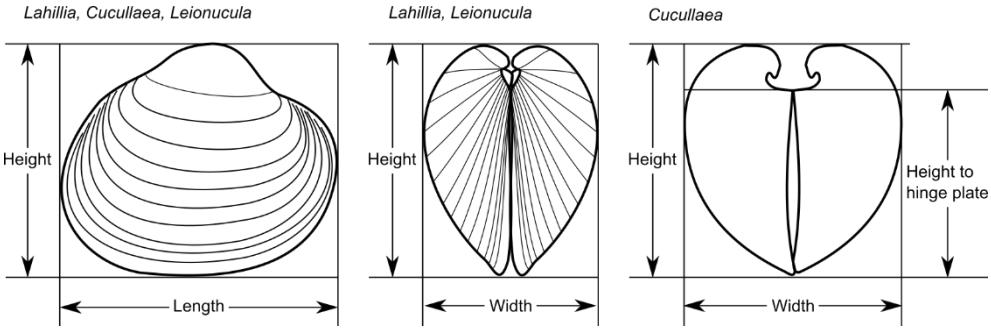

Figure 3.8: Major axis dimensions measured in species of *Lahillia*, *Cucullaea* and *Leionucula*

3.5.2 Results: Ontogeny and Allometry

Major axis dimensions were compiled from over 600 specimens from Seymour Island fossil collections. This data set includes measurements taken by E. M. Harper and J.L.O Hall in 2012 and presented in Hall 2013 (MNatSci dissertation). The collection details and measurements taken for each stratigraphic unit and genus are presented in Appendix B. A census summary of the specimens measured from each stratigraphic unit within each collection is presented in Figure 3.9.

Figure 3.9: Due to the section lines chosen, collections have different numbers of specimens per genus from each stratigraphic interval. Counts for each character may vary within a set as some incomplete specimens were measured.

Bivariate allometry is the analysis of change in shape as size increases and has been used to study morphological measurements from the early 17th century (see Gould 1966 for a review). Bivariate allometry uses the two-parameter allometric equation $y = ax^b$ (Huxley 1932) which is typically rearranged as $\log y = \log a + b \log x$ in order to compute values of b; the ratio of the growth rates of each trait y and x.

In isometric growth, all body parts grow at the same rate and body proportions remain the same throughout the growth of the organism. Therefore, where b=1 where comparing two linear body measurements, and the ratio of two linear measurements remains the same throughout growth. Establishing isometric or near-isometric growth allows the use of one-dimensional measurements of a single character, such as shell length to be used as an indicator of overall shell growth.

Bivariate plots (Figure 3.10) have been used to determine whether the equation $y = ax^b$ is a good fit to linear regression models (ie where b=1). Variance analysis (ANOVA) was used to calculate the R-squared and P values of each of the Maastrichtian and Danian species from the López de Bertodano Formation.

Ontogenetic growth ratios have also been calculated; here shell length (L) has been chosen as the scaling variable and appropriate plots of L against shell height (H) and width (W) have been made to examine change in shell shape over time (Figure 3.10). The change in L/W and L/H ratios with increasing shell length were plotted for individuals from each stratigraphic unit in order to determine whether shell growth was isometric or allometric (Figure 3.11 to Figure 3.13). These ontogenetic plots allow visual trends to be interpreted easily by linear regression analysis; a straight flat line trend (Allometry = 0) shows isometric growth, and a sloped or curved line (Allometry ≠ 0) shows positive or negative growth allometry. These tests also give an indication of whether the specimens examined are likely to be the same or different species across each stratigraphic unit, as the formal taxonomy of some groups is contentious (R. J Whittle, pers. comm. 2015)

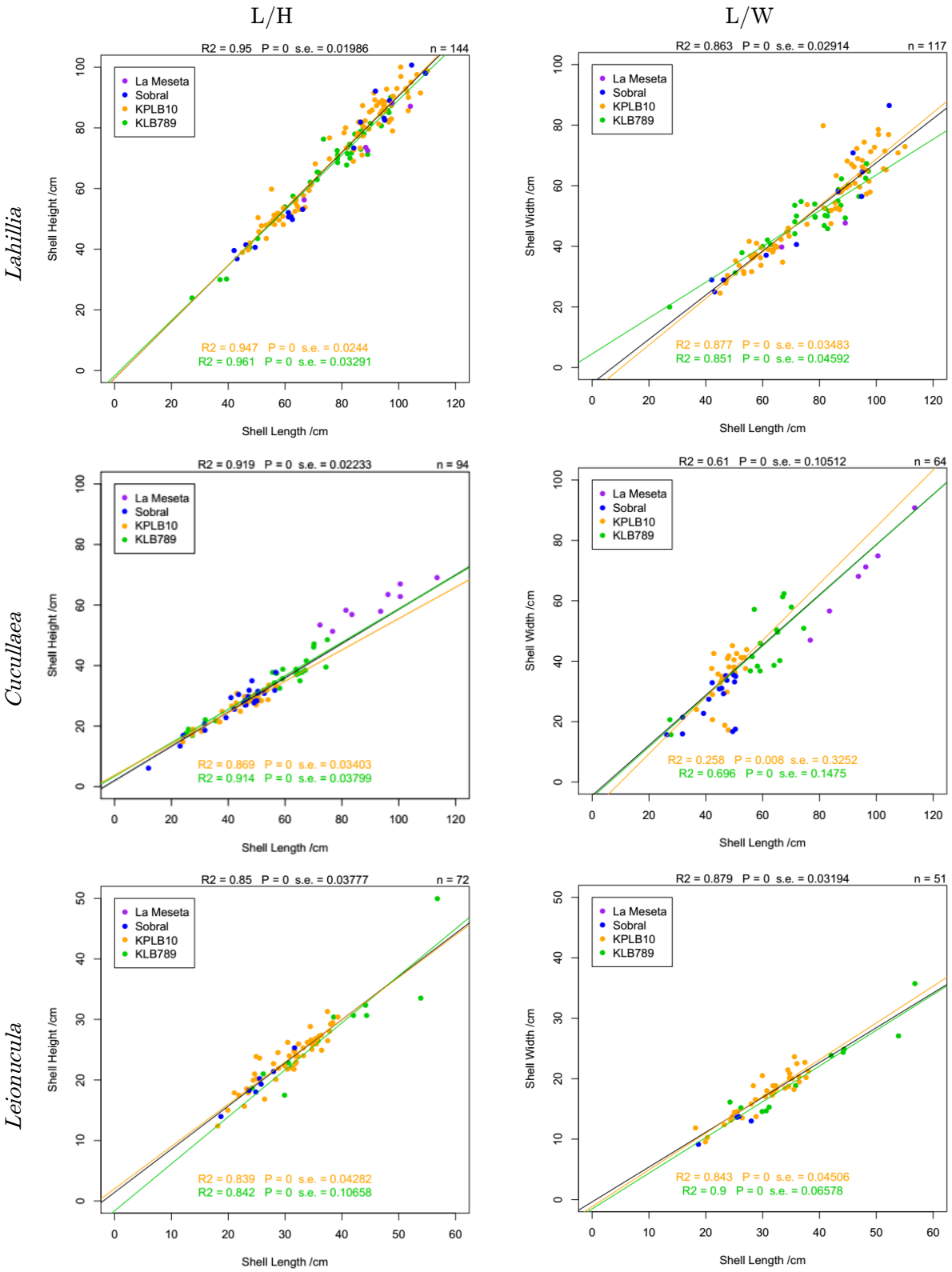

Figure 3.10: Bivariate plots for Length/Width and Length/Height in each genus. Data is colour coded by stratigraphic unit. Trend lines and R-squared values (R2) were calculated by linear regression for all data from the López de Bertodano Formation (black) as well as Maastrichtian and Danian LdB specimens separately (green and orange). P-values (P) and standard error (s.e.) were calculated from ANOVA variance analysis.

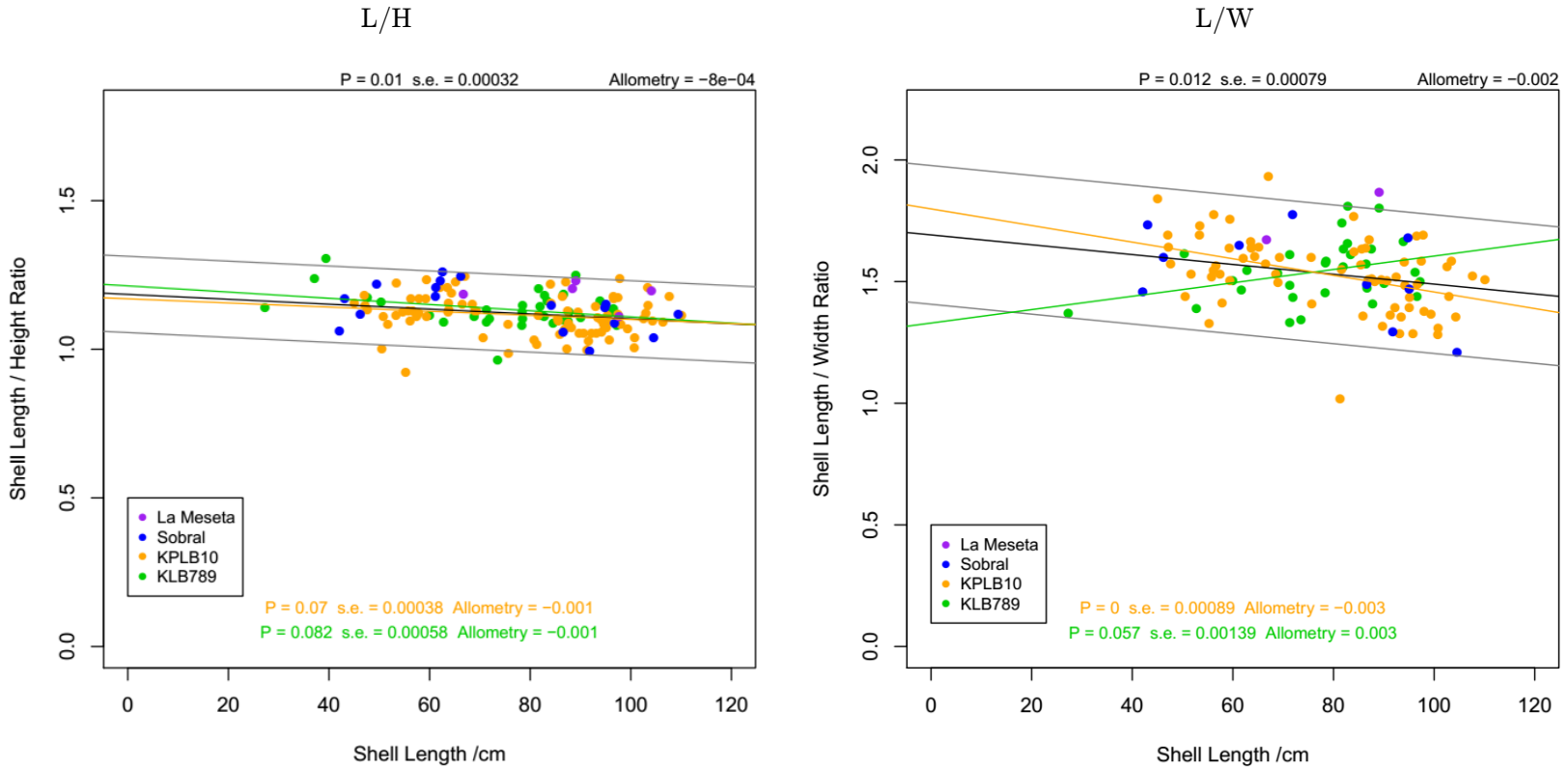

Figure 3.11: ***Lahillia*** **ontogenetic plots of Length/Height and Length/Width against Length coloured by lithostratigraphic unit. Showing number of specimens measured (n) and ontogenetic trend line (black) and 2 standard deviations (grey) from data from the López de Bertodano Formation. Trend for specimens from the Maastrichtian López de Bertodano Formation (green) and Danian López de Bertodano Formation (yellow) are also presented for comparison; trend lines for L/H against L are close to horizontal and have similar trends, trend lines for L/W against L are different although the data plots in a similar location.**

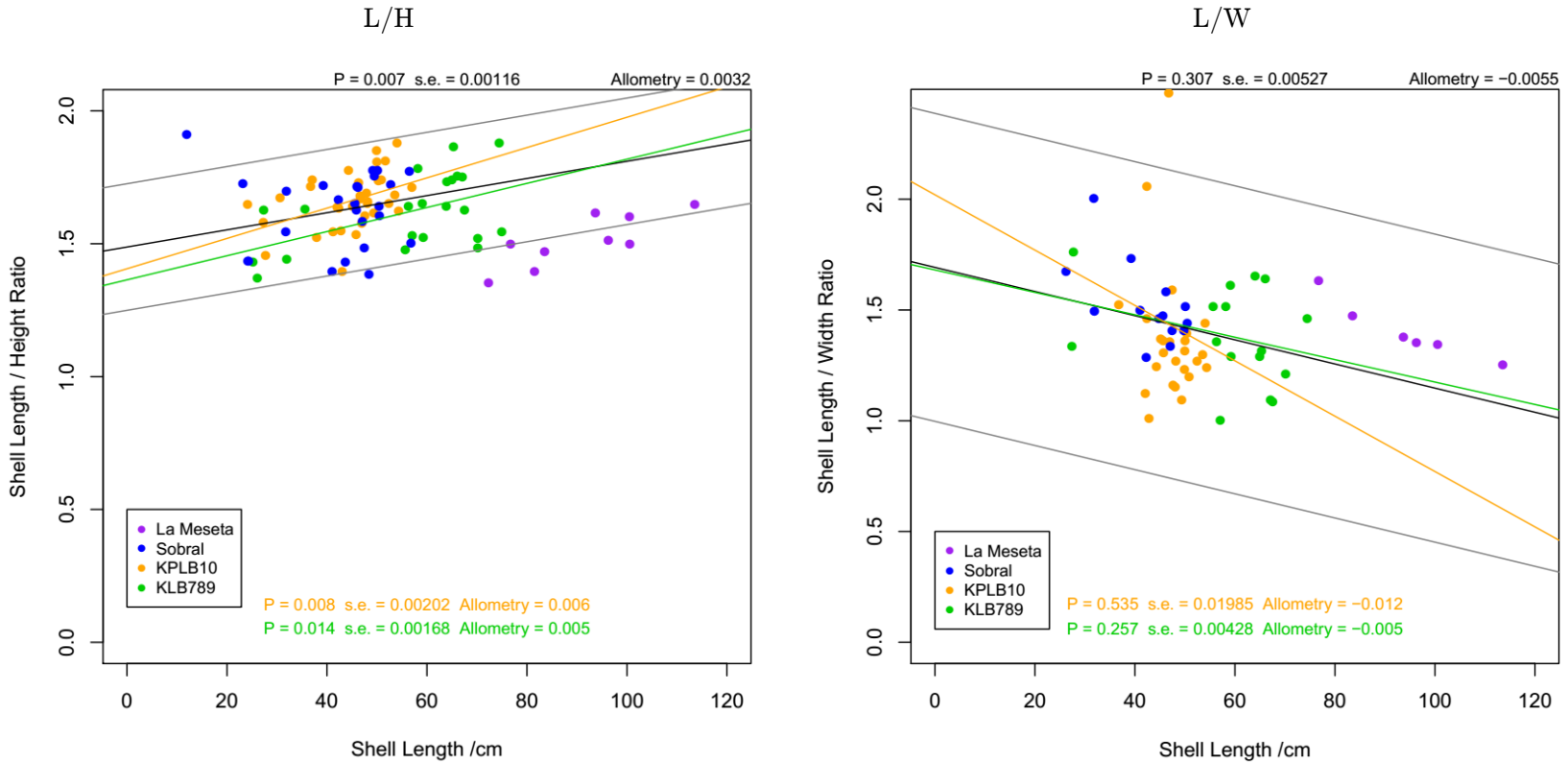

Figure 3.12: ***Cucullaea*** **ontogenetic plots of Length/Height and Length/Width against Length coloured by lithostratigraphic unit. Showing number of specimens measured (n) and ontogenetic trend line for all data points (black) and 3 standard deviations (grey) from data from the López de Bertodano Formation. Trend for specimens from the Maastrichtian López de Bertodano Formation (green) and Danian López de Bertodano Formation (yellow) are also presented for comparison. These trend lines in L/H and L/W have clear slopes and plot with slightly different trends.**

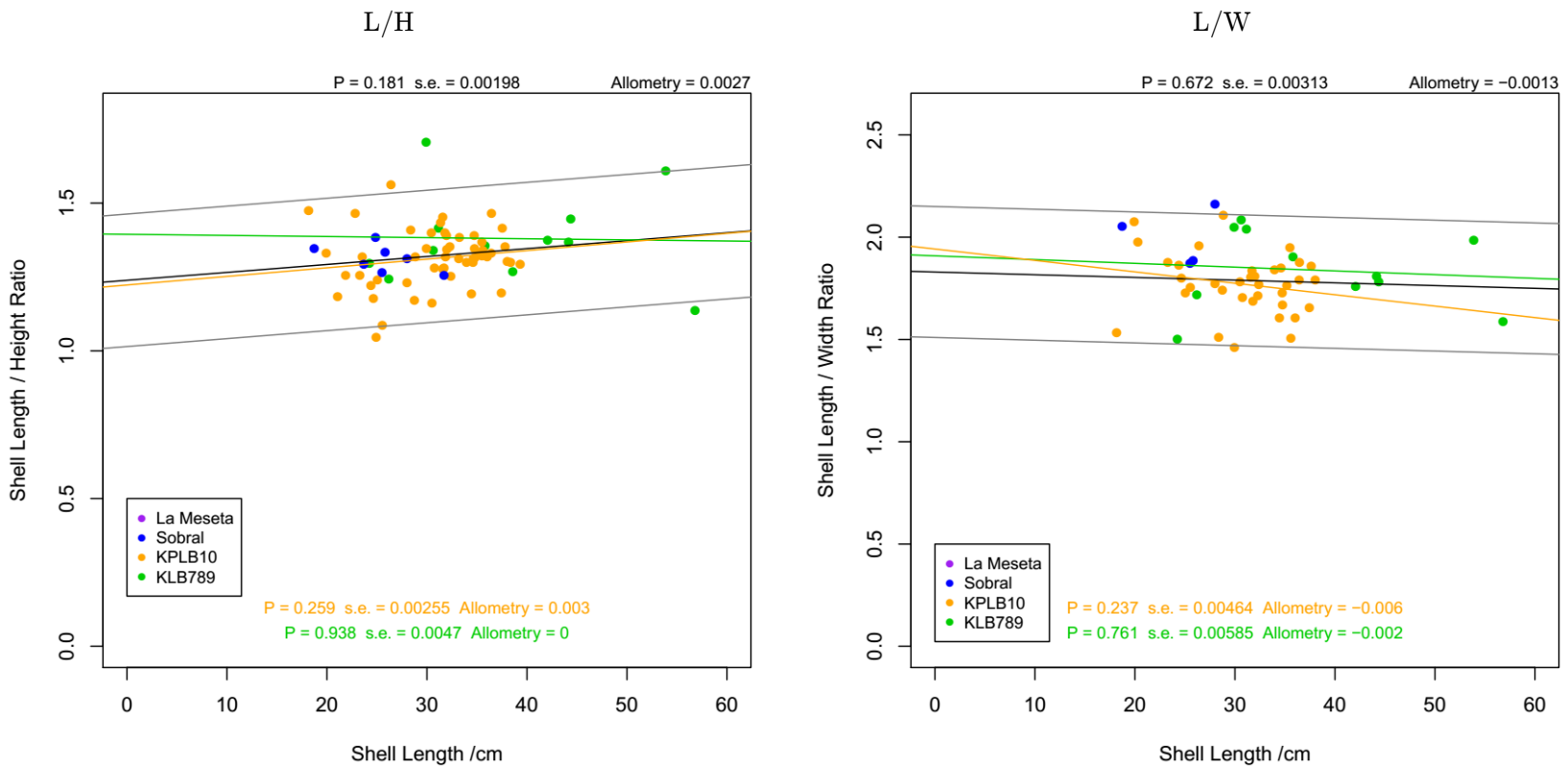

Figure 3.13: ***Leionucula*** **ontogenetic plots of Length/Height and Length/Width against Length coloured by lithostratigraphic unit. Showing number of specimens measured (n) and ontogenetic trend line for all data points (black) and 3 standard deviations (grey) from data from the López de Bertodano Formation. Trend for specimens from the Maastrichtian López de Bertodano Formation (green) and Danian López de Bertodano Formation (yellow) are also presented for comparison; these trend lines are close to horizontal and have similar trends. No specimens of** ***Leionucula*** **from the La Meseta Formation were measured.**

Linear regression was used to calculate the values of b in each plot, while variance analysis (ANOVA) was used to calculate the R-squared and P values of each of the Maastrichtian and Danian species from the López de Bertodano Formation.

In order to confirm whether the change in shell dimension ratios obtained by linear regressions were significantly different from the isometric value, a T-test at a 95% confidence level was used to test the null hypothesis of isometric growth (gradient = 0) according to methods in Sokal & Rohlf (1987). The results of this analysis are presented in Table 3.1.

Table 3.1: Isometry tests for bivalve specimens from the López de Bertodano Formation

	Length/Height		Length/Width	
	gradient	Relationship (T-Test)	gradient	Relationship (T-Test)
Lahillia				
Combined Maastrichtian and Danian Species	-0.002	**Allometric**	-0.001	Isometric
Maastrichtian *L. larseni/ huberi*	-0.001	**Allometric**	-0.003	**Allometric**
Danian *L. larseni/ huberi*	-0.001	**Allometric**	0.003	**Allometric**
Cucullaea				
Combined Maastrichtian and Danian Species	0.003	**Allometric**	-0.006	Isometric
Maastrichtian *C. antarctica*	0.006	**Allometric**	-0.012	Isometric
Danian *C. ellioti*	0.005	**Allometric**	-0.005	Isometric
Leionucula				
Combined Maastrichtian and Danian Species	0.003	Isometric	0.001	Isometric
Maastrichtian *L. suboblongata*	0.003	Isometric	-0.006	Isometric
Danian *L. suboblongata/ hunickeni*	-0.001	Isometric	-0.002	Isometric

3.5.3 Discussion: Ontogeny and Allometry

The results from the bivariate and ontogenetic ratio plots allow patterns of isometric or allometric growth to be determined in each species of bivalve. From the analysis of ontogenetic ratios, only *Leionucula* showed statistically significant isometric growth, although values of b are very close to isometric in several species. However, due to the limited numbers of fossil specimens compared to modern studies, P-values are all reasonably high which suggests these results are not definitive.

Direct bivariate comparisons do have reasonably good R-squared correlations, with all species except for Danian *Cucullaea ellioti* having $R^2 \geq 0.8$. This is consistent with previous assertions that fossils have retained an undeformed three-dimensional shape in the rock (Tobin et al. 2012).

Specimens of *Lahillia* from the López de Bertodano Formation plot with slightly different trends in shell width across the K-Pg boundary (Figure 3.10), with specimens in the Danian tending to grow wider for the same height than Maastrichtian specimens of the same species (*Lahillia larseni*). Specimens of *Lahillia* from the Sobral Formation plot within the same range of shell geometry as the Maastrichtian and Danian *Lahillia* (Figure 3.11), this supports the proposal that the *Lahillia larseni* described from the López de Bertodano Formation, and the *Lahillia huberi* described from the Sobral Formation may be the same species (R. J Whittle, pers. comm. 2015).

For specimens of *Cucullaea* (Figure 3.12), the species distinction is far clearer than in *Lahillia*. Both *Cucullaea antarctica* from the Maastrichtian and *Cucullaea elliotti* from the Danian López de Bertodano and Sobral Formations show allometric growth in both shell L/H and L/W ratios, and appear to plot with different trends, which supports the differentiation of the two species. Eocene *Cucullaea raea* plot at a larger size than each of the previous species and with a different shell length to height allometry.

Leionucula (Figure 3.13) consist of a single species; *L. suboblongata* from the Maastrichtian to the Danian, with the addition of a co-existing species; *L. hunickeni* in the Sobral Formation. *Leionucula* from all stratigraphic intervals show clear isometric growth, with near-flat trend lines produced for L/H and L/W ratios against length. Little to no change was found between the

morphology of Maastrichtian and Danian specimens from the López de Bertodano Formation, however Maastrichtian specimens appeared to reach larger body sizes. This will be discussed further in Section 3.5.4.

3.5.4 Results: Size changes through stratigraphy

As isometric growth could only reliably be established in species of *Leionucula* (Section 3.5.3), all major axes must be examined as indicators of overall shell growth in the other species (Figure 3.14). However, change in shell major axis ratios was found to be sufficiently small that no immature specimens needed to be removed from analysis of size change through stratigraphy. Average and maximum shell dimensions in each species and collection are presented in Figure 3.14. A comparison of the maximum shell size is considered to be more meaningful than average size where populations are unable to be sampled equally (Ridgway et al. 2011).

As the trends for each dimension are similar in each collection, for the remainder of this analysis specimens from measured collections have been combined using the stratigraphic correlation detailed in Section 2.6. Box plots have been constructed using size data from each 50 m stratigraphic interval as described in Figure 2.13 in order to show the change in size and distribution through stratigraphy (Figure 3.15 to Figure 3.17)

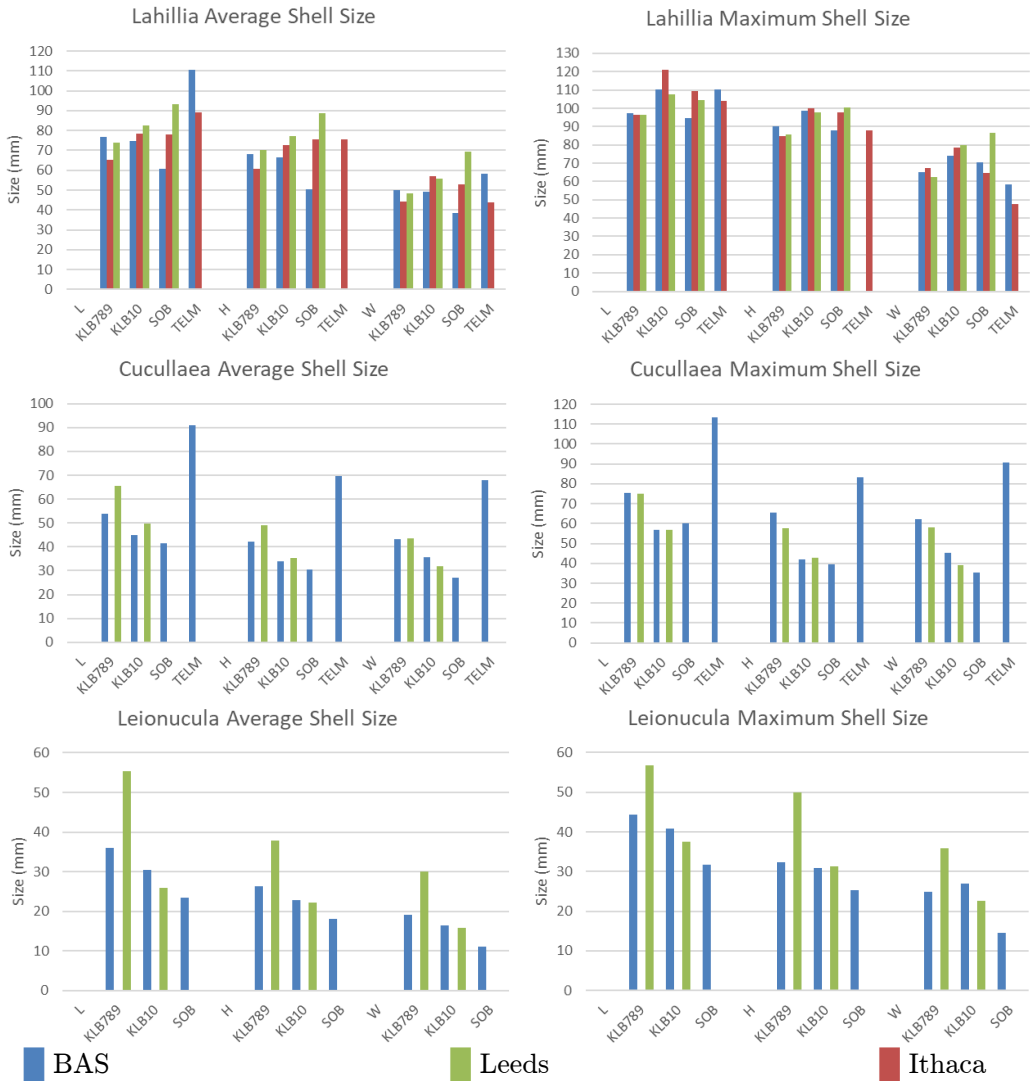

Figure 3.14: Plots of average and maximum shell dimensions measured from each genus coloured by collection (key at base) plotted by lithostratigraphic unit (labelled along x axis). The trends are very similar by collection, which indicates that combining these data sets will not introduce additional bias. Maximum size is a better metric than average size where populations cannot be sampled equally (see text for discussion). Size trends through stratigraphy are discussed further in Section 3.5.5.

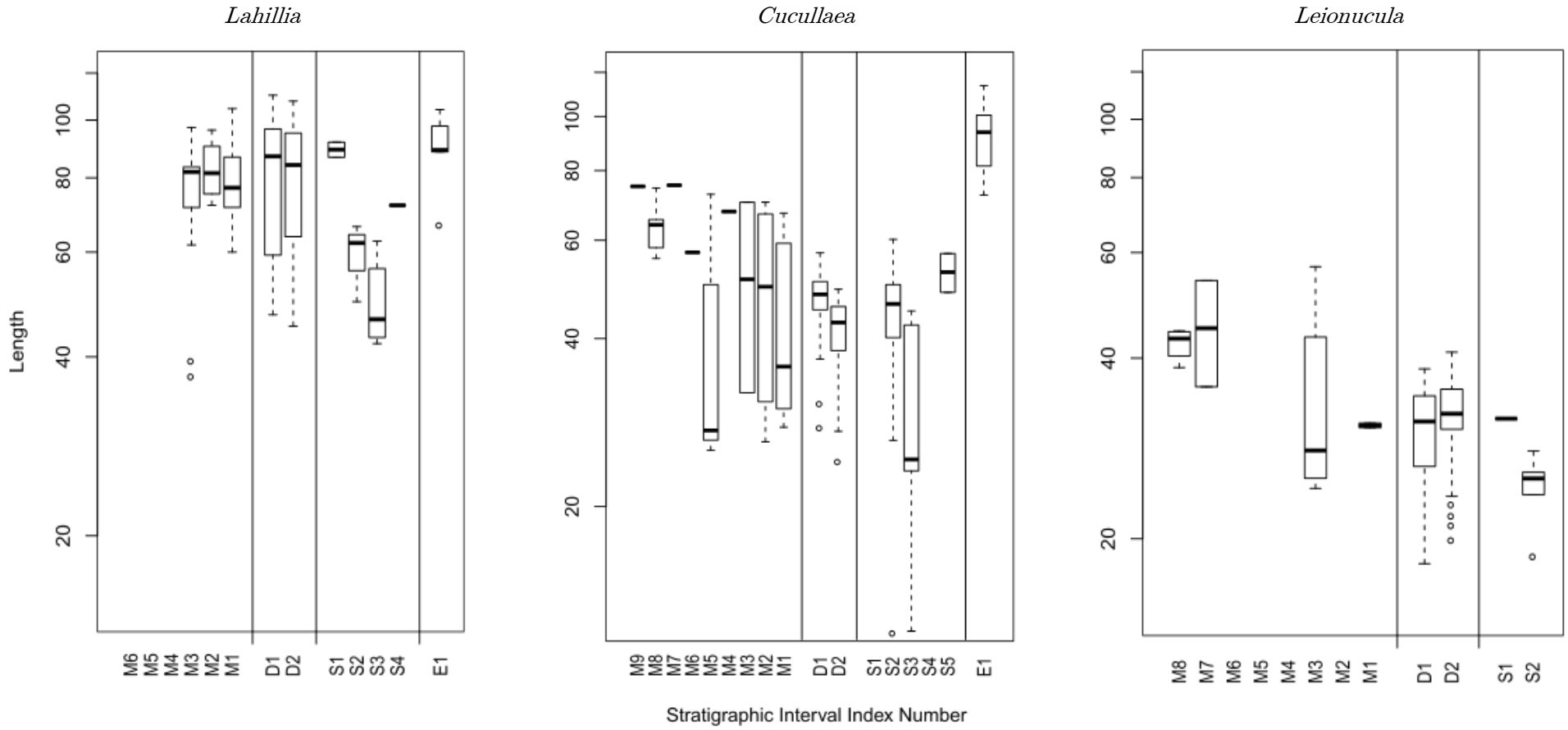

Figure 3.15: External shell length of bivalves within each stratigraphic interval. Left: *Lahillia*; centre: *Cucullaea*; right: *Leionucula*. M1-M9: Maastrichtian López de Bertodano Formation; D1-D2: Danian López de Bertodano Formation; S1-S5: Sobral Formation; E1: La Meseta Formation

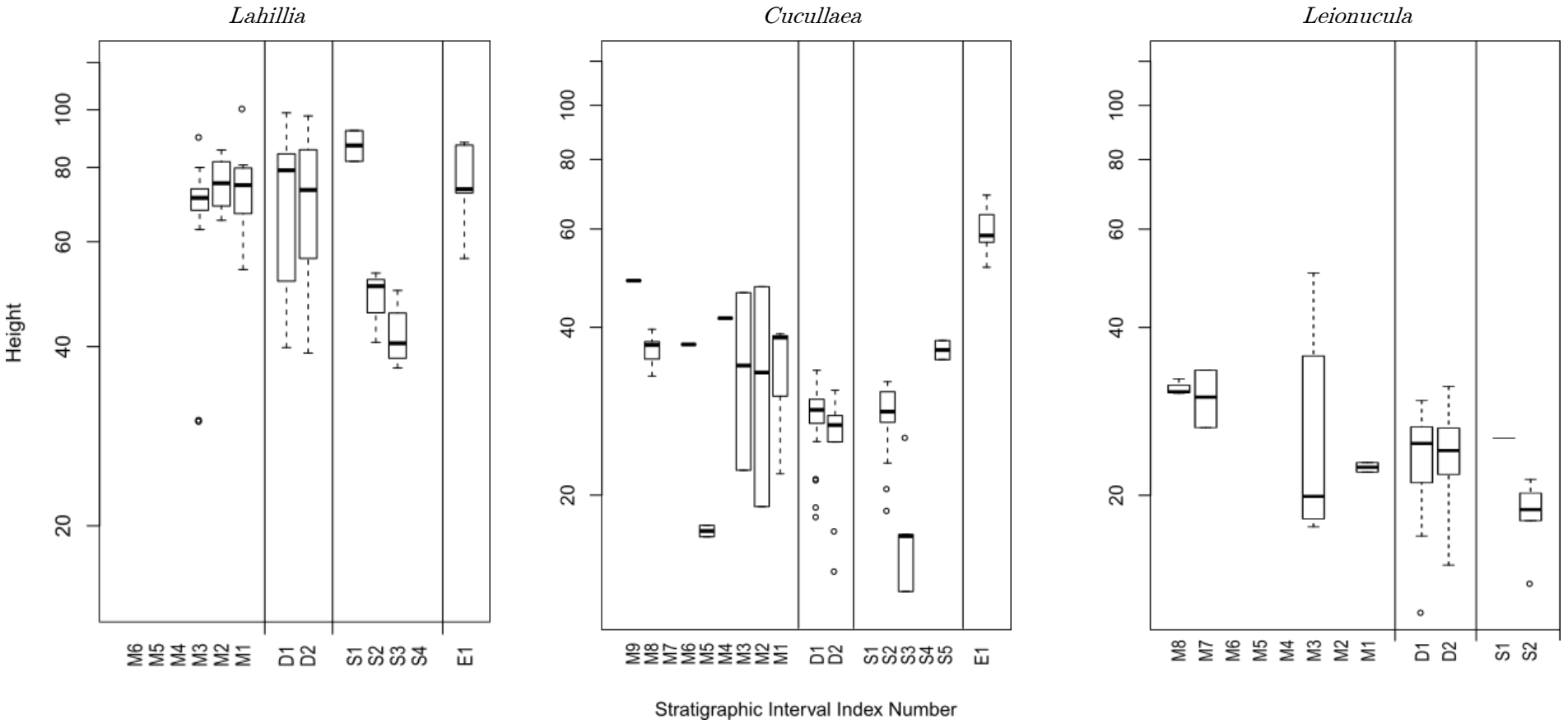

Figure 3.16: External shell height of bivalves within each stratigraphic interval. Left: *Lahillia*; centre: *Cucullaea*; right: *Leionucula*. M1-M9: Maastrichtian López de Bertodano Formation; D1-D2: Danian López de Bertodano Formation; S1-S5: Sobral Formation; E1: La Meseta Formation

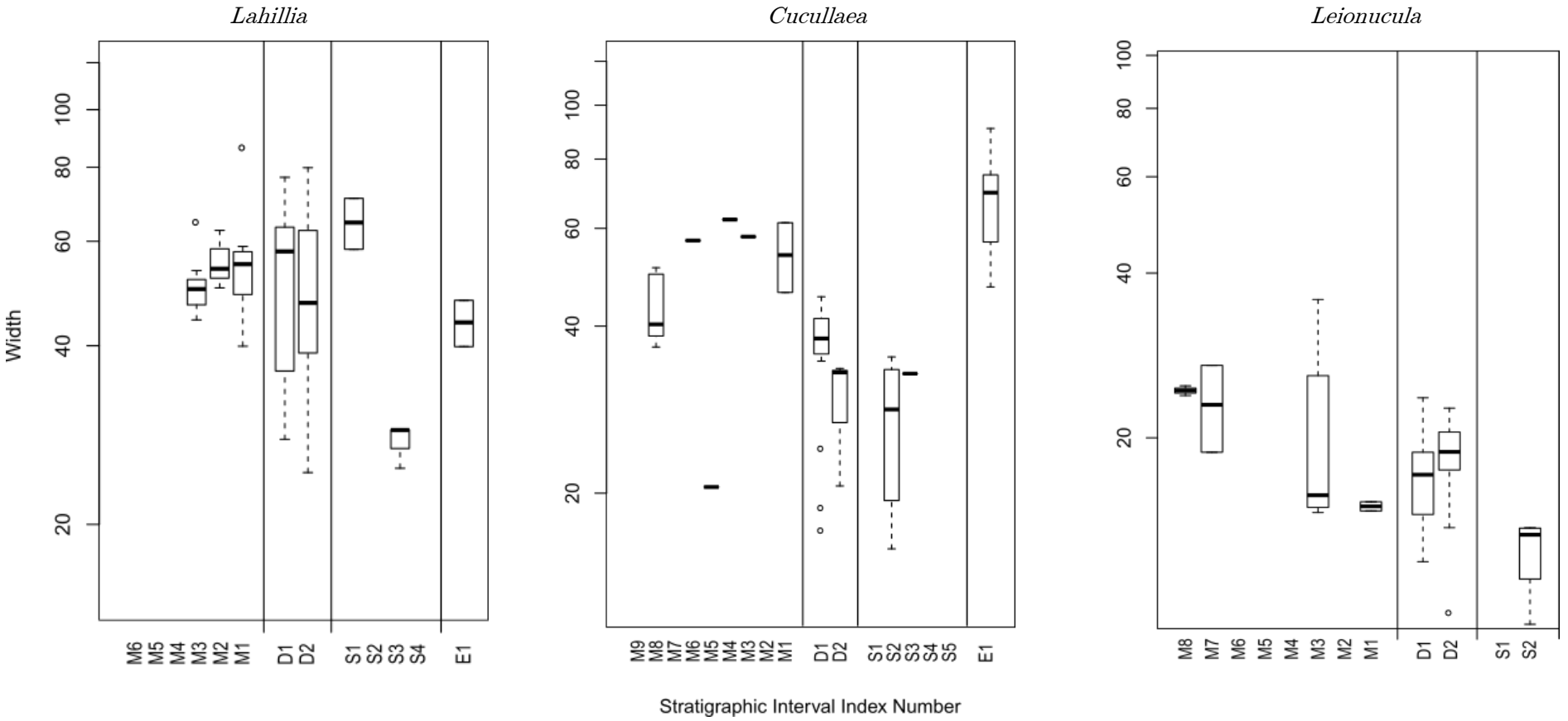

Figure 3.17: External shell width of bivalves within each stratigraphic interval. Left: *Lahillia*; centre: *Cucullaea*; right: *Leionucula*. M1-M9: Maastrichtian López de Bertodano Formation; D1-D2: Danian López de Bertodano Formation; S1-S5: Sobral Formation; E1: La Meseta Formation

3.5.5 Discussion: Size Changes Through Stratigraphy

The similarity of the trends for the change in major axis dimensions within each species supports the observations made in Section 3.5.3 that shell morphometry is fairly consistent throughout the López de Bertodano Formation.

In all species, the main change in maximum shell size is at the K-Pg boundary. In *Lahillia*, the maximum size increases from the Maastrichtian to the Danian, whereas in *Cucullaea* and *Leionucula* the maximum shell size decreases. A change in the width of the interquartile range shown by a change in box size also indicates a change in the distribution of shell sizes at the K-Pg boundary. This will be discussed further in Section 3.7.2

In addition, in all species the smallest specimens tend to be found in the middle to upper levels of the Sobral Formation. This could reflect the shallowing of water in the Sobral Formation compared to the López de Bertodano Formation. Modern marine bivalves can show a marked reduction in maximum size, growth rate and longevity when living in shallower waters (Jones et al 1978), although these specimens of *Spisula solidissima* were found in much shallower waters than the bivalves examined here (15-28m vs 50-200m) and a depth/growth relationship has not been firmly established from studies of other species (e.g. Antsulevich et al. 1999).

During the Eocene, the *Lahillia wilckensi* grew to slightly smaller sizes than the *Lahillia larseni* of the Maastrichtian and Danian López de Bertodano Formation, whereas Eocene *Cucullaea raea* grew to much larger sizes than either the Maastrichtian *Cucullaea antarctica* or Danian *Cucullaea ellioti*. Interestingly, *Lahillia* became extinct from Antarctic faunas during the Eocene, whereas species of *Cucullaea* are still extant (Huber 2010).

Cucullaea size decreases dramatically during interval M5 (between approximately 760 and 810m in stratigraphy). This interval is before the earliest known occurrence of *Lahillia* in the section, and during a period from 630 to 850m in stratigraphy where *Leionucula* occurrence was also extremely limited, so it is not possible to determine the cause of this size decrease. The maximum shell size during this interval remains similar to the rest of the Maastrichtian, so it is possible the low average size may be due to collection of

younger individuals. Other species of bivalve remained abundant throughout this interval (Witts et al. 2016).

3.6 Growth Rates and Longevity

3.6.1 Methods

In Section 3.4 the external and internal growth lines of *Lahillia* and *Cucullaea* were determined to have been produced with annual periodicity. This means that the number and spacing of growth lines can be measured to reconstruct age-at-size histories throughout each specimen's life. In order to do this, major external growth lines were measured using a combination of tiled scaled photographs taken perpendicular to the shell surface and calliper measurements (Valentine et al. 2011). Only *Lahillia* were used for this analysis due to the shell surface ornamentation which obscured the location of true growth lines in specimens of *Cucullaea*.

In addition, *Lahillia* specimens possessing an intact cardinal tooth (Figure 3.3) but incomplete shell were sectioned for study of internal shell growth lines. Acetate peels and thin sections were used to examine sectioned teeth under optical microscopy, details of tooth preparation are given in Appendix B. The tooth was used rather than the valve section because the growth lines are most condensed and easiest to visualise. The hinge and tooth are grown under maximum environmental shielding so are less susceptible to abrasion and removal of juvenile shell layers. The tooth is also less likely to record environmental noise than the valve, where several modern species are known to produce extra growth lines during times of environmental stress, as a result of interaction between the periostracum and secreting mantle lobe (e.g. Lutz & Rhoads 1980; Thompson et al. 1980; Ropes 1984).

In order to determine the age vs size growth curves for these specimens, the distance between successive external growth lines were plotted against total shell size, and internal growth lines were plotted against tooth size. Von Bertalanffy growth functions (von Bertalanffy 1938) were fitted to this data using least squares regression analysis. The von Bertalanffy function (see Section 3.6.3) gives a growth parameter (k) which represents the rate at which

growth rate changes over the course of an organism's lifespan. This growth parameter was then compared in specimens before and after the mass extinction. Some authors have reported issues when applying this function to long-lived organisms with indeterminate as opposed to determinate growth, such as several species of bivalves. These issues will be discussed in Section 3.7.3.

3.6.2 Results

Growth trajectories were constructed from 18 whole-shell *Lahillia* (Figure 3.18) and 22 sectioned hinge-teeth (Figure 3.19). These were distributed fairly evenly between specimens from the Maastrichtian (López de Bertodano Formation) and Danian (López de Bertodano and Sobral Formation) and each Age has been plotted on a separate graph. These trends were used to calculate growth functions (Section 3.6.3) in order to compare the trends in the pre-and post-extinction data sets.

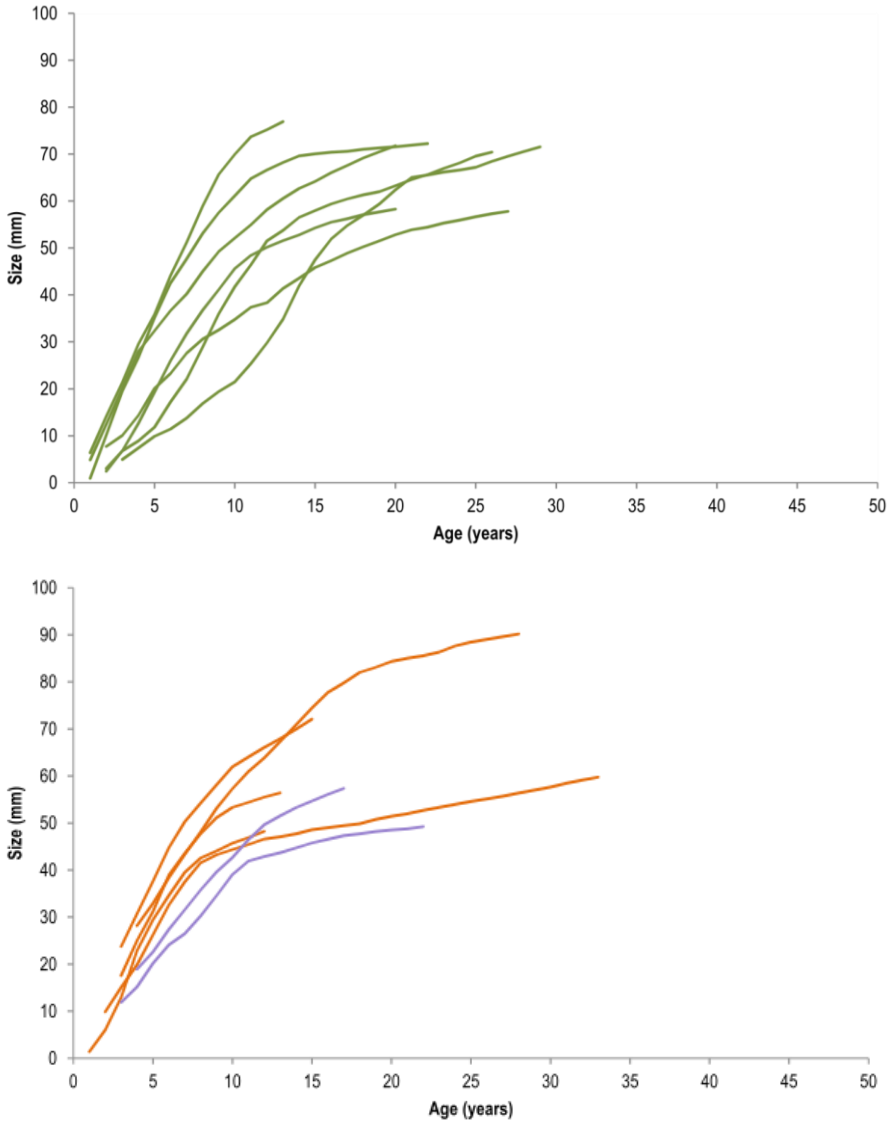

Figure 3.18: Growth trajectories for *Lahillia* valves in Maastrichtian (green), Danian López de Berdotano (orange) and Sobral Formation specimens (purple) showing size at age data determined from visible shell growth lines

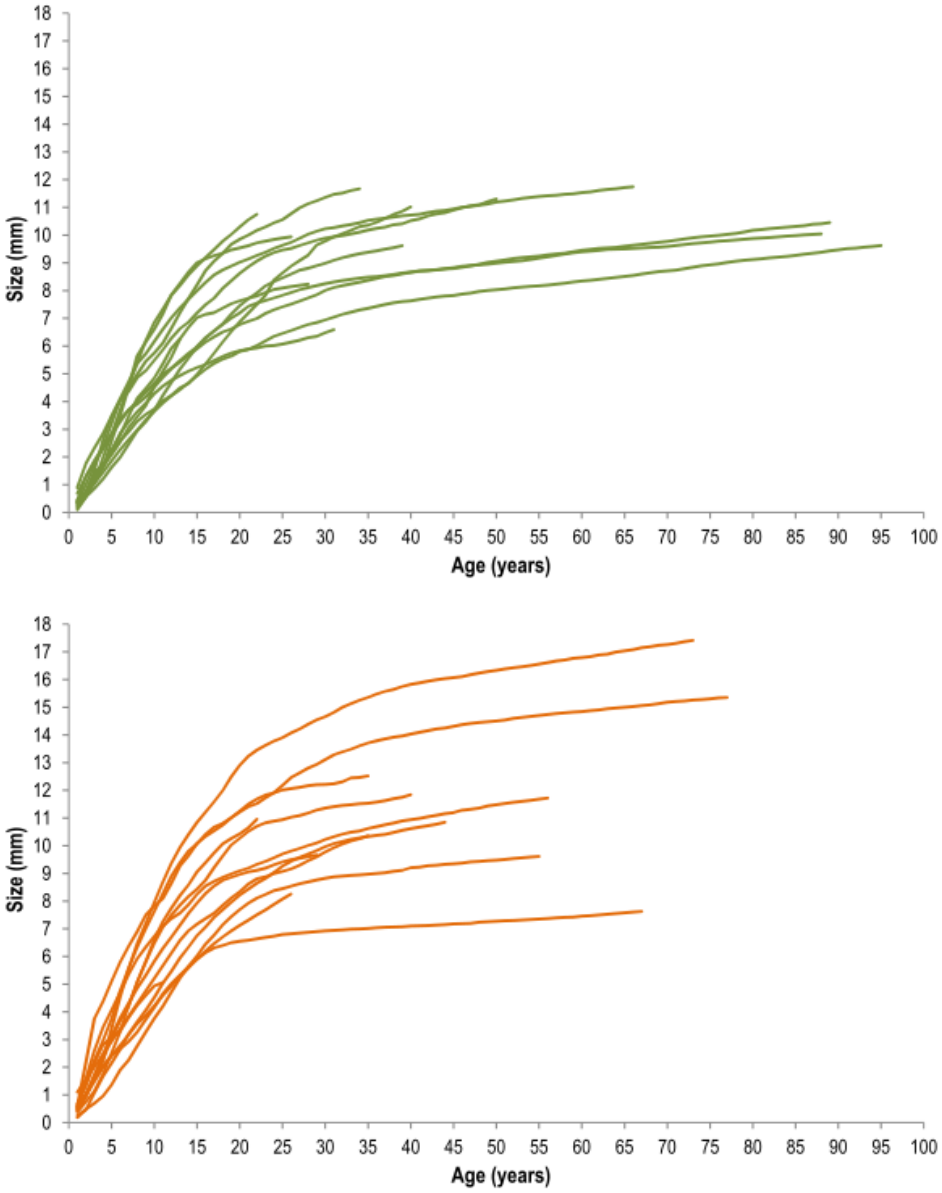

Figure 3.19: Growth trajectories for sectioned *Lahillia* hinge teeth. in Maastrichtian (green), Danian López de Berdotano (orange) and Sobral Formation specimens (purple) showing size at age data determined from visible internal growth lines

3.6.3 Discussion

These size-at-age curves can be used to calculate growth functions, which are equations used to parametrically describe the growth of organisms and compare the growth parameters. The "von Bertalanffy Growth Function" (VBGF) (von Bertalanffy 1938) and variations based on this function have been commonly used to fit growth patterns in bivalves and other organisms and is widely used among fisheries science, due to the ease of its use, and the clear biological interpretability of its parameters, which are described below.

$$L_t = L_{max}\,(1 - e^{-kt})$$

The equation relates the length at time t (L_t) to a theoretical maximum length (L_{max}) and the constant k; a one-dimensional description of the rate at which the organism reaches L_{max} in units of years^{-1}. k values can be used as a way of comparing growth characteristics of populations and allows for comparison of growth measurements in the hinge plate as well as whole shell sizes.

A nonlinear least squares regression model was used to fit this function to the above growth trajectories (Figure 3.18 and Figure 3.19) and generate values of L, k and t for each *Lahillia* specimen. The results from whole shells and teeth from each side of the K-Pg boundary have been compiled in Figure 3.20. Data from each regression model are available in Appendix B.

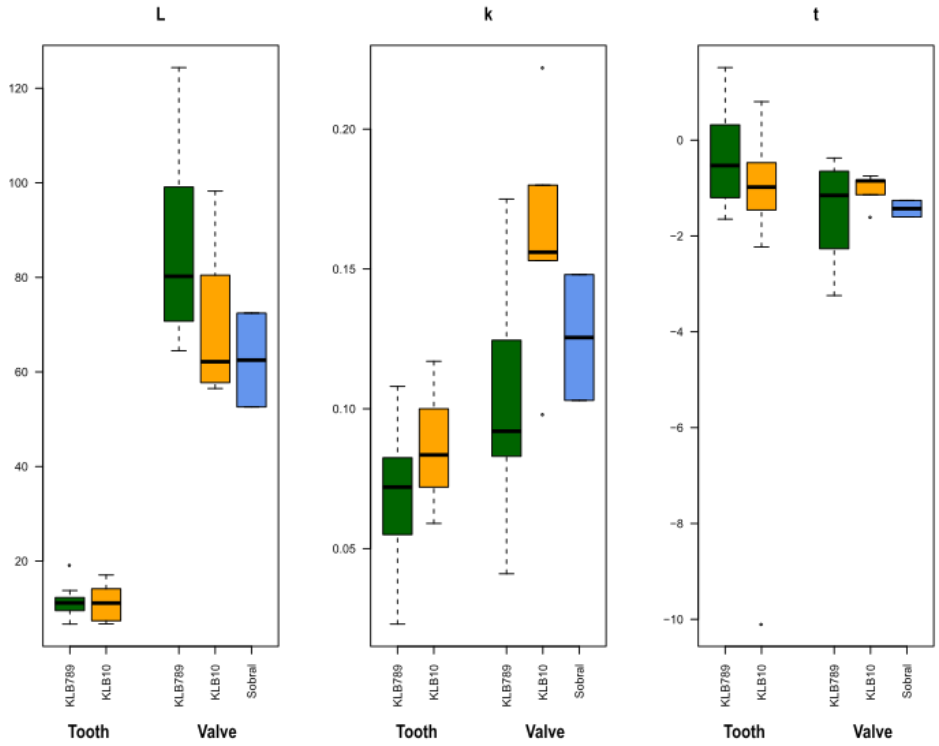

Figure 3.20: Box plots of growth parameters derived from the von Bertalanffy growth function in *Lahillia* from the Maastrichtian López de Berdotano Formation (green) Danian López de Berdotano Formation (yellow) and Sobral Formation (blue). Data produced from hinge teeth and valves over the K-Pg mass extinction interval.

Growth functions are not typically calculated from hinge teeth, but were produced here in order to examine whether the trends were consistent between the valve and the tooth due to the limited numbers able to be examined of each. Size trends are not likely to be reliable in hinge teeth, as in many cases broken or isolated hinges were used and were likely to have come from a mixture of left and right valves which tend to produce different sized teeth. The growth rate (k) increases in both teeth and whole shells across the K-Pg boundary, while t shows no significant change across the boundary. As only two shells from the Sobral Formation were sampled it is difficult to infer trends, however it appears that behaviour was similar to Maastrichtian *Lahillia*.

3.7 Discussion

3.7.1 Morphometric Changes at the K-Pg Boundary

Morphometric data from specimens of *Lahillia*, *Cucullaea* and *Leionucula* from the Maastrichtian Units 7, 8 and 9 of the López de Bertodano Formation have been compared to specimens from the Danian Unit 10 in order to look for changes in shape or size that may have been caused by ecological stress or restructuring across the boundary. *Lahillia larseni* and *Leionucula suboblongata* survive the boundary, whereas Maastrichtian *Cucullaea* antarctica are replaced by *Cucullaea elliotti* during the Danian. Summary figures of this data are presented in Figure 3.21 to Figure 3.23 with the full numerical data presented in Appendix B.

These pairwise analysis plots have been constructed to compare each major axis dimension with every other dimension and represent the change in each dimension in pre- and post- K-Pg faunas. The types of plots include bivariate plots of each pair of major axes, as used in section 3.5.2, the correlation coefficient (R^2 value) for each analysis, frequency curves of size data for each trait in pre- and post- extinction faunas, combined box plots for each dimension and histograms showing the count of each size category and relative proportions of specimens examined overall.

Morphometric data is conventionally examined in log-transformed format, however in these specimens it did not improve the coefficients of fit. This is likely to be due to the close to isometric growth in all genera (ie where b = 1 in the equation $y = ax^b$, no log transformation is required to fit a straight line with slope a).

These plots highlight the difference in size and size distribution in each species of bivalve across the K-Pg boundary. The range of sizes recorded by each species at the K-Pg boundary is different and does not appear to follow any consistent trend across the three genera analysed.

Figure 3.21: ***Lahillia*** **pairwise comparisons of specimen morphology and size distribution from the between pre- and post- extinction López de Bertodano Formation specimens.**

This summary figure uses different plot types to compare corresponding Length (L), width (W), height (H) and frequency data. Each sub-plot compares the relationship between two sets of variables in both the Maastrichtian (green) and the Danian (orange). The pairs used for each grid-wise comparison are listed on the top and right-hand size axis. Size measurements are in mm and frequency measurements in count with corresponding scales along the left and bottom axes of the figure.

Pairwise morphometric comparisons (e.g. L against H) have been previously presented in Figure 3.10 and the corresponding pair (e.g. H against L) shows the correlation coefficient for the comparison. Graphs along the diagonal show frequency distribution of each character, bottom row and right column shows frequency distribution and the bottom right plot represents the total number of specimens examined from KLB789 vs KPLB10.

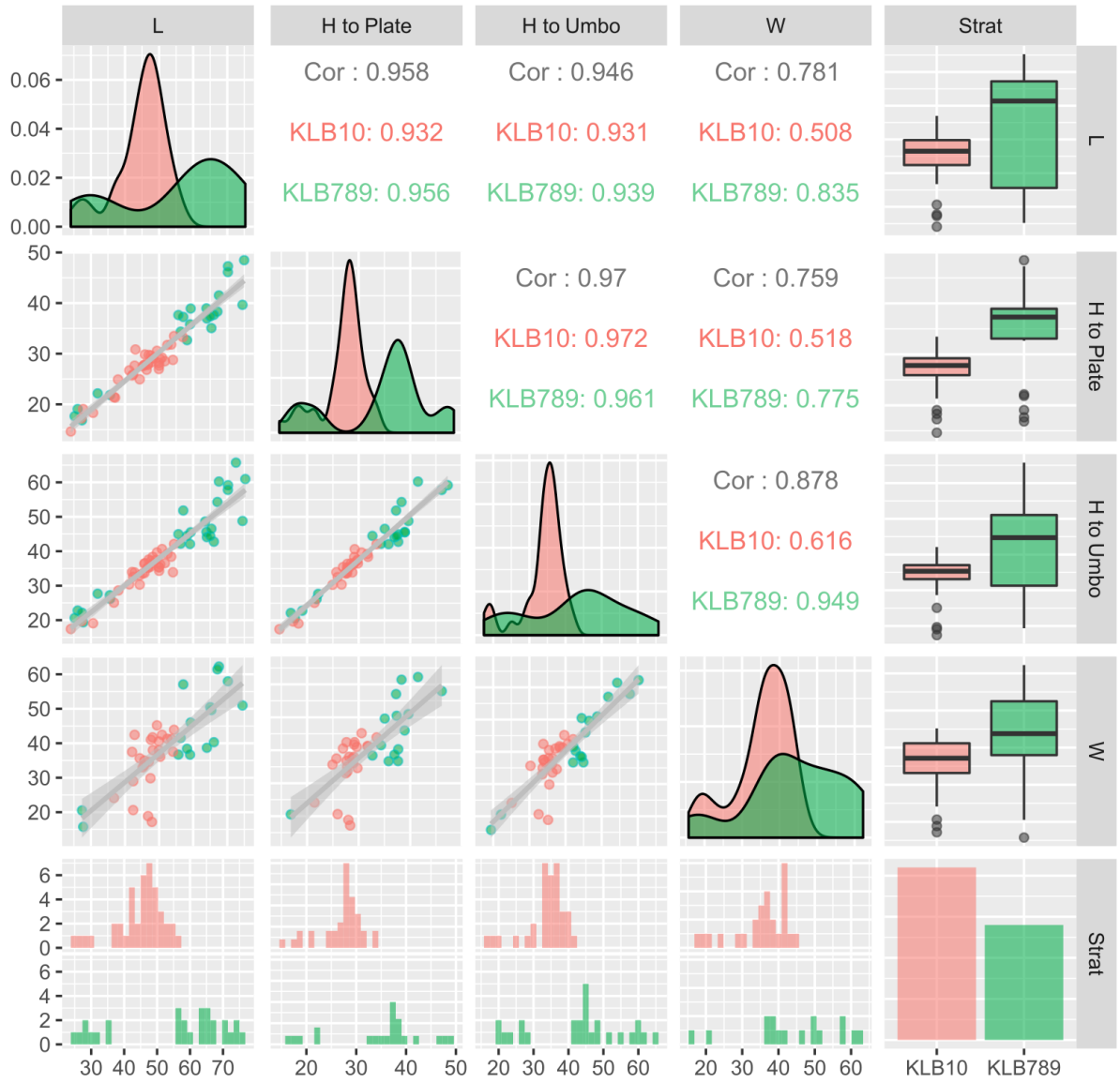

Figure 3.22: ***Cucullaea*** **pairwise comparisons of specimen morphology and size distribution from the between pre- and post- extinction López de Bertodano Formation specimens.**

This summary figure uses different plot types to compare corresponding Length (L), width (W), height (H) and frequency data. Each sub-plot compares the relationship between two sets of variables in both the Maastrichtian (green) and the Danian (orange). The pairs used for each grid-wise comparison are listed on the top and right-hand size axis. Size measurements are in mm and frequency measurements in count with corresponding scales along the left and bottom axes of the figure.

Pairwise morphometric comparisons (e.g. L against H) have been previously presented in Figure 3.10 and the corresponding pair (e.g. H against L) shows the correlation coefficient for the comparison. Graphs along the diagonal show frequency distribution of each character, bottom row and right column shows frequency distribution and the bottom right plot represents the total number of specimens examined from KLB789 vs KPLB10.

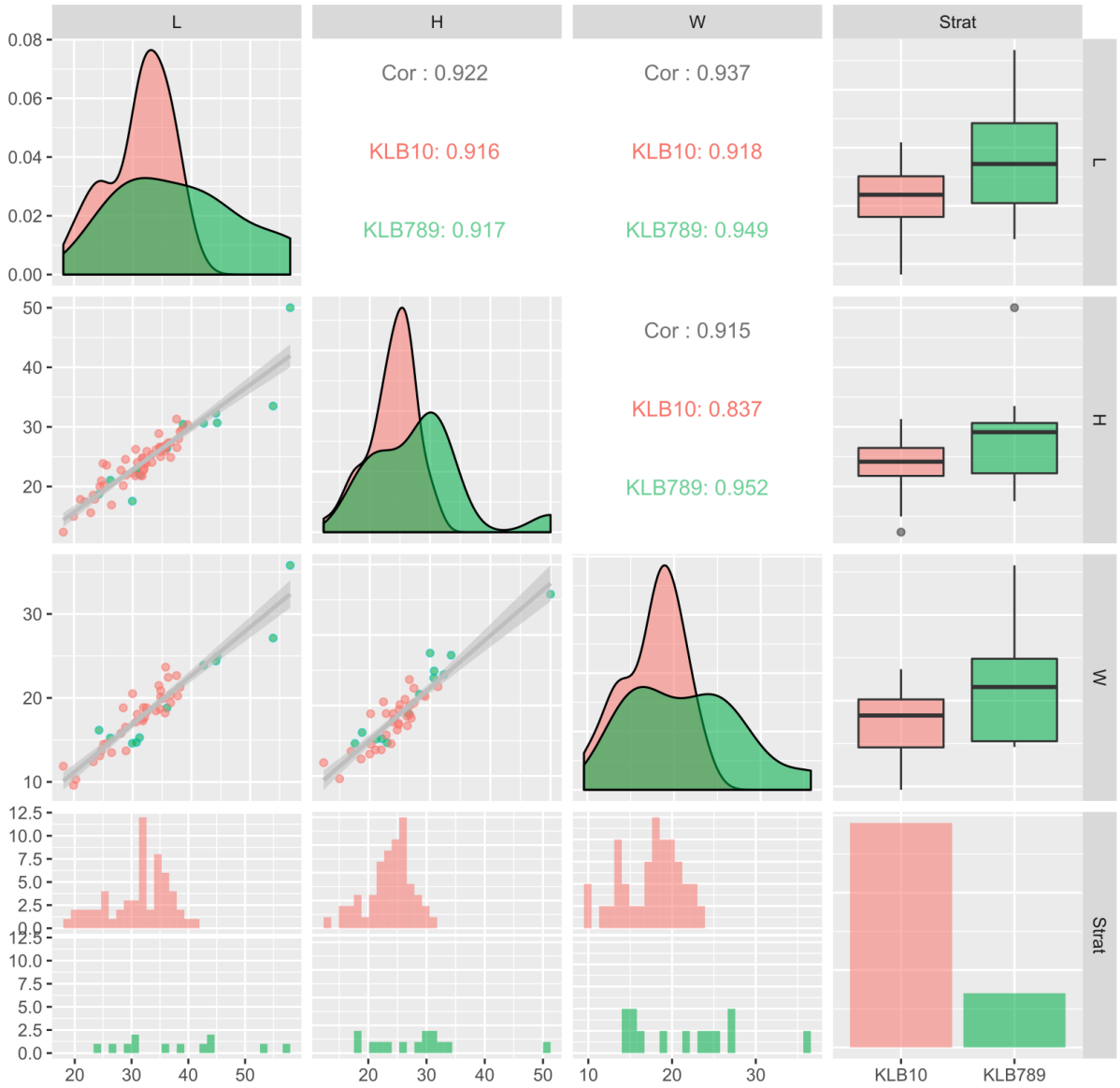

Figure 3.23: ***Leionucula*** **pairwise comparisons of specimen morphology and size distribution from the between pre- and post- extinction López de Bertodano Formation specimens.**

This summary figure uses different plot types to compare corresponding Length (L), width (W), height (H) and frequency data. Each sub-plot compares the relationship between two sets of variables in both the Maastrichtian (green) and the Danian (orange). The pairs used for each grid-wise comparison are listed on the top and right-hand size axis. Size measurements are in mm and frequency measurements in count with corresponding scales along the left and bottom axes of the figure.

Pairwise morphometric comparisons (e.g. L against H) have been previously presented in Figure 3.10 and the corresponding pair (e.g. H against L) shows the correlation coefficient for the comparison. Graphs along the diagonal show frequency distribution of each character, bottom row and right column shows frequency distribution and the bottom right plot represents the total number of specimens examined from KLB789 vs KPLB10.

Table 3.2: Welch's t-test results comparing major axis dimensions in shells from the Cretaceous and Paleogene López de Bertodano Formation. This test is to investigate whether the difference in box plots along the right-hand columns of Figure 3.21-Figure 3.23 are likely to have been produced by statistically different distributions at the 95% confidence level

Species	Dimension	Mean Size (mm)		Welch's t-test Coefficients			95% Significant difference in means
		K	Pg	t	degrees of freedom	p-value	
Lahillia	Length	73.80	79.62	1.70	75.22	0.093	N
	Height	68.01	72.89	1.84	97.41	0.069	N
	Width	50.05	54.02	2.17	159.11	0.031	**Y**
Cucullaea	Length	55.19	44.84	-3.00	33.71	0.005	**Y**
	Height	34.62	27.01	-3.61	26.45	0.001	**Y**
	Width	44.02	35.19	-2.41	21.29	0.025	**Y**
Leionucula	Length	38.16	31.15	-2.26	12.29	0.043	**Y**
	Height	28.17	23.69	-1.99	14.72	0.065	N
	Width	21.53	17.51	-2.13	14.67	0.051	N

Size change in marine bivalves through the Seymour Island K-Pg boundary section was originally investigated in order to determine whether any significant size changes were observable that may have been associated with environmental fluctuations in the latest Maastrichtian or ecosystem-level changes across the mass extinction event itself.

The results of this morphometric study do not show agreement with the Lilliput hypothesis, which predicts significant within-lineage size decrease across the K–Pg boundary. Of the three taxa studied here, the size change was only found to be significant in *Cucullaea*, which change species across the boundary. Whereas of the two species which survive the boundary, in *Leionucula*, the size decrease was only statistically significant in one axis; and in *Lahillia* a significant size increase was found in shell width. The potential for environmental and climate changes across the K-Pg boundary to have influenced size changes in the Seymour Island section will be discussed in greater detail in Chapter 7.

3.7.2 Size Distribution Changes at the K-Pg Boundary

The difference in interquartile ranges of shell dimensions across the Cretaceous-Paleogene boundary in both *Lahillia* and *Cucullaea* is extremely pronounced (Figure 3.15). It is possible that this broader distribution might be influenced by the larger number of specimens from the Danian part of the López de Bertodano Formation collected than Maastrichtian part (130 individuals vs 62), producing a broader range. However, the opposite trend is present in the *Cucullaea* examined; with a broader size range during the Maastrichtian and a far narrower size range during the post-extinction López de Bertodano Formation, even though more Danian *Cucullaea* were also measured (43 vs 32)

The Kolmogorov–Smirnov test, Hartigans' diptest and Shapiro-Wilkes test were used to numerically test the morphometric measurement data from each specimen and age bracket (Maastrichtian López de Bertodano Formation, Danian López de Bertodano Formation, Sobral Formation and Eocene La Meseta Formation) for either bimodality or unimodality. Results and interpretations of these tests are presented in Table 3.3 and Table 3.4.

Table 3.3: P-Value from Shapiro Wilk Test for Normality. Bold values indicate shell length data are not likely to be from a normally distributed population

	KLB789	KPLB10	Sobral	La Meseta
Lahillia	**0.011**	**0.000**	0.181	0.509
Cucullaea	**0.001**	**0.003**	**0.007**	0.802
Leionucula	0.546	**0.022**	0.827	NA

Table 3.4: HDS Value from Hartigan's Dip Test for Bimodality. Bold values indicate shell length data show significant bimodality

	KLB789	KPLB10	Sobral	La Meseta
Lahillia	0.672	**0.014**	0.762	0.554
Cucullaea	**0.038**	0.988	0.956	0.462
Leionucula	0.561	0.485	0.990	NA

Multimodal finite-mixture models were used to produce a graphical and numerical interpretation of the size data by modelling the observed frequency distribution as a mixture of two normally-distributed data sets (Scrucca et al. 2016). The comparison of the original frequency distribution with the modelled normal distributions. This approach is commonly used in biological populations to allow comparison of means in populations where the data is not normally distributed (e.g. Woods et al. 2012).

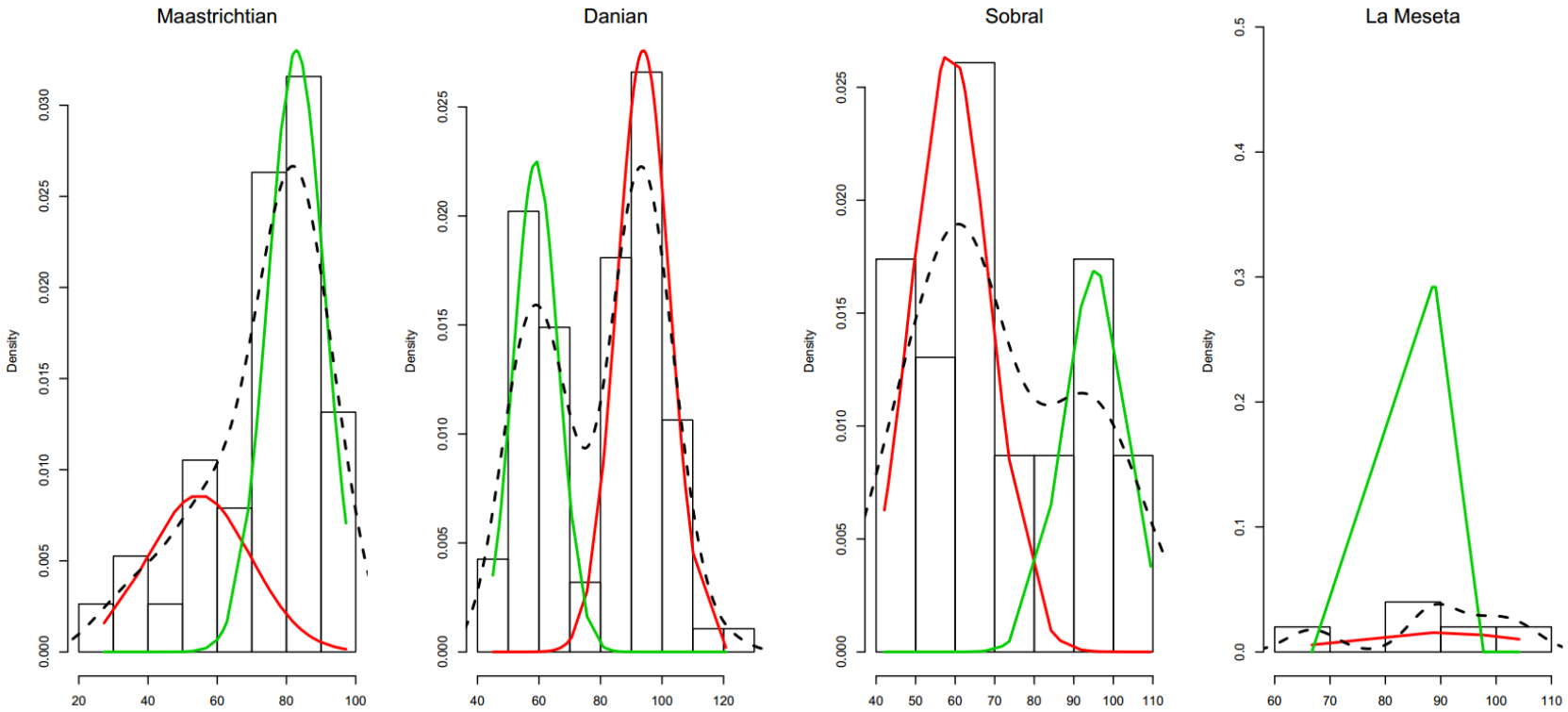

Figure 3.24: ***Lahillia*** **Multimodal finite mixture models for external shell length. Histograms represent the size data split into size categories 10mm wide. The black dashed line represents the size frequency distribution constructed from the discrete data and the red and green curves represent the two modelled normal distributions which best combine to fit the black dashed curve. The colouring of each curve is arbitrary and is just to visually distinguish the two normal distributions. Hartigan's dip test identified** ***Lahillia*** **from the Danian López de Bertodano Formation as significantly bimodal, this test confirms that the bimodality fits an even mixture of two normal distributions with equal numbers of specimens clustered around means at 50-60 mm and 90-100 mm.**

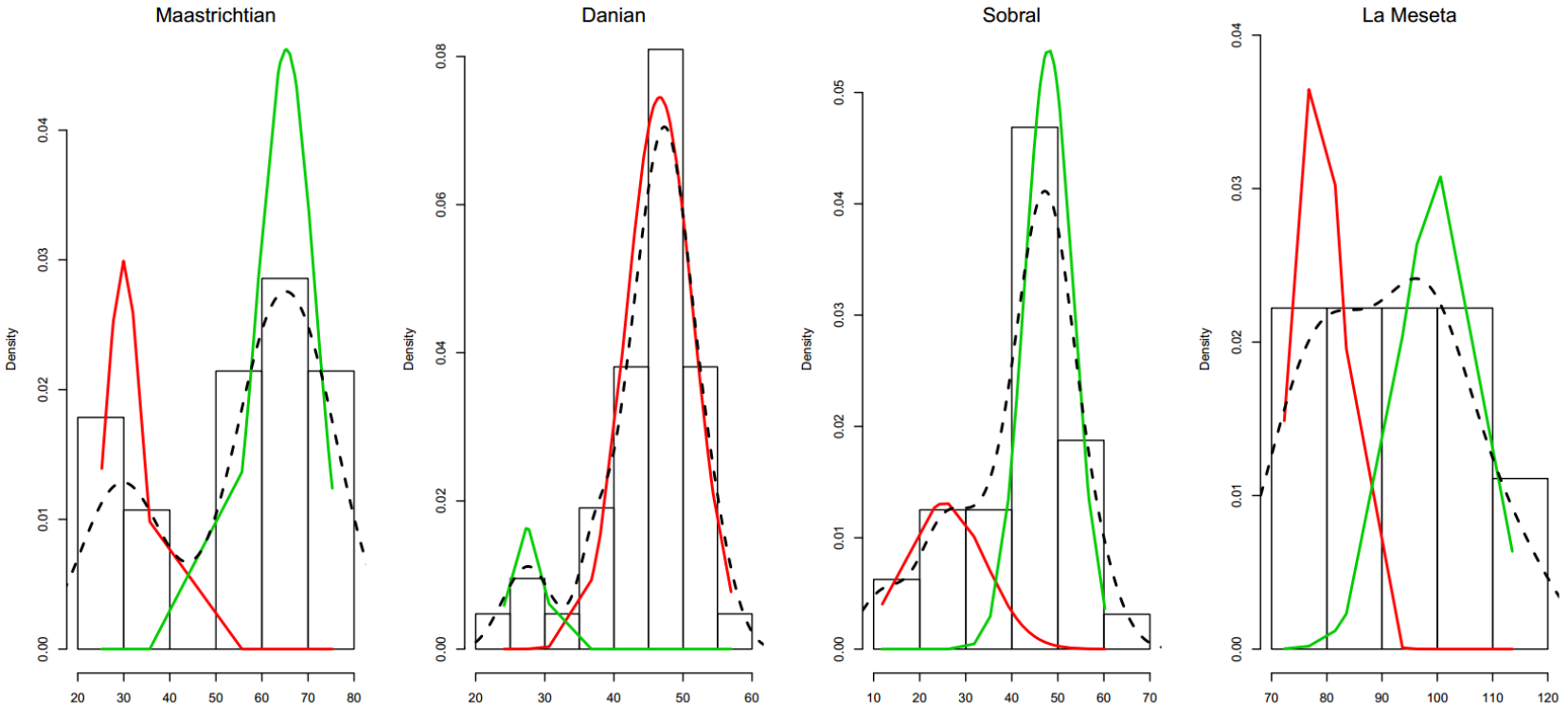

Figure 3.25: ***Cucullaea*** **Multimodal finite mixture models for external shell length. Histograms represent the size data split into size categories 10mm wide. The black dashed line represents the size frequency distribution constructed from the discrete data and the red and green curves represent the two modelled normal distributions which best combine to fit the black dashed curve. The colouring of each curve is arbitrary and is just to visually distinguish the two normal distributions. Hartigan's dip test identified** ***Cucullaea*** **from the Maastrichtian López de Bertodano Formation as significantly bimodal, this test confirms that the bimodality fits a dual-peaked distribution clustered around means of 30 mm and 60-70 mm.**

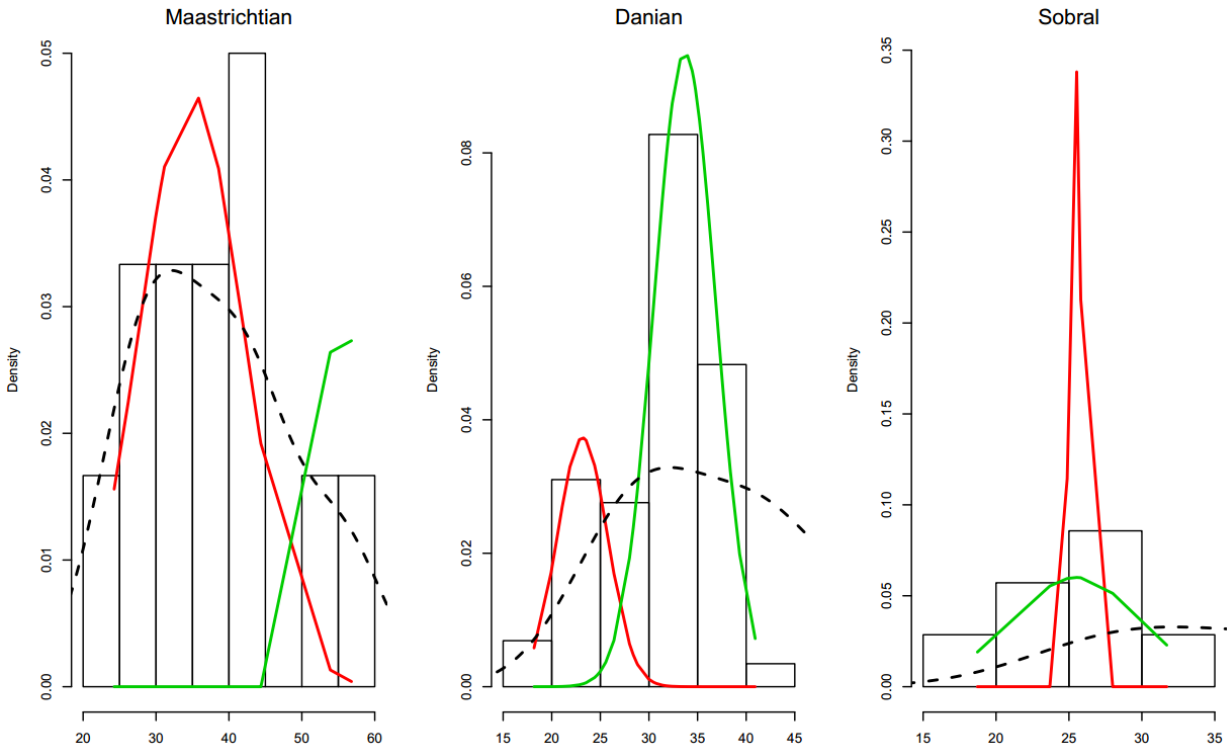

Figure 3.26: ***Leionucula*** **Multimodal finite mixture models for external shell length. Histograms represent the size data split into size categories 10mm wide. The black dashed line represents the size frequency distribution constructed from the discrete data and the red and green curves represent the two modelled normal distributions which best combine to fit the black dashed curve. The colouring of each curve is arbitrary and is just to visually distinguish the two normal distributions. No significant bimodality was found by the Hartigan's dip test and on the whole, size ranges best fit a single peaked distribution.**

Lahillia show an increase in mean shell length and maximum shell size across the K-Pg boundary, with maximum shell sizes increasing from 97.3 to 120.8 mm. There is also an increase in the range of shell sizes collected and the population appears to shift from a single-peaked distribution in the Maastrichtian with a dominant mean shell length of 80-90 mm to a roughly even mix of 2 similar distributions during the Danian, with equal numbers of specimens clustered around means at 50-60 mm and 90-100 mm. By the time of the Sobral, this size distribution becomes dominated by the smaller size individuals, with a dominant mean at 60-70mm and a minor component of larger sized individuals. Shell sizes of Eocene *Lahillia wilckensi* are similar to the larger Danian specimens.

In *Cucullaea* there is little change in mean shell size across the boundary, however almost the opposite trend to *Lahillia* is observed in the size distribution. The size range decreases at the boundary, changing from a dual-peaked distribution in the Maastrichtian clustered around means of 30 mm and 60-70 mm to a normal distribution in unit 10 dominated by specimens 45-50 mm in length. Mean shell length decreases in the 50 m interval immediately prior to the K-Pg boundary, which may reflect changes in environmental conditions during the latest Maastrichtian. Maximum shell length decreases significantly across the boundary from 75.0 mm to 57.0 mm, which is in line with the change in dominant means of the size distribution. Through the Sobral Formation, range and means are similar to the Danian, with a similar single-peaked distribution with a mean of 40-50 mm and a max shell length of 60.2 mm. All distributions from the Maastrichtian to the Sobral Formation have a minor peak centered between 20-30m. In the Eocene, the *Cucullaea raea* produce much larger shells than specimens from the López de Berotodano or Sobral, with a maximum length of 113.6 mm, which could reflect generally warmer climate conditions.

In *Leionucula* the range of sizes is very similar across the K-Pg boundary, like *Cucullaea* the shells reach a much larger maximum size during the Maatrichtian (56.8 mm) than the Danian (max 40.9). There is no obvious change in size distribution across the boundary, unlike *Lahillia* and *Cucullaea*. Far more Danian specimens than Maastrichtian were measured (121 Danian compared to 23 Maastrichtian), although this does not appear to have affected the spread or range of data collected. Specimens measured from the Sobral Formation grow much smaller than any from the López de Bertodano Formation with a maximum size of 31.7 mm.

Table 3.5: Summary table of size changes across the K-Pg boundary from the Maastrichtian to Danian López de Bertodano Formation

	Lahillia	Cucullaea	Leionucula
Species	No species change	Species change	No species change
Shell ratios	significant increase in width	no significant change in dimension	significant decrease in length
Overall size change	larger max size	smaller max size	smaller max size
Max length Maas (mm)	97.3	75.3	56.8
Max length Danian (mm)	120.8	57	40.9
bimodality	change from unimodal to bimodal	change from bimodal to unimodal	change from normal to unimodal
Mean length Maas (mm)	80-90	30 and 60-70	30-40 and 50-60
Mean length Danian (mm)	50-60 and 90-100	45-50	20-25 and 30-35

The lack of a consistent size-change across a boundary has been noted in several within-lineage studies across mass-extinctions; even closely related taxa have been found to respond differently (Huang et al. 2010).

There are many factors which contribute to a bimodal size distribution among living populations of animals (Huston & DeAngelis 1987), and bimodal distributions have been found in many species of modern bivalves. However, in the fossil record it is difficult to determine whether the change in size distribution is a reflection of the composition of the living population or the size at mortality.

It is therefore useful to consider these morphometric changes in conjunction with analysis of growth patterns and maturation rates in order to examine the potential causes. A further discussion of this bimodality with regards to ecosystem-level predation patterns and sedimentary environment is presented in Chapter 7.

3.7.3 Growth Rate and Longevity

In specimens where growth patterns were examined in the tooth, modelled values of L_{max} (the theoretical maximum shell size) have a narrower range in the Maastrichtian López de Bertodano Formation and a wider range in the Danian with similar means for specimens on each side of the boundary (Figure 3.20). This is consistent with the increase in morphometric size distribution of whole specimens across the K-Pg boundary. However, where growth patterns were measured from the valve surface, specimens from the Maastrichtian produce far larger modelled L_{max} values than specimens from the Paleocene, and have a much larger size range. This difference between modelled growth behaviour and observations from morphometric data may be due to a sampling bias; only shells with little umbonal abrasion, and clear visible growth rings were chosen for external growth rate studies. This may produce a bias against older or larger specimens, where there is a greater chance that young growth layers may have been abraded. Sedimentological studies suggest that the environment is likely to have been shallower in the Danian than the Maastrichtian, so abrasion may have a larger effect and bias sampling against larger individuals during this interval.

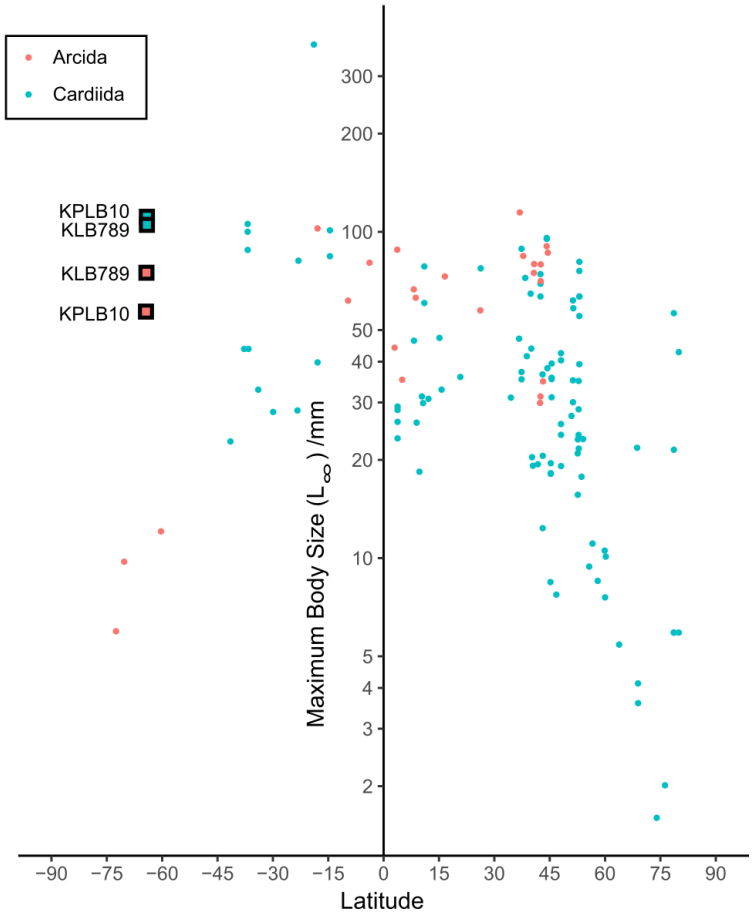

Figure 3.27: Plot of measured or modelled von Bertallanffy L_{max} (maximum mature length) values against latitude for modern species of non-photosymbiotic cardiida and arcida. An inverse trend has been noted by several authors (data from Moss et al 2016). Data points from bivalves in this study presented with black outlines and labelled with the respective stratigraphic units; KLB789 for pre- and KPLB10 for post- extinction specimens.

The maximum size of both *Lahillia* and *Cucullaea* are very different to the maximum sizes of bivalves of the same order (cardiida and arcida respectively) from similar modern high southern latitudes (Figure 3.27). *Lahillia* reached sizes larger than almost all modern cardiida, whereas *Cucullaea* were nearly an order of magnitude larger than modern arcids from the same latitude. Both groups were more similar to modern specimens from Latitudes between 40°S and 55°N. Figure 3.28 highlights this latitude range and shows the annual range of sea surface temperatures predicted from modern model data. This will be compared with the Cretaceous temperature data produced from geochemical

analysis of these shells in Chapter 4 and 5 in order to determine whether temperature is likely to have been a restricting factor in the ability for shells to grow to large sizes.

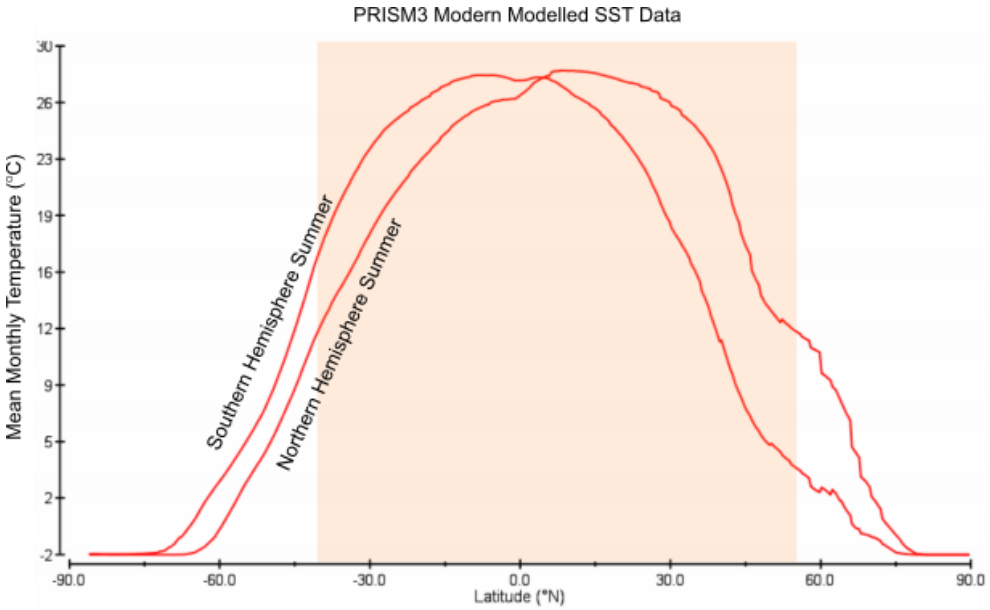

Figure 3.28 Modern simulated warm and cold month mean sea surface temperatures. Orange shading highlights the latitudes at which bivalves with large shell sizes (between 50 and 100 mm) become common in modern oceans

The k-values (representing the rate at which the organism reaches L_{max}) are also relatively different between measurements taken from the tooth and the valve, although they do show a consistent trend across the boundary, with Danian values generally higher than Maastrichtian. This suggests that Danian *Lahillia* may have grown at a faster rate than Maastrichtian specimens. Growth rate has been linked to metabolic rate (Klein et al. 1996) and changes across the K-Pg boundary interval could reflect an increase in nutrient availability, or reduced competition for food as a result of the K-Pg mass extinction's effect on competitor species (Harper et al. in prep).

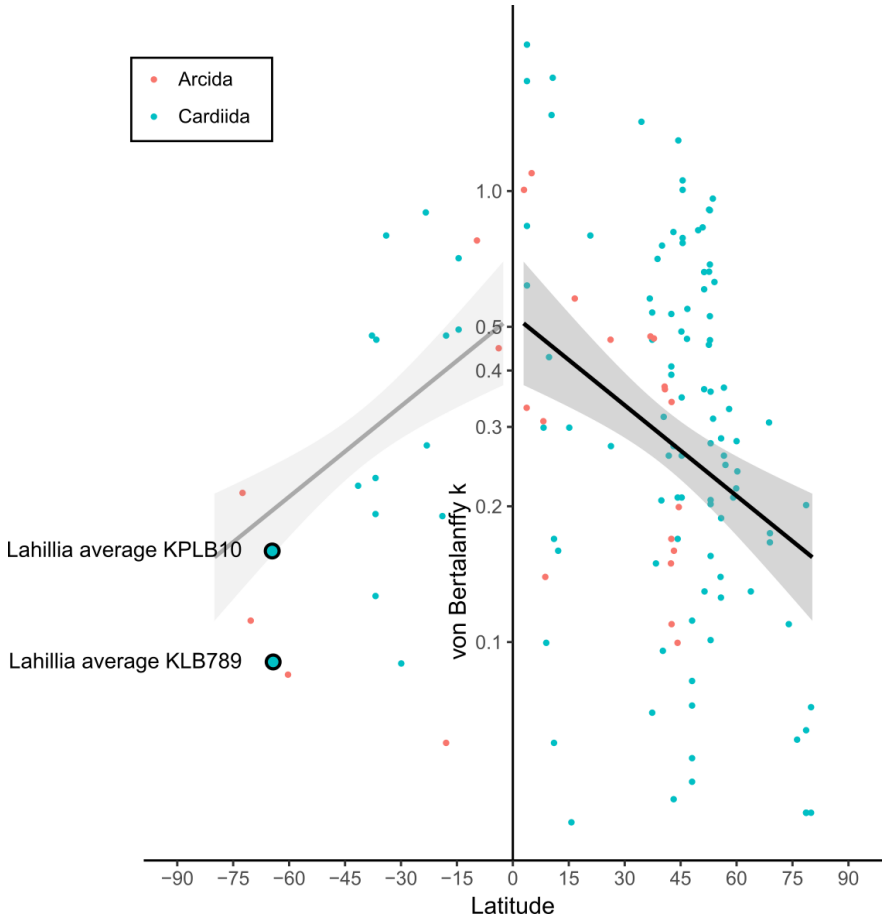

Figure 3.29: Plot of modelled von Bertalanffy k values (rate at which the organism reaches mature size) against latitude for modern species of cardiida and arcida (data from Moss et al 2016). Data points from bivalves presented in this study have black outlines and are labelled with the respective stratigraphic units; KLB789 for pre- and KPLB10 for post- extinction specimens.

A slight trend towards decreased growth rates at higher latitudes has been found for several species of modern bivalve (e.g. Moss et al. 2016). The k-values produced by this study are lower than expected for this latitude (Figure 3.29).

Although this may initially suggest that *Lahillia* may have been growing more slowly than bivalves at modern high latitudes, the difference in size between modern and Cretaceous Antarctic bivalves must be taken into account. The lower k-values are likely to be a result of *Lahillia* spending a long period of life in the juvenile growth phase before growing at a slower mature rate. This would have allowed them to attain their large adult shell sizes, at the expense of short generation times and rapid recruitment. Smaller k-values are associated

with larger shell sizes (Figure 3.30) and longer juvenile growth phases. This pattern of growth behaviour is also more common in modern lower latitudes, whereas modern high latitudes tend to favour faster maturation rates and smaller shell sizes.

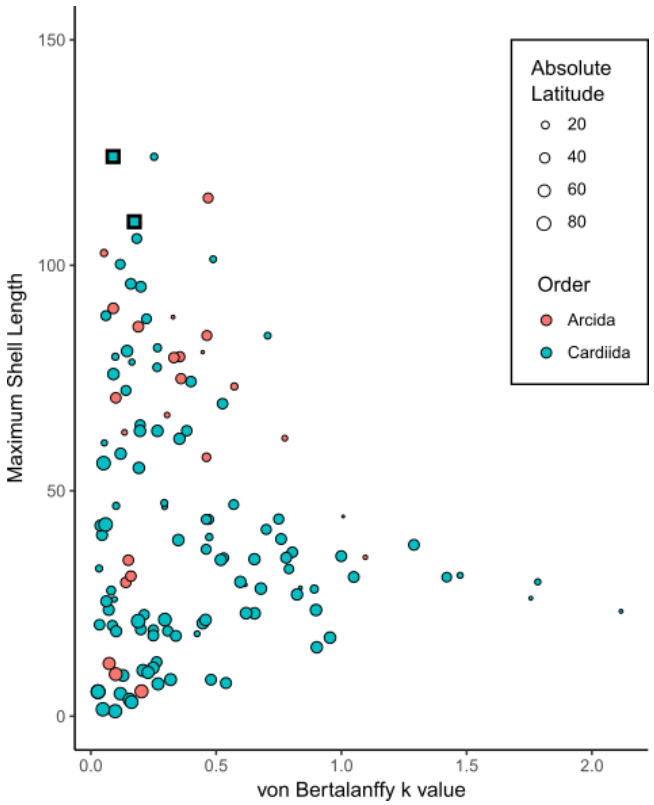

Figure 3.30: Comparison of shell length and k-values in modern arcids and cardiids. Size of each data point represents the approximate value of latitude. Square data points represent *Lahillia* from this study.

Modelled k-values may also have been affected by the relatively poor fit that many of the model calculations produced for the shell data, which will be discussed next.

In spite of the wide application of the von Bertalanffy growth function to invertebrate growth, no explicit validation exists for the legitimacy of its use to parametrise the growth of bivalves in terms of maximum size and rate of growth to this size. However, in organisms with indeterminate growth, such as bivalves, a maximum size may not actually be biologically appropriate. A

number of authors have questioned the applicability of the growth function in bivalves (Knight 1968; Roff 1980) or the assumptions made by von Bertalanffy to construct this model (e.g. Beverton & Holt 1957; Ursin 1967; Ricker 1979).

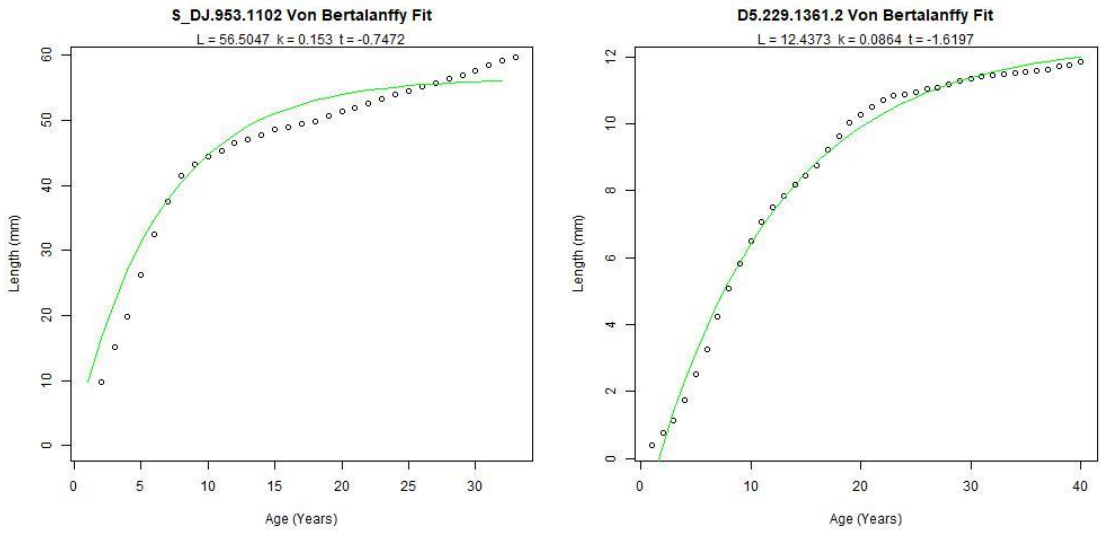

Figure 3.31 examples of poor fit in von Bertalanffy models in specimens of *Lahillia* with a long period of mature growth (A) in which the age of maturation is overestimated and the maximum size is underestimated. S-shaped juvenile growth (B) in which maturation age is underestimated. This illustrates some of the shortcomings of the model.

The model has particular difficulty fitting specimens, such as *Lahillia*, which are long-lived (Roff 1980). In these specimens, rather than growing towards an asymptotic size, as is typical for the VBGF model, bivalves appear to continue growing at a constant rate post-maturity leading to indefinite size (e.g. Figure 3.31). This has led some authors (e.g. Day & Taylor 1997) to suggest that the VBGF should not be used to model growth trajectory and should instead be separated into a pre-maturity and post-maturity equation. This interpretation is more consistent with the energy balance determining the growth rate of bivalve molluscs and gives a more accurate reflection of the effects of postponing maturity (Day & Taylor 1997). The application of a discontinuous function containing separate descriptions of prematurity and post-maturity growth is therefore preferable for comparing the effect of the K-Pg mass extinction on long-lived bivalve specimens, such as *Lahillia*, where there may be great value in postponing maturity during climatically inopportune years.

A number of authors have suggested alternatives to the VBGF in order to deal with its shortcomings, including the Gompertz equation, which includes an early sigmoid growth stage at small size, exhibited in scallops (Orensanz et al. 1991) and in slow growing mussels (Seed & Suchanek 1992). Alternatives such as polynomials have also been suggested, but the factors lack the immediate biological interpretability of the VBGF.

The problem appears to be in attempting to fit a single function to a curve which is in fact governed by two separate functions depending on age; one for pre-maturity and one for post-maturity growth, with a period where the functions combine during maturation. The VBGF is a reasonable fit for the pre-maturity growth curve, however, the point at which each bivalve reaches maturity appears to change from specimen to specimen, and can't be fixed. Beyond this point, a linear fit appears to match the data best.

It may be possible to develop a modified function which fits to pre-maturity and post-maturity growth using statistical techniques such as break function regression (Mudelsee 2009) or least-squares regression in order to produce growth curves with even more biologically relevant parameters, such as mature growth rate, age and duration of maturation, and size at maturation. However, such an undertaking is beyond the scope of this project.

3.8 Summary

Seasonal $\delta^{18}O$ signals are present in shells of both species, and suggest annual periodicity of external and internal shell rings in *Lahillia* and internal rings in *Cucullaea*. Shell growth occurred during the warmer portions of the year, with a hiatus during cooler months. This trend is present in all specimens examined from the López de Bertodano Formation, but may be reversed for specimens in the Sobral and La Meseta Formations.

Morphometric data suggest that shell growth in *Lahillia* and *Leionucula* is isometric or near-isometric, and shell growth is similar either side of the K-Pg boundary. *Cucullaea* shell growth appears to be allometric, and changes with stratigraphy. This is consistent with taxonomical studies suggesting *Lahillia larseni* and *Leionucula suboblongata* continued across the K-Pg boundary, whereas *Cucullaea antarctica* are replaced by *Cucullaea elliotti*.

Lahillia show a general increase in mean size across the K-Pg boundary, as well as an increased range of sizes in the Danian compared to the Maastrichtian whereas *Cucullaea* show the opposite trend, with a decrease in range and mean size across the boundary. *Leionucula* show a reduction in size and slight decrease in size range. *Cucullaea* show significant size reduction in all major axes across the boundary, however this is not a within-species change, as there is a species change across the K-Pg boundary; supported by changes in ontogenetic ratios. *Lahillia* and *Leionucula* do not show significant size change across the K-Pg boundary and are therefore not consistent with the Lilliput effect.

Non-normality tests suggest the change is a result of changing population distributions in *Lahillia* and *Cucullaea*, the biological implications of which will be discussed in greater detail in Chapter 7.

Investigation of whether the size changes in *Lahillia* across the boundary may have been due to changes in juvenile growth duration or rate suggests that *Lahillia* may have been growing faster in the Danian than the Maastrichtian, but tend to grow much more slowly than modern high latitude bivalves, favouring a growth strategy of a long period of slow juvenile growth to reach large body sizes more commonly found in modern mid to low latitude bivalves.

The extended period of non-determinate mature growth in *Lahillia* also causes inaccuracies in the common method of using the von Bertalanffy growth equation to model shell growth. But the fact that it is a good fit to many other species of bivalve suggests that *Lahillia* may have an unusual mode of life or ecological strategy in comparison.

3.9 References

Aberhan, M., Weidemeyer, S., Kiessling, W., Scasso, R. A. and Medina, F. A. (2007) 'Faunal evidence for reduced productivity and uncoordinated recovery in Southern Hemisphere Cretaceous-Paleogene boundary sections', *Geology*, 35(3), 227–230.

Alegret, L., Thomas, E. and Lohmann, K. C. (2012) 'End-Cretaceous marine

mass extinction not caused by productivity collapse', *Proceedings of the National Academy of Sciences*, 109(3), 728–732.

Anderson, T. F. and Arthur, M. A. (1983) 'Stable isotopes of oxygen and carbon and their application to sedimentologic and paleoenvironmental problems', in Arthur, M. A., Anderson, T. F., Kaplan, I. R., Veizer, J., and Land, L. S. (eds) *Stable isotopes in sedimentary Geology*, 1/1-1/151 Short Course.

Antsulevich, A. E., Maximovich, N. V. and Vuorinen, I. (1999) 'Population structure, growth and reproduction of the common mussel (*Mytilus edulis L.*) off the Island of Seili (SW Finland)', *Boreal Environment Research*, 4(4), 367–375.

Arthur, M. A., Zachos, J. C. and Jones, D. S. (1987) 'Primary productivity and the Cretaceous/Tertiary boundary event in the oceans', *Cretaceous Research*, 8(1), 43–54.

von Bertalanffy, L. (1938) 'A quantitative theory of organic growth (inquires on growth laws II)', *Human Biology*, 10, 181–213.

Beverton, R. and Holt, S. (1957) 'On the Dynamics of Exploited Fish Populations, Fishery Investigations', *Ministry of Agriculture, Fisheries and Food*.

Brayard, A., Nutzel, A., Stephen, D. A., Bylund, K. G., Jenks, J. and Bucher, H. (2010) 'Gastropod evidence against the Early Triassic Lilliput effect', *Geology*, 38(2), 147–150.

Brown, J. R. and Hartwick, E. B. (1988) 'Influences of temperature, salinity and available food upon suspended cultre of the Pacific oyster - condition index and survival', *Aquaculture*, 70, 253–267.

Buick, D. P. and Ivany, L. C. (2004) '100 years in the dark: Extreme longevity of Eocene bivalves from Antarctica', *Geology*, 32(10), 921.

Butler, P. G., Richardson, C. A., ., Scourse, J. D., Wanamaker, A. D., Shammon, T. M. and Bennell, J. D. (2010) 'Marine climate in the Irish Sea: analysis of a 489-year marine master chronology derived from growth increments in the shell of the clam Arctica islandica', *Quaternary Science Reviews*, 29(13–14), 1614–1632.

Butler, P. G., Wanamaker, A. D., Scourse, J. D., Richardson, C. A. and Reynolds, D. J. (2013a) 'Variability of marine climate on the North Icelandic Shelf in a 1357-year proxy archive based on growth increments

in the bivalve Arctica islandica', *Palaeogeography, Palaeoclimatology, Palaeoecology*, 373, 141–151.

Butler, P. G., Wanamaker, A. D., Scourse, J. D., Richardson, C. A. and Reynolds, D. J. (2013b) 'Variability of marine climate on the North Icelandic Shelf in a 1357-year proxy archive based on growth increments in the bivalve Arctica islandica', *Palaeogeography, Palaeoclimatology, Palaeoecology*, 373, 141–151.

Case, T. J. (1978) 'A general explanation for insular body size trends in terrestrial vertebrates', *Ecology*, 59, 1–18.

Day, T. and Taylor, P. D. (1997) 'Von Bertalanffy's Growth Equation Should Not Be Used to Model Age and Size at Maturity', *The American Naturalist*, 149(2), 381–393.

Dettman, D. L. and Lohmann, K. C. (1995) 'Microsampling carbonates for stable isotope and minor element analysis; physical separation of samples on a 20 micrometer scale', *Journal of Sedimentary Research*, 65(3a), 566–569.

Epstein, S., Buchsbaum, R., Lowenstam, H. A. (Heinz A. and Urey, H. C. (1953) 'Revised Carbonate-Water Isotopic Temperature Scale', *Bulletin of the geological Society of America*, 64, 1315–1326.

Friedman, M. and Sallan, L. C. (2012) 'Five hundred million years of extinction and recovery: a phanerozoic survey of large-scale diversity patterns in fishes', *Palaeontology*, 55(4), 707–742.

Gould, S. J. (1966) 'Allometry And Size In Ontogeny And Phylogeny', *Biological Reviews*, 41(4), 587–638.

Grossman, E. L. and Ku, T.-L. (1986) 'Oxygen and carbon isotope fractionation in biogenic aragonite: Temperature effects', *Chemical Geology: Isotope Geoscience section*, 59, 59–74.

Hall, J. L. O. (2013) *Giant Antarctic Bivalves: Investigating change over the Cretaceous-Paleogene boundary*.

Hansen, T. A., Farrell, B. R. and Upshaw, B. (1993) 'The first 2 million years after the Cretaceous-Tertiary boundary in east Texas: rate and paleoecology of the molluscan recovery', *Paleobiology*, 19(2), 251–265.

Harries, P. J. and Knorr, P. O. (2009) 'What does the "Lilliput Effect" mean?', *Palaeogeography, Palaeoclimatology, Palaeoecology*, 284(1–2), 4–10.

Heim, N. A., Knope, M. L., Schaal, E. K., Wang, S. C. and Payne, J. L. (2015)

'Animal evolution. Cope's rule in the evolution of marine animals.', *Science*, 347(6224), 867–70.

Huang, B., Harper, D. A. T., Zhan, R. and Rong, J. (2010) 'Can the Lilliput Effect be detected in the brachiopod faunas of South China following the terminal Ordovician mass extinction?', *Palaeogeography, Palaeoclimatology, Palaeoecology*, 285(3), 277–286.

Huber, M. (2010) *Compendium of bivalves. A full-color guide to 3,300 of the World's Marine Bivalves. A status on Bivalvia after 250 years of research*.

Huston, M. A. and DeAngelis, D. L. (1987) 'Size Bimodality in Monospecific Populations: A Critical Review of Potential Mechanisms', *The American Naturalist*, 129(5), 678–707.

Huxley, J. (1932) *Problems of relative growth*.

Immenhauser, A., Schone, B. R., Hoffmann, R. R., Niedermayr, A., Schöne, B. R., Hoffmann, R. R. And Niedermayr, A. (2016) 'Mollusc and brachiopod skeletal hard parts: Intricate archives of their marine environment', *Sedimentology*, 63(1), 1–59.

Jeffery, C. H. (2001) 'Heart urchins at the Cretaceous/Tertiary boundary: a tale of two clades', *Paleobiology*, 27(1), 140–158.

Jones, D. S., Arthur, M. A. and Allard, D. J. (1989) 'Sclerochronological records of temperature and growth from shells of Mercenaria mercenaria from Narragansett Bay, Rhode Island', *Marine Biology*, 102(2), 225–234.

Jones, D. S. and Quitmyer, I. R. (1996) 'Marking Time with Bivalve Shells: Oxygen Isotopes and Season of Annual Increment Formation', *PALAIOS*, 11(4), 340.

Kemp, D. B., Robinson, S. A., Crame, J. A., Francis, J. E., Ineson, J., Whittle, R. J., Bowman, V. and O'Brien, C. (2014) 'A cool temperate climate on the Antarctic Peninsula through the latest Cretaceous to early Paleogene', *Geology*, 42(7), 583–586.

Klein, R. T., Lohmann, K. C. and Thayer, C. W. (1996) 'SrCa and 13C12C ratios in skeletal calcite of Mytilus trossulus: Covariation with metabolic rate, salinity, and carbon isotopic composition of seawater', *Geochimica et Cosmochimica Acta*, 60(21), 4207–4221.

Knight, W. (1968) 'Asymptotic Growth: An Example of Nonsense Disguised as Mathematics', *Journal of the Fisheries Research Board of Canada*, 25(6),

1303–1307.

Lockwood, R. (2005) 'Body size, extinction events, and the early Cenozoic record of veneroid bivalves: a new role for recoveries?', *Paleobiology*, 31(4), 578.

Lutz, R. A. and Rhoads, D. C. D. C. (1980) 'Growth patterns within the molluscan shell. An overview', in *Skeletal growth of aquatic organisms*, 203–254.

McClain, C. R., Boyer, A. G. and Rosenberg, G. (2006) 'The island rule and the evolution of body size in the deep sea.', *Journal of Biogeography*, 33, 1578–1584.

Moss, D. K., Ivany, L. C., Judd, E. J., Cummings, P. W., Bearden, C. E., Kim, W.-J., Artruc, E. G. and Driscoll, J. R. (2016) 'Lifespan, growth rate, and body size across latitude in marine Bivalvia, with implications for Phanerozoic evolution', *Proceedings of the Royal Society of London B: Biological Sciences*, 283(1836).

Mudelsee, M. (2009) 'Break function regression', *The European Physical Journal Special Topics*, 174(1), 49–63.

Orensanz, J. M., Parma, A. M. and Iribarne, O. O. (1991) 'Population dynamics and management of natural stocks', *Scallops: biology, ecology and aquaculture*, 21, 625–713.

Pianka, E. R. (1970) 'On r- and K-Selection', *The American Naturalist*, 104(940), 592–597.

Poole, I., Cantrill, D. J. and Utescher, T. (2005) 'A multi-proxy approach to determine Antarctic terrestrial palaeoclimate during the Late Cretaceous and Early Tertiary', *Palaeogeography, Palaeoclimatology, Palaeoecology*, 222, 95– 121.

Ricker, W. E. (1979) 'Growth rates and models.', in *In Fish Physiology. Vol. VIII. Bioenergetics and Growth*, 678–744.

Ridgway, I. D., Richardson, C. A. and Austad, S. N. (2011) 'Maximum shell size, growth rate, and maturation age correlate with longevity in bivalve molluscs.', *The journals of gerontology. Series A, Biological sciences and medical sciences*, 66(2), 183–90.

Roff, D. A. (1980) 'A Motion for the Retirement of the Von Bertalanffy Function', *Canadian Journal of Fisheries and Aquatic Sciences*, 37(1),

127–129.

Ropes, J. . (1984) 'Procedures for preparing acetate peels and evidence validating the annual periodicity of growth lines formed in the shells of ocean quahogs, *Arctica islandica*.', *Marine Fisheries Review*, 46(2), 27–35.

Schone, B. R., Lega, J., Flessa, K. W., Goodwin, D. H. and Dettman, D. L. (2002) 'Reconstructing daily temperatures from growth rates of the intertidal bivalve mollusk *Chione cortezi* (northern Gulf of California , Mexico)', *Palaeogeography, Palaeoclimatology, Palaeoecology*, 184, 131–146.

Schöne, B. R., Oschmann, W., Tanabe, K., Dettman, D., Fiebig, J., Houk, S. D. and Kanie, Y. (2004) 'Holocene seasonal environmental trends at Tokyo Bay, Japan, reconstructed from bivalve mollusk shells—implications for changes in the East Asian monsoon and latitudinal shifts of the Polar Front', *Quaternary Science Reviews*, 23(9–10), 1137–1150.

Scrucca, L., Fop, M., T.B, M. and A.E, R. (2016) 'mclust 5: clustering, classification and density estimation using Gaussian finite mixture models', *The R Journal*, 8(1), 205–233.

Seed, R. and Suchanek, T. H. (1992) 'Population and community ecology of *Mytilus*', in Gosling, E. M. (ed.) *The mussel Mytilus: ecology, physiology, genetics and culture*. 25th edn, 87–170.

Shirai, K., Schöne, B. R., Miyaji, T., Radarmacher, P., Krause, R. A. and Tanabe, K. (2014) 'Assessment of the mechanism of elemental incorporation into bivalve shells (Arctica islandica) based on elemental distribution at the microstructural scale', *Geochimica et Cosmochimica Acta*, 126, 307–320.

Smith, A. B. and Jeffery, C. H. (1998) 'Selectivity of extinction among sea urchins at the end of the Cretaceous period', *Nature*, 392(6671), 69–71.

Smith, P. E., Evensen, N. M., York, D. and Odin, G. S. (1998) 'Single-Grain 40Ar-39Ar Ages of Glauconies: Implications for the Geologic Time Scale and Global Sea Level Variations', *Science*, 279, 1517–1519.

Sogot, C. E., Harper, E. M. and Taylor, P. D. (2014) 'The Lilliput effect in colonial organisms: cheilostome bryozoans at the Cretaceous-Paleogene mass extinction.', *PloS one*. 9(2), e87048.

Sokal, R. R. and Rohlf, F. J. (1987) *Introduction to Biostatistics*.

Thompson, I., Jones, D. S. and Dreibelbis, D. (1980) 'Annual internal growth

banding and life history of the ocean quahog *Arctica islandica* (Mollusca: Bivalvia)', *Marine Biology*, 57(1), 25–34.

Tobin, T. S., Ward, P. D., Steig, E. J., Olivero, E. B., Hilburn, I. A., Mitchell, R. N., Diamond, M. R., Raub, T. D., *et al.* (2012) 'Extinction patterns, $\delta^{18}O$ trends, and magnetostratigraphy from a southern high-latitude Cretaceous–Paleogene section: Links with Deccan volcanism', *Palaeogeography, Palaeoclimatology, Palaeoecology*, 350, 180–188.

Urbanek, A. (1993) 'Biotic crises in the history of Upper Silurian graptoloids: A Palaeobiological model', *Historical Biology*, 7(1), 29–50.

Urey, H. C. (1947) 'The thermodynamic properties of isotopic substances', *Journal of the Chemical Society*, 562.

Urey, H. C., Epstein, S., Lowenstam, H. A. (Heinz A. and McKinney, C. R. (1951) 'Measurement of paleotemperatures and temperatures of the upper Cretaceous of England, Denmark, and the southeastern United States', *Bulletin of the geological Society of America*, 62(4), 399–416.

Ursin, E. (1967) 'A mathematical model of some aspects of fish growth, respiration and mortality', *J. Fish. Res. Board Can.*, 24, 2355–2453.

Valentine, A., Johnson, A. L. a., Leng, M. J., Sloane, H. J. and Balson, P. S. (2011) 'Isotopic evidence of cool winter conditions in the mid-Piacenzian (Pliocene) of the southern North Sea Basin', *Palaeogeography, Palaeoclimatology, Palaeoecology*, 309(1–2), 9–16.

Witts, J. D., Newton, R. J., Mills, B. J. W., Wignall, P. B., Bottrell, S. H., Hall, J. L. O., Francis, J. E. and Alistair Crame, J. (2018) 'The impact of the Cretaceous–Paleogene (K–Pg) mass extinction event on the global sulfur cycle: Evidence from Seymour Island, Antarctica', *Geochimica et Cosmochimica Acta*, 230, 17–45.

Witts, J. D., Whittle, R. J., Wignall, P. B., Crame, J. A., Francis, J. E., Newton, R. J. and Bowman, V. C. (2016) 'Macrofossil evidence for a rapid and severe Cretaceous–Paleogene mass extinction in Antarctica', *Nature Communications*, 7, 11738.

Woods, P. J., Skúlason, S., Snorrason, S. S., Kristjánsson, B. K., Malmquist, H. J. and Quinn, T. P. (2012) 'Intraspecific diversity in Arctic charr, Salvelinus alpinus, in Iceland: I. Detection using mixture models', *Evolutionary Ecology Research*, 14, 973–992.

Zinsmeister, W. J. and Macellari, C. E. (1988) 'Bivalvia (Mollusca) from Seymour Island , Antarctic Peninsula', *Geological Society of America Memoirs*, (169).

Zolotarev, V. (1980) 'The life span of bivalves from the Sea of Japan and Sea of Okhotsk', *Biologiya morya-Marine Biology*, 6, 3–12.

CHAPTER 4

CLIMATE OF THE JAMES ROSS BASIN

The aim of this chapter is to determine the correlation between model simulations of Maastrichtian climate with geochemically derived proxy temperature estimates and examine whether this provides evidence for or against local ice influence.

4.1 Introduction

Stable oxygen isotopic records from shell carbonates are commonly used to characterize palaeoenvironments and track climate change (see Section 3.3 for further details). Constraining high southern latitude palaeotemperatures is critical for understanding the role of the polar regions in regulating global climate and potentially driving evolutionary change (Bowman et al. 2013).

Some previous temperature reconstructions based on $\delta^{18}O$ proxies have assumed a seawater $\delta^{18}O$ for an ice-free world of a constant -1‰ VSMOW (Shackleton & Kennett 1975), whereas the range in $\delta^{18}O_{sw}$ in the modern ocean is very large, −3 to +2‰ (LeGrande & Schmidt 2006) due to equatorial evaporation and polar ice melt. Recently a number of observations from sedimentology and palynology studies (e.g. Miller et al. 2005; Bowman et al. 2013) have suggested the presence of ephemeral continental Antarctic ice sheets during the latest Cretaceous which through the contribution of isotopically light meltwater could bias $\delta^{18}O$ records in the high latitudes.

Chapters 2 and 3 established the excellent preservation of Seymour Island's fossil *Cucullaea* and *Lahillia* shells and used the presence of cyclic signals in the stable oxygen isotopic data to determine the periodicity of growth line formation. This chapter will convert the geochemical $\delta^{18}O$ data to

temperatures using additional clumped isotope data and isotope enabled modelling of riverine inputs to refine the conversion. Temperature data will be used to examine changes in the shell-derived temperature data through geological time rather than just within single specimens.

Temperature and $\delta^{18}O$ data will then be compared with models of the Maastrichtian climate in order to examine whether simulations are capable of producing similar temperature conditions under reasonable parameters. The combination of proxy data and computer models will allow further information to be gathered about the main processes influencing the stable oxygen isotope data trends through this time, and whether they are likely to have been caused by seasonal changes in water temperature or indicate that additional factors such as freshwater runoff or ice are likely to have been required to produce the data patterns observed.

4.2 Objectives

- Examination of the assumptions made in converting from isotopic data to palaeotemperatures to assess the accuracy of temperatures reconstructed from $\delta^{18}O$ data using additional clumped isotopic data and oxygen isotope enabled models.
- Reconstruction of Maastrichtian climate conditions through geological time using mean annual temperatures derived from stable oxygen isotope and clumped isotope data.
- Comparison of stable oxygen-derived temperature data with climate simulations over a range of scenarios in order to test which model scenario best fits the geological evidence.
- Assess the potential for sea ice formation around the James Ross basin using both proxy and model data.

4.3 Background to Techniques

Stable oxygen isotope and clumped isotope geochemistry were used as proxies for temperature for this study and compared to outputs from isotope-enabled climate models. This section outlines the types of information captured by each proxy, and the details of the models and simulations used. Details of analytical methodology used in this chapter are covered in Section 4.4.

4.3.1 Stable Oxygen Isotope Geochemistry

Seminal papers by Urey (1947) Urey et al (1951) and Epstein et al (1953) showed that oxygen isotope levels in biogenic carbonates are a function of temperature and isotopic composition of the water. Isotopes of oxygen are fractionated as metabolic processes thermodynamically favour the lighter ^{16}O isotope over the heavier ^{18}O. The ratio of ^{16}O to ^{18}O atoms in carbonate compounds, such as the calcium carbonate that makes up aragonite and calcite can be measured using mass spectrometry and calculated to give a $\delta^{18}O$ composition. The amount of fractionation shows strong temperature dependence due to entropy effects in addition to recording source water composition.

$$\delta^{18}O = \left(\frac{\left(\frac{\delta^{18}O}{\delta^{16}O}\right)_{sample}}{\left(\frac{\delta^{18}O}{\delta^{16}O}\right)_{standard}} - 1 \right) * 1000\ ‰$$

The amount of biological fractionation has been experimentally determined in aragonitic (Grossman & Ku 1986) and calcitic (Anderson & Arthur 1983) molluscs. These formulas allow for conversion between the measured $\delta^{18}O$ of shell carbonates to the temperature of water they were mineralised in.

Mollusc Calcite (Anderson & Arthur 1983)

$$T\,(°C) = 16.0 - 4.14\,[\,(\delta^{18}O_{calcite} - \delta^{18}O_{water}] + 0.13\,[\,(\delta^{18}O_{calcite} - \delta^{18}O_{water}]^{2}$$

Inorganic Calcite (Kim & O'Neil 1997)

$$T\,(°C) = \frac{18.03\;E\;3}{1000\ln\alpha\;(\delta^{18}O_{calcite} - \delta^{18}O_{water}) + 32.42}$$

Mollusc Aragonite (Grossman & Ku 1986, modified by Schöne et al. 2005)

$$T\,(°C) = 20.6 - 4.36\,(\delta^{18}O_{aragonite} - (\delta^{18}O_{water} - 0.20))$$

These experimentally-derived relationships have been corroborated with many modern high-resolution studies in a number of species and environments, (e.g. (Wefer & Killingley 1980; Krantz et al. 1987; Jones et al. 1989; Jones & Quitmyer 1996; Dettman et al. 1999; Toland et al. 2000; Goodwin et al. 2001; Schöne et al. 2003; Lorrain et al. 2004; Schöne et al. 2005; Carré et al. 2005; Fenger et al. 2007), which show clear annual cycles of isotopes in the shell and a high level of correlation between recorded water or air temperature and temperatures predicted from the $\delta^{18}O_{shell}$ record.

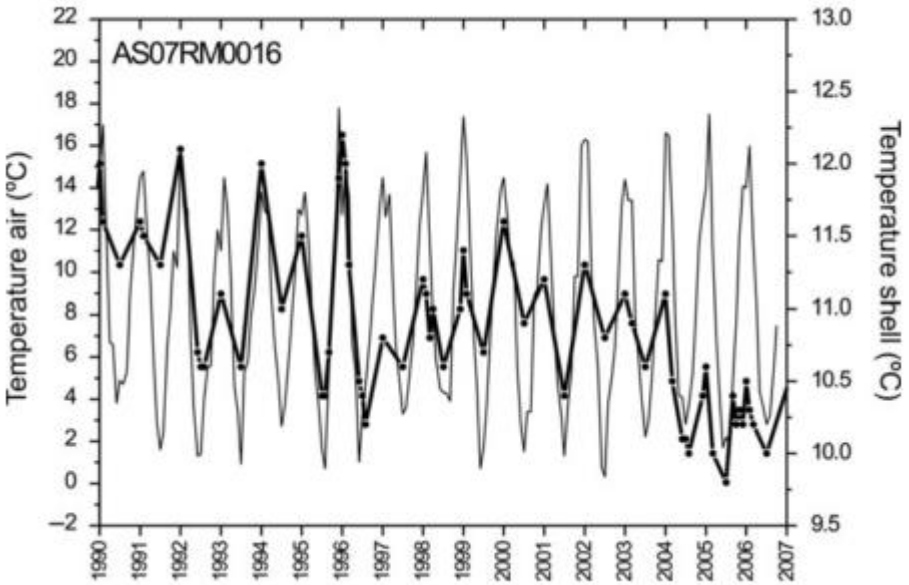

Figure 4.1: Comparison of apparent water temperatures from δ^{18}O of modern Argentinian *Diplodon* (Unionida) bivalve shell (bold dot-point line) and recorded monthly air temperature records from the same location (solid grey line) indicating that the two records show strong correspondence. From Soldati et al 2008.

Fossil bivalve shells have been used to reconstruct seasonal palaeotemperatures in the Pliocene (Jones & Quitmyer 1996; Williams et al. 2010; Valentine et al. 2011), Pleistocene (Krantz et al. 1987), Eocene (Buick & Ivany 2004) and further back into the Mesozoic (Jones & Quitmyer 1996; Steuber 1996, Zacharov et al 2005). However, there are several sources of error which may affect the temperatures reconstructed from δ^{18}O of fossil shell carbonates. It is therefore important to account for the external factors that can affect interpretation of data.

Sources of Error

In fossil studies, the $\delta^{18}O_{water}$ composition is not known and thus is a key source of uncertainty in palaeotemperature conversions. The processes of evaporation and ice formation cause additional fractionation of the ^{16}O and ^{18}O in ambient water. Ice melt water and freshwater from continental runoff tends to have a more negative δ^{18}O signature than ocean water. In ice-free geological systems,

ocean water $\delta^{18}O$ is conventionally taken as -1‰ (Zachos et al. 2001), provided the body of water is considered to have been well-mixed and without significant freshwater input. However, in ice-present conditions or near-shore environments with significant freshwater input, it can be more difficult to deconvolve the effects of water composition and temperature.

This chapter will combine oxygen isotope enabled models with clumped isotope data to attempt to constrain the effect of water $\delta^{18}O$ on palaeotemperature reconstructions.

There are also issues reconstructing palaeotemperatures from marine $\delta^{18}O$ due to the thermal gradients within the water column. This means that organisms mineralising at different water depths may record drastically different temperatures. Determination of depth habits in extinct organisms can also be difficult, as pelagic organisms may migrate within a large vertical section of the water column (e.g. Kobashi et al. 2001). Even for infaunal organisms, the water depth must be estimated from sedimentology and the range is often large compared with typical thermal gradients.

Diagenetic alteration usually changes the composition of the crystals, destroying any original data produced by fractionation and organic processes in the shell or incorporated from environmental conditions attenuating any seasonal data (Ivany 2012). This process occurs by a number of mechanisms and can begin while the organism is still alive (Lécuyer et al. 2004). Alteration causes recrystallization of metastable minerals such as aragonite and high-Mg calcite as more stable minerals.

Depending on the shell microstructure, some areas may undergo diagenesis while other areas retain their original composition. Once identified, structures which have been altered can be mechanically removed prior to chemical analysis. Concerns about the heat generated during high-speed abrasion or microsampling techniques causing transition to calcite when sampling aragonitic material (Waite & Swart 2008) have been addressed and found to be insignificant for oxygen isotopic analysis (Foster et al. 2008). However, rigorous testing is required to verify preservation of original signals particularly in fossil material. Preservation can be tested in a number of ways, depending on the composition of the original shell material.

Preservation tests were conducted for a number of representative specimens of *Lahillia* and *Cucullaea*; details about tests and the results are described in Section 2.7 and Appendix A.

4.3.2 Clumped Isotope Geochemistry

Clumped isotope thermometry can be used to calculate palaeotemperatures without the need to assume a $\delta^{18}O_{sw}$ value (Ghosh et al. 2006). This means that in combination with stable isotope $\delta^{18}O$ values measured simultaneously $\delta^{18}O_{sw}$ can be independently determined. The clumped isotope palaeothermometer is a recent addition to the suite of temperature proxies available to bivalve shell studies. It uses the distribution of ^{12}C and ^{13}C as well as ^{16}O and ^{18}O isotopes in different configurations within isotopologues (molecules with different isotopes) in the carbonate lattice. Clumping of heavy isotopes within carbonate molecules is thermodynamically favourable for the relative stability of the ^{13}C-^{18}O bond at low temperatures, but at high temperatures, entropy effects cause a decrease in clumping leading to a stochastic distribution at high temperatures.

$$Ca^{13}C^{16}O_3 + Ca^{12}C^{18}O^{16}O_2 \rightleftharpoons Ca^{13}C^{18}O^{16}O_2 + Ca^{12}C^{16}O_3$$

This reaction is driven to the right with decreasing temperature, producing proportionally more $Ca^{13}C^{18}O^{16}O$. The Δ47 clumped isotope thermometer measures the atomic mass of CO_2 produced by acid digestion of carbonates and uses the measured abundance of the most common CO_2 isotopologue ($^{13}C^{18}O^{16}O$) with a ^{13}C–^{18}O bond, which is energetically favoured at lower temperatures. A quantitative value (Δ47) indicates the excess or depletion of mass 47 isotopologues (of which the $^{13}C^{18}O^{16}O$ accounts for approximately 97%) relative to a stochastic distribution of all possible isotopologues. This relationship can be described in the below equation, where R_n is the abundance ratio of mass n relative to mass 44 in the sample and R_n^* is the theoretical stochastically distributed ratio.

$$\Delta 47 = \left[\left(\frac{R_{47}}{R_{47}^*} - 1\right) - \left(\frac{R_{46}}{R_{46}^*} - 1\right) - \left(\frac{R_{45}}{R_{45}^*} - 1\right)\right] * 1000$$

Δ47 can be calibrated to carbonate standards precipitated at known temperatures as well as to theoretical predictions. The thermometer is extremely precise and studies across multiple taxonomic orders of carbonate biomineralisers show that the vast majority of species follow the same calibration with little apparent influence from vital effects (e.g. Affek & Zaarur 2014; Tang et al. 2014) so these calibrations can be used with a greater degree of confidence in extinct lineages (Dennis & Schrag 2010).

The temperatures produced are also independent of the $\delta^{18}O$ composition of the source water, making clumped isotope geochemistry an independent constraint on both water $\delta^{18}O$ and temperature. In the production of clumped isotope data, $\delta^{18}O$ and $\delta^{13}C$ are measured simultaneously to Δ47 in the same sample. This can allow clumped isotopes to be used in addition to stable isotopes to deconvolve temperature and water $\delta^{18}O$.

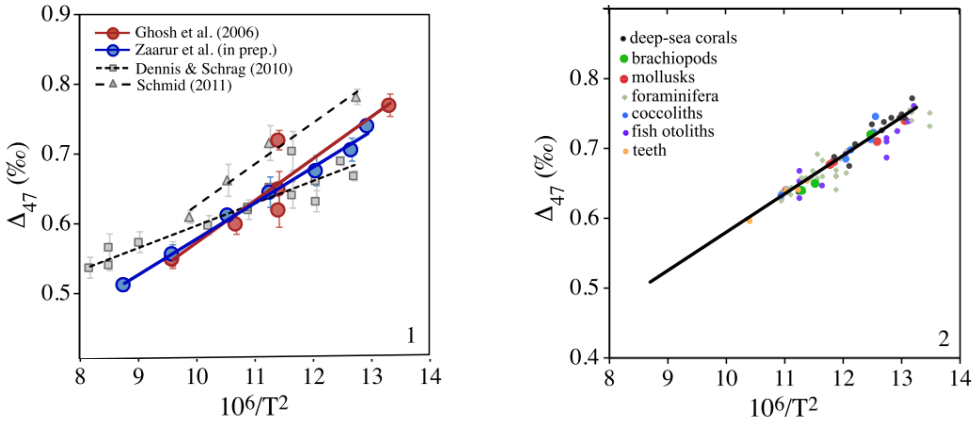

Figure 4.2: Clumped isotope thermometry calibration from synthetic calcite (left) and a variety of biogenic carbonates (right) showing the difference between some of the Δ47 to temperature calibrations that have been used. Taken from Affek (2012).

Current technology requires large sample amounts – an order of magnitude heavier than is required for stable isotope work (Dennis et al. 2013). Machine precisions are also around 0.01‰, roughly equalling a temperature resolution of 2°C). These factors make clumped isotopes an unsuitable palaeothermometer for high resolution inter-annual temperatures in bivalves. However it is likely

that equipment will improve to allow smaller samples to be analysed in future studies (Zaarur et al. 2011).

Sources of Error

Carbonate clumped isotope thermometry is a relatively new proxy, and as such, some of the limitations are clear, but others have yet to be quantified. There are three main sources of error to clumped isotope thermometry; alteration, calibration and vital or disequilibrium effects.

Δ47 data is far more sensitive to diagenetic alteration than other palaeotemperature proxies (e.g. $\delta^{18}O$ or Mg/Ca) (Eiler 2011). Diagenetic re-equilibration of isotopes during diagenesis will overprint the original temperature data with the diagenetic temperature, even without bulk recrystallization (Dennis & Schrag 2010). This makes the presence of original aragonite insufficient to establish the authenticity of the Δ47 data. It is also possible that the standard method of microdrilling may produce heat and shear friction sufficient to alter the aragonite structure (Larkin, 2014). Clumped isotopes have an additional unique alteration pattern; solid state diffusion of the atoms over time within the carbonate lattice, which may be caused by heating or deformation but does not include dissolution or re-precipitation. This makes solid state reordering extremely difficult to detect, although in the absence of high temperatures, solid-state reordering is sufficiently slow to allow use of clumped isotope thermometry on timescales of hundreds of millions of years (Dennis & Schrag 2010).

The calibration of the clumped isotope thermometer for biogenic carbonates is ongoing. Many temperature conversions and calibrations are currently used; each covering different temperature and pressure ranges (Figure 4.2). Using an unsuitable calibration may cause the temperature estimates to vary by more than the standard error of an individual measurement. Differences in equipment configuration or vital effects within different organism groups have also been suggested to cause discrepancies in temperature calibrations (Eagle et al. 2013; Kelson et al. 2016). The use of an absolute reference frame and correction procedures helps to correct for some fractionation and recombination effects and improve inter laboratory correlation, but does not account for all artefacts (Huntington et al. 2009; Dennis et al. 2011). Some laboratory practices introduce additional sources of error related to instrumental

instability, or noise due to sample preparation and contaminants which can raise the uncertainty of an individual analysis to 0.02‰ (equivalent to 4 to 5°C). This amount of potential error highlights the need to replicate the analysis of each sample to obtain climate-relevant data (Zaarur et al. 2013).

Although the calibrations appear to work for many organisms (Figure 4.2), Δ47 temperature dependence may not be assumed if the carbonate is not crystallised in isotopic equilibrium. Speleothems display clumped isotopic disequilibrium and Δ47 does not reflect cave temperatures (Affek et al. 2008). This effect has also been found in some species of deep sea and shallow water corals and several species of mollusc and brachiopod, which all show large deviations towards lower Δ47 values, particularly at low temperatures (Thiagarajan et al. 2011; Zaarur et al. 2011; Saenger et al. 2012; Henkes et al. 2013). This can cause an underestimation of temperature by up to 8°C (Saenger et al. 2012). It is possible that it may reflect differences in laboratory protocols alternatively there may be a systematic difference between these taxa and standard calibrations.

Recent descriptions of anti-clumping (where more than one heavy isotope occurs in a molecule at a frequency that is lower than the predicted abundance for that temperature) have also drawn doubt over the reliability of clumped isotope-derived temperature data from biological sources. Anti-clumping results from enzyme activity controlling the formation of biological compounds away from thermodynamic equilibrium and has been described in CO_2 of exhaled breath, photosynthetic oxygen and microbial methane (Wang et al. 2015; Yeung et al. 2015). Anticlumping produces clumped isotope signatures corresponding to lower temperatures than the true formation temperature of the biomineral and may be the cause of some of the vital effects discussed above. However, many biominerals show only minor departures from equilibrium isotope fractionation (e.g. Guo et al. 2009; Affek & Zaarur 2014; Tang et al. 2014) and the contribution of biological influence and thermodynamic effects to the clumped isotopic composition is not yet known.

4.3.3 Computer Models

The Maastrichtian is generally well-constrained in the model realm compared to earlier time-periods with several high-resolution palaeogeographic

reconstructions available (e.g. Scotese 1991; Markwick & Valdes 2004) and reasonably well-defined boundary conditions (Hunter et al. 2013). As a result, the Maastrichtian has been the subject of numerous model and data studies at a global scale (e.g. Horrell 1991; Upchurch et al. 1999; Markwick 2007; Hunter et al. 2008).

Using different types of climate models has afforded a great deal of information about Cretaceous and early Cenozoic climates and patterns of circulation. This is particularly important at the high latitudes where data from these times is extremely limited, and the use of models can help fit data results from a single location such as Seymour Island into a broader regional climate context. Climate models come in a number of different forms producing different data, but with different errors associated. This study uses the Hadley Centre Coupled Climate Model version 3 with the lower resolution ocean (HadCM3L) (see Section 4.4.3 for further details). HadCM3L is a general circulation model (GCM), but the principles of various climate models are described briefly below.

The simplest climate models are zero-dimensional thermodynamical energy balance models which model the earth as a single box and balance incoming solar radiation against outgoing terrestrial radiation to obtain an estimate of global surface temperature. Various parameters can be added to these models to include layers of atmosphere to provide more accurate estimates of temperatures and heat flux, but little other data can be produced without adding detail to the model.

The principles of these energy balance models can be applied to single-column models which simulate a one-dimensional column through the atmosphere to produce a vertical profile of temperatures and associated radiative and convective fluxes. These models can be produced with a number of vertical layers with physical parameters. However, these can still only represent a small portion of the climate system and any horizontal interactions must be prescribed, which makes them less useful for palaeoclimate studies.

Statistical dynamical models attempt to incorporate atmospheric motions and dynamics to single column models, usually in a two-dimensional plane representing vertical height and latitude, occasionally using a third (time) dimension to track annual changes (Budyko 1969; Sellers 1969). These models

are of limited use and have largely become obsolete when compared to general circulation models.

General circulation models are sophisticated three-dimensional models that attempt to simulate many parts and processes within a climate system. They include elements of energy balance models and consist of a number of vertically layered columns, similar to the single-column energy balance models, distributed around a representation of the surface of the Earth. Energy flow and transport between these boxes or cells is calculated using a variety of fluid dynamical, chemical and sometimes biological physical behaviours and parameters.

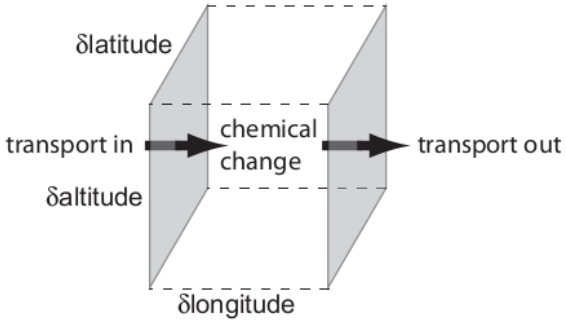

Figure 4.3: Schematic of a numerical model "box" in a model for chemical changes showing the processes that can change the chemical composition within the box. In this case only longitudinal transport is shown, whereas in reality, transport is 3-dimensional and involves thermal changes governed by thermodynamic physics in addition to chemical changes.

GCMs can be used to model the behaviour of the atmosphere (AGCMs) and ocean (OGCMs), or can be coupled together to form an atmosphere-ocean or fully coupled general circulation model. These models include three-dimensional ocean bathymetry and topography, and are extremely useful for simulating past climate conditions.

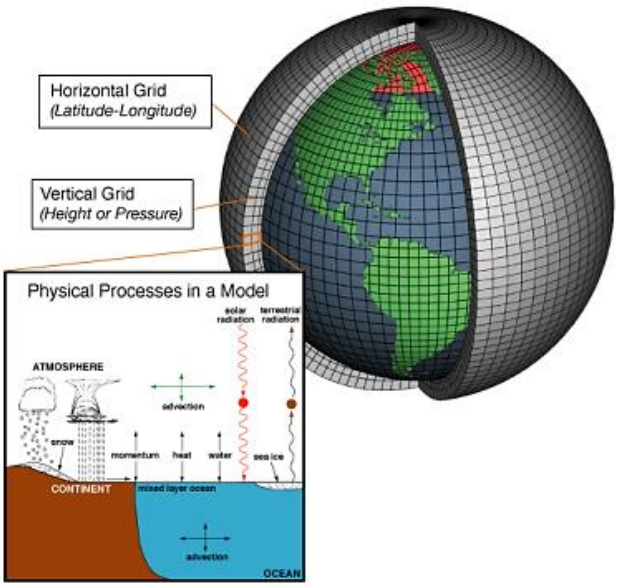

Figure 4.4: Schematic of a typical numerical GCM showing the division of the atmosphere and ocean into a series of grid boxes which are then processed in a manner similar to Figure 4.3. From NOAA

Climate simulations of Cretaceous conditions often feature strong climate equability – a term used to describe reduced seasonal extremes and shallow equator-to-pole thermal gradients. Climate models for the Maastrichtian have also been used to determine the likely patterns of circulation (Bowman et al. 2012; Jung et al. 2013) examine potential for sea ice (Otto-Bliesner & Upchurch 1997; Hunter et al. 2008; Hunter et al. 2013) and the effects of vegetation (Upchurch et al. 1998), hydrology (Markwick et al. 2002) among many other aspects of the Maastrichtian climate system.

Sources of Error

The sources of uncertainty in palaeoclimate modelling can be broadly grouped into three categories. First are structural model uncertainties – differences between different climate models and the ways they are constructed including gridding and resolution, the number of ocean and atmospheric levels, timesteps and differences in computer processing. Secondly are the uncertainties in physical parameters used in the model, including the complexity of physical processes and the way they are simulated. Third are the boundary conditions

used by the simulation including physical parameters, palaeogeography and atmospheric chemistry.

The uncertainty and performance of climate models are conventionally tested by comparison with real modern data. Some of the deficiencies noted in HadCM3L under modern conditions include a general overestimation of global precipitation, weakness in modelled ocean overturning circulation as well as limitations in the treatment of eddy circulation and upwelling. HadAM3, the atmospheric model used by HadCM3 does predict mean annual surface air temperatures with good correlation with real-world datasets where observations are well-constrained and topology is accurately represented. However, it is difficult to compare the performance of climate models in polar regions due to the sparse coverage of observational and historical data sets. The uneven Antarctic topography with rapid elevation changes are also difficult to represent in GCMs, particularly low-resolution models such as HadCM3L which can lead to further issues assessing model uncertainty.

Currently HadCM3L is one of the best climate models for use in deep time scenarios. It is stable across multiple platforms and has a relatively fast spin-up, although this comes as a trade-off in terms of model resolution and complexity. However, in deep time the palaeogeography is a key source of model uncertainty, so use of a higher resolution simulation may not provide more accurate results, except in cases where circulation or flow is restricted by bathymetry. As a result, uncertainty in deep time modelling is more likely to be introduced by physical processes representation within the model and by boundary condition uncertainties rather than by any structural model uncertainty.

Some uncertainty lies in the tuning of model parameters and physical properties to present-day climatology. It is unknown how robust these parametrizations may be under significantly difficult boundary conditions, such as those found in the Maastrichtian. Clouds in particular are a major source of model inaccuracy, as they play a significant role in the transmission and reflectance of solar radiation (Solomon et al. 2007), but there is no proxy data for their behaviour in past climates, and as a result parametrization in palaeoclimate models must be entirely based on modern data.

Perhaps the most significant source of uncertainty in deep time palaeoclimate modelling is the error associated with estimates of boundary conditions. CO_2 is

a large source of error, as it affects climate warming (Forster et al. 2007). In this work, multiple proxies have been used to estimate atmospheric CO_2 concentration and experiments have been run to account for several potential CO_2 concentrations as a variable. These proxies are discussed further in Section 7.3.4. Other greenhouse gases are also important in the modern atmosphere and have fewer or no proxies in the geological past, including CH_4, N_2O and O_3, while CFCs which are important greenhouse gas contributors in the modern atmosphere were not present until the 1980s (Forster et al. 2007). CH_4 and N_2O in particular have atmospheric chemistry feedbacks with the CO_2 cycle: oxidation of methane is the main source of water vapour to the upper stratosphere (e.g. Figure 4.9), which in turn has feedbacks into climate including destruction of stratospheric ozone through radical formation, which leads to additional warming of the troposphere and Earth surface (Blake & Rowland 1988). Without accurate boundary conditions for CH_4 and N_2O concentrations, these chemical processes are extremely difficult to model. Other model boundary conditions such as solar insolation, the solar constant and ocean heat flux also have uncertainties associated, but are better constrained relative to the other sources of error discussed here.

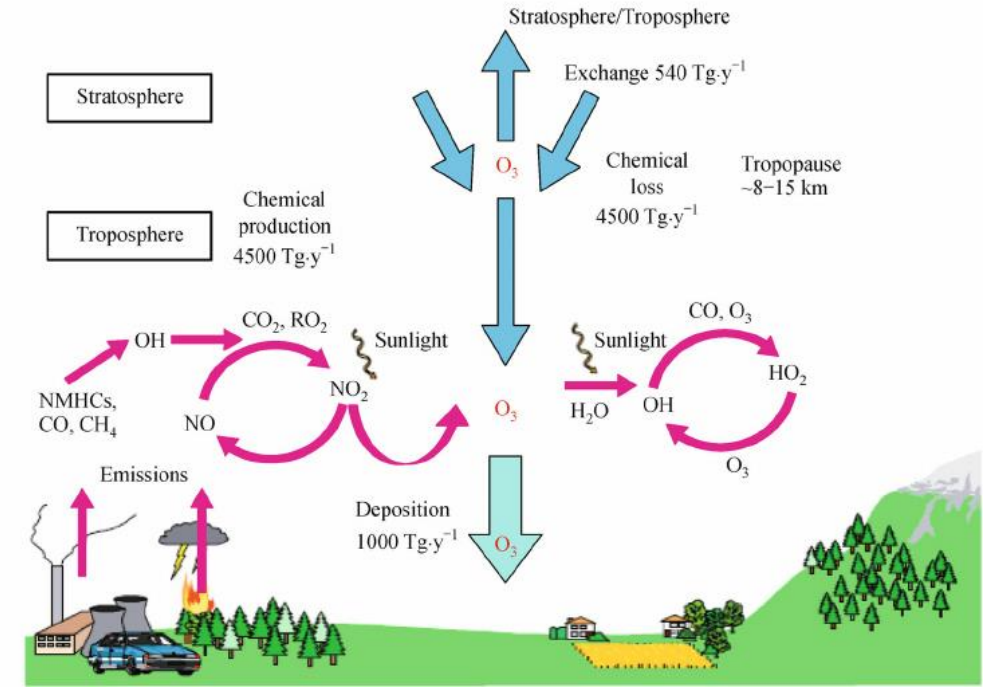

Figure 4.5: Schematic of modern day tropospheric odd-oxygen chemistry and ozone formation showing the interdependence of various atmospheric components to greenhouse gas formation. Taken from Feng et al. (2015).

Palaeogeography is a considerable source of uncertainty and exerts a profound effect on the strength of climate cycles, particularly seasonal cycles as well as climate sensitivity and ocean-atmosphere circulation patterns (e.g. Valdes et al. 1996; Poulsen et al. 1999). Both the accuracy of the reconstruction and the representation of the palaeogeography within the model can cause issues.

Flow can only occur between grid cells linked by a vertical or horizontal edge, therefore palaeogeography must be gridded in order to represent the open channels of flow and prevent restriction. Alternatively, in some cases energy flow may be parametrised and forced to move between cells where the palaeogeography prohibits circulation in order to achieve more realistic results. Within the Maastrichtian palaeogeography used (Markwick & Valdes 2004) there are no regions where flow is specified, aside from the redirection of a river in some experiments.

Sea level and land exposure is also important, as land has less thermal inertia than ocean (Barron et al. 1993; Donnadieu et al. 2006). HadCM3L models the

ocean as a fixed volume with a rigid lid and the Maastrichtian model has been specified as free from permanent ice caps. Potential modelling of effects such as glacioeustatic sea level change is limited by the fidelity of the palaeogeography which does not resolve the shelf or shallow sea bathymetry around the edges of continents.

4.4 Methods

4.4.1 Stable Isotopes

This chapter uses the high resolution and bulk shell carbonate $\delta^{18}O$ data sets used in Chapter 3 to define the seasonality and periodicity of bivalve shell growth.

High resolution stable carbon and oxygen isotope microanalysis was attempted for 29 specimens. The specimens chosen for stable isotope analysis have extremely well preserved original aragonite shell mineralogy which was microsampled following standard procedures (Dettman & Lohmann 1995). Microsampling was undertaken using a Merchantek MicroMill at a resolution of between 5 and 10 samples per visible growth band using an adaptive sampling strategy, i.e. low sampling resolution in fast-growing shell portions, higher resolution in slow-growing portions to give approximately monthly resolution data. Lahillia were polished by dremel to remove any of the previously identified altered surface layers and sampled on the outer surface. Cucullaea were sectioned along the line of maximum growth and sampled from the cut face to avoid the intermittent periostracal layer identified by SEM. The stable oxygen and carbon isotope compositions of the resulting powders were determined using a Micromass Multicarb Sample Preparation System attached to a VG SIRA Mass Spectrometer at the Godwin Laboratory, University of Cambridge. Each run of samples was accompanied by 10 reference carbonates and 2 control samples. The results are reported with reference to the international standard VPDB and the precision is better than +/-0.06‰ for $\delta^{13}C$ and +/-0.08‰ for $\delta^{18}O$.

Additional bulk shell carbonate powders from *Lahillia* and *Cucullaea* were also examined. These were prepared by James Witts for carbon associated sulfate analysis (Witts et al. 2018). Shells were first visually screened for preservation, then crushed whole and washed in an ultrasonic bath to remove the sedimentary matrix from the shell fragments which were hand-crushed into powders. This method of extraction incorporates layers from the entire shell, whereas the high resolution microdrilled specimens sample only the well-preserved outer shell layers. Preservation tests including XRD and trace elemental analysis carried out on bulk powders and shells do confirm the same excellent preservation as in the microdrilled specimens, and the proportion of altered material incorporated appears to be negligible (Appendix A and Witts et al. 2018).

4.4.2 Clumped Isotopes

Two clumped isotope datasets from Seymour Island have been used to provide further constraints on seawater $\delta^{18}O$ composition and temperatures. The first is a published clumped isotope dataset produced by Petersen et al. (2016) using specimens from the Zinsmeister collection of Seymour Island fossils (Zinsmeister & Macellari 1988). Also presented are unpublished data produced by Christina Larkin in 2014 using some of the same *Lahillia* and *Cucullaea* specimens that have been used for high resolution stable isotope thermometry.

The methodology for clumped isotopic analysis is presented modified from Larkin (2014). The automated method from Schmid & Bernasconi (2010) was used coupling a Thermo Scientific Kiel IV Carbonate Device (automated sample preparation device) with a Thermo Scientific MAT 253 Mass Spectrometer. This method used repeated measurements of 160-180 μg aliquots (10 per sample, 8 per standard). The sample gas was fed into the mass spectrometer in 10 cycles against the reference gas. The integration time for measurements was 26 seconds; 10 seconds idle time, with an ion counting time of 288 seconds for 8 cycles per acquisition. This process took approximately 24 hours per sample and the long counting time allowed for shot-noise limit minimisation. Samples weighed 160-180 μg to produce an initial intensity of ~20V on mass 44, where results are more stable (Huntington et al. 2009). Anomalous cycles (where the initial mass 44 intensity was lower than ~12V) were discarded and attributed to problems with the acid drop counter.

Corrections were applied following calculation of Δ47 (Huntington et al. 2009; Dennis et al. 2011). An 'in-house' calibration specific to the instrumentation used was also applied to the data (Figure 4.6).

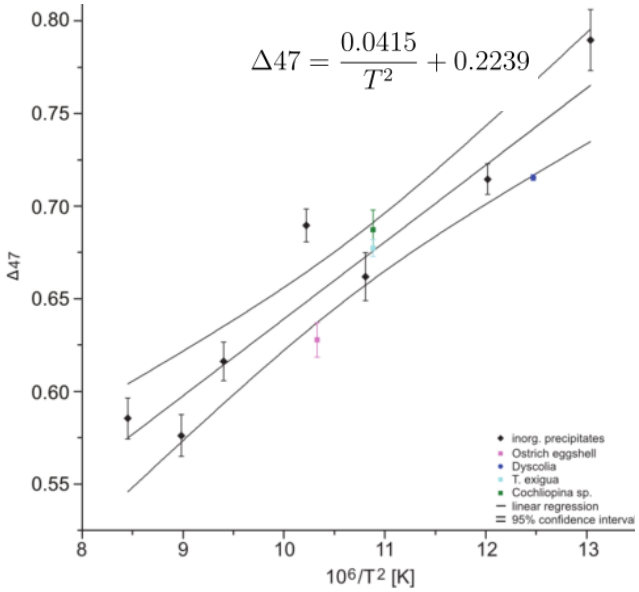

Figure 4.6: Empirical temperature calibration Δ47 is plotted against growing or precipitation temperature with standard error. Linear regression and 95% confidence interval shown in black.

The direct comparison of specimens from the Zinsmeister collections with the specimens presented in this thesis may be problematic due to differences in collection methods. Specimens in Petersen et al. 2016 used point collections which were collected only at GPS points and not from a stratigraphic section, with the relative stratigraphic position of each specimen calculated using the plane projection method (Zinsmeister 2001). This is in contrast to the specimens from the BAS and AFI collections presented here which were taken directly from a measured section in addition to GPS location data. As a result, the stratigraphic heights of the specimens in the clumped isotope dataset (Petersen et al. 2016) are much less reliable than the specimens from measured sections.

In order to determine the extent of this issue when attempting to compare the two datasets, a basic comparison of the stratigraphic ranges of specimens was performed. Taking the K-Pg boundary as a datum and comparing the

stratigraphic ranges of each species used for geochemical analysis with well-established stratigraphic ranges from measured sections (Witts et al. 2016) (Figure 4.7) it becomes evident that the stratigraphic range for several species used for clumped isotopic analysis are not well correlated. *Lahillia* appear around 80m lower, and *Cucullaea ellioti* roughly 30m lower in the stratigraphy constructed by plane projection than the measured stratigraphic section, whereas *Dozyia* extend roughly 60m higher than expected.

The faunal range data, particularly for *Lahillia* and *Cucullaea* have been reliably established in the measured stratigraphy (Zinsmeister 1998; Witts et al. 2016). Therefore, the occurrence of these taxa considerably outside their expected ranges significantly reduces confidence in the plane projection method and the reconstructed heights of the clumped isotope data set. As a result, this dataset is considered less reliable and less useful and will be used only for broad trends and constraining seawater $\delta^{18}O$.

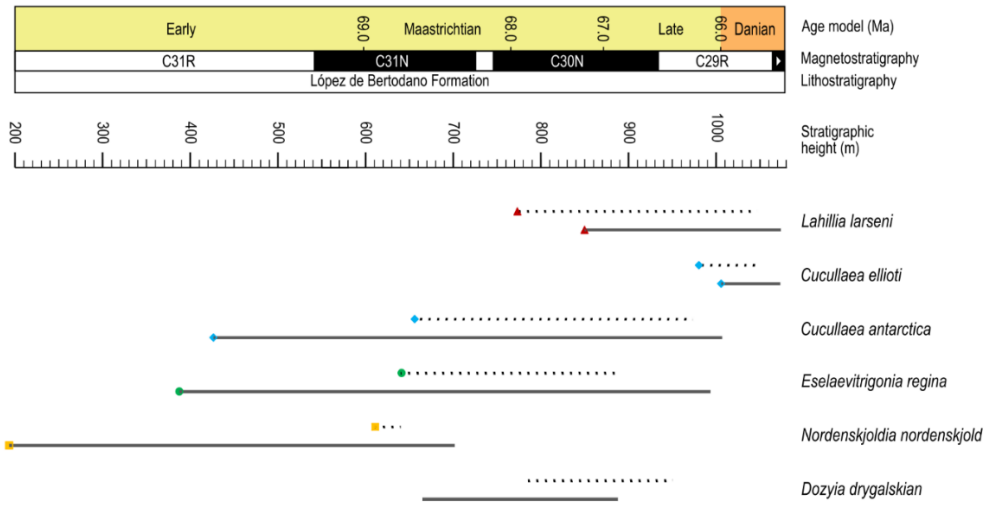

Figure 4.7 Stratigraphic ranges of bivalve species in the measured section (solid line) compared to plane projection reconstructed spot collections (dotted line) showing the large difference in stratigraphic occurrence in species of *Lahillia*, *Cucullaea* and *Dozyia* which suggests the correlation between sections is not particularly good. Stratigraphic heights of each section have been collated using the K-Pg boundary as a datum. Measured section range data from Witts et al. (2016), plane projected section range data from Petersen et al. (2016).

4.4.3 Climate Simulations

Climate simulations for the Maastrichtian were run using the HadCM3L General Circulation Model (GCM), which is a version of the UKMO-HadCM3 Atmosphere-Ocean GCM consisting of a dynamic atmosphere and ocean, with a variety of other optional modules (Gordon et al. 2000). HadCM3L uses a lower resolution ocean model than HadCM3, with a horizontal resolution of 2.5° in latitude by 3.75° in longitude, which is equivalent to a spatial resolution of 278 km north-south by 417 km east-west at the equator and approximately 278 km by 176 km at Seymour Island's palaeolatitude of 60-65°S. In the vertical dimension, there are 19 atmospheric levels and 20 oceanic levels, which are processed with a time step of 30 minutes and coupled once every simulated day. HadCM3L uses identical atmospheric and ocean physics to HadCM3 with modifications to take the reduced spatial resolution into account (Gent & McWilliams 1990) but this trade-off in resolution makes model spin-up times much faster and contributes to the model's stability across multiple platforms.

In this study, climate simulations were performed using parameters selected using the existing palaeoenvironmental data. The model used a Maastrichtian palaeogeography and orography created by Paul Markwick (Markwick & Valdes 2004) which was scaled to the HadCM3L grid (Figure 4.8). Seymour Island's location relative to the Maastrichtian palaeogeography used in the model was calculated by plate rotation from its modern-day position. This gave a palaeolatitude of -59.8 and palaeolongitude of -69.7, which corresponds to cell 16-6 in the schematic illustrated in Figure 4.8. This location is slightly different from the palaeolatitude given from other plate reconstructions (65°S; Lawver et al. 1992; Hay et al. 1999), which would correspond to cell 15-8. Data from both cells have been considered in this chapter, as they encompass the range of possible palaeolatitudes and slightly different modelled water depths (16-6 reaches a depth of 1500m, whereas 15-8 is a shallower 666m).

The majority of experiments used a modern orbit (Table 4.1) but in order to explore the potential temporal variability in sea ice formation around the Larsen Basin, an alternative orbit was used to favour southern hemisphere ice formation. This orbit used insolation and orbital parameters from 207 ka, and was derived to produce the most southern hemisphere sea ice (S.J. Hunter Pers. Comm.). In both cases the model uses modern months as a frame of reference for annual data, with December to February corresponding to

Southern Hemisphere summer, and June to August corresponding to Southern Hemisphere winter. A solar constant of 1358.2 W/m^2 was predicted by stellar evolution models (Gough 1981). The simulation incorporated a static land-ice and dynamic sea ice component (Cattle & Crossley 1995) as well as a tracer scheme that simulates the oxygen isotopic composition throughout the hydrological cycle (Tindall et al. 2009, 2010). Vegetation was predicted dynamically by the interactive vegetation model with HadCM3L.

	Longitude	-125.6	-121.9	-118.1	-114.4	-110.6	-106.9	-103.1	-99.4	-95.6	-91.9	-88.1	-84.4	-80.6	-76.9	-73.1	-69.4	-65.6	-61.9	-58.1	-54.4	-50.6	-46.9
Latitude	Gridref	1	2	3	4	5	6	7	8	9	10	11	12	13	14	15	16	17	18	19	20	21	22
-47.75	1	-4577	-4577	-3962	-3962	-3962	-3962	-3962	-3962	-3347	-3347	-3962	-3962	-3962	-3962	-3962	-3962	-2731	477	53	74	-301	-996
-50.25	2	-4577	-3962	-3962	-3962	-3962	-3962	-3962	-3347	-3347	-3347	-3347	-3347	-3347	-3347	-3347	-3347	-2731	466	-666	132	-447	-996
-52.75	3	-3962	-3962	-3962	-3347	-3347	-3347	-3347	-3347	-2731	-2731	-2731	-2731	-2731	-2731	-2731	-2731	-2731	596	-666	-447	-666	-666
-55.25	4	-2731	-3347	-3347	-3347	-3347	-3347	-2731	-2731	-2731	-2731	-2731	-3347	-3347	-2731	-2731	-2731	-2116	490	-996	-996	-1501	-666
-57.75	5	-3347	-3347	-3347	-3347	-3347	-3347	-2731	-2731	-3347	-3347	-3347	-2731	-2731	-2731	-2116	-2116	-2116	-2116	-1501	-996	-1501	-1501
-60.25	6	-3347	-3347	-3347	-3347	-3347	-2731	-2731	-2731	-3347	-3347	-2731	-2731	-2731	-2116	463	-1501	-2116	-2116	-2116	-2731	-2731	-3347
-62.75	7	-3347	-3347	-3347	-2731	-3347	-2116	-2116	-2116	-2731	-2731	-2731	-2731	155	656	-1501	-1501	-2116	-3347	-3962	-3962	-3962	-3962
-65.25	8	-2731	-2116	-2116	-1501	-1501	-1501	17	-1501	-1501	-2116	-2116	142	487	588	-666	-996	-2731	-3347	-3962	-3962	-3962	-3962
-67.75	9	-1501	-1501	-1501	-666	-996	-996	-996	-996	241	218	303	398	825	-301	-447	-1501	-2116	-3347	-3962	-3962	-3962	-3962
-70.25	10	1	1	-996	-666	-666	-447	-447	-447	-447	-447	-447	-301	-301	-301	-447	-996	-1501	-2116	-2731	-2731	-2731	-2731
-72.75	11	-666	-447	-447	-301	-301	445	684	655	-204	-204	-204	-301	-301	-301	-447	-666	-1501	-2116	-2731	-2731	-2731	-2731
-75.25	12	-204	-204	298	517	453	406	587	-204	-204	-204	-204	-301	-301	-301	-447	-666	-996	-1501	237	220	-2731	-2731
-77.75	13	401	527	632	553	493	301	-139	-139	-204	-204	13	77	316	358	-447	366	450	638	808	945	1055	996
-80.25	14	558	608	567	527	509	425	311	261	271	491	716	822	980	1092	934	936	1082	1107	1041	1072	1117	1008
-82.75	15	528	547	535	497	429	413	515	693	994	1117	1101	1062	1050	1061	1086	1081	1028	1011	1001	1004	1007	1014

Figure 4.8: Maastrichtian Antarctic Peninsula palaeogeography grid used by HadCM3L, from Markwick and Valdes 2004. Orography (greens) and bathymetry (blues) are labelled with height above and below sea level in metres. Grid references (bold numbers across top and left) are consistent throughout. Two possible palaeolocations for Seymour Island are marked in red at 60°S (16-6) and 65°S (15-8).

Variations of this model set-up were chosen to explore various climate scenarios for the Antarctic Peninsula. Atmospheric CO_2 levels are thought to have been variable throughout the Late Cretaceous and Early Paleocene. Estimates of Maastrichtian atmospheric CO_2 vary depending on the proxy record examined, but there is a broad agreement that CO_2 levels during this interval dropped much lower than during the previous ages of the Cretaceous. Stomatal indices give estimates of approximately 500 ppmv (Beerling et al 2002), whereas

pedogenic carbonates give values between 0 and 840 ppmv (Cojan et al 2000, Ghosh et al 2001, Nordt et al 2002, 2003), although the proxy is unlikely to be accurate below 500 ppmv (Ekart et al 1999). More detailed paleosol carbonate records (e.g. Huang et al 2013) suggest variable CO_2 levels throughout the K-Pg boundary interval, with values rising rapidly from around 300 to over 800 ppmv between 69 and 66 Ma and continuing to fluctuate through the early Paleocene. For this set of climate simulations, equilibrium CO_2 levels of 2, 4 and 6x preindustrial concentrations were chosen (560, 1120 and 1680 ppmv). This range of concentrations covers most of the range suggested by proxy data, and the 6xCO_2 concentration simulation is useful to consider the potential effect on atmospheric CO_2 of the Deccan Traps volcanism active immediately prior to the K-Pg (Self et al 2006). The records and effects of different CO_2 concentrations are discussed in more detail in Section 7.3.4.

Initial examinations of model data during spin-up allowed positions of river output to oceans and the drainage basins to be checked, as these are calculated by the model from the palaeogeography and orography rather than being user-defined. Evidence from alternative higher resolution palaeogeographic and basin level reconstruction suggest that the Larsen basin received a large amount of river input from rivers flowing from the Antarctic Peninsula which would have provided the main clastic source for the López de Bertodano Formation (Pirrie 1989; Scasso et al. 1991; Olivero et al. 1992). There is also evidence from sedimentology and palaeontology that Seymour Island was relatively proximal to the source of this clastic input, producing shallow marine deltaic to estuarine deposits with abundant plant material (e.g. Hathway 2000; Francis & Poole 2002; Olivero et al. 2008).

The original modelled drainage produced river output to cell 15-8, but no output to cell 16-6. This may have been caused by uncertainties in palaeogeography which can often lead to differences between modelled and expected drainage patterns. In this case, the drainage basin covering a large amount of the Eastern Antarctic Peninsula was being discharged off the west coast of the peninsula into the Pacific rather than into the Larsen Basin. In order to account for this, the drainage basin covering the Eastern Antarctic Peninsula was rerouted into cell 16-6 in a number of model simulations to provide more realistic results for this location (Figure 4.9).

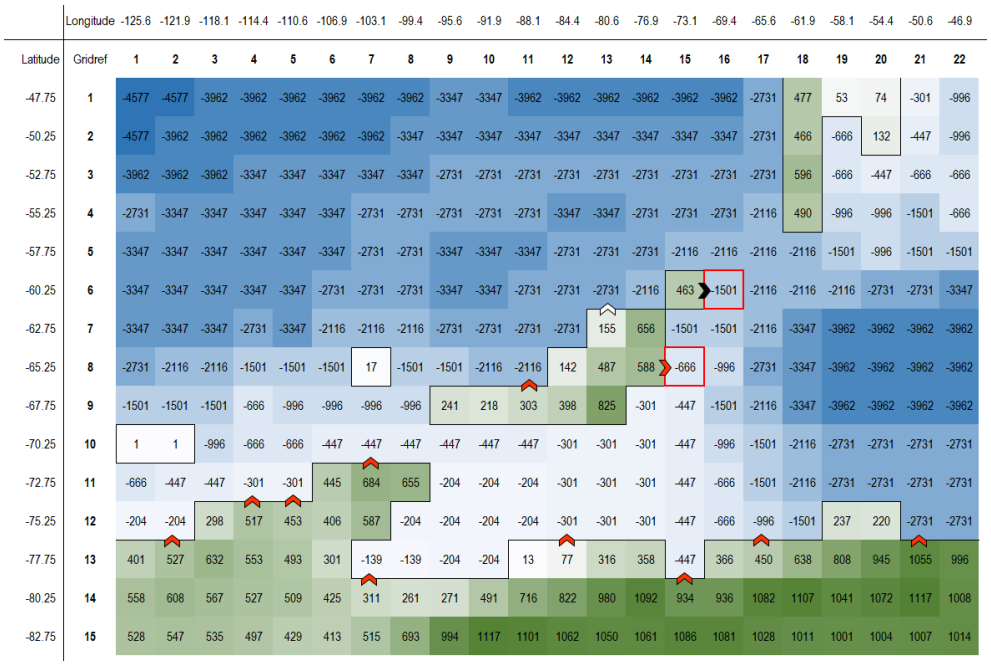

	Longitude	-125.6	-121.9	-118.1	-114.4	-110.6	-106.9	-103.1	-99.4	-95.6	-91.9	-88.1	-84.4	-80.6	-76.9	-73.1	-69.4	-65.6	-61.9	-58.1	-54.4	-50.6	-46.9
Latitude	Gridref	1	2	3	4	5	6	7	8	9	10	11	12	13	14	15	16	17	18	19	20	21	22
-47.75	1	-4577	-4577	-3962	-3962	-3962	-3962	-3962	-3962	-3347	-3347	-3962	-3962	-3962	-3962	-3962	-3962	-2731	477	53	74	-301	-996
-50.25	2	-4577	-3962	-3962	-3962	-3962	-3962	-3962	-3347	-3347	-3347	-3347	-3347	-3347	-3347	-3347	-3347	-2731	466	-666	132	-447	-996
-52.75	3	-3962	-3962	-3962	-3347	-3347	-3347	-3347	-3347	-2731	-2731	-2731	-2731	-2731	-2731	-2731	-2731	-2731	596	-666	-447	-666	-666
-55.25	4	-2731	-3347	-3347	-3347	-3347	-3347	-2731	-2731	-2731	-2731	-2731	-3347	-3347	-2731	-2731	-2731	-2116	490	-996	-996	-1501	-666
-57.75	5	-3347	-3347	-3347	-3347	-3347	-3347	-2731	-2731	-3347	-3347	-3347	-2731	-2731	-2731	-2116	-2116	-2116	-2116	-1501	-996	-1501	-1501
-60.25	6	-3347	-3347	-3347	-3347	-3347	-2731	-2731	-2731	-3347	-3347	-2731	-2731	-2731	-2116	463	-1501	-2116	-2116	-2116	-2731	-2731	-3347
-62.75	7	-3347	-3347	-3347	-2731	-3347	-2116	-2116	-2116	-2731	-2731	-2731	-2731	155	656	-1501	-1501	-2116	-3347	-3962	-3962	-3962	-3962
-65.25	8	-2731	-2116	-2116	-1501	-1501	-1501	17	-1501	-1501	-2116	-2116	142	487	588	-666	-996	-2731	-3347	-3962	-3962	-3962	-3962
-67.75	9	-1501	-1501	-1501	-666	-996	-996	-996	-996	241	218	303	398	825	-301	-447	-1501	-2116	-3347	-3962	-3962	-3962	-3962
-70.25	10	1	1	-996	-666	-666	-447	-447	-447	-447	-447	-447	-301	-301	-301	-447	-996	-1501	-2116	-2731	-2731	-2731	-2731
-72.75	11	-666	-447	-447	-301	-301	445	684	655	-204	-204	-204	-301	-301	-301	-447	-666	-1501	-2116	-2731	-2731	-2731	-2731
-75.25	12	-204	-204	298	517	453	406	587	-204	-204	-204	-204	-301	-301	-301	-447	-666	-996	-1501	237	220	-2731	-2731
-77.75	13	401	527	632	553	493	301	-139	-139	-204	-204	13	77	316	358	-447	366	450	638	808	945	1055	996
-80.25	14	558	608	567	527	509	425	311	261	271	491	716	822	980	1092	934	936	1082	1107	1041	1072	1117	1008
-82.75	15	528	547	535	497	429	413	515	693	994	1117	1101	1062	1050	1061	1086	1081	1028	1011	1001	1004	1007	1014

Figure 4.9 Maastrichtian Antarctic Peninsula bathymetry (blues) and orography (greens) from Figure 4.8 with positions of continental drainage marked with arrows. River draining into 13-6 in original simulation (white) was manually re-routed (black) to drain into Seymour Island's approximate palaeolocation at 16-6 in some simulations.

A summary of the combinations of models and conditions used are presented with the designated names that the scenarios have been refered to throughout the remainder of this thesis. This work also only used model outputs from an area surrounding the Antarctic Peninsula (Figure 4.8), although the model was run to simulate the entire globe.

Table 4.1: List of model parameter combinations used in this study with designated names and the model outputs produced.

	2 x CO_2	4 x CO_2	6 x CO_2
Markwick & Valdes 2004 Maastrichtian palaeogeography and modern orbit	Maas2 Temperature and $\delta^{18}O$	Maas4 Temperature and $\delta^{18}O$	Maas6 Temperature
Markwick & Valdes 2004 palaeogeography and modern orbit with river redirected to drain into Seymour Island's grid location	Maas2 riv Temperature and $\delta^{18}O$	Maas4 riv Temperature and $\delta^{18}O$	
Markwick & Valdes 2004 palaeogeography with redirected river and southern-hemisphere favourable sea-ice orbit (207k)	Maas2 riv 207 Temperature and $\delta^{18}O$		

4.5 Results

4.5.1 Oxygen Isotope Data

This chapter focuses on the stratigraphic context of the sub-annual scale oxygen isotopic data presented in Chapter 3 which were used to determine the seasonality and periodicity of bivalve shell growth.

The range and means of these data have been plotted through the stratigraphic section alongside bulk $\delta^{18}O$ data from a number of additional *Cucullaea* and *Lahillia* shells and other calcifying organisms (Figure 4.10). Also presented are existing climate interpretations from palynology (Bowman et al. 2013) and in particular the *Impletosphaeridium clavus* dinoflagellate record, which has been used as a proxy for the presence of sea ice in the Seymour Island section.

Bulk shell $\delta^{18}O$ data were extremely similar to the microsampled shells. The mean $\delta^{18}O$ of each sub-annually sampled microdrilled shell ranged from 1.68 to -0.61‰, while bulk shell $\delta^{18}O$ was between 1.88 and -0.35‰.

There appears to be little variation in the broad trend of $\delta^{18}O$ through stratigraphy which remains at approximately 0.8‰, even across intervals of changing climate suggested from the palynological data. Specimens from below the 750m level in the section have the most positive $\delta^{18}O$, which suggests that they may have been recording slightly cooler temperatures. From 750 to 830m, there is a large amount of variation in the bulk temperature data, although the single specimen examined at sub annual resolutions from this interval suggests that seasonal temperature variation may have been lower than in specimens from the other climate intervals. Bivalve shells from the K-Pg recovery interval do appear to show a slight trend towards more positive $\delta^{18}O$ compositions into the Danian, and less variability within the interval with values clustered between 1.53 and 0.08‰.

Data from aragonitic gastropods through the section show a systematic trend towards more positive $\delta^{18}O$ compositions than bivalves from the same stratigraphic height with an average shell $\delta^{18}O$ of between 1.0 and 1.6‰ throughout and slightly more variation through stratigraphy (Tobin et al. 2012 and Figure 4.10). The potential causes of this apparent discrepancy will be discussed in Chapter 7.

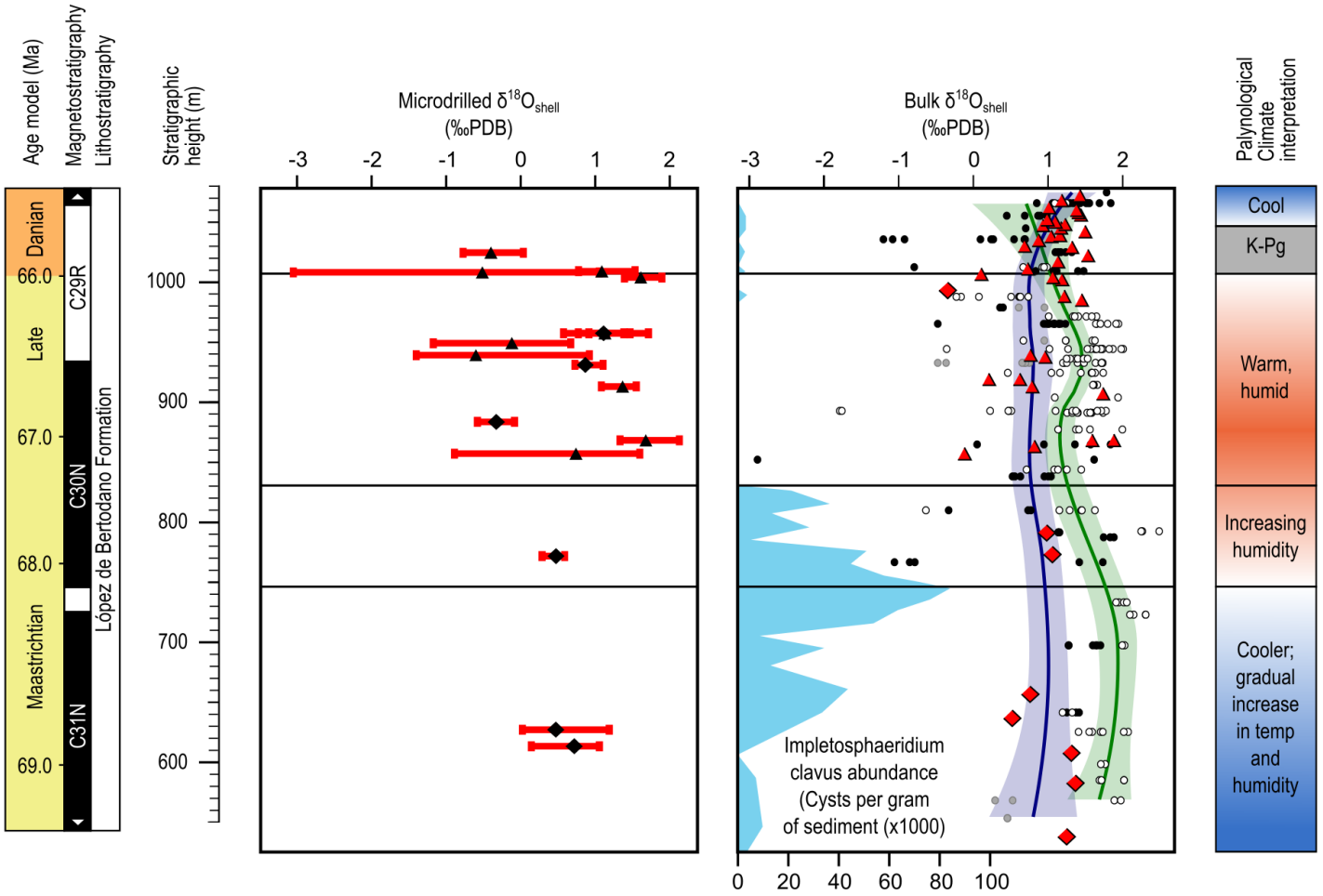

Figure 4.10: Stratigraphic $\delta^{18}O$ and climate trends. Microdrilled shell data from *Cucullaea* (diamonds) and *Lahillia* (triangles) with red horizontal bars representing the range of values found within each shell. Bulk data from *Cucullaea* (red diamonds) and *Lahillia* (red triangles) and additional aragonitic bivalves (filled circles) calcitic bivalves (gray circles) and gastropods (hollow circles) from Tobin et al 2012. Curves are Loess fits for bivalves (blue) and gastropods (green). Blue field indicates *I. clavus* abundance from Bowman et al 2013 and is used as a proxy for sea ice presence.

Work in Chapter 3 established that the shell material in *Lahillia* and *Cucullaea* from the Lopez de Bertodano formation was largely produced during the warm spring to summer period. This means that the peak temperature from the growth increment between each visible growth line gives an indication of the temperature conditions during the warmest months. Similarly, averaging temperature data from readings taken on the growth line will allow an estimate of cool season temperature, allowing the minimum mean seasonality to be determined.

For each specimen with high resolution data, the peak temperatures from each year of shell growth were averaged to give an indication of warm month mean temperature (WMMT) and measurements on each annual growth line were also averaged to estimate cold month mean temperature (CMMT). This raw $\delta^{18}O$ data is presented in Table 4.2.

Table 4.2: $\delta^{18}O$ data from microsampled shells showing the mean $\delta^{18}O$, winter average $\delta^{18}O$ calculated from the average of $\delta^{18}O$ at each growth line, summer average temperature calculated from the average of peak summer $\delta^{18}O$ during each subsequent growth year increment (Y1-Y7)

Specimen	Species	Section Height	Mean δ18O	Winter Avg δ18O	Summer Avg δ18O	Peak δ18O Y1	Y2	Y3	Y4	Y5	Y6	Y7
D9.207.1	*Lahillia*	1026.4	-0.37	0.27	-0.65	-0.50	-0.43	-0.69	-0.78	-0.71	-0.75	
D9.206.152	*Lahillia*	1011	1.06	1.20	0.92	0.84	1.27	0.77	0.86	0.88		
D5.229.1301.2	*Lahillia*	1010	-0.65	0.81	-1.77	-1.86	-3.06	-1.07	-1.07			
DJ.953.746	*Lahillia*	1005.75	1.60	1.77	1.44	1.45	1.44					
D5.222.1248.2	*Cucullaea*	975	0.56	0.58	0.40	0.40						
DJ.953.335	*Lahillia*	959.25	1.03	1.35	0.91	1.15	0.80	0.91	0.77			
DJ.953.456	*Lahillia*	959.25	1.12	1.28	0.95	0.92	0.92	0.96	0.91	1.06		
DJ.953.459-464	*Cucullaea*	959.25	1.10	1.48	0.77	0.98	0.57	0.75				
D5.222.1234.2	*Lahillia*	951	-0.12	0.56	-0.56	0.09	-0.60	-1.18				
D5.220.1226.2	*Lahillia*	941	-0.61	0.63	-1.39	-1.41	-1.37					
D5.220.1214.2	*Lahillia*	915	1.36	1.47	1.10	1.08	1.13					
D5.220.1229.2	*Cucullaea*	885.5	-0.33	-0.14	-0.44	-0.37	-0.51					
DJ.952.523	*Lahillia*	870.05	1.68	2.01	1.48	1.53	1.33	1.67	1.41			
D5.219.1185.2	*Lahillia*	865	0.81	1.04	0.70	0.93	0.86	0.68	0.33			
D5.219.1182.2	*Lahillia*	859	0.78	1.28	0.43	0.68	0.43	0.24	0.52	0.41	0.39	0.32
DJ.957.490	*Cucullaea*	773.75	0.47	0.58	0.38	0.28	0.48					
D5.218.1011.2	*Cucullaea*	629	0.54	0.82	0.02	0.02						
DJ.959.93	*Cucullaea*	615.25	0.67	0.92	-0.86	-1.87	0.14					

4.5.2 Clumped Isotope Data

Temperatures calculated from clumped isotopes have also ben plotted through stratigraphy to examine the broad trends and compare them with the $\delta^{18}O$ record. However, as discussed in Section 4.4.2, the clumped isotope data points taken from Petersen et al. (2016) may not be well correlated with the stratigraphic section used in this study.

The existing clumped isotopic record has been interpreted to show a period of cooling in the last million years of the Maastrichtian and no clear trend of warming or cooling in the K-Pg recovery interval (Petersen et al. 2016). Cooler temperatures in the lower portions of stratigraphy and a slight warming trend to approximately 200m below the K-Pg boundary are also suggested.

The addition of several clumped isotopic data points from specimens collected from measured sections (Larkin 2014) compares fairly well with the original data set. These additional points do appear to corroborate with the observations of temperatures near freezing in the latest Maastrichtian.

Clumped isotope data were also used to constrain seawater $\delta^{18}O$. Estimates of $\delta^{18}O$ varied hugely both through the section, and by species ranging from -3.42 to 1.05 overall (Figure 4.11). Average $\delta^{18}O$ appears to be more positive in the Maastrichtian Lopez de Bertodano Formation, becoming more negative during the Danian Lopez de Bertodano Formation (Table 4.3).

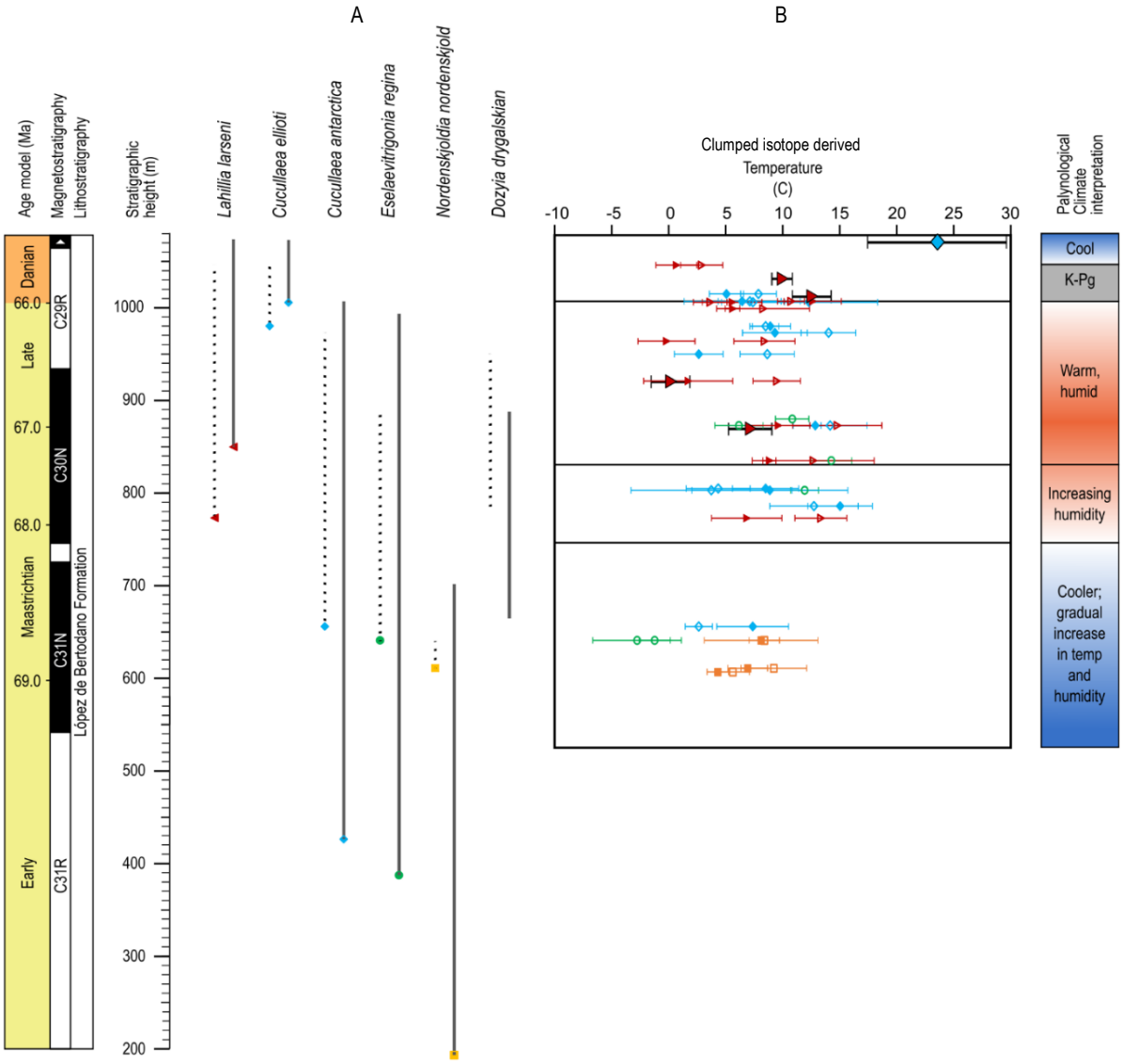

Figure 4.11: (A) Stratigraphic ranges of each bivalve species used for clumped isotopic analysis (see Figure 4.7 for details). (B) Full clumped isotopic temperature data set from Petersen et al. (2016) (no outline) and Larkin (2014) (black outline) colour and shape coded by species using the same key as the stratigraphic range diagram. Filled and open points represent average temperatures with analytical errors plotted as horizontal error bars.

Table 4.3: Average oxygen isotopic composition of shells used for clumped isotopic analysis temperature by species and stratigraphy (data from Petersen et al. (2016) and Larkin (2014). Average $\delta^{18}O_{sw}$ is variable between species, but appears to become more negative from the Maastrichtian to the Danian.

	Maastrichtian Lopez de Bertodano Formation			Danian Lopez de Bertodano Formation		
Species	Average $\delta^{18}O_{sw}$ (‰ PDB)	Average Δ47 Temp. (°C)	n	Average $\delta^{18}O_{sw}$ (‰ PDB)	Average Δ47 Temp. (°C)	n
Cucullaea	-1.26	9.0	63	-2.00	10.1	16
Eselaevitrigonia	-1.22	6.5	21			
Lahillia	-1.24	7.2	59	-1.60	8.3	15
Nordenskjoldia	-1.58	6.5	22			
All Species	-1.29		165	-1.80		31

4.5.3 Model Results

The primary outputs of the modelling work were the water temperature and $\delta^{18}O$ in the two potential grid cells (16-6 and 15-8) identified in Section 4.4.3 as being representative of Seymour Island's palaeolocation. 16-6 is at a palaeolatitude of 59.8°S, but in the James Ross Basin's correct relative palaeogeographic location, whereas 15-8 is closer to the palaeolatitude reported from other plate reconstructions (65°S; Lawver et al. 1992; Hay et al. 1999) but with slightly different relative palaeogeography (Figure 4.8). This chapter also only examines model outputs from an area surrounding the Antarctic Peninsula (Figure 4.8), although the model was run to simulate the entire globe. A summary of the combinations of models and conditions used are presented in Table 4.1.

Data were recorded from the final 450 months of the spun-up simulation under each set of model parameters. Figures 4.12 to 4.14 show the average annual variation in temperature through the top 300m of the water column for each grid location and parameter combination. Maximum temperatures at the surface are reached between January and April, with minimum surface temperatures between July and November. Under all sets of parameters, there is negligible annual temperature variation at water depths greater than 200m.

Figures 4.15 and 4.16 show the annual variation in water $\delta^{18}O$ for each isotope enabled simulation. These show little evidence for seasonal behaviour at any water depth, however there is a marked gradient from more negative surface waters to less negative deep waters, particularly in simulations with direct river output to the cell.

In order to examine the contribution of ^{18}O enriched river water to these trends, the seasonal average outputs of both rivers were also recorded (Figure 4.17). Riverine $\delta^{18}O$ also appears to be seasonally variable, with the most negative compositions between September and February, and less negative compositions between March and June

Modelled air temperatures show a range similar to surface water temperatures, and mean annual temperatures similar to mean annual water temperatures for each model (Figure 4.18).

16-6 Maas2

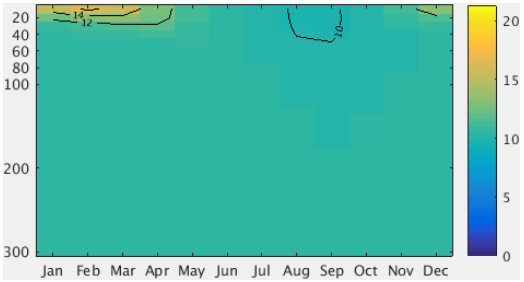

16-6 Maas4

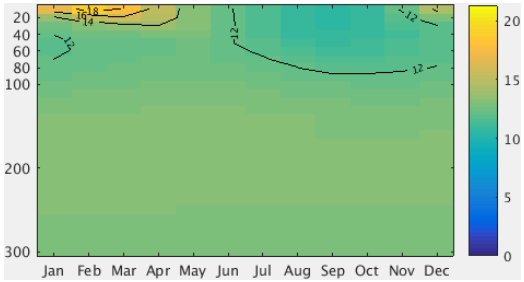

16-6 Maas6

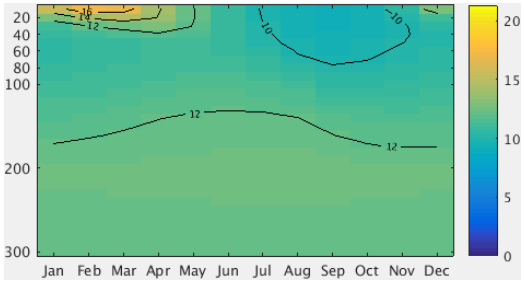

Figure 4.12: Monthly water column temperature profiles at 16-6 modelled using different atmospheric CO_2 concentrations. Temperatures are presented in degrees C using equivalent colour scales.

16-6 Maas2 riv

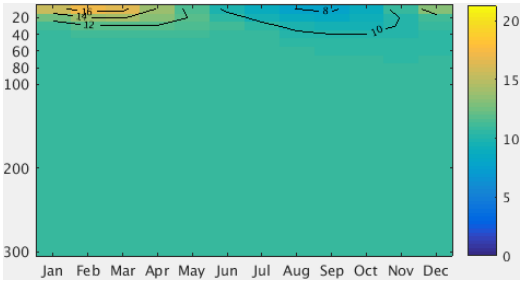

16-6 Maas2 riv 207

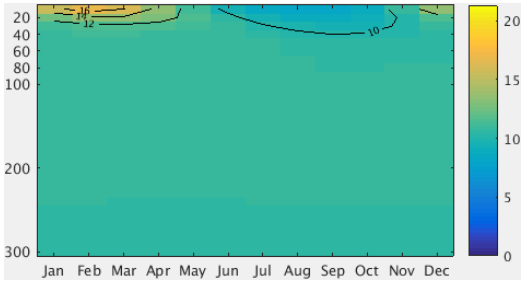

16-6 Maas4 riv

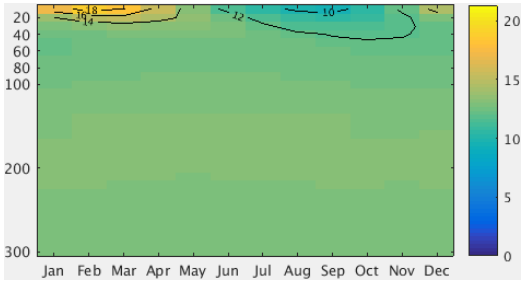

Figure 4.13: Monthly water column temperature profiles at 16-6 modelled using the rerouted drainage to produce river output to 16-6 under different atmospheric CO_2 concentrations and orbital conditions. Temperatures are presented in degrees C using equivalent colour scales.

15-8 Maas2

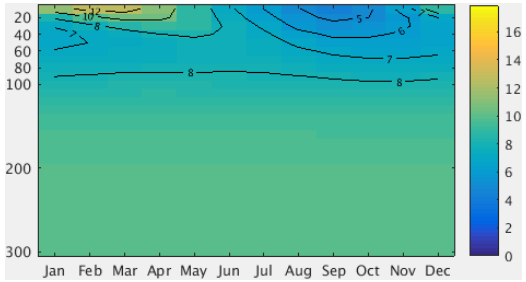

15-8 Maas4

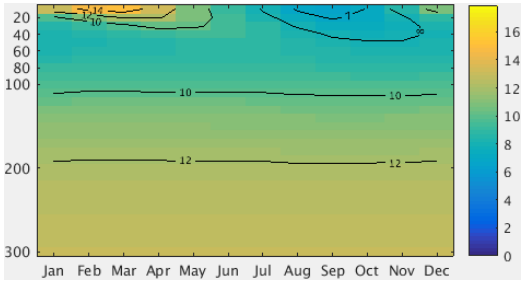

15-8 Maas6

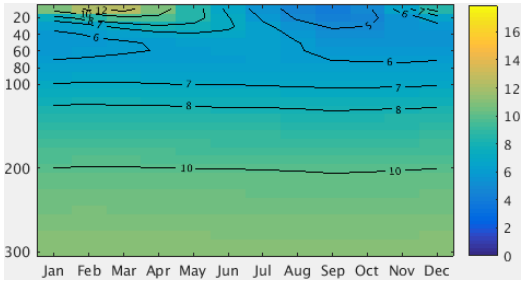

15-8 Maas2 207

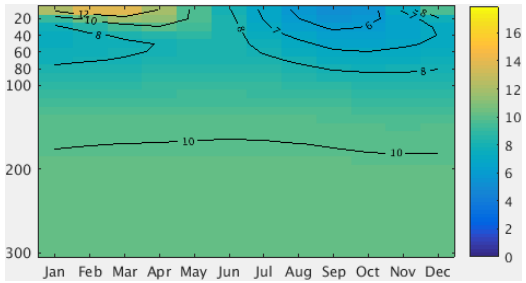

Figure 4.14: Monthly water column temperature profiles 15-8 at Seymour Island's grid location modelled using different atmospheric CO_2 concentrations. Temperatures are presented in degrees C using equivalent colour scales.

16-6 Maas2

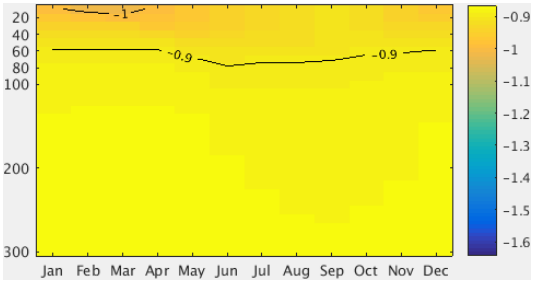

16-6 Maas2 riv

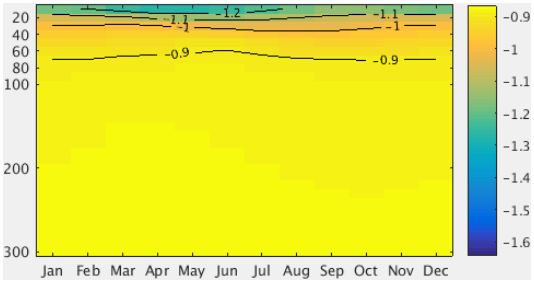

16-6 Maas2 riv 207

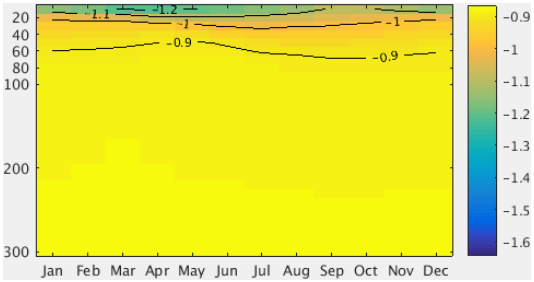

16-6 Maas4

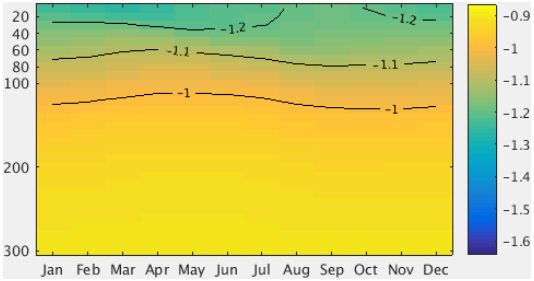

16-6 Maas4 riv

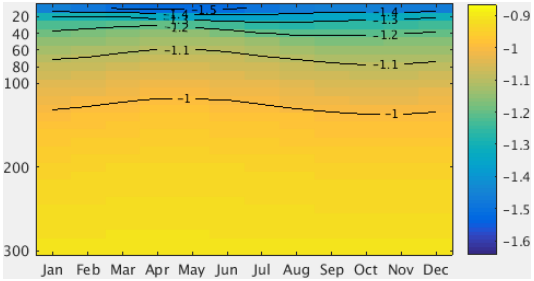

Figure 4.15: Monthly water column $\delta^{18}O$ profiles at 16-6 modelled using different atmospheric CO_2 concentrations, drainage patterns and orbital conditions. $\delta^{18}O$ presented in ‰ relative to V-SMOW.

15-8 Maas2

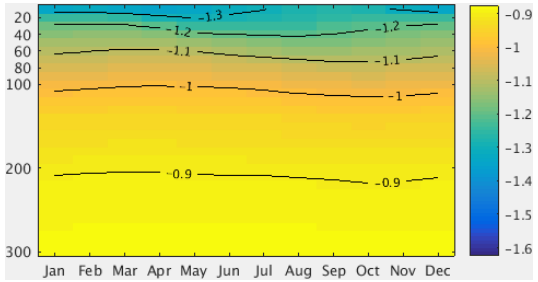

15-8 Maas2 207

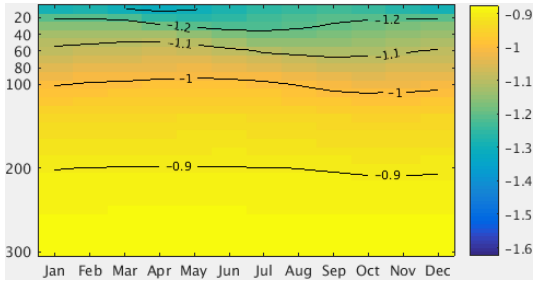

15-8 Maas4

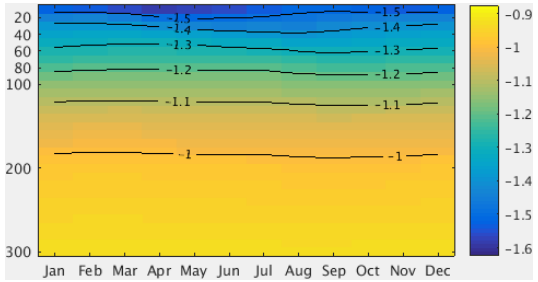

Figure 4.16: Monthly water column $\delta^{18}O$ profiles at 15-8 modelled using different atmospheric CO_2 concentrations, drainage patterns and orbital conditions. $\delta^{18}O$ presented in ‰ relative to V-SMOW.

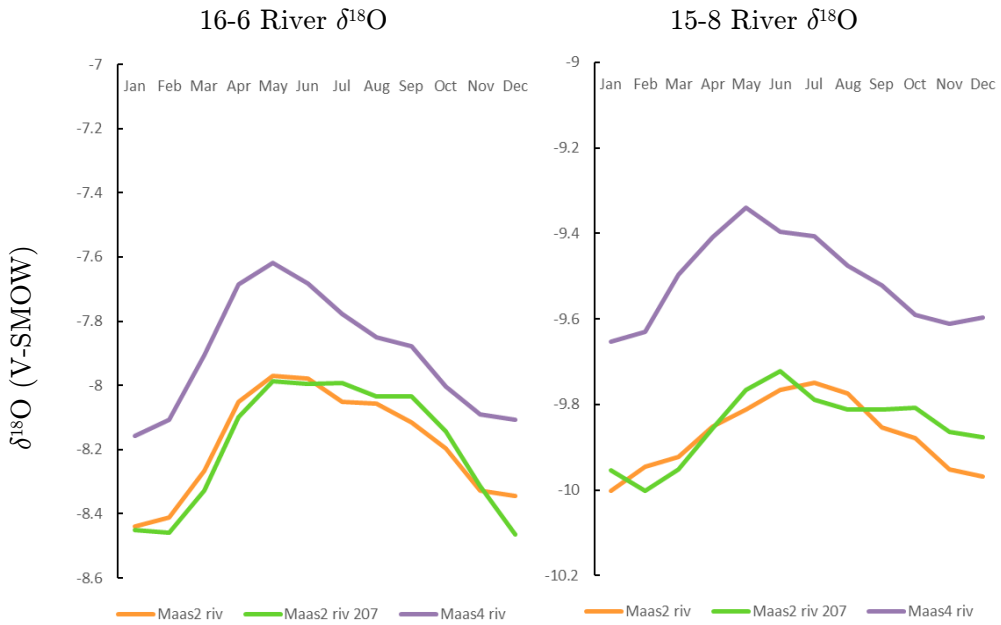

Figure 4.17: Modelled δ^{18}O of rerouted river water redirected into 16-6 and draining into 15-8 under different atmospheric CO_2 concentrations and orbital conditions.

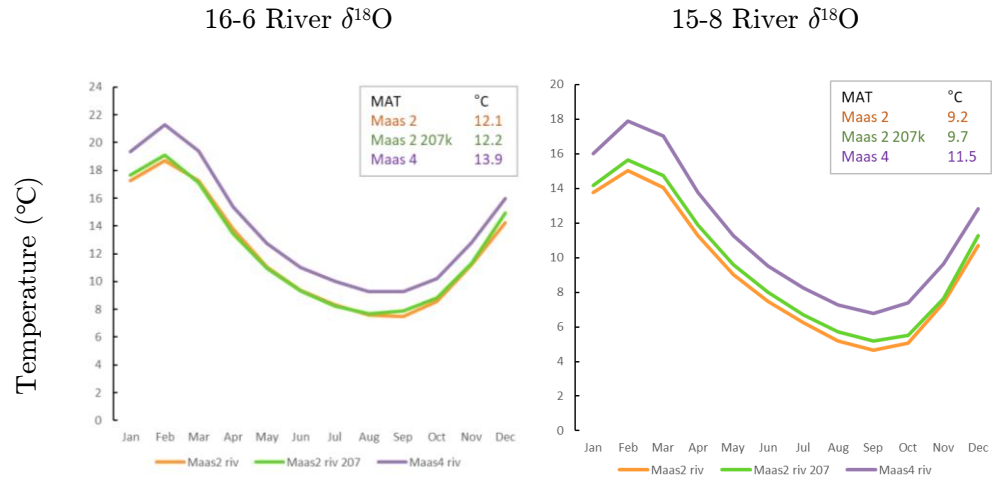

Figure 4.18: Modelled annual and mean annual surface air temperatures under different atmospheric CO_2 concentrations and orbital conditions.

4.6 Discussion

4.6.1 Proxy conversions and assumptions

As discussed in Section 4.3.1, one of the largest sources of error to temperatures reconstructed from shell $\delta^{18}O$ data is the uncertainty in the $\delta^{18}O$ composition of the ambient water. Conventionally, in conditions that can be assumed to be ice-free, $\delta^{18}O_{sw}$ is taken as −1.0‰ (Zachos et al. 2001) but it is likely that at high latitudes where there is existing evidence for sea ice (see Section 2.5) that $\delta^{18}O$ is unlikely to have been constant throughout the section. Additional data from clumped isotopes and isotope enabled modelling allowed approximate upper and lower estimates of $\delta^{18}O$ to be estimated in order to produce a range of more accurate potential temperatures from shell $\delta^{18}O$ data.

Seawater $\delta^{18}O$ calculated from clumped isotope data ranged from –3.42 to 1.05‰ in specimens of *Lahillia* and *Cucullaea*. Both species suggest more negative $\delta^{18}O_{sw}$ compositions in the Danian than the Maastrichtian, however only around 25% of the number of specimens were measured from the Danian than the Maastrichtian in each species (Table 4.3). This large range emphasises the potential variability of water $\delta^{18}O$ compared to the assumption that seawater $\delta^{18}O$ in ice-free conditions can be taken as −1‰ (Zachos et al. 2001). Previous studies have noted a correlation between low clumped isotope temperature and reduced $\delta^{18}O$ of seawater, which has been suggested to be due to seasonal runoff, precipitation or even ice melt (Petersen et al. 2016). This relationship is highlighted by Figure 4.19.

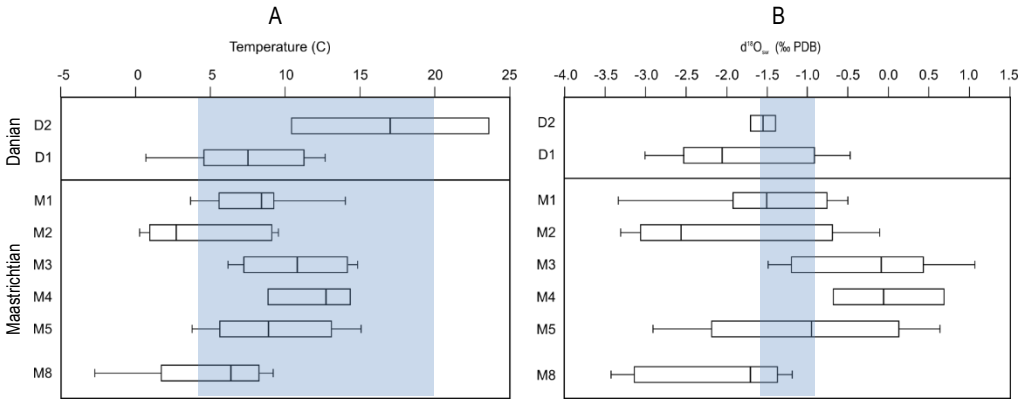

Figure 4.19: Box plots of (A) clumped-isotope derived temperatures and (B) $\delta^{18}O_{sw}$ values calculated from the difference between clumped-isotope derived temperature and $\delta^{18}O$ derived temperature from the same samples (data from Petersen et al. 2016 and Larkin, 2014). Separated into 50m stratigraphic intervals M8 to D2 (see Figure 2.13). Blue shading represents maximum and minimum values of T and $\delta^{18}O_{sw}$ generated across the top 300m in both location cells and all simulation conditions.

In models, the range of seawater $\delta^{18}O$ was lower than predicted by clumped isotopic data, with all simulations falling between −0.9 and −1.6‰ and a trend of more negative $\delta^{18}O$ in surface waters becoming less negative with depth. Experiments at $2xCO_2$ showed less of a range than experiments at $4xCO_2$, and the addition of riverine freshwater input caused the compositions of surface waters to become more enriched in ^{16}O, but had little effect on the composition of modelled waters deeper than approximately 50 m.

The difference between the clumped isotopic and modelled data may arise from a number of issues. Firstly, the model may be overestimating $\delta^{18}O$; the water depth in the modelled cells are deeper than the 70 to 200 m shelf location of Seymour Island was likely to have been (Macellari 1988; Crame et al. 2004), which can result in a dilution of a freshwater signal as it is mixed with a larger volume of marine water than would have been present in real life. However, examination of the modelled $\delta^{18}O$ of the river water only produces $\delta^{18}O$ as low as −8.5‰ in cell 16-6 and −10.0‰ in cell 15-8 (Figure 4.17). This means that in order to produce $\delta^{18}O$ compositions as negative as the clumped isotopic data, a mixture of between 25% and 35% river water in seawater would be required. This amount of freshwater input would produce brackish water conditions, which there is no evidence for in the Lopez de Bertodano Formation on Seymour Island (Crame et al. 2004). It is possible that the model may be underestimating riverine $\delta^{18}O$, factors such as high-altitude glaciation and

meltwater runoff may produce significant volumes of freshwater enriched in ^{16}O. These processes are difficult to model due to the large elevation changes in the mountains of the Antarctic Peninsula, and uncertainties in reconstructing palaeogeographic elevation.

Conversely, the clumped isotopic data may be producing temperature estimations that are too low compared to the temperatures reconstructed from $\delta^{18}O$. This could occur due to several mechanisms discussed in section 4.3.2; the bivalves could be growing under non-equilibrated conditions; an effect which has been observed in some species of bivalve, particularly under low temperature conditions (e.g. Saenger et al. 2012) such as those found in Seymour Island. The effects of anticlumping can also produce a bias towards lower temperatures, and although this effect has not been directly observed in marine bivalves, it has been found in biogenic methane, which may have been a major contributor to shell DIC (see Chapters 6 and 7 for further discussion). Section 4.6.4 uses climate models more to explore the potential for the lower temperatures predicted by clumped isotope data and potential for sea ice formation in the models.

As a result of the uncertainty in seawater composition, a range of water $\delta^{18}O$ from −1 to −2‰ was used for temperature conversion of $\delta^{18}O_{shell}$ data. Seawater of −1 was taken as a conventional top end estimate (Zachos et al. 2001), and a most negative composition of −2 was chosen as it was the lowest average $\delta^{18}O_{seawater}$ derived from clumped isotopes in *Lahillia* and *Cucullaea*. This range also encompasses the majority of modelled water conditions.

Raw $\delta^{18}O$ data from each specimen were converted to temperature data using standard aragonite conversions (Grossman & Ku 1986; Schöne et al. 2002) using two variations of the temperature conversion equation with two values for seawater $\delta^{18}O$ (−1 and −2‰). This produces an approximate upper and lower estimate of each point of temperature data for each shell (Table 4.4).

These data have been plotted through stratigraphy, but do not appear to show any major changes between the climate intervals previously defined by palynology, and little change in WMMT or CMMT over the K-Pg boundary. However, the amount of annual temperature seasonality does appear to increase over the mass extinction. Changes in seasonality will be discussed further in Chapter 5.

Table 4.4: Seasonal temperature data from bivalve specimens sampled at high resolution calculated from $\delta^{18}O$ using two variations of conversion equation to produce a "maximum" and "minimum" temperature estimate under a range of potential water $\delta^{18}O$ conditions

			High Temperature Estimate			**Low Temperature Estimate**		
			Aragonite Mollusc (Grossman and Ku 1986) $\delta^{18}O$ sw = –1			Aragonite General (Grossman and Ku 1986) $\delta^{18}O$ sw = –2		
			T (℃) = 21.8 – 4.69 * ($\delta^{18}O$ shell – ($-\delta^{18}O$ sw – 0.2))			T (℃) = 20.6 – 4.34 * ($\delta^{18}O$ shell – ($-\delta^{18}O$ sw – 0.2))		
Specimen	Species	Section Height	Seasonal Range	Winter Avg	Summer Avg	Seasonal Range	Winter Avg	Summer Avg
D9.207.1	*Lahillia*	1026.4	4.29	14.91	19.20	3.97	9.88	13.85
D9.206.152	*Lahillia*	1011	1.32	10.52	11.84	1.22	5.82	7.05
D5.229.1301.2	*Lahillia*	1010	12.07	12.38	24.45	11.17	7.54	18.72
DJ.953.746	*Lahillia*	1005.75	1.55	7.85	9.40	1.43	3.35	4.78
D5.222.1248.2	*Cucullaea*	975	0.86	13.46	14.32	0.79	8.55	9.34
DJ.953.335	*Lahillia*	959.25	2.07	9.85	11.92	1.92	5.21	7.12
DJ.953.456	*Lahillia*	959.25	1.53	10.17	11.70	1.41	5.50	6.91
DJ.953.459-464	*Cucullaea*	959.25	3.35	9.23	12.58	3.10	4.62	7.73
D5.222.1234.2	*Lahillia*	951	5.29	13.53	18.82	4.89	8.61	13.50
D5.220.1226.2	*Lahillia*	941	9.45	13.22	22.68	8.75	8.32	17.07
D5.220.1214.2	*Lahillia*	915	1.73	9.26	10.99	1.60	4.66	6.26
D5.220.1229.2	*Cucullaea*	885.5	1.40	16.83	18.23	1.29	11.66	12.96
DJ.952.523	*Lahillia*	870.05	2.49	6.72	9.21	2.30	2.31	4.61
D5.219.1185.2	*Lahillia*	865	1.61	11.29	12.89	1.49	6.53	8.02
D5.219.1182.2	*Lahillia*	859	4.00	10.16	14.16	3.70	5.49	9.19
DJ.957.490	*Cucullaea*	773.75	0.95	13.44	14.38	0.88	8.52	9.40
D5.218.1011.2	*Cucullaea*	629	3.76	12.33	16.09	3.48	7.50	10.98
DJ.959.93	*Cucullaea*	615.25	8.38	11.84	20.23	7.76	7.05	14.80

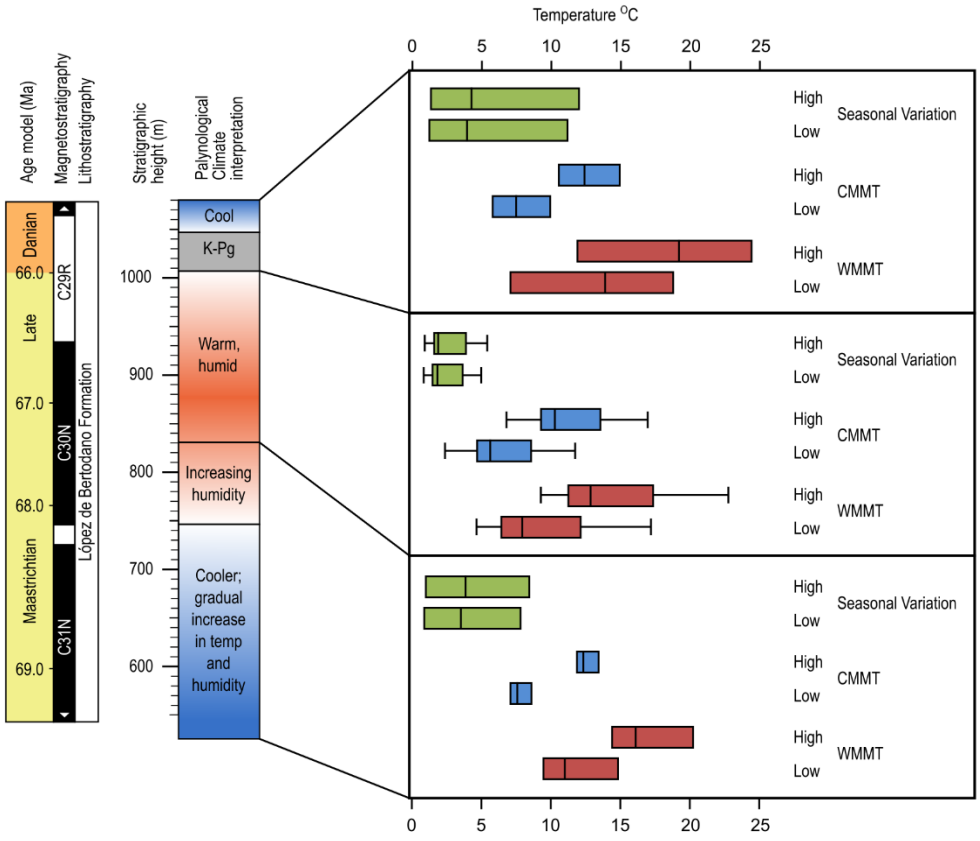

Figure 4.20: High estimate and low estimate δ^{18}O-derived temperature box plots illustrating the data from Table 4.4 separated into broad intervals defined by the local palynological climate interpretation. The changes in the amount of temperature seasonality through stratigraphy will be discussed further in Chapter 5

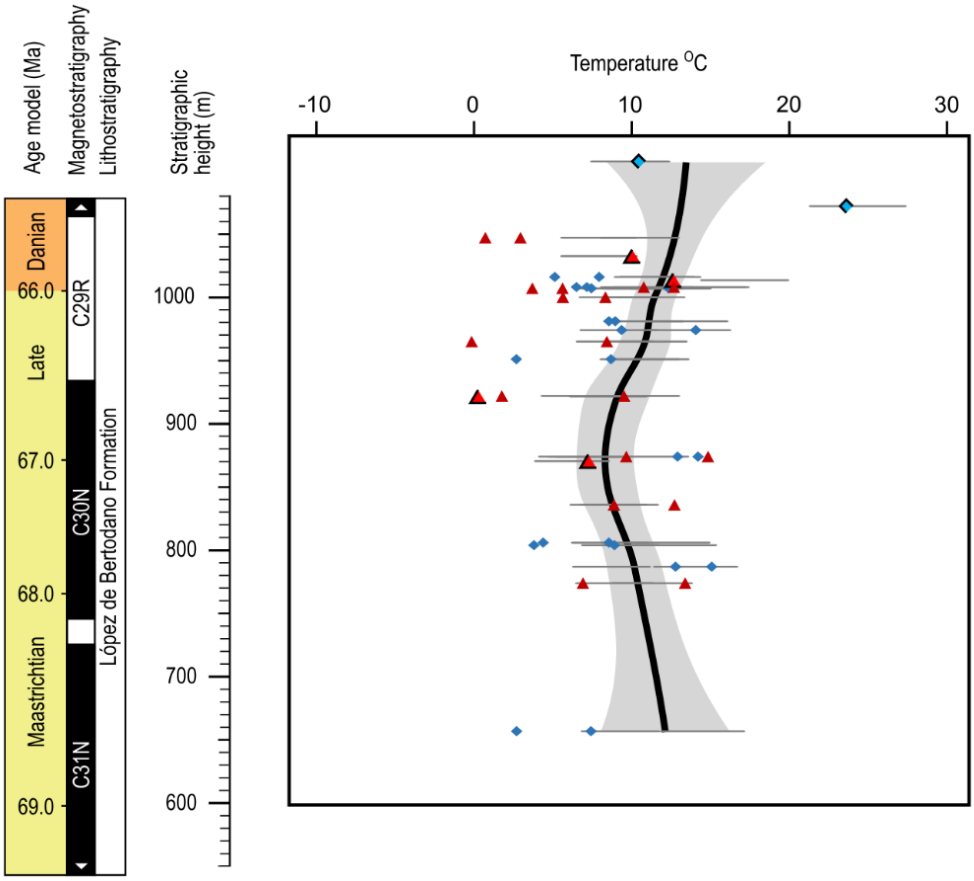

Figure 4.21 Comparison of temperature estimates produced from $\delta^{18}O$ data using the same high and low conversion as Table 4.4 (grey horizontal bars) and clumped isotope data in the same samples of *Lahillia* (red triangles) or *Cucullaea* (blue diamonds). Black trendline represents a 0.3 Loess fit to the midpoints of temperature data converted from $\delta^{18}O$. Data from Petersen et al. (2016) in smaller points with no outline, data from Larkin et al. (2014) in larger points with black outline. Stratigraphic heights are approximate and may not be directly comparable with other data from this study (for further details see discussion in the text).

4.6.2 Maastrichtian climate conditions

Although the stratigraphic heights of the data from Petersen et al. (2016) may be difficult to compare directly with the new data sets presented in this study, useful information can still be gained by examining the broad trends. Figure 4.22 shows the temperature trends in both correlated and plane projected

sections in a number of $\delta^{18}O$ bulk data sets converted using the high estimate and low estimate equations in Table 4.4. The measured section consists of bulk data from *Lahillia* and *Cucullaea* produced in this study, as well as aragonitic bivalves from Tobin et al 2012 (raw $\delta^{18}O$ data shown in Figure 4.10). The plane projected section consists of data from Petersen et al 2016.

From the $\delta^{18}O$ data, the stratigraphic trends show a great deal of consistency in bulk temperature on the whole, with statistical fit curves in both sections showing average temperatures of roughly 10°C throughout the Cretaceous. Most $\delta^{18}O$ data falls within ± 5°C of this 10°C average with a little evidence for increasing temperatures at the very end of the Cretaceous. Both sections also show a trend towards slightly lower temperatures throughout the Danian K-Pg recovery interval, beginning from the K-Pg boundary. A few anomalously high temperatures are present, with 4 specimens producing mean annual temperature ranges greater than 20°C, but these are a minority and may be due to alteration rather than a record of actual temperature conditions.

Clumped isotopic data however show a different trend, with distinctive cooling beginning at a stratigraphic height of approximately 900 m. This is in contrast to the slight warming observed from roughly the same interval in the $\delta^{18}O$ record. Temperatures from Δ47 below this level are in general in good agreement with the ranges calculated from $\delta^{18}O$. It is possible that seawater $\delta^{18}O$ may have dropped in the latest Maastrichtian, causing temperature estimates to be too high. Or it is possible that the clumped isotope pool was out of equilibrium (see Section 7.2 for details). The cooling trend beginning at the K-Pg boundary does however appear to continue into the Danian, in Δ47 as in $\delta^{18}O$ records, although again, Δ47 temperatures can be several degrees lower than the associated $\delta^{18}O$ temperature ranges.

Given the interdependence of these two proxies it is not clear which provides the most accurate representation of climate conditions around the K-Pg boundary interval. Therefore, it will be useful to examine these records against temperature data derived from other proxies from the nearby area (see Section 7.1 for further discussion).

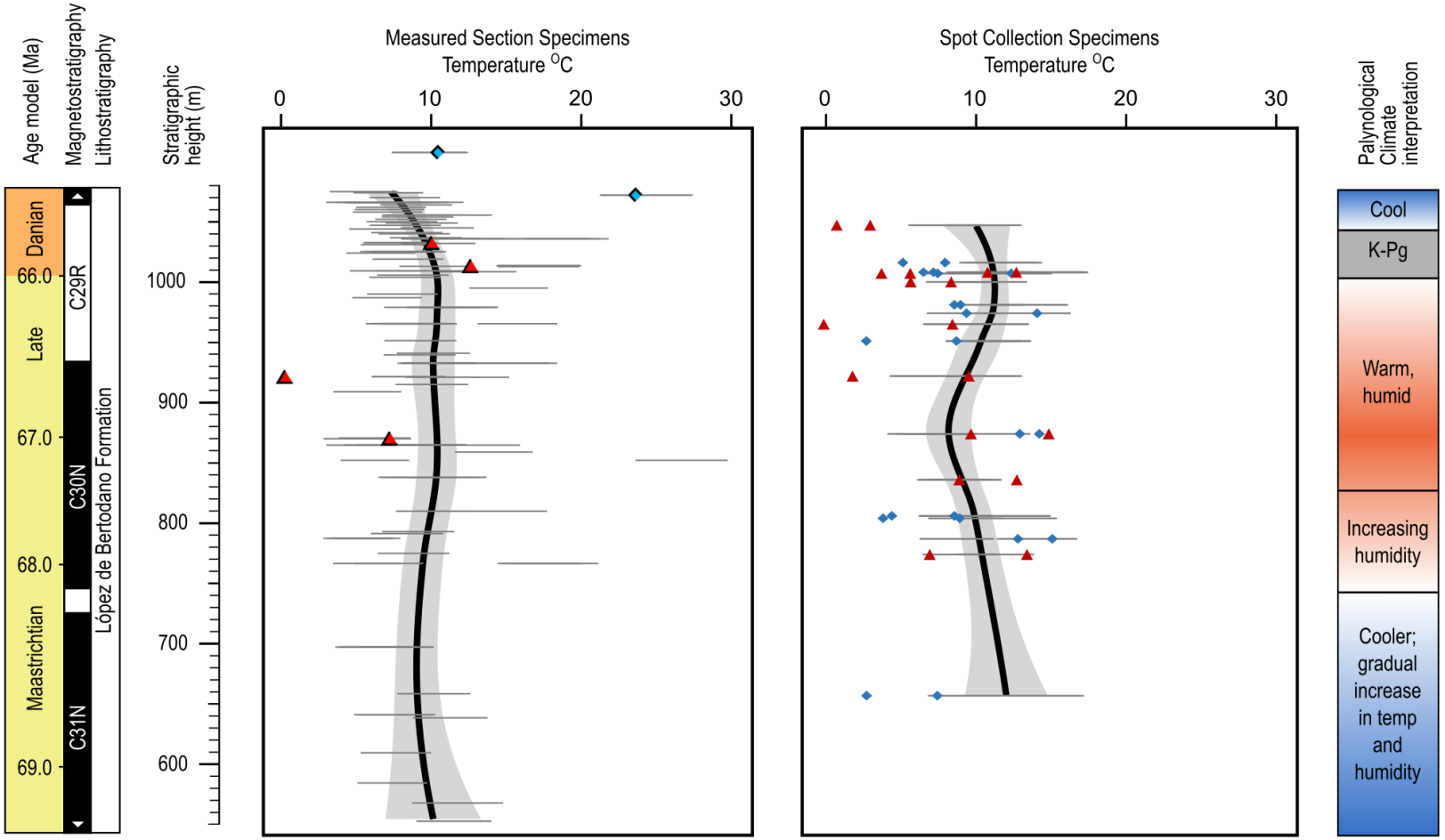

Figure 4.22: Comparison of temperature trends in specimens collected from the correlated section and spot collections with stratigraphic heights reconstructed using the plane projection method (Section 4.4.2). Each panel shows temperature ranges from $\delta^{18}O$ data (grey horizontal bars) and temperature estimates from $\Delta 47$ data in *Lahillia* (red triangles) or *Cucullaea* (blue diamonds). Black curves represent a 0.3 Loess fit to the midpoints of temperature data converted from $\delta^{18}O$. Data from this study, Tobin et al 2012, Larkin 2014 and Petersen et al. 2016.

The temperature data from *Lahillia* and *Cucullaea* can be compared with other $\delta^{18}O$ data in order to determine whether vital effects or similar phenomena may have been affecting clumped isotope temperatures, or if there is additional evidence for colder temperatures or freshwater runoff in the $\delta^{18}O$ record.

There are several sets of $\delta^{18}O$ records from calcite-shelled bivalves from the Lopez de Bertodano formation (Figure 4.10) which show generally more negative $\delta^{18}O$ compositions than the aragonite-shelled bivalves, but this discrepancy is more likely to be due to the different fractionation relationship for calcite versus aragonite. When converted to temperatures using the same -1 to -2‰ range of seawater $\delta^{18}O$, calcite bivalves give temperatures between 14.4 and 2.6°C with an average temperature of 6.0°C. However, these bivalves are likely to be producing similar vital effects to aragonite secreting bivalves, as both forms of mineralisation use biologically-mediated pathways and the same seawater DIC pool to construct their shells.

Gastropods produce aragonitic shells, but the $\delta^{18}O$ data shows a systematic bias towards cooler temperatures (less negative $\delta^{18}O$) than those recorded in aragonitic bivalves (Figure 4.10). This is however, likely to have been due to the production of shell material in *Lahillia* and *Cucullaea* during the warm spring and summer period, with an extended period of growth hiatus during the cold winter months. This may result in a bias towards warmer temperatures in the bulk $\delta^{18}O$ data from bivalves compared to gastropods from the same section.

Overall, the bivalve $\delta^{18}O$ and $\Delta47$ records suggest that Maastrichtian climates on Seymour Island were fairly stable with little variation at seafloor depths. There may have been some cooling and freshwater input during the very latest Maastrichtian interval, or it is possible that other effects were influencing the equilibrium of the clumped isotope proxy record. A slight cooling across the K-Pg boundary has also been noted. The implications of this cooling for the growth trends discussed in Chapter 3 will be expanded upon in the discussion in Chapter 7. The larger scope of Seymour Island's climate conditions within a global climate context will be discussed in Chapter 5.

In the last portion of this chapter, we will attempt to use climate models to explore the potential for seawater and runoff $\delta^{18}O$ variability, as well as the

potential for the colder temperatures predicted from clumped isotopic data to produce sea ice in the models.

4.6.3 Data and Model Comparisons

The work in the previous section suggests that $\delta^{18}O$ temperature estimates are likely to be accurate, and a seawater $\delta^{18}O$ of between -1 and -2 gives a reasonable conversion from shell $\delta^{18}O$ to temperature.

At the predicted depth range of 50-200m that these bivalves were living at (refer to Section 2.4.2 for details), all model scenarios show good agreement with the data, producing mean annual water temperatures of between 10 and 13°C in cell 16-6 and between 6 and 12°C in cell 15-8 slightly further south (Figures 4.12 to 4.14 and Figure 4.23). Both of these estimates are within the range of temperature trends through the Maastrichtian (Figure 4.22)

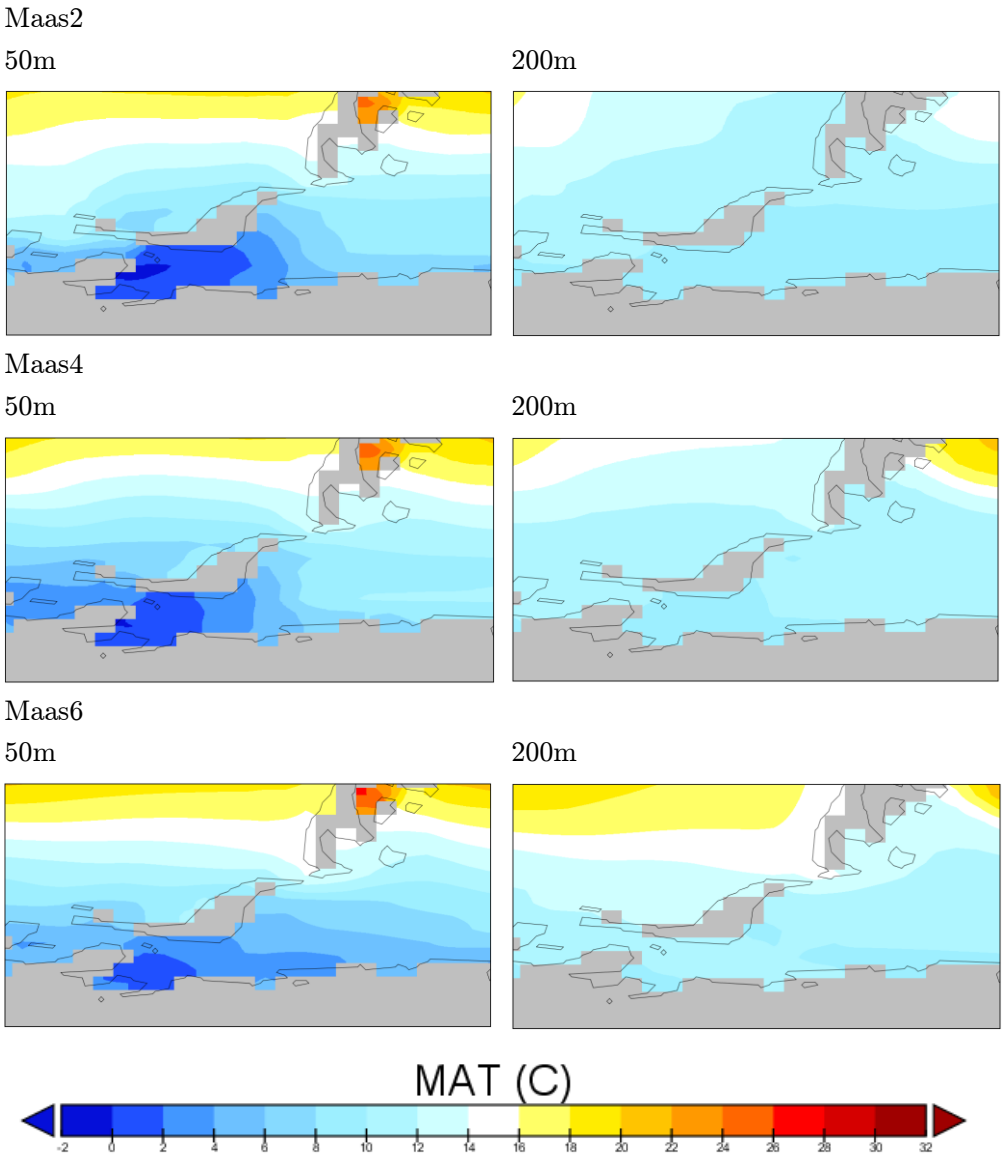

Figure 4.23: Mean annual temperatures around the Antarctic Peninnsula at water depths of 50m and 200m which represent the upper and lower estimates of water depth during the Maastrichtian to Danian deposition of the López de Bertodano Formation on Seymour Island.

Coolest and warmest temperatures within each simulation were found in the surface waters, with less temperature variation lower down. In waters deeper than around 200m in all model scenarios, almost no annual variation in temperature was produced. The coolest bottom water temperatures were found in $2xCO_2$ experiments, whereas the warmest bottom waters were produced

under 4xCO_2 conditions (Figures 4.12 to 4.14). This suggests that in this location, water temperature does not increase linearly with increasing CO_2, and other factors such as circulation affect marine temperatures.

Rerouting riverine input to cell 16-6 did not produce a discernible effect on water temperatures, which does suggest that freshwater input could have occurred without an associated change in temperature. This behaviour conflicts with the interpretation of the Δ47 record, which suggests that significant temperature change occurred during the latest Maastrichtian in addition to enough freshwater input to produce a negative $\delta^{18}O$ signal in the seawater (Petersen et al 2016). A comparison of the modelled temperature profiles with the $\delta^{18}O$ seawater profiles suggests that this may be because the influence of freshwater was confined to the uppermost water layers (e.g. Maas2 riv and Maas4 riv, Figure 4.15); which could be a result of stratification between the two water sources.

Comparison of bulk temperature data alone does not produce enough data to favour a certain set of model conditions, but the close agreement of mean annual temperature data from $\delta^{18}O$ with terrestrial proxies and modelled data is a good indication of their veracity. In the following chapter, seasonal trends will be examined in order to test the model simulations further.

4.6.4 Evidence for Sea Ice

Recent evidence from palaeoenvironmental proxies have suggested that ephemeral continental and sea ice may have been present during the Late Cretaceous, with particular prominence at high latitudes. The proxy record evidence for the presence of sea ice near to the Seymour Island section comes from the dinoflagellate *Impletosphaeridium clavus* record which suggests periodic sea ice influence between 500 and 830m in the section and from the clumped isotopic data in the upper part of the section between 900 and 1050m which gives both low temperatures and ^{18}O depleted seawater results.

But temperatures from the $\delta^{18}O$ record throughout both of these intervals are not low enough to allow sea-ice formation and the temperature ranges inferred are a good fit to many proxies and model scenarios without the need for an additional source of water with more negative $\delta^{18}O$ caused by meltwater input.

Models have been used to examine the potential for sea ice formation in surface waters around the Antarctic Peninsula to see whether it is possible for surface water to be cold enough for sea ice formation when temperatures at depth are much warmer. The Maas2 riv 207 experiment was used to produce a lowest temperature, maximum Antarctic sea ice scenario. This model produced the most cells with sea ice coverage of all of the experiments tested, and the lowest latitude sea ice around the Antarctic Peninsula with ice down to 70°S (Figure 4.24)

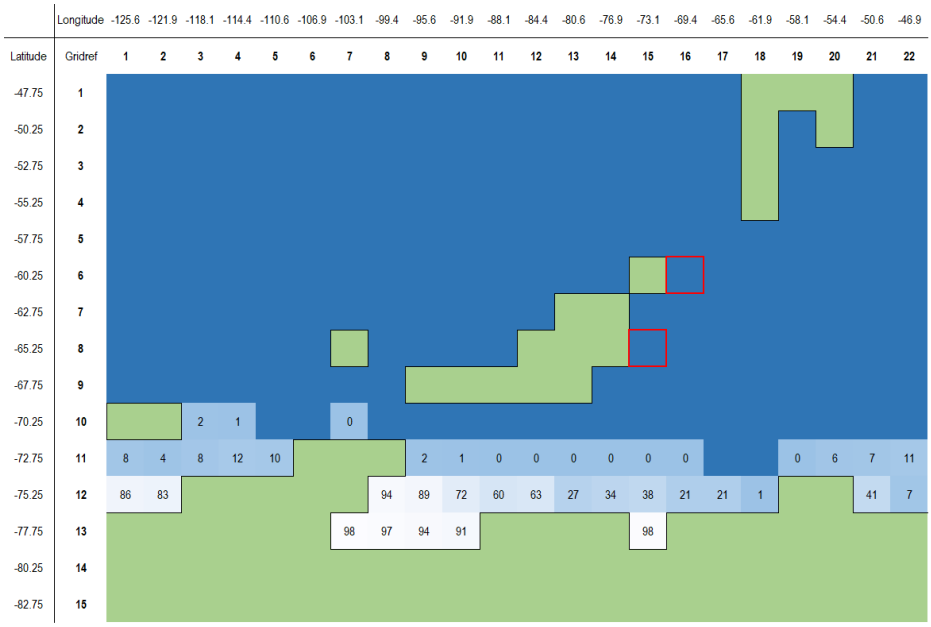

Figure 4.24: Plot of the Antarctic Peninsula area showing cells producing any sea ice in lighter blues annotated with maximum monthly sea ice coverage in percent. Data taken from the Maas2 riv 207 simulation with Seymour Island's possible locations highlighted in red. No sea ice formation was simulated near to either of Seymour Island's potential locations.

However, there was no sea ice produced in either of the grid locations for Seymour Island even under the most ice-favourable conditions tested. The 560 ppmv CO_2 levels led to sea surface temperatures that were too warm at the latitude of the Antarctic Peninsula, and in general, sea ice only formed in cells around the Antarctic contintent at latitudes higher than 72°S or with restricted

waters (e.g. around Australia and the Western Antarctic area, Figure 4.25). Modelled sea surface temperatures also change rapidly through the annual cycle, with even locations with high peak sea ice formation experiencing several ice-free months during the peak of Antarctic summer (Figure 4.26).

As the models do not support the presence of sea ice near to the Antarctic Peninsula, the results from palynology and clumped isotopic data are more likely to be attributed to other effects. Others have suggested that these *Impletosphaeridium clavus* blooms may be related to periods of higher continental nutrient influx and eutrophication, without the need to invoke sea ice formation (Amenábar et al. 2014). Models are not particularly good at recreating the formation and impact of high-elevation ice, due to the inability of low-resolution models to render the rapid changes in elevation over mountainous terrain, but it is possible that high elevation ice on the mountains Antarctic Peninsula may have been a source of depleted freshwater and potential nutrient influx in the absence of evidence for sea ice.

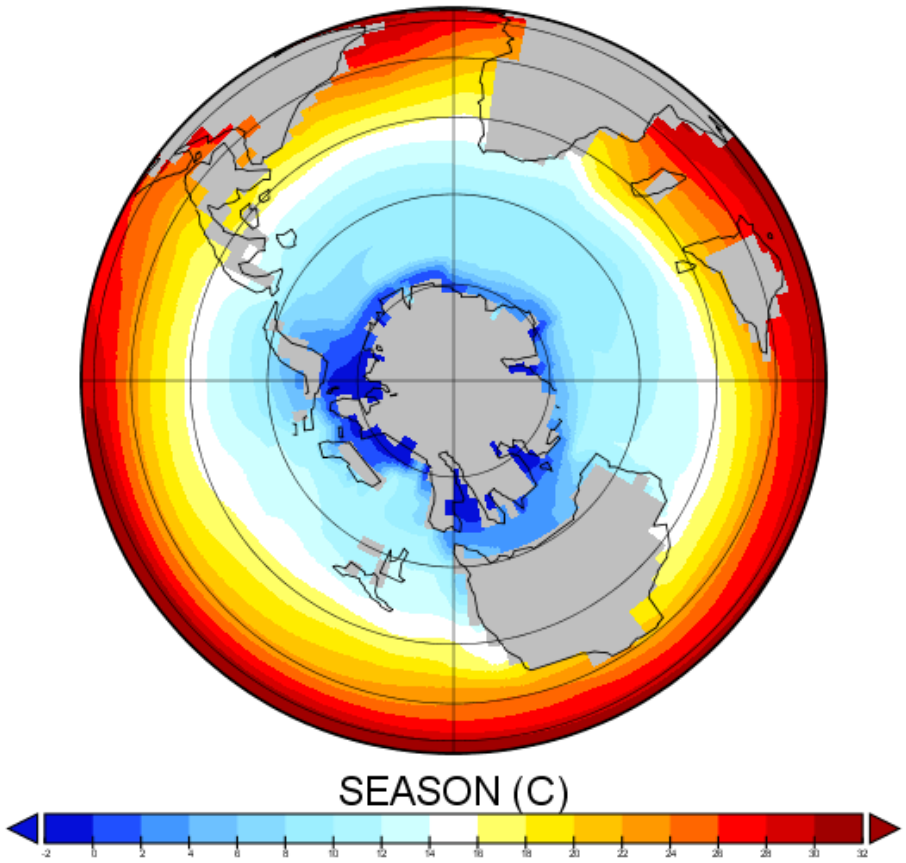

Figure 4.25: Orthographic Austral polar centered projection of Maas2 simulation showing 3-month averaged surface-water temperatures during southern hemisphere winter (September-October-November). Temperatures cold enough to allow sea-ice formation are only found in waters with restricted flow around the Antarctic continent at latitudes greater than 70°S.

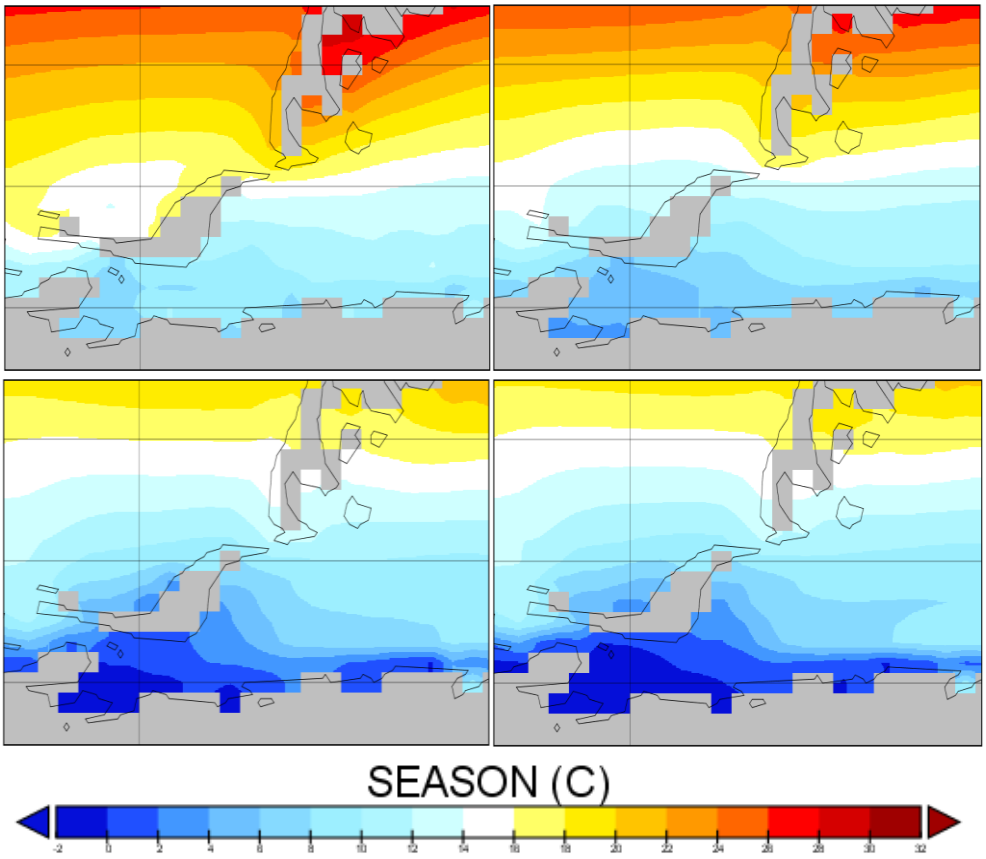

Figure 4.26: Seasonal surface water temperatures around the Antarctic Peninsula in the Maas2 simulation in December-January-February, March-April-May, June-July-August, and September-October-November.

4.7 Summary

Bulk shell $\delta^{18}O$ data from *Lahillia* and *Cucullaea* compares well with the average $\delta^{18}O$ calculated from high resolution sampled shells and with other aragonitic bivalves from the same section. Aragonitic bivalve $\delta^{18}O$ is generally 0.5 to 1‰ more negative than gastropod data, which is could be due to a summer bias of temperatures in bivalve shells and a reduction in the recording of winter temperatures during the growth hiatus discussed in Chapter 3.

Clumped isotopic data suggest that in the latest Maastrichtian, $\delta^{18}O$ may have been considerably more negative than the −1‰ that standard ice-free conversions from shell $\delta^{18}O$ to water temperatures suggest. Isotope enabled models also corroborate these findings, leading to a range of seawater $\delta^{18}O$ compositions from −1 to −2‰ being used for temperature conversions of bulk and seasonal shell $\delta^{18}O$ data.

When examined through stratigraphy, trends in bulk temperatures from $\delta^{18}O$ data show little variation throughout the late Maastrichtian, with indications for a slight temperature decrease from the Maastrichtian to the Danian. Average water temperatures for the Maastrichtian remained around 10°C, with most mean annual $\delta^{18}O$ data falling within ±5 degrees throughout. Comparison with gastropod data suggest that the recorded temperatures are likely to have been between 2 and 4 degrees higher than the actual mean temperatures due to the discussed warm temperature bias of bivalve growth.

Clumped isotopic data are similar to the $\delta^{18}O$ data at stratigraphic heights lower than 900m. At stratigraphic heights above 900m, the clumped isotope temperatures tend to be much lower than the $\delta^{18}O$ temperatures, in several cases close to 0°C, which has been used to suggest the presence of sea ice.

Climate model scenarios showed good agreement with the mean annual temperatures produced from $\delta^{18}O$ data, with modelled water temperatures of between 6 and 13°C across all simulations at the water depths bivalves are thought to have lived in. Due to the uncertainty in the exact water depth, the comparison of temperature means was not sufficient to favour a certain set of model conditions, however extending the comparison to seasonal temperatures in Chapter 5 is likely to provide additional constraints.

The climate simulations did not produce any sea ice near to Seymour Island's palaeolocation at atmospheric CO_2 concentrations of 560ppmv (2xPI CO_2). This could be due to misrepresentation of Antarctic conditions by the models, lower CO_2 conditions than were accounted for, or that the potential proxy evidence for sea ice may have been caused by other effects

4.8 References

Affek, H. P. (2012) 'Clumped isotope palaeothermometry: Principles, applications, and challenges', *Paleontological Society Publications*, 18(18), 101–114.

Affek, H. P., Bar-Matthews, M., Ayalon, A., Matthews, A. and Eiler, J. M. (2008) 'Glacial/interglacial temperature variations in Soreq cave speleothems as recorded by "clumped isotope" thermometry', *Geochimica et Cosmochimica Acta*, 72(22), 5351–5360.

Affek, H. P. and Zaarur, S. (2014) 'Kinetic isotope effect in CO2 degassing: Insight from clumped and oxygen isotopes in laboratory precipitation experiments', *Geochimica et Cosmochimica Acta*. Pergamon, 143, 319–330.

Amenábar, C. R., Candel, M. S. and Guerstein, G. R. (2014) 'Small Antarctic Late Cretaceous chorate dinoflagellate cysts: biological and palaeoenvironmental affinities', *Palynology*. American Association of Stratigraphic Palynologists , 38(2), 303–323.

Anderson, T. F. and Arthur, M. A. (1983) 'Stable isotopes of oxygen and carbon and their application to sedimentologic and paleoenvironmental problems', in Arthur, M. A., Anderson, T. F., Kaplan, I. R., Veizer, J., and Land, L. S. (eds) *Stable isotopes in sedimentary Geology*. Society of Economic Paleontologists and Mineralogists, Tulsa, 1/1-1/151 Short Course.

Barron, E. J., Fawcett, P. J., Pollard, D. and Thompson, S. L. (1993) 'Model simulations of Cretaceous climates: the role of geography and carbon dioxide', *Philosophical Transactions of the Royal Society of London. Series B*, 341, 307–316.

Blake, D. R. and Rowland, F. S. (1988) 'Continuing worldwide increase in tropospheric methane, 1978 to 1987', *Science*. JSTOR, 239(4844), 1129–1131.

Bowman, V. C., Francis, J. E. and Riding, J. B. (2013) 'Late Cretaceous winter sea ice in Antarctica?', *Geology*, 41(12), 1227–1230.

Bowman, V. C., Francis, J. E., Riding, J. B., Hunter, S. J. and Haywood, A. M. (2012) 'A latest Cretaceous to earliest Paleogene dinoflagellate cyst

zonation from Antarctica, and implications for phytoprovincialism in the high southern latitudes', *Review of Palaeobotany and Palynology*. Elsevier B.V., 171, 40–56.

Budyko, M. I. (1969) 'The effect of solar radiation variations on the climate of the earth', *Tellus*. Wiley Online Library, 21(5), 611–619.

Buick, D. P. and Ivany, L. C. (2004) '100 years in the dark: Extreme longevity of Eocene bivalves from Antarctica', *Geology*, 32(10), 921.

Carré, M., Bentaleb, I., Blamart, D., Ogle, N., Cardenas, F., Zevallos, S., Kalin, R. M., Ortlieb, L., *et al.* (2005) 'Stable isotopes and sclerochronology of the bivalve Mesodesma donacium: Potential application to Peruvian paleoceanographic reconstructions', *Palaeogeography, Palaeoclimatology, Palaeoecology*, 228(1–2), 4–25.

Cattle, H. and Crossley, J. (1995) 'Modelling Arctic climate change', *Philosophical Transactions of the Royal Society of London: Physical Sciences and Engineering*, 352(1699), 201–213.

Crame, J. A., Francis, J. E., Cantrill, D. J. and Pirrie, D. (2004) 'Maastrichtian stratigraphy of Antarctica', *Cretaceous Research*, 25(3), 411–423.

Dennis, K. J., Affek, H. P., Passey, B. H., Schrag, D. P. and Eiler, J. M. (2011) 'Defining an absolute reference frame for "clumped" isotope studies of CO2', *Geochimica et Cosmochimica Acta*, 75(22), 7117–7131.

Dennis, K. J., Cochran, J. K., Landman, N. H. and Schrag, D. P. (2013) 'The climate of the Late Cretaceous: New insights from the application of the carbonate clumped isotope thermometer to Western Interior Seaway macrofossil', *Earth and Planetary Science Letters*, 362, 51–65.

Dennis, K. J. and Schrag, D. P. (2010) 'Clumped isotope thermometry of carbonatites as an indicator of diagenetic alteration', *Geochimica et Cosmochimica Acta*. Pergamon, 74(14), 4110–4122.

Dettman, D. L. and Lohmann, K. C. (1995) 'Microsampling carbonates for stable isotope and minor element analysis; physical separation of samples on a 20 micrometer scale', *Journal of Sedimentary Research*. SEPM Society for Sedimentary Geology, 65(3a), 566–569.

Dettman, D. L., Reische, A. K. and Lohmann, K. C. (1999) 'Controls on the stable isotope composition of seasonal growth bands in aragonitic fresh-water bivalves (unionidae)', *Geochimica et Cosmochimica Acta*, 63(7),

1049–1057.

Donnadieu, Y., Pierrehumbert, R., Jacob, R. and Fluteau, F. (2006) 'Modelling the primary control of paleogeography on Cretaceous climate', *Earth and Planetary Science Letters*, 248, 426–437.

Eagle, R. A., Eiler, J. M., Tripati, A. K., Ries, J. B., Freitas, P. S., Hiebenthal, C., Wanamaker, A. D., Taviani, M., *et al.* (2013) 'The influence of temperature and seawater carbonate saturation state on 13C–18O bond ordering in bivalve mollusks', *Biogeosciences*, 10(7), 4591–4606.

Eiler, J. M. (2011) 'Paleoclimate reconstruction using carbonate clumped isotope thermometry', *Quaternary Science Reviews*, 30(25–26), 3575–3588.

Epstein, S., Buchsbaum, R., Lowenstam, H. A. (Heinz A. and Urey, H. C. (1953) 'Revised Carbonate-Water Isotopic Temperature Scale', *Bulletin of the geological Society of America*, 64, 1315–1326.

Fenger, T., Surge, D., Schöne, B. R. and Milner, N. (2007) 'Sclerochronology and geochemical variation in limpet shells (Patella vulgata): A new archive to reconstruct coastal sea surface temperature', *Geochemistry, Geophysics, Geosystems*, 8(7)

Forster, P., Ramaswamy, V., Artaxo, P., Berntsen, T., Betts, R., Fahey, D. W., Haywood, J., Lean, J., *et al.* (2007) 'Changes in atmospheric constituents and in radiative forcing. Chapter 2', in *Climate Change 2007. The Physical Science Basis*.

Foster, L. C., Finch, A. A., Allison, N., Andersson, C. and Clarke, L. J. (2008) 'Mg in aragonitic bivalve shells: Seasonal variations and mode of incorporation in Arctica islandica', *Chemical Geology*, 254(1–2), 113–119.

Francis, J. E. and Poole, I. (2002) 'Cretaceous and early Tertiary climates of Antarctica: evidence from fossil wood', *Palaeogeography, Palaeoclimatology, Palaeoecology*, 182(1), 47–64.

Gent, P. R. and McWilliams, J. C. (1990) 'Isopycnal mixing in ocean circulation models', *Journal of Physical Oceanography*, 20, 150–155.

Goodwin, D. H., Flessa, K. W., Schöne, B. R. and Dettman, D. L. (2001) 'Cross-Calibration of Daily Growth Increments, Stable Isotope Variation, and Temperature in the Gulf of California Bivalve Mollusk Chione cortezi: Implications for Paleoenvironmental Analysis', *PALAIOS*. SEPM

Society for Sedimentary Geology, 16(4), 387–398.

Gordon, C., Cooper, C., Senior, C. A., Banks, H. T., Gregory, J. M., Johns, T. C., Mitchell, J. F. B. and Wood, R. A. (2000) 'The simulation of SST, sea ice extents and ocean heat transports in a version of the Hadley Centre coupled model without flux adjustments', *Climate Dynamics*, 16(2–3), 147–168.

Gough, D. O. (1981) 'Solar interior structure and luminosity variations', *Solar Physics*, 74(1), 21–34.

Grossman, E. L. and Ku, T.-L. (1986) 'Oxygen and carbon isotope fractionation in biogenic aragonite: Temperature effects', *Chemical Geology: Isotope Geoscience section*, 59, 59–74.

Guo, W., Mosenfelder, J. L., Goddard, W. A. and Eiler, J. M. (2009) 'Isotopic fractionations associated with phosphoric acid digestion of carbonate minerals: Insights from first-principles theoretical modeling and clumped isotope measurements', *Geochimica et Cosmochimica Acta*, 73(24), 7203–7225.

Hathway, B. (2000) 'Continental rift to back-arc basin: Jurassic-Cretaceous stratigraphical and structural evolution of the Larsen Basin, Antarctic Peninsula', *Journal of the Geological Society*, 157(2), 417–432.

Hay, W. W., DeConto, R. M., Wold, C. N., Wilson, K. M., S., V., M., S., Wold, A. R., Balukhovsky, A. N., *et al.* (1999) 'Alternative global Cretaceous paleogeography', *Geological Society of America*, Special Pa.

Henkes, G. A., Passey, B. H., Wanamaker, A. D., Grossman, E. L., Ambrose, W. G. and Carroll, M. L. (2013) 'Carbonate clumped isotope compositions of modern marine mollusk and brachiopod shells', *Geochimica et Cosmochimica Acta*, 106, 307–325.

Horrell, M. A. (1991) 'Phytogeography and paleoclimatic interpretation of the Maestrichtian', *Palaeogeography, Palaeoclimatology, Palaeoecology*, 86(1–2), 87–138.

Hunter, S. J., Haywood, A. M., Valdes, P. J., Francis, J. E. and Pound, M. J. (2013) 'Modelling equable climates of the Late Cretaceous: Can new boundary conditions resolve data-model discrepancies?', *Palaeogeography, Palaeoclimatology, Palaeoecology*, 392, 41–51.

Hunter, S. J., Haywood, A. M., Valdes, P. J. and Markwick, P. J. (2008)

'Modelling Maastrichtian Climate: Investigating The Role Of Geography, Atmospheric –"CO″ And Vegetation Treatment.', *Climates of the Past*

Hunter, S. J., Valdes, P. J., Haywood, A. M. and Markwick, P. J. (2008) 'Modelling Maastrichtian climate: investigating the role of geography, atmospheric CO2 and vegetation', *Climate of the Past Discussions*. Copernicus GmbH, 4(4), 981–1019.

Huntington, K. W., Eiler, J. M., Affek, H. P., Guo, W., Bonifacie, M., Yeung, L. Y., Thiagarajan, N., Passey, B., *et al.* (2009) 'Methods and limitations of "clumped" CO 2 isotope (Δ47) analysis by gas-source isotope ratio mass spectrometry', *Journal of Mass Spectrometry*, 44(9), 1318–1329.

Ivany, L. C. (2012) 'Reconstructing paleoseasonality from accretionary skeletal carbonates — challenges and opportunities', 18, 133–165.

Jones, D. S., Arthur, M. A. and Allard, D. J. (1989) 'Sclerochronological records of temperature and growth from shells of Mercenaria mercenaria from Narragansett Bay, Rhode Island', *Marine Biology*, 102(2), 225–234.

Jones, D. S. and Quitmyer, I. R. (1996) 'Marking time with bivalve shells: oxygen isotopes and season of annual increment formation', *Palaios,* 11 (4) 340–346

Jung, C., Voigt, S., Friedrich, O., Koch, M. C. and Frank, M. (2013) 'Campanian-Maastrichtian ocean circulation in the tropical Pacific', *Paleoceanography*, 28(3), 562–573.

Kelson, J., Schauer, A. J., Huntington, K. W., Saenger, C. and Lechler, A. R. (2016) 'Choice of 17O Abundance Correction Affects Δ47 and Thus Calibrations for Paleothermometry', in *American Geophysical Union, Fall General Assembly 2016*.

Kim, S.-T. and O'Neil, J. R. (1997) 'Equilibrium and nonequilibrium oxygen isotope effects in synthetic carbonates', *Geochimica et Cosmochimica Acta*, 61(16), 3461–3475.

Kobashi, T., Grossman, E. L., Yancey, T. E. and Dockery, D. T. (2001) 'Reevaluation of conflicting Eocene tropical temperature estimates: Molluskan oxygen isotope evidence for warm low latitudes', *Geology*, 29(11), 983–986.

Krantz, D. E., Williams, D. F. and Jones, D. S. (1987) 'Ecological and

paleoenvironmental information using stable isotope profiles from living and fossil molluscs', *Palaeogeography, Palaeoclimatology, Palaeoecology*, 58(3), 249–266.

Larkin, C. (2014) *Clumped Isotope analysis of Antarctic Molluscs from the Late Cretaceous to Early Paleogene*, *University of Cambridge*.

Lawver, L. A., Gahagan, L. M. and Coffin, M. F. (1992) 'The development of paleoseaways around Antarctica', in Kennett, J. P. and Warnke, D. A. (eds) *The Antarctic Paleoenvironment: A Perspective on Global Change Antarctic Research Series*, 7–30.

Lécuyer, C., Reynard, B. and Martineau, F. (2004) 'Stable isotope fractionation between mollusc shells and marine waters from Martinique Island', *Chemical Geology*, 213(4), 293–305.

LeGrande, A. N. and Schmidt, G. A. (2006) 'Global gridded data set of the oxygen isotopic composition in seawater', *Geophysical Research Letter*, 33(L12604)

Lorrain, A., Paulet, Y.-M., Chauvaud, L., Dunbar, R., Mucciarone, D. and Fontugne, M. (2004) 'δ13C variation in scallop shells: Increasing metabolic carbon contribution with body size?', *Geochimica et Cosmochimica Acta*, 68(17), 3509–3519.

Macellari, C. E. (1988) 'Stratigraphy, sedimentology, and paleoecology of Upper Cretaceous / Paleocene shelf-deltaic sediments of Seymour Island', *Geological Society of America Memoirs*, 169, 25–54.

Markwick, P. J. (2007) 'The palaeogeographic and palaeoclimatic significance of climate proxies for data-model comparisons', in Williams, M., Haywood, A. M., Gregory, D., and Schmidt, D. N. (eds) *Deep-Time Perspectives on Climate Change: Marrying the Signal from Computer Models and Biological Proxies*. London: Geological Society Publishing House.

Markwick, P. J., Crossley, R. and Valdes, P. J. (2002) 'A Comparison of "Ice-House" (Modern) and "Hot-House" (Maastrichtian) Drainage Systems: the Implications of Large-Scale Changes in the Surface Hydrological Scheme', *American Geophysical Union, Fall Meeting 2002*.

Markwick, P. J. and Valdes, P. J. (2004) 'Palaeo-digital elevation models for use as boundary conditions in coupled ocean–atmosphere GCM experiments: a Maastrichtian (late Cretaceous) example',

Palaeogeography, Palaeoclimatology, Palaeoecology, 213(1), 37–63.

Miller, K. G., Wright, J. D. and Browning, J. V. (2005) 'Visions of ice sheets in a greenhouse world', *Marine Geology*, 217(3–4), 215–231.

Olivero, E. B., Martinioni, D. R. and Mussel, F. J. (1992) 'Upper Cretaceous sedimentology and biostratigraphy of western Cape Lamb (Vega Island, Antarctica). Implications on sedimentary cycles and evolution of the basin', *Geología de la Isla James Ross*, 147–166.

Olivero, E. B., Ponce, J. J. and Martinioni, D. R. (2008) 'Sedimentology and architecture of sharp-based tidal sandstones in the upper Marambio Group, Maastrichtian of Antarctica', *Sedimentary Geology*, 210(1–2), 11–26.

Otto-Bliesner, B. L. and Upchurch, G. R. (1997) 'Vegetation-induced warming of high latitude regions during the Late Cretaceous period', *Nature*, 385, 804–807.

Petersen, S. V., Dutton, A. and Lohmann, K. C. (2016) 'End-Cretaceous extinction in Antarctica linked to both Deccan volcanism and meteorite impact via climate change', *Nature Communications*. Nature Publishing Group 7, 12079

Pirrie, D. (1989) 'Shallow marine sedimentation within an active margin basin, James Ross Island, Antarctica', *Sedimentary Geology*. Elsevier, 63(1–2), 61–82.

Poulsen, C. J., Barron, E. J., Peterson, W. H. and Wilson, P. A. (1999) 'A reinterpretation of mid-Cretaceous shallow marine temperatures through model-data comparison', *Paleoceanography*, 14, 679–697.

Saenger, C., Affek, H. P., Felis, T., Thiagarajan, N., Lough, J. M. and Holcomb, M. (2012) 'Carbonate clumped isotope variability in shallow water corals: Temperature dependence and growth-related vital effects', *Geochimica et Cosmochimica Acta*. Elsevier Ltd, 99, 224–242.

Scasso, R. ., Olivero, E. B. and Buatois, L. . (1991) 'Lithofacies, biofacies, and ichnoassemblage evolution of a shallow submarine volcaniclastic fan-shelf depositional system (Upper Cretaceous, James Ross Island, Antarctica)', *Journal of South American Earth Sciences*. Pergamon, 4(3), 239–260.

Schmid, T. W. and Bernasconi, S. M. (2010) 'An automated method for "clumped-isotope" measurements on small carbonate samples', *Rapid*

Communications in Mass Spectrometry, 24(14), 1955–1963.

Schöne, B. R., Hickson, J. and Oschmann, W. (2005) 'Reconstruction of subseasonal environmental conditions using bivalve mollusk shells—A graphical model'.

Schöne, B. R., Houk, S. D., Freyre Castro, A. D., Fiebig, J., Oschmann, W., Kroncke, I., Dreyer, W. and Gosselck, F. (2005) 'Daily Growth Rates in Shells of Arctica islandica: Assessing Sub-seasonal Environmental Controls on a Long-lived Bivalve Mollusk', *Palaios*, 20(1), 78–92.

Schöne, B. R., K, T. and Dettman, D. L. (2003) 'Environmental controls on shell growth rates and delta O-18 of the shallow-marine bivalve mollusk Phacosoma japonicum in Japan', 142(3), 473–485.

Schöne, B. R., Lega, J., W. Flessa, K., Goodwin, D. H. and Dettman, D. L. (2002) 'Reconstructing daily temperatures from growth rates of the intertidal bivalve mollusk Chione cortezi (northern Gulf of California, Mexico)', *Palaeogeography, Palaeoclimatology, Palaeoecology*, 184(1–2), 131–146.

Scotese, C. R. (1991) 'Jurassic and cretaceous plate tectonic reconstructions', *Palaeogeography, Palaeoclimatology, Palaeoecology*, 87(1–4), 493–501.

Sellers, W. D. (1969) 'A global climatic model based on the energy balance of the earth-atmosphere system', *Journal of Applied Meteorology*, 8(3), 392–400.

Shackleton, N. J. and Kennett, J. P. (1975) 'Paleotemperature history of the Cenozoic and the initiation of Antarctic glaciation: oxygen and carbon isotope analyses in DSDP sites 277, 279 and 281.', in Kennett, J. P. and Houtz, R. E. (eds) *Initial reports of the Deep Sea Drilling Project 29.* Washington: U.S. Government Printing Office, 743–756.

Solomon, S., Qin, D., Manning, M., Chen, Z., Marquis, M., Averyt, K. B., Tignor, M. and Miller, H. L. (2007) *IPCC, 2007: Climate Change 2007: The Physical Science Basis. Contribution of Working Group I to the Fourth Assessment Report of the Intergovernemental Panel on Climate Change*. Cambridge: Cambridge University Press.

Steuber, T. (1996) 'Stable isotope sclerochronology of rudist bivalves : Growth rates and Late Cretaceous seasonality Stable isotope sclerochronology of rudist bivalves : Growth rates and Late Cretaceous seasonality', *Geology*,

24, 315–318.

Tang, J., Dietzel, M., Fernandez, A., Tripati, A. K. and Rosenheim, B. E. (2014) 'Evaluation of kinetic effects on clumped isotope fractionation (Δ47) during inorganic calcite precipitation', *Geochimica et Cosmochimica Acta*. Pergamon, 134, 120–136.

Thiagarajan, N., Adkins, J. and Eiler, J. (2011) 'Carbonate clumped isotope thermometry of deep-sea corals and implications for vital effects', *Geochimica et Cosmochimica Acta*. Elsevier Ltd, 75(16), 4416–4425.

Tindall, J. C., Valdes, P. J. and Sime, L. C. (2009) 'Stable water isotopes in HadCM3: Isotopic signature of El Nino-Southern Oscillation and the tropical amount effect', *Journal of Geophysical Research Atmospheres*, 114(4), 1–12.

Tindall, J., Flecker, R., Valdes, P. J., Schmidt, D. N., Markwick, P. J. and Harris, J. (2010) Modelling the oxygen isotope distribution of ancient seawater using a coupled ocean–atmosphere GCM: Implications for reconstructing early Eocene climate, *Earth and Planetary Science Letters*. 265–273

Tobin, T. S., Ward, P. D., Steig, E. J., Olivero, E. B., Hilburn, I. A., Mitchell, R. N., Diamond, M. R., Raub, T. D., *et al.* (2012) 'Extinction patterns, δ18 O trends, and magnetostratigraphy from a southern high-latitude Cretaceous–Paleogene section: Links with Deccan volcanism', *Palaeogeography, Palaeoclimatology, Palaeoecology*, 350, 180–188.

Toland, H., Perkins, B., Pearce, N., Keenan, F. and Leng, M. J. (2000) 'A study of sclerochronology by laser ablation ICP-MS', *Journal of Analytical Atomic Spectrometry*, 15(9), 1143–1148.

Upchurch, G. R., Otto-Bliesner, B. L. and Scotese, C. R. (1998) 'Vegetation-Atmosphere Interactions and Their Role in Global Warming during the Latest Cretaceous', *Philosophical Transactions of the Royal Society of London. Series B*, 353(1365), 97–112.

Upchurch, G. R., Otto-Bliesner, B. L. and Scotese, C. R. (1999) 'Terrestrial Vegetation and its effect on climate during the latest Cretaceous', in Barrera, E. and Johnson, C. C. (eds) *Evolution of the Cretaceous Ocean-climate System*. Boulder: Geological Society of America.

Urey, H. C. (1947) 'The thermodynamic properties of isotopic substances',

Journal of the Chemical Society, 562.

Urey, H. C., Epstein, S., Lowenstam, H. A. and McKinney, C. R. (1951) 'Measurement of paleotemperatures and temperatures of the upper Cretaceous of England, Denmark, and the southeastern United States', *Bulletin of the geological Society of America*, 62(4), 399–416.

Valdes, P. J., Sellwood, B. W. and Price, D. A. (1996) 'Evaluating Concepts of Cretaceous Equability', *Palaeoclimates*, 2, 139–158.

Valentine, A., Johnson, A., Leng, M. J., Sloane, H. J. and Balson, P. S. (2011) 'Isotopic evidence of cool winter conditions in the mid-Piacenzian (Pliocene) of the southern North Sea Basin', *Palaeogeography, Palaeoclimatology, Palaeoecology*. Elsevier B.V., 309(1–2), 9–16.

Waite, A. and Swart, P. K. (2008) 'Drilling and storage effects on biogenic carbonate mineralogy: Implications for isotope fractionation', *Goldschmidt conference abstracts*, A991.

Wang, D. T., Gruen, D. S., Lollar, B. S., Hinrichs, K.-U., Stewart, L. C., Holden, J. F., Hristov, A. N., Pohlman, J. W., *et al.* (2015) 'Nonequilibrium clumped isotope signals in microbial methane', *Science*, 348(6233), 428–431.

Wefer, G. and Killingley, J. S. (1980) 'Growth histories of strombid snails from Bermuda recorded in their O-18 and C-13 profiles', *Marine Biology*, 60(2–3), 129–135.

Williams, M., Nelson, A. E., Smellie, J. L., Leng, M. J., Johnson, A. L. A., Jarram, D. R., Haywood, A. M., Peck, V. L., *et al.* (2010) 'Sea ice extent and seasonality for the Early Pliocene northern Weddell Sea', *Palaeogeography, Palaeoclimatology, Palaeoecology*, 292(1–2), 306–318.

Witts, J. D., Newton, R. J., Mills, B. J. W., Wignall, P. B., Bottrell, S. H., Hall, J. L. O., Francis, J. E. and Alistair Crame, J. (2018) 'The impact of the Cretaceous–Paleogene (K–Pg) mass extinction event on the global sulfur cycle: Evidence from Seymour Island, Antarctica', *Geochimica et Cosmochimica Acta*, 230, 17–45.

Witts, J. D., Whittle, R. J., Wignall, P. B., Crame, J. A., Francis, J. E., Newton, R. J. and Bowman, V. C. (2016) 'Macrofossil evidence for a rapid and severe Cretaceous–Paleogene mass extinction in Antarctica', *Nature Communications*. Nature Publishing Group, 7, 11738.

Yeung, L. Y., Ash, J. L. and Young, E. D. (2015) 'Biological signatures in clumped isotopes of O2', *Science*, 348(6233), 431–434.

Zaarur, S., Affek, H. P. and Brandon, M. T. (2013) 'A revised calibration of the clumped isotope thermometer', *Earth and Planetary Science Letters*, 382, 47–57.

Zaarur, S., Olack, G. and Affek, H. P. (2011) 'Paleo-environmental implication of clumped isotopes in land snail shells', *Geochimica et Cosmochimica Acta*, 75(22), 6859–6869.

Zachos, J. C., Pagani, M., Sloan, L., Thomas, E. and Billups, K. (2001) 'Trends, rhythms, and aberrations in global climate 65 Ma to present.', *Science (New York, N.Y.)*, 292(5517), 686–93.

Zinsmeister, W. J. (1998) 'Discovery of fish mortality horizon at the K-T Boundary on Seymour Island: Re-evaluation of events at the end of the Cretaceous', *Journal of Paleontology*, 72(3), 556–571.

Zinsmeister, W. J. (2001) 'Late Maastrichtian short-term biotic events on Seymour Island, Antarctic Peninsula', *The Journal of Geology*. The University of Chicago Press, 109(2), 213–229.

Zinsmeister, W. J. and Macellari, C. E. (1988) 'Bivalvia (Mollusca) from Seymour Island , Antarctic Peninsula', *Geological Society of America Memoirs*, (169).

CHAPTER 5

REGIONAL TEMPERATURE SEASONALITY AND VARIABILITY

This chapter's aim is to expand the work in Chapter 4 to include seasonality and climate variability data expressed in bivalve shells in order to look for patterns of change during the K-Pg boundary interval and examine the ability of general Maastrichtian climate simulations to replicate this data.

5.1 Introduction

The Maastrichtian to Danian interval has long been highlighted as a time of extreme temperature seasonality and variability on a scale unseen in modern temperate climates in contrast to more equable Cretaceous conditions (Barrera et al. 1987; Wolfe & Upchurch 1987; Pirrie & Marshall 1990; Barrera 1994; Ditchfield et al. 1994; Huber et al. 1995; Li & Keller 1998; Dingle & Lavelle 2000; Francis & Poole 2002; Gallagher et al. 2008). This potential for heightened seasonal variability is largely overlooked in interpretations of geochemical proxy records which often use modern calibrations to mean annual temperatures and may result in misleading palaeoenvironment reconstructions (Wolfe 1993; Markwick 1996; Price et al. 1997; Pearson et al.a 2001; Huber et al. 2002). In spite of a rich fossil and proxy data record, late Cretaceous climate models often fail to match the conditions expected, with mean annual temperatures often predicted by models to be several degrees cooler than the proxy data suggest (Donnadieu et al. 2006). The effect of seasonality in the proxy interpretation of data may therefore be an important source of data-model discrepancy.

Chapter 3 established the presence of cyclic signals in the stable oxygen isotopic data of *Cucullaea* and *Lahillia* shells, and Chapter 4 expanded on this work to produce estimates of summer temperatures and seasonality from these shells and examine the extent to which the seasonal climate variability can be

accounted for by climate models. In this chapter, the seasonal temperature trends in bivalve shells will be examined through stratigraphy and compared with other local records of seasonality and temperature during the Late Cretaceous and Early Paleocene.

Climate variability can be considered on a number of timescales, from atmospheric evolution taking hundreds of millions of years to tectonic changes and insolation cycles. Annual seasonal temperature change provides one of the largest sources of climate variability on one of the shortest timescales (Figure 5.1). This temperature seasonality is driven largely by changes in solar insolation due to the Earth's axial tilt as it completes each yearly orbit of the sun. Many aspects of the earth climate system are affected by changes in seasonality and extreme temperatures, including ice formation and melt, precipitation extremes, cloud formation and changes in the distribution and albedo of vegetation (Foley et al. 1994; Crowley & Zachos 2000; Bauer et al. 2003; Gerber et al. 2003; Reichstein et al. 2013). This is particularly important in the high latitudes, where the change in insolation is extremely large over the course of a year.

Seasonal temperature variation is also an important driver of physical systems such as ocean currents and nutrient cycling (Marshall & Speer 2012). These systems are important to understand from both a biological and climatic perspective particularly in deep time where changes in temperature extremes have been postulated as a mechanism to drive global patterns of evolution and extinction (Bartlein & Prentice 1989; Sheldon 1996; Li & Keller 1998; Davis et al. 2005).

It has been suggested that seasonality and intra-annual climate change is more important to understand from a palaeoecological angle than longer timescale mean-state climate conditions (e.g. Guthrie 1984). Some studies suggest that seasonal temperatures may have a stronger effect than mean annual temperatures on evolution and diversification (Parmesan et al. 2000; Archibald et al. 2010). Changes to the climate system on longer timescales can alter the magnitude of seasonality and seasonal behaviours. This chapter will aim to examine changes in seasonality recorded in bivalve shell carbonates and other proxies, and look for evidence of seasonal climate variability over the K-Pg boundary interval.

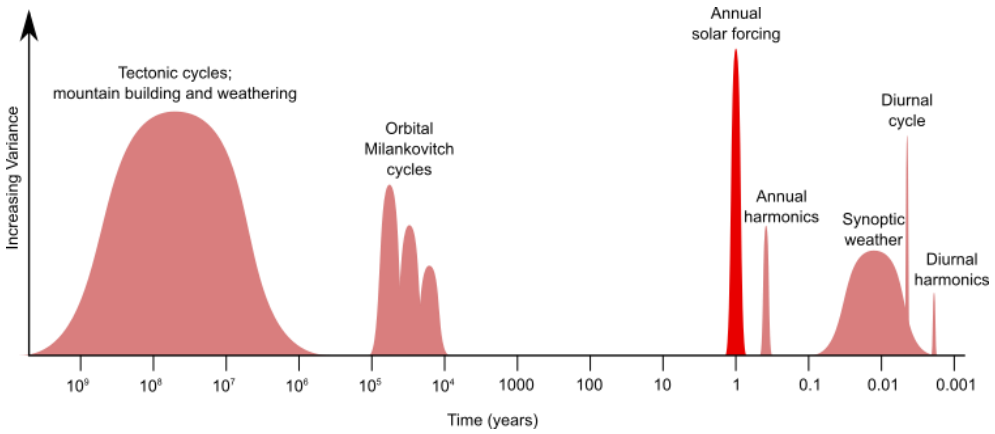

Figure 5.1: Timescales of climate variability, showing the large impact that annual solar forcing (bright red) has on climate compared to other variables. Based on Murray Mitchell (1976).

5.2 Objectives

- To examine how seasonality is expressed in Seymour Island's shell material in terms of stable and clumped isotopes
- To determine how well modelled data is able to fit the patterns of seasonality recorded in shells from Seymour Island
- To examine whether the differences between these two geological time intervals can be reliably detected
- Use of combined mean annual and seasonal temperature data to compare with model simulations over a range of scenarios in order to reconcile the differences between proxy systems.

5.3 Seasonality around Seymour Island

In Chapter 4, the seasonal variation of temperature in shells was used to compare data and models (e.g. Figure 4.19 and Figure 4.22). In this chapter, these trends will be examined through the latest Maastrichtian in the context of local and global climate change.

5.3.1 Methods

This section of the chapter builds on the methods, clumped and stable isotopic proxy data and HadCM3 model data and outputs detailed in Chapter 4.

As shell material in *Lahillia* from the López de Bertodano Formation was established to have a seasonally-determined periodicity (Chapter 3), peak summer temperatures (WMMT) were able to be calculated from the growth increment, and an estimate of winter temperatures (CMMT) gathered from readings at the growth line (Table 4.2). The difference between the two resulting temperatures is an estimate of the maximum seasonality.

In addition, the clumped isotope dataset from Petersen et al. 2016 used in Chapter 4 in comparison with δ^{18}O-derived temperatures also has the ability to give seasonal information. Samples from each specimen were taken from juvenile shell (near the umbo) and more mature shell (near the margin). As bivalves tend to grow for shorter periods of time as they mature, recording a smaller representative section of annual seasonality (Figure 5.2). As a result, the difference between mature and juvenile mean recorded temperatures can give an indication of minimum seasonality (Figure 5.4).

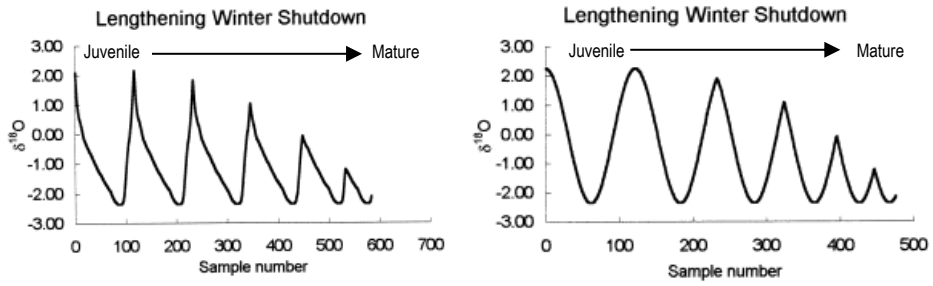

Figure 5.2 Goodwin et al 2003 δ^{18}O models of predicted annual shell growth showing the change in average recorded temperatures between juvenile and mature shell growth.

This interpretation does, however assume that mature bivalves are growing for a shorter period of time than the juveniles, and assumes there is little change in conditions year-on year within the lifespan of one bivalve, which can be up to 80 years (Chapter 3). The amount of expected year-to-year temperature variability will be tested using model data in Section 5.4.

5.3.2 Results

A maximum estimate of seasonality was calculated from the stable isotopic dataset (Figure 5.3) and compared with shells of *Lahillia* and *Cucullaea* within Petersen et al. 2016 (Figure 5.4). The assumptions and potential pitfalls of comparisons made between these two datasets have been discussed in Section 4.4.2. Temperature seasonality from stable isotopic data is fairly constant, remaining at approximately 2 to 4℃ throughout the stratigraphic section, with a few occurrences of higher seasonality of between 5 and 10℃ below 650m and between 930 and 960m with an additional potential spike near the K-Pg boundary, although this is only recorded by a single bivalve with shells at a similar stratigraphic height recording low seasonality.

The summer and winter temperatures derived from $\delta^{18}O$ shell data are presented in Figure 5.3, these temperature estimates include both the warm and cool estimate temperature conversions set out in Section 4.6.1. The seasonality estimate (Figure 5.3 A) assumes a constant water $\delta^{18}O$. Clumped isotopic data has suggested that water $\delta^{18}O$ may be seasonally variable, in which case the temperature seasonality experienced will have been several degrees larger than presented here (up to 4 to 5℃ greater).

The temperature difference and inferred seasonality from the clumped isotope data within one shell are slightly higher than the average annual seasonality derived from $\delta^{18}O$ data (Figure 5.4 A and B). Seasonality in clumped isotope-derived data remains approximately 5℃ through the lower part of the section, falling to between 2 and 3℃ across the K-Pg boundary interval from approximately 980m in stratigraphy. However, there does not appear to be a consistent relationship between which temperature conditions are being favoured by mature or juvenile growth in each species of bivalve.

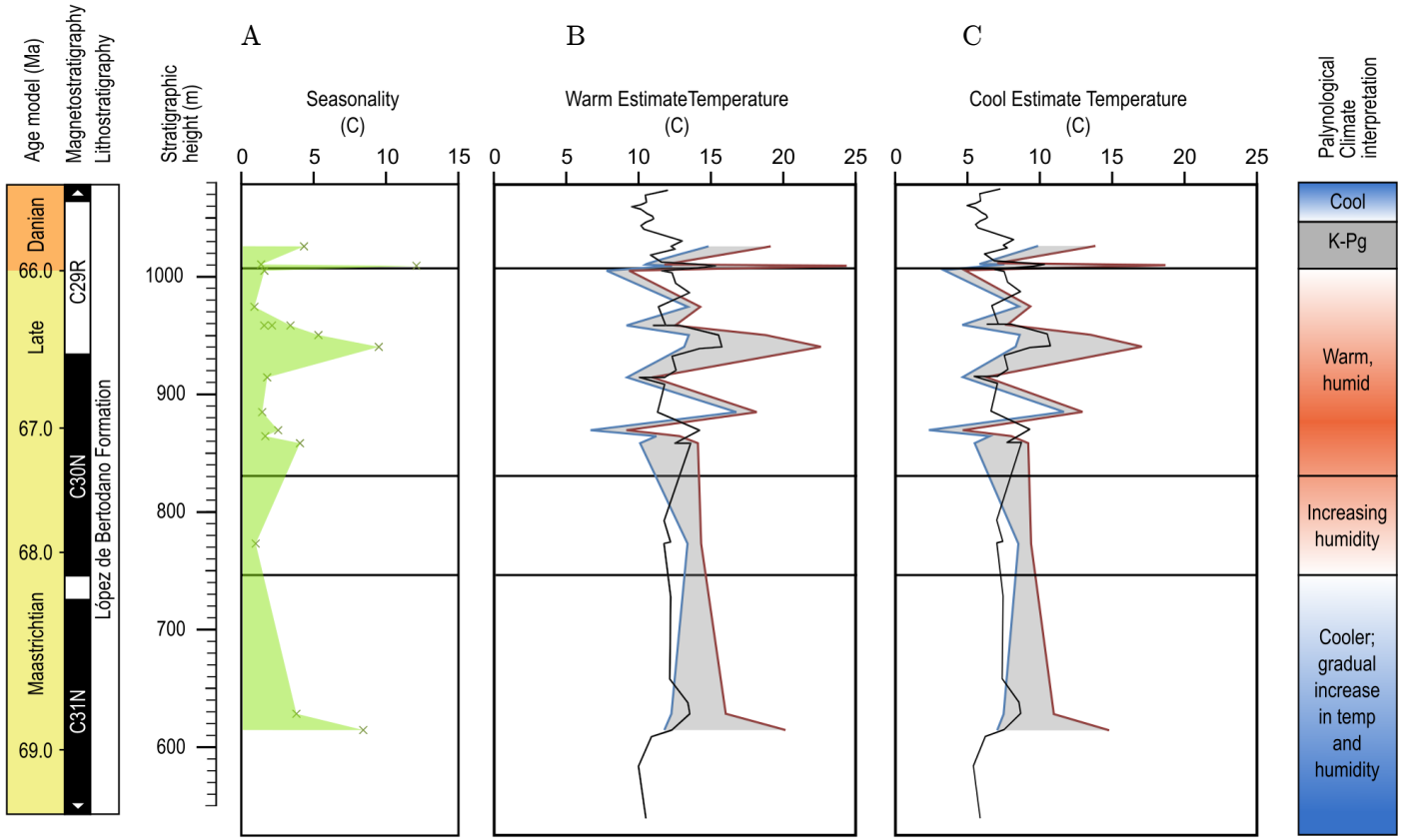

Figure 5.3: Seasonality (A) and warm and cool estimates of temperature from δ^{18}O data through the stratigraphic section. (B and C). Blue curve represents cool month mean temperature (CMMT) from each shell, red curve represents warm month mean temperature (WMMT). Black curve is the 3-point moving average of bulk δ^{18}O data, grey polygon shows the amount of intra-annual seasonality, i.e. the difference between WMMT and CMMT.

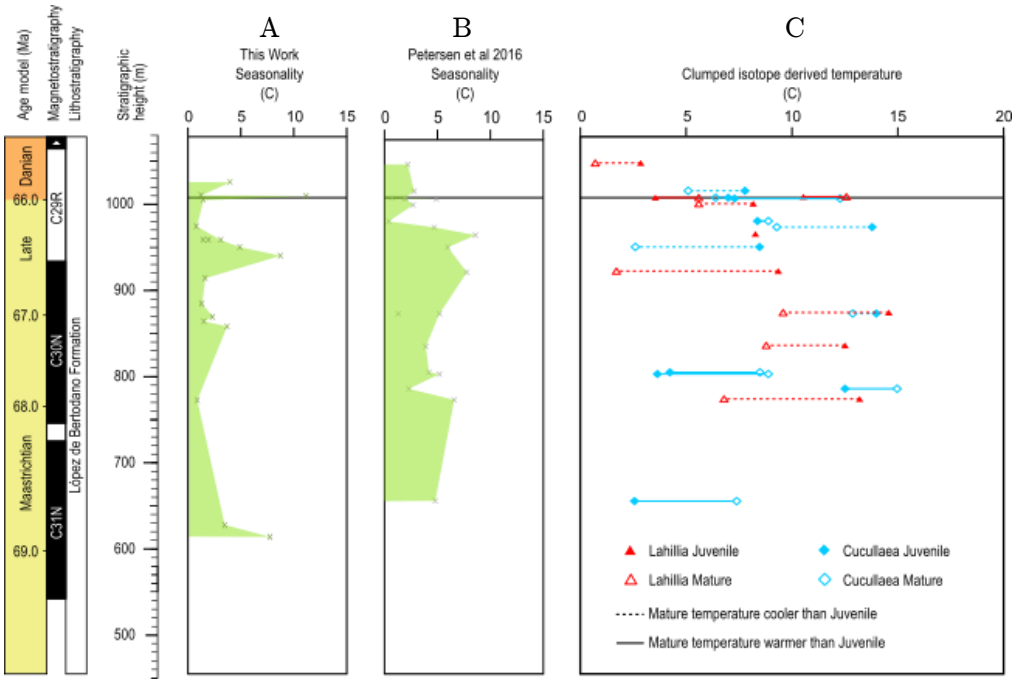

Figure 5.4: Temperature seasonality data from *Lahillia* and *Cucullaea* shells inferred from δ^{18}O data (left column) and clumped isotope data (middle column). Also showing the clumped isotopic data from mature (hollow) and juvenile (filled) *Lahillia* (red) and *Cucullaea* (blue). Dotted or solid lines between corresponding pairs of data from the same shell represent whether temperatures recorded by the mature growth are cooler (dashed) or warmer (solid) than juvenile growth. This graph shows that there does not appear to be a consistent pattern of temperature change as shells mature e.g. Figure 5.2. Data from this study and Petersen et al. (2016).

5.3.3 Discussion

Information relating to seasonality appears to be present in the δ^{18}O data; temperatures taken from the growth line are consistently lower than temperatures from the peak of the growing interval. The difference appears to be on the order of 2 to 3°C, although this seasonality estimate (Figure 5.4 A) assumes a constant water δ^{18}O. Clumped isotopic data have suggested that water δ^{18}O may be seasonally variable, with more negative water δ^{18}O occurring in summer months (Figure 4.18). If this was a significant factor in changing the δ^{18}O of water, the temperature seasonality experienced may have been up to 4 to 5°C lower than presented here.

The temperatures reconstructed from clumped isotopes were found to be in broad agreement with temperatures from $\delta^{18}O$ data below approximately 900m in the stratigraphy. Above this stratigraphic level, it is likely that clumped isotopic temperatures show a cold bias although the effect of this potential bias on seasonality data is unknown and depends on the mechanism (this is discussed further in Sections 4.6.1 and 7.1).

There is, however, a lack of a consistent pattern of temperature change as shells mature (Figure 5.4 C). For example, in *Cucullaea*, mature specimens record warmer temperatures than juveniles in the lower part of the succession; below 850m in the stratigraphy. This suggests that mature specimens could be recording the expected effects of a longer winter shutdown (e.g. Figure 5.2). However, above 850m in the stratigraphy, this trend is largely reversed, with most, but not all mature specimens recording cooler temperatures than the juveniles. *Lahillia* mostly record cooler temperatures in mature specimens than juvenile specimens as well, with the exception of a pair of specimens immediately prior-to and following the mass extinction horizon.

Bivalves are known to change the seasonality of shell growth and spawning under changing temperature and nutrition conditions (Jones & Quitmyer 1996), and commonly pause shell growth under non-ideal temperature conditions (Schöne et al. 2002, 2003). The changes described above could be a result of the cool-temperature bias noticed in the clumped isotopic record during the latest Maastrichtian, or could reflect a change in growth habits as a response to the generally warmer temperatures recorded by juvenile specimens where this behaviour is exhibited. However, the lack of a consistent pattern may also support the tentative conclusion from Chapter 4 that clumped isotope data is not recording an accurate temperature signal through the entire section.

The seasonality data produced from clumped isotopic data is also likely to include some temperature variation on longer temporal scales than just intra-annual temperatures. As a result, these clumped-isotope derived temperatures represent a different type of seasonality than the $\delta^{18}O$ data and are not reliable enough indicators of intra-annual seasonality for comparison with models, although could provide a ballpark estimate of climate variability over longer timescales (Figure 5.5).

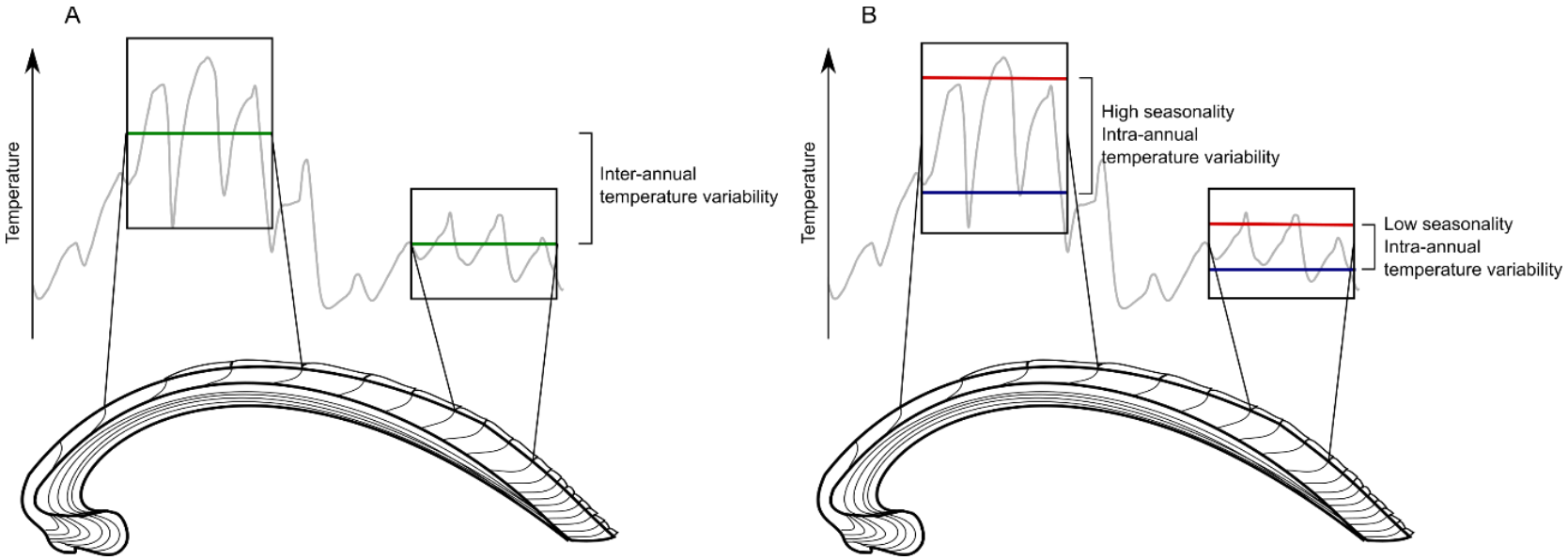

Figure 5.5: Schematic diagram of (A) inter-annual variability data produced from comparison between juvenile and more mature shell-derived temperature data and (B) high and low seasonal intra-annual variability from consecutive-year measurements. Grey curve represents water temperature data recorded by geochemical proxies in the shell. Green lines are MAT estimates from bulk temperature data, red and blue lines are warm month mean temperature (WMMT) and cold month mean temperature (CMMT) estimates from high resolution temperature data. Each method produces different information about climate variability and can be useful in combination.

Other seasonal proxies for temperature have been produced from Seymour Island's fossil material, such as analyses of fossil wood physiognomy and coexistence of flora (Poole et al. 2005). The range of seasonalities predicted from floral analyses is between 11.1 and 15.9°C, however, the comparison of terrestrial and marine seasonal data is not as good as the comparison between terrestrial and marine mean annual temperature data. Although the MAT conditions on land are often similar to the MAT conditions of marine surface waters (as discussed in Chapter 4), seasonality tends to be much larger and more variable on land than in water, due to the high specific heat capacity of water buffering temperature changes. As a result, terrestrial proxy data is unlikely to provide useful constraints on the amount of seasonality in marine data or models.

5.4 Climate Variability

Climate variability refers to the natural short-timescale changes in atmospheric conditions which cause temperature and weather fluctuations on scales of months to up to 30 years (Figure 5.6). This is as opposed to climate change which describes the changes over much longer periods, of over 30 years (as defined by the World Meteorological Organization). The combination of models and high temporal resolution data from bivalves through geological time can give insights on both climate variability and climate change scales.

Climate variability is important to study from a palaeontological point of view, as it represents the distribution of extreme values around the mean value of climate. Climate extremes have the potential to affect biology and ecosystems to a greater extent than mean state climate (Guthrie 1984; Parmesan et al. 2000; Archibald et al. 2010).

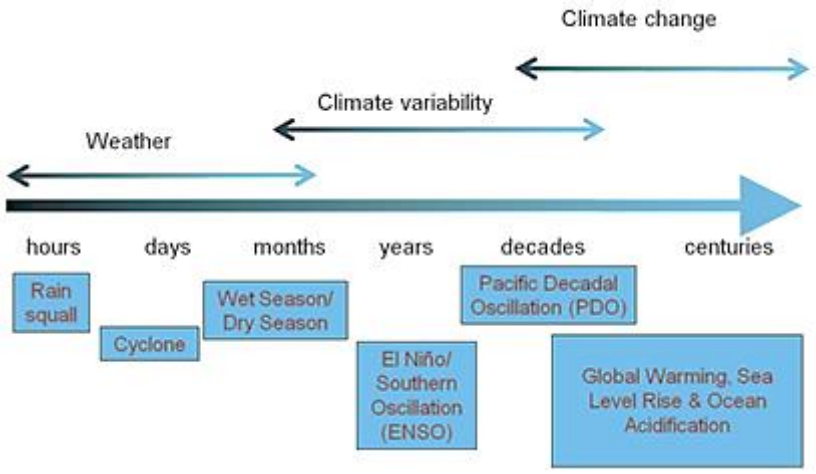

Figure 5.6: Temporal scales of key variations in the Earth's climate system. From the Pacific Climate Change Science Program.

5.4.1 Methods

This section of the chapter compares the monthly temperature data from the final spun-up years of the climate models described in Section 4.4.3 with the sub-annual resolution $\delta^{18}O$ data produced from shells through the geological stratigraphy of Seymour Island presented in Chapter 3. In order to visually confirm whether the models produce temperature variability of a similar timescale and magnitude to the signals preserved in fossil bivalve shells.

Shell data were processed from spatial data (temperature against distance) to temporal data (temperature against approximate time) by splitting the data into annual blocks at each visible growth line. These blocks of data were linearly scaled so that each block of data spanned the same amount of time; representing a year of shell growth. As it has been established that bivalves were not producing shell all year around, each block was then reduced by 70% to represent an active growing period of approximately 8 months out of the entire year, which is in line with estimates for modern bivalves (e.g. Goodwin et al. 2003). This method assumes shell growth was linear with no skewness caused by variable growth rates (Goodwin et al. 2003).

5.4.2 Results

The scaled temporal shell data from the shells which cover several years of growth are presented in Figures 5.7 and 5.8 in stratigraphic order and separated into the 50m stratigraphic intervals used in previous chapters. These clearly show the cycles of annual temperature change and the magnitude of the temperature peaks through the section. In many cases, the amount of temperature variability is greater than the uncertainty in the temperature conversion due to potential changes in water $\delta^{18}O$, which is likely to heighten the observed seasonality.

Temperature data from the simulations have been plotted to the same temporal and temperature scale as the proxy data for ease of comparison. This includes the data from each simulated marine depth slice between 15 and 138.9m. Water depths greater than this range were not investigated due to the small amount of annual variation present at greater depths.

In the northernmost cell (16-6), mean annual temperature and average seasonality generally decreased with depth, whereas in the slightly more southerly cell (15-8), mean temperatures were generally higher with increasing depth, while seasonality decreased.

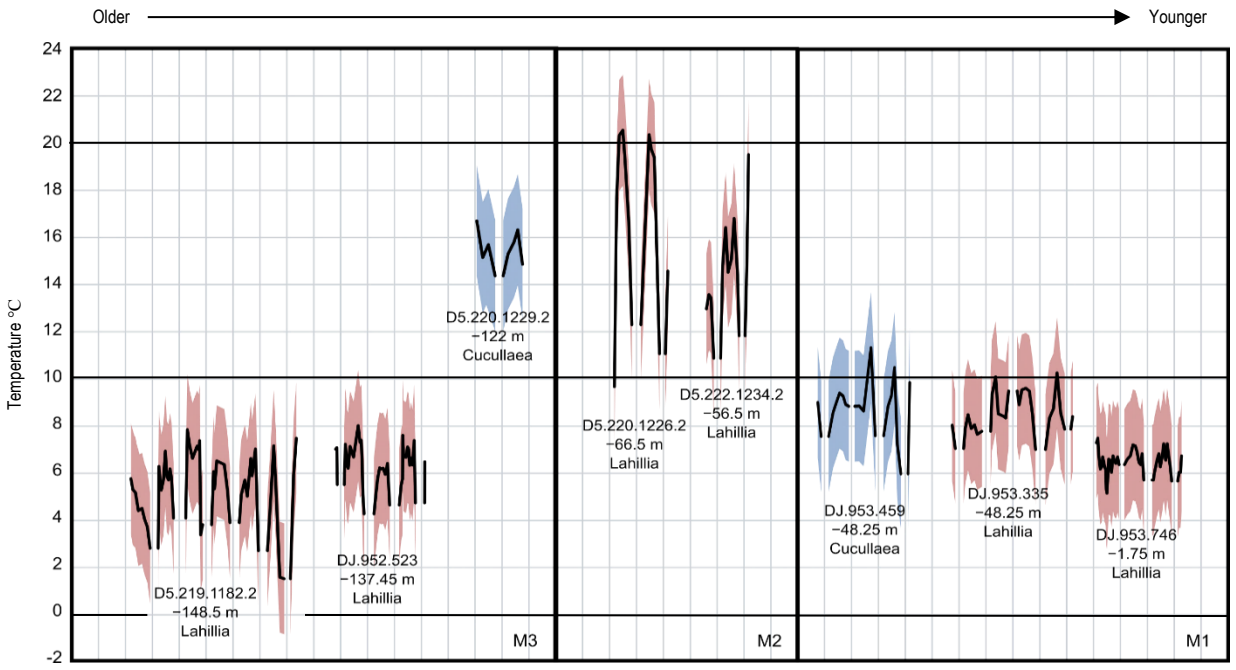

Figure 5.7 Temperature data from pre-extinction Maastrichtian bivalves of the Lopez de Bertodano Formation. Data have been separated at each visible growth line and linearly scaled such that each horizontal grid square represents a year of growth. Each shell has been presented in stratigraphic order with vertical error bands representing the warm and cool temperature conversions in *Lahillia* (red) and *Cucullaea* (blue). M1-M3 represent 50m stratigraphic intervals defined in Figure 2.13

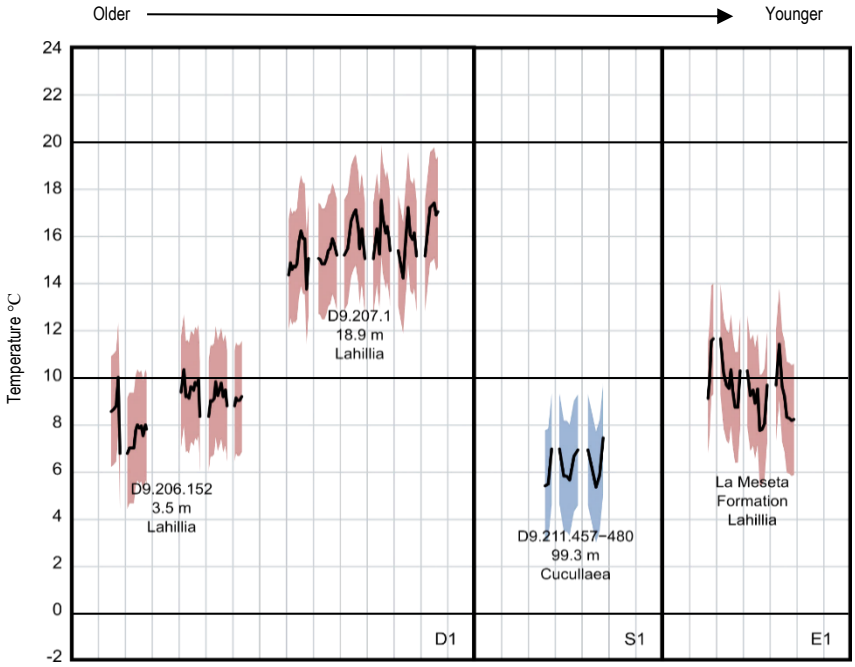

Figure 5.8: Temperature data from post-extinction Danian and Eocene bivalves of Seymour Island. Data have been separated at each visible growth line and linearly scaled such that each horizontal grid square represents a year of growth. Each shell has been presented in stratigraphic order with vertical error bands representing the warm and cool temperature conversions in *Lahillia* (red) and *Cucullaea* (blue). D1, S1 and E1 represent stratigraphic intervals of the post-extinction sediments defined in Figure 2.13

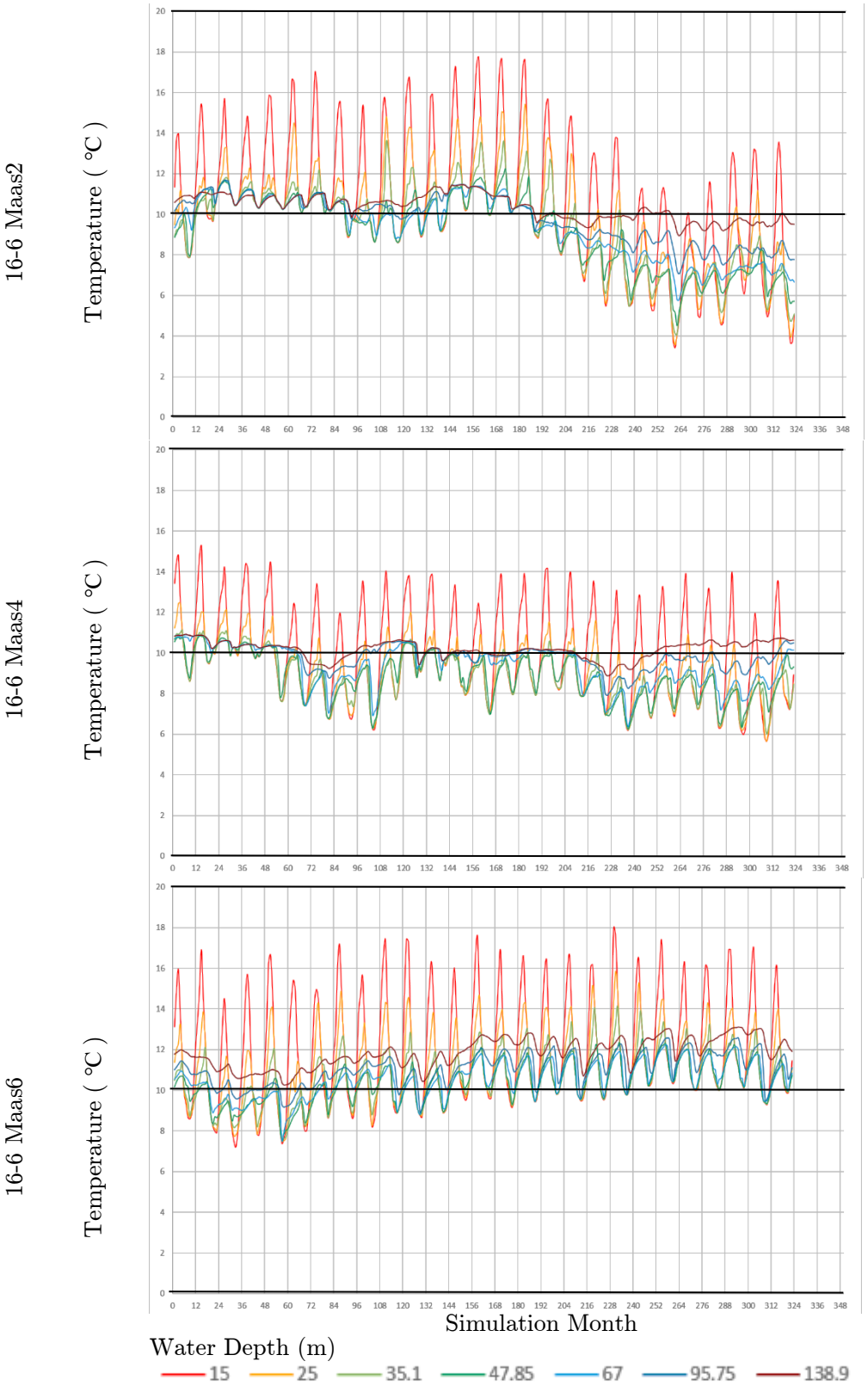

Figure 5.9: Monthly model data from each marine depth slice (colour code in key) at grid square 16-6 under different CO_2 conditions. Temperature data plotted to the same vertical and horizontal scale as shell data in Figures 5.7 and 5.8; each vertical grid line represents one year of data.

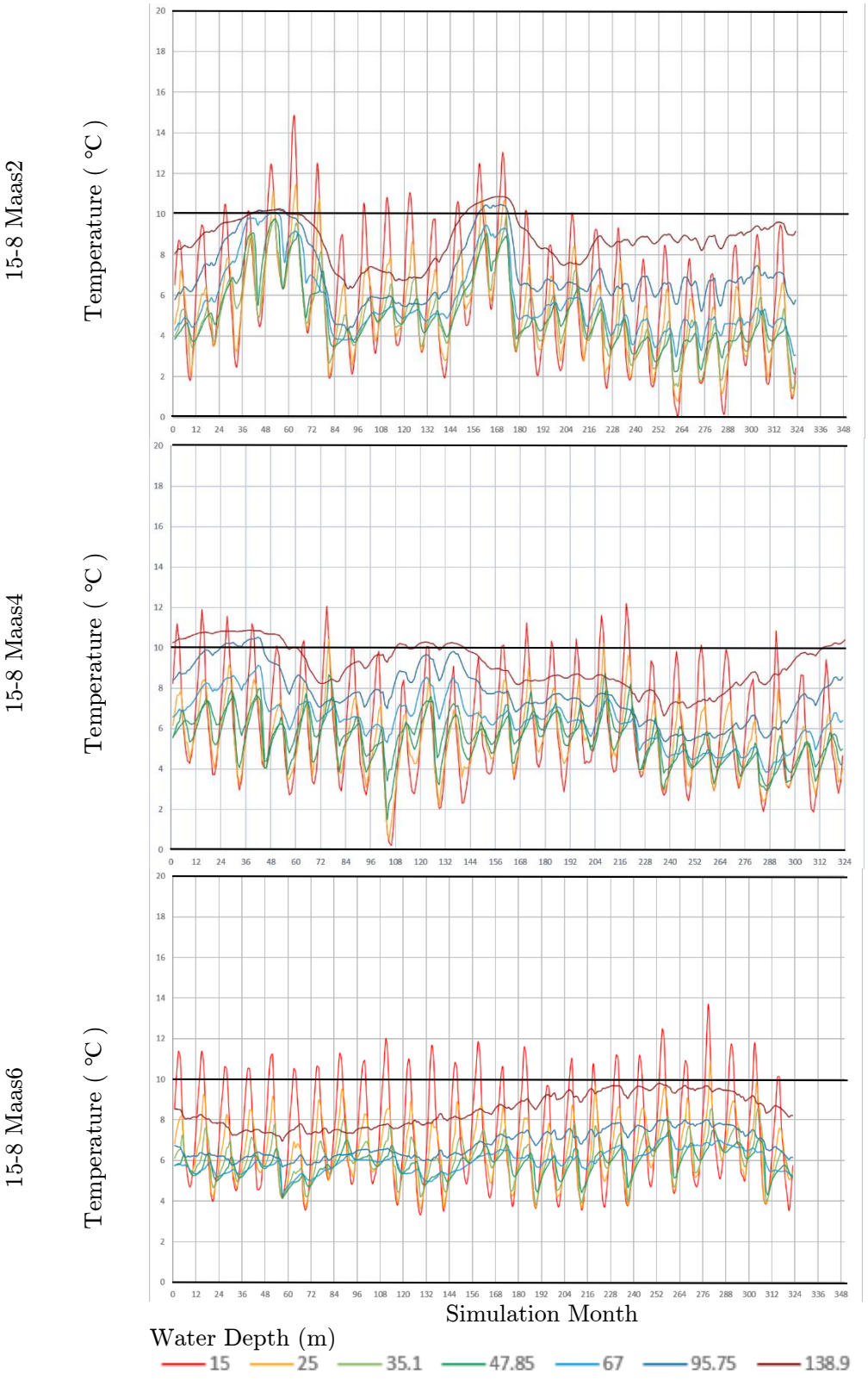

Figure 5.10: Monthly model data from each marine depth slice (colour code in key) at grid square 15-8 under different CO_2 conditions. Temperature data plotted to the same vertical and horizontal scale as shell data in Figures 5.7 and 5.8; each vertical grid line represents one year of data.

5.4.3 Discussion

In general, this comparison shows that the models demonstrate a clear seasonal temperature cycle that has a number of similarities to the temperature data reconstructed in fossils. It is remarkable to see how well the time-scaled proxy data correlate with simulated temperature data, especially because the data capture short snapshots across a span of several million years of geological time but are largely reasonable in comparison to the model. Most of the shells match up with at least one of the experiments within the 25-50m range.

The good fit of the model results to data produced over a large spread of geological time, and likely under different orbital forcing conditions, could imply that orbitally driven variations in seasonality are a second order effect compared to the overall strength of the seasonal cycle at this latitude.

The bivalves and sedimentary deposits are thought to have been produced at water depths between 50-200m (Macellari 1988; Crame et al. 2004), which is slightly deeper than the 20-50m range that is the best fit to the model data. However, this is not to say that the correlation between modelled temperatures and shell data at these depths demonstrates that water depth was actually 20-50m. This is partly a shortcoming of HadCM3L, which has a coarse lateral resolution (3.75 by 2.5°) and supports a minimum water depth of 200m due to model instabilities in shallower conditions. But climate models do have deficiencies in representing shelf systems in general as they lack a physical representation of barotropic scale processes, tides and coastal eddy currents, which are an important driver of bottom-water flow and mixing through turbulent processes (Holt et al. 2017).

Unfortunately, it is difficult to produce more than a visual comparison of individual shell data to show that the amplitude and variability of the proxy data can be simulated fairly well by climate models. The comparison between data and models through geological time will be discussed further in Section 5.5.

5.5 Data Model Comparisons

The uncertainty in the water depth conditions recorded by bivalve shells is high enough that mean annual temperature alone is insufficient to favour a certain set of model conditions (Section 4.6.3). However, the amount of seasonal temperature change did vary greatly with modelled water depth and can provide additional constraints to the data model comparison.

Due to shortcomings in the way HadCM3L handles shelf sections, it is not possible to constrain water depth conditions using climate simulations (Section 5.4.3). It is reasonable however, to compare the modelled temperatures of surface waters to the shell proxy data, even if in reality they were likely to have been produced in deeper waters.

Seasonal temperature variation from $\delta^{18}O$ data were found to be fairly consistent throughout the section (Figure 5.4) and can provide a rough constraint on the performance of each climate experiment (Figure 5.11 and Figure 5.12). This shows that in the northernmost location (16-6), modelled mean summer temperatures in all models were a good match to data at water depths between 30 and 70m, but the seasonality behaviour produced the best match for all model conditions between 30 and 40 m water depth. The highest CO_2 simulation (Maas6) produced the most similar amount of seasonality at deeper water depths, however the addition of riverine input (Maas2 riv, Maas2 riv 207k and Maas4 riv) muted the amount of temperature seasonality in the water at depths greater than 30m. This may be a result of temperature or freshwater causing stratification as mentioned in Section 4.6.3.

In the southernmost location (15-8), which was also modelled with a shallower overall water depth of 666 m compared to the 1500 m water depth in 16-6, simulated mean annual temperatures are a good match to proxy data at all shallow water depths. Seasonality, however is greatest in the low CO_2 (Maas2 and Maas2 207k) experiments and is the best match to data 40 m water depth. In addition, the 207k orbit experiment; designed to produce the coolest southern hemisphere temperatures and maximum sea ice formation produced higher warm month mean (WMMT) temperatures and higher seasonality at this location than the modern-day orbit experiment.

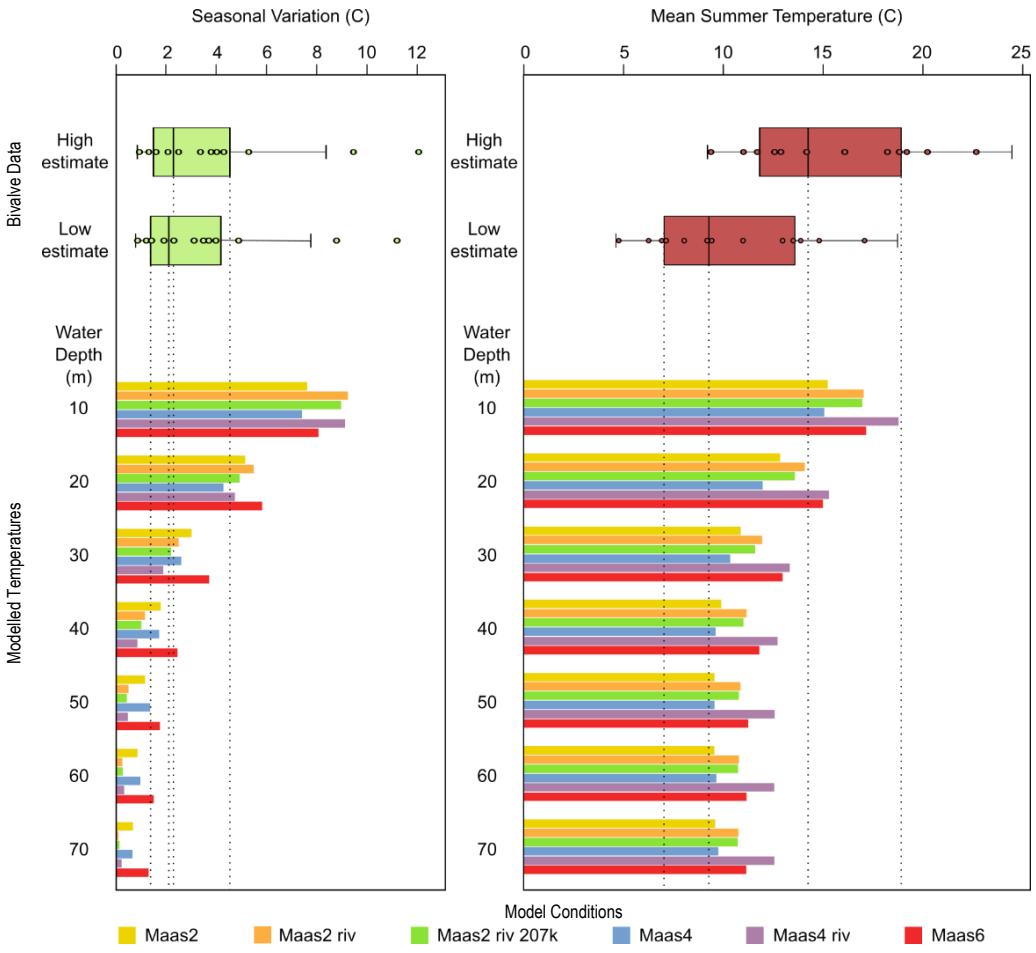

Figure 5.11: Comparison shell δ^{18}O-derived seasonality and mean summer temperature data with depth slice data from cell 16-6 under different model scenarios. Box plots represent high and low temperature estimates from all δ^{18}O data across all Maastrichtian and Danian specimens. Vertical dotted lines show the mean of each box plot as well as lower quartiles of the low temperature estimate and upper quartile of the upper temperature estimate from shell data for comparison with the model data in the lower section of the diagram. Model data has been interpolated into 10m depth slices and each model scenario is colour coded using the key at the bottom.

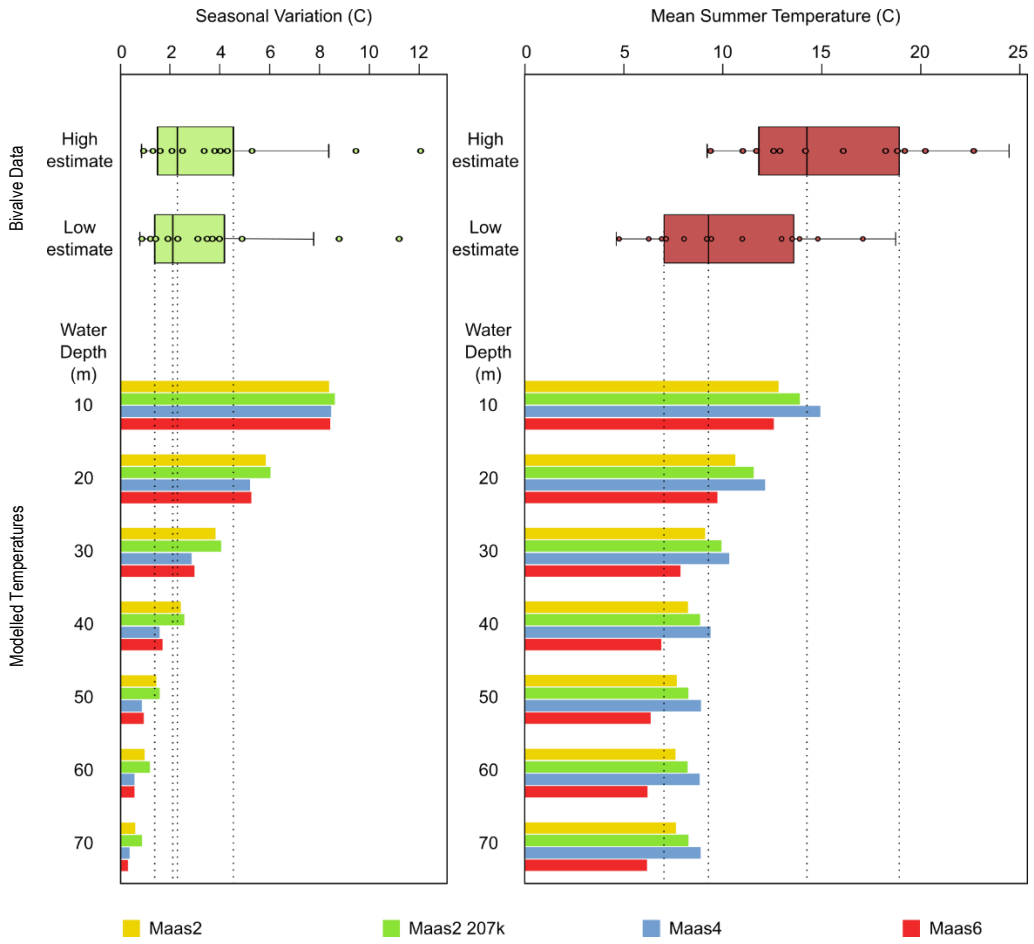

Figure 5.12: Comparison shell δ^{18}O-derived seasonality and mean summer temperature data with depth slice data from cell 15-8 under different model scenarios. Box plots represent high and low temperature estimates from all δ^{18}O data across all Maastrichtian and Danian specimens. Vertical dotted lines show the mean of each box plot as well as lower quartiles of the low temperature estimate and upper quartile of the upper temperature estimate from shell data for comparison with the model data in the lower section of the diagram. Model data has been interpolated into 10m depth slices and each model scenario is colour coded using the key at the bottom.

Depending on the latitude chosen for comparison, either the high CO_2 experiment (Maas6) or the low CO_2 experiment (Maas2) offers the best overall comparison to data from the entire Lopez de Bertodano formation. Proxy information about potential CO_2 conditions throughout this interval will be examined in Chapter 7. Redirecting river input through cell 16-6 does not improve the model's comparison with seasonal variation at reasonable water depths. This study also appears to corroborate with the observation in Section 5.4.3 that orbital conditions do not make much of an impact on either the amount of seasonal variation, or temperatures at this latitude as the signal is dominated by the seasonal cycle.

Although the model is generic for the Maastrichtian within the defined orbital and CO_2 parameters and will not represent changes in conditions over geological time, it is still useful to examine the patterns of data that best fit certain model snapshots. Separating the temperature data through geological time across the K-Pg boundary interval allows a comparison of the variability of the proxy and model data. This is a way of representing and comparing the climate variability data presented in Section 5.4.2.

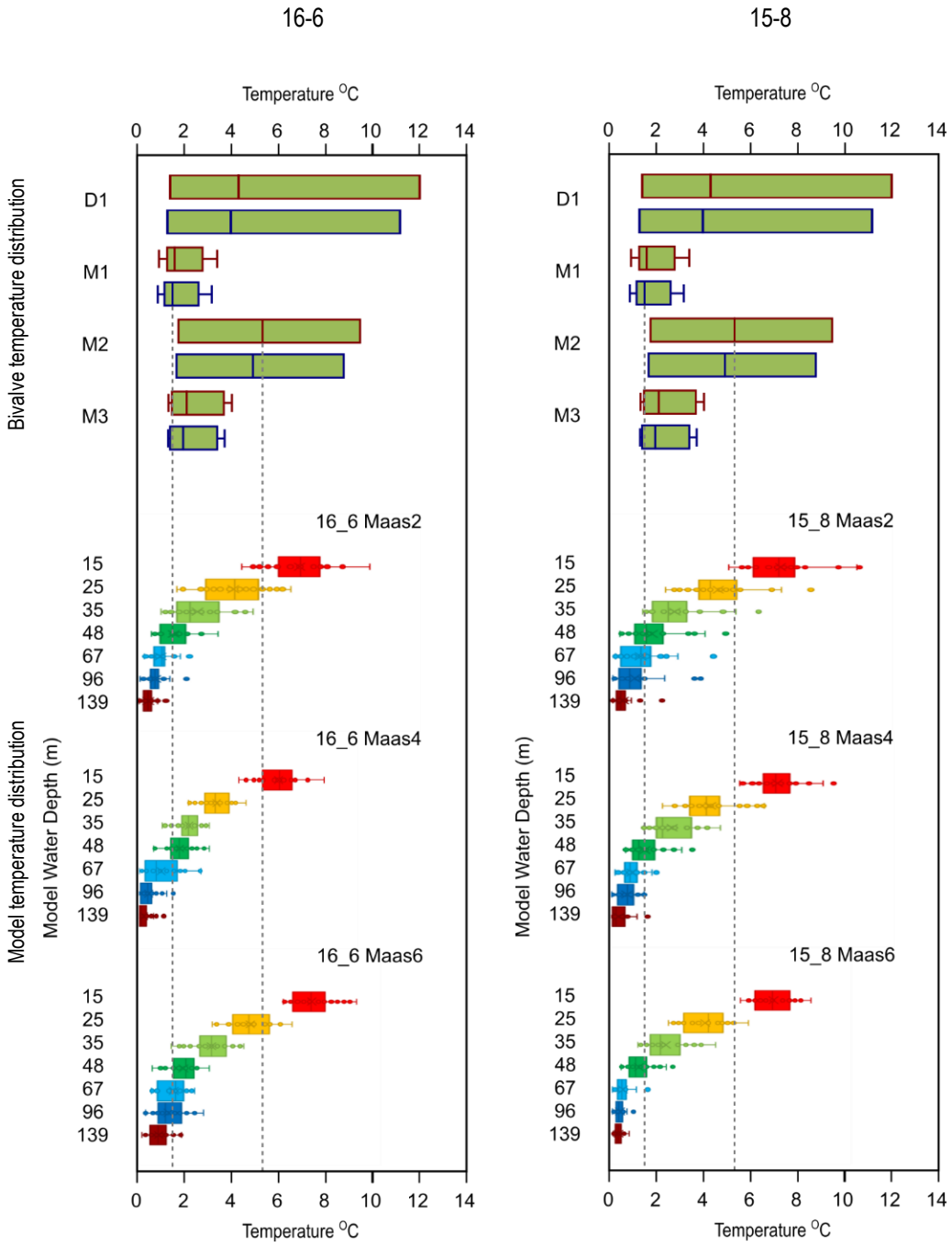

Figure 5.13: Box plots showing high-estimate (red outline) and low estimate (blue outline) seasonal temperature variation in bivalves from stratigraphic intervals around the K-Pg boundary (green) compared to simulated data in grid cells 16-6 (left column) and 15-8 (right column) under different CO_2 concentration conditions and water depths. Dotted vertical lines show the range between the lowest and highest mean amount of seasonal temperature variation found in the data.

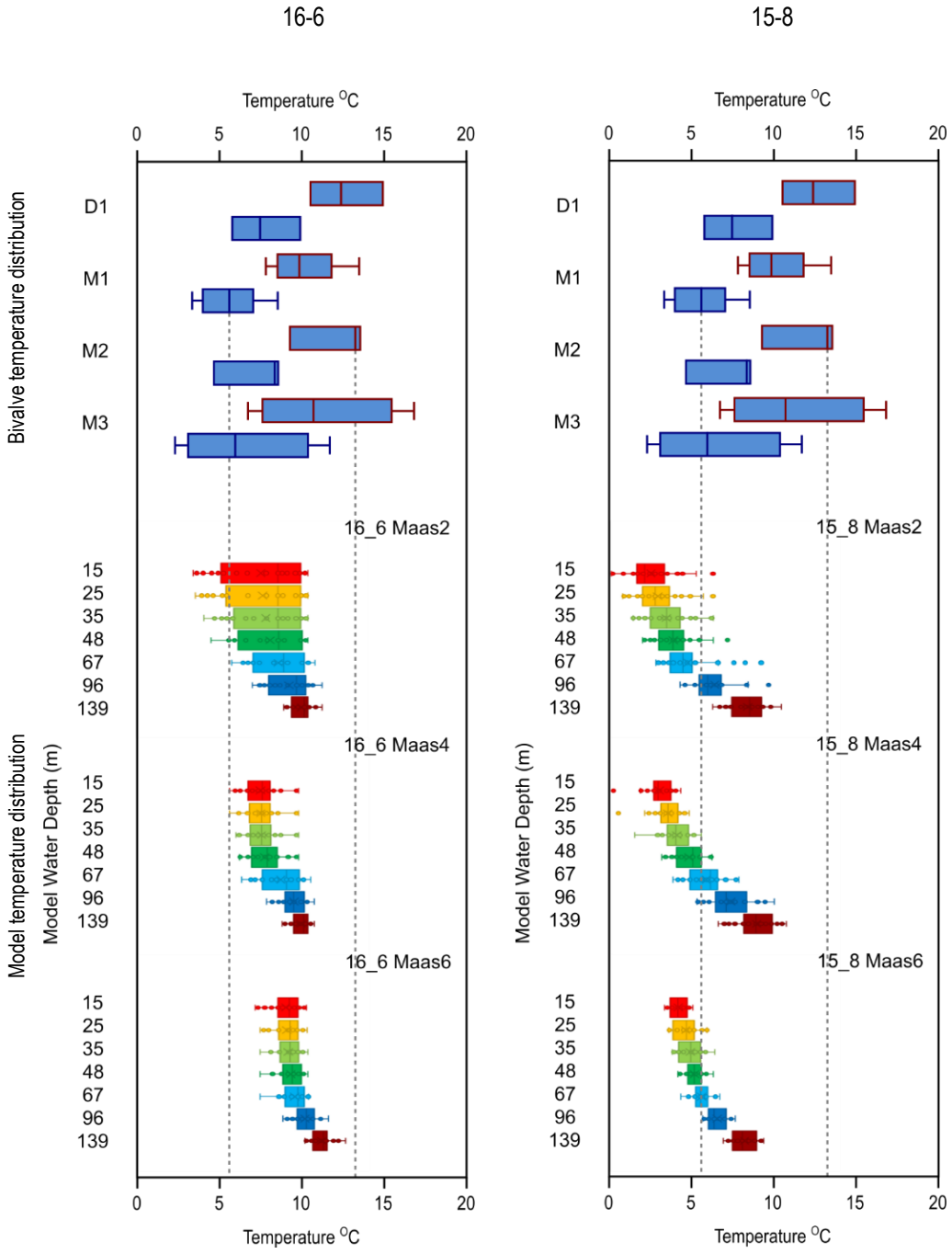

Figure 5.14: Box plots showing high-estimate (red outline) and low estimate (blue outline) CMMT in bivalves from stratigraphic intervals around the K-Pg boundary (blue fill) compared to simulated CMMT data in grid cells 16-6 (left column) and 15-8 (right column) under different CO_2 concentration conditions and water depths. Dotted vertical lines show the range between the lowest and highest average CMMT from shell data.

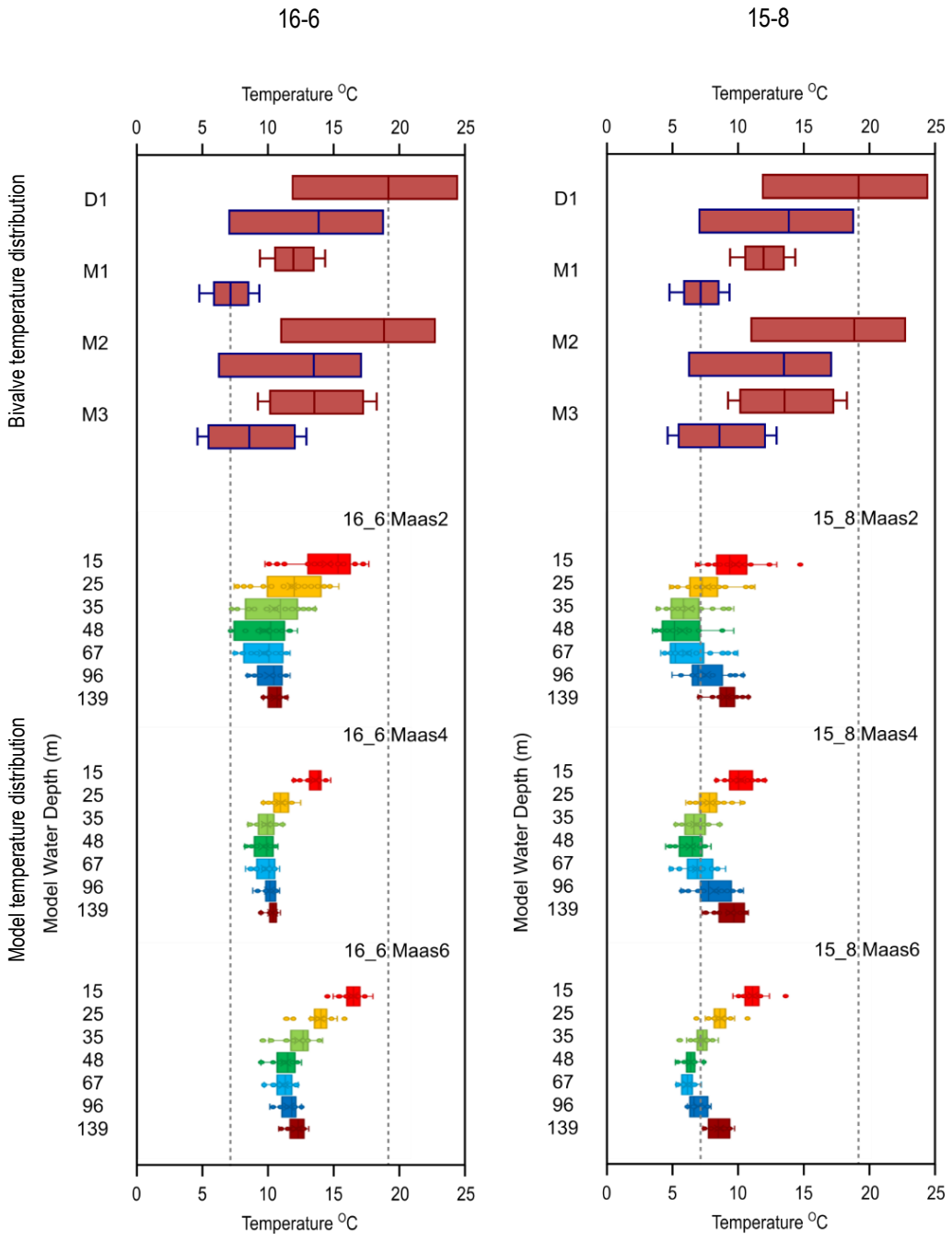

Figure 5.15: Box plots showing high-estimate (red outline) and low estimate (blue outline) WMMT in bivalves from stratigraphic intervals around the K-Pg boundary (red fill) compared to simulated WMMT data in grid cells 16-6 (left column) and 15-8 (right column) under different CO_2 concentration conditions and water depths. Dotted vertical lines show the range between the lowest and highest average WMMT from shell data.

The proxy data show that the variability between CMMT and WMMT in each stratigraphic interval around the K-Pg boundary is on a similar scale to the uncertainty in the temperature conversion due to variable water $\delta^{18}O$. As a result, it is difficult to track any changes in temperature through stratigraphy and correlate it with changes in model conditions.

The highest amounts of seasonality (e.g. shells in D1 and M2) were only able to be produced in the very shallowest waters in the model, which is likely to have been unrealistically shallow, even with the caveat that the models may not represent shelf environments perfectly. Layers this shallow are predominantly influenced by insolation and atmospheric temperatures and are unlikely to be as affected by the cool deeper water column present in the model bathymetry compared to a shallower, warmer real-life shelf bathymetry. This means that the amount of seasonality recorded here by shells may have been affected by factors such as freshwater runoff, causing the amount of seasonality to be overestimated, even in the $\delta^{18}O$ data, which generally shows a far lower amount of temperature seasonality than clumped isotope-derived temperature data (Figure 5.4).

Overall, all simulations at any CO_2 level were capable of producing seasonality and temperatures within the range of the proxy data at reasonable water depths. This suggests either that CO_2 is unlikely to have been a driving factor in any changes in high latitude seasonality and climate conditions during the Maastrichtian and Danian, or alternatively that HadCM3L underestimates the impact of CO_2 on temperatures at this location.

The model experiment at $2xCO_2$ produced a range of WMMT, CMMT and seasonality conditions closest to the distribution of the proxy data, and was able to produce these results at water depths within the 50-200m depth suggested for these bivalves, regardless of the restrictions of the model in simulating shelf environments.

The low CO_2 experiments produced the largest overall range and variance of WMMT and CMMT at most shallow-water depths in both study locations, however the mean year-to-year seasonality in each depth layer was still broadly similar to the higher CO_2 experiments. This suggests that in simulations with lower CO_2, longer timescale climate variability may have a larger effect on temperature than intra-annual seasonality.

The simulations taken at the lower latitude location (16-6) show generally better agreement with proxy data than the higher latitude location (15-8). This is reasonable given that 16-6 is the location that corresponds to the palaeogeographic position of Seymour Island with respect to the global Maastrichtian palaeogeography (Markwick & Valdes 2004). Whereas 15-8 is a similar location given the palaeomagnetic latitude of Seymour Island's sedimentary deposits (Lawver et al. 1992) but will be in a different relative palaeogeographic location and circulatory regime in the model.

5.6 Summary

The $\delta^{18}O$ composition of shells of *Lahillia* and *Cucullaea* can be used to produce CMMT and WMMT data as well as a measure of the intra-annual seasonality. Estimates suggest seasonality of between 2 and 4°C through the section, with the potential for intervals with slightly higher seasonality between approximately 930 and 960m in stratigraphy; around the height of the latest Maastrichtian C30N to C29R geomagnetic reversal.

Due to the method of collecting seasonality data from shells using clumped isotopic data, it is likely that the difference in temperatures found will incorporate longer timescale climate variability in addition to seasonal behaviour. Data from climate simulations suggests that this variability may be larger than the degree of seasonality, depending on the amount of atmospheric CO_2. This means that the estimates of seasonality produced from shells measured several years apart are unlikely to be as reliable as in shells sampled continuously across consecutive growth lines.

As only a limited number of shells from the recovery interval of the Lopez de Bertodano formation were able to be sampled for seasonality data, it is not possible to determine whether there were any changes in seasonal climate behaviour in the aftermath of the K-Pg mass extinction. It is possible that the amount of seasonality increased as a result of warmer summer temperatures while winter temperatures remained similar to Maastrichtian conditions, but too few shells were sampled to conclude this definitively.

Modelled data appears to be a remarkably good fit to the $\delta^{18}O$ derived proxy data, provided slightly shallower depth slices (between 30 and 50m) are considered compared to the suggested living depth for the infaunal bivalves. This does not suggest that the waters were actually these shallow depths in the Seymour Island section, but is more likely to be a reflection on the ability of the model to accurately represent shallow shelf environments. The fact that a general model covering the whole Maastrichtian is capable of producing data comparable to geological data recorded over several million years of geological time, under different orbital conditions could imply that orbitally driven variations in seasonality and temperature are a second order effect compared to the strength of the seasonal cycle at this location.

Models $2xCO_2$ produced the range of WMMT, CMMT and seasonality conditions closest to the distribution of $\delta^{18}O$ derived proxy data at the water depths most similar to the likely shelf environment. This model also produced the largest amount of climate variability on timescales longer than annual seasonality, giving a good match to the larger-amplitude (i.e. 4 to 6°C), longer frequency variability shown in the clumped isotopic data.

The $4xCO_2$ and $6xCO_2$ experiments were also capable of producing seasonality and temperature data within the range of the proxy data at reasonable, if slightly shallower water depths, suggesting that changes in CO_2 do not have a driving effect on temperature in this location.

5.7 References

Archibald, J. D., Clemens, W. A., Padian, K., Rowe, T., Macleod, N., Barrett, P. M., Gale, A. *et al.* (2010) 'Multiple Causes Cretaceous Extinctions : Cretaceous Extinctions ':, *Science*, 328, 973–976.

Barrera, E. (1994) 'Global environmental changes preceding the Cretaceous-Tertiary boundary: Early-late Maastrichtian transition', *Geology*, 22(10), 877–880.

Barrera, E., Huber, B. T., Savin, S. M. and Webb, P. N. (1987) 'Antarctic marine temperatures: Late Campanian through early Holocene', *Paleoceanography*, 2, 21–47.

Bartlein, P. J. and Prentice, I. C. (1989) 'Orbital variations, climate and paleoecology', *Trends in Ecology & Evolution*, 4(7), 195–199.

Bauer, W., Thomas, R. J. and Jacobs, J. (2003) 'Proterozoic-Cambrian history of Dronning Maud Land in the context of Gondwana assembly', *Geological Society, London, Special Publications*, 206(1), 247–269.

Crame, J. A., Francis, J. E., Cantrill, D. J. and Pirrie, D. (2004) 'Maastrichtian stratigraphy of Antarctica', *Cretaceous Research*, 25(3), 411–423.

Crowley, T. J. and Zachos, J. C. (2000) 'Comparison of zonal temperature profiles for past warm time periods', in Huber, B. T., Macleod, K. G., and Wing, S. L. (eds) *Warm Climates in Earth History*. Cambridge: Cambridge University Press, 50–76.

Davis, M. B., Shaw, R. G. and Etterson, J. R. (2005) 'Evolutionary Responses To Changing Climate', *Ecology*. Ecological Society of America, 86(7), 1704–1714.

Dingle, R. V. and Lavelle, M. (2000) 'Antarctic Peninsula Late Cretaceous-Early Cenozoic palꞌoenvironments and Gondwana palꞌogeographies', *Journal of African Earth Sciences*, 31(1), 91–105.

Ditchfield, P. W., Marshall, J. D. and Pirrie, D. (1994) 'High latitude palaeotemperature variation: New data from the Thithonian to Eocene of James Ross Island, Antarctica', *Palaeogeography, Palaeoclimatology, Palaeoecology*, 107(1–2), 79–101.

Donnadieu, Y., Pierrehumbert, R., Jacob, R. and Fluteau, F. (2006) 'Modelling the primary control of paleogeography on Cretaceous climate', *Earth and Planetary Science Letters*, 248, 426–437.

Foley, J. A., Kutzbach, J. E., Coe, M. T. and Levis, S. (1994) 'Feedbacks between climate and boreal forests during the Holocene epoch', *Nature*, 52–54.

Francis, J. E. and Poole, I. (2002) 'Cretaceous and early Tertiary climates of Antarctica: evidence from fossil wood', *Palaeogeography, Palaeoclimatology, Palaeoecology*, 182(1), 47–64.

Gallagher, S. J., Wagstaff, B. E., Baird, J. G., Wallace, M. W. and Li, C. L. (2008) 'Southern high latitude climate variability in the Late Cretaceous greenhouse world', *Global and Planetary Change*, 60(3), 351–364.

Gerber, S., Joos, F., Brügger, P., Stocker, T., Mann, M., Sitch, S. and Scholze, M. (2003) 'Constraining temperature variations over the last millennium by comparing simulated and observed atmospheric CO 2', *Climate Dynamics*. Springer, 20(2), 281–299.

Goodwin, D. H., Schöne, B. R. and DL, D. (2003) 'Resolution and fidelity of oxygen isotopes as paleotemperature proxies in bivalve mollusk shells: Models and observations', *Palaios*, 18(2), 110–125.

Guthrie, R. D. (1984) 'Mosaics, allelochemics and nutrients: an ecological theory of late Pleistocene megafaunal extinctions.', *Quaternary Extinctions: A Prehistoric Revolution. 1984.*

Holt, J., Hyder, P., Ashworth, M., Harle, J., Hewitt, H. T., Liu, H., New, A. L., Pickles, S., *et al.* (2017) 'Prospects for improving the representation of coastal and shelf seas in global ocean models', *Geoscientific Model Development*, 10(1), 499–523.

Huber, B. T., Hodell, D. A. and Hamilton, C. P. (1995) 'Middle-Late Cretaceous climate of the Southern High Latitiudes: Stable isotope evidence for minimal equator-to-pole thermal gradients', *Geological Society of America Bulletin*, 107(10), 1164–1191.

Huber, B. T., Norris, R. D. and MacLeod, K. G. (2002) 'Deep-sea paleotemperature record of extreme warmth during the Cretaceous', *Geology*, 30(2), 123–126.

Jones, D. S. and Quitmyer, I. R. (1996) 'Marking Time with Bivalve Shells: Oxygen Isotopes and Season of Annual Increment Formation', *PALAIOS*, 11(4), 340.

Lawver, L. A., Gahagan, L. M. and Coffin, M. F. (1992) *The Antarctic Paleoenvironment: A Perspective on Global Change: Part One*, *Antarctic Research Series*. Edited by J. P. Kennett and D. A. Warkne. Washington, D. C.: American Geophysical Union (Antarctic Research Series).

Li, L. and Keller, G. (1998) 'Abrupt deep-sea warming at the end of the Cretaceous', *Geology*, 26(11), 995–998.

Macellari, C. E. (1988) 'Stratigraphy, sedimentology, and paleoecology of Upper Cretaceous / Paleocene shelf-deltaic sediments of Seymour Island', *Geological Society of America Memoirs*, 169, 25–54.

Markwick, P. J. (1996) *Late Cretaceous to Pleistocene Climates: Nature of the Transition from 'Hot-House' to an 'Ice-House' World*. University of Chicago.

Markwick, P. J. and Valdes, P. J. (2004) 'Palaeo-digital elevation models for use as boundary conditions in coupled ocean-atmosphere GCM experiments: a Maastrichtian (late Cretaceous) example', *Palaeogeography, Palaeoclimatology, Palaeoecology*, 213(1–2), 37–63.

Marshall, J. and Speer, K. (2012) 'Closure of the meridional overturning circulation through Southern Ocean upwelling', *Nature Geoscience*. Nature Publishing Group, 5(3), 171–180.

Parmesan, C., Root, T. L., Willig, M. R., Parmesan, C., Root, T. L. and Willig, M. R. (2000) 'Impacts of Extreme Weather and Climate on Terrestrial Biota *', *Bulletin of the American Meteorological Society*, 81(3), 443–450.

Pearson, P. N., Ditchfield, P. W., Singano, J., Harcourt-Brown, K. G., Nicholas, C. J., Olsson, R. K., Shackleton, N. J. and Hall, M. A. (2001) 'Warm tropical sea surface temperatures in the Late Cretaceous and Eocene epochs', *Nature*, 413(6855), 481–487.

Pirrie, D. and Marshall, J. D. (1990) 'High-paleolatitude Late Cretaceous paleotemperatures: New data from James Ross Island, Antarctica', *Geology*, 18(1), 31–34.

Poole, I., Cantrill, D. J. and Utescher, T. (2005) 'A multi-proxy approach to determine Antarctic terrestrial palaeoclimate during the Late Cretaceous and Early Tertiary', *Palaeogeography, Palaeoclimatology, Palaeoecology*, 222, 95– 121.

Price, D. A., Valdes, P. J. and Sellwood, B. W. (1997) 'Prediction of modern bauxite occurence: implications for climate reconstruction', *Palaeogeography, Palaeoclimatology, Palaeoecology*, 131, 1–13.

Reichstein, M., Bahn, M., Ciais, P., Frank, D., Mahecha, M. D., Seneviratne, S. I., Zscheischler, J., Beer, C., *et al.* (2013) 'Climate extremes and the carbon cycle', *Nature*, 500(7462), 287–295.

Schöne, B. R., Lega, J., W. Flessa, K., Goodwin, D. H. and Dettman, D. L. (2002) 'Reconstructing daily temperatures from growth rates of the intertidal bivalve mollusk Chione cortezi (northern Gulf of California,

Mexico)', *Palaeogeography, Palaeoclimatology, Palaeoecology*, 184(1–2), 131–146.

Schöne, B. R., Tanabe, K., Dettman, D. L. and Sato, S. (2003) 'Environmental controls on shell growth rates and d 18 O of the shallow-marine bivalve mollusk Phacosoma japonicum in Japan', *Marine Biology*, 142(3), 473–485.

Sheldon, P. R. (1996) 'Plus ça change — a model for stasis and evolution in different environments', *Palaeogeography, Palaeoclimatology, Palaeoecology*, 127(1–4), 209–227.

Wolfe, J. A. (1993) 'A method of obtaining climatic parameters from leaf assemblages', *U.S. Geological Survey Bulletin*, 2040.

Wolfe, J. A. and Upchurch, G. R. (1987) 'North American nonmarine climates and vegetation during the Late Cretaceous', *Palaeogeography, Palaeoclimatology, Palaeoecology*, 61, 33–77.

CHAPTER 6

SULFATE AND SEASONALITY: BIOGEOCHEMICAL CYCLES

6.1 Abstract

In addition to $\delta^{18}O$ data which have been used to reconstruct past temperature conditions in Chapters 3, 4 and 5, bivalve shells can also record $\delta^{13}C$ data and give information about bottom water productivity and redox conditions. These conditions are themselves affected by seasonal variations, as well as major seawater chemistry and biogeochemical cycling.

The late Cretaceous period is likely to have fallen within a period in which marine sulfate concentrations were significantly lower than modern oceans. As sulfate has a major controlling effect on sedimentary carbon cycling, particularly the processes of methane production and oxidation, lower sulfate levels may have led to an increase in sedimentary methane production; the oxidation products of which can conceivably be detected in the carbonate carbon and organic carbon isotopic records of marine organisms.

Here we present the results of high resolution carbonate-carbon isotope records from two species of well-preserved shallow infaunal marine bivalves collected from the marine shelf succession across the Cretaceous-Paleogene (K-Pg) boundary in Seymour Island, Antarctica. Shell carbonate-carbon isotope records vary widely: at one extreme, shells have unremarkable average values and small ranges compatible with a contemporaneous marine dissolved inorganic carbon (DIC) source and modern sedimentary carbon cycling. At the other, the shells have large-amplitude annual cycles of carbon isotopic variability of up to −23.8‰ within a single year of growth and shell carbonate $\delta^{13}C$ compositions as negative as −34‰. Shells with these increased ranges and unusually negative average values are found at discrete intervals within the 3-4 Myr K-Pg boundary sequence and are present in both species of bivalve examined. Mass balance calculations

suggest that these unusual records can only be explained by enhanced supply of sedimentary methane derived DIC. However, a corresponding carbon isotopic depletion is not found in the organic carbon isotopic record which remained between −26.1 and −21.7‰ throughout the sedimentary sequence, suggesting a localized bottom-water signal. We therefore interpret these intervals as periods where carbon derived from the oxidation of methane entered the bottom-water dissolved inorganic carbon pool.

Based on further mass balance calculations, the contribution of methane required to explain the most negative carbonate-carbon isotopic values in the bivalve shells is extremely high (between 30 to 85% of bottom-water DIC). The lack of authigenic carbonate in the section suggests that methane oxidation progressed aerobically. Given the large calculated contribution of methane, this could provide a substantial driver for transient bottom water deoxygenation and introduce seasonality into the bottom water oxygen budget. The seasonality of the carbonate-carbon isotope signal indicates that the system of methane production or oxidation must have been sensitive to environmental variables on annual time scales. This sensitivity precludes control by methane-hydrates and we instead argue that these combined data indicate the shallowing and increased importance of methanogenesis in the sediments enabled by lower ocean sulfate concentrations in the Late Cretaceous. The tendency towards a more dynamic role for marine methane production and oxidation is likely to apply to other times of low marine sulfate in Earth's history.

6.2 Introduction

The sedimentary production and release of methane is largely a function of the depth of penetration of various oxidants into marine sediments, of which sulfate plays a particularly important role. Given the importance of sulfate in sedimentary biogeochemistry, remarkably little is known of the behavior of the marine methane cycle under the lower marine sulfate concentrations that dominated the majority of the Phanerozoic (Horita et al. 2002; Holt et al. 2014)

In the modern ocean, sulfate plays a key role in the oxidation of organic carbon in ocean sediments via microbial sulfate reduction (MSR), which can account for up to ~80% of organic carbon oxidation (Jørgensen & Kasten 2006). Only organic

carbon that survives oxidation by MSR to sedimentary depths where sulfate concentrations have been reduced to zero is then available for methanogenesis. Ocean sulfate concentrations will, therefore, exert a first order control on methane production; by affecting both the amount of organic carbon available for methanogenesis and the sedimentary depth at which methanogenesis becomes the dominant fate for this carbon.

It is therefore reasonable to hypothesize that lower sulfate oceans of the past would have been characterized by greater methane production, with methanogenesis occurring at shallower depths in the sediment. The result of this is likely to be an increased flux of methane across the sediment-water interface (Wortmann & Chernyavsky 2007; Wortmann & Paytan 2012), and the potential for methane-derived dissolved inorganic carbon (DIC) with a characteristic negative $\delta^{13}C$ signature in bottom-waters during these times. This DIC signal can be preserved in the fossil record by biomineralizing organisms which incorporate carbon from the ambient DIC pool into biological compounds such as shell carbonate (McConnaughey & Gillikin 2008).

Infaunal bivalves such as *Lahillia* and *Cucullaea* examined in this thesis represent ideal archives in which to search for the signals of methane oxidation in the benthic boundary layer of the water column. The active pumping of water by bivalves to supply food particles, oxygen, and ions for biomineralization means that the isotope signatures produced in modern shells are dominated by bottom water rather than sedimentary signatures (Klein et al. 1996). Some species do incorporate a small amount of respired organic carbon into their shell carbonate; however, the majority is precipitated from the DIC in inhalant seawater with little carbon isotope fractionation (McConnaughey et al. 1997; Poulain et al. 2010). Even bivalves which derive nutrition from chemosymbiotic methane oxidizing bacteria at modern seeps, have shell-carbonate carbon isotope compositions dominated by DIC from the ambient seawater, with the main isotopic effect of their food source confined to the ^{13}C-depleted signal of their soft tissues. (Paull et al. 1989; Fisher 1995).

Some muted indicators of methane production and oxidation have also been observed at discrete levels within the Lopez de Bertodano Formation, including the appearance of thyasirid, lucinid and solemyid bivalves, which are taxa known to host chemosymbiotic bacteria and occur at sites of modern and Cretaceous methane seepage (Kauffman et al. 1996). Burrow-filling carbonates can also be found concurrent with these bivalve occurrences, and have been found to have

distinctly negative carbon isotope compositions (−24 to −58‰, Little et al. 2015). However, the López de Bertodano formation lacks the abundant authigenic carbonate which characterizes many modern sites of focused marine methane seepage, and which can be found in stratigraphically older early Maastrichtian sediments on nearby Snow Hill Island (Little et al. 2015). This makes it an ideal location to look for the potential effects of late Cretaceous low marine sulfate concentrations on the methane cycle.

Estimates of marine geochemistry from fluid inclusions, proxies and geochemical models suggest that the Late Cretaceous is likely to have been characterized by ocean sulfate concentrations far lower than modern seawater (29 mM). Fluid inclusions in well-preserved halite have been used to extrapolate sulfate concentrations across the Late Cretaceous. The records closest in time to the Maastrichtian are from the Aptian and Albian-Cenomanian (125 to 93.9 Ma); spanning a range of 5-16 mM (Lowenstein et al. 2003; Timofeeff et al. 2006), and the Eocene and Oligocene (56 to 23 Ma); which spans 14-23 mM (Horita et al. 2002). Studies of sulfate-sulfur isotopic rate of change during OAE-2 in the Cenomanian-Turonian (100.5 to 89.8 Ma) suggest sulfate concentrations of 2-7 mM (Adams et al. 2010; Owens et al. 2013). Modelling studies using a variety of methods also suggest low marine sulfate concentrations for the Maastrichtian with estimates of ~5 mM; (Wortmann & Paytan 2012), ~11 mM (Berner 2004) and ~15 mM (Demicco et al. 2005). Taken together, these lines of evidence strongly suggest that while the exact concentration of sulfate in the Late Cretaceous is debatable, concentrations were likely to have been less than half that of modern seawater (i.e. less than 14 mM).

6.3 Methods

6.3.1 Stable Isotopic Analysis

This chapter focuses on examining the high-resolution $\delta^{13}C$ records presented in Chapter 3 and Appendix A. These records were produced by microsampling Lahillia and Cucullaea shells (refer to Section 3.4.1 for methodology) and the

$\delta^{13}C$ data were recorded concurrently with the $\delta^{18}O$ records which have been the focus of Chapter 3, 4 and 5.

6.3.2 Sedimentary Analysis

A total of 133 samples of bulk sediment from composite section D5.251 were analysed for organic carbon isotope content, total organic carbon (TOC) and carbonate content.

Samples were prepared by acidification following standard techniques to remove all carbonate and non-organic material (Appendix C) and analysed using a Micromass Isoprime continuous flow mass spectrometer coupled to a Eurovector or Elementar Pyrocube elemental analyser. $^{13}C/^{12}C$ ratios were calibrated using the international standards ANU-sucrose and IAEA-CH7 to the V-PDB scale with a precision of better than ±0.25‰ for repeat analysis of standard materials during the runs. Calculation of weight percent organic carbon was either derived from the mass spectrometer traces or analysed on a LECO elemental analyser, and corrected for weight loss during the acidification process. Weight percent carbonate was either calculated from weight loss during acidification or from analysing total carbon on the LECO and then calculating total inorganic carbon (TIC) by deducting TOC. TIC was then converted to weight percent carbonate by assuming that it was all present as $CaCO_3$.

6.4 Results

The stable isotopic analysis results are presented in Figures 6.1 to 6.3, with the raw data in Appendix C. These data were processed with the d18O data to remove obvious outliers (Section 3.5.2).

Oxygen isotopic values in all specimens range from 2.84 to −4.44‰, and were used to establish the seasonality of the carbon isotope signals (see Section 3.4.3). More negative carbonate-$\delta^{18}O$ is a common feature of the mid to late portion of the growth increment in both species and smooth cuspate trajectories truncated against visible major growth lines are distinguishable (Figures 6.1 to 6.3).

Carbonate-carbon isotopic records in the nineteen bivalves across both species sampled at high resolution range from +6.3 to −34.2‰ (Figure 6.1 to Figure 6.3 and data in Appendix). Regular patterns of change within growth increments are observed with lower carbonate-δ^{13}C generally observed in earlier part of the growth period and more positive δ^{13}C towards each dark growth ring. The average and range of carbonate- δ^{13}C within each shell varies markedly (average from +4.2 to −23.8, range from 0.4 to 23.5‰). The shells with the most negative mean and the largest ranges of carbonate-carbon isotope composition appear to be clustered around particular stratigraphic intervals (notably 930-970 and 1000-1040m).

Percentages of total organic carbon range between between 0.14 and 0.65% throughout the succession (Figure 6.4 and Appendix C) with an average value of 0.38 wt%. Organic-carbon δ^{13}C ranges from −21.7 to −26.1‰ with an average of −24.8‰ with no clear stratigraphic trend. Weight percent carbonate varies between 6.3 and 22.0% with a particularly carbonate-rich horizon at the Cretaceous-Paleogene boundary, which is likely to be related to a glauconite rich layer at the same position (Zinsmeister 1998).

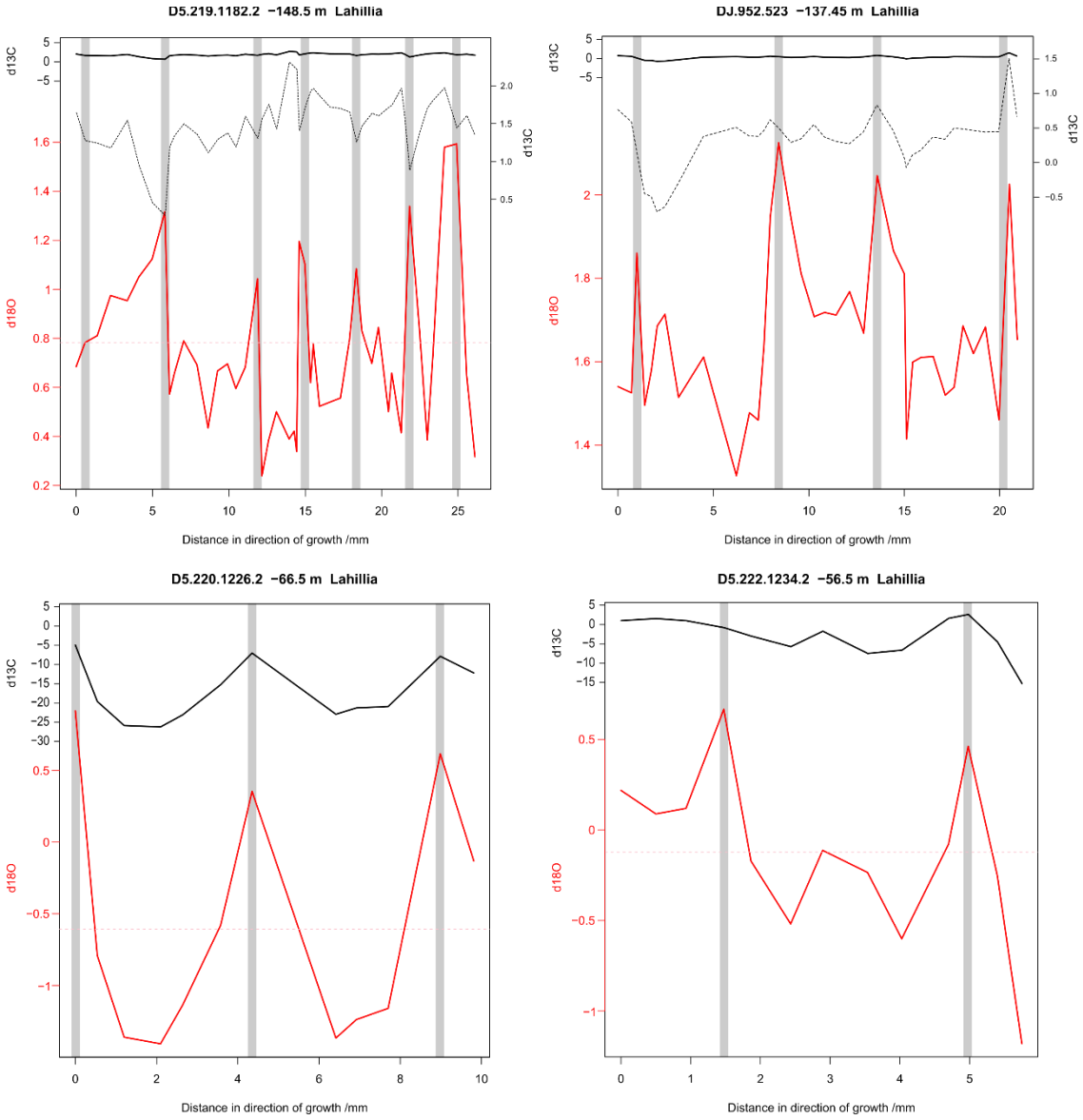

Figure 6.1 A: Stable carbon (black) and oxygen isotope data (red) in specimens of *Lahillia* from the López de Bertodano Formation. Distance axis begins at an arbitrary point within the shell. Vertical gray bars locate positions of annual growth lines. δ^{13}C data presented to the same scale on the top/left axis and an expanded scale (dotted line) on the right axis to show lower amplitude trends and variability

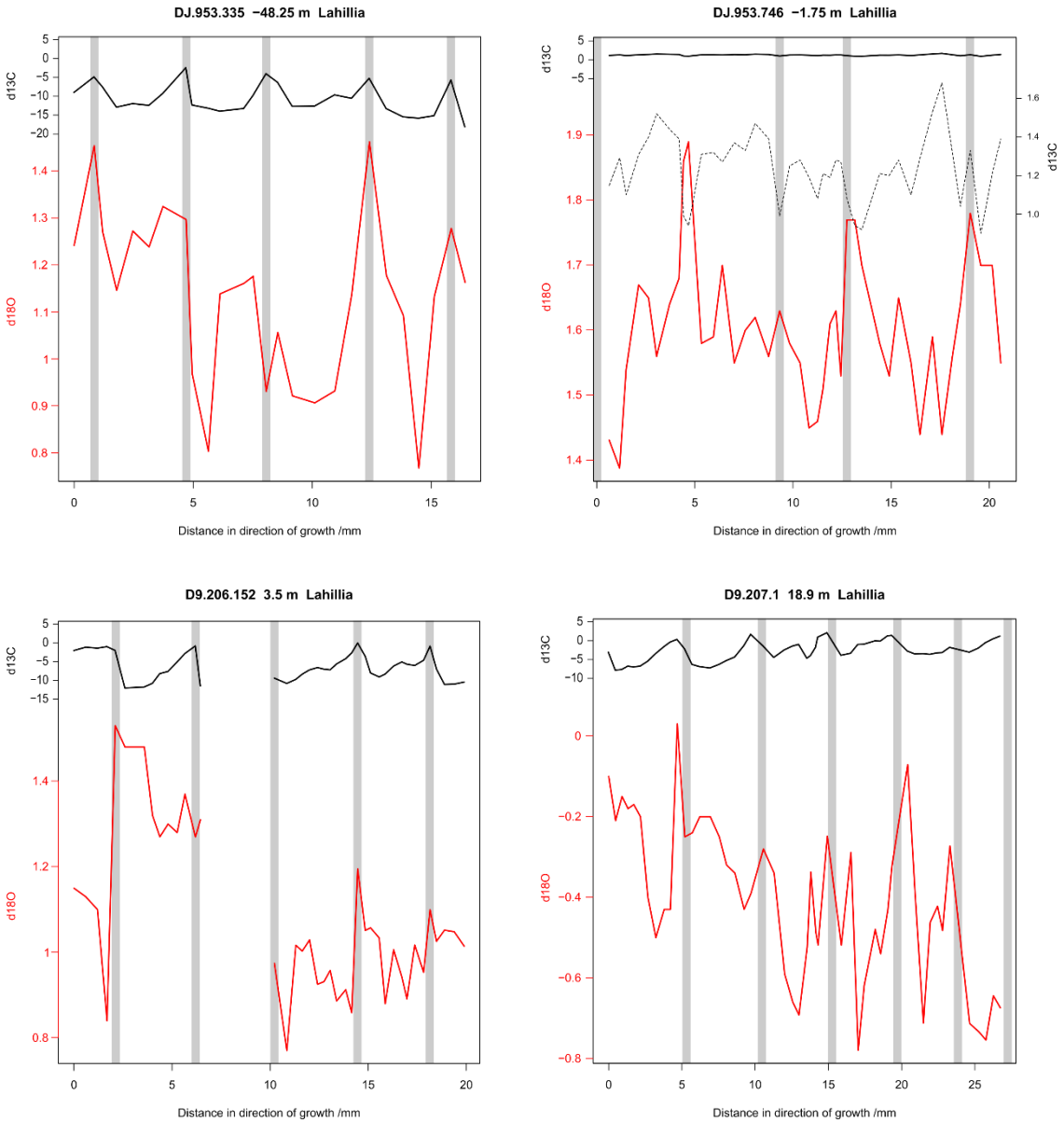

Figure 6.1 B: Stable carbon (black) and oxygen isotope data (red) in specimens of *Lahillia* from the López de Bertodano Formation. Distance axis begins at an arbitrary point within the shell. Vertical gray bars locate positions of annual growth lines. δ^{13}C data presented to the same scale on the top/left axis and an expanded scale (dotted line) on the right axis to show lower amplitude trends and variability

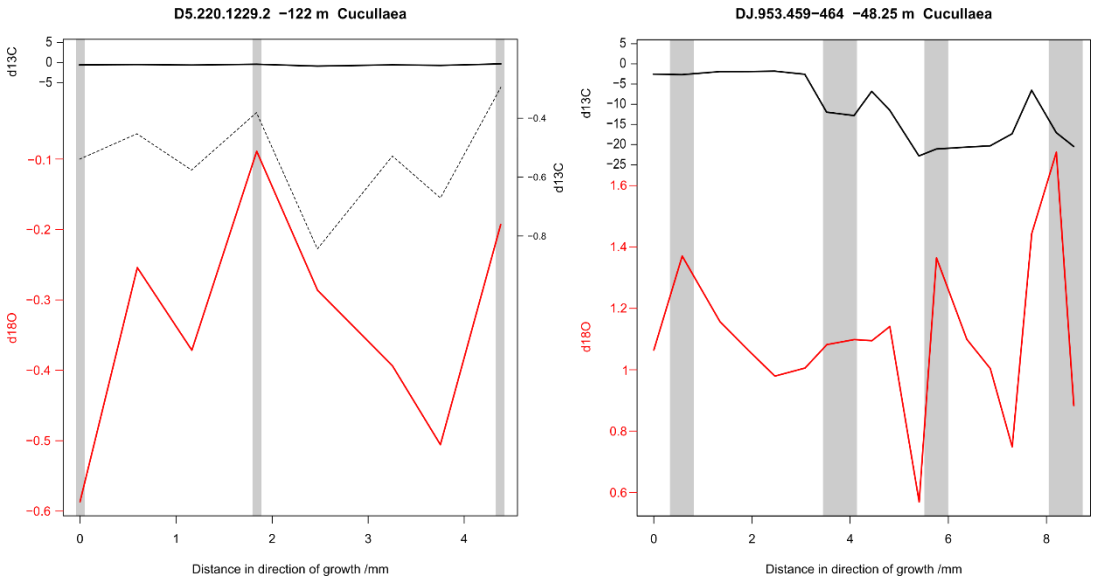

Figure 6.2: Stable carbon (black) and oxygen isotope data (red) in specimens of *Cucullaea* from the López de Bertodano Formation. Distance axis begins at an arbitrary point within the shell. Vertical gray bars locate positions of annual growth lines. δ^{13}C data presented to the same scale on the top/left axis and an expanded scale (dotted line) on the right axis to show lower amplitude trends and variability

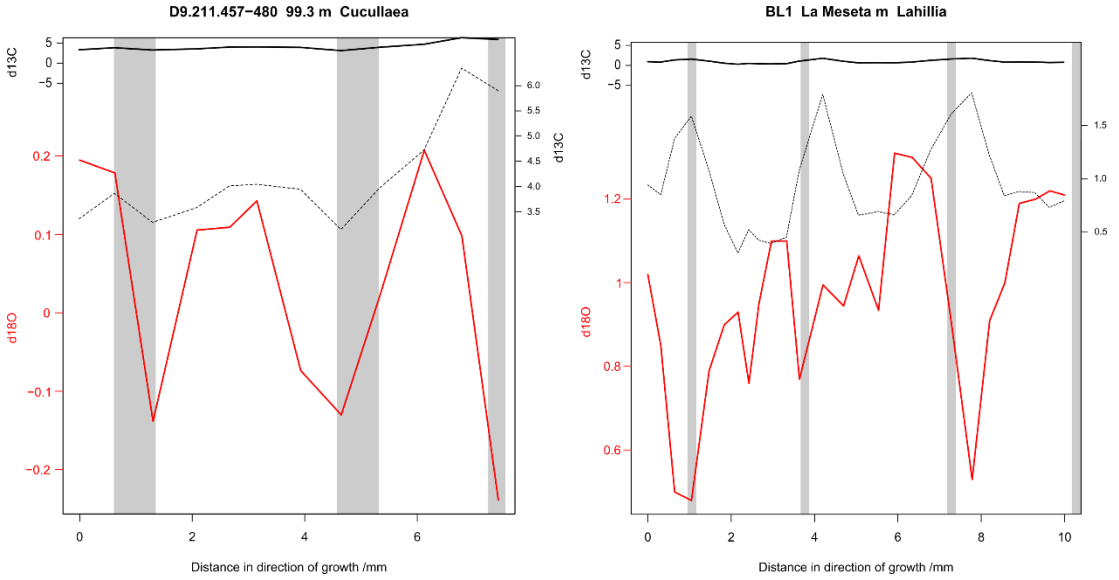

Figure 6.3: Oxygen isotope graphs (red) with approximate temperature conversions (black) in specimens of *Cucullaea* from the Sobral Formation (A) and *Lahillia* from the La Meseta Formation (B). Distance axis begins at an arbitrary point within the shell. Vertical gray bars locate positions of annual growth lines. δ^{13}C data presented to the same scale on the top/left axis and an expanded scale (dotted line) on the right axis to show lower amplitude trends and variability

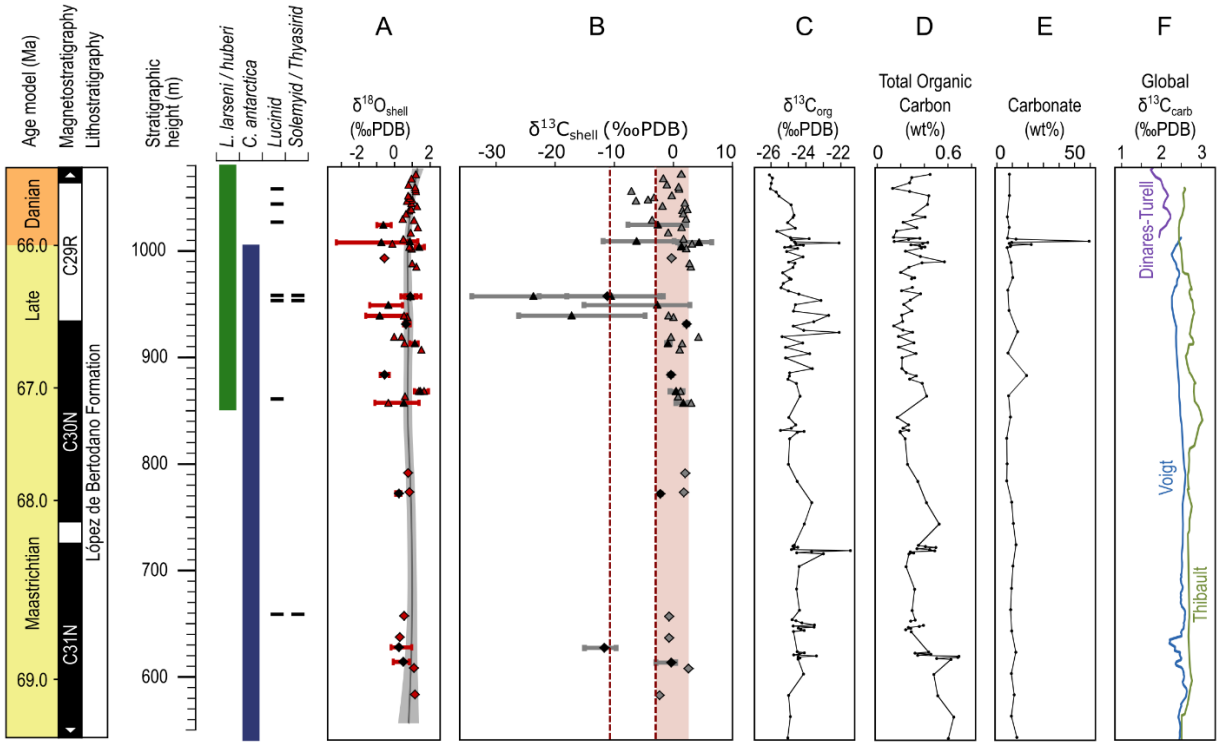

Figure 6.4. Compilation of stable isotope and sedimentary data from Seymour Island. Stratigraphic ranges for selected bivalve species including recorded horizons of chemosymbiotic-associated lucinids, thyasirids and solemyids (Little et al. 2015). (A and B) $\delta^{18}O$ and $\delta^{13}C$ data respectively from *Lahillia* (triangles) and *Cucullaea* (diamonds), horizontal bars with black markers indicate seasonal range and mean values from specimens sampled at high resolution and are not error bars; shaded line in (A) represents the Loess fit through data; shaded field in (B) represents the values within the range of expected shell $\delta^{13}C$ depletion due to metabolic carbon incorporation; dashed vertical lines represent shell $\delta^{13}C$ values calculated for normal (10%) and extreme (37%) fractional incorporation. (C to E) Sedimentary results from composite section D5.251; (C) organic carbon $\delta^{13}C$; (D) weight percent total organic; (E) weight percent carbonate. (F) Synchronus marine bulk carbonate $\delta^{13}C$ values from Voigt et al. (2012); Dinarès-Turell et al. (2014); Thibault et al. (2012).

6.5 Discussion

Notable within the shell $\delta^{13}C$ data are two interesting trends. Firstly the remarkable variation in $\delta^{13}C$ between annual growth lines in several specimens, and secondly the apparent clustering of shells displaying this large variation within the section. The origin of each of these apsects of the data set will be discussed below.

6.5.1 Origins of the Shell Carbonate $\delta^{13}C$ Signal

The carbonate-$\delta^{13}C$ results at the upper end of the end of our reported range of +6.3 to −34.2‰ are typical of modern marine heterotrophic bivalves (Toland et al. 2000; Carré et al. 2005; Schöne et al. 2005) whilst the much more negative data are difficult to explain under normal marine conditions. We used a simple isotopic mass balance (details in supplementary material) incorporating generally accepted values for metabolic carbon contribution to bivalve shells (0 to 10%, McConnaughey et al. 1997; Poulain et al. 2010), isotope compositions of the particulate organic carbon (POC) food source (−28 to −20‰, Mook & Tan 1991), and Cretaceous ambient dissolved inorganic carbon (DIC) (0 to +2.5‰, Voigt et al. 2012), to identify an expected range of $\delta^{13}C_{shell}$ compositions (+2.5 to −2.8‰) for this latitude and geological time period.

Nine of the nineteen bivalves sampled produced several carbonate-$\delta^{13}C$ values significantly more negative than this expected range. Within this set of nine bivalve shells, the mean average shell $\delta^{13}C$ ranges from −23.8 to −0.5‰. Large seasonal cycles in carbon isotopes are an additional remarkable feature of this subset of shells. As a result of this cyclicity, the range of $\delta^{13}C$ data within a single shell is also high and varies between 3.3 and 23.5‰ with the most negative annual carbonate-$\delta^{13}C$ compositions occurring at the beginning of each growth phase and a gradual return to less negative values throughout each growing period.

The remaining ten shells sampled have much more typical $\delta^{13}C$ averages of between −2.3 and +4.2‰, and while seasonal variability is still present, the range of values present within the whole shell is much lower; between 0.4 and 5.8‰.

In these shells, there appears to be a slight anticorrelation between $\delta^{18}O$ and $\delta^{13}C$ (i.e. low $\delta^{13}C$ and high $\delta^{18}O$ at each growth line in comparison to the growing increment). This is typical of a marine productivity signal, where summer productivity causes water $\delta^{13}C$ to become more positive while warm water temperatures produce a more negative $\delta^{18}O$ signal (e.g. Toland et al. 2000; Carré et al. 2005; Schone et al. 2005). A few shells record some anomalously high $\delta^{13}C$ compositions, which may reflect periods of high biological productivity (Alcalá-Herrera et al. 1992; Gillikin et al. 2006) or local diagenetic effects due to cracks or microborings (e.g. Figures 2.15 and 2.16)

Given that preservation tests (Section 2.7) and $\delta^{18}O$ observations show that post-depositional alteration is not a credible explanation for the seasonal $\delta^{13}C$ variability, we need to consider alternate hypotheses for their origin. Most shell carbonate-carbon is derived from bottom water DIC but some metabolic carbon can be incorporated from the organism's POC food source. The isotopic mass balance used earlier to distinguish between expected and abnormal shell $\delta^{13}C$ compositions used an accepted typical value of metabolic carbon contribution, although repeating the calculation using the most extreme metabolic fractionation factor reported in modern bivalves (37%, Gillikin et al. 2007) still only accounts for $\delta^{13}C$ more positive than −10.4‰ by incorporation of metabolic carbon alone. Six of the bivalve shells we report gave at least two $\delta^{13}C$ compositions too negative to have been produced by even this exceptional incorporation of metabolic carbon, and the most negative $\delta^{13}C$ compositions we report are unable to be attained by incorporation of POC with $\delta^{13}C$ in the range we observe in the sediments. Instead, we suggest that the most likely source of the ^{13}C-depleted carbon in the affected bivalve shells is methane-derived carbon, since methane can provide a much more negative range of $\delta^{13}C$ signatures than photosynthetic-derived POC (Whiticar 1999).

The distinct stratigraphic intervals characterized by bivalves with extremely negative shell-$\delta^{13}C$ occur close to, or overlap occurrences of putatively chemosymbiotic bivalves (Figure 6.4, Little et al. 2015). This provides further support for the idea that the $\delta^{13}C$ signals in shells are indicative of an enhanced abundance of shallow sedimentary methane.

Observations of bulk sedimentary TOC, organic-$\delta^{13}C$, and weight percent carbonate from the López de Bertodano formation (Figure 6.4) reveal no corresponding negative carbon isotope excursions concurrent with the episodes

of extreme carbonate-$\delta^{13}C$ behaviour. This suggests that the bivalves are recording a signal localized in bottom-water DIC without propagation into the upper water column.

Shell $\delta^{13}C$ values of the magnitude we observe have not been recorded in any modern heterotrophic bivalves. Even chemosymbiotic bivalves from modern and ancient methane seep sites show little ^{13}C depletion in their shell material (Kauffman et al. 1996; Hein et al. 2006; Lartaud et al. 2010). The most negative $\delta^{13}C$ signatures in seep bivalves appear in their soft tissues, suggesting that in modern seep environments the methane signal is typically incorporated from metabolic carbon rather than from methane-derived DIC (Paull et al. 1989; Fisher 1995). Comparison of $\delta^{18}O$ and $\delta^{13}C$ cross plots from a range of modern cold seep bivalves (Figure 6.5) also show differences in the behaviour recorded by many of Seymour Island's bivalves, suggesting a different environment and scheme for methane release.

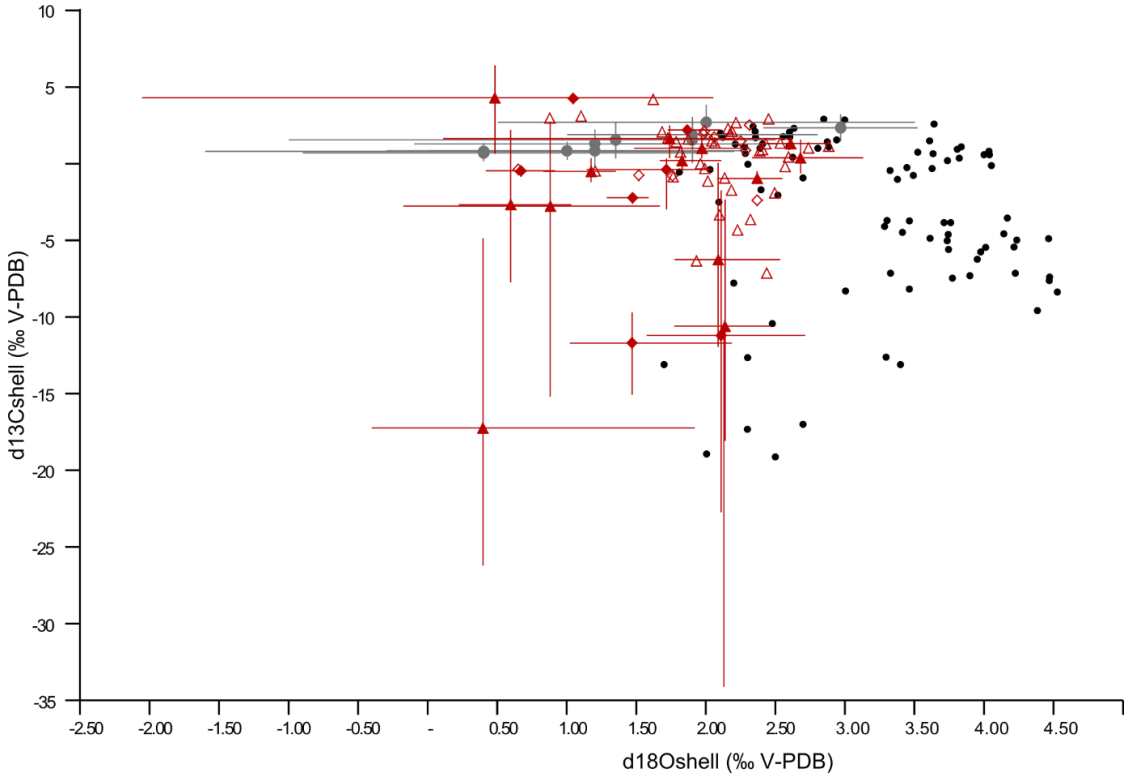

Figure 6.5: Bulk and average shell carbon-oxygen stable isotope cross-plot of δ^{18}O and δ^{13}C produced by this study (red) from *Lahillia* (triangles) and *Cucullaea* (diamonds). Horizontal bars with filled markers represent the mean and range of microsampled data points produced within one shell. Hollow markers represent bulk data from a single shell. This data is compared to modern bivalves from cold seeps (black circles, Lartaud et al. 2010) and modern marine heterotrophs (grey circles with range bars, Krantz et al. 1987; Toland et al. 2000). δ^{18}O data from this study have been shifted by +1.2‰ to account for the difference beteen modern seawater (0‰) and Cretaceous conditions (taken as –1.2‰). This shows that some of Seymour Island's bivalves display a similar isotopic pattern to normal marine bivalves, however the δ^{18}O suggests temperatures far warmer than most modern cold seep environments.

6.5.2 Extreme Seasonality in bottom water DIC-$\delta^{13}C$

One of the most remarkable features of the shell-carbonate data is the magnitude of the seasonal fluctuations in $\delta^{13}C$, which reflect a similar variability in the bottom water DIC. Seasonal $\delta^{13}C$ variability of DIC may be introduced by variation of the $\delta^{13}C$ of the methane itself, or by seasonal modulation of the rate of methane production or methane release. Winter $\delta^{13}C$ depletion of up to 10‰ has been observed in biogenic methane from marine sediments (Martens et al. 1986), but this is insufficient to explain the seasonal variations reported here, which can be as great as 23.5‰, even within the truncated period of spring-summer shell growth.

Since variability of methane $\delta^{13}C$ is unlikely to fully explain the observed signals, we consider mechanisms by which methane flux may be pulsed annually. Annual temperature changes are known to trigger seasonal methane release from methane hydrates in modern high latitude marine settings (Berndt et al. 2014). However, the sedimentology and faunal assemblage of the López de Bertodano Formation suggest a continental shelf setting with water depths of between 70−200m (Macellari 1988; Crame et al. 2004). Under these conditions, sea-bed hydrates would only have been stable at mean-annual temperatures lower than −2°C (Kvenvolden 1993). This is far lower than the existing temperature estimates from this region (Kemp et al. 2014) or the temperatures derived from the carbonate-$\delta^{18}O$ data reported here (19.0 to 5.1°C, see Chapter 4 and 5).

Recent work covering the same latest Cretaceous to Paleogene interval of the Lopez de Bertodano Formation (Petersen et al. 2016) has given evidence for cooler temperatures than produced by this study. Further one-dimensional sedimentary geotherm modelling (Appendix C) was carried out to determine whether the lower temperature estimates produced by the clumped isotope proxy would have been sufficient to allow sedimentary hydrate formation. The results of this investigation (Appendix C) show that even at the lowest temperatures recorded by Lahillia and Cucullaea of −0.2°C no hydrate formation could be replicated at depths which could realistically be affected by seasonal variations in temperature and pressure. From this we can conclude that hydrates were not likely to have been involved in the seasonality of the methane signal.

In addition, the stratigraphic occurrences of the putatively chemosymbiotic fauna (Figure 6.4) occur in multiple section lines spaced between 2-6 km apart. Specimens displaying the unusually negative carbon isotopic compositions and large seasonal variability are also sourced from both sections. The spatial distribution of these methane-related signals across several kilometres of the shelf environment also favors a mechanism generated by a wider change in sediment biogeochemistry rather than a localized occurrence of focused gas seepage. We conclude that the bivalve shells are most likely recording a direct signal of enhanced springtime methane input to bottom-water DIC directly from the sediment.

This bottom-water DIC signal must be due to some combination of methane production or release and eventual oxidation to DIC, but the seasonality is likely to have been driven by factors other than temperature, as there is no observable correlation between temperature and these signals (Figure 6.5). Modern areas of prolific seasonal methane production and release tend to occur in shallow waters such as swamps and marginal marine sites with extremely high organic carbon sedimentation, many of which also have sulfate concentrations lower than marine environments (Crill & Martens 1983; Van der Nat & Middelburg 2000; Zhang et al. 2008). However, to find evidence for seasonal methane release in a high-biodiversity fully marine environment with relatively low sedimentary TOC is extremely unusual.

Annually variable marine methane production could be controlled by organic matter supply or temperature variation; high latitude vegetated continents with temperate summer climates are likely to have experienced a spring pulse of runoff into coastal waters prompting an initial spring bloom and subsequent increase in organic matter delivery to the sediment. Whether these or the associated temperature changes could propagate into the sediment sufficiently quickly to produce an effect on methane production is debatable. The ability for such a signal to be transported fast enough into sediment without being smeared out requires consideration. The presence of anticorrelated seasonal $\delta^{18}O$ and $\delta^{13}C$ patterns in some specimens that do not show methane signals (Figures 6.1 to 6.3) could be the result of a marine productivity signal, which does indicate that seasonal changes in productivity are able to propagate to bottom-water depths. This could be investigated further using trace elemental analysis such as Ba/Ca or Mo/Ca, which have been used as indicators of palaeoproductivity in bivalve shell material (e.g. Gillikin et al. 2008; ThÉbault et al. 2009; Barats et al. 2010; Goodwin et al. 2013).

An alternative to a seasonal control on the production of marine methane would be a seasonal modulation of its release and oxidation by some physical disturbance, perhaps by changing storm frequency. Whilst it is unfortunately not possible to distinguish between these mechanisms with the available data, a low sulfate ocean and shallowing of the methanogenic zone would make all mechanisms more conceivable by bringing methanogenesis and its products closer to the influence of processes operating at the sediment-water interface.

6.5.3 Contribution of methane to bottom water DIC

Extending the mass balance approach introduced earlier allows us to produce an estimate of the amount of methane-derived carbon required to produce shell carbonate signals as depleted as we observe here. A similar mass balance equation (below) was used to determine the amount of methane derived DIC required to produce the bottom-water DIC signal we infer from our $\delta^{13}C_{shell}$ data. Using typical $\delta^{13}C$ for biogenic methane of −50 to −110‰ (Whiticar 1999), these calculations suggest that between 30−85% methane derived DIC is required to account for the most extreme negative shell values. Further details and results tables for all calculations are available in the supplementary material (Tables S1-S3).

$$\delta^{13}C_{\text{bottom water DIC}} = F\ \delta^{13}C_{\text{methane-derived DIC}} + (1\text{-}F)\delta^{13}C_{\text{oceanic DIC}}$$

The strength of the isotopic signals is consistent with our original hypothesis that the low-sulfate conditions of the Cretaceous-Paleocene allowed for a greatly increased flux of methane-derived DIC to bottom-waters. A conceptual model of the normal modern and hypothetical low-sulfate conditions is proposed in Figure 6.6. The inferred isotopically depleted carbon in bottom-water DIC recorded by the bivalve shells is likely to result from some combination of enhanced methane production or release, and its oxidation to bottom-water DIC, but it would be challenging to decouple these effects.

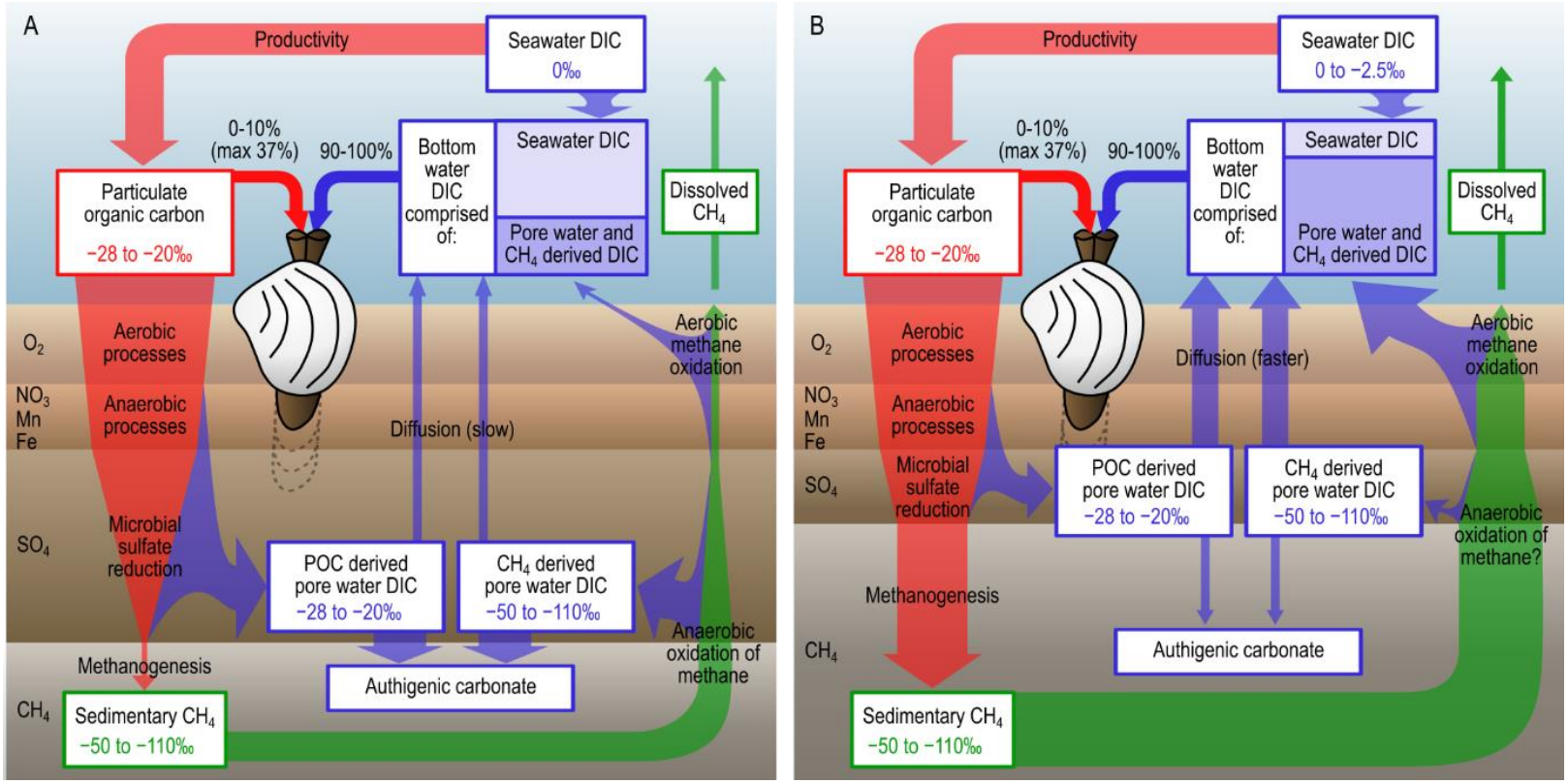

Figure 6.6. Conceptual model of sedimentary carbon cycle under high and low sulfate conditions. Showing fluxes of POC (red), DIC (blue) and methane (green) under (A) modern high sulfate conditions (B) Cretaceous lower sulfate conditions. Thickness of arrows represents relative strength of flux to each reservoir (not to scale). Depth scales are arbitrary; bottom-water reservoir refers to the benthic boundary layer sampled by bivalves and is likely to be only 5-10cm in depth. The depth to the sulfate reduction zone is variable in modern marine sediments depending on factors such as porewater flow and bioturbation. The proportion of pore water DIC that diffuses into bottom water versus burial as authigenic carbonate is unknown, but likely to relate to depth of DIC production, and pore fluid flux from the sediment to bottom water, thus is likely to be faster in low sulfate systems. No significant accumulations of authigenic carbonate have been found at horizons where we see evidence for increased methane flux to bottom-water DIC

In the modern ocean the vast majority of methane produced in sediment is oxidized anaerobically by sulfate (sulfate driven AOM, Reeburgh 2007). Although we calculate a large contribution of oxidised methane to bottom-water DIC, it would be challenging to determine the proportion of this methane-derived DIC produced by AOM versus aerobic oxidation of methane. It has also recently been shown that AOM can be facilitated by other electron acceptors such as iron (e.g. Scheller et al, 2011; Ettwig et al, 2016) further complicating the issue. We can reason that AOM yields only small amounts of energy when compared to bacterial processes fuelled by other electron acceptors (Dale et al. 2006), and in a lower sulfate ocean the shallowing of methane production will bring reactive sedimentary organic matter into competition with methane as a substrate, making it likely that the AOM community would be become outcompeted or marginalized. Alternatively, we could argue that this shallowing of production will bring methane into contact with a greater supply of reactive iron oxides making iron-driven AOM more likely in a low sulfate ocean. The lack of significant authigenic carbonate throughout the López de Bertodano formation perhaps supports a reduced or minor role for either variety of AOM in total methane oxidation since AOM promotes authigenic carbonate precipitation whilst aerobic oxidation does not (Reeburgh 2007). If most of the oxidation is being driven by oxygen, then the large proportion of methane derived DIC we calculate has significant implications for the bottom water oxygen budget, and may indicate that low sulfate conditions indirectly provide a substantial driver for bottom water de-oxygenation. Clearly the continued presence of a diverse benthic fauna throughout the Lopez de Bertodano Formation limits the significance of this process in our study section over long time scales, but is consistent with the presence of indications of transient sedimentary anoxia from geochemical proxies (Witts et al. 2016; Schoepfer et al. 2017).

The episodic nature of seasonal methane release throughout the stratigraphic section is difficult to explain, as an increased methane flux due to a low sulfate biogeochemical regime might be expected to operate throughout the whole mid-Cretaceous to Eocene low-sulfate interval. It is possible that the onset of increased methane flux to DIC may have been influenced by a period of local climate warming observed through the very latest Maastrichtian of this section (Tobin et al. 2012; Bowman et al. 2013; Kemp et al. 2014; Petersen et al. 2016). Periods of elevated sedimentation rate could also increase pore fluid flux; recent studies of modern passive margins (Prouty et al. 2016) suggest that high sedimentation rates, such as those present in the Cretaceous-Paleocene James Ross Basin (up to 0.1–0.2 mm/yr), may enhance pore space compaction and

allow more methane or methane derived DIC to be expelled from sediments. It is also possible that the system in this location is sensitive enough that small changes in the regional sulfate concentration of the ocean may have been enough to drive the change in regime seen here. The development of regional differences in sulfate sulfur isotope composition, with implied spatial differences in sulfate concentration have been indicated for time intervals in the Cretaceous (Owens et al. 2013) and early Jurassic (Newton et al. 2011).

Given the prevalence of low sulfate conditions through the Phanerozoic, the question arises as to why similar extreme shell carbon values have not been documented in previous studies. It is likely that there will have been a tendency to discount unusual isotopic signals from single analyses of bulk shell material as the result of poor preservation, preparation or a productivity signal (Lartaud et al. 2010; Tobin & Ward 2015), especially if, as is seen here, the signals are sporadic in nature and only present in a subset of shells analyzed. Indeed, similarly negative $\delta^{13}C$ data have been reported from the bulk shell carbonate of a number of ammonites, gastropods, and calcitic and aragonitic bivalves from Seymour Island and dismissed as sample preparation error (Tobin & Ward 2015). Our method of micro-analysis lends confidence to the primary nature of the signals and allows the repetitive seasonal patterns within shells to be identified, discriminating between our proposed mechanism and others involving hydrate dissociation. This approach is rarely used for fossil shell material, but may be required in order to detect the extreme seasonal signals which we have used in our calculations to provide diagnostic indicators of methanogenic input to bottom water DIC.

6.6 Conclusions

These isotopic records from latest Cretaceous–early Paleocene bivalves from Antarctica represent the first time that negative carbon isotope signals of this nature have been documented in the fossil record and resolved on a sub-annual scale, revealing both their seasonal and stratigraphically-pulsed characteristics. The shell carbonate-carbon signals are likely to be reflective of localized DIC composition, with extreme springtime carbon isotope depletion suggesting a very large contribution to bottom-water DIC by methane oxidation products. Bulk sediment organic-carbon isotopes indicate that the influence of this process did not extend to the upper water column. The presence of pronounced annual

cyclicity suggests intervals of strong environmental control on the flux of methane derived carbon to the bottom-water DIC pool. A methane hydrate mechanism appears unlikely at the temperatures and water depths indicated for this site, so the signal must be due to some combination of enhanced methane production or release and its subsequent oxidation, facilitated by the low sulfate concentrations of the Cretaceous-Paleocene ocean and the shallowing of the methanogenic zone. The lack of substantial authigenic carbonate supports an aerobic oxidation pathway for the methane and if correct this has significant implications for bottom water oxygen budgets. If low sulfate is indeed the driver for these unusual isotopic records then similar seasonal signals in shell carbonate are likely to be present in other low sulfate intervals of the Phanerozoic, and signify a fundamental difference in marine sedimentary carbon cycling.

6.7 References

Adams, D. D., Hurtgen, M. T. and Sageman, B. B. (2010) 'Volcanic triggering of a biogeochemical cascade during Oceanic Anoxic Event 2', Nature Geoscience. Nature Publishing Group, 3(3), 1–4.

Alcalaȷ-Herrera, J. A., Grossman, E. L. and Gartner, S. (1992) 'Nannofossil diversity and equitability and fine-fraction δ13C across the Cretaceous/Tertiary boundary at Walvis Ridge Leg 74, South Atlantic', Marine Micropaleontology, 20(1), 77–88.

Barats, A., Amouroux, D., Pécheyran, C., Chauvaud, L., Thébault, J. and Donard, O. F. X. (2010) 'Spring molybdenum enrichment in scallop shells: a potential tracer of diatom productivity in temperate coastal environments (Brittany, NW France)', Biogeosciences, 7(1), 233–245.

Berndt, C., Feseker, T., Treude, T., Krastel, S., Liebetrau, V., Niemann, H., Bertics, V. J., Dumke, I., et al. (2014) 'Temporal constraints on hydrate-controlled methane seepage off Svalbard.', Science, 343(6168), 284–7.

Berner, R. A. (2004) 'A model for calcium, magnesium and sulfate in seawater over Phanerozoic time', American Journal of Science, 304(5), 438–453.

Bowman, V. C., Francis, J. E. and Riding, J. B. (2013) 'Late Cretaceous winter sea ice in Antarctica?', Geology, 41(12), 1227–1230.

Carré, M., Bentaleb, I., Blamart, D., Ogle, N., Cardenas, F., Zevallos, S., Kalin,

R. M., Ortlieb, L., et al. (2005) 'Stable isotopes and sclerochronology of the bivalve Mesodesma donacium: Potential application to Peruvian paleoceanographic reconstructions', Palaeogeography, Palaeoclimatology, Palaeoecology, 228(1–2), 4–25.

Crame, J. A., Francis, J. E., Cantrill, D. J. and Pirrie, D. (2004) 'Maastrichtian stratigraphy of Antarctica', Cretaceous Research, 25(3), 411–423.

Crill, P. M. and Martens, C. S. (1983) 'Spatial and temporal fluctuations anoxic coastal marine sediments of methane production in anoxic coastal marine sediments', Limnology and Oceanography, 28(6), 1117–1130.

Dale, A. W., Regnier, P. and Van Cappellen, P. (2006) 'Bioenergetic controls on anaerobic oxidation of methane (AOM) in coastal marine sediments: A theoretical analysis', American Journal of Science, 246–294.

Demicco, R. V., Lowenstein, T. K., Hardie, L. A. and Spencer, R. J. (2005) 'Model of seawater composition for the Phanerozoic', Geology, 33(11), 877–880.

Dinarès-Turell, J., Westerhold, T., Pujalte, V., Röhl, U. and Kroon, D. (2014) 'Astronomical calibration of the Danian stage (Early Paleocene) revisited: Settling chronologies of sedimentary records across the Atlantic and Pacific Oceans', Earth and Planetary Science Letters, 405, 119–131.

Fisher, C. (1995) 'Toward an appreciation of hydrothermal-vent animals: their environment, physiological ecology, and tissue stable isotope values.', in Humphris, S. E., Zierenberg, R. A., Mullineaux, L. S., and Thomson, R. E. (eds) Seafloor Hydrothermal Systems: Physical, Chemical, Biological, and Geological Interactions Geophysical Monograph Series. Washington, D C: AGU, 297–316.

Gillikin, D. P., Lorrain, A., Bouillon, S., Willenz, P. and Dehairs, F. (2006) 'Stable carbon isotopic composition of Mytilus edulis shells: relation to metabolism, salinity, δ13CDIC and phytoplankton', Organic Geochemistry, 37(10), 1371–1382.

Gillikin, D. P., Lorrain, A., Meng, L. and Dehairs, F. (2007) 'A large metabolic carbon contribution to the δ13C record in marine aragonitic bivalve shells', Geochimica et Cosmochimica Acta, 71(12), 2936–2946.

Gillikin, D. P., Lorrain, A., Paulet, Y.-M., André, L. and Dehairs, F. (2008) 'Synchronous barium peaks in high-resolution profiles of calcite and aragonite marine bivalve shells', Geo-Marine Letters. Springer, 28(5), 351–

358.

Goodwin, D. H., Gillikin, D. P. and Roopnarine, P. D. (2013) 'Preliminary evaluation of potential stable isotope and trace element productivity proxies in the oyster Crassostrea gigas', Palaeogeography, Palaeoclimatology, Palaeoecology, 373, 88–97.

Hein, J. R., Normark, W. R., McIntyre, B. R., Lorenson, T. D. and Powell, C. L. (2006) 'Methanogenic calcite, 13C-depleted bivalve shells, and gas hydrate from a mud volcano offshore southern California', Geology, 34(2), 109.

Holt, N. M., García-Veigas, J., Lowenstein, T. K., Giles, P. S. and Williams-Stroud, S. (2014) 'The major-ion composition of Carboniferous seawater', Geochimica et Cosmochimica Acta, 134, 317–334.

Horita, J., Zimmermann, H. and Holland, H. D. (2002) 'Chemical evolution of seawater during the Phanerozoic', Geochimica et Cosmochimica Acta, 66(21), 3733–3756.

Jørgensen, B. B. and Kasten, S. (2006) 'Sulfur Cycling and Methane Oxidation', in Schulz, H. D. and Zabel, M. (eds) Marine Geochemistry. Berlin/Heidelberg: Springer-Verlag, 271–309.

Kauffman, E. G., Arthur, M. A., Howe, B. and Scholle, P. A. (1996) 'Widespread venting of methane-rich fluids in Late Cretaceous (Campanian) submarine springs (Tepee Buttes), Western Interior seaway, U.S.A.', Geology, 24(9), 799–802.

Kemp, D. B., Robinson, S. A., Crame, J.A., Francis, J. E., Ineson, J., Whittle, R. J., Bowman, V. and O'Brien, C. (2014) 'A cool temperate climate on the Antarctic Peninsula through the latest Cretaceous to early Paleogene', Geology, 42(7), 583–586.

Klein, R. T., Lohmann, K. C. and Thayer, C. W. (1996) 'SrCa and 13C12C ratios in skeletal calcite of Mytilus trossulus: Covariation with metabolic rate, salinity, and carbon isotopic composition of seawater', Geochimica et Cosmochimica Acta, 60(21), 4207–4221.

Krantz, D. E., Williams, D. F. and Jones, D. S. (1987) 'Ecological and paleoenvironmental information using stable isotope profiles from living and fossil molluscs', Palaeogeography, Palaeoclimatology, Palaeoecology, 58(3), 249–266.

Kvenvolden, K. A. (1993) 'Gas hydrates—geological perspective and global

change', Reviews of Geophysics, 31(2), 173.

Lartaud, F., de Rafelis, M., Oliver, G., Krylova, E., Dyment, J., Ildefonse, B., Thibaud, R., Gente, P., et al. (2010) 'Fossil clams from a serpentinite-hosted sedimented vent field near the active smoker complex Rainbow, MAR, 36fl13′N: Insight into the biogeography of vent fauna', Geochemistry, Geophysics, Geosystems, 11(8).

Little, C. T. S., Birgel, D., Boyce, A. J., Crame, J. A., Francis, J. E., Kiel, S., Peckmann, J., Pirrie, D., et al. (2015) 'Late Cretaceous (Maastrichtian) shallow water hydrocarbon seeps from Snow Hill and Seymour Islands, James Ross Basin, Antarctica', Palaeogeography, Palaeoclimatology, Palaeoecology, 418, 213–228.

Lowenstein, T. K., Hardie, L. A., Timofeeff, M. N. and Demicco, R. V. (2003) 'Secular variation in seawater chemistry and the origin of calcium chloride basinal brines', Geology, 31(10), 857–860.

Macellari, C. E. (1988) 'Stratigraphy, sedimentology, and paleoecology of Upper Cretaceous / Paleocene shelf-deltaic sediments of Seymour Island', Geological Society of America Memoirs, 169, 25–54.

Martens, C., Blair, N., Green, C. and Des Marais, D. (1986) 'Seasonal variations in the stable carbon isotopic signature of biogenic methane in a coastal sediment', Science, 233(4770), 1300–1303.

McConnaughey, T. A., Burdett, J., Whelan, J. F. and Paull, C. K. (1997) 'Carbon isotopes in biological carbonates: Respiration and photosynthesis', Geochimica et Cosmochimica Acta, 61(3), 611–622.

McConnaughey, T. a. and Gillikin, D. P. (2008) 'Carbon isotopes in mollusk shell carbonates', Geo-Marine Letters, 28(5–6), 287–299.

Mook, W. G. and Tan, F. C. (1991) 'Stable carbon isotopes in rivers and estuaries', in Biogeochemistry of major world rivers, 245–64.

Van der Nat, F.-J. and Middelburg, J. J. (2000) 'Methane emission from tidal freshwater marshes', Biogeochemistry. Kluwer Academic Publishers, 49(2), 103–121.

Newton, R. J., Reeves, E. P., Kafousia, N., Wignall, P. B., Bottrell, S. H. and Sha, J.-G. (2011) 'Low marine sulfate concentrations and the isolation of the European epicontinental sea during the Early Jurassic', Geology. Geological Society of America, 39(1), 7–10.

Owens, J. D., Gill, B. C., Jenkyns, H. C., Bates, S. M., Severmann, S., Kuypers,

M. M. M., Wood, R. G. and Lyons, T. W. (2013) 'Sulfur isotopes track the global extent and dynamics of euxinia during Cretaceous Oceanic Anoxic Event 2', 110(46).

Paull, C. K., Martens, C. S., Chanton, J. P., Neumann, A. C., Coston, J., Jull, A. J. T. and Toolin, L. J. (1989) 'Old carbon in living organisms and young CaC03 cements from abyssal brine seeps', Nature, 342(6246), 166–168.

Petersen, S. V., Dutton, A. and Lohmann, K. C. (2016) 'End-Cretaceous extinction in Antarctica linked to both Deccan volcanism and meteorite impact via climate change', Nature Communications. Nature Publishing Group, 7, 12079.

Poulain, C., Lorrain, a., Mas, R., Gillikin, D. P., Dehairs, F., Robert, R. and Paulet, Y.-M. (2010) 'Experimental shift of diet and DIC stable carbon isotopes: Influence on shell δ13C values in the Manila clam Ruditapes philippinarum', Chemical Geology. Elsevier B.V., 272(1–4), 75–82.

Prouty, N. G., Sahy, D., Ruppel, C. D., Roark, E. B., Condon, D., Brooke, S., Ross, S. W. and Demopoulos, A. W. J. (2016) 'Insights into methane dynamics from analysis of authigenic carbonates and chemosynthetic mussels at newly-discovered Atlantic Margin seeps', Earth and Planetary Science Letters. Elsevier B.V., 1, 1–13.

Reeburgh, W. S. (2007) 'Oceanic methane biogeochemistry.', Chemical reviews, 107(2), 486–513.

Schoepfer, S. D., Tobin, T. S., Witts, J. D. and Newton, R. J. (2017) 'Intermittent euxinia in the high-latitude James Ross Basin during the latest Cretaceous and earliest Paleocene', Palaeogeography, Palaeoclimatology, Palaeoecology. The Authors, 477, 40–54.

Schöne, B. R., Fiebig, J., Pfeiffer, M., Gleβ, R., Hickson, J., Johnson, A. L. A., Dreyer, W. and Oschmann, W. (2005) 'Climate records from a bivalved Methuselah (Arctica islandica, Mollusca; Iceland)', Palaeogeography, Palaeoclimatology, Palaeoecology. Elsevier Science Bv, 228(1–2), 130–148.

Schone, B. R., Houk, S. D., Freyre Castro, a. D., Fiebig, J., Oschmann, W., Kroncke, I., Dreyer, W. and Gosselck, F. (2005) 'Daily Growth Rates in Shells of Arctica islandica: Assessing Sub-seasonal Environmental Controls on a Long-lived Bivalve Mollusk', Palaios, 20(1), 78–92.

ThÉbault, J., Chauvaud, L., L'Helguen, S., Clavier, J., Barats, A., Jacquet, Sé., PÉcheyran, C. and Amouroux, D. (2009) 'Barium and molybdenum records

in bivalve shells: Geochemical proxies for phytoplankton dynamics in coastal environments?', Limnology and Oceanography, 54(3), 1002–1014.

Thibault, N., Husson, D., Harlou, R., Gardin, S., Galbrun, B., Huret, E. and Minoletti, F. (2012) 'Astronomical calibration of upper Campanian–Maastrichtian carbon isotope events and calcareous plankton biostratigraphy in the Indian Ocean (ODP Hole 762C): Implication for the age of the Campanian–Maastrichtian boundary', Palaeogeography, Palaeoclimatology, Palaeoecology, 337–338, 52–71.

Timofeeff, M. N., Lowenstein, T. K., da Silva, M. A. M. and Harris, N. B. (2006) 'Secular variation in the major-ion chemistry of seawater: Evidence from fluid inclusions in Cretaceous halites', Geochimica et Cosmochimica Acta, 70(8), 1977–1994.

Tobin, T. S. and Ward, P. D. (2015) 'Carbon isotope (δ13C) differences between Late Cretaceous ammonites and benthic mollusks from Antarctica', Palaeogeography, Palaeoclimatology, Palaeoecology. Elsevier, 428, 50–57.

Tobin, T. S., Ward, P. D., Steig, E. J., Olivero, E. B., Hilburn, I. A., Mitchell, R. N., Diamond, M. R., Raub, T. D., et al. (2012) 'Extinction patterns, δ18 O trends, and magnetostratigraphy from a southern high-latitude Cretaceous–Paleogene section: Links with Deccan volcanism', Palaeogeography, Palaeoclimatology, Palaeoecology, 350, 180–188.

Toland, H., Perkins, B., Pearce, N., Keenan, F. and Leng, M. J. (2000) 'A study of sclerochronology by laser ablation ICP-MS', Journal of Analytical Atomic Spectrometry, 15(9), 1143–1148.

Voigt, S., Gale, A. S., Jung, C. and Jenkyns, H. C. (2012) 'Global correlation of Upper Campanian – Maastrichtian successions using carbon-isotope stratigraphy: development of a new Maastrichtian timescale', Newsletters on Stratigraphy, 45(1), 25–53.

Whiticar, M. J. (1999) 'Carbon and hydrogen isotope systematics of bacterial formation and oxidation of methane', Chemical Geology, 161(1–3), 291–314.

Witts, J. D., Whittle, R. J., Wignall, P. B., Crame, J. A., Francis, J. E., Newton, R. J. and Bowman, V. C. (2016) 'Macrofossil evidence for a rapid and severe Cretaceous–Paleogene mass extinction in Antarctica', Nature Communications. Nature Publishing Group, 7, 11738.

Wortmann, U. G. and Chernyavsky, B. M. (2007) 'Effect of evaporite deposition

on Early Cretaceous carbon and sulphur cycling', 446(April), 17–19.

Wortmann, U. G. and Paytan, A. (2012) 'Rapid Variability of Seawater Chemistry Over the Past 130 Million Years', Science, 337(6092), 334–336.

Zhang, G., Zhang, J., Liu, S., Ren, J., Xu, J. and Zhang, F. (2008) 'Methane in the Changjiang (Yangtze River) Estuary and its adjacent marine area: riverine input, sediment release and atmospheric fluxes', Biogeochemistry, 91(1), 71–84.

Zinsmeister, W. J. (1998) 'Discovery of fish mortality horizon at the KT boundary on Seymour Island: re-evaluation of events at the end of the Cretaceous', Journal of Paleontology.

CHAPTER 7

DISCUSSION AND CONCLUSIONS

This chapter will bring together and discuss the main findings of each of the preceding data-focused chapters and integrate the data and conclusions with existing evidence for environmental change over the K-Pg mass extinction interval.

The overall aims of this thesis can be expressed in terms of the following research questions:

- What were the climate conditions of the marine environment in the James Ross Basin during the late Maastrichtian and early Paleogene; how seasonal and climatologically variable was it and what were the likely drivers of variability? What is the potential for seasonal bias in temperature proxies at high latitude?
- Can high resolution stable carbon and oxygen isotopic data be used to detect changes in biogeochemical cycling throughout this time period?
- How do global patterns of seasonality from climate models and data throughout the Maastrichtian compare to the data from Seymour Island?
- How did infaunal bivalves respond to climate variability, seasonality and environmental changes in the lead up to and during the aftermath of the K-Pg mass extinction?

7.1 Climate and Palaeoenvironment of the James Ross Basin

7.1.1 Evidence for Seasonal Bias

The potential for seasonal bias in high latitude proxies for temperature has been long recognised (Goodwin et al. 2003; Herman & Spicer 2010). Data produced here in Chapters 4 and 5 show that the bivalve data does indeed show a warm temperature and warm season bias due to shell growth occurring mainly in spring and summer. Use of summer and winter temperatures derived from bivalve shells was considered to be more accurate than a mean annual temperature for comparison with model data.

7.1.1 Mean State Climate Conditions

Shell data (presented in Chapter 4 and 5) allowed estimates of climate conditions from $\delta^{18}O$ incorporating the potential for ranges of water $\delta^{18}O$ predicted from model simulations and clumped isotope data. A summary figure of these results through stratigraphy is presented below (Figure 7.1) with additional temperature proxy data from Seymour Island.

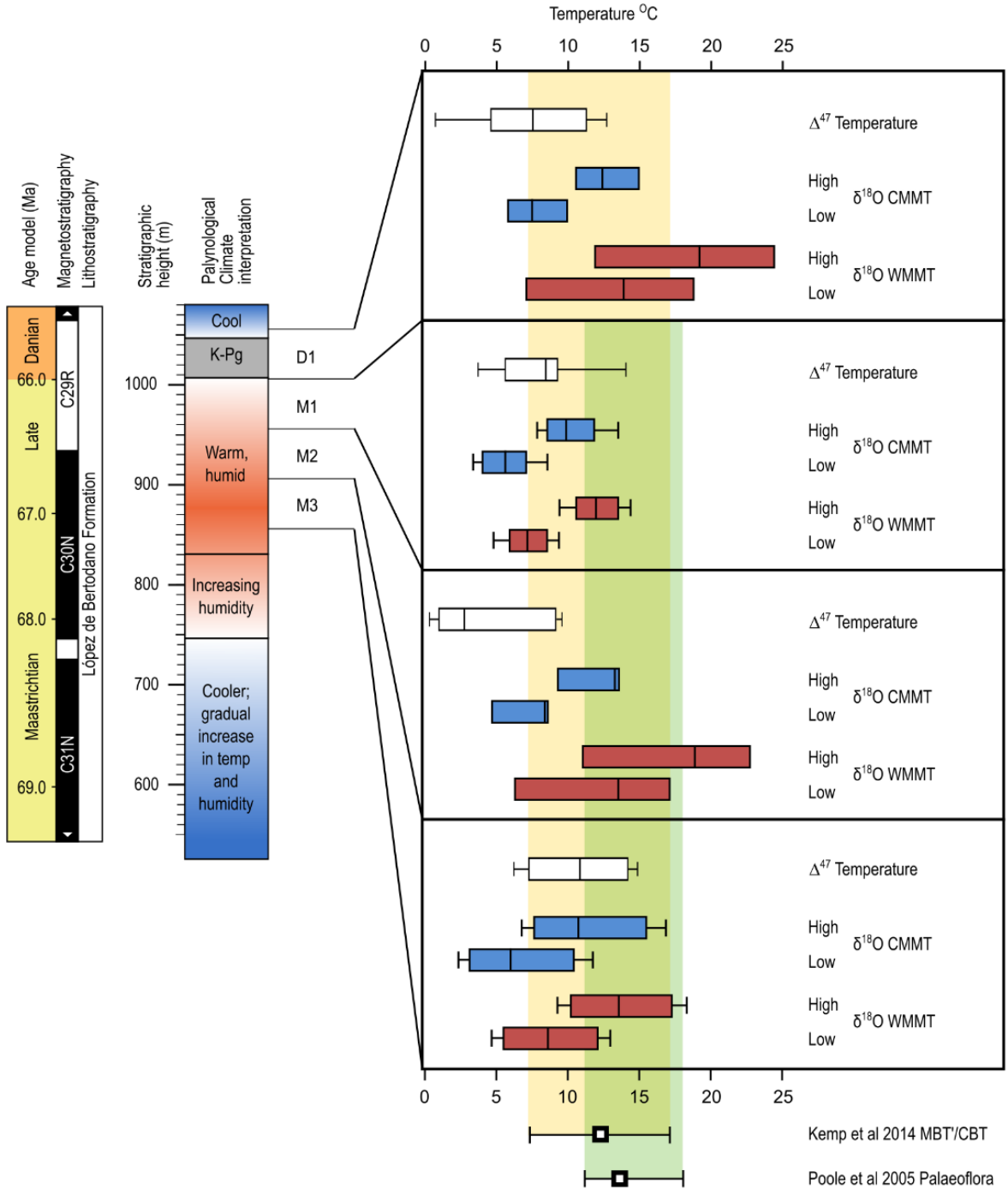

Figure 7.1: Palaeotemperatures in the latest Maastrichtian and early Paleocene recorded through multiple proxies. Box plots of temperature data produced from Δ47, and high and low estimate conversions of cool month mean temperature (CMMT) and warm month mean temperature (WMMT) from δ^{18}O separated into 50 m stratigraphic intervals (M3 to D1) compared to temperature estimates from MBT'/CBT in soil bacteria (yellow) and Palaeofloral (green) analysis. This figure shows that δ^{18}O-derived marine temperatures were within the range of 5 to 15℃ during the winter and may have reached as high as 18 to 25℃ during summers. This range has good agreement to broad continental temperatures from fossil plants and soil algae.

Belemnites collected from approximately 580m below the K-Pg boundary at the López de Bertodano belemnite horizon record rostrum growth at temperatures between 4 and 10°C and mean annual temperature ranges between 2 and 6°C (Dutton et al. 2007). This temperature growth range is slightly lower than bivalve $\delta^{18}O$ estimates from higher up in stratigraphy presented in this study but in line with some of the clumped isotope estimates (Larkin 2014; Petersen et al. 2016). However, belemnites live in deeper waters than bivalves, so tend to record a slightly different water temperature signal, around 1 to 2°C cooler than bivalves from the same location (Anderson et al. 1994). When this difference is accounted for, belemnite temperatures are very similar to those predicted by both stable and clumped isotopes, and as no belemnites have been found from the very latest Maastrichtian they cannot be used to look for evidence of freshwater input or cooler annual temperatures during this interval.

Palynological data provides an alternative source of climate information, and one that is not affected by marine $\delta^{18}O$. The palynological climate interpretation (Bowman et al. 2013, 2014) suggests warming through the latest Maastrichtian which is not convincingly found in either the $\delta^{18}O$ or $\Delta47$ temperature records. This may be due to the bivalves recording temperatures from more thermally insulated deeper water conditions than the dinoflagellates and pollen that the palynological temperature record is based on. The fall in temperatures following the K-Pg mass extinction is, however, found in the $\delta^{18}O$ and palynological interpretation, and to some extent in the $\Delta47$ record which supports the conclusion that climate cooling occurred just after the K-Pg boundary.

The palynological data, in particular the *Impletosphaeridium clavus* dinoflagellate record, have also been used as a proxy for the presence of sea ice as well as temperature records according to Bowman et al. (2012). These records suggest sea ice may have been present during the cooler periods of the late Maastrichtian, with coldest events recorded at around 650 and 740 m in the section. This is in contrast with the $\Delta47$ record, which indicates the lowest temperatures and most depleted freshwater input to seawater occurred during the latest Maastrichtian, with warmer temperatures below the 900m level in stratigraphy.

In addition to these marine proxy data sources, two terrestrial climate data sets have also been produced using sedimentary deposits from Seymour Island (Figure 7.1). Temperature estimates from palaeofloral analyses of plant material from

the Maastrichtian Lopez de Bertodano Formation suggest mean annual temperatures of 11.1 to 18.1℃ and cool month mean temperature (CMMT) of 8.2℃ and estimates of warm month mean temperature (WMMT) between 18.5 and 25℃ (Poole et al. 2005). The MBT'/CBT thermometer has also been used to reconstruct terrestrial mean annual temperatures using membrane lipids from soil bacteria and produces temperature estimates of 12℃, although the error bars are large with uncertainty of +/- 5℃ (Kemp et al. 2014).

These proxies both give estimate of terrestrial air temperatures and the averages are often comparable with shallow-water annual temperatures recorded by bivalves (e.g. Figure 4.1 and Keating-Bitonti et al. 2011). Modelled mean annual terrestrial temperatures are similar to mean annual marine temperatures (Figure 4.22), although the seasonal CMMT and WMMT are likely to be more extreme in terrestrial proxies than the marine record due to the higher thermal capacity of water compared to air.

Overall, the bivalve $\delta^{18}O$ and some $\Delta 47$ records, in addition to other proxy data suggest that Maastrichtian climates on Seymour Island were fairly stable with little variation at seafloor depths. There may have been some cooling and freshwater input during the very latest Maastrichtian interval, which is supported by the $\delta^{18}O$-enabled models, or it is possible that other effects (such as anticlumping, which will be discussed below) were influencing the equilibrium of the clumped isotope proxy record.

Data examined in Chapters 4 and 5 showed that temperatures from $\delta^{18}O$ are likely to have been affected by the $\delta^{18}O$ composition of the water. However, the clumped isotope proxy, which was hoped could be used to determine the seawater $\delta^{18}O$, appeared to produce inaccurate results at stratigraphic heights above 900m (Figure 7.2). Clumped isotope-derived temperatures above this height are consistently lower than both models and proxies suggest. This may be linked to the domination of marine dissolved inorganic carbon (DIC) by methane-derived carbon which begins at approximately 930m in stratigraphy; roughly the level of the C30N to C29R reversal and continues through into the Danian.

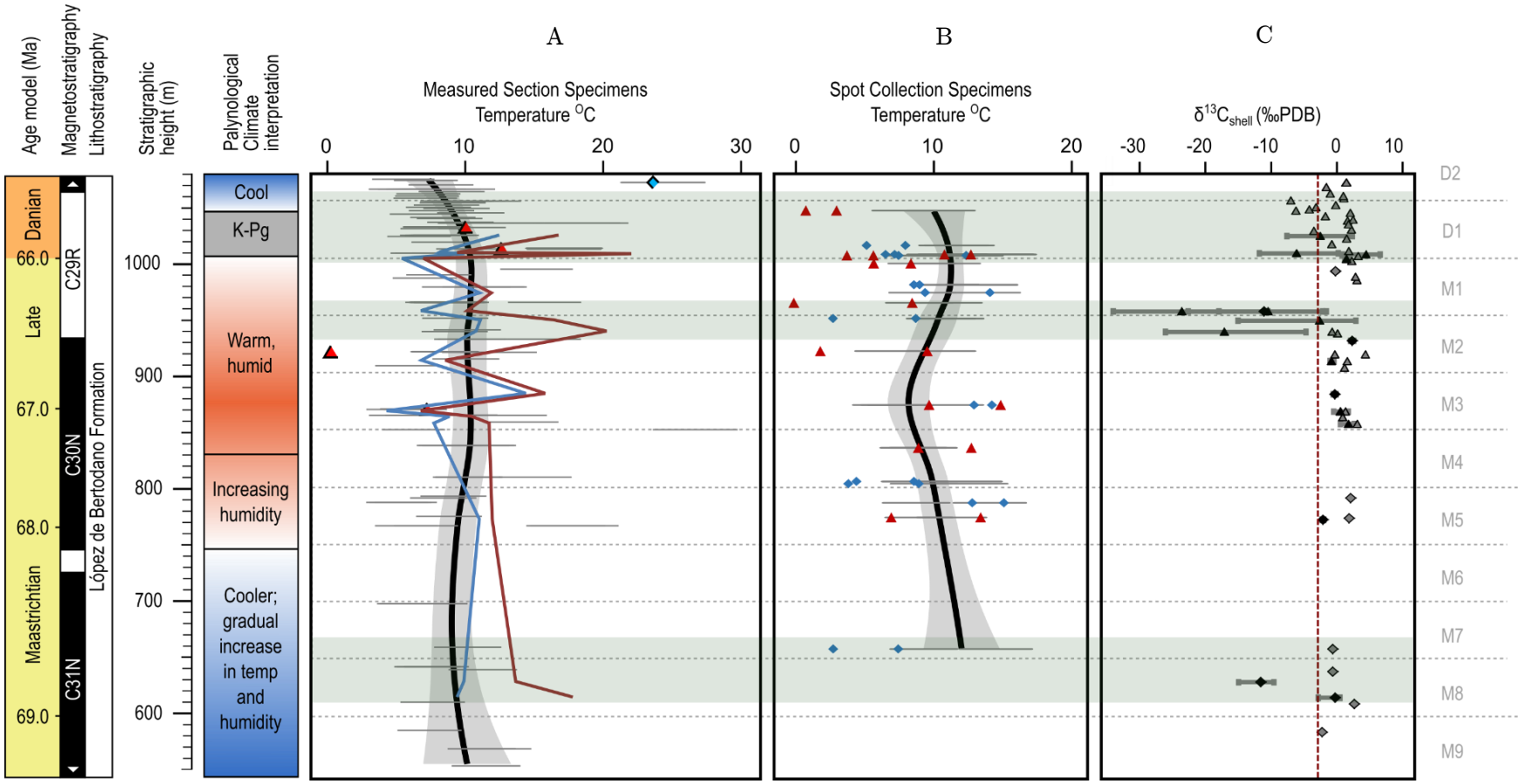

Figure 7.2: Stratigraphic summary of bivalve shell data from Seymour Island. Comparing trends in temperature from (A) correlated measured sections (this study; chapter 4 see discussion for Figures 4.22 and 5.3, with additional data from Tobin et al 2012 and Lakin 2013), (B) spot collected specimens (data from Petersen et al 2016, see discussion for Figure 4.22) and (C) $\delta^{13}C$ (this study; Chapter 6, see discussion for Figure 6.4). Green shading represents intervals with likely methane influence. Light grey dashed lines represent informal stratigraphic intervals with a spacing of approximately 50m. These are used for comparison with growth trends presented in Section 3.5.4.

Microbial methanogenesis has been found to cause anti-clumping in the methane products; i.e. the production of clumped isotope signatures corresponding to lower temperatures than the true formation temperature of the compound (Wang et al. 2015). Calculations in Chapter 6 show that during certain stratigraphic intervals, the majority of DIC incorporated into bivalve shells was derived from the products of methane oxidation. If correct, this implies that the bivalve shells will incorporate an anti-clumped signature from the methane-derived DIC, and therefore the temperatures and water $\delta^{18}O$ composition data produced using this $\Delta 47$ data will not reflect the growing conditions of the shell. Anti-clumping is a relatively novel observation, and the exact impact of processes such as methanogenesis on the clumped isotopic thermometer is not well defined, and due to the periodic nature of the methane-related signal throughout the section, it is possible that not all shells within the section will have been affected by methane.

The $\delta^{18}O$ data is not likely to have been affected by increased methane input to the water column, which affects DIC rather than carbonate ions. Therefore, the $\delta^{18}O$ data is likely to produce the best estimates of temperature, in spite of the large error bars due to uncertainty in water $\delta^{18}O$, which was determined to have a likely composition between −1 and −2‰, in contrast to the constant value of −1.2 ‰ assumed in ice free conditions (Zachos et al. 2001). This translates to a temperature error of approximately ±2°C and a potential seasonal error of up to 4°C, which will be discussed in Section 7.1.3.

To summarise the most likely mean state climate conditions experienced in the marine Seymour Island section, the late Maastrichtian pre-extinction period appears to have been stable and reasonably uniform throughout with mean annual temperatures of approximately 10°C ±5 recorded in bivalves from bulk d18O data. This temperature range is in agreement with Δ47-derived temperatures below the 900 m level of the section (M3-M5; Figure 7.2 C and M3; Figure 7.1) which also average around 10°C ±5. However, above this stratigraphic height, the effects of methane incorporation into shells can be seen in the $\delta^{13}C$ record (M2-D1; Figure 7.2 C) and the clumped isotopic record cannot be considered to be reliable. Terrestrial temperature unaffected by water $\delta^{18}O$ estimates are in agreement with the range of $\delta^{18}O$ and reliable clumped isotope data produced from marine bivalve shells (Figure 7.1). The synthesis of this proxy data concludes that there is no evidence for direct ice influence or water $\delta^{18}O$ compositions more negative than the −1 to −2‰ range considered here.

7.1.2 Evidence for Climate Variability and Seasonality:

Data presented in Chapter 5 show that microsampled $\delta^{18}O$ data can be used to produce estimates of annual seasonality between adjacent years of bivalve shell growth while the method used by Petersen et al 2016 of comparing samples from the umbo and back of the valve is more likely to produce estimates of longer timescale climate variability. Additional data from models presented in chapter 5 suggest that this climate variability is likely to be dependent on CO_2, with lower CO_2 atmospheres producing more inter-annual variability than higher CO_2 conditions. This has been discussed fully in Section 5.4.3.

A comparison of seasonal data from proxies through the section shows that there is little correlation between the amount of intra-annual seasonality (from consecutive-year $\delta^{18}O$ seasonality data presented in Chapter 5) and inter-annual variation (from comparison of umbonal and shell-back $\delta^{18}O$ and $\Delta47$ temperatures Petersen et al. 2016). The amount of variability in water $\delta^{18}O$ compositions predicted from clumped isotopic data (Figure 7.3 D) is also unreasonably large compared to model simulations which typically show between 0.1 and 0.2‰ in water column simulations (Figures 4.14 to 4.15). The variability and water $\delta^{18}O$ data is likely to have been affected by the cold-temperature bias in the clumped isotopic data discussed in Section 7.1.2.

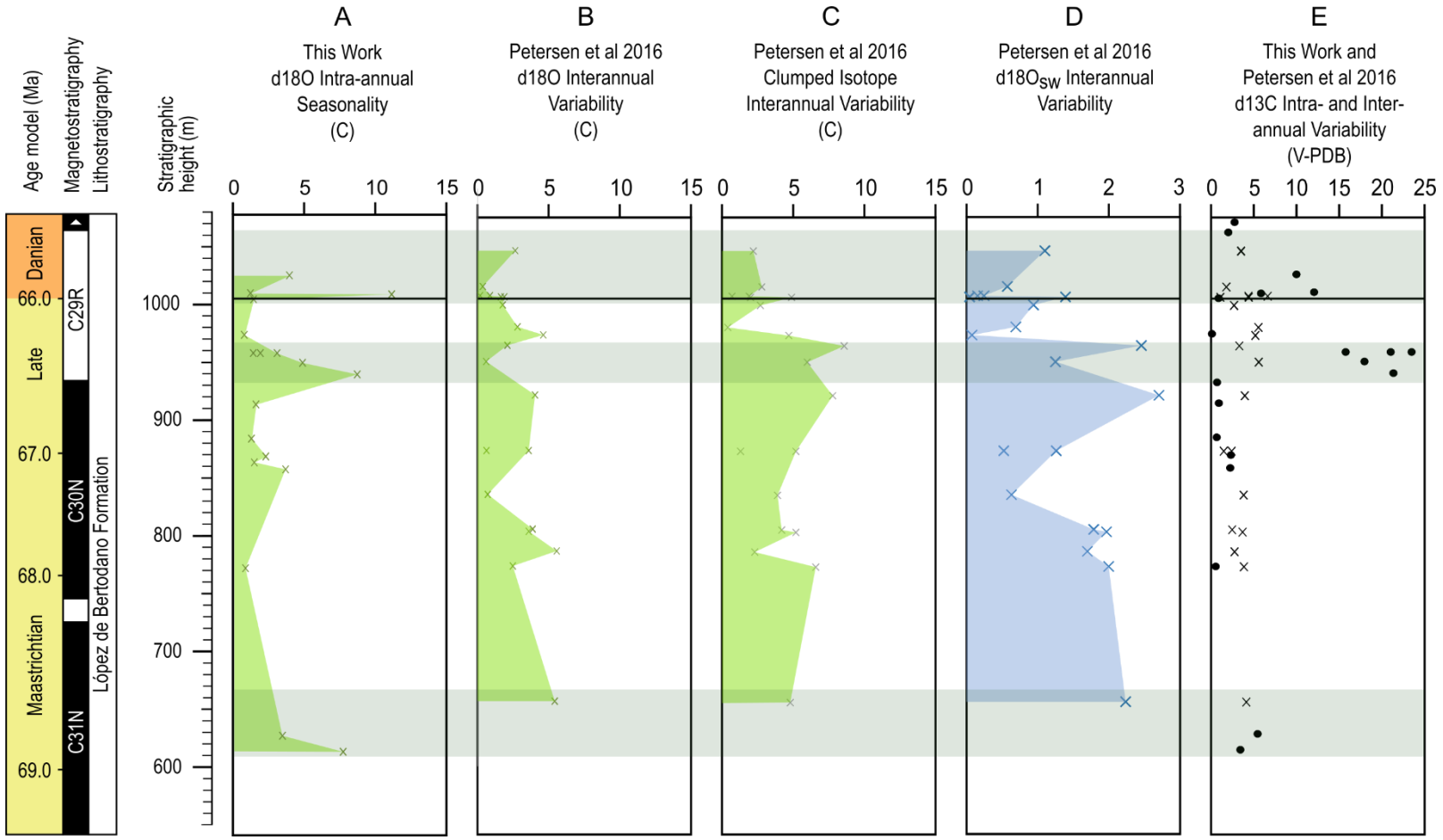

Figure 7.3: Summary figure of shell-derived seasonality and climate variability data (A-C), reported water δ^{18}O variability (D) and shell δ^{13}C variability (E) with dark green shading across all panels to indicate periods of potential methane influence. This shows the difference between intra-annual seasonality, which tends to be approximately 2 to 3℃ (A) and inter-annual variability of between 3 and 6℃ (B and C).

7.2 Biogeochemical Cycling

Use of bivalve shell data to give information about biogeochemical cycles was prompted by the growing number of studies suggesting that sulfate concentrations were much lower across the Cretaceous to Paleogene interval than in modern environments (Reeburgh 2007). Methane production and oxidation in particular are controlled by sulfate in modern oceans. Lower sulfate concentrations may have permitted a stronger and more active methane cycle, the products of which may be recorded in shells. The Seymour Island section is known to have some evidence for local methane release in the form of putatively chemosymbiotic thyasirid, lucinid and solemyid bivalves (Little et al. 2015) but the López de Bertodano formation lacks the abundant authigenic carbonate found in stratigraphically older early Maastrichtian units (Little et al. 2015).

The data presented in Chapter 6 showed that sub-annual resolution $\delta^{18}O$ and $\delta^{13}C$ data can be produced from *Lahillia* and *Cucullaea* to give information about biogeochemical cycling on seasonal and geological timescales. The $\delta^{13}C$ data were determined to most likely be reflective of localised DIC composition rather than caused by metabolic or vital effects in the bivalves, which allowed the data produced from their shells to be used as a proxy for water geochemistry.

Shell-derived $\delta^{13}C$ data showed evidence of periods in which methane oxidation products contributed large amounts of DIC to bottom-waters while bulk sediment organic-carbon isotopes indicated that the influence of this process did not extend to the upper water column. These isotopic records represent the first time that negative carbon isotope signals diagnostic of methane release have been documented in the fossil record and resolved sub-annually, revealing both their seasonal and stratigraphically-pulsed characteristics and the scale of their influence.

This approach would not have been possible without the use of the high resolution microsampling method. Taking only a bulk shell composition resulted in a $\delta^{13}C$ signal that was averaged across multiple years of shell growth producing values that could not be diagnostically linked to methane (Figure 6.4). Indeed, several existing bulk shell data sets from the Seymour Island section have reported negative but not diagnostically methane-influenced $\delta^{13}C$ data and accredited it to sample preparation error (e.g. Tobin & Ward 2015; Petersen et al. 2016).

The incorporation of temperature data from shell $\delta^{18}O$ discussed in Chapters 3 and 4 and the addition of sedimentary geothermal modelling results in Chapter 6 allowed a methane hydrate mechanism to be ruled out for the depths and pressures suggested for deposition in the James Ross Basin (Macellari 1988; Crame et al. 2004). A more likely mechanism to produce the seasonal methane-influenced signal in bivalve shells was a combination of enhanced methane production or release and its subsequent oxidation. This mechanism was likely to have been facilitated by the low sulfate concentrations of the Cretaceous-Paleocene ocean (Schoepfer et al. 2017). However, as methane signals are only present during certain stratigraphic horizons, it is possible that the sediment system in the Seymour Island region was sensitive enough that small changes in sulfate concentration (e.g. Newton et al. 2011; Owens et al. 2013), organic matter or sedimentary supply may have been enough to drive changes in sedimentary methane production or release.

The potential for large amounts of methane-derived DIC in bottom waters provides information about the geochemical processes in the James Ross Basin. This observation also reveals anticlumping introduced from methane-derived DIC used to mineralise shells as a potential mechanism for the large difference between the clumped isotopic record and other temperature proxies from the immediate pre- and post- extinction interval on Seymour Island, as discussed in Section 7.1.2.

The lack of substantial authigenic carbonate in the Lopez de Bertodano Formation supports an aerobic oxidation pathway for the methane which would have significant implications for bottom water oxygen budgets. Despite this assumption that the Lopez de Bertodano Formation was deposited in a fully oxygenated setting, studies of the size range of pyrite framboids provide some evidence for short-term redox fluctuations throughout the section (Witts et al. 2016; Schoepfer et al. 2017), which may be linked to the oxidation of methane.

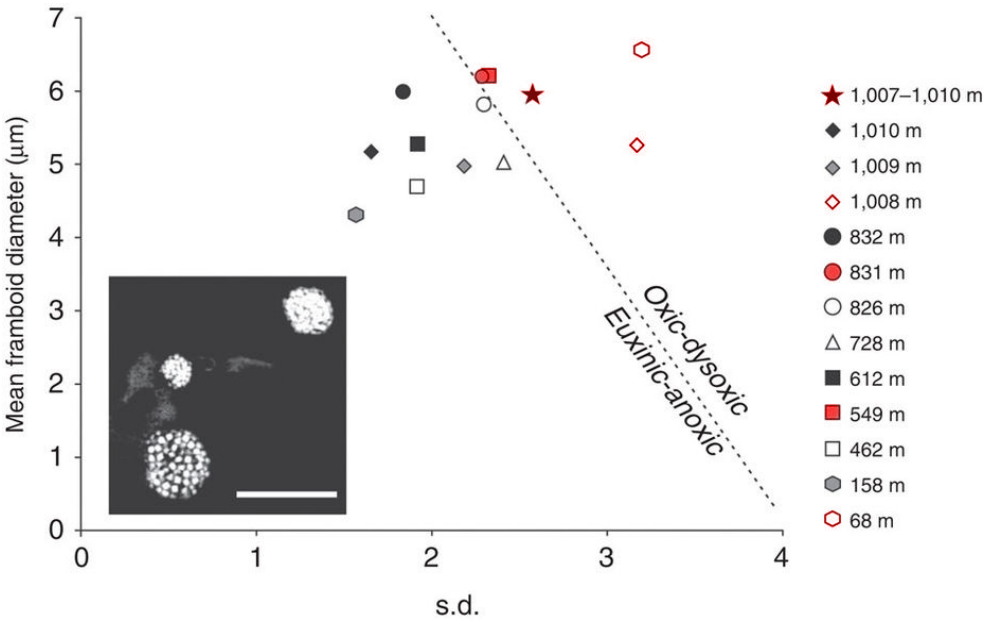

Figure 7.4: Framboid size distribution plot for samples from the Lopez de Bertodano Formation. Symbols represent samples from each stratigraphic height as shown in the column on the right. Dotted line separates redox conditions based on modern calibration (Wilkin et al. 1996). The position of samples on both sides of the line from intermittent stratigraphic heights indicates rapid fluctuations of redox conditions throughout the section rather than in one consistent part of the section. (Figure modified from Witts et al 2016).

Dysoxia in sediments is an environmental stressor for infaunal benthic organisms that are unable to migrate from the affected area. This may have controlled early Maastrichtian diversity, with evidence for recurrence throughout the section (Witts et al. 2016). In bivalves, dysoxia can also reduce individual feeding rates (Sagasti et al. 2001; Riedel et al. 2014) and antipredator responses (Wang et al. 2010, Riedel et al 2014), the potential effects of which will be discussed in Section 7.4.

Estimates of marine seawater sulfate concentrations are variable, but proxy data (e.g. Lowenstein et al. 2003; Timofeeff et al. 2006, Horita et al. 2002, Adams et al. 2010; Owens et al. 2013) and geochemical models (e.g. Berner 2004; Demicco et al. 2005; Wortmann & Paytan 2012) suggest sulfate concentrations were likely to have been approximately half of modern seawater (i.e. 28 mmol/kg), and potentially lower during the interval covered by the Seymour Island section (Figure 7.5). There are no indications that Seymour Island was a particularly

singular environment; sedimentation rates of 0.01 to 0.02cm/a (Tobin et al. 2012) are high compared to modern marine shelf deposits, but not unusually so (Ibach 1982). Therefore, if low sulfate is indeed the driver for these unusual isotopic records then similar seasonal signals in shell carbonate are likely to have been present during many other periods of the Phanerozoic with lower than modern marine sulfate (Figure 7.5).

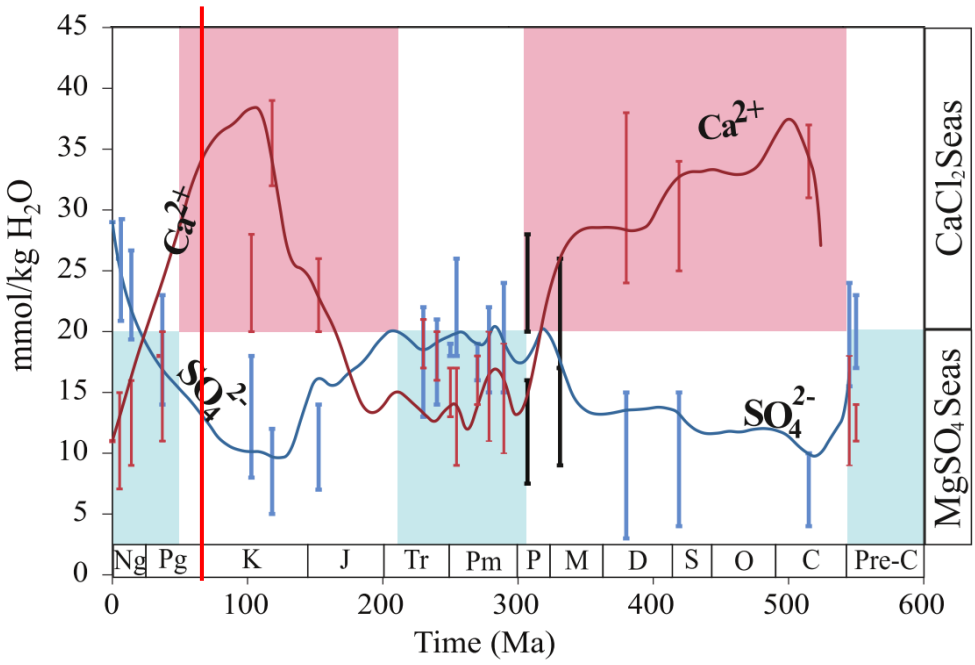

Figure 7.5: Phanerozoic variation in concentrations of marine Ca2+ and SO_4^{2+} estimated from fluid inclusions in marine halite (vertical bars) and geochemical models (curves), highlighting conditions around the time interval covered by this study (red vertical line). Many intervals of the Phanerozoic have SO_4^{2+} concentrations lower than during the K-Pg boundary interval and may show undiscovered evidence for similar biogeochemical processes. Figure from Holt et al. (2014).

7.3 Global Climate Context

As the use of models was important for the interpretation of the data in Chapters 4 and 5, it is useful to test the model performance, particularly with regards to seasonality of temperatures. The new model and proxy data produced in this study were tested by comparison with a database of global seasonal and mean

annual temperature proxies from the Maastrichtian which is available in Appendix D.

7.3.1 Records of Global Temperature and Seasonality

Seasonality is hard to quantify in deep time as it relies on the ability to discern sub-annual variations. Some proxy systems do provide estimates of seasonal (winter and summer) temperature range, such as leaf margin analysis (LMA) and climate leaf analysis multivariate program (CLAMP) (Wolfe 1993, 1995; Spicer et al. 2004; Royer 2012). Some sources provide; for example, warm month temperatures, such as paleosol carbonate nodules (Passey 2012) crocodilian and plant assemblage distributions (Greenwood & Wing 1995; Markwick 1998; Eldrett et al. 2009). These proxies tend to be limited to the terrestrial realm; in marine systems seasonal data can be obtained by high-resolution sampling across annual growth in marine organisms, such as the approach taken with bivalves in this study, or from the temperature range gathered from organisms that grow during a short window of time, such as fish tooth enamel, each of which grows over several weeks to months depending on species (Pucéat et al. 2007).

This study collates and expands upon a number of previous global databases (Goswami 2012; Upchurch et al. 2015) focused on quantitative indicators of Maastrichtian mean annual and seasonal temperatures from marine and terrestrial realms (Figure 7.6). Marine temperatures were based on sedimentary TEX 86 and $\delta^{18}O$ of well-preserved skeletal carbonate from molluscs, belemnites and brachiopods. A limited number of data points from foraminifera with very good preservation were included from data-sparse latitudes (Upchurch et al. 2015) but foraminiferal data were generally excluded due to issues with preservation (e.g. Bernard et al. 2017). Terrestrial seasonal temperatures were based on plant macrofossils, with additional mean annual temperature estimates from $\delta^{18}O$ of vertebrate tooth enamel and pedogenic carbonate. Palaeobotanical temperatures are based on multiple calibration techniques including LMA, digital leaf physiognomy and CLAMP.

Where appropriate, the temperature calibration was re-calculated to standardise all data sets and allow for more reliable comparisons between similar data. Aragonitic shell data was recalibrated to Grossman & Ku (1986), calcitic shell data was recalibrated to Kim & O'Neil (1997). Two calibrations exist for fish tooth data, in this case both calibrations have been used to account for a range

of seawater $\delta^{18}O$ compositions (Pucéat et al. 2007). TEX used the H calibration which has been widely viewed as the most appropriate for greenhouse climates (Kim et al. 2010; Hollis et al. 2012).

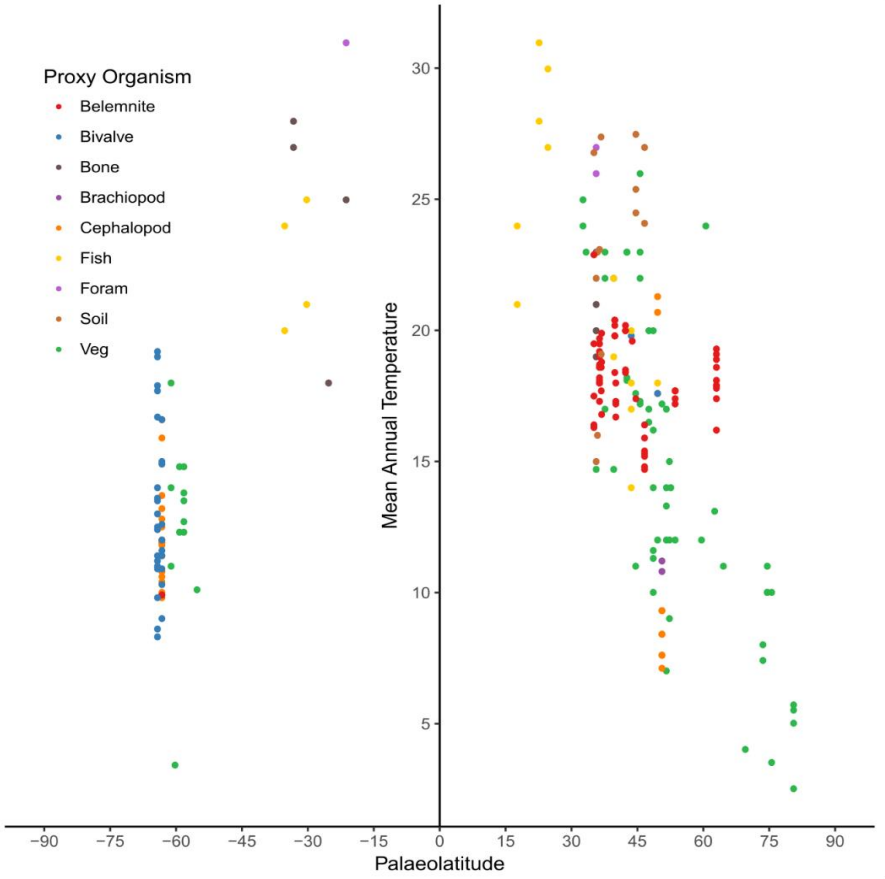

Figure 7.6: Mean annual temperature data for the Maastrichtian from different source organisms and proxies by palaeolatitude. See Appendix D for data sources

Mean annual temperature data from a range of sources for the Maastrichtian is presented in Figures 7.6 and 7.7. There is little difference between mean annual temperature trends from terrestrial and marine proxies at most latitudes, although there is a potential increase in terrestrial MAT recorded in the high northern latitudes (Figure 7.7). This is in line with observations of modern marine and air temperature trends (e.g. Figure 4.1) and supports the assumptions used in Section 7.1.2 for comparisons of Seymour Island's bivalve data with floral temperature proxies.

7.3.2 HadCM3L Simulations of Global Temperatures

Global temperature data from model experiments presented in Chapters 4 and 5 show a number of similarities with the proxy data, including an equatorial temperature peak of around 30 to 35°C and a smooth latitudinal temperature gradient to approximately 8 to 12°C at 60°N and 60°S. Mean annual temperatures show little variation over surface water depths between 5 and 100m (Figure 7.8) and are not particularly dependent on CO_2 concentrations, with only the equatorial latitudes showing a small increase in MAT at experiments with 4x and 6x CO_2 compared to 2x CO_2 experiments (different coloured curves in Figure 7.8).

The lack of any significant change in modelled temperature under a range of different atmospheric CO_2 concentrations is in contrast to recent studies which suggest the CO_2 produced by the Deccan Traps was a driver of significant high latitude climate change during Chron 29R (Petersen et al. 2016). Data presented here do not produce any evidence, for either the significant warming reported, or the potential for any significant CO_2 driven warming at these latitudes.

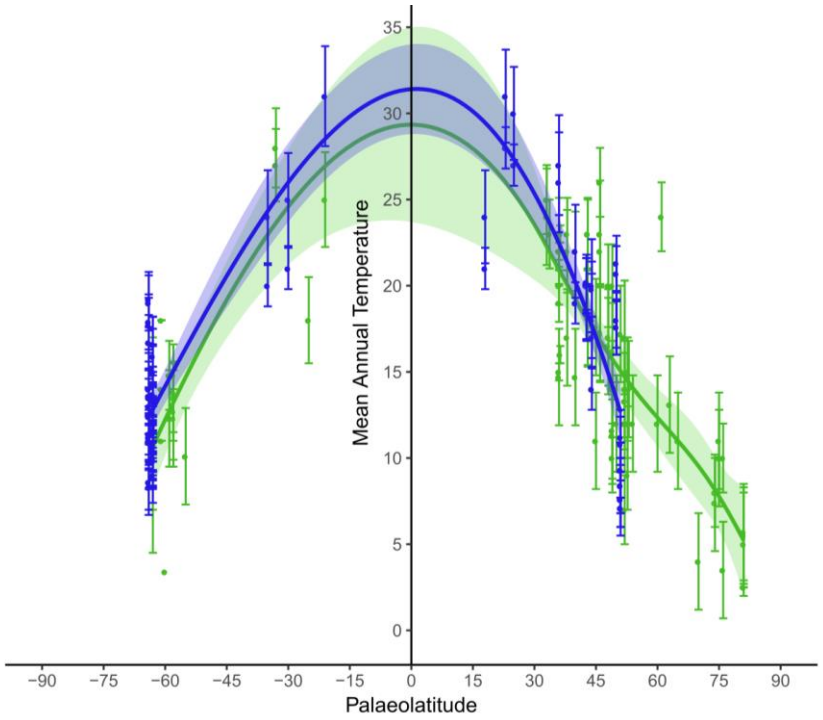

Figure 7.7: Mean annual temperature data for the Maastrichtian from shallow marine (blue) and terrestrial (green) proxy data with the error bars associated with each method of calibration (see Appendix D for details). This dataset omits data from Lowenstam and Epstein 1953 due to calibration discrepancies. See Appendix D for data sources

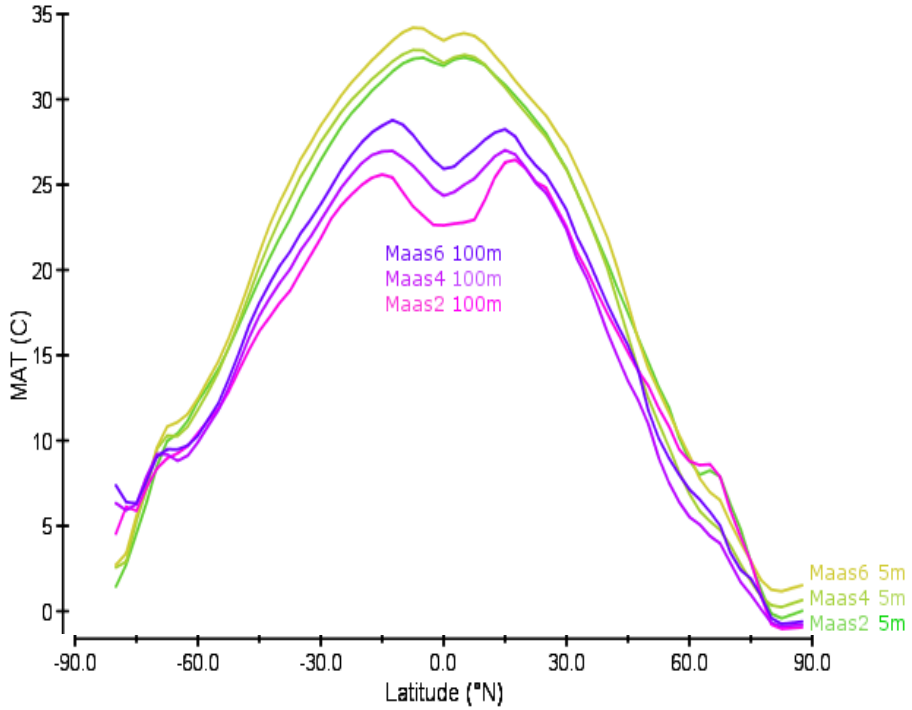

Figure 7.8: Modelled mean annual temperature data for the Maastrichtian from surface marine (greens) and shallow marine (purples) under the 3 different CO_2 concentrations presented in Chapter 4 and 5 (2x, 4x, 6x)

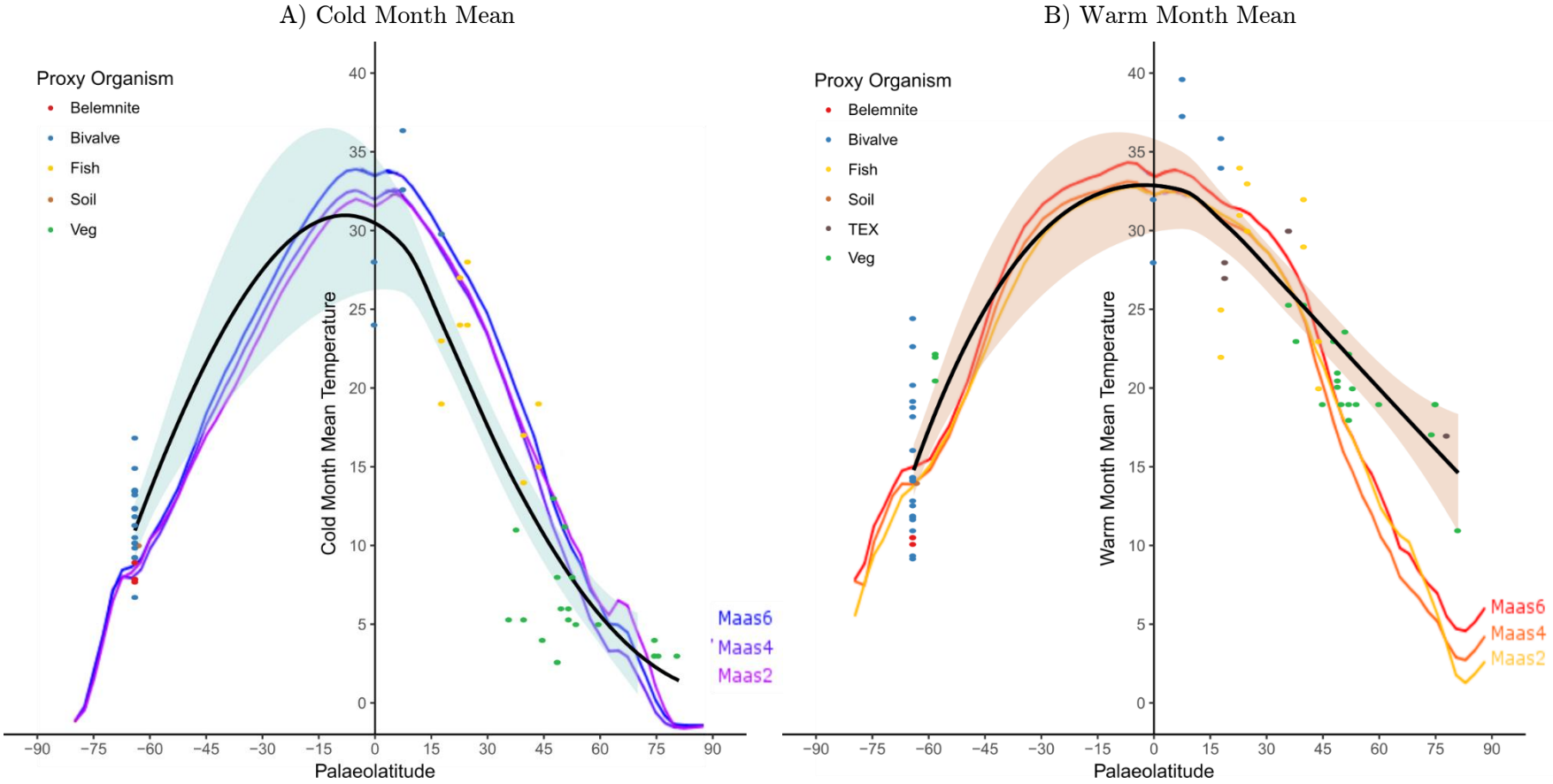

Figure 7.9: Comparison of (A) Maastrichtian cold month mean temperatures and (B) warm month mean temperatures from different proxy systems and organisms by latitude compared to surface water temperatures from climate simulations at different atmospheric CO2 concentrations. There is insufficient data coverage to give meaningful results when marine and terrestrial data points are separated, which may cause mismatch when compared to modelled data (see text for details). See Appendix D for data sources

The seasonal data available for the Maastrichtian also give latitudinal trends that generally compare well to surface-water temperature simulations (Figure 7.9), showing similar trends at equatorial and high southern latitudes in both the warm and cool seasons. The model does however predict high northern latitude summer temperatures between 10 and 15°C cooler than the proxy record suggests.

Unfortunately, the proxy data distribution was too sparse to allow seasonal data to be separated into marine and terrestrial trends like the mean annual data in Figure 7.7, so marine and terrestrial temperatures were plotted together in Figure 7.9. The availability of proxy data sets was also dependent on latitude, with little spatial overlap between data sets from different organisms and methods. The high northern latitudes were dominated by data produced from plant proxies, which are notoriously dependent on modern calibrations (Spicer & Herman 2010). It is also possible that the difference may be caused by terrestrial data recording air temperature conditions, which may be subject to greater seasonal variation than even surface water temperatures (Spicer et al. 2013).

7.3.3 Evidence for Seasonal Ice

Model results presented in Chapter 4 suggest that high latitude seasonal sea ice may have formed at latitudes above 72°S. It is likely that this coincided with the formation of continental Antarctic ice sheets, although these were not explicitly included in the model. The potential for high latitude ice formation is in line with terrestrial proxy records from the Southern Hemisphere, (e.g. Francis & Poole 2002; Amiot et al. 2004) which suggest latitudinal temperature gradients resulting in freezing conditions above 80°S, which are reflected in the global CMMT curves constructed in Figure 7.9. Other proxy records for example sea level curves which show a global 40m drop in sea level between Chron 30N and Chron 28R (Miller et al. 2005) also suggest the existence of Antarctic Ice sheets through the Cretaceous and Paleocene. Although modelling and $\delta^{18}O$ results in this study suggest that ice sheets were not a major influence on marine systems in the Seymour Island area.

7.3.4 The Influence of Atmospheric CO_2

As seen in Chapters 4 and 5, variations in the modelled amount of atmospheric CO_2 between 2 and 6x CO_2 did not appear to have a large effect on either seasonality or mean annual temperatures at any latitude. Data from chapter 5 suggest that the largest effect CO_2 has on modelled climate is in the inter-annual variability of peak seasonal temperatures rather than on the 30-year average climate conditions at any given latitude.

As there was such a small difference between the mean state temperatures predicted by each CO_2 experiment, a comparison of model and proxy data in Chapter 4 did not favour a certain set of conditions. However, both the large range of seasonal temperature variation produced from bivalves sampled across consecutive years of growth in this study, and the amount of longer timescale variability predicted from the shell umbo and shell back dataset produced by Petersen et al. 2016 are a far better match with the 560ppm experiment than the higher CO_2 versions.

Proxy data for atmospheric CO_2 as far back as the Maastrichtian are limited to $\delta^{13}C$ from pedogenic paleosol carbonates (Cerling et al. 1989; Ekart et al. 1999) and the stomatal density index (Gray et al. 2000; Boucot & Gray 2001). The limitations of these proxy records have been discussed in the literature (e.g. Royer et al. 2001). In general, stomatal indices are thought to provide the highest precision data (Beerling et al. 2002), while paleosol-derived results are thought to represent a lower end estimate of atmospheric CO_2 concentration particularly for values below 500ppmv (Ekart et al. 1999). A summary of atmospheric CO_2 estimates from these two proxy methods is presented in Figure 7.10 (Royer 2014).

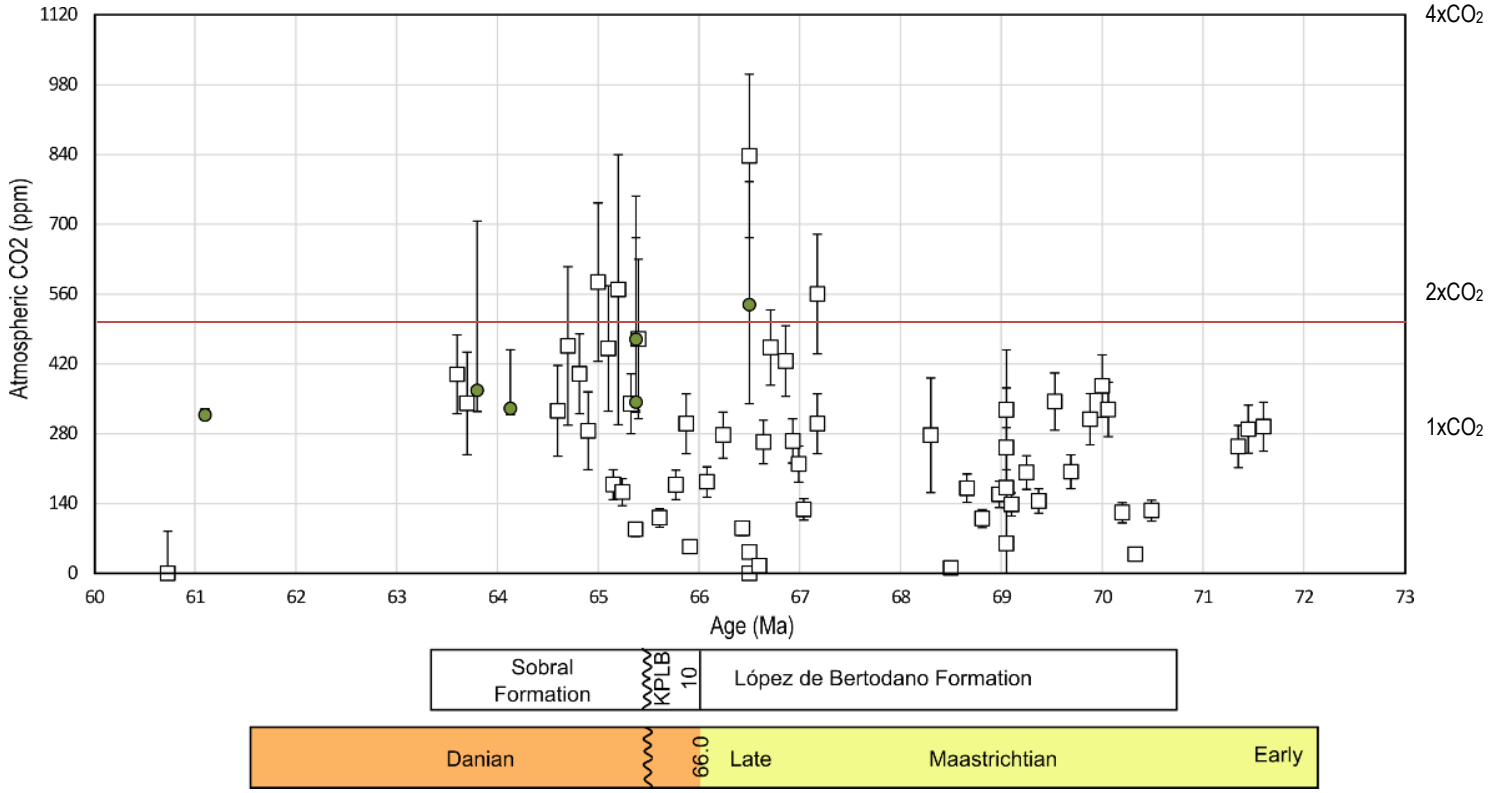

Figure 7.10: Global proxy-derived atmospheric CO_2 record through the Maastrichtian and Danian. Data from paleosols (white squares) and stomatal index data (green circles), data compilation from Royer 2014, for individual data sources see abridged table in Appendix D. Paleosol values below 500ppm (red line) are considered to be unreliable due to proxy limitations (Ekart et al 1999). Atmospheric CO_2 scale is presented at intervals of 0.5xPre-Ind CO_2 for ease of comparison to the experiments used in this study. The maximum 6xCO_2 concentration used for model experiments is off this scale at 1680ppmv.

Proxy data also suggests that atmospheric CO_2 during the time interval immediately prior to and after the K-Pg mass extinction at 66 Ma was likely to have been towards the lower end of the range of model experiments presented in this study. Only three proxy data points in the Maastrichtian suggest CO_2 concentrations higher than 560ppmv (2x Pre-Industrial CO_2). However, as the majority of Maastrichtian data points are derived from pedogenic carbonates (Cojan et al. 2000; Ghosh & Bhattacharya 2001; Nordt et al. 2002, 2003), these estimates may be lower than the actual CO_2 levels, particularly at a range so close to the lower limit of the proxy (Ekart et al. 1999). Models of atmospheric CO_2 conditions suggest end-Cretaceous CO_2 conditions slightly higher than those suggested by the proxy record, with records for the Maastrichtian (e.g. Wallmann 2001) suggesting CO_2 levels between 450 and 650ppm with a general increasing trend from the Maastrichtian through to the Paleocene.

Additional modelling of the effect of the Deccan Traps on atmospheric CO_2 (Henehan et al. 2016) suggest a significant increase in CO_2 concentrations caused by a pulse of volcanism at Chron 29R, which may have released a pulse of between 270 to 900ppm of CO_2 on top of baseline Maastrichtian conditions (Self et al. 2006). The proxy data points in Figure 7.10 with the highest CO_2 levels occur temporally close to the onset of this volcanism. This increase in CO_2 through the last 400ka of the Maastrichtian has been linked to an increase in temperature recorded by benthic foraminifera during this interval of up to 3℃ and a temperature drop through the final 100ka of the stage as carbon was scrubbed from the atmosphere by silicate weathering (Barrera 1994; Abramovich & Keller 2003; Colbourn et al. 2015; Henehan et al. 2016).

A similar warming and cooling trend has been seen in the $\delta^{18}O$-derived temperature data from Seymour Island produced from spot-collected bivalves (e.g. Petersen et al. 2016) but is not reflected in the considerably larger number of specimens examined from the measured section in this study (Figure 7.2) or in the palynological climate interpretation (Bowman et al. 2013, 2014) which shows warming immediately prior to the K-Pg. Other proxy records from Seymour Island do not possess the temporal resolution to be able to discern trends during the few hundred thousand years immediately prior to the mass extinction event.

The HadCM3 climate simulations performed in this study show little temperature change at shallow water depths across all latitudes, even with CO_2

concentrations increasing from 540 to 1680ppmv (Figure 7.8); a far greater change than the Deccan Traps eruption is likely to have caused (Self et al. 2006). The changes to bottom-water temperatures recorded by benthic foraminifera may be larger than the changes in surface waters, but overall the models suggest that increased CO_2 alone is unlikely to have caused the warming suggested by these records. The climate models in this study do not include the effects of potential volcanically-introduced greenhouse gases such as SO_4 and CH_4 due to the great uncertainty in concentrations, it is possible that their inclusion could account for some of the warming, or that the foraminiferal records are recording an effect that is convoluting the temperature record, such as water $\delta^{18}O$ changes. Unfortunately, in the Seymour Island section, the interval prior to the extinction contains the largest signals of methane influence (Chapter 6) which prevents the use of clumped isotopic data to deconvolve the temperature and water $\delta^{18}O$ records.

The press-pulse extinction hypothesis suggests that long-term environmental stresses such as climate destabilization in the run-up to the geologically instantaneous disruption of the Chicxulub impact may have caused the severity of the K-Pg mass extinction event (e.g. Arens & West 2008). Climate change and variability have both been suggested as sources of long-term stress to the environment. The combination of CO_2 proxy observations, drawdown models and climate models suggests that the increase in atmospheric CO_2 caused by the Deccan Traps eruption at the beginning of Chron 29R is more likely to have reduced short-term climate variability than caused it. This is tentatively supported by $\delta^{18}O$ data from Petersen et al. (2016), which shows a decrease in inter-annual temperature variability close to the level of Chron 29R (Figure 7.3). As CO_2 drawdown occurred and atmospheric CO_2 levels dropped to the levels suggested in the proxy record for the several hundred-thousand-year interval either side of the K-Pg boundary (Figure 7.10) climate variability may have increased again, but it is not logistically possible to examine the sub-annual fossil record at this resolution, even in an expanded section such as on Seymour Island.

7.4 Bivalve Responses to Environmental Effects

Combined observations of the climate and environmental conditions in the Seymour Island region over the K-Pg boundary interval presented in Chapters 4, 5 and 6 and expanded upon in this chapter suggest generally stable climates

throughout the latest Maastrichtian. Little climate variability or evidence of rapid temperature or seasonality fluctuations was detected throughout the boundary section with the exception of a couple of spikes in intra-annual seasonality found in single specimens (Figure 7.3). Both warm and cool month temperatures showed less variation through the section than the amount of uncertainty due to potential changes in water composition. Inter-annual variability was found to account for much more variability than annual seasonality Section 5.4.3, particularly during times of low atmospheric CO_2. As a result, it is unlikely that bivalves will have had much of a growth response to changes in the run-up to the K-Pg mass extinction. The molluscan temperature data do however suggest a slight cooling throughout the Danian recovery interval which may be responsible for some of the growth trends presented in Chapter 3.

7.4.1 Size Changes

New data from $\delta^{18}O$ analyses and models allowed reconstruction of seasonal temperature curves for Maastrichtian surface waters (Figure 7.11). When compared to modern latitudinal temperature gradients and the distribution of larger shelled species of bivalves around the mid to low latitudes, it appears that summer temperatures may provide a constraint on the life strategy of producing large sized shells, as large-shelled species of cardiid and arcoids do not tend to be found at modern latitudes where summer temperatures average less than approximately 12℃ (Figure 7.11). However, even the 2 to 3℃ drop in mean annual temperatures through the Danian part of the Lopez de Bertodano Formation is unlikely to have pushed temperatures below this tentatively defined threshold.

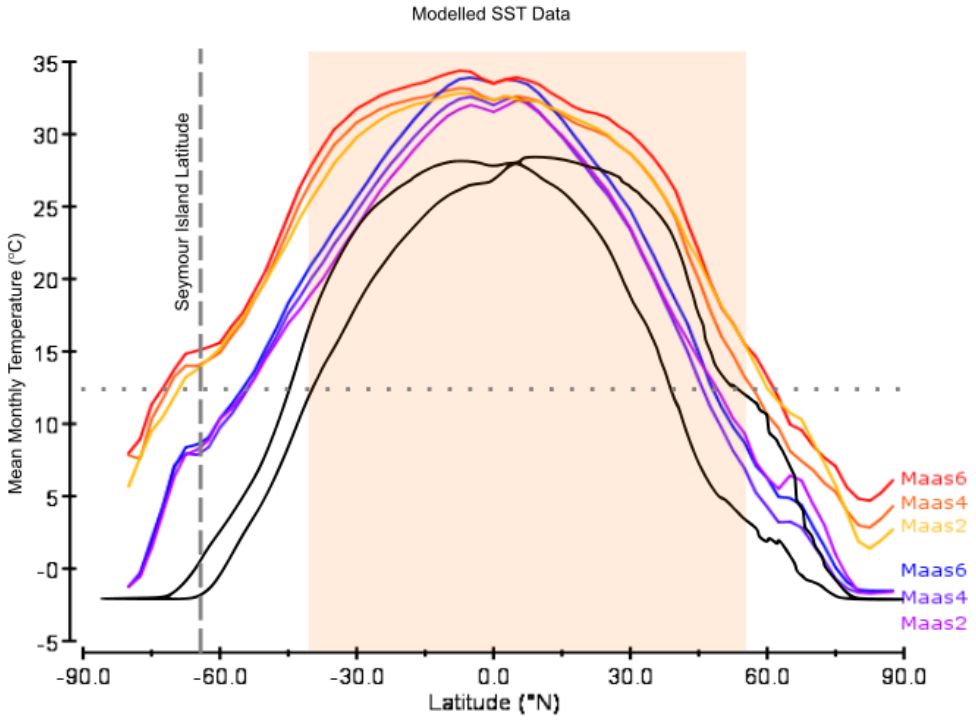

Figure 7.11: Modelled SST data from modern (black) and Maastrichtian simulations in this study (WMMT at each CO2 concentration in reds, CMMT in blues). Also marked is the modern latitudinal range of arcoid and cardiid bivalves able to produce maximum shell sizes of greater than 50 mm (orange field) and the Maastrichtian latitude at which specimens of the large bivalves *Lahillia* and *Cucullaea* lived (dashed grey line). It appears that summer temperatures may provide a constraint on the strategy of large shell size in certain bivalves, as these species do not tend to be found at latitudes where summer temperatures average less than 12°C (dotted grey line).

Size and morphometric analyses of the shells of *Lahillia*, *Cucullaea* and *Leionucula* presented in Chapter 3 did not show any evidence for within-lineage size decrease across the K-Pg boundary, and were not consistent with the Lilliput effect of smaller shell sizes following the K-Pg. It is possible that shell sizes prior to the K-Pg mass extinction were smaller than typical for the environmental conditions due to environmental stresses. Pre-extinction dwarfing has been observed in other taxa (He et al. 2007; Wade & Olsson 2009; O'Dea et al. 2011) where it has been attributed to temperature changes in the latest Maastrichtian, however there was little evidence for similar temperature variability or environmental stressors through the Seymour Island section. Most of the changes in shell dimensions across the K-Pg boundary were morphometric changes, for instance; Danian *Lahillia larseni* growing significantly wider for the same shell

length than Maastrichtian specimens. It is useful to consider such morphometric changes in conjunction with analysis of growth patterns and maturation rates. Other changes in size distribution were also found and will be discussed later in this section.

The Lilliput effect (Urbanek 1993) is a general description for a temporary decrease in body size among post-extinction organisms. The effect has been widely reported in many animal groups, both in holdover taxa and long-term survivors in the aftermaths of all five past mass extinction events including the K-Pg mass extinction (Hansen et al. 1993; Smith & Jeffery 1998; Jeffery 2001; Lockwood 2005; Aberhan et al. 2007). However, many studies of the K-Pg and other mass extinction events dispute the ubiquity of the Lilliput effect; particularly in within-lineage size studies (e.g. Brayard et al. 2010; Sogot et al. 2014). It is becoming more and more accepted that size change at mass extinction horizons is likely to be complex and it cannot be expected that all clades will respond in the same manner, or that all mass extinctions will have the same effects (Harries & Knorr 2009; Friedman & Sallan 2012).

It is therefore useful to examine the environmental and biological context for size change in order to understand the variability of behaviour between clades and extinction events. A reduction in primary productivity following the K-Pg event has been hypothesised as a cause for small organism size (e.g. Smith & Jeffery 1998; Aberhan et al. 2007), although an array of other environmental stresses have been suggested to induce Lilliput effects at mass extinction events, including anoxia, shallow seas and basin restriction, changes in temperature and salinity (Twitchett 2007; Keller et al. 2009). Several other effects have also been hypothesised which may induce the opposite effect; such as changes in ecosystem level predation, food supply and competition (Case 1978; McClain et al. 2006; Harries & Knorr 2009). This study found that changes in temperature across the K-Pg boundary were likely to have been small at the latitude of Seymour Island. However, evidence for anoxia (Witts et al. 2016; Schoepfer et al. 2017), changes in predator distribution (Harper et al. 2018), and food supply (Zachos et al. 1989; D'Hondt 2005; Esmeray-Senlet et al. 2015; Birch et al. 2016) have all been described across the K-Pg boundary and have the potential to affect the mode of life and growth response of infaunal marine bivalves.

7.4.2 Population Distribution and Bimodality

Work in Chapter 3 showed that the most obvious change in bivalve population size-structure across the K-Pg boundary was the change in *Lahillia* between a normally distributed population structure in the Maastrichtian to a bimodally peaked distribution in the Danian, whereas in *Cucullaea* this apparent trend was reversed.

Bivalve populations are known to be extremely unstable, with both short and long-term changes in abundance (Beukema et al. 2010), population size-structure (Strayer & Malcom 2006), and spatial distribution (Herlyn et al. 2008), but the factors governing these fluctuations are still poorly understood, even in modern ecosystems. However, box-plots representing the size distribution of each species of bivalve at several time intervals through stratigraphy (Figures 3.15 to 3.17) do suggest that this trend is more than just a transient anomaly.

Bimodality in population sizes can be produced by a number of interactive and non-interactive inherent and imposed factors (Table 7.1: Biological mechanisms that can produce bimodality annotated with tick and cross marks indicating whether each mechanism is likely to apply to *Lahillia* or *Cucullaea* in this study. Modified from Huston & DeAngelis (1987). It is possible that preservation biases in the fossil record could have introduced additional changes in the preserved versus actual record. Bimodality in the fossil record could come from a combination of several effects; the live population exhibiting a bimodal size distribution, or from time averaging during more transient periods of unimodal smaller and larger shell size, or from the lack of preservation of fossil specimens of intermediate size. However, for relatively long-lived bivalves in modern environments the size frequency distribution of the live populations does tend to be well-reflected in the distribution of dead shells, (e.g. Skazina et al. 2013) so the likelihood is that the patterns observed in the fossil record do represent a real change in population structure across the K-Pg boundary. The most likely causes of such an effect have been marked in Table 7.1 and will be discussed further below.

Table 7.1: Biological mechanisms that can produce bimodality annotated with tick and cross marks indicating whether each mechanism is likely to apply to *Lahillia* or *Cucullaea* in this study. Modified from Huston & DeAngelis (1987).

	Non-interactive		Interactive	
Inherent	Sexual dimorphism	X	Sex change	X
	Genetic variation	✓	Sexual/asexual shifts	X
	Maximum size limits	X	Morphometric change	X
Imposed	Temporal heterogeneity	X	Competition	X
	Hatching/germination		Symmetrical	
	Cohorts		Asymmetrical	
	Temperature			
			Mortality	X
	Spatial heterogeneity	✓	Cannibalism	
	Abiotic resources		Density-dependent	
	Food availability			
	Temperature			
	Mortality	✓		
	Predation			
	Density-independent			

It is unlikely that the stratigraphic intervals captured relatively short-term effects such as temporal or spatial heterogeneity, as such effects would likely average out over such long periods of time (Fürsich & Aberhan 1990; Albano & Sabelli 2011). Sexually dimorphic shell size is also not particularly common among marine bivalves, aside from cases of extreme male dwarfing in commensal species.

Predation is capable of producing a bimodal distribution between smaller dead shells in the sediment and living shells capable of growing to larger size extremes. Size-selective predation is thought to be less of a selection pressure among infaunal and semi-infaunal bivalves (West & Williams 1986) than epifaunal species, although this situation does occur for infaunal bivalves preyed on by naticid gastropods (Kitchell et al. 1981). This scenario is plausible for the Seymour Island section, given that main predation in the post-extinction interval was boring gastropods. Once these bivalves reached sexual maturity, body size increase slowed and shell production thickened the shell rather than increasing

internal volume. This means older and larger sized individuals will be less cost-efficient to predate than smaller, younger ones.

It is, unfortunately not possible to determine the drilling frequencies in Seymour Island's specimens due to the collection methods used, however studies of drilled fossil material from Seymour Island by Harper et al. (2018) show significant correlation between prey size and successful predatory drill hole diameter. This suggests that a size or shell thickness refuge may not have been an effective defence against borers.

Comparisons of shell size frequency distributions and patterns of maturation (Figure 7.12) also suggest that the difference in size distribution is more likely to have been linked to age at maturity, rather than changes in predation or mortality.

In the Maastrichtian part of the López de Bertodano Formation, the juvenile growth rate did not affect the age at which maturity was reached, with even the specimens with the slowest initial growth rates maturing at similar sizes to the fastest growing juveniles. Whereas for *Lahillia* in the Danian part of the López de Bertodano Formation, some specimens matured at a considerably larger size and later age than other specimens which matured much earlier and at a smaller shell size than any Maastrichtian specimens. Two Danian individuals were found to have reached maturity by 8 years of growth with heights below 45 mm, compared to the youngest Maastrichtian specimen to mature at 10 years of growth with a shell height of over 75 mm. This early maturation appears to have created a bimodal size distribution in the Danian, as few specimens which matured early would be able to reach the larger shell sizes of later-maturing specimens at the slower rate of mature shell growth, even if, as suggested by the data, they were able to survive to similarly advanced ages.

In bivalves, a reasonable relationship has been found between later maturation and longevity, as well as slower growth rate and longevity (e.g. Haag & Rypel 2011; Ridgway et al. 2011). This trend does, however explain less of the variation in longevity than in some other taxonomic groups (de Magalhaes et al. 2007) which may be due to confounding factors such as shell thickness and burrowing depth that reduce vulnerability to predation and extrinsic hazards (Kirby 2001).

As growth trajectories were unable to be produced from *Cucullaea* due to the need to destructively section shells, it is not possible to determine whether a

similar, reversed change in maturation sizes occurred at the K-Pg boundary in order to produce the change in size distribution from bimodal in the Maastrichtian to normally distributed in the Danian.

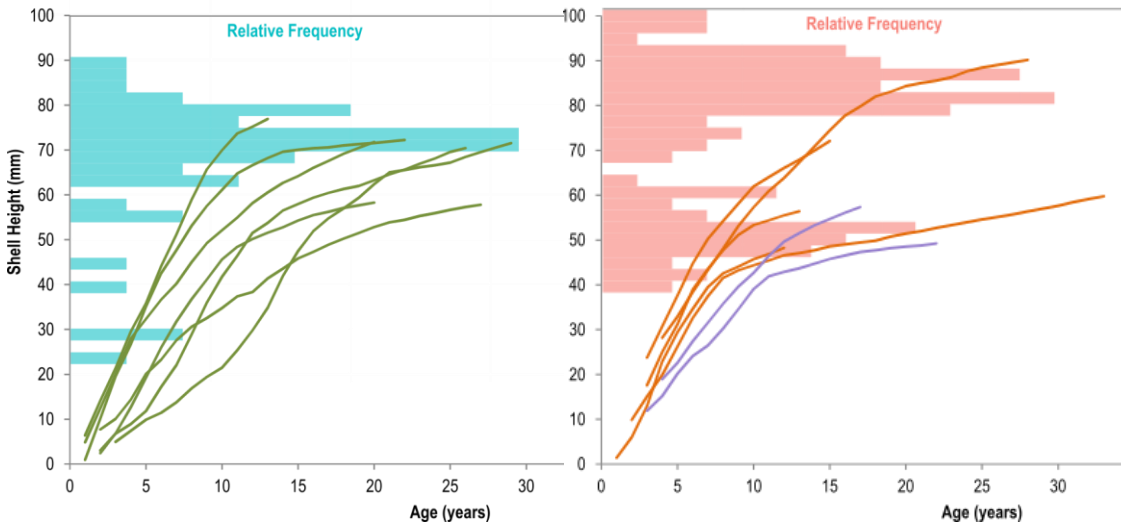

Figure 7.12: Maastrichtian (left) and Danian (right) comparisons of *Lahillia* growth trajectories (curves on lower scale) and frequency distribution (histograms, relative scale). Specimens from the Maastrichtian all show growth trajectories with the potential to reach the size of the peak frequency. Whereas specimens from the Danian show maturity at a smaller size and will only reach the size of the lower frequency peak at the slower rate of mature growth, even if long-lived. This shows that the size distribution is more likely to have been linked to growth rate and maturity rather than changes in mortality which is unlikely to have changed the maturation cycle.

7.4.3 Productivity and Food Supply after the K-Pg

A significant body of evidence suggests that the K-Pg mass extinction event was accompanied by a decrease in primary and export productivity in the oceans (e.g. (Zachos et al. 1989; Kump 1991; D'Hondt 2005; Esmeray-Senlet et al. 2015; Birch et al. 2016). This decrease in productivity was particularly pronounced in lower latitudes (e.g., Barrera & Keller 1994) but may have also been experienced in the higher latitudes.

A lower food supply in the recovery interval may have caused problems for more metabolically-active organisms dependent on organic matter supply from surface waters. Feeding strategy has been found to be a significant factor in the probability of surviving the K-Pg boundary in groups such as echinoids (Smith & Jeffery 1998; Jeffery 2001) and bivalves, where there is evidence that suspension-feeding bivalves suffered much higher rates of extinction than deposit feeders across the K-Pg boundary (61% extinction compared to only 30%). Some of this, however may be attributed to the extinction-resistant characteristics of nuculoids and lucinoids biasing the data (Jablonski & Raup 1995). Species of modern bivalve are known to respond to variations in food supply by changing the timing and rate of shell growth and energy put into reproductive development (e.g. Thompson & Nichols 1988). The increase in shell growth rate in *Lahillia* (VBGF parameter k, see discussion in Section 3.7.3) across the K-Pg boundary may reflect the lower competition for food in post-extinction ecosystems.

7.4.4 Redox and Oxygen Availability

Evidence for hypoxia and euxinia has been found in sedimentary deposits from Seymour Island (see section 7.2 for further details) throughout the Lopez de Bertodano Formation on both sides of the K-Pg boundary. Basinal euxinia does not appear to have increased either across the boundary, or in the pre-extinction period of Deccan Traps eruption, which suggests it played only a minor role in the mass extinction event (Schoepfer et al. 2017). There is little evidence that euxinia was a major driver of marine diversity in the James Ross Basin during deposition of the Molluscan units of the Cretaceous Lopez de Bertodano Formation which are the focus of this study. Euxinic periods may have played a partial role in restricting diversity in the underlying Rotularia units at the base of the section (Schoepfer et al. 2017). Periodic euxinia throughout the upper strata of the Lopez de Bertodano Formation could still have provided an environmental stressor for infaunal benthic organisms unable to migrate away, as hypoxia is known to reduce feeding, reproduction and metabolic rates in benthic fauna (Davis 1975; Herreid 1980; Wang & Widdows 1993; Wiklund & Sundelin 2001).

The presence of long-lived bivalves such as *Lahillia* and *Cucullaea* throughout the section suggests that the infaunal bivalve community was tolerant of short-lived euxinic events in the water column. In general mollusc communities are among the most tolerant of hypoxia, particularly in cooler waters (Gray et al.

2002; Vaquer-Sunyer & Duarte 2008). It is possible that widespread dysoxia in the pre-extinction sediments could have opened up ecological space for *Lahillia*, *Cucullaea* and other benthic fauna that were better able to survive due to their slower metabolisms.

Oxygen concentrations also increase logarithmically with height above the seafloor in modern sediments (Jørgensen 1980; Diaz & Rosenberg 1995), such that the ability to access the water column a few centimetres above the sedimentary surface could have meant the difference between tolerable and lethal conditions during an anoxic event. This may have favoured the survival of larger species of bivalve that had the ability to raise the shell above the sediment surface, or extend siphons or palps higher into the more oxygenated water column (e.g. Sagasti et al. 2001).

7.4.5 Overall Growth Strategy

The low growth rates and slow maturation of *Lahillia* and *Cucullaea* would have allowed them to reach larger body sizes before the growth rate slowed. This strategy is well-suited to an environment with external factors controlling food availability and metabolic rate, such as the periodic anoxia of the pre-extinction times. This tolerance for low food availability may have contributed to their ability to survive the potential productivity collapse of the post-extinction interval. In addition, the thick shells produced by this growth strategy may have shielded them from hazards such as predation and temperature fluctuations during this interval (Kirby 2001). It is possible that the pattern of younger maturation at smaller sizes seen in Danian *Lahillia* could have been due to a reduction in the need to produce such large shells for environmental protection, in favour of shorter generation times.

Deposit feeders such as *Leionucula* tended to survive better across the K-Pg boundary and associated productivity collapse (Jablonski & Raup 1995). However, *Leionucula* is the only taxon analysed here which shows a decrease in overall body size from the Maastrichtian into the Danian, with maximum shell length decreasing significantly by approximately 10%. Relative abundance was greatly increased following the mass extinction (R.J Whittle, pers. comm.), which could suggest that size is not necessarily a good indicator of the success of a species.

Overall, it appears that the lack of a clear trend across the K-Pg boundary within each of these clades of bivalves may be related to their ecological strategy to deal with selective pressures in the pre-extinction ecosystem, more than any environmental effects caused by the K-Pg mass extinction. It appears that for the three taxa of bivalves observed here, there may have been advantages to both increasing or decreasing size in the aftermath of the K-Pg boundary.

7.5 Conclusions

To summarise the main conclusions of this body of work:

- The climate of the James Ross Basin was likely to have been stable and reasonably uniform throughout the late Maastrichtian pre-extinction period with average temperatures of approximately 10°C ± 5 recorded in bivalves throughout with a 2°C temperature decrease during the post-extinction interval.

- New sub-annual resolution temperature data show that Lahillia and Cucullaea bivalves produced their shells during warmer seasons. Use of summer and winter temperatures from high resolution bivalve records is likely to be more reliable than bulk or mean temperatures.

- Annual seasonality of approximately 2 to 5°C produces less temperature variation than year-to-year temperature variability; an effect which appears to be enhanced by potentially lower atmospheric CO_2 conditions than have been explored by models in this study.

- No evidence for the influence of nearby sea ice was produced from either new proxy data or model analyses, or re-evaluation of pre-existing proxy data sets in light of new concerns about their reliability.

- For the first time, seasonal $\delta^{13}C$ signals diagnostic of methane-derived carbon have been found in bivalve shells from several discrete intervals throughout the late Maastrichtian and early Danian. The seasonal nature of the signal allows methane hydrates to be ruled out as a potential cause, and links it to a mechanism likely to have been facilitated by the low

marine sulfate conditions at the time of deposition and could also be related to observations of periodic bottom water anoxia through the section.

- The identification of a significant methane-related signal in a number of bivalve shells provides evidence to suggest that clumped isotopic data produced from these shells may be unreliable and the low temperatures described by previous data sets unrealistic.

- New and compiled seasonal temperature data produce a good fit to modelled latitudinal data showing that both seasonal behaviour and the high southern latitudes are well-represented by behaviour in the climate simulations. In the high northern latitudes, CMMTs are congruent but floral proxies are consistently between 10 and 15℃ warmer than simulated WMMT conditions, potentially due to methods of proxy calibration or continental temperature differences.

- $2xCO_2$ model experiments give the best fit to temperature and temperature variability data as well as the estimates of atmospheric CO_2 during the K-Pg boundary interval. Although both sets of experiments with higher atmospheric CO_2 were also capable of producing seasonality and temperature data within the range of the proxy data at reasonable, if slightly shallower water depths. This suggests that changes in CO_2, for example due to active volcanism in the Deccan Traps do not have a driving effect on high southern latitude temperatures

- Good agreement between proxy data recorded over several million years of geological time and the general climate model covering the entire Maastrichtian could imply that orbitally driven variations in seasonality and temperature are a second order effect compared to the strength of the seasonal cycle and year-to year temperature variability at this location.

- No evidence for Lilliput effect style post-extinction dwarfing was found in any of the three genera of bivalves examined. Size and growth patterns showed a variable response to the mass extinction which may be linked to the ecological strategy of slow growth to large mature shell sizes making these species particularly tolerant of pre- and post-extinction conditions.

Data generated over the course of this thesis have raised several questions which could be explored with further work.

- The development of a more relevant and accurate growth function for indeterminate growth, as found in slow growing long-lived bivalve species. This study is one of a long line which highlights the inadequacies of the commonly used von Bertalanffy Growth Function. It would be more biologically relevant and useful for comparison between taxa to be able to consider juvenile and mature growth trajectories separately, and produce a mathematical function to parametrise the duration and period of overlap of each trajectory.

- Further investigation into changing of bivalve growth patterns and seasonality across major episodes of climate change. A few shells from the Eocene were examined in this thesis, and it was found that these specimens appear to grow with opposite seasonality to specimens of the same taxa from the cooler K-Pg section. It would be interesting to see whether this trend is linked to the warmer climate of the Eocene and is present across other periods of climate change.

- This work only examined a range of atmospheric CO_2 from 2 to 4 times pre-industrial levels, however a large number of estimates from pedogenic carbonates and some from stomatal indices suggest that Maastrichtian CO_2 levels may have been lower than 500ppmv. It would be interesting to examine model results from 1 and 0.5 times pre-industrial concentrations of CO_2 and see whether the effects of seasonal and inter-annual variability were amplified further.

- Examining longer records of seasonal variability from climate simulations in order to look for evidence of regular cyclicity on longer than annual temporal scales. Climate variability caused large temperature differences, particularly in the lower CO_2 experiments and finding cyclicity in these cycles may shed light on their origin and effects on Antarctic ecosystems.

- A similar approach using microsampling could be taken to examine for evidence of methane-related signals in other periods with low marine sulfate concentrations.

- Potential drivers of methane production in the Seymour Island section could be investigated using trace elemental analysis of bivalve shells to measure seasonal changes in Ba/Ca and Mo/Ca which are generally accepted to be linked to changes in productivity. This could allow the propagation of productivity-based changes through the water column to be determined.

7.6 References

Aberhan, M., Weidemeyer, S., Kiessling, W., Scasso, R. A. and Medina, F. A. (2007) 'Faunal evidence for reduced productivity and uncoordinated recovery in Southern Hemisphere Cretaceous-Paleogene boundary sections', *Geology*, 35(3), 227–230.

Abramovich, S. and Keller, G. (2003) 'Planktonic foraminiferal response to the latest Maastrichtian abrupt warm event: a case study from South Atlantic DSDP Site 525A', *Marine Micropaleontology*, 48(3–4), 225–249.

Adams, D. D., Hurtgen, M. T. and Sageman, B. B. (2010) 'Volcanic triggering of a biogeochemical cascade during Oceanic Anoxic Event 2', *Nature Geoscience*. Nature Publishing Group, 3(3), 1–4.

Albano, P. G. and Sabelli, B. (2011) 'Comparison between death and living molluscs assemblages in a Mediterranean infralittoral off-shore reef', *Palaeogeography, Palaeoclimatology, Palaeoecology*, 310(3–4), 206–215.

Amiot, R., Lecuyer, C., Buffetaut, E., Fluteau, F., Legendre, S. and Martineau, F. (2004) 'Latitudinal temperature gradient during the Cretaceous Upper Campanian-Middle Maastrichtian: –"oxy" record of continental vertebrates', *Earth and Planetary Science Letters*, 226(1–2), 255–272.

Anderson, T. F., Popp, B. N., Williams, A. C., Ho, L.-Z. And Hudson, J. D. (1994) 'The stable isotopic records of fossils from the Peterborough Member, Oxford Clay Formation (Jurassic), UK: palaeoenvironmental implications', *Journal of the Geological Society*. Geological Society of London, 151(1), 125–138.

Arens, N. C. and West, I. D. (2008) 'Press-pulse: a general theory of mass extinction?', *Paleobiology*, 34(4), 456–471.

Barrera, E. (1994) 'Global environmental changes preceding the Cretaceous-

Tertiary boundary: Early-late Maastrichtian transition', *Geology*, 22(10), 877–880.

Barrera, E. and Keller, G. (1994) 'Productivity across the Cretaceous/Tertiary boundary in high latitudes', *Geological Society of America* (10).

Beerling, D. J., Lomax, B. H., Royer, D. L., Upchurch, G. R. and Kump, L. R. (2002) 'An Atmospheric p–CO2 reconstruction across the Cretaceous-Tertiary boundary from leaf megafossils', *PNAS*, 99(12), 7836–7840.

Bernard, S., Daval, D., Ackerer, P., Pont, S. and Meibom, A. (2017) 'Burial-induced oxygen-isotope re-equilibration of fossil foraminifera explains ocean paleotemperature paradoxes', *Nature Communications*. Springer US, 8(1), 1–10.

Berner, R. A. (2004) 'A model for calcium, magnesium and sulfate in seawater over Phanerozoic time', *American Journal of Science*, 304(5), 438–453.

Beukema, J. J., Dekker, R. and Philippart, C. J. M. (2010) 'Long-term variability in bivalve recruitment, mortality, and growth and their contribution to fluctuations in food stocks of shellfish-eating birds', *Marine Ecology Progress Series*. Inter-Research Science Center, 117–130.

Birch, H. S., Coxall, H. K., Pearson, P. N., Kroon, D. and Schmidt, D. N. (2016) 'Partial collapse of the marine carbon pump after the Cretaceous-Paleogene boundary', *Geology*, 44(4), 287–290.

Boucot, A. J. and Gray, J. (2001) 'A critique of Phanerozoic climatic models involving changes in the –CO2 content of the atmosphere', *Earth-Science Reviews*, 56(1–4), 1–159.

Bowman, V. C., Francis, J. E., Askin, R. A., Riding, J. B. and Swindles, G. T. (2014) 'Latest Cretaceous–earliest Paleogene vegetation and climate change at the high southern latitudes: palynological evidence from Seymour Island, Antarctic Peninsula', *Palaeogeography, Palaeoclimatology, Palaeoecology*, 408, 26–47.

Bowman, V. C., Francis, J. E. and Riding, J. B. (2013) 'Late Cretaceous winter sea ice in Antarctica?', *Geology*, 41(12), 1227–1230.

Brayard, A., Nutzel, A., Stephen, D. A., Bylund, K. G., Jenks, J. and Bucher, H. (2010) 'Gastropod evidence against the Early Triassic Lilliput effect', *Geology*, 38(2), 147–150.

Case, T. J. (1978) 'A general explanation for insular body size trends in terrestrial

vertebrates', *Ecology*, 59, 1–18.

Cerling, T. E., Quade, J., Wang, Y. and Bowman, J. R. (1989) 'Carbon isotopes in soils and palaeosols as ecology and palaeoecology indicators', *Nature*, 341, 138–139.

Cojan, I., Moreau, M.-G. and Stott, L. E. (2000) 'Stable carbon isotope stratigraphy of the Paleogene pedogenic series of southern France as a basis for continental marine correlation':, *Geology*, 28, 259–262.

Colbourn, G., Ridgwell, A. and Lenton, T. M. (2015) 'The time scale of the silicate weathering negative feedback on atmospheric CO_2', *Global Biogeochemical Cycles*, 29(5), 583–596.

Crame, J. A., Francis, J. E., Cantrill, D. J. and Pirrie, D. (2004) 'Maastrichtian stratigraphy of Antarctica', *Cretaceous Research*, 25(3), 411–423.

D'Hondt, S. (2005) 'Consequences of the Cretaceous/Paleogene Mass Extinction for Marine Ecosystems', *Annual Review of Ecology, Evolution, and Systematics*, 36(1), 295–317.

Davis, J. C. (1975) 'Minimal Dissolved Oxygen Requirements of Aquatic Life with Emphasis on Canadian Species: a Review', *Journal of the Fisheries Research Board of Canada*. NRC Research Press Ottawa, Canada , 32(12), 2295–2332.

Demicco, R. V., Lowenstein, T. K., Hardie, L. A. and Spencer, R. J. (2005) 'Model of seawater composition for the Phanerozoic', *Geology*, 33(11), 877–880.

Diaz, R. J. and Rosenberg, R. (1995) 'Marine benthic hypoxia: a review of its ecological effects and the behavioural responses of benthic macrofauna', *Oceanography and marine biology. An annual review*, 33, 203–245.

Dutton, A. L., Huber, B. T., Lohmann, K. C. and Zinsmeister, W. J. (2007) 'High-resolution stable isotope profiles of a Dimitobelid Belemnite implications for paleodepth habitat and Late Maastrichtian climate Sensitivity', *Palaios*, 22, 642–650.

Ekart, D. D., Cerling, T. E. and Montanez, I. P. (1999) 'A 400 million year carbon isotope record of pedogenic carbonate: implications for palaeoatmmospheric carbon dioxide', *American Journal of Science*, 299, 805–827.

Eldrett, J. S., Greenwood, D. R., Harding, I. C. and Huber, M. (2009) 'Increased seasonality through the Eocene to Oligocene transition in northern high

latitudes', *Nature*, 459(7249), 969–973.

Esmeray-Senlet, S., Wright, J. D., Olsson, R. K., Miller, K. G., Browning, J. V. and Quan, T. M. (2015) 'Evidence for reduced export productivity following the Cretaceous/Paleogene mass extinction', *Paleoceanography*, 30(6), 718–738.

Francis, J. E. and Poole, I. (2002) 'Cretaceous and early Tertiary climates of Antarctica: evidence from fossil wood', *Palaeogeography, Palaeoclimatology, Palaeoecology*, 182(1), 47–64.

Friedman, M. and Sallan, L. C. (2012) 'Five hundred million years of extinction and recovery: a phanerozoic survey of large-scale diversity patterns in fishes', *Palaeontology*, 55(4), 707–742.

Fürsich, F. T. and Aberhan, M. (1990) 'Significance of time-averaging for palaeocommunity analysis', *Lethaia*. 23(2), 143–152.

Ghosh, P. and Bhattacharya, S. K. (2001) '–CO2 levels in the Late Palaeozoic and Mesozoic atmosphere from soil carbonate and organic matter, Satpura basin, Central India', *Palaeogeography, Palaeoclimatology, Palaeoecology*, 170(3–4), 219–236.

Goodwin, D. H., Schöne, B. R. and DL, D. (2003) 'Resolution and fidelity of oxygen isotopes as paleotemperature proxies in bivalve mollusk shells: Models and observations', *Palaios*, 18(2), 110–125.

Goswami, A. (2012) 'Predicting the geographic distribution of ancient soils with special reference to the Cretaceous'. Environmental & Earth Science.

Gray, J., Holroyd, G. H., Van der Lee, F. M., Bahrami, A. R., Sijmons, P. C., Woodward, F. I., Schuch, W. and Hetherington, A. M. (2000) 'The HIC signalling pathway links –CO2 perception to stomatal developement', *Nature*, 408, 713–716.

Gray, J. S., Wu, R. S. and Or, Y. Y. (2002) 'Effects of hypoxia and organic enrichment on the coastal marine environment', *Marine Ecology Progress Series*. Inter-Research Science Center, 249–279.

Greenwood, D. R. and Wing, S. L. (1995) 'Eocene continental climates and latitudinal temperature gradients', *Geology*, 23(11), 1044–1048.

Grossman, E. L. and Ku, T.-L. (1986) 'Oxygen and carbon isotope fractionation in biogenic aragonite: Temperature effects', *Chemical Geology: Isotope Geoscience section*, 59, 59–74.

Haag, W. R. and Rypel, A. L. (2011) 'Growth and longevity in freshwater mussels: evolutionary and conservation implications', *Biological Reviews*. Blackwell Publishing Ltd, 86(1), 225–247.

Hansen, T. A., Farrell, B. R. and Upshaw, B. (1993) 'The first 2 million years after the Cretaceous-Tertiary boundary in east Texas: rate and paleoecology of the molluscan recovery', *Paleobiology*. 19(2), 251–265.

Harper, E. M., Crame, J. A. and Sogot, C. E. (2018) '"Business as usual": Drilling predation across the K-Pg mass extinction event in Antarctica', *Palaeogeography, Palaeoclimatology, Palaeoecology*.

Harries, P. J. and Knorr, P. O. (2009) 'What does the "Lilliput Effect" mean?', *Palaeogeography, Palaeoclimatology, Palaeoecology.*, 284(1–2), 4–10.

He, W., Shi, G. R., Feng, Q., Campi, M. J., Gu, S., Bu, J., Peng, Y. and Meng, Y. (2007) 'Brachiopod miniaturization and its possible causes during the Permian–Triassic crisis in deep water environments, South China', *Palaeogeography, Palaeoclimatology, Palaeoecology*, 252(1–2), 145–163.

Henehan, M. J., Hull, P. M., Penman, D. E., Rae, J. W. B. and Schmidt, D. N. (2016) 'Biogeochemical significance of pelagic ecosystem function: an end-Cretaceous case study', *Philosophical Transactions of the Royal Society B: Biological Sciences*, 371(1694), 20150510.

Herlyn, M., Millat, G. and Petersen, B. (2008) 'Documentation of sites of intertidal blue mussel (Mytilus edulis L.) beds of the Lower Saxonian Wadden Sea, southern North Sea (as of 2003) and the role of their structure for spatfall settlement', *Helgoland Marine Research*, 62(2), 177–188.

Herman, A. B. and Spicer, R. A. (2010) 'Mid-Cretaceous floras and climate of the Russian high Arctic (Novosibirsk Islands, Northern Yakutiya)', *Palaeogeography, Palaeoclimatology, Palaeoecology*, 295(3–4), 409–422.

Herreid, C. F. (1980) 'Hypoxia in invertebrates', *Comparative Biochemistry and Physiology Part A: Physiology*, 67(3), 311–320.

Hollis, C. J., Taylor, K. W. R., Handley, L., Pancost, R. D., Huber, M., Creech, J. B., Hines, B. R., Crouch, E. M., *et al.* (2012) 'Early Paleogene temperature history of the Southwest Pacific Ocean: Reconciling proxies and models', *Earth and Planetary Science Letters*, 349–350, 53–66.

Holt, N. M., García-Veigas, J., Lowenstein, T. K., Giles, P. S. and Williams-Stroud, S. (2014) 'The major-ion composition of Carboniferous seawater',

Geochimica et Cosmochimica Acta, 134, 317–334.

Horita, J., Zimmermann, H. and Holland, H. D. (2002) 'Chemical evolution of seawater during the Phanerozoic', *Geochimica et Cosmochimica Acta*, 66(21), 3733–3756.

Huston, M. A. and DeAngelis, D. L. (1987) 'Size Bimodality in Monospecific Populations: A Critical Review of Potential Mechanisms', *The American Naturalist*. 129(5), 678–707.

Ibach, L. E. J. (1982) 'Relationship between sedimentation rate and total organic carbon content in ancient marine sediments', *AAPG Bulletin*, 66(2), 170–188.

Jablonski, D. and Raup, D. M. (1995) 'Selectivity of end-Cretaceous marine bivalve extinctions', *Science*. 268(5209), 389.

Jeffery, C. H. (2001) 'Heart urchins at the Cretaceous/Tertiary boundary: a tale of two clades', *Paleobiology*, 27(1), 140–158.

Jørgensen, B. B. (1980) 'Seasonal Oxygen Depletion in the Bottom Waters of a Danish Fjord and Its Effect on the Benthic Community', *Oikos*, 34(1), 68.

Keating-Bitonti, C. R., Ivany, L. C., Affek, H. P., Douglas, P. and Samson, S. D. (2011) 'Warm, not super-hot, temperatures in the early Eocene subtropics', *Geology*, 39(8), 771–774.

Keller, G., Abramovich, S., Berner, Z. and Adatte, T. (2009) 'Biotic effects of the Chicxulub impact, K-T catastrophe and sea level change in Texas', *Palaeogeography, Palaeoclimatology, Palaeoecology*, 271(1–2), 52–68.

Kemp, D. B., Robinson, S. a., Crame, J. a., Francis, J. E., Ineson, J., Whittle, R. J., Bowman, V. and O'Brien, C. (2014) 'A cool temperate climate on the Antarctic Peninsula through the latest Cretaceous to early Paleogene', *Geology*, 42(7), 583–586.

Kim, J.-H., van der Meer, J., Schouten, S., Helmke, P., Willmott, V., Sangiorgi, F., Koç, N., Hopmans, E. C., *et al.* (2010) 'New indices and calibrations derived from the distribution of crenarchaeal isoprenoid tetraether lipids: Implications for past sea surface temperature reconstructions', *Geochimica et Cosmochimica Acta*, 74(16), 4639–4654.

Kim, S.-T. and O'Neil, J. R. (1997) 'Equilibrium and nonequilibrium oxygen isotope effects in synthetic carbonates', *Geochimica et Cosmochimica Acta*, 61(16), 3461–3475.

Kirby, M. X. (2001) 'Differences in growth rate and environment between Tertiary and Quaternary Crassostrea oysters', *Paleobiology*, 27(1), 84–103.

Kitchell, J. A., Boggs, C. H., Kitchell, J. F. and Rice, J. A. (1981) 'Prey Selection by naticid gastropods: experimental tests and application to the fossil record', *Paleobiology*. 7(4), 533–552.

Kump, L. R. (1991) 'Interpreting carbon-isotope excursions: Strangelove oceans', *Geology*, 19(4), 299.

Larkin, C. (2014) *Clumped Isotope analysis of Antarctic Molluscs from the Late Cretaceous to Early Paleogene*, *University of Cambridge*.

Little, C. T. S., Birgel, D., Boyce, A. J., Crame, J. A., Francis, J. E., Kiel, S., Peckmann, J., Pirrie, D., *et al.* (2015) 'Late Cretaceous (Maastrichtian) shallow water hydrocarbon seeps from Snow Hill and Seymour Islands, James Ross Basin, Antarctica', *Palaeogeography, Palaeoclimatology, Palaeoecology*, 418, 213–228.

Lockwood, R. (2005) 'Body size, extinction events, and the early Cenozoic record of veneroid bivalves: a new role for recoveries?', *Paleobiology*, 31(4), 578.

Lowenstein, T. K., Hardie, L. A., Timofeeff, M. N. and Demicco, R. V. (2003) 'Secular variation in seawater chemistry and the origin of calcium chloride basinal brines', *Geology*, 31(10), 857–860.

Macellari, C. E. (1988) 'Stratigraphy, sedimentology, and paleoecology of Upper Cretaceous / Paleocene shelf-deltaic sediments of Seymour Island', *Geological Society of America Memoirs*, 169, 25–54.

de Magalhaes, J. P., Costa, J. and Church, G. M. (2007) 'An Analysis of the Relationship Between Metabolism, Developmental Schedules, and Longevity Using Phylogenetic Independent Contrasts', *The Journals of Gerontology Series A: Biological Sciences and Medical Sciences*, 62(2), 149–160.

Markwick, P. J. (1998) 'Fossil crocodilians as indicators of Late Cretaceous and Cenozoic climates: implications for using palaeontological data in reconstructing palaeoclimate', *Palaeogeography, Palaeoclimatology, Palaeoecology*, 137, 205–271.

McClain, C. R., Boyer, A. G. and Rosenberg, G. (2006) 'The island rule and the evolution of body size in the deep sea.', *Journal of Biogeography*, 33, 1578–1584.

Miller, K. G., Kominz, M. A., Browning, J. V, Wright, J. D., Mountain, G. S.,

Katz, M. E., Sugarman, P. J., Cramer, B. S., *et al.* (2005) 'The Phanerozoic record of global sea-level change.', *Science*. American Association for the Advancement of Science, 310(5752), 1293–8.

Newton, R. J., Reeves, E. P., Kafousia, N., Wignall, P. B., Bottrell, S. H. and Sha, J.-G. (2011) 'Low marine sulfate concentrations and the isolation of the European epicontinental sea during the Early Jurassic', *Geology*. Geological Society of America, 39(1), 7–10.

Nordt, L., Atchley, S. and Dworkin, S. (2002) 'Paleosol barometer indicates extreme fluctuations in atmospheric –"CO″ across the Cretaceous-Tertiary boundary', *Geology*, 30(8), 703–706.

Nordt, L., Atchley, S. and Dworkin, S. (2003) 'Terrestrial Evidence for Two Greenhouse Events in the Latest Cretaceous', *GSA Today*, 13(12), 4–9.

O'Dea, A., Håkansson, E., Taylor, P. D. and Okamura, B. (2011) 'Environmental change prior to the K–T boundary inferred from temporal variation in the morphology of cheilostome bryozoans', *Palaeogeography, Palaeoclimatology, Palaeoecology*, 308(3–4), 502–512.

Owens, J. D., Gill, B. C., Jenkyns, H. C., Bates, S. M., Severmann, S., Kuypers, M. M. M., Wood, R. G. and Lyons, T. W. (2013) 'Sulfur isotopes track the global extent and dynamics of euxinia during Cretaceous Oceanic Anoxic Event 2', 110(46).

Passey, B. H. (2012) 'Reconstructing Terrestrial Environments Using Stable Isotopes in Fossil Teeth and Paleosol Carbonates', *The Paleontological Society Papers*. Cambridge University Press, 18, 167–194.

Petersen, S. V., Dutton, A. and Lohmann, K. C. (2016) 'End-Cretaceous extinction in Antarctica linked to both Deccan volcanism and meteorite impact via climate change', *Nature Communications*. Nature Publishing Group, 7(May), 12079.

Poole, I., Cantrill, D. J. and Utescher, T. (2005) 'A multi-proxy approach to determine Antarctic terrestrial palaeoclimate during the Late Cretaceous and Early Tertiary', *Palaeogeography, Palaeoclimatology, Palaeoecology*, 222, 95– 121.

Pucéat, E., Lécuyer, C., Donnadieu, Y., Naveau, P., Cappetta, H., Ramstein, G., Huber, B. T. and Kriwet, J. (2007) 'Fish tooth δ18O revising Late Cretaceous meridional upper ocean water temperature gradients', *Geology*,

35(2), 107–110.

Reeburgh, W. S. (2007) 'Oceanic methane biogeochemistry.', *Chemical reviews*, 107(2), 486–513.

Ridgway, I. D., Richardson, C. A. and Austad, S. N. (2011) 'Maximum shell size, growth rate, and maturation age correlate with longevity in bivalve molluscs.', *The journals of gerontology. Series A, Biological sciences and medical sciences*, 66(2), 183–90.

Riedel, B., Pados, T., Pretterebner, K., Schiemer, L., Steckbauer, A., Haselmair, A., Zuschin, M. and Stachowitsch, M. (2014) 'Effect of hypoxia and anoxia on invertebrate behaviour: Ecological perspectives from species to community level', *Biogeosciences*, 11(6), 1491–1518.

Royer, D. L. (2012) 'Climate Reconstruction from Leaf Size and Shape: New Developments and Challenges', *The Paleontological Society Papers*. 18, 195–212.

Royer, D. L. (2014) 'Atmospheric CO2 and O2 during the Phanerozoic: tools, patterns, and impacts', in *Geochemistry Treatise (Second Edition)*, 251–267.

Royer, D. L., Berner, R. A. and Beerling, D. J. (2001) 'Phanerozoic atmospheric –"CO″ change: evaluating geochemical and paleobiological approaches', *Earth-Science Reviews*, 54(4), 349–392.

Sagasti, A., Schaffner, L. C. and Duffy, J. E. (2001) 'Effects of periodic hypoxia on mortality, feeding and predation in an estuarine epifaunal community', *Journal of Experimental Marine Biology and Ecology*, 258(2), 257–283.

Schoepfer, S. D., Tobin, T. S., Witts, J. D. and Newton, R. J. (2017) 'Intermittent euxinia in the high-latitude James Ross Basin during the latest Cretaceous and earliest Paleocene', *Palaeogeography, Palaeoclimatology, Palaeoecology*. The Authors, 477, 40–54.

Self, S., Widdowson, M., Thordarson, T. and Jay, A. E. (2006) 'Volatile fluxes during flood basalt eruptions and potential effects on the global environment: A Deccan perspective', *Earth and Planetary Science Letters*, 248(1–2), 518–532.

Skazina, M., Sofronova, E. and Khaitov, V. (2013) 'Paving the way for the new generations: Astarte borealis population dynamics in the White Sea', *Hydrobiologia*, 706(1), 35–49.

Smith, A. B. and Jeffery, C. H. (1998) 'Selectivity of extinction among sea urchins at the end of the Cretaceous period', *Nature*, 392(6671), 69–71.

Sogot, C. E., Harper, E. M. and Taylor, P. D. (2014) 'The Lilliput effect in colonial organisms: cheilostome bryozoans at the Cretaceous-Paleogene mass extinction.', *PloS one*, 9(2), e87048.

Spicer, R. a. and Herman, A. B. (2010) 'The Late Cretaceous environment of the Arctic: A quantitative reassessment based on plant fossils', *Palaeogeography, Palaeoclimatology, Palaeoecology*, 295(3–4), 423–442.

Spicer, R. A., Herman, A. B. and Kennedy, E. M. (2004) 'Foliar Physiognomic Record of Climatic Conditions during Dormancy: Climate Leaf Analysis Multivariate Program (CLAMP) and the Cold Month Mean Temperature', *The Journal of Geology*, 112, 685–702.

Spicer, R. A., Herman, A. B., Yang, J., Spicer, T. E. V and Spicer, R. A. (2013) 'Why Future Climate Change is likely to be Underestimated : Evidence from Palaeobotany', *Journal of the Botanical Society of Bengal,* 67(2), 75–88.

Strayer, D. L. and Malcom, H. M. (2006) 'Long-term demography of a zebra mussel (Dreissena polymorpha) population', *Freshwater Biology*. Blackwell Science Ltd, 51(1), 117–130.

Thompson, J. K. and Nichols, F. H. (1988) 'Food availability controls seasonal cycle of growth in Macoma balthica (L.) in San Francisco Bay, California', *Journal of Experimental Marine Biology and Ecology*, 116(1), 43–61.

Timofeeff, M. N., Lowenstein, T. K., da Silva, M. A. M. and Harris, N. B. (2006) 'Secular variation in the major-ion chemistry of seawater: Evidence from fluid inclusions in Cretaceous halites', *Geochimica et Cosmochimica Acta*, 70(8), 1977–1994.

Tobin, T. S. and Ward, P. D. (2015) 'Carbon isotope (δ13C) differences between Late Cretaceous ammonites and benthic mollusks from Antarctica', *Palaeogeography, Palaeoclimatology, Palaeoecology*. Elsevier, 428, 50–57.

Tobin, T. S., Ward, P. D., Steig, E. J., Olivero, E. B., Hilburn, I. A., Mitchell, R. N., Diamond, M. R., Raub, T. D., *et al.* (2012) 'Extinction patterns, δ18 O trends, and magnetostratigraphy from a southern high-latitude Cretaceous–Paleogene section: Links with Deccan volcanism', *Palaeogeography, Palaeoclimatology, Palaeoecology*, 350, 180–188.

Twitchett, R. J. (2007) 'The Lilliput effect in the aftermath of the end-Permian extinction event', *Palaeogeography, Palaeoclimatology, Palaeoecology*, 252(1–2), 132–144.

Upchurch, G. R., Kiehl, J., Shields, C., Scherer, J. and Scotese, C. (2015) 'Latitudinal temperature gradients and high-latitude temperatures during the latest Cretaceous: Congruence of geologic data and climate models', *Geology*, 43(8), 683–686.

Urbanek, A. (1993) 'Biotic crises in the history of Upper Silurian graptoloids: A Palaeobiological model', *Historical Biology*. Taylor & Francis, 7(1), 29–50.

Vaquer-Sunyer, R. and Duarte, C. M. (2008) 'Thresholds of hypoxia for marine biodiversity.', *Proceedings of the National Academy of Sciences of the United States of America*. National Academy of Sciences, 105(40), 15452–7.

Wade, B. S. and Olsson, R. K. (2009) 'Investigation of pre-extinction dwarfing in Cenozoic planktonic foraminifera', *Palaeogeography, Palaeoclimatology, Palaeoecology*, 284(1–2), 39–46.

Wallmann, K. (2001) 'The geological water cycle and the evolution of marine –"oxy" values', *Geochimica et Cosmochimica Acta*, 65(15), 2469–2485.

Wang, T., Surge, D. and Lees, J. M. (2015) 'ClamR: A statistical evaluation of isotopic and temperature records in sclerochronologic studies', *Palaeogeography, Palaeoclimatology, Palaeoecology*, 437, 26–32.

Wang, W. X. and Widdows, J. (1993) 'Metabolic responses of the common mussel Mytilus edulis to hypoxia and anoxia', *Marine Ecology Progress Series*. 205–214.

West, D. L. and Williams, A. H. (1986) 'Predation by Callinectes sapidus (Rathbun) within Spartina alterniflora (Loisel) marshes', *Journal of Experimental Marine Biology and Ecology*, 100(1–3), 75–95.

Wiklund, A.-K. E. and Sundelin, B. (2001) 'Impaired reproduction in the amphipods Monoporeia affinis and Pontoporeia femorata as a result of moderate hypoxia and increased temperature', *Marine Ecology Progress Series*.131–141.

Wilkin, R. T., Barnes, H. L. and Brantley, S. L. (1996) 'The size distribution of framboidal pyrite in modern sediments: An indicator of redox conditions', *Geochimica et Cosmochimica Acta*, 60(20), 3897–3912.

Witts, J. D., Whittle, R. J., Wignall, P. B., Crame, J. A., Francis, J. E., Newton, R. J. and Bowman, V. C. (2016) 'Macrofossil evidence for a rapid and severe Cretaceous–Paleogene mass extinction in Antarctica', *Nature Communications*, 7, 11738.

Wolfe, J. A. (1993) 'A method of obtaining climatic parameters from leaf assemblages', *U.S. Geological Survey Bulletin*, 2040.

Wolfe, J. A. (1995) 'Paleoclimatic estimates from Tertiary leaf assemblages', *Annual Reviews of Earth and Planetary Science*, 23, 119–142.

Wortmann, U. G. and Paytan, A. (2012) 'Rapid Variability of Seawater Chemistry Over the Past 130 Million Years', *Science*, 337(6092), 334–336.

Zachos, J. C, Pagani, M., Sloan, L., Thomas, E. and Billups, K. (2001) 'Trends, rhythms, and aberrations in global climate 65 Ma to present.', *Science*, 292(5517), 686–93.

Zachos, J. C., Arthur, M. A. and Dean, W. E. (1989) 'Geochemical and paleoenvironmental variations across the Cretaceous/Tertiary boundary at Braggs, Alabama', *Palaeogeography, Palaeoclimatology, Palaeoecology*, 69, 245–266.

APPENDIX A

Field Seasons and Collection Data

Zinsmeister Collection

Additional measurements and specimens were acquired from the W. J. Zinsmeister Collection housed in the Palaeontological Research Institution, NY. The collection was assembled from three decades of spot collections, mapped by location rather than collected along a continuous stratigraphic section. In order to back-calculate the approximate stratigraphic height of specimens, dip correction calculations must be utilised from accurate geological maps (e.g. Petersen et al. 2016). These calculations involve a large amount of extrapolation, and have been known to yield stratigraphic heights for fossils which are well outside of the stratigraphic ranges established from other sections (Figure 4.10). As a result, specimens from this collection may only be positioned approximately within stratigraphy.

Preservation Test Methods

Scanning Electron Microscopy

Shell fragments were prepared for SEM in cross section within polyester resin blocks which were polished to P1000 grade and etched in 1% HCl for 20 seconds before being ultrasonically cleaned and mounted on stubs. Fractured surfaces were also prepared similarly by etching, cleaning and mounting. All specimens were gold-coated using an Emitech K550 sputter coater and viewed with a Jeol JSM 820 electron microscope at the University of Cambridge.

Cathodoluminescence

Cold cathode CL work to image uncovered shell sections was undertaken at the University of Edinburgh using a CITL 8200 Mk 3A mounted on a Nikon Optiphot petrological microscope.

X-Ray Diffraction

Shell powders collected by micromilling were prepared for XRD by grinding dry, then with acetone in a pestle and mortar to produce a uniform powder which was wetted with acetone to form a thin paste and spread onto glass sample discs to produce a uniform flat surface when air-dried. XRD analyses at the University of Cambridge used a Bruker D8 diffractometer scanning from 20° to 60° with a 0.02° step size. Results were interpreted using Topas software. Analysis of the crossed-lamellar layers show strong peaks at diffraction angles (2θ) of 26.2° and 27.2° and minor peaks at angles of 33.2° and 36.2°, indicative of aragonite mineralogy.

Dataset A.1: Specimens used for experimental analysis

Specimen No.	Species	Height relative to KPB (m)	Height on composite section (m)	Preservation tests	Longevity	Stable Isotope Analysis	Number of microsamples analysed
DJ.953.1025	*L. larseni/huberi*	29.25	1036.8		Acetate Peel	Bulk	4
D5.229.1320.2	*L. larseni/huberi*	24.5	1032		Acetate Peel	Bulk	5
DJ.953.745	*L. larseni/huberi*	-1.75	1005.8		Acetate Peel	Bulk	4
DJ.953.663	*L. larseni/huberi*	-17.5	990		Acetate Peel	Bulk	4
D5.222.1226.2B	*L. larseni/huberi*	-66.5	941			Bulk	3
D5.220.1217.2	*L. larseni/huberi*	-86.5	921	SEM	Acetate Peel	Bulk	3
DJ.952.516	*L. larseni/huberi*	-137.45	870.1	SEM, XRD		Bulk	30
DJ.952.529	*L. larseni/huberi*	-137.45	870.1	XRD		Bulk	30
D5.218.1011.2	*C. antarctica*	-378.5	629			Bulk	7
D9.211.457	*C. ellioti*	99.3	1106.8	SEM		Micro	12
D9.207.1	*L. larseni/huberi*	18.9	1026.4	XRD		Micro	52
D5.229.1301.2	*L. larseni/huberi*	5.5	1013			Micro	30
D9.206.152	*L. larseni/huberi*	3.5	1011			Micro	41
DJ.953.746	*L. larseni/huberi*	-1.75	1005.8			Micro	42
D5.222.1248.2	*C. antarctica*	-32.5	975			Micro	6
DJ.953.335	*L. larseni/huberi*	-48.25	959.3			Micro	28
DJ.953.456	*L. larseni/huberi*	-48.25	959.3	CL		Micro	49
DJ.953.459	*C. antarctica*	-48.25	959.3			Micro	18
D5.222.1234.2	*L. larseni/huberi*	-56.5	951			Micro	13
D5.222.1226.2A	*L. larseni/huberi*	-66.5	941			Micro	12
D5.222.1223.2	*C. antarctica*	-74.5	933	SEM		Micro	5
D5.220.1214.2	*L. larseni/huberi*	-92.5	915		Acetate Peel	Micro	7
D5.220.1229.2	*C. antarctica*	-122	885.5			Micro	8
DJ.952.523	*L. larseni/huberi*	-137.45	870.1			Micro	37

Specimen No.	Species	Height relative to KPB (m)	Height on composite section (m)	Preservation tests	Longevity	Stable Isotope Analysis	Number of microsamples analysed
D5.219.1185.2	*L. larseni/huberi*	-142.5	865	SEM, XRD		Micro	21
D5.219.1182.2	*L. larseni/huberi*	-148.5	859			Micro	61
DJ.957.490	*C. antarctica*	-233.75	773.8			Micro	10
DJ.959.93	*C. antarctica*	-392.25	615.3			Micro	11
D5.229.1334.2	*L. larseni/huberi*	39.5	1047		Thin section		
D5.229.1351.2	*L. larseni/huberi*	48	1055.5		Acetate peel		
D5. 229.1361.2	*L. larseni/huberi*	55.5	1063				
D5.229.1361.2	*L. larseni/huberi*	55.5	1063		Acetate peel		
D5.229.1361.2	*L. larseni/huberi*	55.5	1063		Acetate peel		
D5.229.1363.2	*L. larseni/huberi*	56.5	1064		Acetate peel		
DJ.953.915	*L. larseni/huberi*	29.25	1036.75		Thin section		
D9.206.95	*L. larseni/huberi*	-1.5	1006	CL	Thin Section		
DJ.953.799	*L. larseni/huberi*	2.5	1010		Acetate peel		
DJ.953.334	*L. larseni/huberi*	-48.25	959.25		Acetate peel		
DJ.953.452	*L. larseni/huberi*	-48.25	959.25		Acetate peel		
DJ.952.712	*L. larseni/huberi*	-98.75	908.75		Acetate peel		
DJ.952.755	*L. larseni/huberi*	-98.75	908.75		Acetate peel		
D5.219.1185.2 B	*L. larseni/huberi*	-142.5	865	SEM, XRD	Thin Section		
3 Danian Hinges D001-D003	*L. larseni/huberi*	Unknown	N/A		Acetate Peel		

APPENDIX B

Taxonomy

Antarctic examples of *Lahillia* (Classification: Mollusca, Bivalvia, Cardiida, Cardiidae) have traditionally been split into two species although taxonomy is currently under review (R.J. Whittle pers. comm. 2015) – *Lahillia larseni* (Sharman & Newton 1897) for specimens in the Lopez de Bertodano Formation and *L. huberi* (Zinsmeister & Macellari 1988) in the Sobral Formation.

Cucullaea (Classification: Mollusca, Bivalvia, Arcoida) are more definitively split. *Cucullaea antarctica* (Wilckens 1907) is present in the upper Maastrichtian of the Lopez de Bertodano Formation. *Cucullaea elliotti* (Zinsmeister & Macellari 1988) which has been found shortly after the boundary, in the Danian of the Lopez de Bertodano Formation and into the Sobral Formation. *Cucullaea raea* (Zinsmeister 1984) and *Cucullaea donaldi* (Sharman and Newton 1894) are found in the lower (I and II) and upper (III) Eocene La Meseta formations respectively.

Leionucula taxa (Classification: Mollusca, Bivalvia, Palaeotaxodonta, Nuculoida, Nuculoidea, Nuculidae, Nuculinae, Nucula (Stilwell et al. 2004) are also easily distinguished; *Leionucula suboblongata* (Wilckens 1907) are present from the Lopez de Bertodano molluscan units to the middle of unit 1 of the Sobral formation, *Leionucula hunickeni* (Zinsmeister & Macellari 1988) are also present in the middle part of unit 1 of the Sobral Formation. Leionucula nova (Wilckens 1911) and *Leionucula palmeri* (Zinsmeister 1984) occur in the Eocene La Meseta, the former has been found in units I-II and the latter only from unit I.

Acetate Peels Method

Hinges were embedded in polyester resin for stabilization and each specimen was sectioned along the axis of maximum growth, ground and polished for production of acetate peels following the procedure described by Kennish et al (1980) with the modification of etching with a 1% HCl solution for 20 seconds. The acetate peels were examined under transmitted light microscope and photographed to produce composites to visualise the entire tooth at high magnification. Sucessive growth lines were marked and measured along the path of maximum tooth growth using ImageJ.

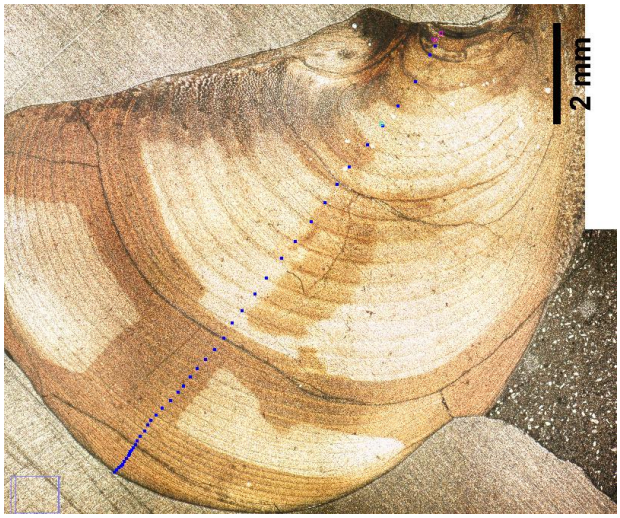

Figure B.1: Example of growth line measurements produced from an acetate peel of a bivalve tooth.

Dataset B.1: Summary of stable isotope data and high and low estimate converted temperatures from bulk and microsampled specimens

Specimen No.	Species	Height relative to KPB (m)	Height on composite section (m)	Stable Isotope Analysis	Number of microsamples	$\delta^{18}O$ minimum (‰V-PDB)	$\delta^{18}O$ maximum (‰V-PDB)	$\delta^{18}O$ range (‰V-PDB)	$\delta^{18}O$ average (‰V-PDB)	$\delta^{13}C$ minimum (‰V-PDB)	$\delta^{13}C$ maximum (‰V-PDB)	$\delta^{13}C$ range (‰V-PDB)	$\delta^{13}C$ average (‰V-PDB)	MAT_Low (°C)	MAT_High (°C)
DJ.953.1025	*L. larseni /huberi*	29.25	1036.8	Bulk	4	0.7	1.03		0.87	1.37	1.72		1.54	9.4	12.1
D5.229.1320.2	*L. larseni /huberi*	24.5	1032	Bulk	5	0.6	0.76		0.68	1.66	2.43		2.01	10.3	13.0
DJ.953.745	*L. larseni /huberi*	-1.75	1005.8	Bulk	4	0.79	1.23		1.06	-1.11	2.74		1.29	8.6	11.2
DJ.953.663	*L. larseni /huberi*	-17.5	990	Bulk	4	1.13	1.31		1.21	2.51	2.7		2.6	8.0	10.5
D5.222.1226.2B	*L. larseni /huberi*	-66.5	941	Bulk	3	0.63	0.86		0.76	-1.34	-0.66		-0.92	9.9	12.6
D5.220.1217.2	*L. larseni /huberi*	-86.5	921	Bulk	3	-0.07	0.44		0.2	-0.96	-0.05		-0.53	12.4	15.2
DJ.952.516	*L. larseni /huberi*	-137.45	870.1	Bulk	30	1.42	1.77		1.59	-0.26	1.01		0.378	6.3	8.7
DJ.952.529	*L. larseni /huberi*	-137.45	870.1	Bulk	30	1.54	2.12		1.88	0.13	2.34		1.08	5.1	7.4
D5.218.1011.2	*C. antarctica*	-378.5	629	Bulk	7	0.02	1.18		0.46	-15.14	-9.78		-11.76	11.2	14.0
D9.211.457	*C. ellioti*	99.3	1106.8	Micro	12	-0.24	0.21	0.45	0.04	3.15	6.35	3.2	4.18	13.0	16.0
D9.207.1	*L. larseni /huberi*	18.9	1026.4	Micro	52	-0.78	0.03	0.81	-0.41	-7.81	2.13	9.94	-2.74	15.0	18.1
D5.229.1301.2	*L. larseni /huberi*	5.5	1013	Micro	30	0.77	1.53	0.76	1.08	-12.01	0	12.01	-6.33	8.5	11.1
D9.206.152	*L. larseni /huberi*	3.5	1011	Micro	41	-3.06	1.05	4.11	-0.52	0.57	6.35	5.77	4.23	15.5	18.6
DJ.953.746	*L. larseni /huberi*	-1.75	1005.8	Micro	42	1.39	1.89	0.5	1.6	0.9	1.68	0.78	1.24	6.3	8.7
D5.222.1248.2	*C. antarctica*	-32.5	975	Micro	6	0.4	0.67	0.28	0.56	-1.79	13.68	15.46	-1.4	10.8	13.5
DJ.953.335	*L. larseni /huberi*	-48.25	959.3	Micro	28	0.77	1.46	0.69	1.13	-18.14	-2.42	15.72	-10.67	8.3	10.9
DJ.953.456	*L. larseni /huberi*	-48.25	959.3	Micro	49	0.91	1.38	0.47	1.12	-34.18	-10.7	23.48	-23.78	8.4	10.9
DJ.953.459	*C. antarctica*	-48.25	959.3	Micro	18	0.57	1.71	1.14	1.1	-22.82	-1.8	21.02	-11.26	8.4	11.0
D5.222.1234.2	*L. larseni /huberi*	-56.5	951	Micro	13	-1.18	0.67	1.84	-0.12	-15.26	2.66	17.92	-2.84	13.7	16.7
D5.222.1226.2A	*L. larseni /huberi*	-66.5	941	Micro	12	-1.41	0.92	2.32	-0.61	-26.27	-4.93	21.34	-17.29	15.9	19.0

Specimen No.	Species	Height relative to KPB (m)	Height on composite section (m)	Stable Isotope Analysis	Number of microsamples	$\delta^{18}O$ minimum (‰V-PDB)	$\delta^{18}O$ maximum (‰V-PDB)	$\delta^{18}O$ range (‰V-PDB)	$\delta^{18}O$ average (‰V-PDB)	$\delta^{13}C$ minimum (‰V-PDB)	$\delta^{13}C$ maximum (‰V-PDB)	$\delta^{13}C$ range (‰V-PDB)	$\delta^{13}C$ average (‰V-PDB)	MAT_Low (°C)	MAT_High (°C)
D5.222.1223.2	*C. antarctica*	-74.5	933	Micro	5	0.72	1.1	0.38	0.86	1.8	2.39	0.59	2.12	9.5	12.1
D5.220.1214.2	*L. larseni /huberi*	-92.5	915	Micro	7	1.08	1.55	0.47	1.36	-1.38	-0.56	0.81	-1.03	7.3	9.8
D5.220.1229.2	*C. antarctica*	-122	885.5	Micro	8	-0.59	-0.09	0.5	-0.33	-0.84	-0.29	0.55	-0.54	14.7	17.7
DJ.952.523	*L. larseni /huberi*	-137.45	870.1	Micro	37	1.33	2.12	0.8	1.68	-0.71	1.511	2.223	0.313	5.9	8.3
D5.219.1185.2	*L. larseni /huberi*	-142.5	865	Micro	21	0.33	1.21	0.88	0.81	-0.97	1.85	2.82	0.69	9.7	12.4
D5.219.1182.2	*L. larseni /huberi*	-148.5	859	Micro	61	-0.89	1.59	2.49	0.73	0.29	2.43	2.139	1.57	10.1	12.7
DJ.957.490	*C. antarctica*	-233.75	773.8	Micro	10	0.28	0.58	0.3	0.47	-2.55	-2.12	0.425	-2.3	11.2	14.0
DJ.959.93	*C. antarctica*	-392.25	615.3	Micro	11	0.14	1.05	0.91	0.71	-3.06	0.26	3.325	-0.45	10.1	12.8

Figure B.2: Micromilled shell $\delta^{18}O$ and $\delta^{13}C$ data.

Stable carbon (black) and oxygen isotope data (red). Distance axis begins at an arbitrary point within the shell. Vertical gray bars locate positions of annual growth lines. $\delta^{13}C$ data presented to the same scale on the top/left axis and an expanded scale (dotted black line) on the right axis to show lower amplitude trends and variability where appropriate.

Cross plots and first difference plots of $\delta^{18}O$ and $\delta^{13}C$ data from each shell have also been plotted and show little evidence for either consistent correlation or anticorrelation patterns across the entire set of shells. Specimen number, height relative to the K-Pg boundary and taxon has been labelled for each specimen.

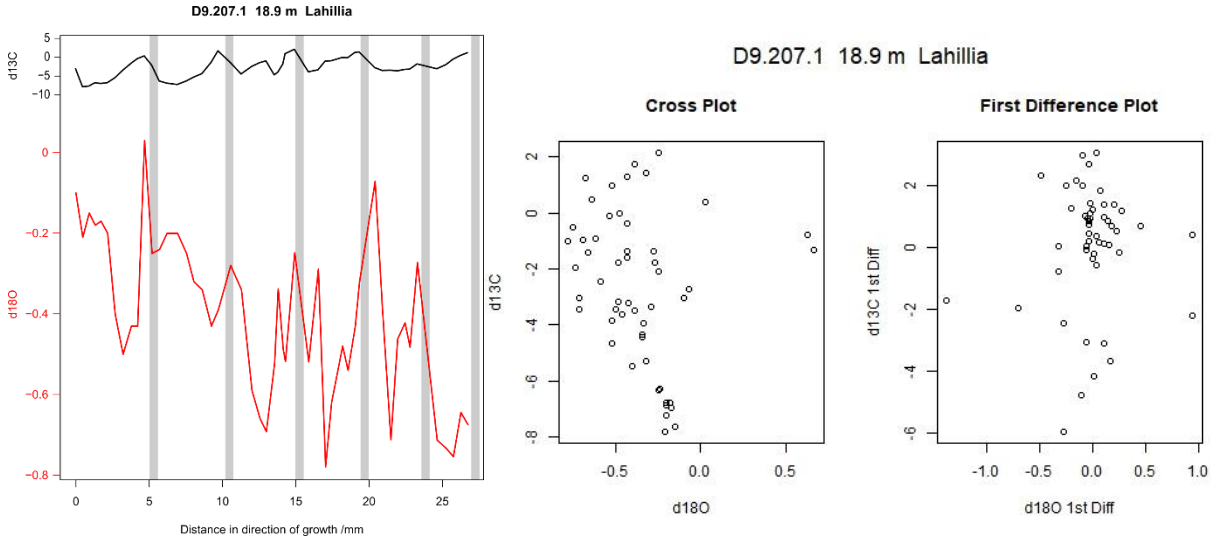

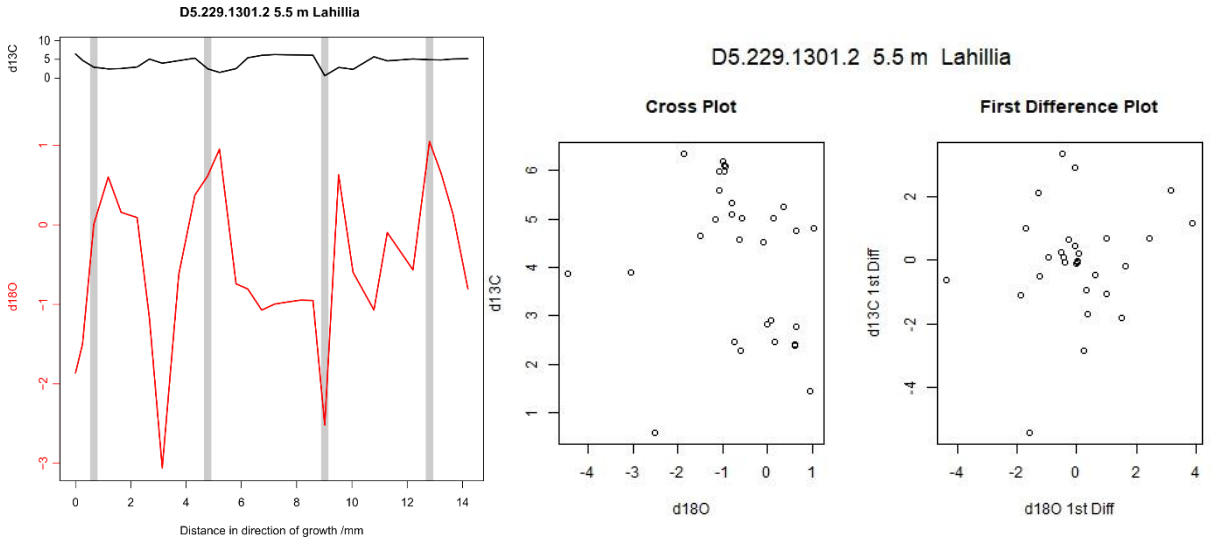

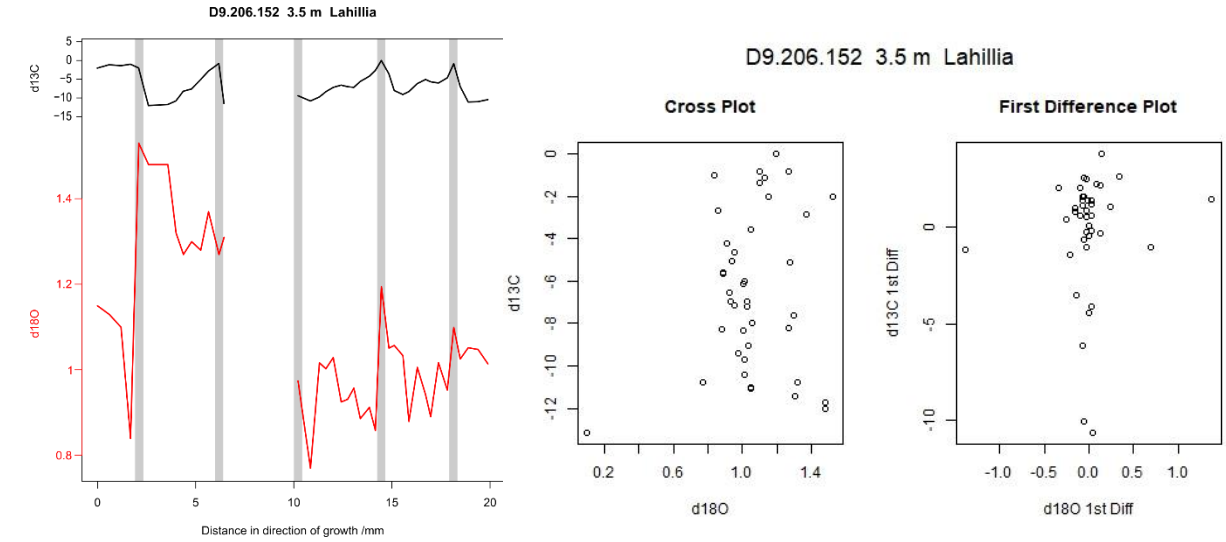
D9.206.152 3.5 m Lahillia
d13C
d18O
Distance in direction of growth /mm
D9.206.152 3.5 m Lahillia
Cross Plot
First Difference Plot
d13C
d18O
d13C 1st Diff
d18O 1st Diff

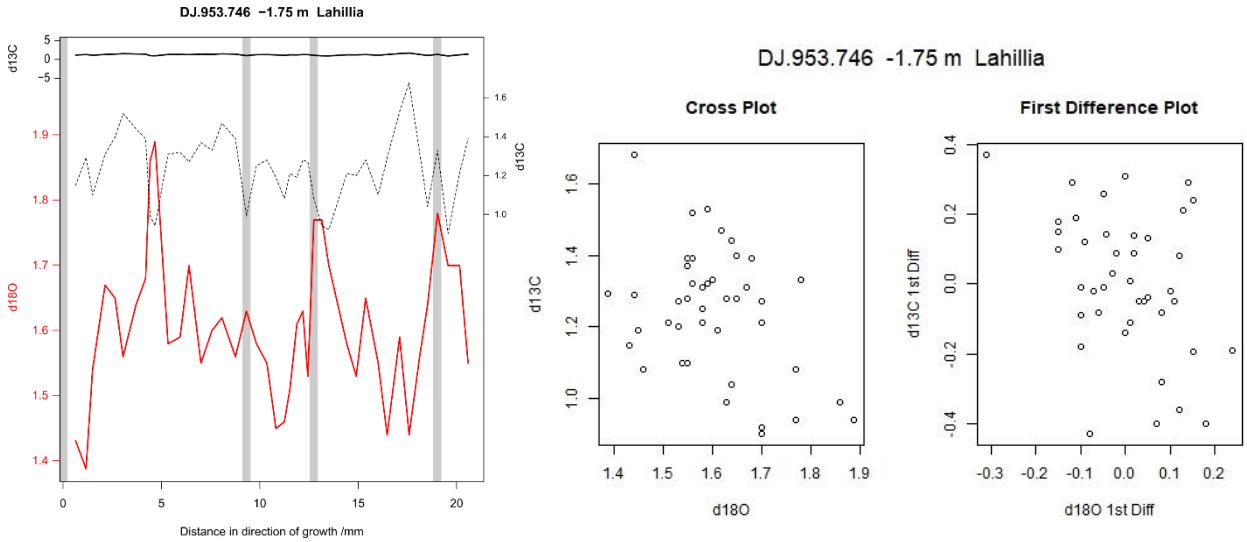
DJ.953.746 −1.75 m Lahillia
d13C
d18O
Distance in direction of growth /mm
DJ.953.746 -1.75 m Lahillia
Cross Plot
First Difference Plot
d13C
d18O
d13C 1st Diff
d18O 1st Diff

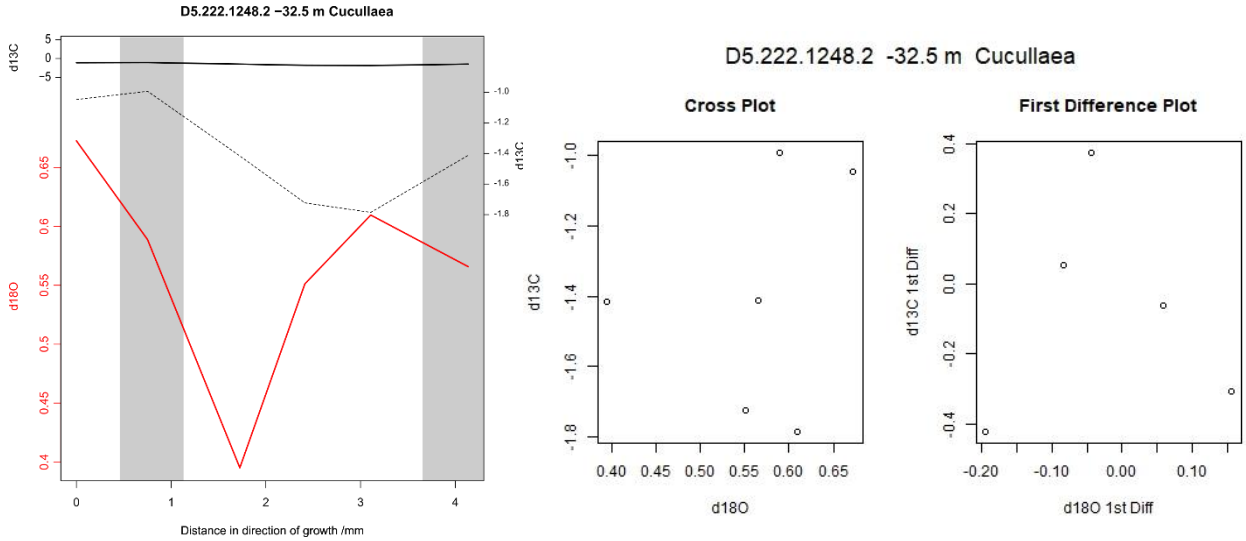
D5.222.1248.2 −32.5 m Cucullaea
d13C
d18O
Distance in direction of growth /mm
D5.222.1248.2 -32.5 m Cucullaea
Cross Plot
First Difference Plot
d13C
d18O
d13C 1st Diff
d18O 1st Diff

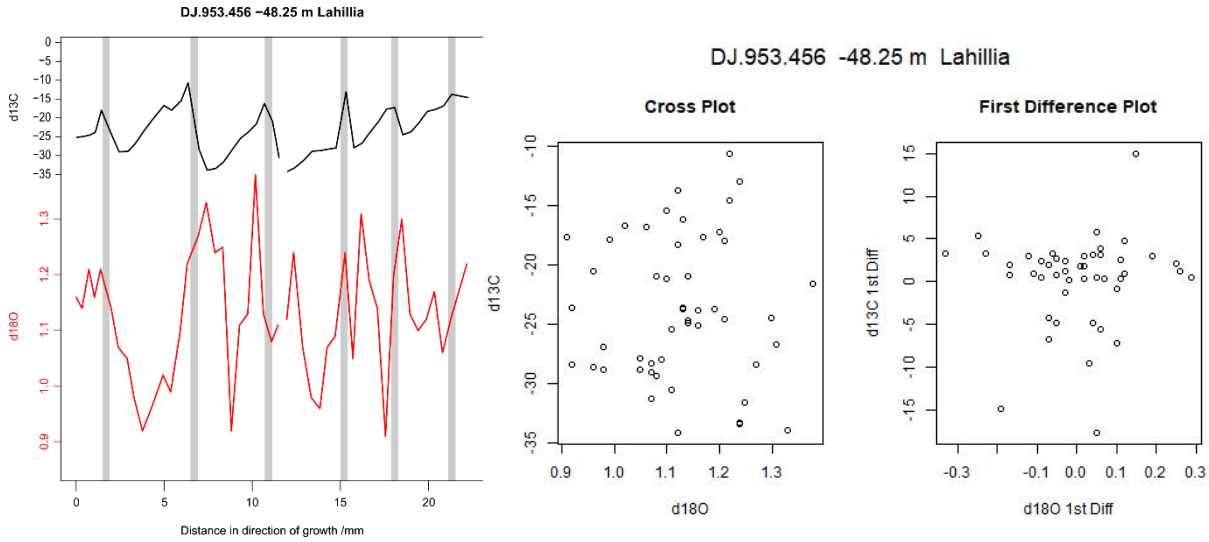
DJ.953.456 −48.25 m Lahillia
d13C
d18O
Distance in direction of growth /mm
DJ.953.456 -48.25 m Lahillia
Cross Plot
First Difference Plot
d13C
d18O
d13C 1st Diff
d18O 1st Diff

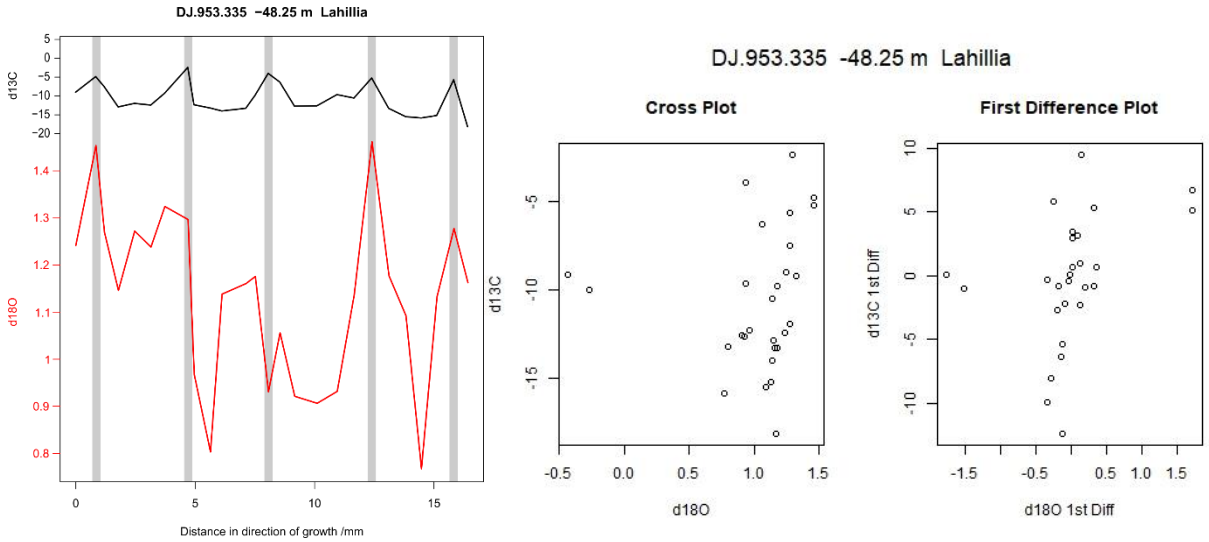
DJ.953.335 −48.25 m Lahillia
d13C
d18O
Distance in direction of growth /mm
DJ.953.335 -48.25 m Lahillia
Cross Plot
First Difference Plot
d13C
d18O
d13C 1st Diff
d18O 1st Diff

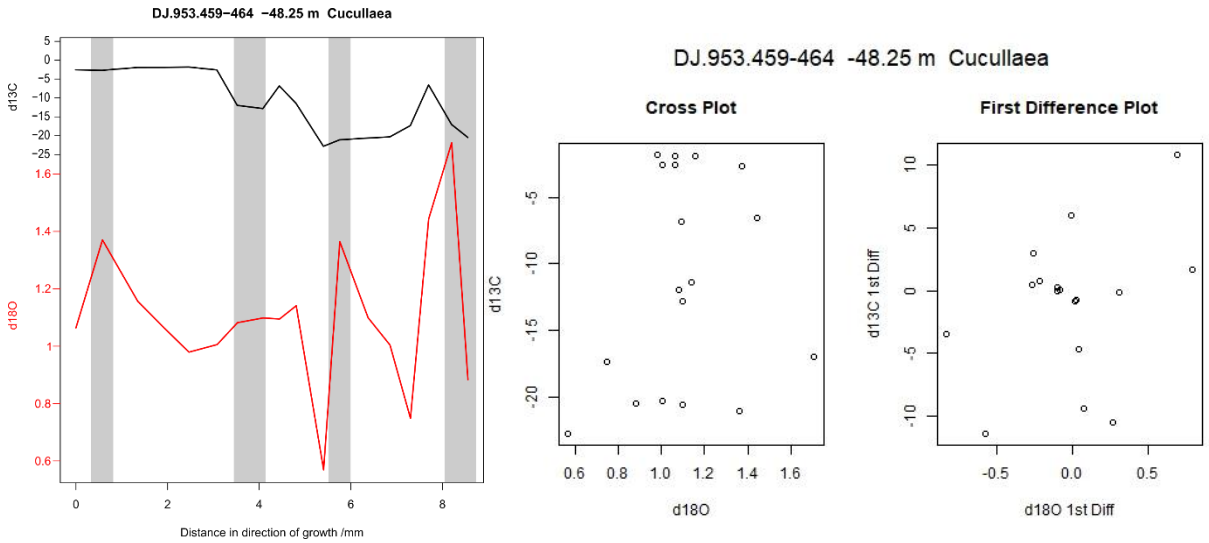
DJ.953.459−464 −48.25 m Cucullaea
d13C
d18O
Distance in direction of growth /mm
DJ.953.459-464 -48.25 m Cucullaea
Cross Plot
First Difference Plot
d13C
d18O
d13C 1st Diff
d18O 1st Diff

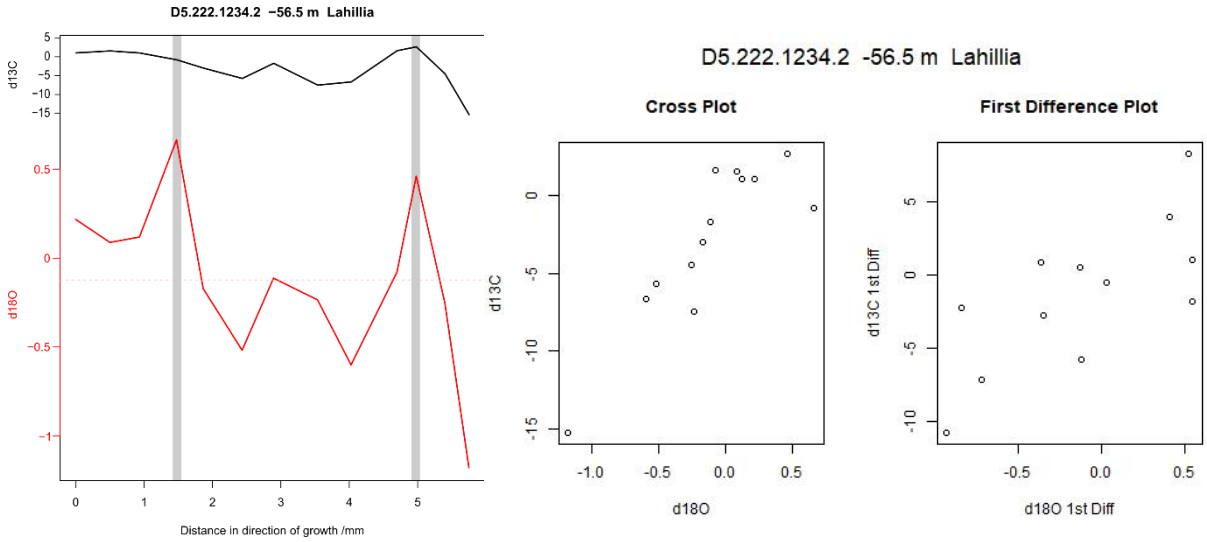
D5.222.1234.2 −56.5 m Lahillia
d13C
d18O
Distance in direction of growth /mm
D5.222.1234.2 -56.5 m Lahillia
Cross Plot
d13C
d18O
First Difference Plot
d13C 1st Diff
d18O 1st Diff

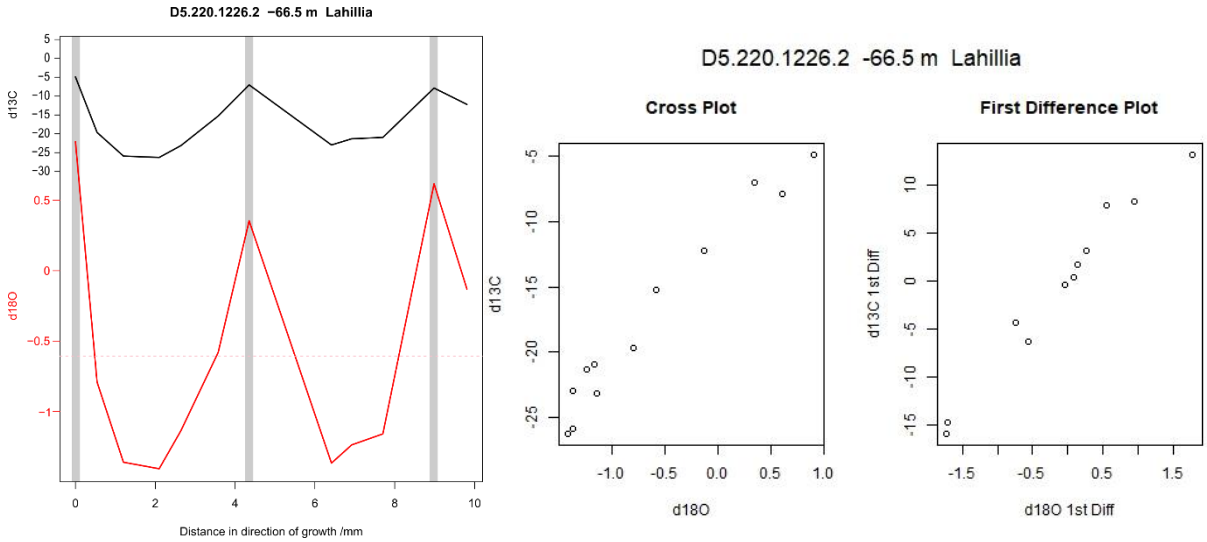
D5.220.1226.2 −66.5 m Lahillia
d13C
d18O
Distance in direction of growth /mm
D5.220.1226.2 -66.5 m Lahillia
Cross Plot
d13C
d18O
First Difference Plot
d13C 1st Diff
d18O 1st Diff

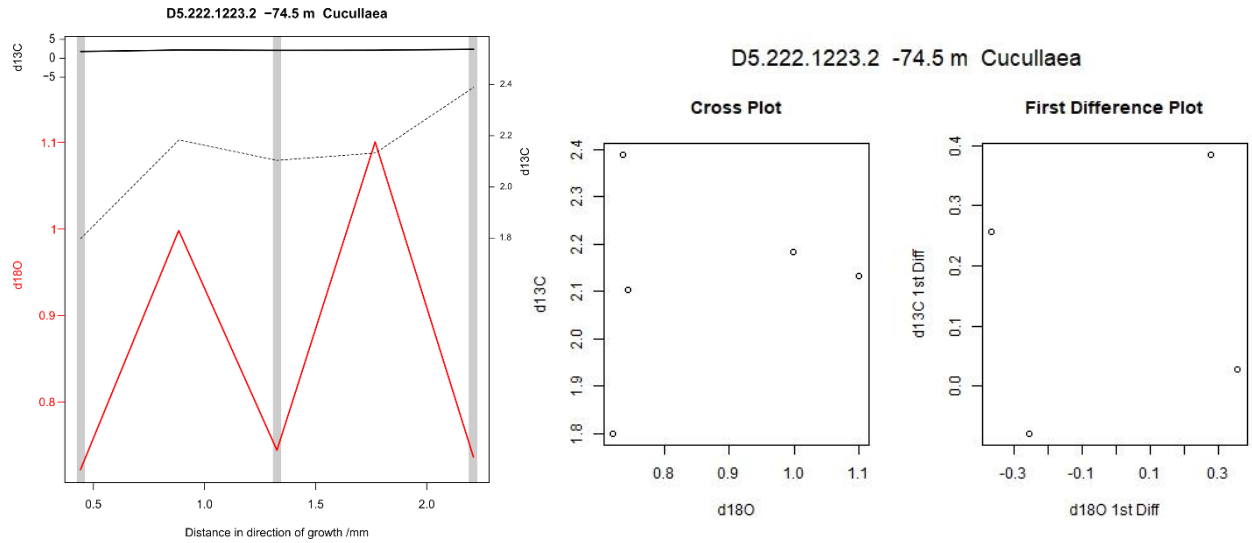
D5.222.1223.2 −74.5 m Cucullaea
d13C
d18O
Distance in direction of growth /mm
D5.222.1223.2 -74.5 m Cucullaea
Cross Plot
d13C
d18O
First Difference Plot
d13C 1st Diff
d18O 1st Diff

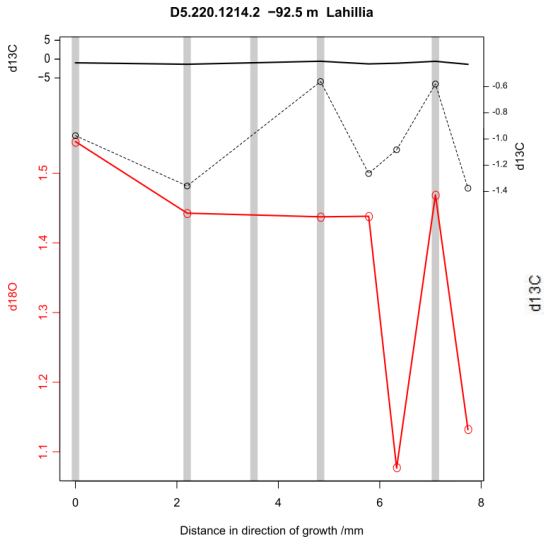
D5.220.1214.2 −92.5 m Lahillia
d13C
d18O
Distance in direction of growth /mm

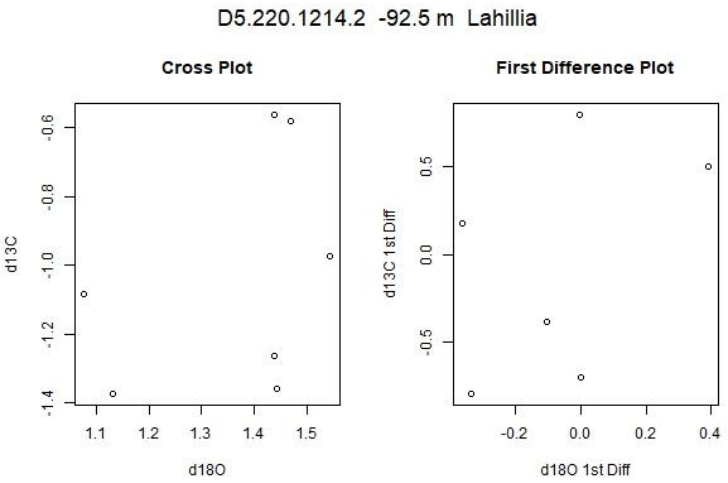
D5.220.1214.2 -92.5 m Lahillia
Cross Plot
First Difference Plot
d13C
d18O
d13C 1st Diff
d18O 1st Diff

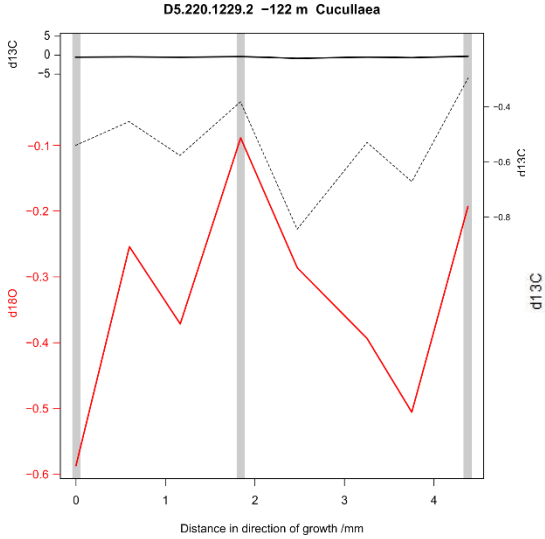
D5.220.1229.2 −122 m Cucullaea
d13C
d18O
Distance in direction of growth /mm

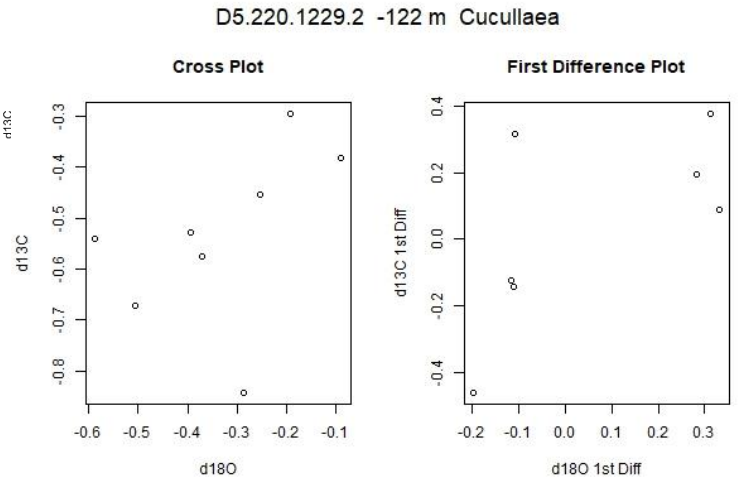
D5.220.1229.2 -122 m Cucullaea
Cross Plot
First Difference Plot
d13C
d18O
d13C 1st Diff
d18O 1st Diff

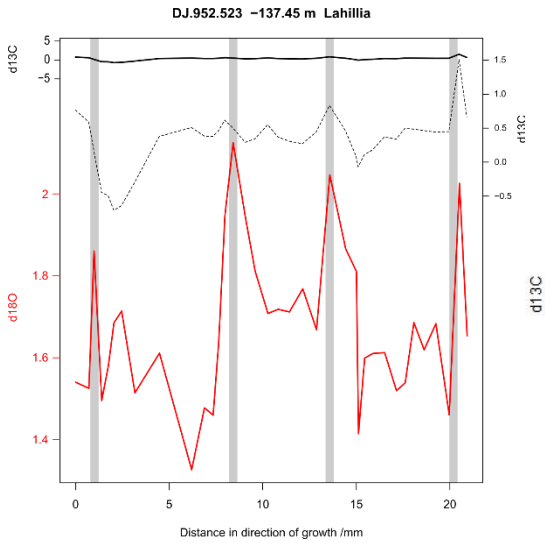
DJ.952.523 −137.45 m Lahillia
d13C
d18O
Distance in direction of growth /mm

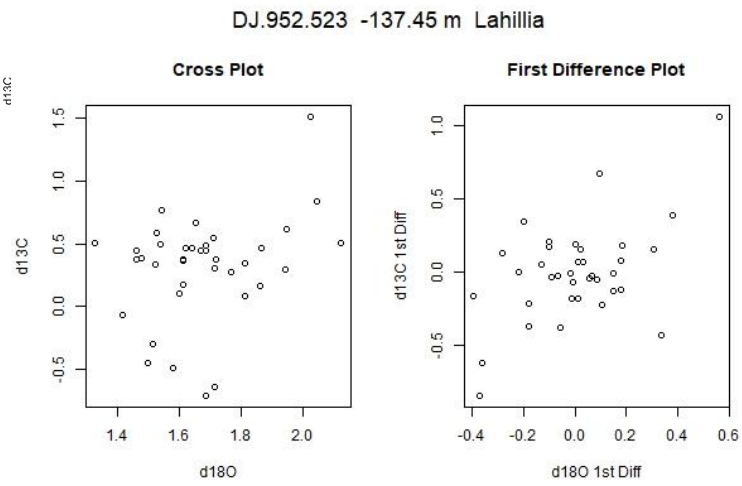
DJ.952.523 -137.45 m Lahillia
Cross Plot
First Difference Plot
d13C
d18O
d13C 1st Diff
d18O 1st Diff

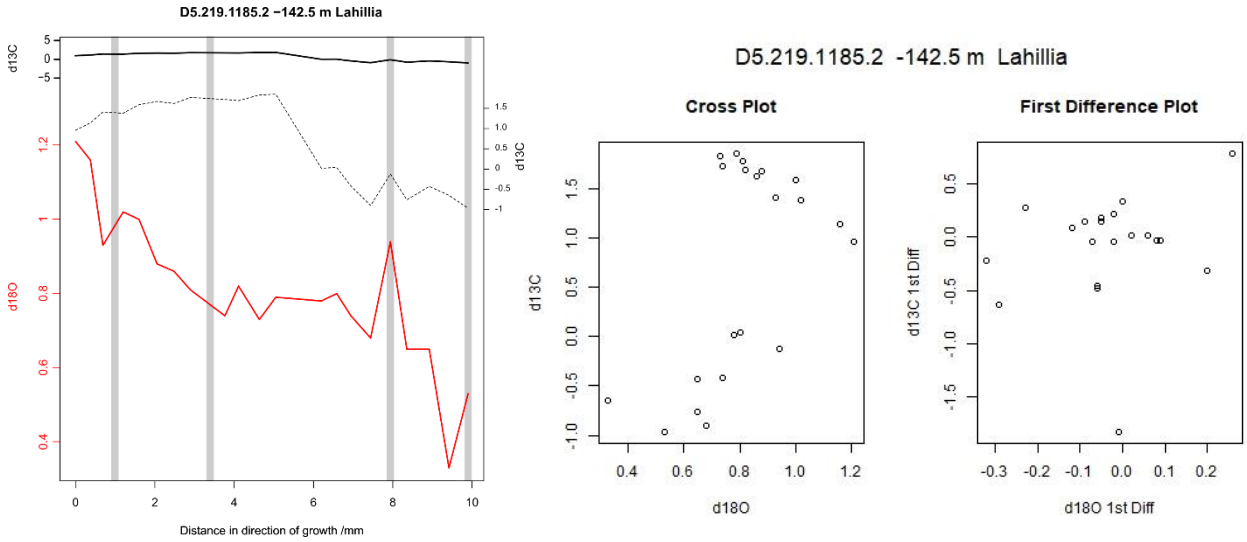
D5.219.1185.2 −142.5 m Lahillia
d13C
d18O
Distance in direction of growth /mm
D5.219.1185.2 -142.5 m Lahillia
Cross Plot
First Difference Plot
d13C
d18O
d13C 1st Diff
d18O 1st Diff

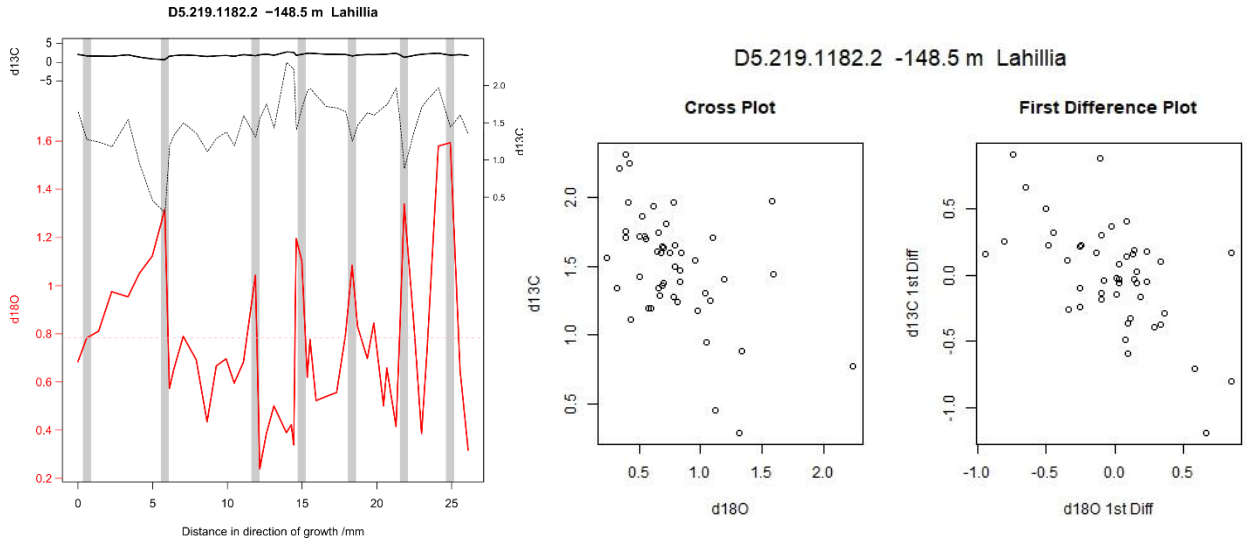
D5.219.1182.2 −148.5 m Lahillia
d13C
d18O
Distance in direction of growth /mm
D5.219.1182.2 -148.5 m Lahillia
Cross Plot
First Difference Plot
d13C
d18O
d13C 1st Diff
d18O 1st Diff

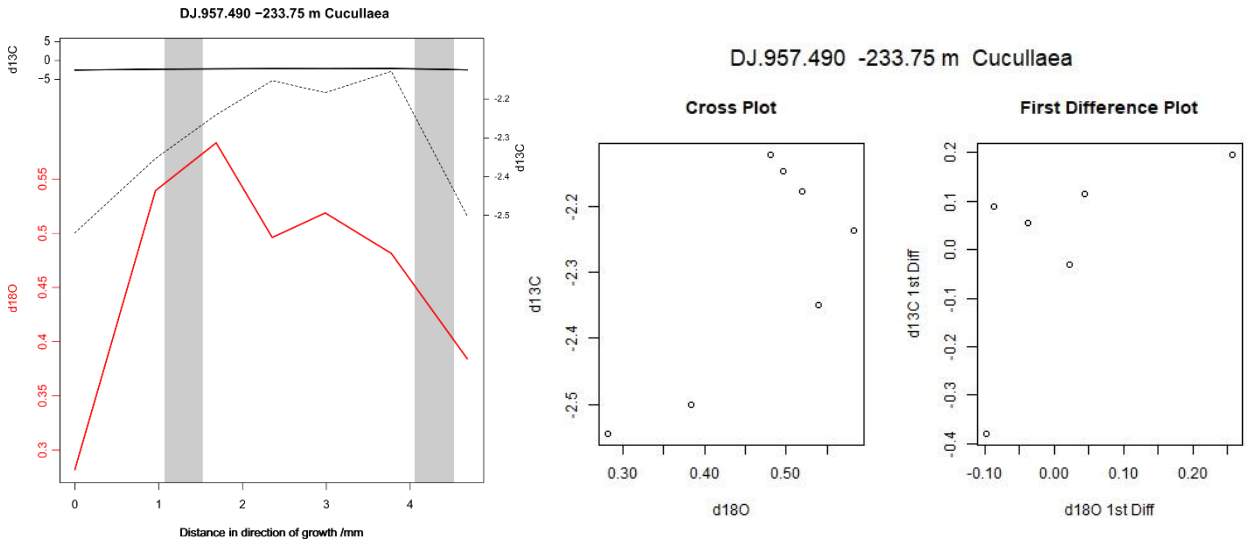
DJ.957.490 −233.75 m Cucullaea
d13C
d18O
Distance in direction of growth /mm
DJ.957.490 -233.75 m Cucullaea
Cross Plot
First Difference Plot
d13C
d18O
d13C 1st Diff
d18O 1st Diff

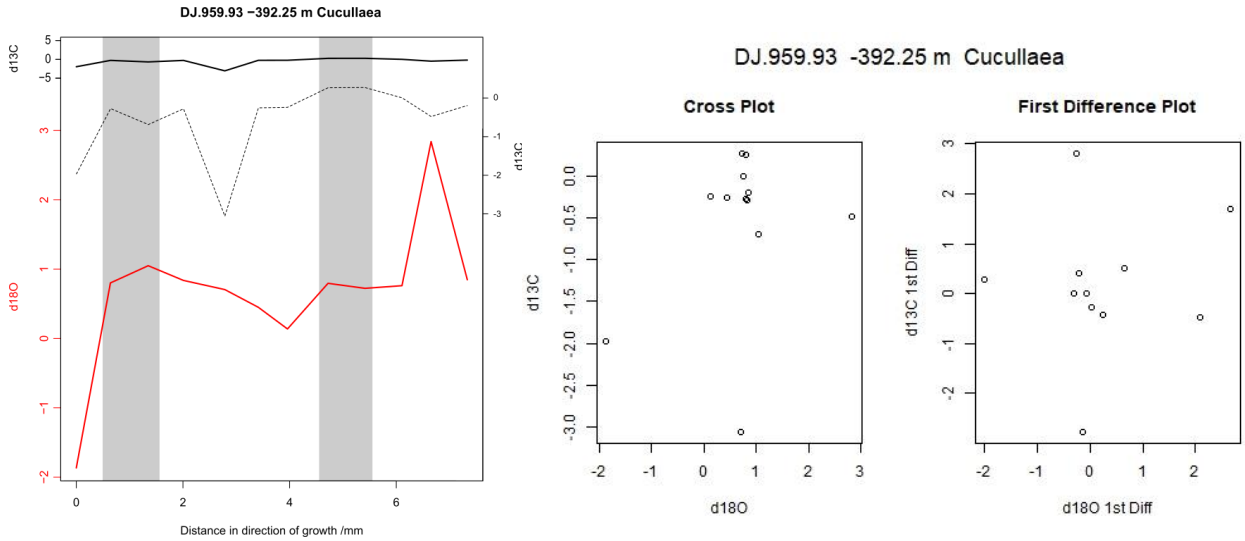
DJ.959.93 −392.25 m Cucullaea
d13C
d18O
d13C
Distance in direction of growth /mm
DJ.959.93 -392.25 m Cucullaea
Cross Plot
d13C
d18O
First Difference Plot
d13C 1st Diff
d18O 1st Diff

Dataset B.2: High resolution microsampled bivalve stable isotope raw data set

D5.219.1182.2 *Lahillia* -148.5

SIRA_Number	Distance	Number	d18OCalcite	d18O_Raw	d18O	d13C	TMollusc
G14 1643	0	1	0.605	9.670481	0.684336	1.6434	12.96246
G14 1644	0.5811	2	0.7032	9.769571	0.782544	1.275	12.50187
G14 1645	1.3818	3	0.7316	9.798228	0.810946	1.2406	12.36866
G14 1646	2.2548	4	0.8954	9.963512	0.974759	1.1784	11.60038
G14 1647	3.3428	5	0.874	9.941918	0.953357	1.5436	11.70075
G14 1648	4.1049	6	0.9708	10.0396	1.050165	0.9496	11.24673
G14 1649	4.9756	7	1.044	10.11346	1.123371	0.4556	10.90339
G14 1650	5.8101	8	1.2368	10.30801	1.316186	0.2874	9.999087
G14 1651	6.1182	9	0.4936	9.558072	0.572927	1.197	13.48497
G14 1652	6.4263	10	0.5762	9.64142	0.655534	1.3388	13.09755
G14 1653	7.0436	11	0.71	9.776433	0.789344	1.4972	12.46998
G14 1654	7.9143	12	0.6126	9.67815	0.691937	1.3566	12.92682
G14 1655	8.6402	13	0.3552	9.418418	0.434516	1.1128	14.13412
G14 1656	9.2575	14	0.5876	9.652924	0.666935	1.2916	13.04408
G14 1657	9.911	15	0.6166	9.682186	0.695937	1.3764	12.90806
G14 1658	10.4559	16	0.516	9.580675	0.595329	1.1918	13.37991
G14 1659	11.0732	17	0.6032	9.668665	0.682536	1.5958	12.97091
G14 1660	11.8739	18	0.9634	10.03213	1.042764	1.3052	11.28144
G14 1661	12.1661	19	0.1596	9.221046	0.238901	1.563	15.05156
G14 1662	12.6026	20	0.3054	9.368167	0.384712	1.7534	14.3677
G14 1663	13.1114	21	0.421	9.484814	0.500321	1.4282	13.82549
G14 1666	13.9459	24	0.3102	9.37301	0.389513	2.3106	14.34519
S14 1051	14.2741	25	0.342414	9.405516	0.421729	2.248895	14.19409
S14 1052	14.4382	26	0.259269	9.321618	0.338578	2.211712	14.58407
S14 1053	14.6023	27	1.11595	10.18606	1.195327	1.404372	10.56592
S14 1054	14.9798	28	1.022811	10.09208	1.102181	1.709966	11.00277
S14 1055	15.3441	29	0.539737	9.604628	0.619068	1.932432	13.26857
S14 1056	15.5289	30	0.696552	9.762863	0.775896	1.962046	12.53305
S14 1057	15.9342	31	0.443433	9.507451	0.522756	1.8664	13.72027
S14 1058	16.6026	32	0.46027	9.52444	0.539595	1.718822	13.6413
S14 1059	17.3064	33	0.477108	9.54143	0.556433	1.699661	13.56233
S14 1060	17.8965	34	0.713915	9.780383	0.79326	1.65166	12.45161
S14 1061	18.3449	35	1.004405	10.0735	1.083772	1.254315	11.08911
S14 1062	18.7092	36	0.751275	9.818081	0.830622	1.46901	12.27638
S14 1063	19.3617	37	0.618129	9.68373	0.697466	1.636845	12.90088
S14 1064	19.7967	38	0.764956	9.831886	0.844304	1.602587	12.21221
S14 1065	20.4502	39	0.421827	9.485648	0.501148	1.713311	13.82162
S14 1066	20.6677	40	0.578652	9.643895	0.657986	1.742925	13.08604
S14 1067	21.2839	41	0.33551	9.39855	0.414825	1.967988	14.22647
S14 1068	21.5014	42	0.672325	9.738416	0.751666	1.595555	12.64669
S14 1069	21.8296	43	1.259129	10.33054	1.338517	0.882916	9.894355
S14 1070	22.4821	44	0.756	9.82285	0.835348	1.384311	12.25422
S14 1071	22.9909	45	0.306536	9.369313	0.385848	1.707585	14.36237
S14 1072	23.3534	46	0.643364	9.709193	0.722703	1.806028	12.78252
S14 1073	24.1155	47	1.500186	10.57378	1.579593	1.972511	8.763709
S14 1074	24.6604	48	2.167022	11.24666	2.246482	0.775568	5.635999

SIRA_Number	Distance	Number	d18OCalcite	d18O_Raw	d18O	d13C	TMollusc
S14 1075	24.9141	49	1.513876	10.58759	1.593284	1.442572	8.6995
S14 1076	25.5666	50	0.57072	9.635891	0.650053	1.605686	13.12325
S14 1077	26.1115	51	0.237556	9.299708	0.316862	1.341504	14.68592

D5.219.1185.2 *Lahillia* -142.5

SIRA_Number	Distance	Number	d18OCalcite	d18O_Raw	d18O	d13C	TMollusc
S12 2471	0	1	1.13	10.20024	1.209378	0.96	10.50002
S12 2472	0.3732	2	1.08	10.14978	1.159374	1.14	10.73454
S12 2473	0.6902	3	0.85	9.917701	0.929355	1.41	11.81332
S12 2474	1.2009	4	0.94	10.00852	1.019363	1.38	11.39119
S12 2475	1.6008	5	0.92	9.988335	0.999361	1.59	11.485
S12 2476	2.0558	6	0.8	9.867248	0.879351	1.67	12.04784
S12 2477	2.4833	7	0.78	9.847067	0.85935	1.62	12.14165
S12 2478	2.897	8	0.73	9.796614	0.809346	1.77	12.37617
S12 2479	3.7663	9	0.66	9.72598	0.73934	1.72	12.70449
S12 2480	4.1111	10	0.74	9.806704	0.819347	1.69	12.32926
S12 2481	4.635	11	0.65	9.715889	0.72934	1.83	12.7514
S12 2482	5.0494	12	0.71	9.776433	0.789344	1.85	12.46998
S12 2483	6.1987	14	0.7	9.766342	0.779343	0.02	12.51688
S12 2484	6.5856	15	0.72	9.786523	0.799345	0.04	12.42307
S12 2485	6.9442	16	0.66	9.72598	0.73934	-0.42	12.70449
S12 2486	7.4411	17	0.6	9.665436	0.679336	-0.9	12.98592
S12 2487	7.9403	18	0.86	9.927792	0.939356	-0.12	11.76642
S12 2488	8.3547	19	0.57	9.635164	0.649333	-0.76	13.12663
S12 2489	8.9205	20	0.57	9.635164	0.649333	-0.43	13.12663
S12 2490	9.4169	21	0.25	9.312265	0.329308	-0.65	14.62755
S12 2491	9.8995	22	0.45	9.514077	0.529324	-0.97	13.68947

D5.220.1214.2 *Lahillia* -92.5

SIRA_Number	Distance	Number	d18OCalcite	d18O_Raw	d18O	d13C	TMollusc
G14 2276	0	1	1.466	10.53928	1.545404	-0.975	8.924054
G14 2277	2.2023	2	1.3632	10.43555	1.442596	-1.3582	9.406224
G14 2273	4.8336	3	1.358	10.4303	1.437396	-0.5628	9.430614
G14 2278	5.7819	4	1.3588	10.43111	1.438196	-1.2634	9.426862
G14 2279	6.3331	5	0.9972	10.06623	1.076567	-1.0824	11.1229
G14 2274	7.0981	6	1.3894	10.46199	1.468798	-0.5812	9.283337
G14 2275	7.7402	7	1.0522	10.12173	1.131571	-1.3754	10.86493

D5.220.1226.2 *Lahillia* -66.5

SIRA_Number	Distance	Number	d18OCalcite	d18O_Raw	d18O	d13C	TMollusc
G14 2293	0	1	0.8364	9.903978	0.915754	-4.9258	11.87711
G14 2294	0.5416	2	-0.8706	8.181512	-0.79138	-19.6424	19.88358
G14 2295	1.2021	3	-1.4398	7.607155	-1.36063	-25.901	22.55334
G14 2296	2.0972	4	-1.4862	7.560335	-1.40703	-26.27	22.77097
G14 2297	2.6429	5	-1.2156	7.833387	-1.13641	-23.1236	21.50176
G14 2298	3.5762	6	-0.66	8.39402	-0.58076	-15.2836	18.89578
G14 2299	4.3518	7	0.2748	9.33729	0.35411	-7.0304	14.51123

G14 2300	6.4148	8	-1.446	7.600899	-1.36683	-22.9602	22.58242
G14 2301	6.9224	9	-1.31662	7.731451	-1.23744	-21.3176	21.97558
G14 2302	7.7028	10	-1.23858	7.810198	-1.15939	-20.9548	21.60954
G14 2303	8.9856	11	0.53758	9.60245	0.616911	-7.8718	13.27869
G14 2304	9.8105	12	-0.21054	8.847553	-0.13127	-12.2112	16.78765

D5.222.1223.2 *Cucullaea* -74.5

SIRA_Number	Distance	Number	d18OCalcite	d18O_Raw	d18O	d13C	TMollusc
S14 3079	0.442	1	0.642535	9.708356	0.721874	1.798516	12.78641
S14 3078	0.884	2	0.918658	9.986981	0.998019	2.182913	11.49129
S14 3077	1.326	3	0.664855	9.730879	0.744196	2.103657	12.68172
S14 3076	1.768	4	1.020964	10.09021	1.100333	2.132201	11.01144
S14 3075	2.21	5	0.657179	9.723134	0.73652	2.388408	12.71772

D5.222.1234.2 *Lahillia* -56.5

SIRA_Number	Distance	Number	d18OCalcite	d18O_Raw	d18O	d13C	TMollusc
G14 2280	0	1	0.1388	9.200058	0.218099	1.0564	15.14912
G14 2281	0.5	2	0.0092	9.069283	0.088489	1.5836	15.75699
G14 2282	0.9319	3	0.0396	9.099959	0.118891	1.0388	15.6144
G14 2283	1.474	4	0.5862	9.651511	0.665534	-0.768	13.05064
G14 2284	1.8644	5	-0.251	8.806726	-0.17173	-2.9632	16.97742
G14 2285	2.4329	6	-0.5978	8.456784	-0.51856	-5.6982	18.60404
G14 2286	2.8922	7	-0.192	8.86626	-0.11273	-1.6996	16.70069
G14 2287	3.5361	8	-0.3142	8.742953	-0.23494	-7.4612	17.27385
G14 2288	4.0262	9	-0.68	8.373839	-0.60077	-6.6216	18.98959
G14 2289	4.6979	10	-0.1578	8.90077	-0.07852	1.6484	16.54028
G14 2290	4.9794	11	0.3822	9.445663	0.461518	2.6644	14.00748
G14 2291	5.3984	12	-0.333	8.723983	-0.25374	-4.4758	17.36203
G14 2292	5.7493	13	-1.2584	7.790199	-1.17921	-15.2592	21.7025

D5.222.1248.2 *Cucullaea* -32.5

SIRA_Number	Distance	Number	d18OCalcite	d18O_Raw	d18O	d13C	TMollusc
S14 3074	0	1	0.593351	9.658727	0.672686	-1.04681	13.0171
S14 3073	0.7509	2	0.509526	9.574143	0.588855	-0.99268	13.41027
S14 3072	1.7254	3	0.31572	9.378581	0.395033	-1.4164	14.31929
S14 3071	2.412	4	0.471857	9.536132	0.551182	-1.72353	13.58696
S14 3070	3.1076	5	0.530332	9.595137	0.609662	-1.78566	13.31268
S14 3069	4.1367	6	0.486502	9.55091	0.565829	-1.41186	13.51826

D5.229.1301.2 *Lahillia* 5.5

SIRA_Number	Distance	Number	d18OCalcite	d18O_Raw	d18O	d13C	TMollusc
S14 0961	0	1	-1.94155	7.100861	-1.86241	6.345252	24.90672
S14 0962	0.254	2	-1.57658	7.469134	-1.49742	4.644428	23.19489
S14 0963	0.6614	3	-0.07181	8.987542	0.007475	2.830156	16.13694
S14 0964	1.1842	4	0.523133	9.587873	0.602463	2.373599	13.34645
S14 0965	1.6493	5	0.078249	9.138957	0.157543	2.465855	15.43312

S14 0966	2.2286	6	0.012	9.072109	0.091289	2.896	15.74385
S14 0967	2.6732	7	-1.25147	7.797194	-1.17228	4.987446	21.66999
S14 0968	3.1371	8	-3.13616	5.895429	-3.05712	3.887015	30.50988
S14 0969	3.7361	9	-0.70148	8.352167	-0.62225	4.577527	19.09033
S14 0970	4.3183	10	0.293423	9.356082	0.372734	5.241803	14.42388
S14 0971	4.7834	11	0.538518	9.603397	0.617849	2.393852	13.27429
S14 0972	5.2087	12	0.873522	9.941436	0.95288	1.443099	11.70299
S14 0973	5.8086	13	-0.82124	8.231315	-0.74202	2.455135	19.65208
S14 0974	6.2339	14	-0.8862	8.165769	-0.80698	5.338371	19.95676
S14 0975	6.7364	15	-1.15114	7.898431	-1.07194	5.981037	21.19941
S14 0976	7.2003	16	-1.07611	7.974138	-0.99691	6.194849	20.84751
S14 0977	7.6642	17	-1.05	8.000487	-0.9708	6.123	20.72503
S14 0978	8.1474	18	-1.02605	8.024656	-0.94684	6.090772	20.61269
S14 0979	8.5916	19	-1.03101	8.019646	-0.95181	5.99694	20.63597
S14 0980	9.0169	20	-2.59586	6.440622	-2.51678	0.57286	27.97569
S14 0981	9.5194	21	0.549028	9.614002	0.62836	2.763653	13.22499
S14 0982	10.0412	22	-0.67586	8.378016	-0.59663	2.272274	18.97018
S14 0983	10.7966	23	-1.1508	7.898773	-1.0716	5.59751	21.19782
S14 0984	11.2798	24	-0.17581	8.882595	-0.09654	4.518083	16.62476
S14 0985	11.6858	25	-4.5206	4.498447	-4.44167	3.875319	37.00342
S14 0986	12.2076	26	-0.64572	8.408431	-0.56648	5.020179	18.8288
S14 0987	12.8066	27	0.969268	10.03805	1.048633	4.815547	11.25391
S14 0988	13.2319	28	0.563	9.628101	0.642333	4.756	13.15946
S14 0989	13.6567	29	0.0554	9.115902	0.134692	5.014	15.54029
S14 0990	14.1974	30	-0.88557	8.166406	-0.80635	5.09105	19.9538

D9.206.152 *Lahillia* 3.5

SIRA_Number	Distance	Number	d18OCalcite	d18O_Raw	d18O	d13C	TMollusc
S13 2153	0	1	1.07	10.13969	1.149373	-2.02	10.78144
S13 2152	0.5998	2	1.05	10.11951	1.129371	-1.13	10.87525
S13 2151	1.1991	3	1.02	10.08924	1.099369	-1.38	11.01596
S13 2150	1.6855	4	0.76	9.826886	0.839348	-0.98	12.23546
S13 2157	2.1042	5	1.45	10.52314	1.529403	-1.99	8.9991
S13 2149	2.6019	6	1.4	10.47268	1.479399	-12.01	9.233619
S13 2148	3.1447	7	0.02	9.080181	0.09929	-13.17	15.70633
S13 2147	3.586	8	1.4	10.47268	1.479399	-11.74	9.233619
S13 2146	4.0042	9	1.24	10.31123	1.319386	-10.77	9.984078
S13 2145	4.3786	10	1.19	10.26078	1.269382	-8.19	10.2186
S13 2144	4.7968	11	1.22	10.29105	1.299385	-7.6	10.07789
S13 2143	5.2606	12	1.2	10.27087	1.279383	-5.09	10.17169
S13 2142	5.6567	13	1.29	10.36169	1.36939	-2.83	9.74956
S13 2158	6.1889	14	1.19	10.26078	1.269382	-0.8	10.2186
S13 2141	6.449	15	1.23	10.30114	1.309386	-11.45	10.03098
S13 1993	10.2179	23	0.894253	9.962355	0.973612	-9.38581	11.60576
S13 1994	10.8508	24	0.690489	9.756745	0.769832	-10.8004	12.56149
S13 1995	11.3086	25	0.936671	10.00516	1.016034	-9.72593	11.4068
S13 1996	11.6363	26	0.922884	9.991246	1.002246	-8.33236	11.47147
S13 1997	12.0099	27	0.949093	10.01769	1.028456	-7.17557	11.34854
S13 1998	12.4168	28	0.845314	9.912973	0.924669	-6.56017	11.8353
S13 1999	12.7447	29	0.851525	9.919239	0.93088	-6.98657	11.80617
S13 2000	13.0613	30	0.877733	9.945686	0.957091	-7.1568	11.68324

S13 2001	13.389	31	0.80637	9.873676	0.885722	-5.59696	12.01796
S13 2002	13.8524	32	0.832579	9.900122	0.911933	-4.19401	11.89504
S13 2003	14.1577	33	0.778792	9.845848	0.858141	-2.64923	12.14732
S13 2004	14.4628	34	1.114986	10.18509	1.194363	-0.00462	10.57044
S13 2005	14.8471	35	0.971204	10.04	1.050569	-3.55091	11.24483
S13 2006	15.1183	36	0.977415	10.04627	1.05678	-8.00125	11.2157
S13 2007	15.5596	37	0.953626	10.02227	1.03299	-9.06876	11.32728
S13 2008	15.8655	38	0.79984	9.867086	0.879191	-8.29113	12.04859
S13 2009	16.2955	39	0.926047	9.994437	1.005409	-6.15311	11.45663
S13 2010	16.7137	40	0.862258	9.93007	0.941615	-5.05746	11.75583
S13 2011	16.9738	41	0.810887	9.878234	0.890239	-5.67078	11.99678
S13 2012	17.3699	42	0.937098	10.00559	1.016461	-6.00492	11.4048
S13 2013	17.8224	43	0.873307	9.941219	0.952664	-4.62031	11.70401
S13 2014	18.1503	44	1.019521	10.08876	1.098889	-0.8348	11.01821
S13 2015	18.4788	45	0.945728	10.0143	1.025091	-6.96275	11.36432
S13 2016	18.8862	46	0.971939	10.04074	1.051304	-11.0714	11.24138
S13 2017	19.3839	47	0.968149	10.03692	1.047514	-10.9838	11.25916
S13 2018	19.8925	48	0.934357	10.00282	1.013719	-10.4242	11.41766

D9.207.1 *Lahillia* 18.9

SIRA_Number	Distance	Number	d18OCalcite	d18O_Raw	d18O	d13C	TMollusc
S12 2151	0	1	-0.18	8.878369	-0.10073	-3.04	16.64441
S12 2152	0.4693	2	-0.29	8.767373	-0.21074	-7.81	17.16035
S12 2153	0.9083	3	-0.23	8.827916	-0.15073	-7.64	16.87892
S12 2154	1.3171	4	-0.26	8.797644	-0.18073	-6.76	17.01964
S12 2155	1.7132	5	-0.25	8.807735	-0.17073	-6.96	16.97273
S12 2156	2.1649	6	-0.28	8.777463	-0.20073	-6.75	17.11344
S12 2157	2.6771	7	-0.48	8.575651	-0.40075	-5.46	18.05152
S12 2158	3.2196	8	-0.58	8.474745	-0.50076	-3.44	18.52055
S12 2159	3.7874	9	-0.51	8.545379	-0.43075	-1.59	18.19223
S12 2160	4.2138	10	-0.51	8.545379	-0.43075	-0.36	18.19223
S12 2161	4.6831	11	-0.05	9.009547	0.029284	0.36	16.03466
S12 2162	5.1953	12	-0.33	8.72701	-0.25074	-2.11	17.34796
S12 2163	5.7075	13	-0.32	8.737101	-0.24074	-6.29	17.30106
S12 2164	6.2197	14	-0.28	8.777463	-0.20073	-6.87	17.11344
S12 2165	6.9338	15	-0.28	8.777463	-0.20073	-7.23	17.11344
S12 2166	7.5494	16	-0.33	8.72701	-0.25074	-6.3	17.34796
S12 2167	8.049	17	-0.4	8.656376	-0.32074	-5.28	17.67629
S12 2168	8.6168	18	-0.42	8.636195	-0.34075	-4.35	17.7701
S12 2169	9.2451	19	-0.51	8.545379	-0.43075	-1.36	18.19223
S12 2170	9.7144	20	-0.47	8.585742	-0.39075	1.71	18.00461
S12 2171	10.5622	21	-0.36	8.696738	-0.28074	-1.39	17.48867
S12 2172	11.2939	22	-0.42	8.636195	-0.34075	-4.44	17.7701
S12 2173	12.013	23	-0.67	8.38393	-0.59077	-2.44	18.94269
S12 2174	12.5681	24	-0.74	8.313296	-0.66077	-1.42	19.27101
S13 1992	12.9925	25	-0.77174	8.281269	-0.69251	-0.96266	19.41988
S13 2020	13.5535	26	-0.60333	8.451207	-0.52409	-4.6642	18.62997
S13 2051	13.8013	27	-0.41759	8.638628	-0.33833	-3.95609	17.75879
S13 2052	14.1458	28	-0.56782	8.487035	-0.48858	-1.7688	18.46343
S13 2053	14.2963	29	-0.59807	8.456515	-0.51883	0.949521	18.6053
S13 2054	14.927	30	-0.32835	8.728673	-0.24909	2.127351	17.34023

S13 2055	15.885	31	-0.59857	8.456009	-0.51933	-3.8574	18.60764
S13 2056	16.5417	32	-0.36885	8.68781	-0.28959	-3.33102	17.53017
S13 2057	17.0344	33	-0.85904	8.193182	-0.77982	-1.00382	19.82933
S13 2058	17.4449	34	-0.69931	8.354358	-0.62007	-0.92455	19.08015
S13 2059	18.1979	35	-0.55957	8.495355	-0.48033	-0.04198	18.42475
S13 2060	18.5673	36	-0.61982	8.434567	-0.54058	-0.10509	18.70731
S13 2061	19.0599	37	-0.51058	8.544791	-0.43134	1.290309	18.19497
S13 2062	19.3475	38	-0.40085	8.65552	-0.32159	1.424779	17.68027
S13 2160	19.6895	39	0.55	9.614983	0.629332	-0.79	13.22043
S13 2063	20.4148	40	-0.15113	8.907499	-0.07186	-2.73682	16.509
S13 2064	20.921	41	-0.47134	8.58439	-0.39209	-3.49744	18.0109
S13 2065	21.489	42	-0.79155	8.26128	-0.71232	-3.43405	19.5128
S13 2066	21.9544	43	-0.54183	8.513259	-0.46259	-3.60395	18.34153
S13 2067	22.4538	44	-0.50209	8.553363	-0.42284	-3.22098	18.15512
S13 2068	22.7961	45	-0.56233	8.492575	-0.48309	-3.15567	18.43768
S13 2069	23.3023	46	-0.35261	8.704197	-0.27335	-1.76179	17.454
S13 2159	23.9592	47	0.59	9.655345	0.669335	-1.34	13.03282
S13 2070	24.6455	48	-0.7928	8.260017	-0.71358	-3.04273	19.51867
S13 2071	25.2772	49	-0.81355	8.23908	-0.73433	-1.94259	19.61599
S13 2072	25.7563	50	-0.8338	8.218649	-0.75458	-0.50885	19.71096
S13 2073	26.2655	51	-0.72406	8.329378	-0.64483	0.492442	19.19626
S13 2074	26.7452	52	-0.75431	8.298857	-0.67508	1.220223	19.33813

D9.211.457-480 *Cucullaea* 99.3

SIRA_Number	Distance	Number	d18OCalcite	d18O_Raw	d18O	d13C	TMollusc
S14 1951	0	1	0.115361	9.176407	0.194659	3.358187	15.25905
S14 1952	0.6261	2	0.098988	9.159885	0.178284	3.863544	15.33585
S14 1953	1.3038	3	-0.21743	8.840597	-0.13816	3.28754	16.81998
S14 1954	2.0868	4	0.026229	9.086466	0.105519	3.580784	15.67712
S14 1955	2.6678	5	0.029853	9.090123	0.109143	4.010543	15.66012
S14 1956	3.1494	6	0.063482	9.124057	0.142775	4.043358	15.50238
S14 1957	3.9288	7	-0.15295	8.905665	-0.07367	3.945515	16.51753
S14 1958	4.6486	8	-0.20935	8.848754	-0.13008	3.146743	16.78206
S14 1959	5.3426	9	-0.05569	9.003805	0.023593	3.978028	16.06135
S14 1960	6.1241	10	0.127984	9.189143	0.207282	4.722682	15.19985
S14 1961	6.7922	11	0.018795	9.078965	0.098084	6.347573	15.71198
S14 1962	7.4396	12	-0.31773	8.739391	-0.23847	5.900677	17.29041

DJ.952.523 *Lahillia* -137.45

SIRA_Number	Distance	Number	d18OCalcite	d18O_Raw	d18O	d13C	TMollusc
S14 1911	0	1	1.4608	10.53403	1.540203	0.766528	8.948446
S14 1912	0.7097	2	1.445927	10.51903	1.52533	0.590219	9.018204
S14 1913	0.984	3	1.781027	10.85716	1.860456	0.166625	7.446461
S14 1914	1.3944	4	1.416182	10.48901	1.495582	-0.44736	9.157721
G14 1591	1.7493	5	1.5007	10.5743	1.580107	-0.4924	8.761298
G14 1592	2.0496	6	1.606	10.68055	1.685415	-0.712	8.267402
G14 1593	2.4591	7	1.6345	10.70931	1.713918	-0.6412	8.133727
G14 1594	3.1694	8	1.435	10.508	1.514402	-0.2966	9.069456
G14 1596	4.4803	10	1.5318	10.60568	1.611209	0.3782	8.615428
G14 1598	6.2009	12	1.2472	10.3185	1.326587	0.5092	9.950308

G14 1599	6.8839	13	1.3983	10.47097	1.477699	0.3844	9.241592
G14 1550	7.3488	14	1.3804	10.45291	1.459797	0.3792	9.32555
G14 0691	7.6503	15	1.5612	10.63534	1.640612	0.4622	8.477531
G14 0692	7.979	16	1.868	10.94492	1.947436	0.6196	7.038525
G14 0693	8.4166	17	2.0454	11.12393	2.12485	0.5052	6.206453
G14 0694	9.074	18	1.8628	10.93968	1.942236	0.2912	7.062915
G14 0695	9.5934	19	1.7318	10.80749	1.811225	0.343	7.677353
G14 0696	10.2764	20	1.6286	10.70336	1.708017	0.551	8.1614
G14 0697	10.823	21	1.6388	10.71365	1.718218	0.3714	8.113558
G14 0698	11.4242	22	1.6324	10.70719	1.711817	0.308	8.143576
G14 0699	12.136	23	1.6888	10.7641	1.768222	0.271	7.879039
G14 0700	12.873	24	1.589	10.6634	1.668414	0.4438	8.347138
G14 0701	13.5833	25	1.9668	11.04462	2.046244	0.8346	6.575116
G14 0702	14.43	26	1.7866	10.86279	1.86603	0.466	7.420321
G14 0703	15.0033	27	1.7312	10.80688	1.810625	0.0866	7.680168
G14 1631	15.1159	28	1.3354	10.4075	1.414794	-0.0708	9.536617
G14 1632	15.4435	29	1.5196	10.59337	1.599008	0.1096	8.67265
G14 1633	15.8811	30	1.531	10.60487	1.610409	0.1796	8.61918
G14 1634	16.5143	31	1.533	10.60689	1.61241	0.3708	8.609799
G14 1635	17.1475	32	1.4402	10.51325	1.519602	0.3378	9.045066
G14 1636	17.6116	33	1.4594	10.53262	1.538804	0.4956	8.955011
G14 1637	18.0765	34	1.6064	10.68095	1.685815	0.4872	8.265526
G14 1638	18.6231	35	1.54	10.61395	1.61941	0.4656	8.576967
G14 1639	19.2515	36	1.6038	10.67833	1.683215	0.4424	8.277721
G14 1640	19.9633	37	1.3816	10.45412	1.460998	0.4496	9.319922
G14 1641	20.512	38	1.9462	11.02383	2.025642	1.5108	6.671738
G14 1642	20.9224	39	1.5738	10.64806	1.653213	0.668	8.418432

DJ.953.335 *Lahillia* -48.25

SIRA_Number	Distance	Number	d18OCalcite	d18O_Raw	d18O	d13C	TMollusc
S14 1081	0	1	1.162197	10.23273	1.241577	-8.99456	10.34901
S14 1082	0.4854	2	-0.35141	8.705408	-0.27215	-10.0101	17.44837
S14 1083	0.8428	3	1.374401	10.44685	1.453798	-4.85358	9.353689
S14 1084	1.1987	4	1.190554	10.26134	1.269936	-7.51919	10.216
S14 1085	1.7847	5	1.066694	10.13636	1.146067	-12.8942	10.79695
S14 1086	2.465	6	1.192794	10.2636	1.272177	-11.9534	10.20549
S14 1087	3.1476	7	1.15892	10.22942	1.2383	-12.409	10.36437
S14 1088	3.73	8	1.245028	10.31631	1.324415	-9.2623	9.960496
S14 1089	4.183	9	-0.50861	8.546784	-0.42936	-9.15679	18.1857
S14 1090	4.7007	10	1.217273	10.2883	1.296657	-2.41639	10.09068
S14 1930	4.9596	11	0.88843	9.956479	0.967788	-12.3252	11.63307
S14 1931	5.6399	12	0.723791	9.790349	0.803136	-13.1821	12.40529
S14 1932	6.1253	13	1.058925	10.12852	1.138297	-13.9697	10.83339
S14 1915	7.1289	14	1.08133	10.15113	1.160704	-13.2525	10.7283
S14 1916	7.5185	15	1.096454	10.16639	1.175829	-9.82317	10.65736
S14 1917	8.0686	16	0.851592	9.919307	0.930948	-3.99829	11.80586
S14 1918	8.554	17	0.976708	10.04556	1.056074	-6.2985	11.21901
S14 1919	9.1688	18	0.841838	9.909465	0.921193	-12.6784	11.85161
S14 1920	10.1072	19	0.826961	9.894454	0.906315	-12.6086	11.92138
S14 1921	10.9485	20	0.852328	9.92005	0.931684	-9.62955	11.8024
S14 1922	11.6604	21	1.057446	10.12703	1.136818	-10.5412	10.84032

S14 1923	12.4046	22	1.382564	10.45509	1.461962	-5.22767	9.315399
S14 1924	13.1172	23	1.097693	10.16764	1.177068	-13.2724	10.65155
S14 1925	13.8291	24	1.012817	10.08199	1.092185	-15.48	11.04965
S14 1926	14.4763	25	0.687941	9.754174	0.767283	-15.8279	12.57344
S14 1927	15.1267	26	1.053063	10.1226	1.132435	-15.1716	10.86088
S14 1928	15.8393	27	1.198188	10.26904	1.277571	-5.6883	10.18019
S14 1929	16.4226	28	1.08331	10.15313	1.162684	-18.138	10.71901

DJ.953.456 *Lahillia* -48.25

SIRA_Number	Distance	Number	d18OCalcite	d18O_Raw	d18O	d13C	TMollusc
S12 2501	0	1	1.08	10.14978	1.159374	-25.17	10.73454
S12 2502	0.3358	2	1.06	10.1296	1.139372	-24.95	10.82835
S12 2503	0.7248	3	1.13	10.20024	1.209378	-24.57	10.50002
S12 2504	1.0414	4	1.08	10.14978	1.159374	-23.82	10.73454
S12 2505	1.3853	5	1.13	10.20024	1.209378	-18	10.50002
S12 2506	1.9917	6	1.06	10.1296	1.139372	-24.74	10.82835
S12 2507	2.3899	7	0.99	10.05897	1.069366	-29.02	11.15667
S12 2508	2.8968	8	0.97	10.03879	1.049365	-28.89	11.25048
S12 2509	3.2859	9	0.9	9.968154	0.979359	-26.96	11.5788
S12 2510	3.7657	10	0.84	9.90761	0.919355	-23.66	11.86023
S12 2511	4.2634	11	0.88	9.947973	0.959358	-20.57	11.67261
S12 2512	4.9334	12	0.94	10.00852	1.019363	-16.72	11.39119
S12 2513	5.368	13	0.91	9.978245	0.98936	-17.95	11.5319
S12 2514	5.9111	14	1.02	10.08924	1.099369	-15.42	11.01596
S12 2515	6.3049	15	1.14	10.21033	1.219378	-10.7	10.45312
S12 2516	6.9292	16	1.19	10.26078	1.269382	-28.4	10.2186
S12 2517	7.3909	17	1.25	10.32133	1.329387	-33.9	9.937174
S12 2518	7.8795	18	1.16	10.23051	1.23938	-33.4	10.35931
S12 2519	8.3236	19	1.17	10.2406	1.249381	-31.66	10.3124
S12 2520	8.8122	20	0.84	9.90761	0.919355	-28.4	11.86023
S12 2521	9.2739	21	1.03	10.09933	1.10937	-25.44	10.96906
S12 2522	9.7444	22	1.05	10.11951	1.129371	-23.67	10.87525
S12 2523	10.1787	23	1.3	10.37178	1.379391	-21.59	9.702656
S12 2524	10.6314	24	1.05	10.11951	1.129371	-16.17	10.87525
S12 2525	11.0929	25	1	10.06906	1.079367	-20.94	11.10977
S12 2526	11.4643	26	1.03	10.09933	1.10937	-30.53	10.96906
S12 2527		27	1	10.06906	1.079367	-29.38	11.10977
S12 2528	11.9529	28	1.04	10.10942	1.11937	-34.18	10.92215
S12 2529	12.3465	29	1.16	10.23051	1.23938	-33.27	10.35931
S12 2530	12.8622	30	0.99	10.05897	1.069366	-31.26	11.15667
S12 2492	13.3418	31	0.9	9.968154	0.979359	-28.85	11.5788
S12 2493	13.8395	32	0.88	9.947973	0.959358	-28.66	11.67261
S12 2494	14.2466	33	0.99	10.05897	1.069366	-28.29	11.15667
S12 2495	14.699	34	1.01	10.07915	1.089368	-27.99	11.06286
S12 2496	15.2692	35	1.16	10.23051	1.23938	-13.07	10.35931
S12 2497	15.7125	36	0.97	10.03879	1.049365	-27.93	11.25048
S12 2631	16.17463	37	1.23	10.30114	1.309386	-26.71	10.03098
S12 2632	16.63676	38	1.11	10.18006	1.189376	-23.75	10.59383
S12 2633	17.0989	39	1.06	10.1296	1.139372	-21.01	10.82835
S12 2634	17.56103	40	0.83	9.89752	0.909354	-17.67	11.90713
S12 2635	18.02316	41	1.12	10.19015	1.199377	-17.25	10.54692

S12 2636	18.48529	42	1.22	10.29105	1.299385	-24.46	10.07789
S12 2637	18.94743	43	1.05	10.11951	1.129371	-23.7	10.87525
S12 2638	19.40956	44	1.02	10.08924	1.099369	-21.25	11.01596
S12 2639	19.87169	45	1.04	10.10942	1.11937	-18.29	10.92215
S12 2640	20.33382	46	1.09	10.15988	1.169374	-17.74	10.68763
S12 2641	20.79596	47	0.98	10.04888	1.059366	-16.83	11.20357
S12 2642	21.25809	48	1.04	10.10942	1.11937	-13.74	10.92215
S12 2643	22.18235	49	1.14	10.21033	1.219378	-14.6	10.45312

DJ.953.459 *Cucullaea* -48.25

SIRA_Number	Distance	Number	d18OCalcite	d18O_Raw	d18O	d13C	TMollusc
S14 1950	0	1	0.984499	10.05342	1.063865	-2.53043	11.18248
S14 1949	0.5786	2	1.290848	10.36254	1.370238	-2.67111	9.745582
S14 1948	1.3483	3	1.077189	10.14695	1.156562	-1.9167	10.74772
S14 1947	1.9288	4	0.983534	10.05244	1.0629	-1.90474	11.187
S14 1946	2.4672	5	0.899882	9.968035	0.979241	-1.7968	11.57936
S14 1945	3.0817	6	0.926224	9.994615	1.005585	-2.57014	11.45581
S14 1944	3.5262	7	1.002557	10.07164	1.081925	-11.971	11.09777
S14 1943	4.0848	8	1.018894	10.08813	1.098263	-12.8083	11.02115
S14 1942	4.4436	9	1.015233	10.08443	1.094601	-6.80627	11.03832
S14 1941	4.8079	10	1.061561	10.13118	1.140933	-11.4225	10.82102
S14 1940	5.4057	11	0.489862	9.5543	0.569189	-22.8158	13.50251
S14 1939	5.7596	12	1.284801	10.35644	1.364191	-21.103	9.773943
S14 1938	6.3771	13	1.019659	10.0889	1.099028	-20.6281	11.01756
S14 1937	6.8549	14	0.924531	9.992907	1.003892	-20.3194	11.46375
S14 1936	7.3017	15	0.669394	9.735458	0.748735	-17.3295	12.66043
S14 1935	7.6996	16	1.36431	10.43667	1.443707	-6.54717	9.401016
S14 1934	8.2012	17	1.629199	10.70396	1.708616	-17.0402	8.15859
S14 1933	8.5564	18	0.804037	9.871322	0.883389	-20.4746	12.02891

DJ.953.746 *Lahillia* -1.75

SIRA_Number	Distance	Number	d18OCalcite	d18O_Raw	d18O	d13C	TMollusc
S14 1079	0.6347	2	1.351251	10.42349	1.430646	1.148948	9.46227
S14 1080	1.1667	3	1.308093	10.37994	1.387485	1.292343	9.664696
G14 0641	1.4995	4	1.46	10.53323	1.539404	1.1	8.952196
G14 0642	2.1342	5	1.59	10.66441	1.669414	1.31	8.342448
G14 0643	2.641	6	1.57	10.64422	1.649412	1.4	8.436255
G14 0644	3.049	7	1.48	10.55341	1.559405	1.52	8.858389
G14 0645	3.7089	8	1.56	10.63413	1.639412	1.44	8.483159
G14 0646	4.1925	9	1.6	10.6745	1.679415	1.39	8.295544
G14 0647	4.4217	10	1.78	10.85613	1.859429	0.99	7.451277
G14 0648	4.6748	11	1.81	10.8864	1.889432	0.94	7.310566
G14 0649	5.3347	12	1.5	10.57359	1.579407	1.31	8.764582
G14 0650	5.9441	13	1.51	10.58368	1.589408	1.32	8.717678
G14 0651	6.3996	14	1.62	10.69468	1.699416	1.27	8.201737
G14 0652	7.0075	15	1.47	10.54332	1.549405	1.37	8.905293
G14 0653	7.5648	16	1.52	10.59377	1.599409	1.33	8.670774
G14 0654	8.0734	17	1.54	10.61395	1.61941	1.47	8.576967
G14 0655	8.7585	18	1.48	10.55341	1.559405	1.39	8.858389
G14 0656	9.3175	19	1.55	10.62404	1.629411	0.99	8.530063

G14 0657	9.8261	20	1.5	10.57359	1.579407	1.25	8.764582
G14 0658	10.3599	21	1.47	10.54332	1.549405	1.28	8.905293
G14 0659	10.8161	22	1.37	10.44241	1.449397	1.19	9.37433
G14 0660	11.247	23	1.38	10.4525	1.459397	1.08	9.327426
G14 0661	11.5265	24	1.43	10.50296	1.509401	1.21	9.092908
G14 0662	11.8817	25	1.53	10.60386	1.609409	1.19	8.62387
G14 0663	12.1864	26	1.55	10.62404	1.629411	1.28	8.530063
G14 0664	12.4407	27	1.45	10.52314	1.529403	1.27	8.9991
G14 0665	12.7454	28	1.69	10.76531	1.769422	1.08	7.873411
G14 0666	13.1511	29	1.69	10.76531	1.769422	0.94	7.873411
G14 0667	13.5063	30	1.62	10.69468	1.699416	0.92	8.201737
G14 0668	14.4177	31	1.5	10.57359	1.579407	1.21	8.764582
G14 0669	14.8992	32	1.45	10.52314	1.529403	1.2	8.9991
G14 0670	15.3807	33	1.57	10.64422	1.649412	1.28	8.436255
G14 0671	16.0139	34	1.47	10.54332	1.549405	1.1	8.905293
G14 0672	16.4701	35	1.36	10.43232	1.439396	1.29	9.421234
G14 0673	17.105	36	1.51	10.58368	1.589408	1.53	8.717678
G14 0674	17.5865	37	1.36	10.43232	1.439396	1.68	9.421234
G14 0675	18.1203	38	1.48	10.55341	1.559405	1.32	8.858389
G14 0676	18.526	39	1.56	10.63413	1.639412	1.04	8.483159
G14 0677	19.0328	40	1.7	10.7754	1.779423	1.33	7.826507
G14 0678	19.5666	41	1.62	10.69468	1.699416	0.9	8.201737
G14 0679	20.1508	42	1.62	10.69468	1.699416	1.21	8.201737
G14 0680	20.584	43	1.47	10.54332	1.549405	1.39	8.905293

DJ.957.490 *Cucullaea* -233.75

SIRA_Number	Distance	Number	d18OCalcite	d18O_Raw	d18O	d13C	TMollusc
S14 3090	0	1	0.202469	9.264303	0.281773	-2.54545	14.85049
S14 3091	0.9619	2	0.46	9.524168	0.539324	-2.35	13.64257
S14 3092	1.6858	3	0.504114	9.568681	0.583442	-2.23521	13.43566
S14 3093	2.3546	4	0.416777	9.480553	0.496098	-2.14538	13.8453
S14 3094	2.987	5	0.439423	9.503404	0.518746	-2.17697	13.73908
S14 3095	3.7753	6	0.402079	9.465721	0.481398	-2.12093	13.91424
S14 3096	4.6824	7	0.304742	9.367503	0.384054	-2.50161	14.37078

DJ.959.93 *Cucullaea* -392.25

SIRA_Number	Distance	Number	d18OCalcite	d18O_Raw	d18O	d13C	TMollusc
S14 1976	0	1	-1.94545	7.096923	-1.86632	-1.97013	24.92503
S14 1977	0.6403	2	0.722694	9.789241	0.802039	-0.28059	12.41044
S14 1978	1.348	3	0.970711	10.03951	1.050076	-0.69252	11.24715
S14 1979	2.0087	4	0.758695	9.825569	0.838043	-0.28623	12.24158
S14 1980	2.7844	5	0.626683	9.692361	0.706021	-3.06127	12.86076
S14 1981	3.4138	6	0.370649	9.434007	0.449967	-0.26057	14.06166
S14 1982	3.9597	7	0.058608	9.119139	0.137901	-0.24689	15.52525
S14 1983	4.7198	8	0.716685	9.783178	0.796029	0.258431	12.43862
S14 1984	5.4118	9	0.644673	9.710514	0.724012	0.264003	12.77638
S14 1985	6.1065	10	0.682676	9.748861	0.762018	-0.00171	12.59813
S14 1986	6.6524	11	2.760987	11.846	2.840494	-0.48621	2.850084
S14 1987	7.3315	12	0.768685	9.83565	0.848034	-0.20169	12.19472

D5.220.1229.2 *Cucullaea* -122

SIRA_Number	Distance	Number	d18OCalcite	d18O_Raw	d18O	d13C	TMollusc
S14 3105	0	1	-0.666	8.387963	-0.58677	-0.53925	18.92394
S14 3106	0.5968	2	-0.33339	8.723585	-0.25413	-0.45291	17.36388
S14 3107	1.1646	3	-0.45073	8.605182	-0.37148	-0.57608	17.91425
S14 3108	1.8399	4	-0.16812	8.890359	-0.08884	-0.38103	16.58867
S14 3109	2.4728	5	-0.36545	8.69124	-0.28619	-0.84395	17.51423
S14 3110	3.2524	6	-0.47279	8.582926	-0.39354	-0.52871	18.0177
S14 3111	3.7521	7	-0.58484	8.469863	-0.5056	-0.67092	18.54325
S14 3112	4.3801	8	-0.27222	8.785313	-0.19295	-0.29496	17.07696

D5.218.1011.2 *Cucullaea* -378.5

SIRA_Number	Distance	Number	d18OCalcite	d18O_Raw	d18O	d13C	TMollusc
S14 3084	0	1	1.103191	10.17319	1.182567	-11.3302	10.62576
S14 3085	0.03399	2	0.929371	9.997791	1.008732	-13.7665	11.44105
S14 3083	0.14399	3	-0.02436	9.03542	0.054926	-10.6544	15.91439
S14 3082	0.18124	4	0.461747	9.525931	0.541072	-10.0417	13.63437
S14 3081	0.25238	5	-0.06203	8.997412	0.017257	-9.78001	16.09106
S14 3080	0.34042	6	0.376409	9.439819	0.455727	-11.0642	14.03464

Dataset B.3: Morphometric Data: *Lahillia* External Shells

Collection	Station /Section	Full Code	KPBHeight	L	H	W
Cambridge	957	DJ.957.408	-265.25	47.64	40.61	
Cambridge	951	DJ.951.15	-199.75	87.77	78.05	62.25
Cambridge	952	DJ.952.517	-137.45		77.08	45.78
Cambridge	952	DJ.952.518	-137.45			51.80
Cambridge	952	DJ.952.520	-137.45			55.43
Cambridge	952	DJ.952.521	-137.45	37.12	30.03	
Cambridge	952	DJ.952.522	-137.45		73.30	49.76
Cambridge	952	DJ.952.523	-137.45	78.44	69.74	49.77
Cambridge	952	DJ.952.527	-137.45			58.53
Cambridge	952	DJ.952.578	-128.2	82.85	70.06	45.78
Cambridge	952	DJ.952.579	-128.2	78.50	71.10	
Cambridge	952	DJ.952.580	-128.2			49.50
Cambridge	952	DJ.952.581	-128.2	89.12	71.37	49.42
Cambridge	952	DJ.952.582	-128.2	97.23	90.13	64.80
Cambridge	952	DJ.952.583	-128.2			53.22
Cambridge	952	DJ.952.584	-128.2	83.40	71.63	51.73
Cambridge	952	DJ.952.585	-128.2		72.06	43.38
Cambridge	952	DJ.952.586	-128.2	71.31	62.90	44.22
Cambridge	952	DJ.952.587	-128.2	81.97	73.65	50.20
Cambridge	952	DJ.952.588	-128.2		75.40	52.66
Cambridge	952	DJ.952.589	-128.2	87.55	79.98	53.56
Cambridge	952	DJ.952.591	-128.2	82.82	74.66	49.94
Cambridge	952	DJ.952.592	-128.2	81.68	67.77	46.89
Cambridge	952	DJ.952.593	-128.2		63.67	42.88
Cambridge	952	DJ.952.673	-117			42.69
Cambridge	953	DJ.953.87	-76		73.39	56.21
Cambridge	953	DJ.953.171	-64.75	78.36	72.62	53.93
Cambridge	953	DJ.953.208	-53.5	71.92	65.18	50.08
Cambridge	953	DJ.953.209	-53.5			64.87
Cambridge	953	DJ.953.332	-48.25	71.30		53.56
Cambridge	953	DJ.953.335	-48.25	93.88	80.76	56.45
Cambridge	953	DJ.953.451	-48.25	86.67	73.03	58.81
Cambridge	953	DJ.953.454	-48.25	78.51	68.47	49.56
Cambridge	953	DJ.953.455	-48.25		67.98	58.72
Cambridge	953	DJ.953.456	-48.25	86.50	78.82	55.02
Cambridge	205	D9.205.297	-8.85			45.14
Cambridge	953	DJ.953.697	-4.5			54.42
Cambridge	953	DJ.953.699	-4.5			45.90
Cambridge	953	DJ.953.741	-1.75	60.00	53.88	39.93
Cambridge	953	DJ.953.744	-1.75	73.56	76.37	54.80
Cambridge	953	DJ.953.746	-1.75		71.18	52.18
Cambridge	953	DJ.953.747	-1.75	71.32	65.34	48.05
Cambridge	953	DJ.953.748	-1.75			46.66
Cambridge	206	D9.206.12	-1.5	75.41		
Cambridge	953	DJ.953.795	2.5		83.63	
Cambridge	206	D9.206.169	3.5			11.99
Cambridge	953	DJ.953.810	4.125			61.90
Cambridge	953	DJ.953.811	4.125			64.19
Cambridge	953	DJ.953.812	4.125		84.22	62.27
Cambridge	953	DJ.953.813	4.125		82.74	61.74

Cambridge	953	DJ.953.814	4.125		72.17	55.41
Cambridge	953	DJ.953.815	4.125		78.03	62.40
Cambridge	953	DJ.953.816	4.125			71.36
Cambridge	953	DJ.953.817	4.125		89.00	66.36
Cambridge	953	DJ.953.818	4.125		88.81	67.91
Cambridge	953	DJ.953.819	4.125			65.55
Cambridge	953	DJ.953.825	8.25	96.68	82.64	64.95
Cambridge	953	DJ.953.826	8.25	94.20	89.02	63.50
Cambridge	953	DJ.953.827	8.25	103.44	90.09	65.29
Cambridge	953	DJ.953.828	8.25	87.60	80.47	57.91
Cambridge	953	DJ.953.829	8.25	110.14	98.76	72.98
Cambridge	206	D9.206.183	10		52.74	40.00
Cambridge	953	DJ.953.934	29.25	47.65	42.10	30.28
Cambridge	953	DJ.953.941	29.25			60.60
Cambridge	953	DJ.953.943	29.25			63.99
Cambridge	953	DJ.953.944	29.25			73.21
Cambridge	953	DJ.953.946	29.25	97.85	79.09	57.89
Cambridge	953	DJ.953.947	29.25	75.72	76.70	53.75
Cambridge	953	DJ.953.948	29.25	89.55	79.70	59.47
Cambridge	953	DJ.953.1033	29.25	57.44	51.80	37.53
Cambridge	953	DJ.953.1035	29.25	47.07	39.85	27.82
Cambridge	953	DJ.953.1036	29.25	56.17	51.25	36.30
Cambridge	953	DJ.953.1037	29.25	51.71	47.74	33.82
Cambridge	953	DJ.953.1038	29.25	55.27	59.90	41.58
Cambridge	953	DJ.953.1039	29.25	59.30	50.75	36.24
Cambridge	953	DJ.953.1040	29.25	67.06	53.81	34.69
Cambridge	953	DJ.953.1078	29.25		98.61	
Cambridge	953	DJ.953.1079	29.25	102.99	91.78	71.54
Cambridge	953	DJ.953.1080	29.25			72.80
Cambridge	953	DJ.953.1081	29.25			65.00
Cambridge	953	DJ.953.1087	29.25		78.33	55.75
Cambridge	207	D9.207.117	42.5	59.42	48.18	33.82
Cambridge	953	DJ.953.1088	51	98.06	90.45	71.21
Cambridge	953	DJ.953.1089	51	103.41	85.65	
Cambridge	953	DJ.953.1090	51	107.67	91.53	70.77
Cambridge	953	DJ.953.1092	51	87.12	71.04	52.11
Cambridge	953	DJ.953.1092	51	84.10	72.75	51.79
Cambridge	953	DJ.953.1093	51	96.55	82.00	57.26
Cambridge	953	DJ.953.1094	51	94.11	85.64	59.56
Cambridge	953	DJ.953.1095	51	86.41	73.33	52.77
Cambridge	953	DJ.953.1096	51	75.60	69.75	47.25
Cambridge	953	DJ.953.1097	51	84.06	68.91	47.58
Cambridge	953	DJ.953.1098	51	87.46	77.37	
Cambridge	953	DJ.953.1099	51			39.29
Cambridge	953	DJ.953.1100	51	64.34	54.15	40.16
Cambridge	953	DJ.953.1101	51	69.30	61.46	43.37
Cambridge	953	DJ.953.1102	51	69.00	61.06	46.11
Cambridge	953	DJ.953.1103	51	59.42	53.45	39.51
Cambridge	953	DJ.953.1104	51	63.82	56.27	38.87
Cambridge	953	DJ.953.1105	51	57.86	51.67	40.95
Cambridge	953	DJ.953.1106	51		49.18	33.02
Cambridge	953	DJ.953.1107	51		50.69	37.67
Cambridge	953	DJ.953.1108	51		41.42	28.78

Cambridge	953	DJ.953.1175	51		47.96	36.50
Cambridge	953	DJ.953.1176	51	45.03	39.00	24.46
Cambridge	953	DJ.953.1195	60.75	97.45	82.92	
Cambridge	953	DJ.953.1200	60.75	55.80	49.48	36.76
Cambridge	953	DJ.953.1201	60.75		90.85	70.64
Cambridge	209	D9.209.284	76.1			59.62
Cambridge	209	D9.209.451	121.8	49.51	40.67	
Cambridge	211	D9.211.330	123.3			21.00
Cambridge	211	D9.211.331	123.3	62.16	50.52	
Cambridge	211	D9.211.333	123.3	66.21	53.17	
Cambridge	209	D9.209.721	141.3		57.99	
Cambridge	209	D9.209.732	157.8			
Cambridge	209	D9.209.782	174.3	43.10	36.81	24.87
Cambridge	209	D9.209.783	174.3	46.25	41.37	28.91
Cambridge	209	D9.209.872	190.8		55.51	39.46
Cambridge	209	D9.209.875	190.8			
Cambridge	209	D9.209.877	190.8	56.27		
Cambridge	209	D9.209.957	203.55	42.09	39.65	28.84
Cambridge	209	D9.209.959	203.55	62.60	49.70	
Cambridge	209	D9.209.960	203.55		57.65	
Cambridge	209	D9.209.1021	218.55	71.91		40.51
Cambridge	209	D9.209.1025	218.55		41.91	
Ithaca	477	62030		92.21	87.41	66.29
Ithaca	1133	62025		100.74	100.11	78.56
Ithaca	1134	62017		99.39	92.88	72.83
Ithaca	1134	62017		91.61	89.30	
Ithaca	1134	62017		120.79		
Ithaca	1134	62017		97.03		
Ithaca	1134	62017		93.19		
Ithaca	1135	62028		94.62	87.27	
Ithaca	1135	62028		63.28		
Ithaca	1135	62028		69.05		
Ithaca	1135	62018		95.79	92.77	74.40
Ithaca	1135	62018		66.50	57.75	42.31
Ithaca	1135	62018		100.80	96.96	77.00
Ithaca	1135	62018		81.64	73.29	52.63
Ithaca	1135	62018		50.83	45.74	
Ithaca	1135	62018		63.78	55.22	
Ithaca	1430	60944		68.52	59.47	44.77
Ithaca	1430	60944		65.18	53.10	39.73
Ithaca	1430	60944		50.56	50.48	35.11
Ithaca	1430	60944		47.18	41.06	28.73
Ithaca	1430	60944		56.29	48.11	
Ithaca	1430	60944		57.95	49.53	
Ithaca	1473	61778			61.04	43.66
Ithaca	1501	61737		53.38	47.90	31.54
Ithaca	1430 (4458)	65729		54.67	48.51	
Ithaca	PU 1532	61788		52.80		
Ithaca	PU 477 (4346)	58774			79.15	57.33
Ithaca	PU 477 (4346)	58774			72.78	55.90
Ithaca	PU 477 (4346)	58774		97.50	87.25	61.53
Ithaca	PU 477 (4346)	58774			85.46	66.87
Ithaca	PU 477 (4346)	58774		85.44	77.40	54.41

Ithaca	PU 477 (4346)	58774		95.10	86.18	68.33
Ithaca	PU 477 (4346)	58774			84.09	60.29
Ithaca	PU 477 (4346)	58774			79.46	61.33
Ithaca	PU 477 (4346)	58774		93.46	84.56	69.03
Ithaca	PU 477 (4346)	58774		89.75	85.16	68.25
Ithaca	PU 477 (4346)	58774			80.67	61.32
Ithaca	PU 477 (4346)	58774		88.24	82.27	58.78
Ithaca	40	58499		90.05	81.41	60.29
Ithaca	189	58451		52.75		37.93
Ithaca	360	58185		62.83	57.60	40.67
Ithaca	1119	58784		96.61	85.03	67.21
Ithaca	1406	60879		27.28	23.90	19.91
Ithaca	1499	60631		50.37	43.46	31.19
Ithaca	K - 119	58613		56.81		
Ithaca	K - 119	58610		68.90	62.00	44.94
Ithaca	Z - 40	58592		81.96	71.57	52.45
Ithaca	9	58840		61.24	50.71	37.10
Ithaca	9	58840		73.70		
Ithaca	9	58840		57.33		
Ithaca	9	58840		67.63		
Ithaca	9	58840		57.25		
Ithaca	746	62029		109.47	97.90	
Ithaca	746	62029		96.78	89.09	
Ithaca	746	62029		84.25	73.31	
Ithaca	1192	62277		61.22	52.01	
Ithaca	1510	60614		95.10	82.60	64.70
Ithaca	1414 (4743)	60890		94.84	83.27	56.47
Ithaca	19	59408		89.08	72.48	47.72
Ithaca	19	59408		66.71	56.24	39.87
Ithaca	1676	62905		88.45	73.55	
Ithaca	IPS - 443V	59686		97.72	88.09	
Ithaca	IPS - 460-V1	63574		104.16	87.18	
Ithaca	1161	58785		91.52	77.07	57.01
Ithaca	1161	58785		81.90	69.99	53.20
Ithaca	1523	60538		90.98	74.01	60.53
Ithaca	1852			65.21	59.88	40.65
Leeds	219	1179.2	-154.5			45.52
Leeds	219	1179.2	-154.5		68.22	
Leeds	219	1182.2	-148.5		73.75	
Leeds	219	1182.2	-148.5			48.33
Leeds	219	1185.2	-142.5			42.87
Leeds	219	1185.2	-142.5		73.93	52.81
Leeds	219	1185.2	-142.5	61.68		42.05
Leeds	220	1202.2	-111.5	39.42	30.2	
Leeds	220	1214.2	-92.5	96.25	85.6	62.61
Leeds	220	1214.2	-92.5		79.43	
Leeds	222		-59.5	84.57	77.88	
Leeds	229	1426.2	-33.5	104.56	100.6	86.53
Leeds	222	1255.2	-20.5		54.46	45.4
Leeds	229	1307.2	14.5	85.65	78.16	52.42
Leeds	229	1313.2	17.5	107.52		
Leeds	229	1327.2	29.5	86.93	81.19	57.69
Leeds	229	1327.2	29.5	85.9	81.91	63.26

Leeds	229	1327.2	29.5	90.65	85.97	60.21
Leeds	229	1329.2	33.5		61.85	
Leeds	229	1333.3A	38.5	104.31	95.11	76.91
Leeds	229	1343.2	46.5	92.48		60.88
Leeds	229	1351.2	50.5	106.4	97.62	
Leeds	229	1355.2	52.5	87.35	87.35	
Leeds	229	1355.2	52.5	91.34	91.46	67.09
Leeds	229	1353.2	52.5		87.82	61.51
Leeds	229	1359.2	54.5		81.09	60.81
Leeds	229	1359.2	54.5		85.28	63.86
Leeds	229	1359.2	54.5		80.98	
Leeds	229	1359.2	54.5	93.03	81.31	
Leeds	229	1361.2	55.5			
Leeds	229	1361.2	55.5	95.14	88.65	
Leeds	229	1361.2	55.5	81.3	80.05	79.85
Leeds	229	1361.2	55.5	56.64	50.19	36.2
Leeds	229	1361.2	55.5	95.11	87.16	66.29
Leeds	229	1361.2	55.5	95.37	85.61	
Leeds	229	1361.2	55.5	93.15	88.44	72.35
Leeds	229	1361.2	55.5	53.43	43.63	30.91
Leeds	229	1361.2	55.5		95.97	73.74
Leeds	229	1361.2	55.5		80.08	64.56
Leeds	229	1361.2	55.5	63.68	56.6	38.89
Leeds	229	1363.2	56.5		82.65	59.47
Leeds	229	1363.2	56.5	102.58	92.98	65.63
Leeds	229	1375.2	62.5	80.84	78.46	
Leeds	229	1375.2	62.5	56.19		31.63
Leeds	229	1375.2	62.5	70.64	68.09	
Leeds	229	1375.2	62.5	63.57	52.55	38.18
Leeds	229	1375.2	62.5	62.07	51.32	38.91
Leeds	229	1375.2	62.5		81.54	
Leeds	229	1375.2	62.5		84.8	
Leeds	229	1379.2	72.5			62.7
Leeds	229	1379.2	72.5		83.35	65.26
Leeds	229	1379.2	72.5	91.82	92.22	70.89
Leeds	229	1379.2	72.5	86.61	81.88	58.17
Leeds	230	1333.3A		88.2	85.85	68.1

Dataset B.4: Morphometric Data Set: *Lahillia* Internal Moulds

Collection	Station/Section	Full Code	KPBHeight	L	H	W
Cambridge	952	DJ.952.526	-137.45	97.25	84.44	57.99
Cambridge	952	DJ.952.528	-137.45	68.03	61.93	47.32
Cambridge	952	DJ.952.530	-137.45	67.83	57.05	38.14
Cambridge	952	DJ.952.670	-117		70.48	49.56
Cambridge	952	DJ.952.670	-117			
Cambridge	952	DJ.952.671	-117			46.31
Cambridge	952	DJ.952.672	-117		65.85	47.49
Cambridge	952	DJ.952.674	-117		54.53	38.16
Cambridge	952	DJ.952.711	-98.75	88.63	81.75	
Cambridge	952	DJ.952.712	-98.75	95.16	83.26	56.38
Cambridge	952	DJ.952.713	-98.75	82.04	73.49	52.65

Cambridge	952	DJ.952.714	-98.75	81.4	70.95	47.61
Cambridge	953	DJ.953.34	-84.25	83.75	72.73	
Cambridge	953	DJ.953.35	-84.25		53.92	41.02
Cambridge	953	DJ.953.88	-76	84.02	73.14	51.45
Cambridge	953	DJ.953.169	-64.75	61.53	55.1	
Cambridge	953	DJ.953.207	-53.5	87.88	72.63	
Cambridge	953	DJ.953.210	-53.5	84.13	76.08	55.18
Cambridge	953	DJ.953.211	-53.5	69.95	59.65	46.72
Cambridge	953	DJ.953.452	-48.25	79.02	69.6	53.48
Cambridge	953	DJ.953.656	-17.5	68.63	64.18	42.49
Cambridge	953	DJ.953.660	-17.5	71.28	61.5	46.95
Cambridge	205	D9.205.249	-8.85	64.26	60.93	42.15
Cambridge	205	D9.205.251	-8.85			43.22
Cambridge	205	D9.205.252	-8.85	82.75		
Cambridge	205	D9.205.296	-8.85	68.83		50.31
Cambridge	953	DJ.953.696	-4.5		62.32	46.8
Cambridge	953	DJ.953.698	-4.5	70.62	62.38	46.08
Cambridge	953	DJ.953.700	-4.5			45.24
Cambridge	953	DJ.953.742	-1.75	42.23	36.83	
Cambridge	953	DJ.953.743	-1.75	83.22	68.58	49.16
Cambridge	953	DJ.953.793	2.5	93.55	76.91	50.28
Cambridge	953	DJ.953.794	2.5	74.27	67.92	50.68
Cambridge	206	D9.206.151	3.5	78.18		46.39
Cambridge	206	D9.206.181	10			74.19
Cambridge	206	D9.206.185	10		75.02	61.75
Cambridge	207	D9.207.2	18.9	53.58	43.44	29.14
Cambridge	207	D9.207.3	18.9	56.18	45.62	29.68
Cambridge	207	D9.207.4	18.9	60.53	50.6	35.41
Cambridge	207	D9.207.5	18.9	33.28	29.4	19.4
Cambridge	207	D9.207.53	18.9	36.1	29.53	20.57
Cambridge	953	DJ.953.942	29.25	81.19		59.69
Cambridge	953	DJ.953.945	29.25	95.11	87.39	62.57
Cambridge	953	DJ.953.1031	29.25		45.14	33.21
Cambridge	953	DJ.953.1034	29.25	47.73	45.11	28.88
Cambridge	953	DJ.953.1082	29.25		72.96	47.29
Cambridge	207	D9.207.55	30.15	101.21		61.13
Cambridge	207	D9.207.129	42.5		50.45	35.31
Cambridge	953	DJ.953.1173	51	56.71	50.74	36.18
Cambridge	207	D9.207.178	55.25	69.85	58.43	42.41
Cambridge	953	DJ.953.1198	60.75	58.57	49.21	33.74
Cambridge	953	DJ.953.1199	60.75	59.15	56.16	34.3
Cambridge	953	DJ.953.1292	69	94.5	89.81	69.13
Cambridge	211	D9.211.456	99.3	76.06	60.69	
Cambridge	211	D9.211.332	123.3	62.85	56.16	38.13
Cambridge	211	D9.211.139	136.8		41.12	26.94
Cambridge	211	D9.211.41	138.3	64.97	54.23	35.4
Cambridge	209	D9.209.611	141.3			43.06
Cambridge	209	D9.209.612	141.3	76.95	64.48	
Cambridge	209	D9.209.733	157.8		42.99	27.97
Cambridge	209	D9.209.1024	218.55		51.37	
Cambridge	209	D9.209.1123	273.3			70.44
Cambridge	209	D9.209.1136	287.55			45.5
Cambridge	209	D9.209.1138	287.55	94.46	88.08	66.63

Cambridge	210		351.8	34.2	24.5	15.35
Cambridge	200	D9.200.9		77.3	67.17	48.44
Cambridge	212	D9.212.31		110.46		58.4
Leeds	220	1200.2	-111.5	79.87	71.38	40
Leeds	220	1223.2A	-80.5		78.7	
Leeds	222	1245.2	-38.5	82.96	76.26	55.4
Leeds	229	1307.2	14.5	97.95	88.3	57.34
Leeds	229	1307.2	14.5	91.69	81.32	52.68
Leeds	229	1313.2	17.5	85.44	80.65	
Leeds	229	1313.2	17.5	100.01	86.96	
Leeds	229	1320.2	24.5	78.62	73.01	51.48
Leeds	229	1320.2	24.5	83.48	76.85	
Leeds	229	1320.2	24.5	70.16	63.41	
Leeds	229	1320.2	24.5	79.36	75.01	57.08
Leeds	229	1320.2	24.5	75.1	66.95	51.45
Leeds	229	1320.2	24.5	91.36		62.38
Leeds	229	1334.2	39.5	91.01	83.55	
Leeds	229	1351.2	50.5	57.47	49.7	35.22
Leeds	229	1359.2	54.5	56.14		38.44
Leeds	229	1359.2	54.5	83.7	80.82	60.21
Leeds	229	1359.2	54.5	72.57	73.7	
Leeds	229	1361.2	55.5	92.45	75.46	54.95
Leeds	229	1361.2	55.5	53.58	51.5	34.63
Leeds	229	1363.2	56.5	79.55	76.99	78.38
Leeds	229	1379.2	72.5	90.65	85.38	71.54

Dataset B.5: Morphometric Data Set: *Cucullaea* External Shells

Collection	Section	Specimen #	KPBHeight	L	H to Plate	H to Umbo	W
Cambridge	203	43	-8.85	27.74		19.37	15.76
Cambridge	206	130	0.5	27.72	19.06		
Cambridge	206	189	10	45.84	29.85	36.5	
Cambridge	206	197	10	37.09	21.32		
Cambridge	207	62	30.15	46.35	26.82		
Cambridge	207	63	30.15	30.62	18.32	19.1	
Cambridge	207	165-170	55.25	47.47		35.51	29.85
Cambridge	207	165-170	55.25	44.29		32.97	
Cambridge	207	165-170	55.25	38.06		28.63	
Cambridge	207	165-170	55.25	49.02		37.45	
Cambridge	209	730	157.8	46.01	26.8	31.9	
Cambridge	209	1027	273.3	56.8	37.84		
Cambridge	209	1028	273.3	48.4	34.98	39.66	
Cambridge	209	803-814	174.3	42.29	25.41	32.46	32.85
Cambridge	209	803-814	174.3	44.82		32.06	30.7
Cambridge	209	803-814	174.3	23.17	13.43	16.37	
Cambridge	209	878-883	190.8	11.96	6.26		
Cambridge	209	962-964	203.55	24.36	16.99	18.7	
Cambridge	209	962-964	203.55	24.22	16.88		
Cambridge	211	142	136.8	49.5	28.2	33.85	16.78
Cambridge	211	143	136.8	50.49	31.48	38.47	35.02
Cambridge	211	144	136.8	39.25	22.83	27.38	22.68
Cambridge	211	145	136.8	50.45	30.73	37.76	17.48

Cambridge	211	146	136.8	41.06	29.44	34.11	27.42
Cambridge	211	148	136.8	47.09	29.75	35.49	35.2
Cambridge	211	149	136.8	60.22		38.75	
Cambridge	211	150	136.8	45.93	28.22	34.02	
Cambridge	211	151	136.8	31.9	18.79	22.07	21.32
Cambridge	211	152	136.8	50.12	28.23	33.82	33.1
Cambridge	211	154	136.8	42.05		34.95	
Cambridge	211	158	136.8	47.46	31.94	36.83	33.72
Cambridge	211	159	136.8	46.25	27.01	32.71	29.2
Cambridge	211	161	136.8	43.68	30.55	33.29	
Cambridge	211	164	136.8	31.8	20.57	23.74	15.88
Cambridge	211	165	136.8	45.6	27.61	35.51	30.98
Cambridge	211	356	123.3	11.88		8.04	
Cambridge	211	363 A-F	123.3	52.76	30.64	38.48	
Cambridge	211	363 A-F	123.3	49.16	27.69		
Cambridge	211	363 A-F	123.3	35.34		25	
Cambridge	211	363 A-F	123.3	26.26		19.45	15.68
Cambridge	211	363 A-F	123.3	56.47	31.89		
Cambridge	211	94-98	138.3	49.82			35.4
Cambridge	212	2748		72.31	53.5	64.84	
Cambridge	214	2		100.6	67.09	83.44	
Cambridge	214	4		83.53	56.79	66.05	56.72
Cambridge	214	5		113.6	68.98		90.82
Cambridge	214	7		76.76	51.22		47.06
Cambridge	215	4-16		81.52	58.39	64.61	
Cambridge	215	4-16		96.3	63.66	71.72	71.1
Cambridge	215	4-16		93.69	57.92	66.04	68.06
Cambridge	215	4-16		100.6	62.83		74.9
Cambridge	952	280	-165.5	67.55	41.51	60.23	62.24
Cambridge	952	534	-137.45	31.98	22.16	27.68	
Cambridge	953	164	-64.75	63.52		48.64	
Cambridge	953	248	-53.5	70.21	47.28	59.17	
Cambridge	953	252	-53.5	35.54		27.23	
Cambridge	953	253	-53.5	26.11	19.07	22.8	
Cambridge	953	345	-48.25	67.11	38.32	54.3	61.42
Cambridge	953	717	-4.5	29.94			
Cambridge	953	754	-1.75	59.26	38.92	45.51	46
Cambridge	953	765	-1.75	35.63	21.84	26.19	
Cambridge	953	798	2.5	56.98	33.28		
Cambridge	953	822	4.125	48.1	29.14	38.36	41.72
Cambridge	953	1145-1152	51	46.68	27.77	35.36	
Cambridge	953	1145-1152	51	41.24	26.7	30.39	
Cambridge	953	1145-1152	51	45.17	27.51	33.58	33.01
Cambridge	953	1145-1152	51	45.65	27.82	36.39	33.56
Cambridge	953	1145-1152	51	37.95	24.9		
Cambridge	953	1221-1237	60.75	43.06	30.83		
Cambridge	953	1221-1237	60.75	42.41			29
Cambridge	953	1221-1237	60.75	27.28	17.27	19.67	
Cambridge	953	1221-1237	60.75	24.11	14.63	17.44	
Cambridge	953	866-882	29.25	52.42	31.71	39.24	41.28
Cambridge	953	866-882	29.25	50.86	29.23	40.63	42.44
Cambridge	953	866-882	29.25	54.38	33.48	42.1	43.9
Cambridge	953	866-882	29.25	46.95	29.76	37.57	34.6

Cambridge	953	866-882	29.25	49.96	28.17	35.31	38
Cambridge	953	866-882	29.25	50.02	27.65	34.32	36.8
Cambridge	953	866-882	29.25	46.77	28	35.17	18.87
Cambridge	953	866-882	29.25	42.82	27.64	33.86	42.44
Cambridge	953	866-882	29.25	51.69	28.51	36.52	
Cambridge	953	866-882	29.25	47.89	28.35		17.18
Cambridge	953	866-882	29.25	45.72	27.77	33.68	34.98
Cambridge	953	883-893	29.25	42.08	25.69	33.96	37.48
Cambridge	953	883-893	29.25	48.18	29.07	36.44	38
Cambridge	953	883-893	29.25	49.93	26.96	35.44	40.54
Cambridge	953	883-893	29.25	47.61	29.64	37.2	41
Cambridge	953	883-893	29.25	53.58	31.82	38.42	41.22
Cambridge	953	883-893	29.25	49.38	30.57	39.67	45.18
Cambridge	953	883-893	29.25	44.32	24.94	30.31	35.64
Cambridge	953	883-893	29.25	50.33	28.95	36.19	36.08
Cambridge	953	894-896	29.25	54.06	28.77	33.9	37.55
Cambridge	953	894-896	29.25	36.75	21.43	25.08	24.13
Cambridge	957	41	-322.25	75.29		60.96	
Cambridge	957	409	-265.25	57.09	37.26	51.82	57.06
Cambridge	957	486	-233.75	27.38	16.84	22.15	20.52
Cambridge	957	495	-220.5	72.55		65.72	
Cambridge	957	536	-206.5	25.23	17.65	20.62	
Cambridge	959	87	-392.25	55.66	37.64	44.95	36.7
Cambridge	959	92	-392.25	66.07	37.68	42.77	40.3
Cambridge	959	95	-392.25	63.89	38.96	45.61	
Cambridge	959	142	-381.25	74.47	39.65	48.79	50.96
Cambridge	959	183-186	-369.75	59.08	35.81	42.1	36.68
Cambridge	959	183-186	-369.75	64.02	36.96	44.09	38.68
Cambridge	959	190-194	-369.75	65	37.37	44.45	50.46
Cambridge	959	190-194	-369.75	65.34	35.06	46.53	49.62
Cambridge	959	190-194	-369.75	58.2	32.67	44.49	38.4
Cambridge	959	96-99	-392.25	56.32	34.34	42.2	41.52
Leeds	215	672.2	-423	74.95	48.47		
Leeds	219	1182.2	-149	70.18	46.12	57.8	57.97
Leeds	229	1359.2	54.5	42.39	25.92	32.56	20.61

Dataset B.6: Morphometric Data Set: *Cucullaea* Internal Moulds

Collection	Section	Specimen #	KPBHeight	L	H to Plate	H to Umbo	W
Leeds	215	686.2	-408	62.86		40.96	26
Leeds	215	332.2A	-495	53.71	26.81		31.9
Leeds	218	1027.2	-364	63.65	40.76		42
Leeds	220	1226.2	65.5		35.12	45.89	50.2
Leeds	229	1301	5.5		37.29	43.03	39.22
Leeds	229	1301	5.5	56.96	23.78	30.74	35.62
Leeds	215	672.2	-423	68.39	43.25	51.31	54.06

Dataset B.7: Morphometric Data Set: Leionucula External Shells

Collection	Section	Specimen #	KPBHeight	L	H	W

Cambridge	959	101-108	-392.25	42.07	30.6	23.89
Cambridge	959	101-108	-392.25	44.17	32.3	24.4
Cambridge	959	130	-381.25	44.38	30.67	24.89
Cambridge	959	130-134	-381.25	38.58	30.44	
Cambridge	959	210-213	-369.75		28.23	21.59
Cambridge	959	326-330	-347.5	35.83	26.42	18.82
Cambridge	952	499-505	-146	26.19	21.06	15.24
Cambridge	952	499-505	-146	29.93	17.54	14.6
Cambridge	952	499-505	-146	24.26	18.72	16.16
Cambridge	203	11	-8.85	31.16	22	15.27
Cambridge	203	12	-8.85	30.64	22.87	14.7
Cambridge	207	11	18.9	34.6	26.65	18.7
Cambridge	207	24	18.9	31.63		
Cambridge	207	28	18.9	34.8	26.47	
Cambridge	207	47	18.9	37.53	26.53	
Cambridge	953	1066-1076	29.25	23.28	18.55	12.4
Cambridge	953	1066-1076	29.25	20.31		10.28
Cambridge	953	897-911	29.25	35.6	26.58	23.67
Cambridge	953	897-911	29.25	34.45	28.88	21.48
Cambridge	953	897-911	29.25	28.39	20.14	18.82
Cambridge	953	912-914	29.25	36.42	27.35	20.34
Cambridge	953	949-972	29.25	28	22.74	15.8
Cambridge	953	949-972	29.25	31.59	24.75	17.49
Cambridge	953	949-972	29.25	29.97	22.27	20.5
Cambridge	953	949-972	29.25	33.97	26.17	18.46
Cambridge	953	972-999	29.25	25.04	20.21	14.48
Cambridge	953	972-999	29.25	24.41	20	13.1
Cambridge	953	972-999	29.25	30.5	26.24	17.12
Cambridge	953	972-999	29.25	31.37	21.89	
Cambridge	207	69	30.15	38.38	29.54	
Cambridge	207	110	42.5	26.4	16.89	13.49
Cambridge	207	111	42.5	32.4	25.9	
Cambridge	207	112	42.5	35.52	25.95	
Cambridge	953	1110-1144	51	38.05	29.2	21.27
Cambridge	953	1110-1144	51	31.82	22.72	18.85
Cambridge	953	1110-1144	51	31.86	24.16	
Cambridge	953	1110-1144	51	32.31	23.91	18.84
Cambridge	953	1110-1144	51	34.75	25	20.11
Cambridge	953	1110-1144	51	36.04	27.32	22.45
Cambridge	953	1110-1144	51	37.65		20.24
Cambridge	953	1110-1144	51	28.85	21.9	13.7
Cambridge	953	1110-1144	51	34.63	26.37	
Cambridge	953	1110-1144	51	33.26	24.05	
Cambridge	953	1110-1144	51	33.21	25.3	
Cambridge	207	136	55.25	39.33	30.39	
Cambridge	207	137	55.25	30.45	21.78	
Cambridge	207	138	55.25	31.59	21.77	
Cambridge	207	139	55.25	40.93		
Cambridge	207	140	55.25	37.83	27.99	
Cambridge	207	144	55.25	22.84	15.6	
Cambridge	207	154	55.25	31.95	22.97	
Cambridge	207	156	55.25	21.87	17.43	
Cambridge	207	157	55.25	32	23.82	17.67

Cambridge	953	1204-1220	60.75	36.17	26.86	20.04
Cambridge	953	1204-1220	60.75	23.65	18.55	
Cambridge	953	1204-1220	60.75	32.31	22.32	18.54
Cambridge	953	1204-1220	60.75	32.48	25.88	17.06
Cambridge	953	1204-1220	60.75	24.56		20.72
Cambridge	953	1204-1220	60.75	19.96	15.02	9.74
Cambridge	953	1204-1220	60.75	32.35	23.5	19.22
Cambridge	953	1204-1220	60.75	19.93	14.98	9.6
Cambridge	953	1204-1220	60.75	23.54	17.87	
Cambridge	953	1204-1220	60.75	34.77	25.84	20.86
Cambridge	953	1204-1220	60.75	35.5	26.88	18.2
Cambridge	953	1204-1220	60.75	30.76	24.02	18.05
Cambridge	953	1204-1220	60.75	31.71	24.78	17.26
Cambridge	953	1204-1220	60.75	35.19	26.57	19.94
Cambridge	207	223	64	31.71	25.28	
Cambridge	953	1310-1319	69	32.4		18.34
Cambridge	953	1310-1319	69	36.45	24.88	19.43
Cambridge	209	444-446	121.8	18.72	13.91	9.12
Cambridge	211	366	123.3	28	21.34	12.95
Cambridge	211	367	123.3	25.53	20.16	13.64
Cambridge	211	370	123.3	23.69	18.33	
Cambridge	211	371	123.3	25.81	19.34	13.7
Cambridge	211	386	123.3	24.88	17.99	
Leeds	215	667.2	-428		30.01	27.43
Leeds	218	1066	-324	53.9	33.5	27.13
Leeds	219	1185.2	-145	56.81	50	35.79
Leeds	229	1336.2	41.5	18.18	12.34	11.87
Leeds	229	1336.2	41.5	28.76	24.55	16.52
Leeds	229	1336.2	41.5	25.56	23.55	14.57
Leeds	229	1351.2	50.5	24.66	20.96	13.7
Leeds	229	1351.2	50.5	24.93	23.87	
Leeds	229	1361.2	55.5	21.08	17.83	
Leeds	229	1361.2	55.5	37.46	31.31	22.66

Dataset B.8: Morphometric Data Set: Leionucula Internal Moulds

Collection	Section	Specimen #	KPBHeight	L	H	W
Cambridge	959	101-108	-392.25	43.06	31.5	24.28
Cambridge	959	101-108	-392.25	35.67	28.25	20.7
Cambridge	959	101-108	-392.25	37.53	27.21	
Cambridge	959	130-134	-381.25	36.92	25.45	19.02
Cambridge	959	130-134	-381.25	40.7	26.92	
Cambridge	959	130-134	-381.25	40.15	28.9	
Cambridge	959	210	-369.75	35.65	27.15	17.3
Cambridge	959	210-213	-369.75	28.02	23.32	14.5
Cambridge	959	326-330	-347.5	38.22	28.49	18.99
Cambridge	959	326-330	-347.5	34.07	23.83	
Cambridge	959	326-330	-347.5	38.29	28.79	20.04
Cambridge	953	359-361	-48.25	18.91	15.12	11.66
Cambridge	207	25	18.9	31.85	23.36	
Cambridge	207	27	18.9	33.1	23.13	15.8
Cambridge	207	31	18.9	34.13	23.59	16.44

Cambridge	207	21a	18.9	24.98	18.42	11.58
Cambridge	207	33-45	18.9	38.2	27.73	18.48
Cambridge	953	1043	29.25	29.52	23.17	16.98
Cambridge	953	1044	29.25	22.5	17.3	11.55
Cambridge	953	1066-1076	29.25	26.06	20.86	14.03
Cambridge	953	1066-1076	29.25	28.69	20.31	12.66
Cambridge	953	897-911	29.25	29.46	21.19	14.6
Cambridge	953	897-911	29.25	23.92	18.12	13.42
Cambridge	953	897-911	29.25	24.42	19.72	10.11
Cambridge	953	897-911	29.25	24.43	17.48	
Cambridge	953	897-911	29.25	28.05	21.54	14.44
Cambridge	953	897-911	29.25	29.45	22.58	14.92
Cambridge	953	949-972	29.25	24.82	19.62	11.59
Cambridge	953	949-972	29.25	29.72	20.78	16.26
Cambridge	953	949-972	29.25	34.24	23.78	17.37
Cambridge	953	949-972	29.25	34.32	24.02	19.88
Cambridge	953	949-972	29.25	29.8	22.1	15.73
Cambridge	953	972-999	29.25	19.56	14.52	9.59
Cambridge	953	972-999	29.25	29.38	21.81	15.71
Cambridge	953	972-999	29.25	33.03	22.99	
Cambridge	953	972-999	29.25	27.49	19.19	13.02
Cambridge	953	972-999	29.25	24.91	19.34	12.9
Cambridge	953	972-999	29.25	26.5	21.16	14.58
Cambridge	953	972-999	29.25	26.79	19.83	13.03
Cambridge	207	130	42.5	26.04	15.11	12.28
Cambridge	953	1110-1144	51	31.71	24.31	17.42
Cambridge	953	1110-1144	51	31.77	24.42	16.44
Cambridge	953	1110-1144	51	25.27	18.6	12.88
Cambridge	953	1110-1144	51	33.48	26.48	
Cambridge	953	1110-1144	51	32.19	23.64	15.71
Cambridge	953	1110-1144	51	31.48	24.67	
Cambridge	207	145	55.25	29.69	20.49	13.58
Cambridge	207	158a	55.25	31.84		14.82
Cambridge	953	1204-1220	60.75	28.61		15.29
Cambridge	953	1204-1220	60.75	33.29		17.44
Cambridge	953	1204-1220	60.75	30.52		16.95
Cambridge	953	1204-1220	60.75	21.6	14.63	11.5
Cambridge	953	1204-1220	60.75	31.28		17.25
Cambridge	953	1204-1220	60.75	31.3	24.2	18
Cambridge	953	1204-1220	60.75	33.46	23.68	18.1
Cambridge	953	1204-1220	60.75	34.24	26.32	17.18
Cambridge	953	1204-1220	60.75	21.21	14.8	12.4
Cambridge	953	1204-1220	60.75	33.28	23.55	17.47
Cambridge	953	1204-1220	60.75	33.37	23.35	17.92
Cambridge	953	1204-1220	60.75	34.26	23.71	17.25
Cambridge	953	1204-1220	60.75	31.21	21.77	17.63
Cambridge	953	1204-1220	60.75	31.48	23.65	17.25
Cambridge	953	1204-1220	60.75	23.7	30.77	26.85
Cambridge	953	1204-1220	60.75	32.64	25.21	17.68
Cambridge	953	1310-1319	69	33.8	24.45	19.7
Cambridge	953	1310-1319	69	34.9	25.41	16.74
Cambridge	953	1310-1319	69	33.3	26.55	17.79
Cambridge	209	283	76.1	15.97	14.18	8.29

Cambridge	211	488-490	99.3	30.24	22.71	14.08
Cambridge	209	444-446	121.8	18.37	13.27	7.29
Cambridge	211	368	123.3	24.81	20.7	12.65
Cambridge	211	369	123.3	25.24	18.63	12.1
Cambridge	211	372	123.3	18.55	14.35	8.33
Cambridge	211	375	123.3	24.14	17.86	10.64
Cambridge	211	324	136.8	27.67	21.69	14.54
Cambridge	211	327	136.8	17.34	13.82	8.89
Cambridge	211	58	138.3	21.24	16.15	
Cambridge	209	794	174.3	21.11	16.61	9.24
Leeds	237	1428.2			22.13	15.54
Leeds	237	1432.2		34.87	23.48	18.24

Table B.1 A-C: Summary of morphometric measurements in Datasets B3 to B8 analysed by collection and stratigraphy. Measurements are in mm

A) *Lahillia*	KLB789		KLB10		SOB		TELM	
	Average	Max	Average	Max	Average	Max	Average	Max
Cambridge								
L	76.8	97.3	74.6	110.1	60.6	94.5	110.5	110.5
H	68.0	90.1	66.4	98.8	50.4	88.1		
W	50.0	64.9	49.3	74.2	38.3	70.4	58.4	58.4
Ithaca								
L	65.3	96.6	78.6	120.8	78.1	109.5	89.2	104.2
H	60.7	85.0	72.6	100.1	75.6	97.9	75.5	88.1
W	44.3	67.2	57.2	78.6	52.8	64.7	43.8	47.7
Leeds								
L	74.1	96.3	82.4	107.5	93.4	104.6		
H	70.0	85.6	77.3	97.6	88.7	100.6		
W	48.3	62.6	55.9	79.9	69.2	86.5		
Overall L	74.9	97.3	78.1	120.8	71.4	109.5	92.8	110.5
Overall H	67.6	90.1	71.1	100.1	61.9	100.6	75.5	88.1
Overall W	49.2	67.2	52.3	79.9	47.4	86.5	48.7	58.4

B) *Cucullaea*	KLB789		KLB10		SOB		TELM	
	Average	Max	Average	Max	Average	Max	Average	Max
Cambridge								
L	53.9	75.3	44.9	57.0	41.5	60.2	91.0	113.6
H to Umbo	42.3	65.7	33.8	42.1	30.6	39.7	69.5	83.4
W	43.1	62.2	35.8	45.2	27.1	35.4	68.1	90.8
Leeds								
L	65.6	75.0	49.7	57.0				
H to Umbo	49.0	57.8	35.4	43.0				
W	43.7	58.0	31.8	39.2				
Overall L	56.1	75.3	45.1	57.0	41.5	60.2	91.0	113.6
Overall H to Umbo	43.3	65.7	34.0	43.0	30.6	39.7	69.5	83.4
Overall W	43.3	62.2	35.4	45.2	27.1	35.4	68.1	90.8

C) *Leionucula*	KLB789		KLB10		SOB	
	Average	Max	Average	Max	Average	Max
Cambridge						
L	36.0	44.4	30.5	40.9	23.5	31.7
H	26.4	32.3	22.8	30.8	18.1	25.3
W	19.1	24.9	16.4	26.9	11.1	14.5
Leeds						
L	55.4	56.8	25.8	37.5		
H	37.8	50.0	22.1	31.3		
W	30.1	35.8	15.9	22.7		
Overall L	37.7	56.8	30.2	40.9	23.5	31.7
Overall H	27.8	50.0	22.7	31.3	18.1	25.3
Overall W	20.7	35.8	16.4	26.9	11.1	14.5

Dataset B.9: Acetate peel ontogenetic data from Maastrichtian bivalve teeth (measurements in mm)

Specimen / Year	DJ.953. 663	D5.220. 1214.2	D5.220. 1214.2.A	DJ.952. 712.A	DJ.952. 712.B	DJ.953. 452A	DJ.953. 452B	DJ.952. 755	DJ.953. 745	D5.220. 1217.2	D5.219. 1185.2
1	0.8891	0.3479	0.6892	0.4246	0.3559	0.2598	0.2191	0.392	0.1582	0.0974	0.3564
2	1.7602	1.0127	1.2988	1.2927	0.6577	0.6728	0.6856	0.7104	0.5715	0.5602	0.7611
3	2.3142	1.6938	1.874	1.8125	1.0324	1.2669	1.1294	1.0787	1.0981	1.5081	1.3878
4	2.8467	2.3711	2.3626	2.293	1.4416	1.7396	1.6628	1.6044	1.9939	2.6105	1.7575
5	3.4755	3.2065	2.8419	2.8149	1.8557	2.2252	2.5603	2.2443	2.8098	3.4642	2.1357
6	4.1016	4.0383	3.3722	3.2695	2.2585	2.7763	3.4532	2.8476	3.7013	4.0298	2.5802
7	4.7134	4.363	3.6847	3.6989	2.6181	3.4624	4.483	3.2541	4.5616	4.495	2.9061
8	5.3627	4.8553	4.0028	3.9043	2.9594	4.112	5.6311	3.6268	5.367	4.971	3.2776
9	5.7249	5.1146	4.3349	4.1604	3.3404	4.4716	6.1534	3.9359	6.2031	5.4502	3.5393
10	6.1695	5.4906	4.6691	4.5226	3.6469	4.8505	6.6072	4.2861	6.8545	5.7487	3.7304
11	6.6065	5.8644	4.9853	4.8727	3.9425	5.3524	7.1571	4.5584	7.3248	6.1093	4.0254
12	7.016	6.2832	5.1975	5.1803	4.2078	5.9104	7.8426	4.7642	7.8272	6.6398	4.2114
13	7.374	6.628	5.4796	5.4219	4.4348	6.2633	8.2561	4.9391	8.1836	7.2075	4.4925
14	7.6926	6.8649	5.7367	5.6611	4.6729	6.6721	8.6656	5.0991	8.5655	7.7135	4.6524
15	7.9978	7.1931	5.9627	5.8954	4.9243	7.0252	9.0038	5.2226	8.8972	8.2018	4.9741
16	8.2942	7.4885	6.2877	6.1408	5.1677	7.1397	9.1501	5.3269	9.1885	8.7157	5.3597
17	8.5587	7.729	6.5418	6.3358	5.374	7.2017	9.2576	5.4816	9.4767	9.06	5.7417
18	8.7425	8.0796	6.7777	6.5023	5.5292	7.3666	9.3497	5.6297	9.7829	9.3426	6.151
19	8.8869	8.3522	7.0062	6.6147	5.6338	7.5216	9.4666	5.7468	10.023	9.6654	6.5262
20	9.0201	8.6252	7.1971	6.7799	5.807	7.6316	9.537	5.8252	10.294	9.8478	6.8689
21	9.1402	8.8509	7.427	6.887	5.8776	7.7213	9.6172	5.8863	10.552	9.9964	7.1837
22	9.2708	9.0683	7.5557	6.9982	6.0174	7.8077	9.7199	5.9321	10.754	10.175	7.5096
23	9.382	9.2451	7.6366	7.1774	6.1799	7.9234	9.7835	5.9981		10.294	7.8271
24	9.5195	9.3759	7.7318	7.3123	6.3527	8.0404	9.8439	6.0177		10.447	8.3807

Specimen	DJ.953. 663	D5.220. 1214.2	D5.220. 1214.2.A	DJ.952. 712.A	DJ.952. 712.B	DJ.953. 452A	DJ.953. 452B	DJ.952. 755	DJ.953. 745	D5.220. 1217.2	D5.219. 1185.2
Year											
25	9.6363	9.4576	7.8268	7.4125	6.4557	8.0912	9.8944	6.0741		10.558	8.6283
26	9.7426	9.5225	7.9277	7.5077	6.5615	8.1485	9.9397	6.1447		10.775	8.8861
27	9.8841	9.6242	8.0283	7.6212	6.6729	8.1847		6.2067		10.986	9.0824
28	10.032	9.7201	8.1086	7.7351	6.776	8.2276		6.296		11.13	9.2789
29	10.139	9.8146	8.179	7.8451	6.8498			6.3485		11.238	9.6421
30	10.223	9.8823	8.2492	8.0078	6.9407			6.4779		11.362	9.7847
31	10.27	9.9347	8.312	8.1066	7.0368			6.5904		11.473	9.9346
32	10.328	9.9826	8.3597	8.1797	7.1401					11.517	10.056
33	10.385	10.042	8.4074	8.2442	7.2216					11.599	10.175
34	10.443	10.108	8.4451	8.3015	7.2957					11.668	10.306
35	10.535	10.183	8.4852	8.3745	7.3562						10.36
36	10.576	10.24	8.5003	8.4395	7.4308						10.466
37	10.61	10.291	8.5355	8.5071	7.5034						10.597
38	10.657	10.373	8.5782	8.543	7.5638						10.748
39	10.7	10.409	8.631	8.605	7.6023						10.864
40	10.721	10.519	8.6686	8.6613	7.6315						11.017
41	10.752	10.583	8.7063	8.699	7.6786						
42	10.813	10.69	8.7314	8.7186	7.7272						
43	10.858	10.766	8.7565	8.7478	7.7727						
44	10.893	10.806	8.7916	8.7827	7.8007						
45	10.936	10.895	8.8217	8.7976	7.8221						
46	10.999	10.986	8.8719	8.8444	7.8749						
47	11.037	11.052	8.9021	8.8927	7.9115						
48	11.078	11.097	8.9297	8.9491	7.9694						
49	11.127	11.208	8.9523	9.0166	8.0083						
50	11.194	11.303	8.9924	9.0548	8.0335						

Specimen	DJ.953. 663	D5.220. 1214.2	D5.220. 1214.2.A	DJ.952. 712.A	DJ.952. 712.B	DJ.953. 452A	DJ.953. 452B	DJ.952. 755	DJ.953. 745	D5.220. 1217.2	D5.219. 1185.2
Year											
51	11.224		9.0225	9.0986	8.0599						
52	11.272		9.0476	9.1583	8.1001						
53	11.321		9.0728	9.1886	8.129						
54	11.358		9.1181	9.2144	8.1518						
55	11.39		9.1713	9.2447	8.1722						
56	11.418		9.2139	9.2861	8.1929						
57	11.433		9.2716	9.3178	8.2301						
58	11.47		9.3169	9.3504	8.2636						
59	11.489		9.3671	9.4012	8.3097						
60	11.53		9.3973	9.4553	8.3464						
61	11.56		9.4275	9.4823	8.3734						
62	11.612		9.4551	9.5172	8.4036						
63	11.649		9.4852	9.5397	8.4374						
64	11.675		9.4956	9.5588	8.4786						
65	11.713		9.5059	9.5993	8.5078						
66	11.744		9.521	9.632	8.5432						
67			9.5387	9.6722	8.5945						
68			9.5538	9.7044	8.644						
69			9.5666	9.7388	8.6842						
70			9.5893	9.7762	8.7069						
71			9.6244	9.8212	8.7392						
72			9.6621	9.8628	8.7894						
73			9.6922	9.9009	8.8433						
74			9.7173	9.9357	8.8905						
75			9.7475	9.9622	8.9275						
76			9.7777	9.9929	8.9651						

Specimen	DJ.953. 663	D5.220. 1214.2	D5.220. 1214.2.A	DJ.952. 712.A	DJ.952. 712.B	DJ.953. 452A	DJ.953. 452B	DJ.952. 755	DJ.953. 745	D5.220. 1217.2	D5.219. 1185.2
Year											
77			9.7953	10.028	9.0175						
78			9.828	10.062	9.0566						
79			9.8556	10.112	9.094						
80			9.8758	10.17	9.1181						
81			9.8961	10.215	9.1428						
82			9.9136	10.257	9.1841						
83			9.9363	10.295	9.2045						
84			9.9639	10.33	9.2294						
85			9.9865	10.356	9.2676						
86			10.012	10.387	9.3125						
87			10.024	10.422	9.3477						
88			10.045	10.456	9.3807						
89				10.506	9.4371						
90					9.4716						
91					9.5097						
92					9.5315						
93					9.5607						
94					9.5921						
95					9.6236						

Dataset B.10: Acetate peel ontogenetic data from Danian bivalve teeth (measurements in mm)

Specimen	D001	D001e	D5.229. 1363.2	D5.229. 1361.2	D5.229. 1351.2	D5.229. 1334.2.A	D5.229. 1334.2.B	DJ.953. 799.II	D5.229. 1320.2	D002	D003	D5.229. 1361.2.8
Year												
1	0.4481	0.4481	0.6014	0.3798	0.507	0.4904	0.5277	0.1837	0.558	0.6763	0.431	0.4878
2	1.0024	1.0024	2.1705	0.7499	0.9381	0.927	1.5783	0.4911	1.49	1.3179	0.9535	1.013
3	1.4915	1.4915	3.7514	1.1383	1.4288	1.5537	2.5824	0.6942	2.2574	2.139	1.6535	1.739
4	1.9931	1.9931	4.3797	1.7551	1.8192	2.2565	3.4509	0.9576	2.9723	2.8097	2.293	2.4692
5	2.4111	2.4111	5.1048	2.519	2.2276	3.4039	4.0636	1.3547	3.7469	3.091	3.041	3.1451
6	2.6524	2.9263	5.7954	3.2748	2.5418	4.5369	4.7033	1.8952	4.7532	3.2981	3.6565	3.7831
7	2.9263	3.2695	6.3656	4.2306	2.886	5.5379	5.3437	2.2592	5.5735	3.7976	4.1882	4.3143
8	3.2695	3.7232	6.8864	5.0621	3.172	6.4712	5.9132	2.7615	6.3204	4.2293	5.0683	4.8476
9	3.7232	4.159	7.5019	5.8102	3.4387	7.1966	6.338	3.2707	7.015	4.5997	5.8287	5.3246
10	4.159	4.6515	7.8243	6.4814	3.6875	7.9501	6.7317	3.7655	7.628	4.9404	6.6297	5.8262
11	4.6515	5.0149	8.0887	7.0566	3.9079	8.685	7.095	4.2004	8.2636	5.058	7.252	6.2929
12	5.0149	5.3334	8.6389	7.4932	4.1238	9.3621	7.3651	4.714	8.8958		7.7437	6.6908
13	5.3334	5.6227	9.2639	7.8537	4.2904	9.9347	7.5728	5.2288	9.3921		8.2061	7.1358
14	5.6227	5.8954	9.6343	8.1689	4.5104	10.408	7.8779	5.6443	9.8119		8.5902	7.5611
15	5.8954	6.1281	10.085	8.435	4.7376	10.846	8.2512	6.0283	10.073		9.055	7.9263
16	6.1281	6.3071	10.332	8.758	4.9151	11.207	8.5421	6.4422	10.414		9.3906	8.2768
17	6.3071	6.3935	10.54	9.2096	5.0572	11.582	8.7089	6.7658	10.668		9.739	8.5435
18	6.3935	6.5004	10.753	9.6276	5.1797	11.996	8.8565	7.1436	10.813		10.071	8.75
19	6.5004	6.5473	10.998	10.029	5.3054	12.488	8.9783	7.4423	11.016		10.265	8.8581
20	6.5473	6.5878	11.216	10.267	5.4404	12.902	9.0961	7.6938	11.25		10.427	8.9615
21	6.5878	6.635	11.409	10.514	5.5508	13.232	9.1889	7.9195	11.501		10.649	9.054
22	6.635	6.6852	11.527	10.702	5.6286	13.458	9.3267	8.1064	11.686		10.955	9.1081
23	6.6852	6.736	11.73	10.83	5.701	13.621	9.4359	8.2358	11.831			9.1938
24	6.736	6.7905	11.917	10.89	5.7539	13.78	9.5628	8.3789	11.912			9.3119
25	6.7905	6.8218	12.177	10.94	5.8049	13.906	9.7038	8.4522	12.015			9.4119
26	6.8218	6.8469	12.465	11.032	5.8504	14.077	9.8071	8.5394	12.069			9.4949

Specimen	D001	D001e	D5.229. 1363.2	D5.229. 1361.2	D5.229. 1351.2	D5.229. 1334.2.A	D5.229. 1334.2.B	DJ.953. 799.II	D5.229. 1320.2	D002	D003	D5.229. 1361.2.8
Year												
27	6.8469	6.8736	12.633	11.09	5.8849	14.216	9.9008	8.6211	12.11			9.549
28	6.8736	6.9016	12.804	11.175	5.9545	14.393	10.01	8.6962	12.17			9.6077
29	6.9016	6.9208	12.931	11.285	6.0354	14.547	10.098	8.7658	12.2			9.6649
30	6.9208	6.94	13.111	11.356	6.0952	14.665	10.227	8.8243	12.214			
31	6.94	6.9592	13.287	11.415	6.1475	14.818	10.326	8.8772	12.236			
32	6.9592	6.9872	13.387	11.456	6.1969	14.996	10.42	8.8983	12.304			
33	6.9872	6.9961	13.489	11.485	6.2513	15.127	10.492	8.9253	12.445			
34	6.9961	7.014	13.603	11.512	6.325	15.256	10.534	8.9464	12.463			
35	7.014	7.0348	13.71	11.535		15.361	10.618	8.9679	12.519			
36	7.0348	7.0586	13.788	11.576		15.478	10.687	9.0023				
37	7.0586	7.0661	13.861	11.625		15.578	10.753	9.0234				
38	7.0661	7.0749	13.923	11.702		15.648	10.82	9.0736				
39	7.0749	7.0975	13.967	11.755		15.753	10.895	9.107				
40	7.0975	7.1079	14.031	11.845		15.825	10.945	9.2045				
41	7.1079	7.1204	14.092			15.877	10.985	9.227				
42	7.1204	7.1297	14.157			15.941	11.045	9.2767				
43	7.1297	7.1523	14.213			15.991	11.098	9.2947				
44	7.1523	7.176	14.254			16.038	11.159	9.3281				
45	7.176	7.1894	14.314			16.075	11.192	9.3493				
46	7.1894	7.1987	14.371			16.11	11.28	9.3688				
47	7.1987	7.2398	14.415			16.177	11.313	9.4144				
48	7.2398	7.2594	14.449			16.24	11.363	9.4357				
49	7.2594	7.2757	14.481			16.289	11.439	9.4605				
50	7.2757	7.2904	14.504			16.335	11.483	9.4748				
51	7.2904	7.3008	14.538			16.382	11.527	9.5059				
52	7.3008	7.3188	14.596			16.426	11.567	9.5352				

Specimen Year	D001	D001e	D5.229. 1363.2	D5.229. 1361.2	D5.229. 1351.2	D5.229. 1334.2.A	D5.229. 1334.2.B	DJ.953. 799.II	D5.229. 1320.2	D002	D003	D5.229. 1361.2.8
53	7.3188	7.3338	14.636			16.467	11.605	9.5621				
54	7.3338	7.3488	14.671			16.509	11.642	9.5934				
55	7.3488	7.3684	14.702			16.563	11.685	9.6114				
56	7.3684	7.3935	14.736			16.612	11.721					
57	7.3935	7.4086	14.771			16.672						
58	7.4086	7.419	14.796			16.71						
59	7.419	7.4561	14.826			16.765						
60	7.4561	7.4757	14.846			16.796						
61	7.4757	7.5029	14.879			16.83						
62	7.5029	7.5262	14.905			16.892						
63	7.5262	7.5487	14.949			16.92						
64	7.5487	7.5812	14.973			16.998						
65	7.5812	7.5999	14.996			17.036						
66	7.5999	7.6265	15.026			17.082						
67	7.6265		15.059			17.148						
68			15.09			17.19						
69			15.135			17.236						
70			15.18			17.267						
71			15.211			17.308						
72			15.23			17.371						
73			15.262			17.417						
74			15.282									
75			15.302									
76			15.337									
77			15.354									

Dataset B.11: Valve surface ontogenetic data from Maastrichtian, Danian KLB10 and Sobral bivalve shells (measurements in mm)

Specimen	DJ.952.578	DJ.952.585	DJ.952.584	DJ.952.517	D5.1214.2	DJ.953.451	DJ.952.581	D5.1361.2	DJ.953.1102	DJ.953.1175	DJ.953.1088	DJ.953.1093	D9.209.872	D9.211.140
Stage	Maa	Maa	Maa	Maa	Maa	Maa	Maa	Dan	Dan	Dan	Dan	Dan	Sob	Sob
Year														
1	3.0157	NA	0.9301	6.366	NA	4.8464	2.423	NA	NA	1.3957	NA	NA	NA	NA
2	6.7944	4.931166	10.171	14.14	7.72	12.45	6.8153	NA	9.8623	6.0622	NA	NA	NA	NA
3	8.9075	7.384096	19.5331	21.4	10.09	20.08	12.6299	17.5568	15.097	12.9584	NA	23.7733	NA	11.9061
4	11.8379	9.905646	26.6533	29.56	14.33	28	19.2568	25.01	19.8894	22.8945	28.1743	30.7623	18.96	15.1952
5	17.211	11.45185	35.0993	35.84	20.06	32.33	26.0007	31.2	26.2584	29.4167	32.914	37.6116	22.6	20.1698
6	22.0864	13.75645	42.5513	44.16	23.3	36.67	31.7804	38.95	32.5662	34.605	38.4102	44.7501	27.43	24.1197
7	28.8996	16.85958	47.6917	51.2	27.6	40.19	36.7465	43.52	37.4923	39.5307	43.3674	50.27	31.57	26.4661
8	36.0108	19.38404	53.1061	58.94	30.59	45.01	41.148	47.71	41.5447	42.5514	48.071	54.2369	35.81	30.247
9	41.764	21.49556	57.5581	65.7	32.53	49.24	45.6122	51.17	43.2464	44.0857	53.1394	58.1149	39.62	34.5978
10	46.3594	25.36677	61.1335	69.97	34.78	52.11	48.3889	53.32	44.3791	45.71	57.2815	61.9725	42.67	39.0295
11	51.5199	29.77612	64.7586	73.7	37.34	54.93	50.1606	54.38	45.4139	46.8638	60.9401	64.0279	46.47	41.9
12	53.7593	34.80766	66.5914	75.19	38.34	58.19	51.5858	55.49	46.5972	48.2317	63.8288	66.0548	49.65	42.8754
13	56.4946	41.92628	68.1915	76.92	41.39	60.53	52.7861	56.39	47.1006		67.3073	67.8932	51.53	43.6958
14	57.961	47.48741	69.604		43.58	62.68	54.2717		47.7094		70.8697	69.9614	53.3	44.7183
15	59.3725	51.88229	70.061		45.83	64.19	55.4938		48.5886		74.4685	72.08	54.69	45.7808
16	60.4291	54.75417	70.3713		47.32	66.05	56.2271		48.9945		77.7622		56.08	46.547
17	61.3102	56.98752	70.6091		48.88	67.6	57.1024		49.4483		79.7851		57.35	47.2952
18	62.0159	59.35942	71.0039		50.26	69.16	57.6862		49.8542		81.9927			47.7202
19	63.2481	62.37767	71.3033		51.51	70.5	58.27		50.7441		83.0919			48.2006
20	64.5961	64.99829	71.5659		52.84	71.78			51.4219		84.3161			48.5324
21	65.6527	65.56239	71.878		53.84				51.9529		85.0118			48.7921
22	66.9474	66.18222	72.23		54.43				52.6737		85.535			49.246
23	68.1196	66.62149			55.28				53.303		86.3026			

Specimen	DJ.952.578	DJ.952.585	DJ.952.584	DJ.952.517	D5.1214.2	DJ.953.451	DJ.952.581	D5.1361.2	DJ.953.1102	DJ.953.1175	DJ.953.1088	DJ.953.1093	D9.209.872	D9.211.140
Stage	Maa	Maa	Maa	Maa	Maa	Maa	Maa	Dan	Dan	Dan	Dan	Dan	Sob	Sob
Year														
24	69.5895	67.20288			55.93				53.9447		87.6283			
25	70.41	68.43982			56.64				54.6011		88.433			
26		69.52101			57.29				55.1321		89.0553			
27		70.55868			57.8				55.7116		89.611			
28		71.55							56.3893		90.18			
29									56.9876					
30									57.6169					
31									58.476					
32									59.1538					
33									59.76					

Table B.2: Summary of coeffecients (L, k and t) of the von Bertalanffy growth equation generated by least squares regression analysis of annual growth data (Datasets B.9 to B.11)

Shell	Specimen	Species	Unit	L	k	t
Tooth	D001	*Lahillia*	KPLB10	7.394	0.1	-0.851
Tooth	D001e	*Lahillia*	KPLB10	7.357	0.11	-0.881
Tooth	D5.229.1363.2	*Lahillia*	KPLB10	15.159	0.066	0.804
Tooth	D5.229.1361.2	*Lahillia*	KPLB10	12.437	0.086	-1.62
Tooth	D5.229.1351.2	*Lahillia*	KPLB10	6.704	0.081	-10.1
Tooth	D5.229.1334.2.A	*Lahillia*	KPLB10	17.056	0.071	-1.295
Tooth	D5.229.1334.2.B	*Lahillia*	KPLB10	11.476	0.08	0.265
Tooth	DJ.953.799.II	*Lahillia*	KPLB10	9.92	0.073	-2.231
Tooth	D5.229.1320.2	*Lahillia*	KPLB10	13.125	0.1	-1.036
Tooth	D002	*Lahillia*	KPLB10	7.057	0.117	-0.09
Tooth	D003	*Lahillia*	KPLB10	15.816	0.059	-1.047
Tooth	D5.229.1361.2.8	*Lahillia*	KPLB10	10.755	0.089	-0.925
Valve	S˙D5.1361.2	*Lahillia*	KPLB10	62.159	0.222	-1.604
Valve	S˙DJ.953.1102	*Lahillia*	KPLB10	56.505	0.153	-0.747
Valve	S˙DJ.953.1175	*Lahillia*	KPLB10	57.729	0.18	-1.141
Valve	S˙DJ.953.1088	*Lahillia*	KPLB10	98.252	0.098	-0.849
Valve	S˙DJ.953.1093	*Lahillia*	KPLB10	80.468	0.156	-0.835
Valve	S˙D9.209.872	*Lahillia*	KPLB10	72.438	0.103	-1.258
Valve	S˙D9.211.140	*Lahillia*	Sobral	52.59	0.148	-1.604
Tooth	DJ.953.663	*Lahillia*	KLB789	11.496	0.075	0.124
Tooth	D5.220.1214.2	*Lahillia*	KLB789	11.306	0.072	-0.53
Tooth	D5.220.1214.2.A	*Lahillia*	KLB789	9.713	0.061	0.686
Tooth	DJ.952.712.A	*Lahillia*	KLB789	10.112	0.049	1.513
Tooth	DJ.952.712.B	*Lahillia*	KLB789	9.237	0.045	0.514
Tooth	D5.220.1217.2	*Lahillia*	KLB789	13.111	0.07	-1.084
Tooth	DJ.953.452A	*Lahillia*	KLB789	9.327	0.089	-1.319
Tooth	DJ.953.452B	*Lahillia*	KLB789	11.164	0.106	-1.65
Tooth	DJ.952.755	*Lahillia*	KLB789	6.669	0.108	-0.92
Tooth	DJ.953.745	*Lahillia*	KLB789	13.779	0.076	-1.486
Tooth	D5.219.1185.2	*Lahillia*	KLB789	19.169	0.023	-0.172
Valve	S˙DJ.952.578	*Lahillia*	KLB789	80.221	0.092	-2.422
Valve	S˙DJ.952.585	*Lahillia*	KLB789	116.673	0.041	-3.244
Valve	S˙DJ.952.584	*Lahillia*	KLB789	75.81	0.175	-1.153
Valve	S˙DJ.952.517	*Lahillia*	KLB789	124.362	0.083	-0.569
Valve	S˙D5.1214.2	*Lahillia*	KLB789	65.652	0.083	-0.729
Valve	S˙DJ.953.451	*Lahillia*	KLB789	81.565	0.107	-0.373
Valve	S˙DJ.952.581	*Lahillia*	KLB789	64.468	0.142	-2.112

APPENDIX C

Organic Carbon Analysis

Samples of bulk sediment from composite section D5.251 were analysed for their organic carbon isotope content. Approximately 1 g of bulk sediment was weighed and then reacted for 24 hours with ~5 ml of 10% HCl to remove all carbonate and non-organic material. Excess liquid was drawn off and the samples washed 3 times with milli-Q de-ionised water to remove residual acid and dissolved species. Samples were then dried at 85°C in a heating cabinet for 36 hours and reweighed to establish the mass of carbonate removed. 4-5 mg of this acid-washed sediment was then weighed out into tin cups and run in sequence with standards on a Micromass Isoprime continous flow mass spectrometer coupled to a Eurovector or Elementar Pyrocube Elemental Analyser. Organic carbon was completely combusted at 1020°C to CO_2 in a medium of pure oxygen injected into a stream of helium. Excess oxygen was removed by reaction with metallic copper heated to 650°C, H_2O was removed in a magnesium perchlorate trap and the CO_2 separated from other impurities using a chromatographic column. $^{13}C/^{12}C$ is derived from the integrated mass 44, 45 and 46 signals from the pulse of sample CO_2, compared to those in an independently introduced pulse of CO_2 reference gas. These ratios are then calibrated using the international standards ANU-sucrose (-10.47‰) and IAEA-CH7 (polyethylene film, -31.83‰) to the Vienna-Pee Dee Belemnite (V-PDB) scale in per mille notation (‰). The precision obtained for repeat analysis of standard materials during the runs performed was less than 0.25‰ (1 standard deviation). Calculation of weight percent organic carbon was either derived from the mass spectrometer traces or analysed on a LECO elemental analyser, and corrected for weight loss during the acidification process. Weight percent carbonate was either calculated from weight loss during acidification or from analyzing total carbon on the LECO and then calculating total inorganic carbon (TIC) by deducting TOC. TIC was then converted to weight percent carbonate by assuming that it was all present as $CaCO_3$.

Carbon Isotope Mass Balance Calculations

It is well known that mollusc shells can incorporate carbon both from the dissolved inorganic carbon pool and from organic carbon metabolized as a food source. To explore whether our shell carbon isotope compositions could be explained by metabolic input we used a simple isotope mass balance equation (S1), where F is the proportion of metabolic carbon incorporated into shells, $\delta^{13}C_{shell}$ $\delta^{13}C_{DIC}$ $\delta^{13}C_{POC}$ are the $\delta^{13}C$ values of the aragonite shell, the dissolved inorganic carbon incorporated directly into the shell and the particulate organic carbon incorporated from metabolic processes respectively.

$$\delta^{13}C_{arag} = F\ \delta^{13}C_{DIC} + (1\text{-}F)\delta^{13}C_{POC}$$

[S1]

The normal contribution of respired carbon to bivalve shell carbonate (F) is around 10% (McConnaughey et al. 1997), which typically produces a $\delta^{13}C$ depletion in shells of less than 2‰ relative to seawater under modern oceanic conditions. Cretaceous surface ocean DIC values can be estimated from marine bulk carbonate (Figure 6.4) $\delta^{13}C_{DIC}$ and produce a late Cretaceous average of around +2.5‰ (Voigt et al. 2012; Dinarès-Turell et al. 2014; Thibault et al. 2012). Bottom waters are likely to be depleted relative surface waters so we used a value of 0‰ to represent a lower limit on the DIC experienced by the organism. Modern temperate marine phytoplankton produces organic carbon with a $\delta^{13}C$ of around −20‰, whereas Antarctic phytoplankton produces a greater depletion of around −28‰, (Mook & Tan 1991). This range of values of $\delta^{13}C_{POC}$ encompasses the observed bulk $\delta^{13}C_{org}$ data presented in the main body of the thesis, so low and high estimates have both been included in the calculation. Applying these values to equation 1 produces expected shell carbonate values of between +2.5 and -2.8‰. This range covers 8 of the 19 shells sampled at high resolution. 2 shells have some carbon isotopic values more positive than this range. The 9 shells we define as "extreme" have values more negative than this range, and all have a seasonal $\delta^{13}C$ range of greater than 3‰.

The maximum contribution (F) of metabolically derived carbon into bivalve shells has been calculated as 37% (Gillikin et al. 2007). With this extreme value for the fraction of metabolized carbon, our calculations still only produce a minimum shell values of −10.4‰. This is still ~24‰ heavier than our most negative recorded value. These calculations demonstrate that we must invoke a highly ^{13}C depleted carbon source to explain our data. Methane derived DIC provides the only credible explanation for our carbon isotope data with values of less than −11‰. Since there is not a mechanism to incorporate methane directly into shell carbonate, methane carbon must have.

To explore the contribution of methane derived DIC to the total DIC pool we first applied equation 1 again, this time using shell values of −10 and −34‰ and solving for $\delta^{13}C_{DIC}$ to produce an estimate of bottom water DIC that accounts for any contribution of metabolized carbon in the shell. The shell values of −34‰ observed in this study require oceanic DIC with a carbon isotope composition at least as depleted as the shell carbonate, even assuming no contribution of metabolic carbon. Using contributions of metabolized carbon from 0 to 37% to explain our most negative shell value produces bottom water DIC estimates of between −35‰ and −42.2‰ (Table C.1-C.3). For a shell value of −10‰ we can only produce a DIC value in the range expected for the late Cretaceous (0 to +2.5‰) if we have the most extreme value of 37% incorporation of metabolic carbon and the most depleted particulate organic carbon value (-28‰). Other combinations of variables used to achieve a shell composition of −10‰ produce estimates of bottom water DIC between −4 and −10‰

$$\delta^{13}C_{\text{bottom water DIC}} = F\ \delta^{13}C_{\text{methane-derived DIC}} + (1\text{-}F)\delta^{13}C_{\text{oceanic DIC}} \quad [S2]$$

If we assume that local bottom water DIC is produced by combining ocean DIC in our expected isotopic range (0 to +2.5‰) with DIC derived from the oxidation of methane (equation S2), we can work out the fraction of each component that is required to account for the range of bottom water DIC isotope values produce by the calculation above. The full range of biogenic methane $\delta^{13}C$ spans −50 to −110‰ (Whiticar 1999). For the most extreme negative shell values, between 30-85% methane derived DIC is required, depending on its isotopic composition. Carbon isotope values from authigenic carbonate in burrow fills from stratigraphically lower in the same section of −58.0 and −24.6‰ (Little et al. 2015) are indicative of sedimentary methane and the most negative of these provide a possible estimate of our methane source carbon isotope composition. Using a value of −60‰ in our calculation produces a fraction of methane-derived DIC contribution to bottom-water in the range of 57 to 71%.

Hydrate Modelling

Down-column hydrate stability modelling was used to examine the possibility of seasonally influenced shallow hydrates as the source of seasonal methane-derived DIC. Estimates of representative mean annual bottom water temperatures of 0 to 20°C in 5°C steps were derived from shell $\delta^{18}O$ data using a standard conversion (Grossman & Ku 1986). For bottom-water depths shallower than 200 m, sea-bed methane hydrates are unstable at mean annual temperatures less than −2°C (Kvenvolden 1993). To explore the effect of bottom-water depths deeper than 200m, the top and bottom of the hydrate stability zone were computed following the methods described in (Hunter et al., 2013) using the empirical 3-phase hydrate stability solution of (Tishchenko et al. 2005). We performed a sensitivity analysis with this model that incorporated uncertainty in the geothermal gradient (20, 30, 40, 50°C km^{-1}), water depth (200 to 240 m in 10 m steps). The sensitivity analysis identified that the only conditions which allowed for a hydrate stability zone within the sediment column was at a bottom-water temperature lower than −0.2°C under the lowest geothermal gradient (20°C km^{-1}) and deepest water depth (240 m). Even then, the minimum hydrate zone depth was 28.8 m below the sea-bed, which is too deep for a response to annual fluctuations in bottom-water temperature to drive seasonal release of methane.

Temperatures down to −3°C were also considered following recent work covering the same section (Petersen et al. 2016) which suggests shell $\delta^{18}O$ derived temperatures may produce a warm bias. However, even minimum clumped-isotope derived temperatures of −0.2°C from *Lahillia* and *Cucullaea* and −2.8°C from other bivalve species are likely to have been too warm for shallow hydrate formation at water depths of 70-200 m suggested from the sedimentology and faunal assemblage of the López de Bertodano Formation (Macellari 1988; Crame et al. 2004).

Dataset C.1: Bulk sedimentary weight percent organic carbon and carbon isotope data from sedimentary section D5.251 used in Figure 6.4

		wt% $C_{organic}$			$\delta^{13}C_{organic}$ (‰V-PDB)		
Specimen No.	Height on composite section (m)	(1)	(2)	(average)	(1)	(2)	(average)
D5.229.1377.1	1072	0.45		0.45	-26.14		-26.14
D5.229.1373.1	1069	0.29		0.29	-25.98		-25.98
D5.229.1363.1	1064	0.27		0.27	-26.04		-26.04
D5.229.1353.1	1059	0.14	0.12	0.13	-26.07	-26.09	-26.08
D5.229.1347.1	1056	0.27		0.27	-25.77		-25.77
D5.229.1339.1	1052	0.44		0.44	-25.62		-25.62
D5.229.1331.1	1044	0.33	0.53	0.43	-24.65	-25.28	-24.96
D5.229.1320.1	1034	0.30		0.30	-24.81		-24.81
D5.229.1318.1	1032	0.41		0.41	-24.86		-24.86
D5.229.1312.1	1027	0.22		0.22	-25.16		-25.16
D5.229.1307.1	1022	0.34		0.34	-24.73		-24.73
D5.229.1304.1	1019	0.16	0.17	0.16	-25.65	-25.82	-25.73
D5.229.1298.1	1013	0.17	0.11	0.14	-24.15	-25.86	-25.00
D5.229.1297.1	1012	0.36		0.36	-23.98		-23.98
D5.229.1296.1	1011	0.26		0.26	-24.94		-24.94
D5.229.1294.1	1009	0.14		0.14	-24.77		-24.77
D5.229.1293.1	1008	0.43		0.43	-22.37		-22.37
D5.229.1292.1	1007	0.39		0.39	-24.70		-24.70
D5.229.1291.1	1006	0.29		0.29	-24.29		-24.29
D5.229.1290.1	1005	0.36		0.36	-24.98		-24.98
D5.229.1289.1	1004	0.40		0.40	-25.30		-25.30
D5.229.1288.1	1003	0.37		0.37	-24.61		-24.61
D5.229.1285.1	1000	0.26	0.22	0.24	-25.17	-25.24	-25.20
D5.229.1280.1	995	0.37		0.37	-24.32		-24.32
D5.229.1275.1	990	0.57		0.57	-25.10		-25.10
D5.229.1274.1	989	0.38		0.38	-24.75		-24.75
D5.229.1269.1	985	0.27		0.27	-24.86		-24.86
D5.229.1264.1	980	0.17	0.22	0.20	-25.57	-25.27	-25.42
D5.229.1259.1	975	0.32		0.32	-25.06		-25.06
D5.229.1258.1	974	0.38	0.21	0.29	-25.03	-24.89	-24.96
D5.222.1244.1	970				-25.23	-25.53	-25.38
D5.222.1241.1	966	0.27	0.32	0.30	-25.66	-25.35	-25.50
D5.222.1240.1	963	0.21		0.21	-25.11		-25.11
D5.222.1238.1	960	0.37		0.37	-24.54		-24.54
D5.222.1234.1	954	0.23	0.33	0.28	-23.50	-23.19	-23.35
D5.222.1232.1	950	0.24	0.21	0.22	-25.00	-24.45	-24.72
D5.220.1227.1	944	0.29		0.29	-24.83		-24.83
D5.220.1225.1	940	0.29	0.12	0.21	-21.52	-24.34	-22.93
D5.220.1222.1	934	0.25	0.18	0.22	-23.61	-23.87	-23.74
D5.220.1220.1	930	0.15	0.13	0.14	-24.70	-24.98	-24.84

Specimen No.	Height on composite section (m)	wt% $C_{organic}$ (1)	(2)	(average)	$\delta^{13}C_{organic}$ (‰V-PDB) (1)	(2)	(average)
D5.220.1218.1	926	0.32	0.12	0.22	-23.64	-24.92	-24.28
D5.220.1217.1	924	0.30		0.30	-22.36		-22.36
D5.220.1215.1	920	0.19	0.17	0.18	-25.46	-25.43	-25.45
D5.220.1212.1	914	0.31		0.31	-24.34		-24.34
D5.220.1210.1	910	0.19	0.17	0.18	-25.33	-25.19	-25.26
D5.220.1207.1	904	0.33		0.33	-23.96		-23.96
D5.220.1205.1	900	0.21	0.21	0.21	-25.39	-25.13	-25.26
D5.220.1198.1	890	0.21		0.21	-23.81		-23.81
D5.220.1196.1	886	0.25		0.25	-25.04		-25.04
D5.220.1194.1	883	0.33		0.33	-25.05		-25.05
D5.220.1192.1	880	0.27		0.27	-25.13		-25.13
D5.220.1190.1	876	0.24	0.52	0.38	-24.67	-24.68	-24.68
D5.219.1183.1	864	0.42		0.42	-24.48		-24.48
D5.219.1173.1	844	0.17		0.17	-25.09		-25.09
D5.219.1169.1	837	0.27		0.27	-24.70		-24.70
D5.219.1166.2	834	0.22		0.22	-24.95		-24.95
D5.219.1164.1	832	0.27		0.27	-25.54		-25.54
D5.219.1163.1	831	0.19		0.19	-24.26		-24.26
D5.219.1162.1	830	0.19		0.19	-24.63		-24.63
D5.219.1159.1	824	0.24		0.24	-25.04		-25.04
D5.219.1150.1	800	0.26		0.26	-25.10		-25.10
D5.219.1141.1	784	0.34		0.34	-24.63		-24.63
D5.219.1131.1	764	0.42		0.42	-23.84		-23.84
D5.219.1120.1	744	0.53		0.53	-24.24		-24.24
D5.219.1104.1	724	0.35		0.35	-24.78		-24.78
D5.219.1103.1	723	0.41		0.41	-24.87		-24.87
D5.219.1102.1	722	0.50		0.50	-24.60		-24.60
D5.219.1101.1	721	0.34		0.34	-24.81		-24.81
D5.219.1100.1	720	0.45		0.45	-24.94		-24.94
D5.219.1099.1	719	0.49		0.49	-21.74		-21.74
D5.219.1098.1	718	0.28		0.28	-23.85		-23.85
D5.219.1097.1	717	0.31		0.31	-24.66		-24.66
D5.219.1096.1	716	0.27		0.27	-23.22		-23.22
D5.219.1085.1	704	0.24		0.24	-24.52		-24.52
D5.218.1063.1	683	0.32		0.32	-24.67		-24.67
D5.218.1042.1	663	0.30		0.30	-24.50		-24.50
D5.218.1033.1	654	0.32		0.32	-24.91		-24.91
D5.218.1032.1	653	0.28		0.28	-24.70		-24.70
D5.218.1031.1	651				-24.37		-24.37
D5.218.1030.1	649	0.39		0.39	-23.70		-23.70
D5.218.1029.1	648	0.36		0.36	-24.85		-24.85
D5.218.1028.1	647	0.26		0.26	-23.72		-23.72
D5.218.1027.1	646	0.28		0.28	-24.57		-24.57

Specimen No.	Height on composite section (m)	wt% $C_{organic}$ (1)	(2)	(average)	$\delta^{13}C_{organic}$ (‰V-PDB) (1)	(2)	(average)
D5.218.1026.1	645	0.26	0.22	0.24	-23.94	-24.92	-24.43
D5.218.1025.1	644				-24.25		-24.25
D5.218.1024.1	643	0.29		0.29	-24.83		-24.83
D5.218.1004.1	624	0.44		0.44	-24.63		-24.63
D5.218.1003.1	623	0.32		0.32	-24.24		-24.24
D5.218.1002.1	622	0.45		0.45	-24.50		-24.50
D5.218.1001.1	621	0.34		0.34	-24.82		-24.82
D5.215.704.1	620	0.69		0.69	-23.59		-23.59
D5.215.703.1	619	0.68		0.68	-24.57		-24.57
D5.215.702.1	618	0.50		0.50	-24.49		-24.49
D5.215.701.1	617	0.62		0.62	-24.59		-24.59
D5.215.687.1	603	0.48		0.48	-24.29		-24.29
D5.215.668.1	583	0.51		0.51	-25.09		-25.09
D5.215.384.1	563	0.65		0.65	-25.00		-25.00
D5.215.364.1	543	0.60		0.60	-25.14		-25.14
D5.215.348.1	528	0.52		0.52	-24.89		-24.89
D5.215.347.1	527	0.56		0.56	-25.10		-25.10
D5.215.346.1	526	0.51		0.51	-24.35		-24.35
D5.215.345.1	525	0.61		0.61	-25.37		-25.37
D5.215.344.1	524	0.57		0.57	-25.14		-25.14
D5.215.343.1	523	0.58		0.58	-25.41	-25.48	-25.45
D5.215.342.1	522	0.66		0.66	-25.30		-25.30
D5.215.341.1	521	0.63		0.63	-25.38		-25.38
D5.215.340.1	520	0.62		0.62	-25.38		-25.38
D5.215.323.1	503	0.45		0.45	-24.96		-24.96
D5.215.303.1	481	0.57		0.57	-25.39		-25.39
D5.215.984.1	461	0.47		0.47	-25.35		-25.35
D5.215.966.1	443	0.65		0.65	-25.60		-25.60
D5.215.961.1	438	0.09		0.09	-25.00		-25.00
D5.215.956.1	433	0.09		0.09	-25.33		-25.33
D5.215.951.1	428	0.81		0.81	-25.31		-25.31
D5.215.946.1	423	0.77		0.77	-24.94		-24.94
D5.215.941.1	418	0.79		0.79	-25.16		-25.16
D5.215.936.1	413	0.47		0.47	-24.76		-24.76
D5.215.931.1	408	0.48		0.48	-25.16		-25.16
D5.215.926.1	403	0.82		0.82	-25.04		-25.04
D5.215.921.1	398	0.66		0.66	-25.04		-25.04
D5.215.916.1	393	0.51		0.51	-24.88		-24.88
D5.215.913.2	390	0.97		0.97	-25.24		-25.24
D5.215.910.11	387	0.53		0.53	-24.70		-24.70
D5.212.889.1	366	0.53		0.53	-25.44		-25.44
D5.212.879.1	356	0.52		0.52	-25.02		-25.02
D5.212.869.1	346	0.39		0.39	-25.46		-25.46

Specimen No.	Height on composite section (m)	wt% $C_{organic}$ (1)	(2)	(average)	$\delta^{13}C_{organic}$ (‰V-PDB) (1)	(2)	(average)
D5.212.860.1	337	0.24		0.24	-25.05		-25.05
D5.212.839.1	316	0.37		0.37	-25.36		-25.36
D5.212.832.1	309	0.45		0.45	-25.95		-25.95
D5.212.570.1	246	0.28		0.28	-25.67		-25.67
D5.212.528.1	206	0.50		0.50	-25.03		-25.03
D5.212.489.3	165	0.24		0.24	-25.73		-25.73

Dataset C.2 Bulk sedimentary weight percent carbonate used in Figure 6.4

Specimen No.	Height (m)	wt% Carbonate
D5.229.1377.1	1072	8
D5.229.1339.1	1052	8
D5.229.1318.1	1032	6.6
D5.229.1307.1	1022	7.9
D5.229.1297.1	1012	6.7
D5.229.1296.1	1011	12.2
D5.229.1294.1	1009	59.4
D5.229.1293.1	1008	9.5
D5.229.1292.1	1007	7.9
D5.229.1291.1	1006	22
D5.229.1290.1	1005	8.9
D5.229.1289.1	1004	8.5
D5.229.1288.1	1003	6.5
D5.229.1274.1	989	9
D5.229.1259.1	975	10.1
D5.222.1240.1	963	6.9
D5.220.1227.1	944	7.7
D5.220.1217.1	924	13.2
D5.220.1207.1	904	7.1
D5.220.1194.1	883	19
D5.219.1173.1	844	8.6
D5.219.1159.1	824	6.3
D5.219.1150.1	800	6.5
D5.219.1141.1	784	6.3
D5.219.1131.1	764	9.5
D5.219.1120.1	744	10.5
D5.219.1104.1	724	12.2
D5.219.1085.1	704	10.2
D5.218.1063.1	683	9.3
D5.218.1042.1	663	8.8
D5.218.1024.1	643	9.5
D5.218.1003.1	623	12.1
D5.215.687.1	603	9.2
D5.215.668.1	583	11
D5.215.384.1	563	9.2
D5.215.364.1	543	12.8

Table C.1: Mass balance calculations using equation [S1] solving for modelled shell $\delta^{13}C$

ocean DIC $\delta^{13}C$ (‰)	fraction	POC $\delta^{13}C$ (‰)	fraction	Calculated shell $\delta^{13}C$ (‰)
No incorporation of metabolic carbon				
2.5	1	-28	0	**2.5**
0	1	-28	0	**0.0**
2.5	1	-20	0	**2.5**
0	1	-20	0	**0.0**
10% contribution of metabolic carbon				
2.5	0.9	-28	0.1	**-0.6**
0	0.9	-28	0.1	**-2.8**
2.5	0.9	-20	0.1	**0.3**
0	0.9	-20	0.1	**-2.0**
37% contribution of metabolic carbon				
2.5	0.63	-28	0.37	**-8.8**
0	0.63	-28	0.37	**-10.4**
2.5	0.63	-20	0.37	**-5.8**
0	0.63	-20	0.37	**-7.4**

Table C.2: Mass balance calculation using equation [S1] solving for $\delta^{13}C$ of bottom water DIC

bottom water DIC calculated $\delta^{13}C$ (‰)	fraction	POC $\delta^{13}C$ (‰)	fraction	shell $\delta^{13}C$ (‰)
0.6	0.63	-28	0.37	-10.0
-8.0	0.9	-28	0.1	-10.0
-10.0	1	-28	0	-10.0
-4.1	0.63	-20	0.37	-10.0
-8.9	0.9	-20	0.1	-10.0
-10.0	1	-20	0	-10.0
-37.5	0.63	-28	0.37	-34.0
-34.7	0.9	-28	0.1	-34.0
-34.0	1	-28	0	-34.0
-42.2	0.63	-20	0.37	-34.0
-35.6	0.9	-20	0.1	-34.0
-34.0	1	-20	0	-34.0

Table C.3: Mass balance calculation using equation [S2] solving for fractions of methane derived DIC and oceanic DIC required to recreate modeled local bottom water conditions.

bottom water DIC $\delta^{13}C$ (‰)	Methane DIC $\delta^{13}C$ (‰)	calculated fraction	Ocean DIC $\delta^{13}C$ (‰)	calculated fraction
-34.0	-50	**0.70**	2.5	0.30
-34.0	-50	**0.68**	0.0	0.32
-34.0	-60	**0.58**	2.5	0.42
-34.0	-60	**0.57**	0.0	0.43
-34.0	-110	**0.32**	2.5	0.68
-34.0	-110	**0.31**	0.0	0.69
-42.0	-50	**0.85**	2.5	0.15
-42.0	-50	**0.84**	0.0	0.16
-42.0	-60	**0.71**	2.5	0.29
-42.0	-60	**0.70**	0.0	0.30
-42.0	-110	**0.40**	2.5	0.60
-42.0	-110	**0.38**	0.0	0.62

APPENDIX D

Dataset D.1: Maastrichtian global seasonal and mean annual temperature proxy-derived data set.

Organism	Method	Reference	Year	Pal˙Lat	Local˙Name	Country	MAT	MAT error	CMMT	WMMT
Belemnite	Belemnite d18O	Lowenstam & Epstein	1954	35.49	Macon	USA	16.3	1.6		
Belemnite	Belemnite d18O	Lowenstam & Epstein	1954	37.23	Starkville	USA	19.9	1.6		
Belemnite	Belemnite d18O	Lowenstam & Epstein	1954	37.23	Starkville	USA	18.8	1.6		
Belemnite	Belemnite d18O	Lowenstam & Epstein	1954	37.23	Starkville	USA	16.8	1.6		
Belemnite	Belemnite d18O	Lowenstam & Epstein	1954	37.15	Cape Fear River	USA	18.6	1.6		
Belemnite	Belemnite d18O	Lowenstam & Epstein	1954	35.49	Macon	USA	19.5	1.6		
Belemnite	Belemnite d18O	Lowenstam & Epstein	1954	35.49	Macon	USA	17.5	1.6		
Belemnite	Belemnite d18O	Lowenstam & Epstein	1954	35.49	Macon	USA	16.4	1.6		
Belemnite	Belemnite d18O	Lowenstam & Epstein	1954	35.49	Macon	USA	22.9	1.6		
Belemnite	Belemnite d18O	Lowenstam & Epstein	1954	36.76	Pee Dee River	USA	19.2	1.6		
Belemnite	Belemnite d18O	Lowenstam & Epstein	1954	36.76	Pee Dee River	USA	18	1.6		
Belemnite	Belemnite d18O	Lowenstam & Epstein	1954	36.76	Pee Dee River	USA	19.5	1.6		
Belemnite	Belemnite d18O	Lowenstam & Epstein	1954	36.76	Pee Dee River	USA	18.1	1.6		
Belemnite	Belemnite d18O	Lowenstam & Epstein	1954	36.76	Pee Dee River	USA	18.6	1.6		
Belemnite	Belemnite d18O	Lowenstam & Epstein	1954	36.76	Pee Dee River	USA	18.6	1.6		
Belemnite	Belemnite d18O	Lowenstam & Epstein	1954	36.76	Pee Dee River	USA	18.7	1.6		
Belemnite	Belemnite d18O	Lowenstam & Epstein	1954	36.76	Pee Dee River	USA	18.2	1.6		
Belemnite	Belemnite d18O	Lowenstam & Epstein	1954	36.76	Pee Dee River	USA	18	1.6		
Belemnite	Belemnite d18O	Lowenstam & Epstein	1954	36.76	Pee Dee River	USA	19	1.6		
Belemnite	Belemnite d18O	Lowenstam & Epstein	1954	36.76	Pee Dee River	USA	19.7	1.6		
Belemnite	Belemnite d18O	Lowenstam & Epstein	1954	36.76	Pee Dee River	USA	17.3	1.6		
Belemnite	Belemnite d18O	Lowenstam & Epstein	1954	37.15	Cape Fear River	USA	17.7	1.6		

Organism	Method	Reference	Year	Pal˙Lat	Local˙Name	Country	MAT	MAT error	CMMT	WMMT
Belemnite	Belemnite d18O	Lowenstam & Epstein	1954	40.46	Cream Ridge	USA	17.3	1.6		
Belemnite	Belemnite d18O	Lowenstam & Epstein	1954	40.46	Cream Ridge	USA	18	1.6		
Belemnite	Belemnite d18O	Lowenstam & Epstein	1954	40.46	Cream Ridge	USA	16.7	1.6		
Belemnite	Belemnite d18O	Lowenstam & Epstein	1954	40.46	Cream Ridge	USA	17.2	1.6		
Belemnite	Belemnite d18O	Lowenstam & Epstein	1954	63.42	Hornerstown	USA	17.9	1.6		
Belemnite	Belemnite d18O	Lowenstam & Epstein	1954	63.42	Hornerstown	USA	18.6	1.6		
Belemnite	Belemnite d18O	Lowenstam & Epstein	1954	63.42	Hornerstown	USA	17.4	1.6		
Belemnite	Belemnite d18O	Lowenstam & Epstein	1954	63.42	Hornerstown	USA	18.9	1.6		
Belemnite	Belemnite d18O	Lowenstam & Epstein	1954	63.42	Hornerstown	USA	17.9	1.6		
Belemnite	Belemnite d18O	Lowenstam & Epstein	1954	63.42	Hornerstown	USA	19.1	1.6		
Belemnite	Belemnite d18O	Lowenstam & Epstein	1954	63.42	Hornerstown	USA	17.8	1.6		
Belemnite	Belemnite d18O	Lowenstam & Epstein	1954	63.42	Hornerstown	USA	18.1	1.6		
Belemnite	Belemnite d18O	Lowenstam & Epstein	1954	63.42	Hornerstown	USA	16.2	1.6		
Belemnite	Belemnite d18O	Lowenstam & Epstein	1954	63.42	Hornerstown	USA	19.3	1.6		
Belemnite	Belemnite d18O	Lowenstam & Epstein	1954	40.24	Mullica Hill	USA	20.4	1.6		
Belemnite	Belemnite d18O	Lowenstam & Epstein	1954	40.24	Mullica Hill	USA	18.4	1.6		
Belemnite	Belemnite d18O	Lowenstam & Epstein	1954	40.24	Mullica Hill	USA	19.8	1.6		
Belemnite	Belemnite d18O	Lowenstam & Epstein	1954	40.24	Mullica Hill	USA	20.2	1.6		
Belemnite	Belemnite d18O	Lowenstam & Epstein	1954	40.24	Mullica Hill	USA	20.4	1.6		
Belemnite	Belemnite d18O	Lowenstam & Epstein	1954	40.24	Mullica Hill	USA	19.8	1.6		
Belemnite	Belemnite d18O	Lowenstam & Epstein	1954	54	Bjernum	Sweden	17.7	1.6		
Belemnite	Belemnite d18O	Lowenstam & Epstein	1954	54	Bjernum	Sweden	17.2	1.6		
Belemnite	Belemnite d18O	Lowenstam & Epstein	1954	54	Bjernum	Sweden	17.4	1.6		
Belemnite	Belemnite d18O	Lowenstam & Epstein	1954	54	Bjernum	Sweden	17.7	1.6		
Belemnite	Belemnite d18O	Lowenstam & Epstein	1954	47.03	Moens Klint	Denmark	15.2	1.6		
Belemnite	Belemnite d18O	Lowenstam & Epstein	1954	47.03	Moens Klint	Denmark	15.4	1.6		
Belemnite	Belemnite d18O	Lowenstam & Epstein	1954	47.03	Moens Klint	Denmark	16.4	1.6		
Belemnite	Belemnite d18O	Lowenstam & Epstein	1954	47.03	Moens Klint	Denmark	14.8	1.6		

Organism	Method	Reference	Year	Pal˙Lat	Local˙Name	Country	MAT	MAT error	CMMT	WMMT
Belemnite	Belemnite d18O	Lowenstam & Epstein	1954	47.03	Moens Klint	Denmark	15.9	1.6		
Belemnite	Belemnite d18O	Lowenstam & Epstein	1954	47.03	Moens Klint	Denmark	15.3	1.6		
Belemnite	Belemnite d18O	Lowenstam & Epstein	1954	47.03	Moens Klint	Denmark	14.7	1.6		
Belemnite	Belemnite d18O	Lowenstam & Epstein	1954	44.21	St. Pietersberg	Holland	19.6	1.6		
Belemnite	Belemnite d18O	Lowenstam & Epstein	1954	45.04	Trimingham	England	17.4	1.6		
Soil	Carbonate d18O	Lowenstam & Epstein	1954	35.49	Macon	USA	26.8	0.5		
Soil	Carbonate d18O	Lowenstam & Epstein	1954	36.76	Pee Dee River	USA	23.1	0.5		
Soil	Carbonate d18O	Lowenstam & Epstein	1954	37.15	Cape Fear River	USA	19.1	0.5		
Soil	Carbonate d18O	Lowenstam & Epstein	1954	37.11	Columbus	USA	27.4	0.5		
Soil	Carbonate d18O	Lowenstam & Epstein	1954	47.03	Moens Klint	Denmark	24.1	0.5		
Soil	Carbonate d18O	Lowenstam & Epstein	1954	47.03	Moens Klint	Denmark	27	0.5		
Soil	Carbonate d18O	Lowenstam & Epstein	1954	45.04	Trimingham	England	24.5	0.5		
Soil	Carbonate d18O	Lowenstam & Epstein	1954	45.04	Trimingham	England	25.4	0.5		
Soil	Carbonate d18O	Lowenstam & Epstein	1954	45.04	Trimingham	England	27.5	0.5		
Belemnite	Belemnite d18O	Bowen	1961	42.68		Belgium	20	1.6		
Belemnite	Belemnite d18O	Bowen	1961	42.68		Belgium	20.2	1.6		
Belemnite	Belemnite d18O	Bowen	1961	42.68		Belgium	18.4	1.6		
Belemnite	Belemnite d18O	Bowen	1961	42.68		Belgium	18.5	1.6		
Belemnite	Belemnite d18O	Bowen	1961	42.68		Belgium	20	1.6		
Veg		Spicer	1987	81	Prince Creek Formation	USA	2.5	0		
Veg	Macroflora Life Form Analysis	Parrish and Spicer	1988	81	Prince Creek Formation	USA	5	3		
Belemnite	Belemnite d18O	Pirrie and Marshall	1990	-63	Vega Island	Antarctica	9.9	1.6		
Bivalve	Bivalve d18O	Pirrie and Marshall	1990	-63	Vega Island	Antarctica	12	1.6		
Bivalve	Bivalve d18O	Pirrie and Marshall	1990	-63	Vega Island	Antarctica	10.3	1.6		
Bivalve	Bivalve d18O	Pirrie and Marshall	1990	-63	Vega Island	Antarctica	12.6	1.6		
Bivalve	Bivalve d18O	Pirrie and Marshall	1990	-63	Vega Island	Antarctica	10.9	1.6		

Organism	Method	Reference	Year	Pal˙Lat	Local˙Name	Country	MAT	MAT error	CMMT	WMMT
Bivalve	Bivalve d18O	Pirrie and Marshall	1990	-63	Vega Island	Antarctica	11.4	1.6		
Bivalve	Bivalve d18O	Pirrie and Marshall	1990	-63	Vega Island	Antarctica	9	1.6		
Bivalve	Bivalve d18O	Pirrie and Marshall	1990	-63	Vega Island	Antarctica	14.9	1.6		
Bivalve	Bivalve d18O	Pirrie and Marshall	1990	-63	Vega Island	Antarctica	11.6	1.6		
Bivalve	Bivalve d18O	Pirrie and Marshall	1990	-63	Vega Island	Antarctica	15	1.6		
Bivalve	Bivalve d18O	Pirrie and Marshall	1990	-63	Vega Island	Antarctica	16.6	1.6		
Cephalopod	Ammonoid d18O	Pirrie and Marshall	1990	-63	Vega Island	Antarctica	16.6	1.6		
Cephalopod	Ammonoid d18O	Pirrie and Marshall	1990	-63	Vega Island	Antarctica	15.9	1.6		
Cephalopod	Ammonoid d18O	Pirrie and Marshall	1990	-63	Vega Island	Antarctica	10.8	1.6		
Cephalopod	Ammonoid d18O	Pirrie and Marshall	1990	-63	Vega Island	Antarctica	13.7	1.6		
Cephalopod	Ammonoid d18O	Pirrie and Marshall	1990	-63	Vega Island	Antarctica	12.5	1.6		
Cephalopod	Ammonoid d18O	Pirrie and Marshall	1990	-63	Vega Island	Antarctica	10.6	1.6		
Cephalopod	Ammonoid d18O	Pirrie and Marshall	1990	-63	Vega Island	Antarctica	10.8	1.6		
Cephalopod	Ammonoid d18O	Pirrie and Marshall	1990	-63	Vega Island	Antarctica	13.2	1.6		
Cephalopod	Ammonoid d18O	Pirrie and Marshall	1990	-63	Vega Island	Antarctica	9.8	1.6		
Cephalopod	Ammonoid d18O	Pirrie and Marshall	1990	-63	Vega Island	Antarctica	10	1.6		
Cephalopod	Ammonoid d18O	Pirrie and Marshall	1990	-63	Vega Island	Antarctica	11.9	1.6		
Cephalopod	Ammonoid d18O	Pirrie and Marshall	1990	-63	Vega Island	Antarctica	11.9	1.6		
Cephalopod	Ammonoid d18O	Pirrie and Marshall	1990	-63	Vega Island	Antarctica	11.4	1.6		
Cephalopod	Ammonoid d18O	Pirrie and Marshall	1990	-63	Vega Island	Antarctica	11.8	1.6		
Cephalopod	Ammonoid d18O	Pirrie and Marshall	1990	-63	Vega Island	Antarctica	10.4	1.6		
Cephalopod	Ammonoid d18O	Pirrie and Marshall	1990	-63	Vega Island	Antarctica	12.8	1.6		
Veg	CLAMP	Wolfe	1990	49	Lance		16.2	2.8		
Veg	CLAMP	Wolfe	1990	48	Medicine Bow		16.5	2.8		

Organism	Method	Reference	Year	Pal˙Lat	Local˙Name	Country	MAT	MAT error	CMMT	WMMT
Veg	CLAMP	Wolfe	1990	46	Laramie		17.2	2.8		
Veg	CLAMP	Wolfe	1990	46	Littleton		17.3	2.8		
Veg	CLAMP	Wolfe	1990	45	Rockdale		17.6	2.8		
Veg	CLAMP	Wolfe	1990	43	Lower Raton		18.1	2.8		
Veg	CLAMP	Wolfe	1990	43	Vermejo		18.2	2.8		
Bivalve	Bivalve d18O	Wilson and Opdyke	1996	0	Wodejebato	PACIFIC		1.6	28	32
Bivalve	Bivalve d18O	Wilson and Opdyke	1996	0	Wodejebato	PACIFIC		1.6	24	28
Veg	CLAMP	Golovneva	2000	38	Ripley Fm	USA	17	2.8	11	23
Veg	CLAMP	Golovneva	2000	75	Rarytkin	NE Asia	11	2.8	4	19
Veg	CLAMP	Golovneva	2000	49	Lance	USA	14	2.8	8	21
Veg	CLAMP	Golovneva	2000	52	Hell Creek	USA	12	2.8	6	19
Veg	CLAMP	Golovneva	2000	48	Medicine Bow Fm	USA	17	2.8	13	23
Veg	CLAMP	Golovneva	2000	52	Lance Fm	USA	14	2.8		
Veg	CLAMP	Golovneva	2000	53	Sakhalin	Russia	14	2.8	8	20
Veg	CLAMP	Golovneva	2000	60	Edmonton Fm	Canada	12	2.8	5	19
Veg	CLAMP	Golovneva	2000	45	Zaisan Fm	Russia	11	2.8	4	19
Veg	CLAMP	Golovneva	2000	75	Kakanaut	NE Asia	10	2.8	3	19
Veg	multivariate physignomics	Golovneva	2000	76	Koryak Kakanaut Flora	Russia	10	2	3	
Foram	Foram d18O	Pearson et al	2001	-21		Tanzania	31	2.9		
Veg	CLAMP	Kennedy et al	2002	-59	Pakawau Gp	New Zealand	12.3	2.8		
Veg	CLAMP	Kennedy et al	2002	-58	Pakawu Bush Road	New Zealand	13.8	2.8		20.5
Veg	CLAMP	Kennedy et al	2002	-58	Pakawu Bush Road	New Zealand	12.7	2.8		22
Veg	CLAMP	Kennedy et al	2002	-58	Pakawu Bush Road	New Zealand	12.3	2.8		22.2
Veg	CLAMP	Kennedy et al	2002	-55	Taratu Fm	New Zealand	10.1	2.8		
Veg	LMA	Kennedy et al	2002	-59	Pakawau Gp	New Zealand	14.8	2		
Veg	LMA (NH scale)	Kennedy et al	2002	-58	Pakawu Bush Road	New Zealand	14.8	0.8		
Veg	LMA (SH scale)	Kennedy et al	2002	-58	Pakawu Bush Road	New Zealand	13.5	2		

Organism	Method	Reference	Year	Pal˙Lat	Local˙Name	Country	MAT	MAT error	CMMT	WMMT
Veg	Wood	Francis & Poole	2002	-60	Lopez de Bertodano Fm	Antarctica	3.4	4		
Fish	Fish Otolith d18O	Carpenter et al	2003	50	Fox Hills	USA	18	1.6		
Foram	Foram d18O	Maestas et al	2003	36	Rosario Fm	USA	26	2.9		30
Veg	LMA	Wilf et al	2003	49	Fort Union Formation	USA	10	2		
Veg	LMA	Wilf et al	2003	52	Hell Creek Formation	USA	7	2		18
Veg	LMA	Wilf et al	2003	52.7	Hell Creek	North Dakota	12	2		
Veg	LMA	Wilf et al	2003	52.7	Hell Creek	North Dakota	15	2		
Veg	LMA	Wilf et al	2003	52.7	Hell Creek	North Dakota	9	2		
Bone	Crocodile d18O	Amiot et al	2004	36	France	France	21	1		
Bone	Crocodile d18O	Amiot et al	2004	36	Texas	USA	19	1.1		
Bone	Crocodile d18O	Amiot et al	2004	-33		Madagascar	27	2.1		
Bone	Crocodile d18O	Amiot et al	2004	-25	Lameta Fm	India	18	2.5		
Bone	Crocodile d18O	Amiot et al	2004	-21		Bolivia	25	2.75		
Bone	Dinosaur d18O	Amiot et al	2004	36	France	France	23	2.1		
Bone	Dinosaur d18O	Amiot et al	2004	36	Texas	USA	20	1.1		
Bone	Dinosaur d18O	Amiot et al	2004	-33		Madagascar	28	2.3		
TEX	TEX H86H	Jenkyns et al	2004	78	Alpha Ridge					17
Rudist	Bivalve d18O	Steuber et al	2005	18	Marchmont	Jamaica		1.6	29.8	35.9
Rudist	Bivalve d18O	Steuber et al	2005	18	Jerusalem Mt,	Jamaica		1.6	29.8	34.0
Rudist	Bivalve d18O	Steuber et al	2005	7.7	Jebel Rawdah	Oman		1.6	36.3	39.6
Rudist	Bivalve d18O	Steuber et al	2005	7.7	Jebel Rawdah	Oman		1.6	32.6	37.3
Soil	Carbonate d18O	Dworkin et al	2005	36.3	Big Bend		16	0.5		
Soil	Carbonate d18O	Dworkin et al	2005	36.3	Big Bend		23	0.5		
Soil	Soil Carbonate d18O	Dworkin et al	2005	36	Big Bend	USA	15	0.5		
Soil	Soil Carbonate d18O	Dworkin et al	2005	36	Big Bend	USA	22	0.5		
Veg	CLAMP	Wolfe	2005	33	Olmos		24	2.8		
Veg	CLAMP	Moiseeva	2005	70	Koryak	Russia	4	2.8		

Organism	Method	Reference	Year	Pal˙Lat	Local˙Name	Country	MAT	MAT error	CMMT	WMMT
Veg	Coexistence Intervals	Poole et al	2005	-60.9	King George Island	James Ross Basin	14	0		
Veg	Coexistence Intervals	Poole et al	2005	-60.9	King George Island	James Ross Basin	18	0		
Veg	Wood	Poole et al	2005	-63	Lopez de Bertodano Fm	Antarctica	9.9	5.4		
Veg	Wood	Poole et al	2005	-60.9	King George Island	James Ross Basin	11	0		
Bivalve	Bivalve d18O	Zakharov et al	2006	44	South Netherlands	Netherlands	19.8	1.6		
Bivalve	Bivalve d18O	Zakharov et al	2006	50	Deway Fm Fox Hills	USA	17.6	1.6		
Brachiopod	Brach d18O	Zakharov et al	2006	51	Naiba River	Russia	10.8	1.6		
Brachiopod	Brach d18O	Zakharov et al	2006	51	Naiba River	Russia	11.2	1.6		
Cephalopod	Ammonoid d18O	Zakharov et al	2006	51	Naiba River	Russia	8.4	1.6		
Cephalopod	Ammonoid d18O	Zakharov et al	2006	51	Naiba River	Russia	8.4	1.6		
Cephalopod	Ammonoid d18O	Zakharov et al	2006	51	Naiba River	Russia	7.1	1.6		
Cephalopod	Ammonoid d18O	Zakharov et al	2006	51	Naiba River	Russia	9.3	1.6		
Cephalopod	Ammonoid d18O	Zakharov et al	2006	50	Deway Fm Fox Hills	USA	17.6	1.6		
Cephalopod	Ammonoid d18O	Zakharov et al	2006	50	Deway Fm Fox Hills	USA	21.3	1.6		
Cephalopod	Ammonoid d18O	Zakharov et al	2006	50	Deway Fm Fox Hills	USA	20.7	1.6		
Cephalopod	Ammonoid d18O	Zakharov et al	2006	51	Naiba River	Russia	7.6	1.6		
Cephalopod	Ammonoid d18O	Zakharov et al	2006	51	Naiba River	Russia	9.3	1.6		
Cephalopod	Ammonoid d18O	Zakharov et al	2006	51	Naiba River	Russia	7.6	1.6		
Belemnite	Belemnite d18O	Dutton et al	2007	-64	Seymour Island	Antarctica		1.6	8.9	10.6
Belemnite	Belemnite d18O	Dutton et al	2007	-64	Seymour Island	Antarctica		1.6	7.9	10.1
Belemnite	Belemnite d18O	Dutton et al	2007	-64	Seymour Island	Antarctica		1.6	7.7	10.5
Fish	Fish Tooth Enamel d18O	Puceat et al	2007	-30	Las Tablas	Chile	21	1.2		
Fish	Fish Tooth Enamel d18O	Puceat et al	2007	-30	Las Tablas	Chile	25	2.7		
Fish	Fish Tooth Enamel d18O	Puceat et al	2007	-35	Algarrobo	Chile	20	1.2		

Organism	Method	Reference	Year	Pal˙Lat	Local˙Name	Country	MAT	MAT error	CMMT	WMMT
Fish	Fish Tooth Enamel d18O	Puceat et al	2007	-35	Algarrobo	Chile	24	2.7		
Fish	Fish Tooth Enamel d18O	Puceat et al	2007	44	Maastricht	Netherlands	14	1.2		
Fish	Fish Tooth Enamel d18O	Puceat et al	2007	44	Maastricht	Netherlands	18	2.7		
Fish	Fish Tooth Enamel d18O	Puceat et al	2007	44	Nasilov	Poland	17	1.2	15	20
Fish	Fish Tooth Enamel d18O	Puceat et al	2007	44	Nasilov	Poland	20	2.7	19	23
Fish	Fish Tooth Enamel d18O	Puceat et al	2007	40	New Jersey		19	1.2	14	29
Fish	Fish Tooth Enamel d18O	Puceat et al	2007	40	New Jersey		22	2.7	17	32
Fish	Fish Tooth Enamel d18O	Puceat et al	2007	23		Morocco	28	1.2	24	31
Fish	Fish Tooth Enamel d18O	Puceat et al	2007	23		Morocco	31	2.7	27	34
Fish	Fish Tooth Enamel d18O	Puceat et al	2007	18		Israel	21	1.2	19	22
Fish	Fish Tooth Enamel d18O	Puceat et al	2007	18		Israel	24	2.7	23	25
Fish	Fish Tooth Enamel d18O	Ounis et al	2008	25		Tunisia	27	1.2	24	30
Fish	Fish Tooth Enamel d18O	Ounis et al	2008	25		Tunisia	30	2.7	28	33
Veg	LMA	Estrada-Ruiz et al	2008	33	Olmos		25	2		
Veg	LMA	Estrada-Ruiz et al	2008	33.7	Olmos		23	2		
Veg	CLAMP	Spicer and Herman	2010	40	Ripley Fm	USA	14.7	2.8	5.3	25.3
Veg	CLAMP	Tomsich et al	2010	74	Cantwell	Alaska	7.4	2.8	-2.3	17.1
Veg	CLAMP	Tomsich et al	2010	50	Hell Creek	USA	12	2.8	6	19
Veg	CLAMP	Spicer & Herman	2010	65	Vilui	Russia	11	2.8		
Veg	CLAMP	Tomsich et al	2010	76	Koryak,	Russia	3.5	2.8		
Veg	CLAMP	Tomsich et al	2010	81	Prince Creek		5.5	2.8	3	11
Veg	CLAMP	Spicer and Herman	2010	52	Lance	USA	13.3	2.8	5.3	22.2
Veg	CLAMP	Spicer and Herman	2010	36	Cooper Pit	USA	14.7	2.8	5.3	25.3
Veg	CLAMP	Spicer and Herman	2010	51	Medicine Bow Fm	USA	17.2	2.8	11.2	23.6
Veg	CLAMP	Tomsich et al	2010	54	Edmonton	Canada	12	2.8	5	19

Organism	Method	Reference	Year	Pal˙Lat	Local˙Name	Country	MAT	MAT error	CMMT	WMMT
Veg	CLAMP	Tomsich et al	2010	75	Kakanaut	Russia	10	2.8	3	19
Veg	Extrapolated	Spicer & Herman	2010	81	Prince Creek		5.7	2.8		
Veg	LMA	Tomisch, McCarthy et al	2010	74	Cantwell Fm	Alaska	8	2		
Veg	CLAMP	Hofmann et al	2011	63	Chirimyi Fm	Russia	13.1	2.8		
Veg	Digital Leaf Physiognomy	Peppe et al	2011	52	Fox Hills	USA	17	3.3		
TEX	TEX H86H	Alsenz et al	2013	19	Aderet 1	Israel				28
TEX	TEX H86H	Alsenz et al	2013	19	PAMA Quarry	Israel				27
Foram	Foram d18O	Ashckenazi Polivoda et al	2014	36	Falls County	USA	27	2.9		
Soil	MBT/CBT	Kemp et al	2014	-63	Seymour Island	Antarctica	12	5	10	14
TEX	TEX H86H	Linnert et al	2014	36	Shuqualak Core	USA				30
TEX	TEX H86H	Vellekoop et al	2014	36	Corsicana Fm					30
Veg	CLAMP	Arens and Allen	2014	49	Hell Creek Formation		11.3	2.8	2.6	20.5
Veg	CLAMP	Arens and Allen	2014	49	Hell Creek Formation		11.6	2.8	2.6	20.1
Veg	LMA	Upchurch et al	2015	40	McRae Fm Jose Creek Member		22	2.3		
Veg	LMA	Upchurch et al	2015	38	Ripley Cooper		22	2.4		
Veg	LMA	Upchurch et al	2015	38	Ripley Perry		23	2.1		
Veg	LMA	Upchurch et al	2015	48	Medicine Bow Fm	USA	20	2.4		
Veg	LMA	Upchurch et al	2015	49	Lance Fm	USA	20	2.4		
Veg	LMA	Upchurch et al	2015	46	Littleton		22	2		
Veg	LMA	Upchurch et al	2015	46	Laramie lower		26	2		
Veg	LMA	Upchurch et al	2015	46	Laramie broomfield		23	3.1		
Veg	LMA	Upchurch et al	2015	43	Vermejo		23	2		
Veg	LMA	Upchurch et al	2015	43	Lower Raton		23	2.1		
Veg	LMA	Upchurch et al	2015	61	Lower Atanikerdluk	Greenland	24	2		

Dataset D.2: Paleosol pedogenic carbonate-derived Maastrichtian atmospheric CO_2 data set.

Reference	Age (Ma)	Age old	Age young	CO2 (ppm)	CO2 low (ppm)	CO2 high (ppm)	CO2 low err	CO2 high err
Ekart et al., 1999	61	62.2	59.2	0	0	84	0	84
Huang et al., 2013	64			399	320	478	79	79
Huang et al., 2013	64			341	238	444	103	103
Huang et al., 2013	65			326	235	417	91	91
Huang et al., 2013	65			456	297	615	159	159
Nordt et al., 2002	65	65.0	64.7	400	320	480	80	80
Huang et al., 2013	65			286	208	364	78	78
Huang et al., 2013	65			584	425	743	159	159
Huang et al., 2013	65			451	325	577	126	126
Nordt et al., 2003	65	66.2	64.2	178	148	208	30	30
Huang et al., 2013	65			569	298	840	271	271
Nordt et al., 2003	65	66.2	64.2	163	136	190	27	27
Nordt et al., 2002	65	65.7	65.0	340	280	400	60	60
Nordt et al., 2003	65	66.4	64.4	88	73	103	15	15
Huang et al., 2013	65			470	310	630	160	160
Nordt et al., 2003	66	66.6	64.6	111	93	130	19	19
Nordt et al., 2003	66	66.8	64.8	178	148	207	30	30
Nordt et al., 2002	66	66.3	65.5	300	240	360	60	60
Nordt et al., 2003	66	66.9	64.9	54	45	63	9	9
Nordt et al., 2003	66	67.1	65.1	183	153	214	31	31
Nordt et al., 2003	66	67.2	65.2	277	231	324	46	46
Nordt et al., 2003	66	67.4	65.4	90	75	105	15	15
Nordt et al., 2003	67	67.5	65.5	0	0	0	0	0
Nordt et al., 2003	67	67.5	65.5	42	35	50	7	7
Huang et al., 2013	67			837	673	1001	164	164
Nordt et al., 2003	67	67.6	65.6	15	12	17	2	2
Nordt et al., 2003	67	67.6	65.6	263	219	307	44	44
Nordt et al., 2003	67	67.7	65.7	453	377	528	75	75
Nordt et al., 2003	67	67.9	65.9	426	355	497	71	71
Nordt et al., 2003	67	67.9	65.9	265	221	310	44	44
Nordt et al., 2003	67	68.0	66.0	219	183	256	37	37
Nordt et al., 2003	67	68.0	66.0	128	107	150	21	21
Nordt et al., 2002	67	68.1	66.3	560	440	680	120	120
Nordt et al., 2002	67	68.1	66.3	300	240	360	60	60
Huang et al., 2013	68			277	162	392	115	115
Nordt et al., 2003	69	69.5	67.5	10	9	12	2	2
Nordt et al., 2003	69	69.7	67.7	171	142	199	28	28
Nordt et al., 2003	69	69.8	67.8	110	91	128	18	18
Nordt et al., 2003	69	70.0	68.0	158	132	185	26	26
Andrews et al., 1995	69	72.1	66.0	60	0	260	60	200
Ekart et al., 1999	69	72.1	66.0	328	208	448	120	120
Ekart et al., 1999	69	72.1	66.0	172	52	292	120	120
Ekart et al., 1999	69	72.1	66.0	252	132	372	120	120
Nordt et al., 2003	69	70.1	68.1	138	115	161	23	23
Nordt et al., 2003	69	70.3	68.3	202	169	236	34	34
Nordt et al., 2003	69	70.4	68.4	145	121	169	24	24
Nordt et al., 2003	70	70.5	68.5	345	287	402	57	57
Nordt et al., 2003	70	70.7	68.7	204	170	238	34	34
Nordt et al., 2003	70	70.9	68.9	309	258	361	52	52

Nordt et al., 2003	70	71.0	69.0	375	313	438	63	63
Nordt et al., 2003	70	71.1	69.1	329	274	383	55	55
Nordt et al., 2003	70	71.2	69.2	122	101	142	20	20
Nordt et al., 2003	70	71.3	69.3	38	32	45	6	6
Nordt et al., 2003	70	71.5	69.5	126	105	147	21	21
Nordt et al., 2003	71	72.4	70.4	254	212	297	42	42
Nordt et al., 2003	71	72.5	70.5	289	241	337	48	48
Nordt et al., 2003	72	72.6	70.6	294	245	343	49	49

Dataset D.3: Stomatal index proxy-derived Maastrichtian atmospheric CO_2 data set.

Reference	Age (Ma)	Age old	Age young	CO2 (ppm)	CO2 low (ppm)	CO2 high (ppm)
Royer, 2003 (updated by Beerling et al., 2009)	61.1	64.8	57.4	317	308	330
Beerling et al., 2002 (updated by Beerling et al., 2009)	63.8	66.0	61.6	367	324	707
Beerling et al., 2002 (updated by Beerling et al., 2009)	64.1	64.3	63.9	330	317	448
Beerling et al., 2002 (updated by Beerling et al., 2009)	65.4	66.0	64.8	343	323	673
Beerling et al., 2002 (updated by Beerling et al., 2009)	65.4	66.0	64.8	470	327	757
Beerling et al., 2002 (updated by Beerling et al., 2009)	66.5	67.0	66.0	539	340	786

References

Crame, J. A., Francis, J. E., Cantrill, D. J. and Pirrie, D. (2004) 'Maastrichtian stratigraphy of Antarctica', *Cretaceous Research*, 25(3), 411–423.

Dennis, K. J., Affek, H. P., Passey, B. H., Schrag, D. P. and Eiler, J. M. (2011) 'Defining an absolute reference frame for "clumped" isotope studies of CO2', *Geochimica et Cosmochimica Acta*, 75(22), 7117–7131.

Dettman, D. L. and Lohmann, K. C. (1995) 'Microsampling carbonates for stable isotope and minor element analysis; physical separation of samples on a 20 micrometer scale', *Journal of Sedimentary Research*. SEPM Society for Sedimentary Geology, 65(3a), 566–569.

Dinarès-Turell, J., Westerhold, T., Pujalte, V., Röhl, U. and Kroon, D. (2014) 'Astronomical calibration of the Danian stage (Early Paleocene) revisited: Settling chronologies of sedimentary records across the Atlantic and Pacific Oceans', *Earth and Planetary Science Letters*, 405, 119–131.

Gillikin, D. P., Lorrain, A., Meng, L. and Dehairs, F. (2007) 'A large metabolic carbon contribution to the δ13C record in marine aragonitic bivalve shells', *Geochimica et Cosmochimica Acta*, 71(12), 2936–2946.

Grossman, E. L. and Ku, T.-L. (1986) 'Oxygen and carbon isotope fractionation in biogenic apetite: temperature effects', *Chemical Geology*, 59, 59–74.

Huntington, K. W., Eiler, J. M., Affek, H. P., Guo, W., Bonifacie, M., Yeung, L. Y., Thiagarajan, N., Passey, B., *et al.* (2009) 'Methods and limitations of "clumped" CO 2 isotope (Δ 47) analysis by gas-source isotope ratio mass spectrometry', *Journal of Mass Spectrometry*, 44(9), 1318–1329.

Kvenvolden, K. A. (1993) 'Gas hydrates—geological perspective and global change', *Reviews of Geophysics*, 31(2), 173.

Little, C. T. S., Birgel, D., Boyce, A. J., Crame, J. A., Francis, J. E., Kiel, S., Peckmann, J., Pirrie, D., *et al.* (2015) 'Late Cretaceous (Maastrichtian) shallow water hydrocarbon seeps from Snow Hill and Seymour Islands, James Ross Basin, Antarctica', *Palaeogeography, Palaeoclimatology, Palaeoecology*, 418, 213–228.

Macellari, C. E. (1988) 'Stratigraphy, sedimentology, and paleoecology of Upper Cretaceous / Paleocene shelf-deltaic sediments of Seymour Island', *Geological Society of America Memoirs*, 169, 25–54.

McConnaughey, T. A., Burdett, J., Whelan, J. F. and Paull, C. K. (1997) 'Carbon isotopes in biological carbonates: Respiration and photosynthesis', *Geochimica et Cosmochimica Acta*, 61(3), 611–622.

Mook, W. G. and Tan, F. C. (1991) 'Stable carbon isotopes in rivers and estuaries', in *Biogeochemistry of major world rivers*, 245–64.

Petersen, S. V., Dutton, A. and Lohmann, K. C. (2016) 'End-Cretaceous extinction in Antarctica linked to both Deccan volcanism and meteorite impact via climate change', *Nature Communications*. Nature Publishing Group, 7(May), 12079.

Schmid, T. W. and Bernasconi, S. M. (2010) 'An automated method for "clumped-isotope" measurements on small carbonate samples', *Rapid Communications in Mass Spectrometry*, 24(14), 1955–1963.

Sharman, G. and Newton, E. J. (1897) 'Notes on some additional fossils collected at Seymour Island, Graham's Land, by Dr Donald and Captain Larsen.', *Proceedings of the Royal Society of Edinburgh*, 22, 58–61.

Stilwell, J. D., Zinsmeister, W. J. and Oleinik, A. E. (2004) 'Early Paleocene Mollusks of Antarctica: systematics, paleoecology and paleobiogeographic significance', 369(365).

Thibault, N., Husson, D., Harlou, R., Gardin, S., Galbrun, B., Huret, E. and Minoletti, F. (2012) 'Astronomical calibration of upper Campanian–Maastrichtian carbon isotope events and calcareous plankton biostratigraphy in the Indian Ocean (ODP Hole 762C): Implication for the age of the Campanian–Maastrichtian boundary', *Palaeogeography, Palaeoclimatology, Palaeoecology*, 337–338, 52–71.

Tishchenko, P., Hensen, C., Wallmann, K. and Wong, C. S. (2005) 'Calculation of the stability and solubility of methane hydrate in seawater', *Chemical Geology*, 219(1–4), 37–52.

Voigt, S., Gale, A. S., Jung, C. and Jenkyns, H. C. (2012) 'Global correlation of Upper Campanian – Maastrichtian successions using carbon-isotope stratigraphy: development of a new Maastrichtian timescale', *Newsletters on Stratigraphy*, 45(1), 25–53.

Whiticar, M. J. (1999) 'Carbon and hydrogen isotope systematics of bacterial formation and oxidation of methane', *Chemical Geology*, 161(1–3), 291–314.

Wilckens, O. (1907) 'Die Lamellibranchiaten, Gastropoden, etc. der oberen Kreide Südpatagoniens', *Berlin natf*, 15, 97–166.

Zinsmeister, W. J. (1984) 'Late Eocene bivalves (mollusca) from the La Meseta formation, collected during the 1974-1975 joint Argentine-American expedition to Seymour Island, Antarctic Peninsula', *Journal of Paleontology*, 58(6), 1497–1527.

Zinsmeister, W. J. and Macellari, C. E. (1988) 'Bivalvia (Mollusca) from Seymour Island , Antarctic Peninsula', *Geological Society of America Memoirs*, (169).